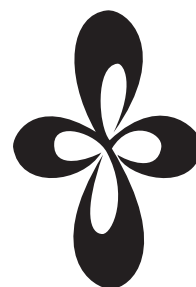


# ***ANNUAL REVIEW***

***INSTITUTE  
FOR  
MOLECULAR  
SCIENCE***



***2005***  
*(Sep. 2004 ~ Aug. 2005)*

Published by

Institute for Molecular Science

National Institutes of Natural Sciences

Myodaiji, Okazaki 444-8585, Japan

Phone: +81-564-55-7418 (Secretary Room)

Fax: +81-564-54-2254 (Secretary Room)

URL: <http://www.ims.ac.jp/>

## Editorial Committee 2005

Chairperson

SHIGEMASA, Eiji

Vice-Chairperson

TSUKUDA, Tatsuya

YAMASHITA, Yasufumi

IMURA, Kohei

JUDAI, Ken

YAMAMOTO, Kaoru

AKITA, Motoko

JIANG, Donglin

TAKAHASHI, Eiji J.

MIURA, Shinichi

MATSUO, Tsukasa

NAGASAWA, Takayuki

NEGISHI, Yuichi

ITO, Takahiro

ISHIZUKI, Hideki

YOSHIOKA, Shiro

KAMO, Kyoko

NAKAMURA, Rie

## IMS 2005

On May 20, 2005, we celebrated the 30<sup>th</sup> anniversary of IMS. The laboratory visit, the commemorative ceremony, and the celebration party were held successfully with the attendance of about 300 people from all over Japan. I would like to take this opportunity to express my deep appreciation again. Thanks to the supports from the Government, the molecular science community, city of Okazaki, and many other organizations and people, IMS could make a big progress as COE in molecular science in the last 30 years.

It is expected that new sciences will be born in this new century based on the wholistic view of the world. Molecular science should play a fundamental role for this birth as a basic science covering from materials to life. In order to contribute to this, we have to refresh our spirits and to have our own philosophy. This is especially important in the present severe circumstances for basic sciences. We always have to pursue “truth, good and beauty,” and furthermore the consciousness of “妙”(myoh: no appropriate translation) higher than the former three. Since international collaborations are also crucial for the promotion of sciences, the new program started last year should be further promoted.

This volume of Annual Review is a comprehensive summary of research activities carried out at IMS in the period of September 2004–August 2005. As usual, a lot of activities are going on and we are proud of that. Any constructive comments and/or questions are heartily welcome. It is also a great pleasure to announce that many colleagues received various prizes as explained in the end of this volume.

October, 2005



*H. Nakamura*

NAKAMURA, Hiroki  
Director General, Institute for Molecular Science



# CONTENTS

IMS 2005 .....	iii
CONTENTS .....	v
ORGANIZATION AND STAFF .....	1
COUNCIL .....	13
BUILDINGS AND CAMPUS .....	15
RESEARCH ACTIVITIES I .....	17

## Department of Theoretical Studies

<b>I-A Theoretical Study and Design of Functional Molecular Systems: New Bonding, Structures, and Reactions .....</b>	<b>17</b>
I-A-1 Counterion-Driven Spontaneous Polymerization of the Linear $C_{60}^{n-}$ Chains in the fcc Fullerides and Its Magic Number Behavior .....	17
I-A-2 Amphoteric and Controllable Doping of Carbon Nanotubes by Encapsulation of Organic and Organometallic Molecules .....	17
I-A-3 Electronic Excited States and Stabilities of Fullerenes: Isomers of $C_{78}$ and $Mg@C_{72}$ .....	17
I-A-4 1,6,7-Trigermabicyclo[4.1.0]hept-3-en-7-yl: The Isolable Bicyclic Germyl Radical .....	17
I-A-5 Isolation of a <i>Se</i> -Nitrososelenol: A New Class of Reactive Nitrogen Species Relevant to Protein <i>Se</i> -Nitrosation .....	18
I-A-6 A New Approach to Simulate the Depolymerization Process of a Two-Dimensional Hexagonal $C_{60}$ Polymer .....	18
I-A-7 Chemical Reactivity and Redox Property of $Sc_3@C_{82}$ .....	18
I-A-8 Reduction of Endohedral Metallofullerenes: A Convenient Method for Isolation .....	18
I-A-9 Dispersion of Single-Walled Carbon Nanotube Bundles in Nonaqueous Solution .....	18
I-A-10 Regioselective Carbon–Carbon Bond Cleavage of an Open-Cage Diketone Derivative of [60]Fullerene by Reaction with Aromatic Hydrazones .....	19
I-A-11 Gibbs Energy-Based Treatment of Metallofullerenes: $Ca@C_{72}$ , $Ca@C_{74}$ , $Ca@C_{82}$ , and $La@C_{82}$ .....	19
I-A-12 Chemical Reactivities of the Cation and Anion of $M@C_{82}$ ( $M = Y, La, \text{ and } Ce$ ) .....	19
I-A-13 Systematic Studies on Redox Behavior of Homonuclear Double-Bond Compounds of Heavier Group 15 Elements .....	19
I-A-14 Syntheses and Structures of Hypervalent Pentacoordinate Carbon and Boron Compounds Bearing an Anthracene Skeleton—Elucidation of Hypervalent Interaction Based on X-Ray Analysis and DFT Calculation .....	19
I-A-15 Adsorption Configuration of $NH_3$ on Single-Wall Carbon Nanotubes .....	20
I-A-16 Structural Characterization of $Y@C_{82}$ .....	20
I-A-17 Synthesis and Characterization of Exohedrally Silylated $M@C_{82}$ ( $M = Y \text{ and } La$ ) .....	20
I-A-18 Synthesis and Characterization of Stable Hypervalent Carbon Compounds (10-C-5) Bearing a 2,6-Bis( <i>p</i> -substituted phenyloxymethyl)benzene Ligand .....	20
I-A-19 Practical Performance Assessment of Accompanying Coordinate Expansion Recurrence Relation Algorithm for Computation of Electron Repulsion Integrals .....	20
I-A-20 2D NMR Characterization of the $La@C_{82}$ Anion .....	20
I-A-21 Open-Cage Fullerene Derivatives Suitable for the Encapsulation of a Hydrogen Molecule .....	21
I-A-22 Computed Structure and Energetics of $La@C_{60}$ .....	21
I-A-23 Metallic Phase in the Metal-Intercalated Higher Fullerene $Rb_{8,8(7)}C_{84}$ .....	21
I-A-24 Interplay of Single-Wall Carbon Nanotubes and Encapsulated $La@C_{82}$ , $La_2@C_{80}$ , and $Sc_3N@C_{80}$ .....	21
I-A-25 Structural Evolution of [2+1] Cycloaddition Derivatives of Single-Wall Carbon Nanotubes: From Open Structure to Closed Three-Membered Ring Structure with Increasing Tube Diameter .....	22
I-A-26 Missing Metallofullerene $La@C_{74}$ .....	22
I-A-27 Chemical Reactivity of $Sc_3N@C_{80}$ and $La_2@C_{80}$ .....	22
I-A-28 Large-Scale Separation of Metallic and Semiconducting Single-Walled Carbon Nanotubes .....	22
I-A-29 Encapsulation of $La@C_{82}$ and $La_2@C_{80}$ inside Single-Walled Boron Nitride Nanotubes .....	22
<b>I-B Prediction of Protein Tertiary Structures and Protein Folding Problem .....</b>	<b>24</b>
I-B-1 Classification and Prediction of Low-Energy Membrane Protein Helix Configurations by Replica-Exchange Monte Carlo Method .....	24

I-B-2	Combination of the Replica-Exchange Monte Carlo Method and the Reference Interaction Site Model Theory for Simulating a Peptide Molecule in Aqueous Solution	-----24
I-B-3	Multi-Overlap Molecular Dynamics Methods for Biomolecular Systems	-----24
I-B-4	Secondary-Structure Preferences of Force Fields for Proteins	
	Evaluated by Generalized-Ensemble Simulations	-----24
<b>I-C</b>	<b>Development of Simulation Algorithms for Complex Systems</b>	<b>-----25</b>
I-C-1	Liquid-Gas Phase Transitions Studied by Multibaric-Multithermal Monte Carlo Simulations	-----25
<b>I-D</b>	<b>Other Results on Molecular Simulations</b>	<b>-----25</b>
I-D-1	Comparisons between a Molecular Dynamics and Hydrodynamics Treatment of Non-Stationary Thermal Processes in a Liquid	-----25
<b>I-E</b>	<b>Applications of the Zhu-Nakamura Theory to Nonadiabatic Chemical Dynamics</b>	<b>-----26</b>
I-E-1	Nonadiabatic Transition and Chemical Dynamics: Multi-Dimensional Tunneling Theory and Applications of the Zhu-Nakamura Theory	-----26
I-E-2	Electron Transfer Rate to Cover the Whole Range from Adiabatic to Nonadiabatic Regime Based on the Zhu-Nakamura Theory	-----26
I-E-3	Semiclassical Theory of Electron Transfer Beyond the Perturbation Theory	-----26
I-E-4	Generalized Trajectory Surface Hopping Approach	-----26
I-E-5	Semiclassical Theory of Thermal Rate Constant for Multi-Surface Processes	-----26
<b>I-F</b>	<b>Theory of Nonadiabatic Transition</b>	<b>-----27</b>
I-F-1	Rabi Dynamics of Coupled Atomic and Molecular Bose-Einstein Condensates	-----27
I-F-2	A Basic Two-State Model for Bosonic Field Theories with a Cubic Nonlinearity	-----27
I-F-3	Incorporation of Nonadiabatic Transition into Wave Packet Dynamics	-----27
<b>I-G</b>	<b>Theory of Multi-Dimensional Tunneling</b>	<b>-----27</b>
I-G-1	Instanton Theory for the Tunneling Splitting of Low Vibrationally Excited States	-----27
I-G-2	Effect of Out-Of Plane Vibration on the Hydrogen Atom Transfer Reaction in Malonaldehyde	-----27
I-G-3	Ground State and Vibrationally Assisted Tunneling in the Formic Acid Dimer	-----28
<b>I-H</b>	<b>Laser Control of Molecular Processes</b>	<b>-----28</b>
I-H-1	Laser Control of Electronic Transitions of Wave Packet by Using Quadratically Chirped Pulses	-----28
I-H-2	Semiclassical Guided Optimal Control of Molecular Dynamics	-----28
<b>I-I</b>	<b>Development of New Molecular Functions</b>	<b>-----29</b>
I-I-1	A Theoretical Study of Cyclohexadiene/ Hexatriene Photochemical Interconversion: Miltireference Configuration Interaction Potential Energy Surfaces and Transition Probabilities for the Radiationless Decays	-----29
I-I-2	Reaction Dynamics of Cyclohexadiene/Hexatriene Ultrafast Photoisomerization through Conical Intersections	-----29
I-I-3	Encapsulation of Hydrogen Atoms by Fullerenes and Carbon Nanotubes with the Use of Nonadiabatic Transition	-----29
<b>I-J</b>	<b>Theoretical Studies of Electron Dynamics in Molecular Systems</b>	<b>-----30</b>
I-J-1	High-Order Harmonic Generation from Silver Clusters: Laser-Frequency Dependence and the Screening Effect of d Electrons	-----30
I-J-2	Multiple Ionization of a Silver Diatomic Molecule in an Intense Laser Field	-----30
<b>I-K</b>	<b>Electronic Structures and Photochemical Properties of Nanometer-Sized Metal Clusters</b>	<b>-----30</b>
I-K-1	Electronic Structure and Photochemical Properties of a Monolayer-Protected Gold Cluster	-----30
I-K-2	Glutathione-Protected Gold Clusters Revisited: Bridging the Gap between Gold(I)-Thiolate Complexes and Thiolate-Protected Gold Nanocrystals	-----31
I-K-3	Gold-Thiolate Nanoring: Electronic Structure and Photochemical Properties	-----31
<b>I-L</b>	<b>Electronic Structure of a Molecule in Solution</b>	<b>-----32</b>
I-L-1	Electronic Structure Calculation of a Solvated Macro Molecule by Using Three-Dimensional Reference Interaction Site Model Combined with <i>Ab Initio</i> Molecular Orbital Theory	-----32
I-L-2	New Theoretical Approach for the Diastereoselectivity of H/D Exchange Reaction on Methyl 3-Fluorobutanoate Anion	-----32
<b>I-M</b>	<b>Solvation Thermodynamics of Protein and Related Molecules</b>	<b>-----33</b>
I-M-1	Hydrophobic Effects on Partial Molar Volume	-----33
I-M-2	Partial Molar Volume of Proteins Studied by the 3D-RISM Theory	-----33
I-M-3	Theoretical Study of Volume Changes Associated with the Helix-Coil Transition of an Alanine-Rich Peptide in Aqueous Solution	-----33
I-M-4	Combination of the Replica-Exchange Monte Carlo Method and the Reference Interaction Site Model Theory for Simulating a Peptide Molecule in Aqueous Solution	-----34
I-M-5	Water Molecules in a Protein Cavity Detected by a Statistical-Mechanical Theory	-----34

<b>I-N Collective Density Fluctuations in Polar Liquids and Their Response to Ion Dynamics</b> .....	<b>34</b>
I-N-1 Site-Site Memory Equation Approach in Study of Density/Pressure Dependence of Translational Diffusion Coefficient and Rotational Relaxation Time of Polar Molecular Solutions: Acetonitrile in Water, Methanol in Water, and Methanol in Acetonitrile .....	35
I-N-2 Theoretical Study on the Dynamic Properties of Compressed Water and Water-Hydrophobic Solute Mixtures .....	35
I-N-3 Solvation Dynamics in Water Investigated by RISM/Mode-Coupling Theory .....	35
<b>I-O Statistical Mechanics of Interfacial Fluids</b> .....	<b>36</b>
I-O-1 A Molecular Theory of Liquid Interfaces .....	36
<b>I-P Photoinduced Phase Transitions in Molecular Materials</b> .....	<b>37</b>
I-P-1 Photoinduced Dynamics and Nonequilibrium Characteristics in Quasi-One-Dimensional Electron Systems: Mott Insulators vs. Band Insulators .....	37
I-P-2 Optical Responses of Photoexcited States in the One-Dimensional Ionic Hubbard Model ----	37
I-P-3 Quantum Ising Model Coupled with Conducting Electrons .....	37
I-P-4 Photoinduced Metallic Properties of One-Dimensional Strongly Correlated Electron Systems .....	37
I-P-5 Interchain-Coupling Effects on Photoinduced Neutral-Ionic Transition Dynamics in Mixed-Stack Charge-Transfer Complexes .....	38
I-P-6 Theory of Photoinduced Phase Transitions .....	38
<b>I-Q Collective Transport through Metal-Insulator Interfaces</b> .....	<b>38</b>
I-Q-1 Mechanism of Ambipolar Field-Effect Carrier Injections in One-Dimensional Mott Insulators .....	38
<b>I-R Strongly Correlated Electron Systems with Frustrations</b> .....	<b>39</b>
I-R-1 Frustration-Induced $\eta$ Inversion in the $S = 1/2$ Bond-Alternating Spin Chain .....	39
I-R-2 Field-Induced Phase Transitions and Long-Range Orders in the $S = 1/2$ Spin Bond-Alternating Chain with Frustrating Interaction .....	39
I-R-3 Field-Induced Incommensurate Order in Frustrated Spin Chain .....	39
I-R-4 Phase Diagram of the Excitonic Insulator .....	39
I-R-5 Effective Interaction between the Interpenetrating Kagome Lattices in $\text{Na}_x\text{CoO}_2$ .....	39
I-R-6 Magnetism in Strongly Correlated and Frustrated Systems .....	40
<b>I-S Theory and Applications of Relativistic Quantum-Chemical Methods to Molecular Properties of Compounds Containing Heavy Elements</b> .....	<b>41</b>
I-S-1 Theoretical Studies on Circular Dichroism Spectra of Linear and Cyclic Dichalcogenide Compounds (Chalcogen = S, Se, Te) by the SAC and SAC-CI Methods .....	41
I-S-2 Theoretical Studies on Magnetic Circular Dichroism by the Finite Perturbation Method with Relativistic Corrections .....	42
I-S-3 $^{13}\text{C}$ NMR Chemical Shifts of Small Molecules Interacting with Metal Complexes in Heme Proteins and Metal Enzymes .....	42
<b>I-T Polymorphism in Molecular Liquids</b> .....	<b>43</b>
I-T-1 Construction of an Interaction-Site Model for Molecular Systems .....	43
<b>I-U Nonlinear Processes Induced by Ultrafast Laser Pulses</b> .....	<b>44</b>
I-U-1 Few-Cycle Effects in the Low Intensity Regime .....	44
<b>I-V Control of Photoionization Processes Using Lasers</b> .....	<b>44</b>
I-V-1 Control of the Spin-Polarization of Photoelectrons/Photoions Using Short Laser Pulses ----	44
I-V-2 Control of Photoelectron Angular Distributions Using a Dressing Laser .....	44
<b>I-W Theoretical Studies on Dynamical Foundation of Chemical Reactions and Proteins</b> .....	<b>46</b>
I-W-1 Phase Space Reaction Network on Multibasin Energy Landscapes .....	46
I-W-2 A Construction of Multidimensional Free Energy Landscape from an Ensemble of Single Molecule Time Series .....	46
I-W-3 A New Technique to Differentiate the Origin of Observed non-Brownian Dynamics in the Principal Component Space .....	46
I-W-4 Polypeptide in Water on the Lagrange Picture in Fluid Dynamics .....	47
<b>RESEARCH ACTIVITIES II</b> .....	<b>49</b>

## Department of Molecular Structure

<b>II-A Development of Dynamic Near-Field Spectroscopy and Application to Nanometric Systems</b> ----	<b>49</b>
II-A-1 Morphological and Spectroscopic Properties of Thin Films of Self-Assembling Amphiphilic Porphyrins on Hydrophilic Surface as Revealed by Scanning Near-Field Optical Microscopy ---	49
II-A-2 Scanning Near-Field Optical Microscopic Study of Porphyrin Nanowire .....	49
II-A-3 Imaging of Plasmon Modes in Gold Nanorods .....	50
II-A-4 Near-Field Two-Photon Induced Photoluminescence from Single Gold Nanorods .....	50
II-A-5 Dispersion Relation of Plasmon Modes in the Gold Nanorods .....	50
II-A-6 Imaging and Dispersion Relations of Surface Plasmon Modes in Silver Nanorods by Near-Field Spectroscopy .....	51

II-A-7 Ultrafast Near-Field Imaging of Single Gold Nanorods and Nanoplates	51
II-A-8 Near-Field Spectroscopy of Close-Packed Self-Assembled Monolayer Films of Gold Nanoparticles	52
<b>II-B Spectroscopic Studies on Atoms and Ions in Liquid Helium</b>	<b>53</b>
II-B-1 Laser Spectroscopic Studies of Mg Atoms in Pressurized Liquid Helium	53
<b>II-C Magnetic Structures of Magnetic Thin Films Studied by Using a Depth-Resolved XMCD Technique</b>	<b>54</b>
II-C-1 Direct Observation of an Oscillatory Behavior in the Surface Magnetization of Fe Thin Films Grown on a Ni/Cu(100) Film	54
II-C-2 Spin Reorientation Transition of Ni/Cu(100) and Co/Ni/Cu(100): Separation of the Surface and Bulk Components of the X-Ray Magnetic Circular Dichroism Spectrum	54
<b>II-D Structure and Function of Metalloproteins and Its Molecular Design</b>	<b>56</b>
II-D-1 L358P Mutation on P450cam Simulates Structural Changes upon Putidaredoxin Binding. The Structural Changes Trigger Electron Transfer to Oxy-P450cam from Electron Donors	56
II-D-2 Structural Diversities of Active Site in Clinical Azole Bound Forms between Sterol 14 $\alpha$ -demethylases (CYP51) from Human and <i>Mycobacterium tuberculosis</i>	56
II-D-3 Two Heme Binding Sites Are Involved in the Regulated Degradation of the Bacterial Iron Response Regulator (Irr) Protein	57
II-D-4 Involvement of Heme Regulatory Motif in Heme-Mediated Ubiquitination and Degradation of IRP2	57
<b>II-E Structure and Energy Changes during Protein Reaction Dynamics</b>	<b>58</b>
II-E-1 Hydrogen Bonding Dynamics During Protein Folding of Reduced Cytochrome <i>c</i> : Temperature and Denaturant Concentration Dependence	58
II-E-2 Conformational Dynamics of Phototropin 2 LOV2 Domain with the Linker upon Photoexcitation	58
<b>II-F Controllable Magnetic Properties of Ultrathin Magnetic Films Using Surface Chemical Techniques</b>	<b>59</b>
II-F-1 MOKE and XMCD Study on K Adsorption on Fe Ultrathin Films on Cu(001)	59
II-F-2 Spin Reorientation Transition in Ag-Covered Co Films Grown on Vicinal Cu(001) Surface Studied by Means of XMCD	60
II-F-3 Drastic Magnetization Change Observed in NO Adsorption on Co/Cu(1 1 17)	60
II-F-4 Direct Observation of Biquadratic Exchange Interaction in Fe/Ni/Cu(001) by Using MSHG	61
<b>II-G Local Structures of Molecular-Based Magnetic Materials Studied by X-Ray Absorption Fine Structure Spectroscopy</b>	<b>62</b>
II-G-1 Molecular Structure of Single-Molecule Magnet Mn <sub>11</sub> Cr, Mn <sub>11</sub> Cr <sup>-</sup> and Mn <sub>10</sub> Fe <sub>2</sub>	62
II-G-2 Photoinduced Phase Transition of CuMo Cyanides Studied by XAFS Spectroscopy	63
<b>II-H Development of Fluorescent and Bioluminescent Proteins for Imaging Intracellular Molecular Dynamics</b>	<b>64</b>
II-H-1 Quantitative Determination of Protein Nuclear Transport Induced by Phosphorylation or by Proteolysis	64
II-H-2 A Stress Indicator for Noninvasively Imaging Endogenous Corticosterone in Living Mice	64
<b>RESEARCH ACTIVITIES III</b>	<b>65</b>
<b>Department of Electronic Structure</b>	
<b>III-A Synthesis and Characterization of Exotic Molecule Based Nano-Crystals of Metal Acetylides: Toward Carbon Encapsulated Metal Dot Array, Metal Nano-Networks and Metal-Carbon Hybrid Systems</b>	
III-A-1 Self-Assembled Nanowire Synthesis of Highly-Anisotropic Copper Acetylide Molecules	65
III-A-2 Photochemical Conversion of (Cu <sup>+</sup> C $\equiv$ C <sup>-</sup> - <i>t</i> -Butyl) <sub>24</sub> Cluster Molecules to Cu Metallic Nano-Sheets Embedded in Polymer Nano-Film	66
III-A-3 Guest Controlled Magnetism of CoC <sub>2</sub> Nanoparticles	66
III-A-4 Formation of Carbon-Encapsulated Metallic Nano-Particles from Metal Acetylides by Electron Beam Irradiation	67
III-A-5 Reexamination of the Structures and Energies of Li <sub>2</sub> C <sub>2</sub> and Li <sub>4</sub> C <sub>4</sub>	67
<b>III-B Ultrafast Dynamics and Scanning Tunneling Microscopy</b>	<b>68</b>
III-B-1 Excited-State Double-Proton Transfer in the 7-Azaindole Dimer in Gas Phase 3. Reaction Mechanism Studied by Picosecond Time-Resolved REMPI Spectroscopy	68
III-B-2 Ultrafast Excited-State Dynamics in Photochromic <i>N</i> -Salicylideneaniline Studied by Femtosecond Time-Resolved REMPI Spectroscopy	68
III-B-3 Orientation of Nitrous Oxide on Palladium(1 1 0) by STM	68
<b>III-C Spectroscopic and Dynamical Studies of Molecular Cluster Ions</b>	<b>69</b>
III-C-1 Infrared Photodissociation Spectra and Solvation Structure of Mg <sup>+</sup> (CH <sub>3</sub> OH) <sub><i>n</i></sub> ( <i>n</i> = 1–4)	69

III-C-2 Infrared Photodissociation Spectroscopy of $\text{Mg}^+(\text{NH}_3)_n$ ( $n = 3-6$ ): Direct Coordination or Solvation through Hydrogen Bonding -----	69
III-C-3 Electronic Spectra of Jet-Cooled 3-Methyl-7-Azaindole Dimer. Symmetry of the Lowest Excited Electronic State and Double-Proton Transfer -----	69
III-C-4 Structures of $[(\text{CO}_2)_n(\text{H}_2\text{O})_m]^-$ ( $n = 1-4, m = 1, 2$ ) Cluster Anions. I. Infrared Photodissociation Spectroscopy -----	70
<b>III-D Development of High-Precision Coherent Control and Its Application -----</b>	<b>71</b>
III-D-1 Space- and Time- Resolved Observation of Molecular Wave-Packet Interference on Femtosecond and Picometric Scales -----	71
III-D-2 Real-Time Observation of Phase-Controlled Molecular Wave-Packet Interference -----	71
III-D-3 Development of Quantum Gate Operations with Vibrational Eigenstates of Molecules -----	71
<b>III-E Quantum-State Manipulation of Molecular Motions -----</b>	<b>72</b>
III-E-1 Femtosecond Random-Phase Interferometry of Jet-Cooled Polyatomic Molecules -----	72
III-E-2 Wavepacket Observation of Methyl Internal Rotation in <i>o</i> -Fluorotoluene -----	72
III-E-3 Construction of an Experimental Apparatus for Nonadiabatic Quantum-State Manipulation of Molecular Motions -----	73
III-E-4 Development of High-Resolution Coherent Pulsed Laser -----	73
III-E-5 Laser Spectroscopy of the van der Waals Vibrations of Benzene-Water -----	74
<b>III-F Photophysics and Photochemistry of Aromatic Molecules in the Condensed Phase -----</b>	<b>75</b>
III-F-1 Excited-State Dynamics of 4-Thiothymidine with UVA Light Irradiation -----	75
III-F-2 Photochemical Reaction Dynamics of <i>o</i> -Quinones -----	75
III-F-3 Evidence of Phenoxymethyl Radical Formation in Laser Photolysis of Anisole in Solution -----	76
III-F-4 Production and Excited State Dynamics of the Photorearranged Isomer of Benzyl Chloride and Its Methyl Derivatives Studied by Stepwise Two-Color Laser Excitation Techniques -----	76
<b>III-G Spectroscopy and Excited State Dynamics of Jet-Cooled Aromatic Molecules -----</b>	<b>76</b>
III-G-1 Spectroscopy and Relaxation Dynamics of Photoexcited Anisole and Anisole- $\text{d}_3$ Molecules in a Supersonic Jet -----	77
III-G-2 Internal Rotational Motion of the Chloromethyl Group of the Jet-Cooled Benzyl Chloride Molecule -----	77
III-G-3 Molecular Structure and Excited State Dynamics of Jet-Cooled <i>o</i> -, <i>m</i> - and <i>p</i> -Fluoroanisole -----	77
III-G-4 Evidence for a Non-Planar Conformer and Conformational Isomerization of <i>o</i> -Fluoroanisole in a Low-Temperature Ar Matrix -----	77
III-G-5 Molecular Structure and Puckering Vibration of 1-Aminoindan in a Supersonic Jet -----	78
<b>III-H Photochemical Reactions in Microreactors -----</b>	<b>78</b>
III-H-1 Application of Microfabricated Reactors for Asymmetric Photoreaction -----	78
III-H-2 Photocatalytic Reaction in Microfabricated Reactors -----	78
<b>III-I In-Situ Observation of Surface Reactions by Variable Temperature Scanning Tunneling Microscopy -----</b>	<b>80</b>
III-I-1 In-Situ Observation of CO Oxidation on $\text{Ag}(110)(2\times 1)\text{-O}$ by Scanning Tunneling Microscopy: Structural Fluctuation and Catalytic Activity -----	80
III-I-2 Propagation of Reaction Front in the Disproportionate Reaction of $\text{H}_2\text{O}$ on $\text{Ag}(110)(5\times 1)\text{-O}$ Surface: Role of Hydrogen Bonding Interaction -----	80
<b>RESEARCH ACTIVITIES IV -----</b>	<b>81</b>

### Department of Molecular Assemblies

<b>IV-A Optical Study of Charge Ordering States in Organic Conductors -----</b>	<b>81</b>
IV-A-1 Examination of the Charge-Sensitive Vibrational Modes in ET Molecule -----	81
IV-A-2 Infrared and Raman Studies of $\theta\text{-(BEDT-TTF)}_2\text{CsZn(SCN)}_4$ : Comparison with the Frozen State of $\theta\text{-(BEDT-TTF)}_2\text{RbZn(SCN)}_4$ -----	81
IV-A-3 Robust Superconducting State in the Low-Quasiparticle-Density Organic Metals $\beta''\text{-(BEDT-TTF)}_4[(\text{H}_3\text{O})M(\text{C}_2\text{O}_4)_3]\cdot Y$ : Superconductivity due to Proximity to a Charge-Ordered State -----	82
IV-A-4 Influence of the Cooling Rate on Low-Temperature Raman and Infrared-Reflection Spectra of Partially Deuterated $\kappa\text{-(BEDT-TTF)}_2\text{Cu}[\text{N}(\text{CN})_2]\text{Br}$ -----	82
IV-A-5 Optical Second Harmonic Generation in a Charge-Ordered Organic Conductor $\alpha\text{-(BEDT-TTF)}_2\text{I}_3$ -----	83
IV-A-6 Correlation between Structural Instabilities and Raman Shift and Width in $\beta\text{-(ET)}_2\text{I}_3$ and $\kappa\text{-(ET)}_2\text{Cu}[\text{N}(\text{CN})_2]\text{I}$ -----	83
IV-A-7 Inhomogeneous Charge Distribution in $(\text{EDO-TTF})_2\text{X}$ ( $\text{X} = \text{ReO}_4$ and $\text{GaCl}_4$ ) -----	84
IV-A-8 Re-Examination of the Site Charge Difference in $\text{TEA}(\text{TCNQ})_2$ -----	84

IV-A-9 Spectroscopic Evidence for the Monovalent-to-Divalent Phase Transition of Biferrocenium (F <sub>1</sub> TCNQ) <sub>3</sub> .....	84
IV-A-10 Phase Separation in the Monovalent-to-Divalent Phase Transition of Biferrocenium-(F <sub>1</sub> TCNQ) <sub>3</sub> .....	85
<b>IV-B Magnetic Resonance Studies for Molecular-Based Conductors .....</b>	<b>86</b>
IV-B-1 Charge Disproportionation in (TMTTF) <sub>2</sub> SCN Observed by <sup>13</sup> C NMR .....	86
IV-B-2 Redistribution of Electronic Charges in the Spin-Peierls State in (TMTTF) <sub>2</sub> AsF <sub>6</sub> Observed by <sup>13</sup> C NMR .....	86
IV-B-3 Deuteration Effect and Possible Origin of the Charge-Ordering Transition of (TMTTF) <sub>2</sub> X .....	87
IV-B-4 Redistribution of Electronic Charge in (TMTTF) <sub>2</sub> ReO <sub>4</sub> : <sup>13</sup> C NMR Investigation .....	87
IV-B-5 Spin Structure of Organic Conductors (TMTTF) <sub>2</sub> X .....	87
IV-B-6 Multi-Frequency ESR Measurements for (TMTTF) <sub>2</sub> X .....	88
IV-B-7 Extremely Slow Charge Fluctuations in the Metallic State of the Two-Dimensional Molecular Conductor θ-(BEDT-TTF) <sub>2</sub> RbZn(SCN) <sub>4</sub> .....	88
IV-B-8 Sliding Spin-Density Wave of (TMTSF) <sub>2</sub> PF <sub>6</sub> Studied with Narrow-Band Noise .....	88
<b>IV-C Synchrotron X-Ray Diffraction Experiments and MEM Analyses for Single Crystals of Organic Conductors .....</b>	<b>88</b>
IV-C-1 Low-Temperature Charge-Ordering State of (TMTTF) <sub>2</sub> PF <sub>6</sub> .....	89
<b>IV-D EPR Study toward Molecular Biology as Microscopic and Selective Probes Measurements ----</b>	<b>89</b>
IV-D-1 First Detection of the Multiline Signal from the S <sub>2</sub> -State Manganese Cluster of Photosystem II by Single-Crystal W-Band EPR Spectroscopy .....	90
<b>IV-E Development of Multi-Functional Molecular Systems .....</b>	<b>91</b>
IV-E-1 Dielectric Properties of Porous Molecular Crystals Containing Polar Molecules .....	91
IV-E-2 Giant Dielectric Constants of Porous Molecular Crystal with Guest Water Cluster .....	91
IV-E-3 Synthesis and Characterization of a Porous Magnetic Diamond Framework Compound, Co <sub>3</sub> (HCOO) <sub>6</sub> , and Its N <sub>2</sub> Sorption Characteristic .....	92
IV-E-4 Superconductivity and Vortex Phases in the Two-Dimensional Organic Conductor λ-(BETS) <sub>2</sub> Fe <sub>x</sub> Ga <sub>1-x</sub> Cl <sub>4</sub> (x = 0.45) .....	92
IV-E-5 Constant Resistivity State in the Field-Induced Organic Superconductor, λ-(BETS) <sub>2</sub> Fe <sub>x</sub> Ga <sub>1-x</sub> Cl <sub>4</sub> .....	93
IV-E-6 (Tetrathiafulvalene)[Fe <sup>III</sup> (C <sub>2</sub> O <sub>4</sub> )Cl <sub>2</sub> ]: An Organic-Inorganic Hybrid Exhibiting Canted Antiferromagnetism .....	93
IV-E-7 Development of Single-Component Molecular Metals .....	94
IV-E-8 Crystal Structures and Physical Properties of Single-Component Molecular Conductors Consisting of Nickel and Gold Complexes with Bis(trifluoromethyl)tetrathiafulvalenedithiolate Ligands .....	94
IV-E-9 <i>Ab Initio</i> Electronic Structure Calculation of Single-Component Molecular Conductor Au(tmdt) <sub>2</sub> (Tmdt = Trimethylenetetrathiafulvalenedithiolate) .....	95
IV-E-10 The Light-Induced Excited Spin State Trapping Effect on Ni(dmit) <sub>2</sub> Salt with an Fe(III) Spin-Crossover Cation: [Fe(qsal) <sub>2</sub> ][Ni(dmit) <sub>2</sub> ·2CH <sub>3</sub> CN] .....	95
IV-E-11 Synergic Behavior between Spin and Conducting Property in Ni(dmit) <sub>2</sub> Salt with Fe(III) Spin-Crossover Cation .....	96
IV-E-12 Synthesis and Molecular Structure of a Novel PROXYL-Fused π-Electron Donor, PROXYL-ET-STF .....	96
<b>IV-F Electronic and Magnetic Properties of π-Electron-Based Molecular Systems .....</b>	<b>98</b>
IV-F-1 Metal-Insulator Transition in Iodinated Amorphous Conducting Carbon Films .....	98
IV-F-2 Magnetic Resonance Study of Nanodiamonds .....	98
IV-F-3 d-Electron-Induced Negative Magnetoresistance of π-d Interaction System Including Brominated-TTF Donor .....	98
IV-F-4 Electronic and Magnetic Properties of π-d Interaction System (EDTDM) <sub>2</sub> FeBr <sub>4</sub> .....	99
IV-F-5 Observation of Zigzag- and Armchair-Edges of Graphite .....	99
<b>IV-G Progress of Conjugated Phenomena Coupled with Spin and Photon for Assembled Hetero-Molecular System .....</b>	<b>100</b>
IV-G-1 Reversible Photomagnetism in a Cobalt Layered Compound Coupled with Photo-Chromic Diarylethene .....	100
<b>IV-H Molecular Crystals toward Nano-Devices by Use of d-π Interaction, Crystal Designing and Optical Doping .....</b>	<b>101</b>
IV-H-1 Light-Induced Transformation of Molecular Materials into Devices .....	101
IV-H-2 Molecular Conductors Containing Photoreactive Species .....	101
IV-H-3 A New Optical Doping Method toward Molecular Electronics .....	102
IV-H-4 Photochemical Method of Device Fabrication Starting from Molecular Crystals .....	102
IV-H-5 Photochemical Control of Dark Conductivity —A New Approach to Devices Based on Molecular Crystals .....	102
IV-H-6 Molecular Unit Based on Metal Phthalocyanine; Designed for Molecular Electronics .....	102

IV-H-7 Anisotropic Giant Magnetoresistance Originating from the $\pi$ -d Interaction in a Molecule	103
IV-H-8 Phthalocyanine-Pphthalocyanine Salt Crystal: A Unique Assembly Design	103
IV-H-9 Physical Properties of Electrically Conducting and Stable Molecular Neutral Radical Solid [Co(2,3-Nc)(CN) <sub>2</sub> ]CH <sub>3</sub> CN (2,3-Nc = 2,3-Naphthalocyanine)	103
IV-H-10 Charge Disproportionation and Anomalous Giant Magnetoresistance in a One-dimensional Conductor, TPP[Co(Pc)(CN) <sub>2</sub> ] <sub>2</sub>	104
IV-H-11 Structural, Electrical and Magnetic Properties of $\alpha$ -(ET) <sub>7</sub> [MnCl <sub>4</sub> ] <sub>2</sub> ·(1,1,2-C <sub>2</sub> H <sub>3</sub> Cl <sub>3</sub> ) <sub>2</sub> (ET = bis(ethylenedithio)tetrathiafulvalene)	104
IV-H-12 New Binuclear Copper Complexes [(9S3)Cu(CN)Cu(9S3)]X <sub>n</sub> (X = BF <sub>4</sub> , n = 1; X = TCNQ, n = 2) (9S3 = 1,4,7-trithiacyclononane): Syntheses, Crystal Structures and Magnetic Properties	104
IV-H-13 Crystal Design of Cation-Radical Salts Based on the Supramolecular Self-Organizing Arrangement of Mellitate Anions	105
IV-H-14 A Helical $\pi$ -Radical Cation Column in the Double Helix of Mellitate Anions	105
IV-H-15 Network Formation of Mellitate Anions ([C <sub>6</sub> (COO) <sub>6</sub> H <sub>6-n</sub> ] <sup>n-</sup> ) in the Salts with Piperidinium Derivatives and <i>o</i> -Phenylenediammonium	106
<b>IV-I Charge and Spin Dynamics of Organic Conductors</b>	<b>107</b>
IV-I-1 Electron Delocalization on $\kappa$ -(BEDT-TTF) <sub>2</sub> Cu <sub>2</sub> (CN) <sub>3</sub> under Pressure	107
IV-I-2 Coherent-Incoherent Crossover Behavior of Electron on $\kappa$ -(BEDT-TTF) <sub>2</sub> Ag(CN) <sub>2</sub> ·H <sub>2</sub> O	107
IV-I-3 Charge Ordering State on (BEDT-TTF) <sub>3</sub> Cl <sub>2</sub> ·2H <sub>2</sub> O	107

## RESEARCH ACTIVITIES V -----109

### Department of Applied Molecular Science

<b>V-A Molecular Design and Functions of Photoactive and Spin-Active Supramolecular Assemblies</b>	<b>109</b>
V-A-1 Molecular Design of Light-Harvesting Antennae	109
<b>V-B Bioinorganic Chemistry and Structural Biology of Heme Proteins</b>	<b>110</b>
V-B-1 Proton Transfer at Helium Temperatures during Dioxygen Activation by Heme Monooxygenases	110
V-B-2 Roles of Distal Asp in Heme Oxygenase from <i>Corynebacterium diphtheriae</i> , HmuO: A Water-Driven Oxygen Activation Mechanism	110
V-B-3 O <sub>2</sub> - and H <sub>2</sub> O <sub>2</sub> -Dependent Verdoheme Degradation by Heme Oxygenase: Reaction Mechanisms and Potential Physiological Roles of the Dual Pathway Degradation	110
<b>V-C Pro-Oxidants-Induced Iron Release from the Fe-S Cluster of Mitochondrial Aconitase and Its Prevention by Flataxin</b>	<b>111</b>
V-C-1 Reversible Redox-Dependent Modulation of Mitochondrial Aconitase and Proteolytic Activity during <i>In Vivo</i> Cardiac Ischemia/Reperfusion	111
<b>V-D Quantum Emissions from Solid in Femtosecond Intense Laser Field and Its Application to Dynamic Imaging</b>	<b>112</b>
V-D-1 Picosecond Time-Resolved X-Ray Diffraction from a Laser-Shocked Germanium Crystal over Hugoniot Elastic Limit	112
V-D-2 Enhanced Generation of Fast Protons from a Polymer-Coated Metal Foil by a Femtosecond Intense Laser Field	112
V-D-3 Electron Imaging of Charge Separated Field on a Copper Film Induced by Femtosecond Laser Irradiation	112

## RESEARCH ACTIVITIES VI -----113

### Department of Vacuum UV Photochemistry

<b>VI-A Electronic Structure and Decay Mechanism of Inner-Shell Excited Molecules</b>	<b>113</b>
VI-A-1 Development of a Transmission-Grating Spectrometer for Soft-X-Ray Emission Studies	113
VI-A-2 Application of R Matrix/MQDT Method to both Valence and Core Excitations in NO	113
<b>VI-B Soft X-Ray Photoelectron-Photoabsorption Spectroscopy and Electronic Structure of Molecular Solids and Clusters</b>	<b>114</b>
VI-B-1 Photoionization of Small Krypton Clusters in the Kr 3d Regime: Evidence for Site-Specific Photoemission	114
VI-B-2 Core Excitation in O <sub>3</sub> Localized to One of Two Symmetry-Equivalent Chemical Bonds—Molecular Alignment through Vibronic Coupling	114
<b>VI-C Ultrafast Dynamics of Molecules in Intense Laser Fields</b>	<b>115</b>
VI-C-1 Probing the Ultrafast Nuclear Motion in CS <sub>2</sub> <sup>2+</sup> in Intense Laser Fields	115
VI-C-2 Concerted and Sequential Coulomb Explosion Processes of N <sub>2</sub> O in Intense Laser Fields by Coincidence Momentum Imaging	115

VI-C-3 Development of an Intense Sub-10fs Laser Source with a Hollow Fiber/Chirped Mirror Compressor .....	115
<b>VI-D Synchrotron Radiation Stimulated Surface Reaction and Nanoscience .....</b>	<b>117</b>
VI-D-1 Synchrotron Radiation Induced Si-H Dissociation on H-Si(111)-1×1 Surfaces Studied by In-Situ Monitoring in the Undulator-STM System .....	117
VI-D-2 Giant Vesicle Fusion on the Microelectrodes Fabricated by Femto-Second Laser Ablation Followed by Synchrotron Radiation Etching .....	117
<b>VI-E Noble Semiconductor Surface Vibration Spectroscopy .....</b>	<b>118</b>
VI-E-1 Orientation of Avidin Molecules Immobilized on the COOH-Modified SiO <sub>2</sub> /Si(100) Surface .....	118
VI-E-2 Hydrogen-Atom-Induced Oxidation Reaction on Water-Terminated Si Surface, 2H+H <sub>2</sub> O/Si(100)-(2×1): A Theoretical Study .....	118
<b>VI-F Integration and Characterization of Bio-Functional Materials on Silicon Surfaces .....</b>	<b>119</b>
VI-F-1 Fabrication of Avidin Single Molecular Layer on Silicon Oxide Surfaces and Formation of Tethered Lipid Bilayer Membranes .....	119
VI-F-2 Deposition of Lipid Bilayers on OH-Density-Controlled Silicon Dioxide Surfaces .....	119
VI-F-3 Supported Lipid Bilayer Formation by the Vesicle Fusion Induced by the Vesicle-Surface Electrostatic Attractive Interaction .....	120
VI-F-4 The Current Noise Characteristic of a Single Ion Channel .....	120
VI-F-5 A New Type of Fluorescence Recovery After Photobleaching Apparatus Using both Illumination Arrangements of UV Lamp and 560 nm Laser .....	121
<b>VI-G Photoionization and Photodissociation Dynamics Studied by Electron and Fluorescence Spectroscopy .....</b>	<b>122</b>
VI-G-1 Photofragmentation Mechanisms of H <sub>2</sub> O Studied by Ultraviolet Dispersed Spectroscopy .....	122
<b>VI-H Extreme UV Photoionization Studies of Fullerenes by Using a Grazing-Incidence Monochromator and High-Temperature Mass Spectrometer .....</b>	<b>122</b>
VI-H-1 Absolute Photoabsorption Cross Section of C <sub>60</sub> in the Extreme Ultraviolet .....	123
VI-H-2 Photofragmentation of C <sub>60</sub> in Valence Ionization .....	123
VI-H-3 Photofragmentation of C <sub>60</sub> in the Extreme Ultraviolet: Statistical Analysis on the Appearance Energies of C <sub>60-2n</sub> <sup>z+</sup> (n ≥ 1, z = 1-3) .....	124
VI-H-4 Fragmentation Mechanism of Highly Excited C <sub>70</sub> Cations in the Extreme Ultraviolet .....	124
VI-H-5 4d → 4f Dipole Resonance of the Metal Atom Encapsulated in a Fullerene Cage: Ce@C <sub>82</sub> .....	124
VI-H-6 Photoion Yield Curves of Dy@C <sub>82</sub> in the Vacuum UV Region .....	125
VI-H-7 4d-4f Dipole Resonance of the Pr Atom in an Endohedral Metallofullerene, Pr@C <sub>82</sub> .....	125
<b>VI-I Kinetic Energy Analysis of the Fragment Ions Produced from Fullerenes .....</b>	<b>126</b>
VI-I-1 Development of the Photofragment Imaging Apparatus to Measure Scattering Distributions of the C <sub>60-2n</sub> <sup>z+</sup> and C <sub>70-2n</sub> <sup>z+</sup> Fragments Produced by Dissociative Photoionization of C <sub>60</sub> and C <sub>70</sub> .....	126

## **RESEARCH ACTIVITIES VII .....**

### **Department of Computational Molecular Science**

<b>VII-A Computer Simulation of Quantum Systems in Condensed Phase .....</b>	<b>129</b>
VII-A-1 A Study of Molecular Vibrational Relaxation Mechanism in Condensed Phase Based upon Mixed Quantum-Classical Molecular Dynamics: I. A Test of IBC Model for the Relaxation of a Nonpolar Solute in Nonpolar Solvent at High Density .....	129
VII-A-2 A Study of Molecular Vibrational Relaxation Mechanism in Condensed Phase Based upon Mixed Quantum-Classical Molecular Dynamics: II. Non-Collisional Mechanism for the Relaxation of a Polar Solute in Supercritical Water .....	129
<b>VII-B Molecular Dynamics Study of Classical Complex Systems .....</b>	<b>130</b>
VII-B-1 A Large-Scale Molecular Dynamics Study of Dynamic Structure Factor and Dispersion Relation of Acoustic Mode in Liquid and Supercritical Water .....	130
<b>VII-C Development of Simulation Algorithms for Quantum Many-Body Systems .....</b>	<b>130</b>
VII-C-1 Quantum Rotation of Carbonyl Sulfide Molecules in Superfluid Helium Clusters: A Path Integral Hybrid Monte Carlo Study .....	130
<b>VII-D Theory of Sum Frequency Generation Spectroscopy .....</b>	<b>131</b>
VII-D-1 Improved Computation of Sum Frequency Generation Spectrum of Water Surface .....	131
<b>VII-E Theory of Mass Transfer Kinetics at Liquid-Vapor Interfaces .....</b>	<b>131</b>
VII-E-1 Mass Accommodation Coefficient of Water .....	131
<b>VII-F Theoretical Studies on Electronic Structure and Dynamics of Electronically Excited States .....</b>	<b>132</b>
VII-F-1 Encapsulation of Hydrogen Atoms by Fullerenes and Carbon Nanotubes with the Use of Nonadiabatic Transition .....	132
VII-F-2 Ab Initio Calculated Structures of Conformers for 1,3-Dimethoxy-p-tert-Butylcalix[4] Crown-5-Ether Complexed with Potassium Cation .....	132

VII-F-3 Theoretical Transition Probabilities for the $\tilde{A}^2A_1-\tilde{X}^2B_1$ System of $H_2O^+$ and $D_2O^+$ and Related Franck-Condon Factors Based on Global Potential Energy Surfaces	-----132
VII-F-4 Analysis of the Ultraviolet Absorption Cross Sections of Six Isotopically Substituted Nitrous Oxide Specie Using 3D Wavepacket Propagation	-----132
VII-F-5 Theoretical Study of the Oxidation Reaction for the H Atom-Induced Water-Terminated Si Surface $2H+H_2O/Si(100)-(2\times 1)$	-----133

## RESEARCH ACTIVITIES VIII -----135

### Coordination Chemistry Laboratories

<b>VIII-A Reduction of CO<sub>2</sub> and Oxidation of Organic Molecules Aiming at Energy Conversion between Chemical Energy and Electricity</b>	<b>-----135</b>
VIII-A-1 Redox Behavior of New Ru-Dioxolene-Ammine Complexes and Catalytic Activity toward Electrochemical Oxidation of Alcohol under Mild Conditions	-----135
VIII-A-2 Equilibrium of Low- and High-Spin States of Ni(II) Complexes Controlled by the Donor Ability of the Bidentate Ligands	-----135
VIII-A-3 A Platinum-Ruthenium Dinuclear Complex Bridged by Bis(terpyridyl)xanthene	-----136
VIII-A-4 Immobilization of a High-Valent Rhenium Complex on an Indium-Doped Tin-Oxide Electrode: Enhanced Catalytic Activity of a <i>trans</i> -Dioxorhenium(V) Complex in Electrochemical Oxidation of Alcohols	-----136
VIII-A-5 Synthesis, Chemical- and Electrochemical Properties of Ruthenium(II) Complexes Bearing 2,6-Bis(2-naphthyridyl)pyridine	-----136
VIII-A-6 Synthesis, Structures and Electrochemical Properties of Ruthenium (II) Complexes Bearing Bidentate 1,8-Naphthyridine and Terpyridine Analogous (N,N,C)-Tridentate Ligands	-----136
VIII-A-7 Synthesis and Electrochemical Properties of Bis(bipyridine)ruthenium(II) Complexes Bearing Pyridinyl- and Pyridinylidene Ligands Induced by Cyclometalation of N'-Methylated Bipyridinium Analogs	-----137
VIII-A-8 Electronic Structural Changes Between Nickel(II)-Semiquinonato and Nickel(III)-Catecholato states Driven by Chemical and Physical Perturbation	-----137
VIII-A-9 Synthesis and Crystal Structures of $[W(3,6\text{-Dichloro-1,2-Benzenedithiolate})_3]^{n-}$ ( $n = 1, 2$ ) and $[Mo(3,6\text{-Dichloro-1,2-Benzenedithiolate})_3]^{2-}$ : Dependence of the Coordination Geometry on the Oxidation Number and Counter-Cation in Trigonal-Prismatic and Octahedral Structures	-----137
VIII-A-10 Dioxo-Molybdenum(VI) and Mono-oxo-Molybdenum(IV) Complexes Supported by New Aliphatic Dithiolene Ligands: New Models with Weakened Mo=O Bond Characters for the Arsenite Oxidase Active Site	-----137
VIII-A-11 Electrochemical Hydrogenation of $[Ru(bpy)_2(napy-kN)(CO)]^{2+}$ : Inhibition of Reductive Ru-CO Bond Cleavage by a Ruthenacycle	-----138
VIII-A-12 Stabilization and Destabilization of the Ru-CO Bond During the 2,2'-Bipyridin-6-onato (bpyO)-Localized Redox Reaction of $[Ru(terpy)(bpyO)(CO)](PF_6)$	-----138
<b>VIII-B Coordination Chemistry of Sterically Hindered Ligands and Multidentate Ligands, and Activation of Small Molecules</b>	<b>-----139</b>
VIII-B-1 Synthesis of a Vanadium(III) Tris(arylthiolato) Complex and Its Reactions with Azide and Azo Compounds; Formation of a Sulfenamide Complex <i>via</i> Cleavage of an Azo N=N Bond	-----139
VIII-B-2 Titanium and Zirconium Complexes of Preorganized Tripodal Triaryloxo Ligands	----139
<b>VIII-C Preparation and Properties of the Homo- and Heterometallic Clusters</b>	<b>-----141</b>
VIII-C-1 A Dinuclear Ru(II) $\kappa^2$ -Diamido/ $\eta^6$ -Naphthalene Complex Featuring a Coordinatively Unsaturated Yet Highly p-Basic ( $\eta^5$ -C <sub>5</sub> Me <sub>5</sub> )Ru Diamide Fragment	-----141
VIII-C-2 Dinuclear Ruthenium(II) Catecholato and 2,3-Naphthalenediolato Complexes Featuring $\kappa^2$ -Diaryloxo/ $\eta^6$ -Arene Coordination Mode	-----141
<b>VIII-D Modification of Myoglobin by Replacing the Native Heme with Metalloporphyrinoids</b>	<b>-----143</b>
VIII-D-1 Ligand Binding Properties of Myoglobin Reconstituted with Iron Porphycene: Unusual O <sub>2</sub> Binding Selectivity against CO Binding	-----143
VIII-D-2 Unusual Ligand Discrimination by a Myoglobin Reconstituted with a Hydrophobic Domain-Linked Heme	-----143
VIII-D-3 Enhancement of Peroxidase Activity of Myoglobin Reconstituted with Iron Porphycene: Compound III Formation due to the Reaction of Ferric Myoglobin with Hydrogen Peroxide	---143
VIII-D-4 Preparation and O <sub>2</sub> Binding Study of Myoglobin Having a Cobalt Porphycene	-----144

<b>VIII-E Synthesis of Transition Metal Complexes Containing a Novel Metal-Silicon and Metal-Gallium Bonding</b> .....	<b>145</b>
VIII-E-1 Synthesis of a Cofacial Schiff-Base Dimanganese(III) Complex for Asymmetric Catalytic Oxidation of Sulfides .....	145
VIII-E-2 Synthesis and Structure of a Base-Stabilized Silyl(silylene)tantalum Complex .....	145
VIII-E-3 Synthesis and Structures of the First Titanium(IV) Complexes with Cyclic Tetrasiloxide Ligands: Incomplete and Complete Cage Titanosiloxanes .....	145
<b>VIII-F Syntheses, Structures, and Reactivities of Multinuclear Transition Metal Complexes with O- and N-Donor Ligands</b> .....	<b>147</b>
VIII-F-1 A Cyanamido-Bridged Diiridium Complex: A Reactive Building Block for Polynuclear Cyanamido Complexes .....	147
VIII-F-2 Synthesis, Structures, and Solution Behavior of Di- and Trinuclear Titanium(IV)-Cyclophosphato Complexes .....	147
<b>VIII-G Organometallic Chemistry: Synthesis, Characterization, and Catalysts</b> .....	<b>148</b>
VIII-G-1 Living Polymerization of 1-Hexene Catalyzed by Half-Metallocene Dimethyl Complexes of Hafnium with Bidentate N-Substituted Iminomethylpyrrolyl Ligands .....	148
VIII-G-2 Unique Preferential Conformation and Movement of Ru(acac) <sub>2</sub> Fragment(s) Coordinated in an η <sup>4</sup> -s-trans Fashion to All Diene Unit(s) of α,ω-Diphenylpolyenes .....	148
VIII-G-3 A Topological Isomer of Ferrocene: Theoretical Approach for Transition Metal Complexes with Conjugated All Trans Cyclodecapentaene .....	148
<b>VIII-H Development of Metal-Conjugated Multi-Electron Redox Systems in Metal-Dioxolene Complexes and Activation of Water Ligand</b> .....	<b>150</b>
VIII-H-1 Synthesis of a Ru-OH <sub>2</sub> Complex Bearing a Ferrocene-Attached Catecholato Ligand and Its Spontaneous Proton Release .....	150
<b>RESEARCH ACTIVITIES IX</b> .....	<b>151</b>
<b>Research Center for Molecular-Scale Nanoscience</b>	
<b>IX-A Nano-Science and Nano-Technology toward Molecular Scale Electronics</b> .....	<b>151</b>
IX-A-1 Photo Precursor for Pentacene .....	151
IX-A-2 Synthesis and Self-Assembly of Novel Porphyrin Molecular Wires .....	151
IX-A-3 Molecular Junctions Composed of Oligothiophene Dithiol Bridged Gold Nanoparticles Exhibiting Photoresponsive Properties .....	152
IX-A-4 Simple Preparation Method for Supramolecular Porphyrin Arrays on Mica Using Air/Water Interface .....	152
IX-A-5 Novel Photochemical Synthesis of Pentacene and Its Derivatives .....	152
IX-A-6 Porphyrin Molecules Working as Nanodevice on Single-Walled Carbon Nanotube Wiring .....	153
IX-A-7 Electronic Properties of Single-Walled Carbon Nanotube/Porphyrin Polymer Complex Measured by Point-Contact Current Imaging Atomic Force Microscopy .....	153
IX-A-8 Preparation of Very Reactive Thiol-Protected Gold Nanoparticles: Revisiting the Brust-Schiffrin Method .....	153
<b>IX-B Development of Organic Semiconductors for Molecular Thin-Film Devices</b> .....	<b>155</b>
IX-B-1 Organic Thin-Film Transistors with High Electron Mobility Based on Perfluoropentacene .....	155
IX-B-2 Organic Light-Emitting Diodes Using Multifunctional Phosphorescent with Iridium-Complex Core and Charge-Transporting Dendrons .....	155
<b>IX-C Field-Effect Transistors with Organic Semiconductors</b> .....	<b>156</b>
IX-C-1 Preparation of Organic Light-Emitting Field-Effect Transistors with Asymmetric Electrodes .....	156
IX-C-2 Field-Effect Transistors Based on Single-Crystalline Wires of Bis-(1, 2, 5-Thiadiazolo)-p-Quinobis(1, 3-Dithiole) .....	156
<b>IX-D Molecular Assemblies on Silicon Surfaces via Silicon-Carbon Covalent Bonds</b> .....	<b>157</b>
IX-D-1 Characterization of Molecular Assemblies on Silicon Surfaces by Attenuated Total Reflectance Infrared Spectroscopy .....	157
<b>IX-E Low Temperature Scanning Tunneling Microscopy and Spectroscopy of Organic Molecules on Metal Surfaces</b> .....	<b>157</b>
IX-E-1 Scanning Tunneling Microscopy and Spectroscopy of Phthalocyanine Molecules on Metal Surfaces .....	157
<b>IX-F Ratchet Motions of a Droplet Caused by Electrochemical Reaction of Monolayers</b> .....	<b>158</b>
IX-F-1 Electrochemically Generated Wetting Gradient and Its Application for the Transport of Droplets .....	158
IX-F-2 Transport of a Droplet by Directional Deformations with Asymmetric Electrode .....	159

<b>IX-G Development of Multi-Function Integrated Macromolecules and Their Organization on Substrate Surfaces for Planar Molecular-Scale Electronics Circuits</b>	<b>160</b>
IX-G-1 Step-Wised Synthesis of Multifunctional Molecular Wires for Planar Metal-Molecule-Metal Junctions	160
<b>IX-H Heterogeneous Aquacatalysis</b>	<b>161</b>
IX-H-1 PS-PEG Resin-Supported Palladium-MOP Complexes. Application in Asymmetric $\pi$ -Allylic Reduction	161
IX-H-2 Hydrogenation and Dehalogenation under Aqueous Conditions with an Amphiphilic Polymer-Supported Nanopalladium Catalyst	161
IX-H-3 Cycloisomerization of 1,6-Enynes: Asymmetric Multi-Step Preparation of a Hydrindane Framework in Water with Polymeric Catalysts	161
IX-H-4 Controlled Monoarylation of Dibromoarenes in Water with a Polymeric Palladium Catalyst	161
<b>IX-I Development of New Nanomaterials as Components in Advanced Molecular Systems</b>	<b>162</b>
IX-I-1 Gold Nanoparticles Stabilized by Tripod Thioether Oligomers: Synthesis and Molecular Dynamics Studies	162
<b>IX-J Designing Artificial Photosynthesis at Molecular Dimensions</b>	<b>162</b>
IX-J-1 Electrochemical Properties of Ferrocene-Dendrimer-Porphyrins	163
<b>IX-K Development of New Metal Complexes as Redox Catalysts</b>	<b>163</b>
IX-K-1 Synthesis, Structure and Electrochemistry of New Cobalt Complexes with Cyclopentadienyl and Bidentate Ligands	164
<b>IX-L Photochemistry on Well-Defined Surfaces</b>	<b>165</b>
IX-L-1 Photochemistry of Cyclohexane on Cu(111)	165
<b>IX-M Ultrafast Dynamics at Well-Defined Surfaces</b>	<b>165</b>
IX-M-1 Femtosecond Wavepacket Dynamics of Cs Adsorbates on Pt(111): Coverage and Temperature Dependences	165
IX-M-2 Mode Selective Excitation of Coherent Surface Phonons on Alkali-Covered Metal Surfaces	166
IX-M-3 Excitation Mechanism of Coherent Surface Phonons on Alkali-Metal Covered Surfaces	166
<b>IX-N Multiphoton Photoelectron Spectroscopy of Electronic States of Nano-Structured Materials on Surfaces</b>	<b>166</b>
IX-N-1 The Electronic Structure and Femtosecond Electron Transfer Dynamics at Noble Metal/tris-(8-hydroxyquinoline) Aluminum Interfaces	166
<b>IX-O Chemistry of One-Dimensional Nano-Surface Compounds Studied by Scanning Tunneling Microscopy</b>	<b>167</b>
IX-O-1 In-Situ Observation of CO Oxidation on Ag(110)(2 $\times$ 1)-O by Scanning Tunneling Microscopy: Structural Fluctuation and Catalytic Activity	167
<b>IX-P Structures, Stabilities and Physicochemical Properties of Organometallic Hybrid Clusters</b>	<b>168</b>
IX-P-1 Glutathione-Protected Gold Clusters Revisited: Bridging the Gap between Gold(I)-Thiolate Complexes and Thiolate-Protected Gold Nanocrystals	168
IX-P-2 Large-Scale Synthesis of Thiolated Au <sub>25</sub> Clusters <i>via</i> Ligand Exchange Reactions of Phosphine-Stabilized Au <sub>11</sub> Clusters	168
IX-P-3 Subnanometer-Sized Gold Clusters with Dual Molecular Receptors: Synthesis and Assembly in One-Dimensional Arrangements	169
IX-P-4 Size-Specific Catalytic Activity of Polymer-Stabilized Gold Nanoclusters for Aerobic Alcohol Oxidation in Water	169
IX-P-5 Fabrication of Two dimensional Arrays of Size-Selected Gold Clusters	169
<b>IX-Q Structural Analyses of Biological Macromolecules by Ultra-High Field NMR Spectroscopy</b>	<b>170</b>
IX-Q-1 Ultra-High Field NMR Study of Carbohydrate-Protein Interactions	170
IX-Q-2 Ultra-High Field NMR Study of Glycoproteins	170
<b>IX-R Electronic Structure and Collision Dynamics of Atoms and Molecules Studied by Electron Impact at Large Momentum Transfer</b>	<b>172</b>
IX-R-1 Development and Use of a Multichannel ( <i>e</i> ,2 <i>e</i> ) Spectrometer for Electron Momentum Densities of Molecules	172
IX-R-2 Observation of Molecular Frame ( <i>e</i> ,2 <i>e</i> ) Cross Section Using an Electron-Electron-Fragment Ion Triple Coincidence Apparatus	172
IX-R-3 ( <i>e</i> ,3 <i>e</i> ) Collisions on Mg in the Impulsive Regime Studied by Second Born Approximation	172
IX-R-4 Electron Momentum Spectroscopy of Valence Satellites of Neon	172
IX-R-5 Theoretical Fine Spectroscopy with Symmetry-Adapted-Cluster Configuration-Interaction Method: Outer- and Inner-Valence Ionization Spectra of Furan, Pyrrole, and Thiophene	173
IX-R-6 Observation of a Molecular Frame ( <i>e</i> ,2 <i>e</i> ) Cross Section: An ( <i>e</i> ,2 <i>e</i> +M) Triple Coincidence Study on H <sub>2</sub>	173
IX-R-7 ( <i>e</i> ,2 <i>e</i> ) and ( <i>e</i> ,3-1 <i>e</i> ) Studies on Double Processes of He at Large Momentum Transfer	173

IX-R-8	Electron Momentum Spectroscopy of the HOMO of Acetone	173
IX-R-9	$(e,3-1e)$ Reactions at Large Momentum Transfer: The Plane-Wave Second Born Approximation	174
IX-R-10	Binary $(e,2e)$ Study on Xe: Momentum Profile for the 4d Orbital Revisited	174
IX-R-11	Binary $(e,2e)$ Study on Inner Shell Orbitals of Ar and Xe	174
IX-R-12	Construction of a New $(e,2e+M)$ Apparatus for Complete Imaging of Molecular Orbitals	174
<b>IX-S</b>	<b>Electronic Structure and Collision Dynamics of Atoms and Molecules</b>	
	<b>Studied by Photon Impact</b>	<b>174</b>
IX-S-1	Inner-Shell Photoelectron Angular Distributions from Fixed-in-Space OCS Molecules	175
IX-S-2	Coincidence Velocity Imaging Apparatus for the Study of Angular Correlations between Photoelectrons and Photofragments	175
IX-S-3	Non-Dipole Effects in the Angular Distribution of Photoelectrons from the K-Shell of $N_2$ Molecule	175
IX-S-4	Direct Observation of a Symmetry Lowering in Core-Electron Ionization for Highly Symmetric Molecules	175
<b>IX-T</b>	<b>Study of Electronic Structure of Organic Thin Film and Organic/Inorganic Interface</b>	<b>176</b>
IX-T-1	Deep Insight into a Valence Hole in Organic Semiconductors: High-Resolution Ultraviolet Photoemission Study	176
IX-T-2	UPS Fine Structures of Highest Occupied Band in Vanadyl-Phthalocyanine Ultrathin Film	176
IX-T-3	Fine Structure of the Highest Occupied Band in OTi-Phthalocyanine Monolayer	176
IX-T-4	Hole/Vibration Coupling of the Highest Occupied Band in Pentacene Thin Film	176
IX-T-5	Quantitative Analysis of Photoelectron Angular Distribution of a Single Domain Organic Monolayer Film: NTCDA on GeS(001)	177
IX-T-6	UPS Study of VUV-Photodegradation of Polytetrafluoroethylene (PTFE) Ultrathin Film by Using Synchrotron Radiation	177
IX-T-7	Site-Specific Ion Desorption of Fluorinated Phthalocyanine Studied with Electron-Ion Coincidence Spectroscopy	177
IX-T-8	Polarized Near-Edge X-Ray-Absorption Fine Structure Spectroscopy of $C_{60}$ -Functionalized 11-Amino-1-Undecane Thiol Self-Assembled Monolayer: Molecular Orientation and Evidence for $C_{60}$ Aggregation	177
<b>UVSOR Facility</b>		
<b>IX-U</b>	<b>Development of the UVSOR Light Source</b>	<b>179</b>
IX-U-1	Successful Commissioning of New RF Cavity	179
IX-U-2	Ion Trapping Phenomena at UVSOR-II	179
<b>IX-V</b>	<b>Researches by the Use of UVSOR</b>	<b>179</b>
IX-V-1	Development of Velocity Imaging Spectrometer for Observing Negative Fragment Ions	179
IX-V-2	Dynamics of Double Photoionization near the Ar 2p Threshold Investigated by Threshold Electron-Auger Electron Coincidence Spectroscopy	179
IX-V-3	Origin of Threshold Electrons Produced in Decay of the Xe $4d^{-1}np$ Resonance	180
IX-V-4	Coincidence Auger Spectroscopy	180
IX-V-5	Collision Dynamics of the $Kr^{8+} + N_2$ System Studied by a Multi-Coincidence Technique	180
IX-V-6	Collision Dynamics of MCI-Molecule Systems Studied by Multi-Coincidence Technique	180
IX-V-7	Optical Investigations of the Clathrate $\alpha-Eu_8Ga_{16}Ge_{30}$	180
IX-V-8	Influence of Cage Distortions on the Electronic Structure and Optical Properties of $Ba_6Ge_{25}$	181
IX-V-9	Indirect and Direct Energy Gaps in Kondo Semiconductor $YbB_{12}$	181
IX-V-10	Kondo Ground States and Non-Fermi-Liquid Behavior in $CeNi_{1-x}Co_xGe_2$	181
IX-V-11	Infrared Spectroscopy under Multiextreme Conditions: Direct Observation of Pseudogap Formation and Collapse in CeSb	181
IX-V-12	Infrared Study on CeSb under High Pressures	182
IX-V-13	Electronic Structure of Bulk Metallic Glass $Zr_{55}Al_{10}Cu_{30}Ni_5$	182
IX-V-14	Carrier-Induced Infrared Magnetic Circular Dichroism in the Magnetoresistive Pyrochlore $Tl_2Mn_2O_7$	182
IX-V-15	Magnetic Ordering in Frustrated $Ce_5Ni_2Si_3$	182
IX-V-16	Features of Fluorescence Spectra of Polyethylene Terephthalate Films	182
IX-V-17	Anomalous Magnetic Properties and Non-Fermi-Liquid Behavior in Single Crystals of the Kondo Lattice $CeNiGe_{2-x}Si_x$	183
IX-V-18	Sub-Natural Linewidth Auger Electron Spectroscopy of the 2s Hole Decay in HCl	183

## Laser Research Center for Molecular Science

<b>IX-W Developments and Researches of New Laser Materials</b> .....	<b>184</b>
IX-W-1 Growth and Scintillation Properties of Yb Doped Aluminate, Vanadate and Silicate Single Crystals .....	184
IX-W-2 Onset Detection of Solid-State Phase Transition in Estrogen-Like Chemical <i>via</i> Terahertz Transmission Spectroscopy .....	184
IX-W-3 Design Principle of Wide-Gap Fluoride Hetero-Structures for Deep Ultraviolet Optical Devices .....	184
IX-W-4 Terahertz Time-Domain Spectroscopy of Amino Acids and Polypeptides .....	184
<b>IX-X Development and Research of Advanced Tunable Solid State Lasers</b> .....	<b>186</b>
IX-X-1 Spectroscopic Properties of Yb:GdVO <sub>4</sub> Single Crystal: Stark Levels, Selection Rules, and Polarized Cross Sections .....	186
IX-X-2 Spectroscopic Properties of All-Ceramic Composite with Layer-by-Layer of Nd:Y <sub>3</sub> Al <sub>5</sub> O <sub>12</sub> and Nd:Y <sub>3</sub> ScAl <sub>4</sub> O <sub>12</sub> .....	186
IX-X-3 Hybrid Process for Measurement of Spectroscopic Properties of Nd:GdVO <sub>4</sub> .....	187
IX-X-4 Absorption, Emission Spectrum Properties and Efficient Laser Performances of Yb:Y <sub>3</sub> ScAl <sub>4</sub> O <sub>12</sub> Ceramics .....	187
IX-X-5 Passive Mode Locking of a Mixed Garnet Yb:Y <sub>3</sub> ScAl <sub>4</sub> O <sub>12</sub> Ceramic Laser .....	187
IX-X-6 High-Power Operation of Diode Edge-Pumped, Glue-Bonded, Composite Yb:Y <sub>3</sub> Al <sub>5</sub> O <sub>12</sub> Microchip Laser with Ceramic, Undoped YAG Pump Light-Guide .....	187
IX-X-7 Continuous-Wave Deep Blue Generation in a Periodically Poled MgO:LiNbO <sub>3</sub> Crystal by Single-Pass Frequency Doubling of a 912-nm Nd:GdVO <sub>4</sub> Laser .....	188
IX-X-8 Continuous-Wave Ultraviolet Generation at 354-nm in a Periodically Poled MgO:LiNbO <sub>3</sub> by Frequency Tripling of a Diode End-Pumped Nd:GdVO <sub>4</sub> Microlaser .....	188
IX-X-9 High-Power Continuous-Wave Intracavity Frequency-Doubled Nd:GdVO <sub>4</sub> -LBO Laser under Diode Pumping into the Emitting Level .....	188
IX-X-10 Deep Blue Generation at 456 nm in a Periodically Poled MgO:LiNbO <sub>3</sub> Ridge-Type Waveguide by Single-Pass Frequency Doubling of a Nd:GdVO <sub>4</sub> Micro-Laser .....	188
IX-X-11 Efficient 1.06 and 1.34- $\mu$ m Laser Emission of Highly-Doped Nd:YAG under 885-nm Diode Pumping into the Emitting Level .....	188
IX-X-12 High-Power Multi-Pass Pumped Microchip Nd:GdVO <sub>4</sub> Laser .....	189
IX-X-13 Highly Efficient New Pumping Configuration for Microchip Solid State Laser .....	189
IX-X-14 High Energy Quasi-Phase-Matched Optical Parametric Oscillation in a 3-mm-Thick Periodically Poled MgO:LiNbO <sub>3</sub> Device .....	189

## Equipment Development Center

<b>IX-Y Development of New Instruments and Experimental Devices</b> .....	<b>190</b>
IX-Y-1 Development of a High-Precision Slit Blade for the Transmission-Grating Spectrometer .....	190
IX-Y-2 Manufacture of Glass Microreactor Chips .....	191
IX-Y-3 Micro Processing by a Femto-Second Laser .....	191
IX-Y-4 Development of Electrical Control System of Fluorescence Recovery after Photobleaching Apparatus Using Semiconductor Laser for Illumination .....	192

## Safety Office

<b>IX-Z Development of Novel Heterocyclic Compounds and Their Molecular Assemblies for Advanced Materials</b> .....	<b>193</b>
IX-Z-1 Molecular Arrangement in the Cocrystals of 1,1',3,3'-Tetramethyl-2,2'-bi-1 <i>H</i> -imidazolium Bis(tetraphenylborate) with Ketone, Aldehyde, and Nitrile as Guest Molecules .....	193
IX-Z-2 Macrocyclic and Acyclic Bis(2,5-diphenyl-1,3,4-oxadiazole)s with Electron-Transporting and Hole-Blocking Ability in Organic Electroluminescent Devices .....	193
IX-Z-3 Synthesis, Characterization and FET Properties of Novel Dithazolybenzothiadiazole Derivatives .....	193

## RESEARCH ACTIVITIES X

### Okazaki Institute for Integrative Bioscience

<b>X-A Single-Molecule Physiology</b> .....	<b>195</b>
X-A-1 One Rotary Mechanism for F <sub>1</sub> -ATPase over ATP Concentrations from Millimolar down to Nanomolar .....	195
X-A-2 ATP-Driven Stepwise Rotation of F <sub>0</sub> F <sub>1</sub> -ATP Synthase .....	195
X-A-3 Activation of Pausing F <sub>1</sub> Motor by External Force .....	195

<b>X-B Bioinorganic Chemistry of Heme-Based Sensor Proteins</b> .....	<b>197</b>
X-B-1 Spectroscopic and Redox Properties of a CooA Homologue from <i>Carboxydotherrnus hydrogenoformans</i> .....	197
X-B-2 Oxygen Sensing Mechanism of HemAT from <i>B. subtilis</i> : A Resonance Raman Spectroscopic Study .....	197
X-B-3 Structure and Function of a Novel Redox Sensor DcrA Containing a C-Type Heme .....	197
<b>X-C Bioinorganic Chemistry of a Novel Heme Enzyme that Catalyzes the Dehydration Reaction</b> --	<b>198</b>
X-C-1 Regulation of Aldoxime Dehydratase Activity by Redox-Dependent Change in the Coordination Structure of the Aldoxime-Heme Complex .....	198
<b>X-D Reaction Mechanism of Metalloenzymes Related to Oxygen Activation</b> .....	<b>199</b>
X-D-1 Oxidizing Intermediates from the Sterically Hindered Salen Iron Complexes Related to the Oxygen Activation by Nonheme Iron Enzymes .....	199
X-D-2 Synthesis of Sterically Hidered Tris(4-imidazolyl)carbinol Ligands and their Copper(I) Complexes Related to Metalloenzymes .....	199
X-D-3 O <sub>2</sub> - and H <sub>2</sub> O <sub>2</sub> -Dependent Verdoheme Degradation by Heme Oxygenase: Reaction Mechanisms and Potential Physiological Roles of the Dual Pathway Degradation ---	200
<b>X-E Reaction Mechanism of Metalloenzymes related to Global Nitrogen Cycle</b> .....	<b>200</b>
X-E-1 Spectroscopic Characterization of Reaction Intermediates in a Model for Copper Nitrite Reductase .....	200
<b>X-F Biomolecular Science</b> .....	<b>202</b>
X-F-1 Resonance Raman Characterization of the P Intermediate in the Reaction of Bovine Cytochrome <i>c</i> Oxidase .....	202
X-F-2 Core Structure of Amyloid Fibril Proposed from IR-Microscope Linear Dichroism .....	202
X-F-3 Activation of Heme-Regulated Eukaryotic Initiation Factor 2 $\alpha$ Kinase (HRI) Activation by Nitric Oxide Is Induced by the Formation of a Five-Coordinate NO-Heme Complex: Optical Absorption, Electron Spin Resonance and Resonance Raman Spectral Studies .....	203
X-F-4 Steric and Hydrogen-Bonding Effects on the Stability of Copper Complexes with Small Molecules .....	203
X-F-5 Identification of Crucial Histidines Involved in Carbon-Nitrogen Triple Bond Synthesis by Aldoxime Dehydratase .....	203
X-F-6 Thermal Stability of Mononuclear Hydroperoxocopper(II) Species. Effects of Hydrogen Bonding and Hydrophobic Field .....	204
X-F-7 Energy Funneling of IR Photons Captured by Dendritic Antennae and Acceptor Mode Specificity: Anti-Stokes Resonance Raman Studies on Iron(III) Porphyrin Complexes with a Poly(Aryl Ether) Dendrimer Framework .....	204
X-F-8 Structural Model of the Amyloid Fibril Formed by $\beta_2$ -Microglobulin #21-31 Fragment Based on Vibrational Spectroscopy .....	204
X-F-9 Excited State Property of Hardly Photodissociable Heme-CO Adduct Studied by Time-Dependent Density Functional Theory .....	205
X-F-10 Mechanism for Transduction of the Ligand-Binding Signal in Heme-Based Gas Sensory Proteins Revealed by Resonance Raman Spectroscopy .....	205
X-F-11 UV Resonance Raman Study of Model Complexes of the Cu <sub>B</sub> Site of Cytochrome <i>c</i> Oxidase .....	205
X-F-12 Resonance Raman Investigation on the Specific Sensing Mechanism of a Target Molecule by Gas Sensory Proteins .....	206
X-F-13 Communication Pathway between Heme and Protein in Myoglobin .....	206
X-F-14 FT-IR Approaches on Amyloid Fibril Structure .....	206
X-F-15 Structural and Spectroscopic Characterization of ( $\mu$ -Hydroxo or $\mu$ -Oxo)( $\mu$ -Peroxo)Diiron(III) Complexes: Models for Peroxo Intermediates of Non-Heme Diiron Proteins Structural and Spectroscopic Characterization of ( $\mu$ -Hydroxo or $\mu$ -Oxo)( $\mu$ -Peroxo)Diiron .....	206
X-F-16 Axial Ligand Substituted Nonheme Fe <sup>IV</sup> =O complexes: Observation of Near-UV LMCT Bands and Fe=O Raman Vibrations .....	206
X-F-17 Reversible O–O Bond Cleavage and Formation of a Peroxo Moiety of a Peroxocarbonate Ligand Mediated by an Iron(III) Complex .....	207
X-F-18 Synthesis and Reactivity of a ( $\mu$ -1,1-Hydroperoxo)( $\mu$ -Hydroxo)Dicopper(II) Complex: Ligand Hydroxylation by a Bridging Hydroperoxo Ligand .....	207
X-F-19 Spectroscopic and Redox Properties of a CooA Homologue from <i>Carboxydotherrnus hydrogenoformans</i> .....	207
X-F-20 Structural Diversities of Active Site in Clinical Azole-Bound Forms between Sterol 14 $\alpha$ -Demethylases (CYP51s) from Human and <i>Mycobacterium tuberculosis</i> --	208
X-F-21 Stopped-Flow Spectrophotometric and Resonance Raman Analyses of Aldoxime Dehydratase Involved in Carbon-Nitrogen Triple Bond Synthesis .....	208

X-F-22 Synthesis, Characterization, and Thermal Stability of New Mononuclear Hydrogenperoxocopper(II) Complexes with N <sub>3</sub> O-Type Tripodal Ligands Bearing Hydrogen-Bonding Interaction Sites -----	208
X-F-23 Spectroscopic Characterization of the Isolated Heme-Bound PAS-B Domain of Neuronal PAS Domain Protein 2 (NPAS2) Associated with Circadian Rhythms -----	209
X-F-24 Covalent Cofactor Attachment to Proteins: Cytochrome <i>c</i> Biogenesis -----	209
X-F-25 Structure and Dioxygen-Reactivity of Copper(I) Complexes Supported by Bis(6-methylpyridin-2-yl-methyl)amine Tridentate Ligands -----	209
X-F-26 Resonance Raman and FT-IR Studies on Proximal and Distal Histidine Environment of Cytochrome <i>c</i> and Neuroglobin -----	210
X-F-27 Dynamic Ligation Properties of the <i>Escherichia coli</i> Heme Chaperone CcmE to Non-Covalently Bound Heme -----	210
<b>X-G Collaborative Research with FANTOM Consortium -----</b>	<b>211</b>
X-G-1 The international Consortium, FANTOM*, Discovered UBL Domains Interspersed over Mammalian Genomes -----	211

## **RESEARCH FACILITIES -----213**

Research Center for Molecular-scale Nanoscience -----	213
UVSOR Facility -----	213
Laser Research Center for Molecular Science -----	214
Equipment Development Center -----	214
Safety Office -----	214
Research Center for Computational Science -----	214

## **SPECIAL RESEARCH PROJECTS -----217**

<b>(a) Chemical Reaction Dynamics -----</b>	<b>217</b>
Folding Mechanism of Protein Molecules Studied by Generalized-Ensemble Algorithms -----	217
Electronic Structure and Decay Mechanism of Inner-Shell Excited Molecules -----	217
Computational Study of Quantum Dynamics of a Solute in Solution -----	217
Chemical Reactions at Surfaces and Nano-Structured Materials Studied by Spatio-Temporally Resolved Spectroscopy -----	218
Towards Complete Imaging of Molecular Orbital Patterns: Development of Molecular Frame ( <i>e,2e</i> ) Spectroscopy -----	218
<b>(b) Molecular Photophysics and Science -----</b>	<b>219</b>
Theoretical Studies of Quantum Many-Particle Dynamics in Open Systems -----	219
Spatiotemporal Dynamics in Nanometric Molecular Assemblies by Near-Field Spectroscopy -----	219
Studies on Laser Cooling and Trapping of Metastable Helium Atoms and Laser Spectroscopic Studies of Atoms and Ions in Liquid Helium -----	219
Methods of Analysis for Protein Dynamics in Living Cells -----	219
Development of Attosecond Coherent Control and Its Application -----	220
Laser Manipulation of Molecular Motions and Its Application to Reaction Dynamics Studies -----	220
Probing Ultrafast Molecular Dynamics by Extremely Short Laser Pulses -----	220
Photoionization and Photodissociation of Fullerenes and Metal Encapsulated Fullerenes, Their Mechanisms, Kinetics, and Dynamics -----	220
Theoretical Development of Interfacial Sum Frequency Generation Spectroscopy -----	221
Decay and Dissociation Dynamics of Core Excited Molecules -----	221
<b>(c) Novel Materials Science -----</b>	<b>222</b>
Quantum Chemistry Calculations of Large Molecular Systems -----	222
Theory for Equilibrium and Non-Equilibrium Properties of Low-Dimensional Molecular Materials with Strong Correlation -----	222
UHV Systems for MOKE, MSHG, XMCD and STM Measurements -----	222
Development and Characterization of Metal/Carbon Hybrid Nano-Systems -----	223
Charge ordering in Organic Conductors -----	223
Multi-Frequency and Pulsed ESR Investigation for Molecular-Based Materials -----	224
Broad-Line Solid State NMR Investigation of Molecular-Based Conductors -----	224
Synchrotron X-Ray Diffraction Experiments and MEM Analyses for Single Crystals of Organic Conductors -----	225
Development of New Functional Molecular Systems -----	225
Synthesis and Properties of Novel Chiral Organic-Inorganic Molecule-Based Magnets -----	225
Design and Functions of Novel Soft Nanomaterials Based on Molecular Programming -----	226
Giant Vesicle Fusion on Microelectrodes Fabricated by Femtosecond Laser Ablation Followed by Synchrotron Radiation Etching -----	226
Reduction of CO <sub>2</sub> and Oxidation of Organic Molecules Aiming at Reversible Conversion between Chemical and Electrical Energies -----	227

Coordination Chemistry of New Multidentate Ligands and Activation of Small Molecules -----	227
Studies on Development of Molecules and the Device Fabrications for Molecular Scale Electronics -----	227
Synthesis of Perfluorinated Fluorene Oligomers and Applications for Organic Light-Emitting Diodes -----	228
Novel Pincer Complexes and Their Catalytic Properties -----	228
Asymmetric Aquacatalysis with Polymeric Palladium Complexes -----	228
Construction of Advanced Redox Materials Based on Organic Molecules and Metal Complexes, as Basis of Chemical Energy Conversion Systems -----	229
Synthesis of Buckybowls and Heterobuckybowls -----	229
Tuning Catalytic Activities of Gold Clusters <i>via</i> Hybridization of Functional Molecules -----	229
Structural Analyses of Multi-Domain Proteins by Use of Ultra-High Field NMR Spectroscopy Measured at 920 MHz <sup>1</sup> H Resonance Frequency -----	229
Observation of Intense Bursts of Terahertz Synchrotron Radiation at UVSOR-II -----	230
Optical and Photoelectrical Studies on Fermiology of Strongly Correlated Electron Systems -----	230
Developments and Researches of New Laser Materials -----	230
Development and Research of Advanced Tunable Solid State Lasers -----	230
Regulation of Biological Function by the Heme-Based Gas-Molecule Sensor Proteins -----	231
Molecular Mechanism of Metalloenzymes Related to Oxygen Activation and Denitrification Processes -----	231
Molecular Science of Proteins Based on Vibrational Spectroscopy -----	231
<b>JOINT STUDIES PROGRAMS -----</b>	<b>233</b>
(1) Special Projects -----	233
(2) Research Symposia -----	235
(3) Cooperative Research -----	235
(4) Use of Facility -----	236
(5) Invited Research -----	236
(6) Use of UVSOR Projects -----	236
(7) Use of Facility Program of the Computer Center -----	236
<b>FOREIGN SCHOLARS -----</b>	<b>237</b>
<b>AWARDS -----</b>	<b>241</b>
<b>LIST OF PUBLICATIONS -----</b>	<b>245</b>
<b>REVIEW ARTICLES AND TEXTBOOKS -----</b>	<b>265</b>
<b>AUTHOR INDEX -----</b>	<b>269</b>

## Abbreviations

IMS: Institute for Molecular Science  
SOKENDAI: The Graduate University for Advanced Studies

# ORGANIZATION AND STAFF

## Organization

The Institute for Molecular Science comprises twenty research laboratories, each staffed by a professor, an associate professor, two research associates and several technical associates, and two research laboratories with foreign visiting professors and five research facilities.

**The laboratories are grouped into seven departments and one facility for coordination chemistry:**

Department of Theoretical Studies	Theoretical Studies I Theoretical Studies II Theoretical Studies III Theoretical Studies IV <sup>1)</sup>
Department of Molecular Structure	Molecular Structure I Molecular Structure II <sup>1)</sup> Molecular Dynamics
Department of Electronic Structure	Excited State Chemistry Excited State Dynamics Electronic Structure <sup>1)</sup> Molecular Energy Conversion <sup>2)</sup>
Department of Molecular Assemblies	Solid State Chemistry Molecular Assemblies Dynamics Molecular Assemblies <sup>1)</sup>
Department of Applied Molecular Science	Applied Molecular Science I Applied Molecular Science II <sup>1)</sup>
Department of Vacuum UV Photoscience	Photochemistry Chemical Dynamics Synchrotron Radiation Research <sup>2)</sup>
Department of Computational Molecular Science	Computational Molecular Science I Computational Molecular Science II Computational Molecular Science III <sup>1)</sup>
Coordination Chemistry Laboratories	Functional Coordination Chemistry Coordination Bond <sup>1)</sup> Complex Catalysis

**The research facilities are:**

- Research Center for Molecular-scale Nanoscience    Molecular-scale Electronics  
Nanocatalysis and Biomolecular Devices  
Nano-scale Photoscience  
Advanced Molecular Science<sup>3)</sup>
- UVSOR Facility
- Laser Research Center for Molecular Science    Advanced Lasers for Chemical Reaction Studies  
Advanced Lasers for Synchrotron Radiation Applications  
Advanced UV and IR Tunable Lasers
- Equipment Development Center
- Safety Office

**Okazaki research facilities (related to IMS) are:**

- Okazaki Institute for Integrative Bioscience
- Research Center for Computational Science

1) Professors and associate professors are visiting professors from other universities.

2) Research laboratories with foreign visiting professors.

3) Professors, associate professors, and research associates, along with their positions, are transferred from other universities.

## Scientific Staff

**NAKAMURA, Hiroki**

**Professor, Director-General**

NAGAKURA, Saburo  
HIROTA, Eizi

The Japan Academy  
Professor Emeritus, The Graduate University for Advanced  
Studies

KIMURA, Katsumi

Senior Researcher, Molecular Photonics & Photoelectron Group,  
Communications Research Laboratory

MOROKUMA, Keiji  
INOKUCHI, Hiroo

Professor, Emory University, U. S. A.  
Chief Scientist of Space Utilization Research Program, Japan  
Aerospace Exploration Agency

MARUYAMA, Yusei  
YOSHIHARA, Keitaro  
HANAZAKI, Ichiro

Professor, Hosei University  
Professor, Japan Advanced Institute of Science and Technology  
Professor Emeritus, The Graduate University for Advanced  
Studies

IWAMURA, Hiizu  
SAITO, Shuji  
IWATA, Suehiro  
ITO, Mitsuo

Professor, University of the Air  
Professor, Fukui University  
Professor, National Institution for Academic Degree  
Professor Emeritus, The Graduate University for Advanced  
Studies, Tohoku University

KAYA, Koji

Director, RIKEN Wako Institute, RIKEN Discovery Institute

### *Department of Theoretical Studies*

#### *Theoretical Studies I*

NAGASE, Shigeru  
OKAMOTO, Yuko  
KOBAYASHI, Kaoru  
OKUMURA, Hisashi  
ISHIMURA, Kazuya  
PULAY, Peter  
ANANT, Dattatraya Kulkarni  
SLANINA, Zdenek  
TAKAGI, Nozomi

Professor  
Associate Professor (–March '05)<sup>1)</sup>  
Research Associate  
Research Associate  
Technical Associate  
Visiting Professor (May–August '05)  
Post-Doctoral Fellow (November '04–March '05)  
Post-Doctoral Fellow (September '04–)  
JSPS Post-Doctoral Fellow (–March '05), Post-Doctoral Fellow  
(April '05–)  
Post-Doctoral Fellow (–March '05)<sup>2)</sup>  
Post-Doctoral Fellow (–March '05)<sup>1)</sup>  
Research Fellow  
Research Fellow (–March '05)<sup>3)</sup>  
Post-Doctoral Fellow (–March '05)<sup>4)</sup>  
Post-Doctoral Fellow (April '05–)  
Graduate Student (–March '05)<sup>1)</sup>  
Graduate Student

RE, Suyong  
KAWASHIMA, Yukio  
KATOUDA, Michio  
KOKUBO, Hironori  
ONO, Yuriko  
SUMIMOTO, Michinori  
ITO, Satoru  
MIZOROGI, Naomi

#### *Theoretical Studies II*

NAKAMURA, Hiroki  
NOBUSADA, Katsuyuki  
TAKAMI, Toshiya  
MIL'NIKOV, Gennady  
YASUIKE, Tomokazu  
ZOU, Shiyang  
Zhao, Yi  
CHIKAZUMI, Shinpei  
TAMURA, Hiroyuki  
PARK, Tae Jun  
ISHKHANYAN, Artur  
KONDORSKY, Alexey  
KUBOTA, Yoji  
OLOYEDE, Oluwaponmile  
SHIRATORI, Kazuya  
IWASA, Takeshi

Professor  
Associate Professor  
Research Associate (–December '04)  
Research Associate  
Research Associate (July '05–)  
IMS Fellow (–March '05), Post-doctoral Fellow (April '05)  
JSPS Post-Doctoral Fellow (–May '05)  
Post-Doctoral Fellow  
Post-Doctoral Fellow  
Visiting Scientist (December '04–February '05)  
Visigint Scientist (September–December '04)  
Post-Doctoral Fellow  
Post-Doctoral Fellow (April '05–)  
Graduate Student  
Graduate Student (April '05–)  
Graduate Student (April '05–)

*Theoretical Studies III*

HIRATA, Fumio  
 YONEMITSU, Kenji  
 CHONG, Song-Ho  
 YAMASHITA, Yasufumi  
 LEE, Jin Yong  
 MONDAL, Chandan Kumar  
 OTSUKA, Yuichi  
 KOBRYN, Oleksandr  
 YOSHIDA, Norio  
 IKUTA, Yasuhiro  
 MAESHIMA, Nobuya  
 MARUYAMA, Yutaka  
 MIYATA, Tatsuhiko  
 INOUE, Hitoshi  
 MIYASHITA, Satoshi  
 TANIMURA, Ayumi  
 MATSUGAMI, Masaru  
 ISHIZUKA, Ryosuke

Professor  
 Associate Professor  
 Research Associate  
 Research Associate  
 MONKASHO Invited Fellow (June–August '05)  
 MONKASHO Invited Fellow (June–August '05)  
 IMS Fellow(–October, '04)<sup>5)</sup>  
 IMS Fellow  
 Post-Doctoral Fellow  
 Post-Doctoral Fellow  
 Post-Doctoral Fellow  
 Post-Doctoral Fellow  
 Post-Doctoral Fellow  
 Post-Doctoral Fellow(–May '05)  
 Post-Doctoral Fellow(June '05–)  
 Post-Doctoral Fellow(April '05–)  
 Graduate Student  
 Graduate Student

*Theoretical Studies IV*

HADA, Masahiko  
  
 NAKAJIMA, Takashi  
  
 FUCHIZAKI, Kazuhiro  
 KOMATSUZAKI, Tamiki

Visiting Associate Professor (from Tokyo Metropolitan University) (–March '05)  
 Visiting Associate Professor (from Kyoto University) (–March '05)  
 Visiting Professor (from Ehime University) (April '05–)  
 Visiting Associate Professor (from Kobe University) (April '05–)

**Department of Molecular Structure***Molecular Structure I*

OKAMOTO, Hiromi  
 MORITA, Norio  
 IMURA, Kohei  
 NAGAHARA, Tetsuhiko  
 HORIMOTO, Noriko  
 LIM, Jong Kuk

Professor  
 Associate Professor (–November '04)  
 Research Associate  
 IMS Fellow (–March '05)  
 IMS Fellow (April '05–)  
 Visiting Graduate Student (from Seoul National University) (–October '04)

*Molecular Structure II*

OHTA, Toshiaki  
 TERAZIMA, Masahide  
 ISHIMORI, Koichiro

Visiting Professor (from The University of Tokyo) (–March '05)  
 Visiting Professor (from Kyoto University) (April '05–)  
 Visiting Associate Professor (from Kyoto University) (–March '05), Visiting Professor (from Hokkaido University) (April '05–)

*Molecular Dynamics*

KITAGAWA, Teizo  
 YOKOYAMA, Toshihiko  
 OZAWA, Takeaki  
 UCHIDA, Takeshi  
 NAKAGAWA, Takeshi  
 WATANABE, Hirokazu  
 MARUYAMA, Koichi  
 MATSUOKA, Hideto  
 MA, Xiaodong

Professor (Okazaki Institute for Integrative Bioscience)  
 Professor  
 Associate Professor (April '05–)  
 Research Associate (–August '05)  
 Research Associate  
 Technical Associate  
 IMS Fellow  
 JSPS Post-Doctoral Fellow (–March '05)  
 Graduate Student

**Department of Electronic Structure***Excited State Chemistry*

NISHI, Nobuyuki  
 BOO, Bong Hyun  
  
 JUDAI, Ken  
 NISHIJO, Junichi  
 OISHI, Osamu

Professor  
 Visiting Professor (from Chungnam National University, South Korea) (December '04–February '05)  
 Research Associate  
 Research Associate  
 Technical Associate (April '05–)

OKABE, Chie  
WATANABE, Michio

IMS Fellow  
Research Fellow

*Excited State Dynamics*

OHMORI, Kenji  
OHSHIMA, Yasuhiro  
KATSUKI, Hiroyuki  
HASEGAWA, Hirokazu  
HOSAKA, Kouichi  
MIYAZAKI, Mitsuhiro  
MIYAKE, Shinichiro  
DELANGNES, Jean-Christophe

Professor  
Professor (September '04–)  
Research Associate  
Research Associate (April '05–)  
IMS Fellow (April '05–)  
IMS Fellow (April '05–)  
Graduate Student (from Kyoto University)\* (April '05–)  
Visiting Scientist (April '05–June '05)

*Electronic Structure*

ICHIMURA, Teijiro  
TAKAGI, Noriaki

Visiting Professor (from Tokyo Institute of Technology)  
Visiting Associate Professor (from The University of Tokyo)

*Molecular Energy Conversion*

KWON, Yong-Seung  
  
OSHEROV, Vladimir Iosiphovich  
  
STANKEVICH, Vladimir, G.  
  
PULAY, Peter  
  
COUPRIE, Marie Emmanuelle  
  
TANATAR, Makariy  
  
VAROTSIS, Constantinos

Visiting Professor (from Sungkyunkwan University, South Korea) (–September '04)  
Visiting Professor (from Institute of Problems of Chemical Physics, Russia) (September '04–January '05)  
Visiting Professor (from Kurchatov Synchrotron Radiation Center, RRC Kurchatov Institute, Russia) (January '05–July '05)  
Visiting Professor (from University of Arkansas, U.S.A.) (May '05–August '05)  
Visiting Associate Professor (from LURE, France) (–September '04)  
Visiting Associate Professor (from National Ukrainian Academy of Sciences, Ukraine) (February '05–)  
Visiting Associate Professor (from University of Crete, Greece) (October '04–January '05)

***Department of Molecular Assemblies****Solid State Chemistry*

YAKUSHI, Kyuya  
NAKAMURA, Toshikazu  
YAMAMOTO, Kaoru  
FURUKAWA, Ko  
URUICHI, Mikio  
YAMAMOTO, Takashi  
HARA, Toshifumi  
NAKANO, Chikako  
SIMONYAN, Mkhitar  
BOYKO, Sergiy  
DROZDOVA, Olga  
MATSUOKA, Hideto  
MAEDA, Keisuke  
TANAKA, Masayuki

Professor  
Associate Professor  
Research Associate  
Research Associate  
Technical Associate  
IMS Fellow (–March '05)  
IMS Fellow  
Research Fellow  
Research Fellow (October '04–December '04)  
Research Fellow (July '05–August '05)  
Research Fellow  
Research Fellow (April '05–)  
Graduate Student  
Graduate Student (April '05–)

*Molecular Assemblies Dynamics*

KOBAYASHI, Hayao  
TAKAHASHI, Kazuyuki  
OKANO, Yoshinori  
OTSUKA, Takeo  
CUI, Heng-Bo  
MIYAMOTO, Akihito  
OTSUBO, Saika

Professor  
Research Associate  
Technical Associate  
JSPS Post-Doctoral Fellow (–March '05)  
JST Post-Doctoral Fellow  
Visiting Scientist (October '04–)  
Graduate Student

*Molecular Assemblies*

ENOKI, Toshiaki

Visiting Professor (from Tokyo Institute of Technology) (–March '05)

NAITO, Toshio	Visiting Associate Professor (from Hokkaido University) (–March '05)
KOJIMA, Norimichi	Visiting Professor (from The University of Tokyo) (April '05–)
KAWAMOTO, Atsushi	Visiting Associate Professor (from Hokkaido University) (April '05–)

**Department of Applied Molecular Science***Applied Molecular Science I*

KINOSHITA, Kazuhiko, Jr.	Professor (Okazaki Institute for Integrative Bioscience) (–March '05)
AONO, Shigetoshi	Professor (Okazaki Institute for Integrative Bioscience)
INOUE, Katsuya	Professor (–September '04)
JIANG, Donglin	Associate Professor (May '05–)
ADACHI, Kengo	Research Associate (Okazaki Institute for Integrative Bioscience) (–March '05)
AKITA, Motoko	Research Associate
YOSHIOKA, Shiro	Research Associate (Okazaki Institute for Integrative Bioscience)
OKUDA, Kazuki	Graduate Student
NUMATA, Yohei	Graduate Student

*Applied Molecular Science II*

IKEDA-SAITO, Masao	Visiting Professor (from Tohoku University)
NAKAMURA, Kazutaka	Visiting Associate Professor (from Tokyo Institute of Technology)

**Department of Vacuum UV Photochemistry***Photochemistry*

KOSUGI, Nobuhiro	Professor
HISHIKAWA, Akiyoshi	Associate Professor
HATSUI, Takaki	Research Associate
TAKAHASHI, Eiji	Research Associate
HIYAMA, Miyabi	Research Associate
SETOYAMA, Hiroyuki	IMS Fellow (–September '04)
MATSUDA, Akitaka	IMS Fellow (April '05–)
MASUDA, Suomi	Graduate Student (–March '05)

*Chemical Dynamics*

URISU, Tsuneo	Professor
MITSUKE, Koichiro	Associate Professor
NONOGAKI, Youichi	Research Associate (–March '05)
KATAYANAGI, Hideki	Research Associate (October '04–)
TERO, Ryugo	Technical Associate
LEI, Shenbin	Post-Doctoral Fellow (–November '04)
YOSHIMURA, Daisuke	Post-Doctoral Fellow (–March '05)
UNO, Hidetaka	Research Fellow
SUGA, Yasuhiro	Visiting Scientist (from AISIN COSMOS R&D CO., LTD.) (–March '05)
ITO, Masayuki	Visiting Scientist (from AISIN COSMOS R&D CO., LTD.) (–March '05)
SUZUKI, Akira	Visiting Scientist (from AISIN COSMOS R&D CO.,LTD.) (–March '05)
MO, Yu-Jun	Visiting Scientist (from Henan University) (February '05–March '05)
FUJIKI, Satoshi	Graduate Student (–September '04)
RAHMAN, Mashiur	Graduate Student
KIM, Yong-Hoon	Graduate Student
MISAWA, Nobuo	Graduate Student
SUZUKI, Masanori	Graduate Student (from Toyohashi University of Technology)* (–March '05)
YOGI, Osamu	Graduate Student (from Toyohashi University of Technology)* (–March '05)
ZHANG, Zhenlong	Graduate Student (November '04–)
KAFLE, Bhim Prasad	Graduate Student (October '04–)

\* persons carrying out graduate research of IMS on Cooperative Education Program of IMS with other graduate schools

NAKAI, Naohito Graduate Student (April '05–)

*Synchrotron Radiation Research*

WAN, Lijun Visiting Professor (from Institute of Chemistry, Chinese Academy of Sciences, China) (–October '04)  
 LONG, La-Sheng Visiting Associate Professor (from Xiamen University, China) (May '05–)  
 SUN, Wei-Yin Visiting Professor (from Nanjing University, China) (–February '05, June–August '05)  
 AKA, Gerard, Philippe Visiting Professor (from ECOLE NATIONALE SUPERIEURE DE CHIMIE DE PARIS, France) (March–May '05)  
 LABLANQUIE, Pascal Visiting Associate Professor (from LURE, France) (September '04–February '05)

***Department of Computational Molecular Science***

*Computational Molecular Science I*

OKAZAKI, Susumu Professor (Research Center for Computational Science)  
 MORITA, Akihiro Associate Professor (Research Center for Computational Science)  
 NANBU, Shinkoh Research Associate (–March '05)  
 TAKAMI, Toshiya Research Associate (–September '04)  
 MIURA, Shinichi Research Associate  
 ISHIDA, Tateki Research Associate (November '04–)  
 IWAHASHI, Kensuke Post-Doctoral Fellow  
 YOSHII, Noriyuki Post-Doctoral Fellow  
 YAMADA, Atsushi Post-Doctoral Fellow  
 MIKAMI, Taiji Post-Doctoral Fellow  
 ISHIYAMA, Tatsuya Post-Doctoral Fellow (January '05–)  
 LI, Hongzhen Research Fellow (April '05–)  
 KOMATSU, Takahiro Graduate student (from Tokyo Institute of Technology)\* (–March '05); Research Fellow (June '05–)  
 SATO, Masahiro Graduate student (from Tokyo Institute of Technology)\* (–March '05)

***Coordination Chemistry Laboratories***

TANAKA, Koji Director

*Functional Coordination Chemistry*

TANAKA, Koji Professor  
 KAWAGUCHI, Hiroyuki Associate Professor  
 SUN, Wei-Yin Visiting Professor (from Nanjing University) (April '05–)  
 WADA, Tohru Research Associate  
 MATSUO, Tsukasa Research Associate  
 MIYASATO, Yuji Post-Doctoral Fellow (–March '05), IMS Fellow (April '05–)  
 WATANABE, Takahito IMS Fellow (April '05–)  
 KOMURO, Takashi JSPS Post-Doctoral Fellow (–September '04)<sup>6)</sup>  
 OKAMURA, Rei Post-Doctoral Fellow  
 TANNAI, Hidenori Post-Doctoral Fellow (April '05–)  
 FUJITA, Mitsuharu Post-Doctoral Fellow (April '05–)  
 KOIZUMI, Takeaki Post-Doctoral Fellow (–April '05)<sup>7)</sup>  
 ZHANG, Dao Post-Doctoral Fellow (–March '05)<sup>8)</sup>  
 TSUTSUI, Kanako Research Fellow  
 TAKUMA, Motoki Research Fellow (April '05–)  
 HINO, Takami Graduate Student (–March '05), Research Fellow (April '05–)  
 INOUE, Ayako Graduate Student (April '05–)  
 FUKUSHIMA, Takashi Graduate Student (April '05–)

*Coordination Bond*

MATSUSAKA, Hiroyuki Visiting Professor (from Osaka Prefecture University) (–March '05)  
 UENO, Keiji Visiting Professor (from Gunma University) (–March '05)  
 ISHII, Youichi Visiting Professor (from Chuo University) (April '05–)  
 HAYASHI, Takashi Visiting Professor (from Osaka University) (April '05–)

*Complex Catalysis*

MASHIMA, Kazushi  
KURIHARA, Masato

Visiting Professor (from Osaka University)  
Visiting Associate Professor (from Yamagata University)

**Research Facilities***Research Center for Molecular-scale Nanoscience*

OGAWA, Takuji Director

*Molecular-scale Electronics*

OGAWA, Takuji	Professor
TADA, Hirokazu	Associate Professor (–March '05)
SUZUKI, Toshiyasu	Associate Professor
TANAKA, Shoji	Research Associate
SAKAMOTO, Youichi	Research Associate
TANAKA, Hirohumi	Research Associate
YAMADA, Ryo	Research Associate (–May '05)
HUANG, Wei	IMS Fellow
ARA, Masato	Graduate Student (–April '05)
TAKADA, Masaki	Graduate Student (–April '05)
SAKANOUE, Tomo	Graduate Student (–April '05)
KAWAO, Masahiro	Graduate Student (from Ehime University)*
MIZUGUCHI, Eisuke	Graduate Student (from Ehime University)* (–March '05)
OZAWA, Hiroaki	Graduate Student (from Ehime University)*
SATOU, Hirokazu	Graduate Student (from Ehime University)*
YAJIMA, Takashi	Graduate Student
SHIMADA, Kazuhiro	Graduate Student (from JAIST)*

*Nanocatalysis and Biomolecular Devices*

UOZUMI, Yasuhiro	Professor
NAGATA, Toshi	Associate Professor
FUJII, Hiroshi	Associate Professor (Okazaki Institute for Integrative Bioscience)
SAKURAI, Hidehiro	Associate Professor
KURAHASHI, Takuya	Research Associate (Okazaki Institute for Integrative Bioscience)
NAGASAWA, Takayuki	Research Associate
YAMADA, Youich	Research Associate
HIGASHIBAYASHI, Shuhei	Research Associate
MAKI, Suguru	IMS Fellow
KAMIYA, Ikuyo	IMS Fellow (April '05–)
TAKENAKA, Kazuhiro	Post-Doctoral Fellow
SUZUKA, Toshimasa	Post-Doctoral Fellow
OHDAKA, Atsushi	Post-Doctoral Fellow (April '05–)
MAEDA, Yasunari	Post-Doctoral Fellow (April '05–)
KIMURA, Tsutomu	Post-Doctoral Fellow (April '05–)
SUGUHARA, Takahiro	Post-Doctoral Fellow (April '05–)
KIMURA, Masahiro	Graduate Student
SAKAMAKI, Junichiro	Graduate Student
MINAKAWA, Maki	Graduate Student
ARAKAWA, Takayasu	Graduate Student
BEPPU, Tomohiko	Graduate Student
FUKUYAMA, Naoshi	Graduate Student (April '05–)
KAWADE, Rei	Graduate Student (April '05–)
TAKIZAWA, Ryu	Graduate Student

*Nano-scale Photoscience*

MATSUMOTO, Yoshiyasu	Professor
TSUKUDA, Tatsuya	Associate Professor
WATANABE, Kazuya	Research Associate
MATSUMOTO, Taketoshi	Research Associate
NEGISHI, Yuichi	Research Associate
NAGAO, Masashi	IMS Fellow
TSUNOYAMA, Hironori	IMS Fellow
NAKAO, Satoru	IMS Fellow (April '05–)

\* persons carrying out graduate research of IMS on Cooperative Education Program of IMS with other graduate schools

SAWADA, Takeshi	Post-Doctoral Fellow
KAI, Noriko	Visiting Scientist (February '05–)
FUYUKI, Masanori	Graduate Student
YAMAGUCHI, Dai	Graduate Student
YANAGIMOTO, Yasushi	Graduate Student (from Okayama University)* (June '05–)

*Advanced Molecular Science*

KATO, Koichi	Professor (from Nagoya City University) (October '04–)
TAKAHASHI, Masahiko	Associate Professor (from Tohoku University) (–March '05)
SASAGAWA, Hiroaki	Research Associate (from Nagoya City University) (April '05–)
KERA, Satoshi	Research Associate (from Chiba University) (–March '05)
WATANABE, Noboru	Research Associate (from Tohoku University) (–March '05)
KHAJURIA, Yugal	IMS Fellow (–March '05)
KAMIYA, Yukiko	Graduate Student (from Nagoya City University)* (April '05–)
YAGI, Hirokazu	Graduate Student (from Nagoya City University)* (April '05–)
YAMADA, Kenzo	Graduate Student (from Nagoya City University)* (April '05–)
NISHI, Yohei	Graduate Student (from Nagoya City University)* (April '05–)
SUZUKI, Maiko	Graduate Student (from Nagoya City University)* (April '05–)
MAENO, Aya	Graduate Student (from Nagoya City University)* (April '05–)
NAGANO, Mayumi	Graduate Student (from Nagoya City University)* (April '05–)
SUMIYOSHI, Akira	Graduate Student (from Nagoya City University)* (April '05–)

*UVSOR Facility*

KOSUGI, Nobuhiro	Director
KATOH, Masahiro	Professor
SHIGEMASA, Eiji	Associate Professor
KIMURA, Shin-ichi	Associate Professor
ITO, Kenji	Visiting Associate Professor (from Photon Factory) (–March '05)
HARA, Toru	Visiting Associate Professor (from RIKEN) (April '05–)
COUPRIE, Marie-Emmanuelle	Visiting Professor (from CEA/DSM/DRECAM/SPAM, France) (December '04)
NOH, Tae Won	Visiting Professor (from Seoul National University, Korea) (February–March '05)
HOSAKA, Masahito	Research Associate
MOCHIHASHI, Akira	Research Associate
ITO, Takahiro	Research Associate
HIKOSAKA, Yasumasa	Research Associate
SAKURAI, Yoko	IMS Fellow
KANAYASU, Tatsuo	IMS Fellow (June '05–)
SICHELSCHMIT, Joerg	Visiting Scientist (from Max Planck Institut fuer Chemische Physik fester Stoffe, Germany) (February '05)
MEYER, Michael	Visiting Scientist (from LURE, Centre Universitaire Paris-Sud, France) (November–December '04)
BIELAWSKI, Serge	Visiting Scientist (from Universite des Sciences et Technologies de Lille, France) (December '04)
SZWAJ, Christophe	Visiting Scientist (from Universite des Sciences et Technologies de Lille, France) (December '04)
SIMON, Marc	Visiting Scientist (from LCPMR, France) (January '05)
ZHANG, Shancai	Visiting Scientist (from National Synchrotron Radiation Laboratory, University of Science and Technology of China, China) (March '05)
FENG, Guangyao	Visiting Scientist (from National Synchrotron Radiation Laboratory, University of Science and Technology of China, China) (March '05)
NISHI, Tatsuhiko	Graduate Student
IM, Hojun	Graduate Student

*Laser Research Center for Molecular Science*

MATSUMOTO, Yoshiyasu	Director
----------------------	----------

*Advanced Lasers for Chemical Reaction Studies*

*Advanced Lasers for Synchrotron Radiation Applications*

SARUKURA, Nobuhiko	Associate Professor
ONO, Shingo	Research Associate
ESTACIO, Elmer	IMS Fellow
QUEMA, Alex	JSPS Post-Doctoral Fellow
MURAKAMI, Hidetoshi	Research Fellow
DIWA, Girbert	Graduate Student
PONSECA Jr., Carlito	Graduate Student (April '05–)
de los REYES, Glenda	Graduate Student (April '05–)

*Advanced UV and IR Tunable Lasers*

TAIRA, Takunori	Associate Professor
LUPEI, Voicu	Visiting Professor (from Institute of Atomic Physics, Romania) (March '05)
ISHIZUKI, Hideki	IMS Fellow (–September '04); Research Associate (October '04–)
TSUNEKANE, Masaki	Post-Doctoral Fellow
DASCALU, Traian	Post-Doctoral Fellow (–March '05)
SATO, Yoichi	Post-Doctoral Fellow
SAIKAWA, Jiro	Research Fellow (–March '05); Post-Doctoral Fellow (from Tokyo Institute of Technology) (April '05–)
PAVEL, Nicolaie	Visiting Scientist (from Institute of Atomic Physics, Romania) (–March '05)

*Equipment Development Center*

URISU, Tsuneo	Director
---------------	----------

*Safety Office*

OGAWA, Takuji	Director
TOMURA, Masaaki	Research Associate

**Okazaki Research Facilities (related to IMS)***Okazaki Institute for Integrative Bioscience**Department of Strategic Methodology*

KINOSITA, Kazuhiko, Jr.	Professor (–March '05)
AONO, Shigetoshi	Professor
FUJII, Hiroshi	Associate Professor
ADACHI, Kengo	Research Associate (–March '05)
YOSHIOKA, Shiro	Research Associate
KOBAYASHI, Katsuaki	IMS Fellow
KUJIME, Masato	IMS Fellow
FUJIWARA, Ikuko	JSPS Post-Doctoral Fellow (–March '05)
SHIROGUCHI, Katsuyuki	JSPS Post-Doctoral Fellow (–March '05)
PATRA, Digambara	Visiting Scientist; JSPS Post-Doctoral Fellow (–August '05)
KON, Rieko	Post-Doctoral Fellow (–March '05)
FURUIKE, Shou	Post-Doctoral Fellow (–March '05)
OKAMOTO, Tetsuaki	Post-Doctoral Fellow (–March '05)
OZAWA, Kazumichi	Post-Doctoral Fellow (April '05–)
KANDA, Ritsuko	Research Fellow (–March '05)
YOGO, Katsunori	Graduate Student (from Waseda University)*
SAKAKI, Naoyoshi	Graduate Student
ONOUE, Yasuhiro	Graduate Student
INAGAKI, Sayaka	Graduate Student
YOSHIMURA, Hideaki	Graduate Student
HOSSAIN, Mohammad Delawar	Graduate Student
NISHIMURA, Muneto	Graduate Student (April '05–)

*Department of Bio-environmental Science*

KITAGAWA, Teizo	Professor
HAYASHIZAKI, Yoshihide	Visiting Professor (from RIKEN Genomic Sciences Center) (–March '05)
TAKAGI, Junichi	Visiting Professor (from Osaka University) (April '05–)
UCHIDA, Takeshi	Research Associate (–August '05) <sup>9)</sup>

\* persons carrying out graduate research of IMS on Cooperative Education Program of IMS with other graduate schools

KUBO, Minoru	IMS Fellow
VAROTSIS, Constantinos	Visiting Scientist; MONKASHO Invited Fellow (from University of Crete, Greece) (September '04–January '05), Visiting Scientist; JSPS Invited Fellow (from University of Crete, Greece) (February–April '05)
MAHINAY, Myrna Sillero	Visiting Scientist; JSPS Post-Doctoral Fellow (from Mindanao State University-Iligan Institute of Technology, Philippine) (–June '05), Visiting Scientist (June–July '05)
GU, Yuzong	Visiting Scientist; JSPS Post-Doctoral Fellow (from Henan University, China)
EL-MASHTOLY, Samir Fathy Abd El-Monem	Visiting Scientist (from Ain Shams University, Egypt) (July–September '04), Visiting Scientist; JSPS Post-Doctoral Fellow
OHTA, Takehiro	JSPS Post-Doctoral Fellow (–March '05) <sup>10)</sup>
NAGANO, Yasutomo	JSPS Post-Doctoral Fellow (–March '05), Post-Doctoral Fellow (April '05–)
HIRAMATSU, Hirotsugu	JSPS Post-Doctoral Fellow (–August '05) <sup>11)</sup>
TOSHA, Takehiko	JSPS Post-Doctoral Fellow
KIM, Younkyoo	Research Fellow (from Hankuk University of Foreign Studies, Korea) (July–August '05)
DASKALAKIS, Evangelos	Visiting Scientist (from University of Crete, Greece) (March–June '05)
GAO, Ying	Graduate Student
LI, Jiang	Graduate Student
LV, Ming	Graduate Student

***Research Center for Computational Science***

NAGASE, Shigeru	Director (Department of Theoretical Studies)
OKAZAKI, Susumu	Professor
MORITA, Akihiro	Associate Professor
NANBU, Shinkoh	Research Associate (Department of Computational Molecular Science) (–March '05)
TAKAMI, Toshiya	Research Associate (Department of Computational Molecular Science) (–September '04)
OONO, Hitoshi	Research Associate
MIURA, Shinichi	Research Associate (Department of Computational Molecular Science)
ISHIDA, Tateki	Research Associate (Department of Computational Molecular Science) (November '04–)

## Technical Staff

KATO, Kiyonori	Technical Division Head
SUZUI, Mitsukazu	Technical Section Chief
YOSHIDA, Hisashi	Technical Section Chief
HORIGOME, Toshio	Technical Section Chief
YAMANAKA, Takaya	Technical Section Chief
MIZUTANI, Fumiyasu	Technical Section Chief
MIZUTANI, Nobuo	Equipment Development Center (Unit Chief)
AOYAMA, Masaki	Equipment Development Center (Unit Chief)
YANO, Takayuki	Equipment Development Center
KONDOU, Takuhiko	Equipment Development Center
NAGATA, Masaaki	Equipment Development Center (Unit Chief)
UCHIYAMA, Kouichi	Equipment Development Center
TOYODA, Tomonori	Equipment Development Center
HASUMOTO, Masami	UVSOR facility (Unit Chief)
YAMAZAKI, Jun-ichiro	UVSOR facility (Unit Chief)
NAKAMURA, Eiken	UVSOR facility (Unit Chief)
SAKAI, Masahiro	UVSOR facility
KONDOU, Naonori	UVSOR facility
HAYASHI, Kenji	UVSOR facility
CHIBA, Hisashi	Laser Research Center for Molecular Science
UEDA, Tadashi	Laser Research Center for Molecular Science
TESHIMA, Fumitsuna	Research Center for Computational Science
NAITOU, Shigeki	Research Center for Computational Science
SAWA, Masataka	Research Center for Computational Science
MINAMINO, Satoshi	Research Center for Computational Science
TAKAYAMA, Takashi	Research Center for Molecular-scale Nanoscience (Unit Chief)
MIZUKAWA, Tetsunori	Research Center for Molecular-scale Nanoscience
MAKITA, Seiji	Research Center for Molecular-scale Nanoscience
FUJIWARA, Motoyasu	Research Center for Molecular-scale Nanoscience
NAKANO, Michiko	Research Center for Molecular-scale Nanoscience
HARADA, Miyuki	Public Affairs Office

## List of Present Addresses

- 1) Department of Physics, Graduate School of Science, Nagoya University, Furo-cho, Chikusa-ku Nagoya, 464-8602
- 2) Departement de Chimie, Ecole Normale Supérieure 24, ru Lhomond 75231 Paris, Cedex 05, France
- 3) Department of Chemistry, University of Houston, 4800 Calhoun Rd., Houston, TX 77204, U.S.A.
- 4) Division of Chemistry, Graduate School of Science, Hokkaido University, Kita 8 Nishi 5, Sapporo, 060-0808
- 5) Institute for Solid State Physics, University of Tokyo, Kashiwanoha 5-1-5, Kashiwa, 277-8581
- 6) Tohoku University, 6-3 Aoba, Aramaki, Aoba-ku, Sendai, 980-8578
- 7) Tokyo Institute of Technology, 4259 Nagatsuta, Midori-ku, Yokohama, 226-8503
- 8) Department of Chemistry, Fudan University, China
- 9) Division of Chemistry, Graduate School of Science, Hokkaido University, Sapporo, 060-0810
- 10) Department of Chemistry, Stanford University, Stanford, California 94305, U.S.A.
- 11) Graduate School of Pharmaceutical Sciences, Tohoku University, Aoba-ku, Sendai, 980-8578



## COUNCIL

**NAKAMURA, Hiroki**

**Director-General**

## Councillors

TSUCHIYA, Soji  
KATO, Shinichi

Invited Professor, Josai University  
Chief Executive Officer, Toyota Central Research &  
Development Laboratories, Inc.

KOMA, Atsushi  
MASUDA, Takashi  
FLEMING, Graham R.\*  
(–March '05)

Director, Institute of Materials Structure Science  
President, The University of Electro-Communications  
Professor, University of California, Berkeley

JORTNER, Joshua\*  
(–March '05)

Professor, Tel Aviv University

NORDGREN, Joseph\*  
(April '05–)

Professor, Uppsala University

CASTLEMAN, A. Welford Jr.\*  
(April '05–)

Professor, The Pennsylvania State University

The Council is the advisory board for the Director-General.

\* Two of the councillors are selected among distinguished foreign scientists.

## Distinguished Consultants

NAGAKURA, Saburo  
INOKUCHI, Hiroo

The Japan Academy  
Chief Scientist of Space Utilization Research Program,  
Japan Aerospace Exploration Agency

ITO, Mitsuo

Professor Emeritus, Institute for Molecular Science, The  
Graduate University for Advanced Studies, Tohoku  
University

KAYA, Koji

Director, RIKEN Discovery Research Institute

## Research Consultants

HIROTA, Noboru  
KONDOW, Tamotsu  
TAMAOKI, Kohei

Professor Emeritus, Kyoto University  
Visiting Professor, Toyota Technological Institute  
Director, RIKEN Frontier Research System

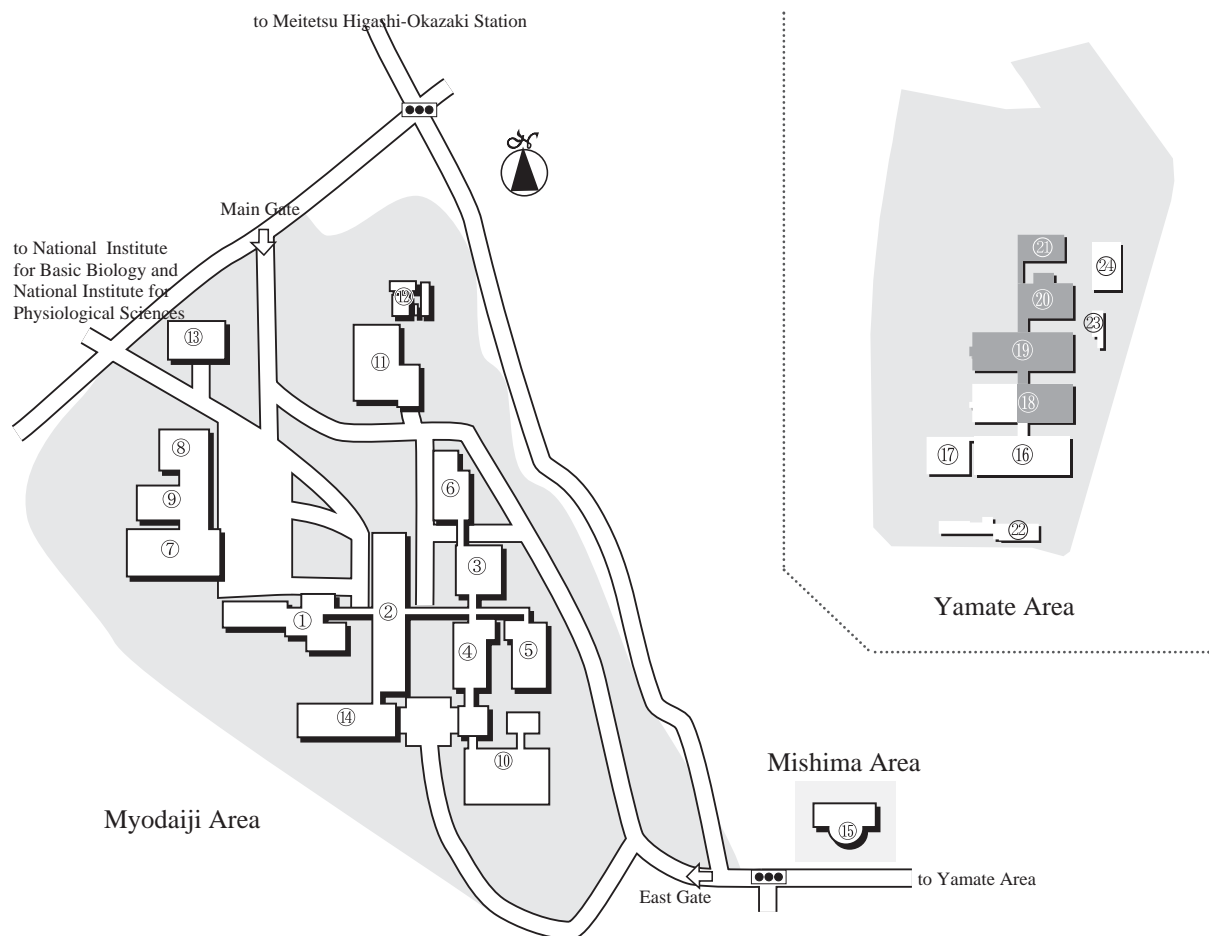
## **Administration Bureau**

KURIKI, Shigeo	Director, Okazaki Administration Office
	Director, General Affairs Department
HARUHATA, Fumio	Director, Financial Affairs Department
TAKYOU, Moriyasu	Head, General Affairs Division
HIRAO, Koji	Head, International Relations and Research Cooperation Division
HAYASHI, Masanori	Head, Financial Affairs Division
KASSAI, Isamu	Head, Procurement Division
WATANABE, Toshio	Head, Facilities Division

## BUILDINGS AND CAMPUS

The IMS campus covering 62,343 m<sup>2</sup> is situated on a low hill in the midst of Okazaki city. The inequality in the surface of the location, the hill and growing trees are preserved as much as possible, and low-storied buildings are adopted for conservation of the environment. The buildings of IMS are separated according to their functions as shown in the map below. The Research Office Building and all Research Facilities, except for the Computer Center, are linked organically to the Main Laboratory Buildings by corridors. The computer Center, Library and Administration Buildings are situated between IMS and neighboring National Institute for Basic Biology and National Institute for Physiological Sciences, since the latter two facilities are for common use amongst these three institutes.

The lodging facility of IMS called Yamate Lodge, located within ten minutes' walk, has sleeping accommodations for 15 guests and two families. Mishima Lodge, located within four minutes' walk east of IMS can accommodate 74 guests and 20 families. Scientists visiting IMS, as well as the two other institutes, can make use of these facilities. Foreign visiting scientists can also live in these lodgings with their families during their stays. The Okazaki Conference Center, with four conference rooms capable of attendance between 50~250, was built in April, 1997 in the Mishima area. The two buildings, Center for Integrative Bioscience, and Research Center for Computational Science, and research facilities of ONRI were built in February, 2002 in the Yamate Area. Four other buildings were also built in March, 2004 in the Yamate Area.



- |  |  |
|--|--|
| 1. Research Office Building                        | 13. Faculty Club                       |
| 2. Main Laboratory Building                        | 14. South Laboratory Building          |
| 3. Equipment Development Center                    | 15. Okazaki Conference Center          |
| 4. Laser Research Center for Molecular Science     | 16. Yamate Bldg. 1A                    |
| 5. Research Center for Molecular-scale Nanoscience | 17. Yamate Bldg. 1B                    |
| 6. Low-Temperature Facilities Building             | 18. Yamate Bldg. 2                     |
| 7. Computer Center                                 | 19. Yamate Bldg. 3                     |
| 8. Library   | 20. Yamate Bldg. 4                     |
| 9. Central Administration                          | 21. Yamate Bldg. 5                     |
| 10. UVSOR Facility                                 | 22. Yamate Lodge                       |
| 11. Power Station                                  | 23. Waste-Water Disposition Facilities |
| 12. Waste-Water Disposition Facilities             | 24. Power Station                      |



Okazaki (population 351,000) is 260 km west of Tokyo, and can be reached by train in approximately 3 hours from Tokyo via Shinkansen and the Meitetsu Line. The nearest large city is Nagoya, about 40 km northwest of Okazaki.



# RESEARCH ACTIVITIES I

## Department of Theoretical Studies

### I-A Theoretical Study and Design of Functional Molecular Systems: New Bonding, Structures, and Reactions

In theoretical and computational chemistry, it is an important goal to develop functional molecules with novel bonding and structures before or in cooperation with experiment. Thus, novel bonds and structures provided by heavier atoms are investigated, which are expected to serve as new building blocks for the design of functional molecules. In addition, unique spaces and flexible structures provided by large molecules and clusters are highly emphasized to develop functional molecular systems by modulating the electronic properties. Efficient computational methods are investigated to perform reliable quantum chemistry calculations of large molecular systems.

#### I-A-1 Counterion-Driven Spontaneous Polymerization of the Linear $C_{60}^{n-}$ Chains in the fcc Fullerides and Its Magic Number Behavior

LU, Jing<sup>1</sup>; NAGASE, Shigeru; ZHANG, Shuang<sup>2</sup>; PENG, Lianmao<sup>2</sup>  
(<sup>1</sup>IMS and Peking Univ.; <sup>2</sup>Peking Univ.)

[*Chem. Phys. Lett.* **395**, 199–204 (2004)]

Polymerization of  $C_{60}$  has attracted considerable interest in recent years. By using the first principle energy band calculations, it is found that the injection of electron alone into  $C_{60}$  increases the instability of the polymeric  $C_{60}$  chain, despite a decrease in the polymerization energy barrier, and cannot cause a spontaneous polymerization as previously proposed. However, inclusion of the electrostatic attraction between the  $C_{60}^{n-}$  and counterions can dramatically stabilize the polymeric  $C_{60}^{n-}$  chains at  $n = 1$  and 3, accompanied by a further decrease in the polymerization energy barrier, and eventually drives an observable spontaneous polymerization of the  $C_{60}^{n-}$  chains in the fcc fullerides at these two doping levels.

#### I-A-2 Amphoteric and Controllable Doping of Carbon Nanotubes by Encapsulation of Organic and Organometallic Molecules

LU, Jing<sup>1</sup>; NAGASE, Shigeru; YU, Dapeng<sup>2</sup>; YE, Hengqiang<sup>2</sup>; HAN, Rushan<sup>2</sup>; GAO, Zhengxiang<sup>2</sup>; ZHANG, Shuang<sup>2</sup>; PENG, Lianmao<sup>2</sup>  
(<sup>1</sup>IMS and Peking Univ.; <sup>2</sup>Peking Univ.)

[*Phys. Rev. Lett.* **93**, 116804 (4 pages) (2004)]

Single-wall carbon nanotubes (SWNTs) have attracted considerable interest as a possible application to molecular electronics. For this application, it is important to obtain both *p*- and *n*-type air-stable SWNTs and control their carrier densities. By performing density functional calculations, we show that controllable *p*- and *n*-type doping can be realized by tuning the electron affinities or ionization potentials of the organic and organometallic molecules encapsulated inside SWNTs.

This novel type of SWNT-based material offers great promise for molecular electronics because of its air stability, synthetic simplicity and the abundance of organic and organometallic molecules.

#### I-A-3 Electronic Excited States and Stabilities of Fullerenes: Isomers of $C_{78}$ and $Mg@C_{72}$

SLANINA, Zdenek; UHLÍK, Filip<sup>1</sup>; ADAMOWICZ, Ludwik<sup>2</sup>; KOBAYASHI, Kaoru; NAGASE, Shigeru  
(<sup>1</sup>Charles Univ.; <sup>2</sup>Univ. Arizona)

[*Int. J. Quantum Chem.* **100**, 610–616 (2004)]

There is one factor in relative stabilities of isomeric fullerenes that has rarely been studied so far—the contribution of excited electronic states. The contribution is clearly quantified by the electronic partition function, supposing the related excitation energies can be evaluated. As temperatures in fullerene synthesis are high, the term should be taken into account. In this article the problem is studied on two isomeric systems. One is the set of five isolated pentagon rule isomers of  $C_{78}$ , relatively well known from experiments. The other is a model set of four isomers of  $Mg@C_{72}$  (not isolated yet). It is found that the electronic partition function can cause significant changes in the computed equilibrium relative concentrations of isomers at high temperatures.

#### I-A-4 1,6,7-Trigermabicyclo[4.1.0]hept-3-en-7-yl: The Isolable Bicyclic Germyl Radical

ISHIDA, Yutaka<sup>1</sup>; SEKIGUCHI, Akira<sup>1</sup>; KOBAYASHI, Kaoru; NAGASE, Shigeru  
(<sup>1</sup>Univ. Tsukuba)

[*Organometallics* **23**, 4891–4896 (2004)]

The one-electron oxidation reaction of potassium 3,4-dimethyl-1,6,7-tris(tri-tert-butylsilyl)-1,6,7-trigermabicyclo[4.1.0]hept-3-en-7-ide with tris(pentafluorophenyl)borane in THF results in the formation of stable 3,4-dimethyl-1,6,7-tris(tri-tert-butylsilyl)-1,6,7-trigermabicyclo-[4.1.0]hept-3-en-7-yl, representing the first bicyclic germyl radical with the bicyclo[4.1.0]-

hept-3-ene skeleton. The electronic and structural aspects of the germyl radical were characterized by density functional calculations as well as X-ray crystallographic analysis and ESR spectroscopy.

#### I-A-5 Isolation of a Se-Nitrososelenol: A New Class of Reactive Nitrogen Species Relevant to Protein Se-Nitrosation

SHIMADA, Keiichi<sup>1</sup>; GOTO, Kei<sup>1</sup>; KAWASHIMA, Takayuki<sup>1</sup>; TAKAGI, Nozomi; CHOE, Yoong-Kee; NAGASE, Shigeru  
(<sup>1</sup>Univ. Tokyo.)

[*J. Am. Chem. Soc.* **126**, 13238–13239 (2004)]

Nitric oxide (NO) is a messenger molecule implicated in a number of physiological processes. In several recent reports, it has been suggested that the interactions of NO (or NO-derived species) with the SeH groups of selenoproteins are involved in NO-mediated cellular functions. To elucidate the mechanism of NO-mediated modification of selenoproteins, a stable Se-nitrosated derivative of an organoselenol, a Se-nitrososelenol (RseNO) is successfully synthesized. The observed <sup>77</sup>Se NMR and UV-vis spectra are analyzed by the gauge-including atomic orbital (GIAO) calculations at the B3LYP/6-311G (3d)[Se]:6-311G(d)[C, O, N, H]/B3LYP/6-31G(d) level and time-dependent density functional (TD-DFT) calculations at the B3LYP/6-311+G(2d)/B3LYP/6-31G(d) levels, respectively.

#### I-A-6 A New Approach to Simulate the Depolymerization Process of a Two-Dimensional Hexagonal C<sub>60</sub> Polymer

LU, Jing<sup>1</sup>; NAGASE, Shigeru; ZHANG, Shuang<sup>2</sup>; PENG, Lianmao<sup>2</sup>  
(<sup>1</sup>IMS and Peking Univ.; <sup>2</sup>Peking Univ.)

[*Chem. Phys. Lett.* **398**, 486–488 (2004)]

In a recent study, the depolymerization process of a two-dimensional hexagonal C<sub>60</sub> polymer was modeled by increasing stepwise the lattice constant, and a considerably high barrier for polymerization was calculated. In the present study, all degrees of freedom (including the lattice constant) are allowed to relax for each distance between fullerenes in order to simulate the depolymerization process of a two-dimensional hexagonal C<sub>60</sub> polymer. The resulting depolymerization barrier is significantly improved compared with the previous study in which the lattice constant was fixed though the atomic positions were relaxed.

#### I-A-7 Chemical Reactivity and Redox Property of Sc<sub>3</sub>@C<sub>82</sub>

WAKAHARA, Takatsugu<sup>1</sup>; SAKURABA, Akihiro<sup>2</sup>; IIDUKA, Yuko<sup>1</sup>; OKAMURA, Mutsuo<sup>2</sup>; TSUCHIYA, Takahiro<sup>1</sup>; MAEDA, Yutaka<sup>1</sup>; AKASAKA, Takeshi<sup>1</sup>; OKUBO, Shingo; KATO, Tatsuhisa; KOBAYASHI, Kaoru; NAGASE, Shigeru; KADISH, Karl M.<sup>3</sup>

(<sup>1</sup>Univ. Tsukuba; <sup>2</sup>Niigata Univ.; <sup>3</sup>Univ. Houston)

[*Chem. Phys. Lett.* **398**, 553–556 (2004)]

The redox property of Sc<sub>3</sub>@C<sub>82</sub> is investigated by using disilirane as a chemical probe. The redox potential of Sc<sub>3</sub>@C<sub>82</sub> in *o*-dichlorobenzene shows a high reactivity attributable to its high electron-accepting and -donating ability. No ESR signal is observed at room temperature for Sc<sub>3</sub>@C<sub>82</sub> in the presence of pyridine, indicating formation of the diamagnetic Sc<sub>3</sub>@C<sub>82</sub> anion. The diamagnetic Sc<sub>3</sub>@C<sub>82</sub> anion is also prepared electrochemically in 1,2-dichlorobenzene. The reactivity and redox properties of Sc<sub>3</sub>@C<sub>82</sub> are characterized by calculating the electron affinity and ionization potentials using density functional theory.

#### I-A-8 Reduction of Endohedral Metallofullerenes: A Convenient Method for Isolation

TSUCHIYA, Takahiro<sup>1</sup>; WAKAHARA, Takatsugu<sup>1</sup>; SHIRAKURA, Shingo<sup>2</sup>; MAEDA, Yutaka<sup>1</sup>; AKASAKA, Takeshi<sup>1</sup>; KOBAYASHI, Kaoru; NAGASE, Shigeru; KATO, Tatsuhisa; KADISH, Karl M.<sup>3</sup>  
(<sup>1</sup>Univ. Tsukuba; <sup>2</sup>Niigata Univ.; <sup>3</sup>Univ. Houston)

[*Chem. Mater.* **16**, 4343–4346 (2004)]

Isolation of endohedral metallofullerenes has been often carried out using a multistage high-performance liquid chromatography (HPLC) method. However, this method is tedious and time-consuming work, making it difficult to obtain macroscopic quantities of pure endohedral metallofullerene samples. We report herein a selective electrochemical reduction of endohedral metallofullerenes from extracts of carbon soot and a convenient separation method of endohedral metallofullerenes and empty fullerenes. A chemical oxidation of the endohedral metallofullerene anions is also discussed.

#### I-A-9 Dispersion of Single-Walled Carbon Nanotube Bundles in Nonaqueous Solution

MAEDA, Yutaka<sup>1</sup>; KIMURA, Shin-ichi<sup>2</sup>; HIRASHIMA, Yuya<sup>1</sup>; KANDA, Makoto<sup>1</sup>; LIAN, Yongfu<sup>2</sup>; WAKAHARA, Takatsugu<sup>2</sup>; AKASAKA, Takeshi<sup>2</sup>; HASEGAWA, Tadashi<sup>1</sup>; TOKUMOTO, Hiroshi<sup>3</sup>; SHIMIZU, Tetsuo<sup>4</sup>; KATAURA, Hiromichi<sup>4</sup>; MIYAUCHI, Yuhei<sup>5</sup>; MARUYAMA, Shigeo<sup>5</sup>; KOBAYASHI, Kaoru; NAGASE, Shigeru  
(<sup>1</sup>Tokyo Gakugei Univ.; <sup>2</sup>Univ. Tsukuba; <sup>3</sup>Hokkaido Univ.; <sup>4</sup>AIST; <sup>5</sup>Univ. Tokyo)

[*J. Phys. Chem. B* **108**, 18395–18397 (2004)]

Although single-walled carbon nanotubes (SWNTs) have interesting mechanical and electrical properties, their practical applications have been hindered by the poor dispersibility and solubility. Therefore, the effective dispersion of bundled SWNTs in organic solvents is important, which makes homogenous chemical reac-

tions possible. We report the observation of photoluminescence from SWNTs dispersed in a tetrahydrofuran(THF)/octylamine solution, providing the first clear evidence for individual SWNTs in nonaqueous solution. We also report the effective amine-assisted dispersion of C<sub>60</sub> and La@C<sub>82</sub> peapods. This solution phase handling is applicable to the analysis of the electronic properties and modification of SWNTs and peapods.

#### I-A-10 Regioselective Carbon–Carbon Bond Cleavage of an Open-Cage Diketone Derivative of [60]Fullerene by Reaction with Aromatic Hydrazones

IWAMATSU, Sho-ichi<sup>1</sup>; KUWAYAMA, Toshiki<sup>1</sup>; KOBAYASHI, Kaoru; NAGASE, Shigeru; MURATA, Shizuaki<sup>1</sup>  
(<sup>1</sup>Nagoya Univ.)

[*Synthesis* 2962–2964 (2004)]

Opening a hole on the fullerene cage by a controlled carbon–carbon bond cleavage is of current interest. It is found that the addition of an aromatic hydrazone to the diketone derivative of C<sub>60</sub> takes place with a regioselective C–C bond scission, which leads to a ring-expanded product having a 16-membered ring orifice.

#### I-A-11 Gibbs Energy-Based Treatment of Metallofullerenes: Ca@C<sub>72</sub>, Ca@C<sub>74</sub>, Ca@C<sub>82</sub>, and La@C<sub>82</sub>

SLANINA, Zdenek<sup>1</sup>; ADAMOWICZ, Ludwik<sup>2</sup>; KOBAYASHI, Kaoru; NAGASE, Shigeru  
(<sup>1</sup>IMS and Academia Sinica; <sup>2</sup>Univ. Arizona)

[*Mol. Sim.* 31, 71–77 (2005)]

The paper surveys ongoing computations on endohedral fullerene systems, combining the treatments of quantum chemistry and statistical mechanics. Relative concentrations of four isomers of Ca@C<sub>72</sub>, six isomers of Ca@C<sub>74</sub>, nine isomers of Ca@C<sub>82</sub>, and four isomers of La@C<sub>82</sub> are evaluated using the Gibbs energy based on density-functional theory computations. The results illustrate the enthalpy–entropy interplay in the systems produced under high temperatures. Approximations for description of the encapsulate motions are analyzed.

#### I-A-12 Chemical Reactivities of the Cation and Anion of M@C<sub>82</sub> (M = Y, La, and Ce)

MAEDA, Yutaka<sup>1</sup>; MIYASHITA, Jun<sup>1</sup>; HASEGAWA, Tadashi<sup>1</sup>; WAKAHARA, Takatsugu<sup>2</sup>; TSUCHIYA, Takahiro<sup>2</sup>; FENG, Lai<sup>2</sup>; LIAN, Yongfu<sup>2</sup>; AKASAKA, Takeshi<sup>2</sup>; KOBAYASHI, Kaoru; NAGASE, Shigeru; KAKO, Masahiro<sup>3</sup>; YAMAMOTO, Kazunori<sup>4</sup>; KADISH, Karl M.<sup>5</sup>  
(<sup>1</sup>Tokyo Gakugei Univ.; <sup>2</sup>Univ. Tsukuba; <sup>3</sup>Univ. Electro-Communications; <sup>4</sup>Japan Nuclear Fuel Cycle Development Inst.; <sup>5</sup>Univ. Houston)

[*J. Am. Chem. Soc.* 127, 2143–2146 (2005)]

The chemical reduction and oxidation of M@C<sub>82</sub> (M = Y, La, and Ce) afford the corresponding anion and cation, respectively, which show unique and interesting chemical reactivities. It is found that the successful reversible gain or loss of electrons by ionization is useful for controlling the stability and reactivity of M@C<sub>82</sub> toward both nucleophiles and electrophiles. The reactivity is discussed by calculating the HOMO and LUMO energy levels.

#### I-A-13 Systematic Studies on Redox Behavior of Homonuclear Double-Bond Compounds of Heavier Group 15 Elements

SASAMORI, Takahiro<sup>1</sup>; MIEDA, Eiko<sup>1</sup>; NAGAHORA, Noriyoshi<sup>1</sup>; TAKEDA, Nobuhiro<sup>1</sup>; TAKAGI, Nozomi; NAGASE, Shigeru; TOKITOH, Norihiro<sup>1</sup>  
(<sup>1</sup>Kyoto Univ.)

[*Chem. Lett.* 166–167 (2005)]

Stable double bonds between heavier group 15 elements have long attracted considerable interest in main group chemistry. The electronic properties of RE=ER (E = P, Sb, and Bi; R = 2,6-bis[bis(trimethylsilyl)methyl]-4-[tris(trimethylsilyl)6-methyl]phenyl) synthesized recently are systematically investigated based on the measurement of cyclic voltammetry and density functional calculations. It is emphasized that relativistic effects are very important for the systematic understanding of the nature of double bonds in RM=MR.

#### I-A-14 Syntheses and Structures of Hypervalent Pentacoordinate Carbon and Boron Compounds Bearing an Anthracene Skeleton—Elucidation of Hypervalent Interaction Based on X-Ray Analysis and DFT Calculation

YAMASHITA, Makoto<sup>1</sup>; YAMAMOTO, Yohsuke<sup>1</sup>; AKIBA, Kin-ya<sup>2</sup>; HASHIZUME, Daisuke<sup>3</sup>; IWASAKI, Fujiko<sup>3</sup>; TAKAGI, Nozomi; NAGASE, Shigeru  
(<sup>1</sup>Hiroshima Univ.; <sup>2</sup>Waseda Univ.; <sup>3</sup>Univ. Electro-Communications)

[*J. Am. Chem. Soc.* 127, 4354–4371 (2005)]

Pentacoordinate and tetracoordinate carbon and boron compounds bearing an anthracene skeleton with two oxygen or nitrogen atoms at the 1,8-positions are synthesized by the use of four newly synthesized tridentate ligand precursors, and characterized by X-ray crystallographic analysis. To provide theoretical insight into the nature of hypervalent interactions, the topology of electron density distributions around hypervalent bonds is analyzed using density functional calculations and X-ray results. The existence of weak apical hypervalent bonds of considerable ionic character is reported.

**I-A-15 Adsorption Configuration of NH<sub>3</sub> on Single-Wall Carbon Nanotubes**

LU, Jing<sup>1</sup>; NAGASE, Shigeru; MAEDA, Yutaka<sup>2</sup>; WAKAHARA, Takatsugu<sup>3</sup>; NAKAHODO, Tsukasa<sup>3</sup>; AKASAKA, Takeshi<sup>3</sup>; YU, Dapeng<sup>4</sup>; GAO, Zhengxiang<sup>4</sup>; HAN, Rushan<sup>4</sup>; YE, Hengqiang<sup>4</sup>

(<sup>1</sup>IMS and Peking Univ.; <sup>2</sup>Tokyo Gakugei Univ.; <sup>3</sup>Univ. Tsukuba; <sup>4</sup>Peking Univ.)

[*Chem. Phys. Lett.* **405**, 90–92 (2005)]

The electronic properties of single-wall carbon nanotubes (SWNTs) are significantly changed when NH<sub>3</sub> molecules are adsorbed on the surface of SWNTs. Density functional calculations show that the absorption energies depend on the electronic structures of SWNTs that are metallic or semiconducting. Metallic SWNTs interact more strongly with NH<sub>3</sub> than semiconducting SWNTs, when comparison is made for SWNTs having similar diameters. Hydrogen-bond-like links dominate the attraction between NH<sub>3</sub> and SWNTs.

**I-A-16 Structural Characterization of Y@C<sub>82</sub>**

FENG, Lai<sup>1</sup>; WAKAHARA, Takatsugu<sup>1</sup>; TSUCHIYA, Takahiro<sup>1</sup>; MAEDA, Yutaka<sup>2</sup>; LIAN, Yongfu<sup>1</sup>; AKASAKA, Takeshi<sup>1</sup>; MIZOROGI, Naomi; KOBAYASHI, Kaoru; NAGASE, Shigeru; KADISH, Karl M.<sup>3</sup>

(<sup>1</sup>Univ. Tsukuba; <sup>2</sup>Tokyo Gakugei Univ.; <sup>3</sup>Univ. Houston)

[*Chem. Phys. Lett.* **405**, 274–277 (2005)]

The cation and anion of Y@C<sub>82</sub> are prepared by controlled potential electrolysis, and their stabilities are investigated. The anion is found to be much more stable than the cation under an air atmosphere. These are confirmed by performing theoretical calculations. It is determined that the cage structure of Y@C<sub>82</sub> has C<sub>2v</sub> symmetry by observing the <sup>13</sup>C NMR spectrum of the stable diamagnetic anion. This agrees well with theoretical prediction.

**I-A-17 Synthesis and Characterization of Exohedrally Silylated M@C<sub>82</sub> (M = Y and La)**

YAMADA, Michio<sup>1</sup>; FENG, Lai<sup>1</sup>; WAKAHARA, Takatsugu<sup>1</sup>; TSUCHIYA, Takahiro<sup>1</sup>; MAEDA, Yutaka<sup>2</sup>; LIAN, Yongfu<sup>1</sup>; KAKO, Masahiro<sup>3</sup>; AKASAKA, Takeshi<sup>2</sup>; KATO, Tatsuhisa<sup>4</sup>; KOBAYASHI, Kaoru; NAGASE, Shigeru

(<sup>1</sup>Univ. Tsukuba; <sup>2</sup>Tokyo Gakugei Univ.; <sup>3</sup>Univ. Electro-Communications; <sup>4</sup>Josai Univ.)

[*J. Phys. Chem. B* **109**, 6049–6051 (2005)]

The silylation of endohedral mono-metallofullerenes (Y@C<sub>82</sub> and La@C<sub>82</sub>) is carried out, and the adducts are isolated by HPLC separation. As the first examples of the tuning of electronic properties of mono-metallofullerenes by exohedral addition, it is shown that the

bis-silylated derivatives of Y@C<sub>82</sub> and La@C<sub>82</sub> have significantly lower oxidation and higher reduction potentials than Y@C<sub>82</sub> and La@C<sub>82</sub>. Bis-silylation is very effective for modifying the electronic properties of endohedral metallofullerenes as well as empty fullerenes.

**I-A-18 Synthesis and Characterization of Stable Hypervalent Carbon Compounds (10-C-5) Bearing a 2,6-Bis(*p*-substituted phenyloxymethyl)benzene Ligand**

AKIBA, Kin-ya<sup>1</sup>; MORIYAMA, Yuji<sup>2</sup>; MIZOZOE, Mitsuhiro<sup>2</sup>; INOHARA, Hideki<sup>2</sup>; NISHII, Takako<sup>2</sup>; YAMAMOTO, Yohsuke<sup>2</sup>; MINOURA, Mao<sup>2</sup>; HASHIZUME, Daisuke<sup>3</sup>; IWASAKI, Fujiko<sup>3</sup>; TAKAGI, Nozomi; ISHIMURA, Kazuya; NAGASE, Shigeru

(<sup>1</sup>Waseda Univ.; <sup>2</sup>Hiroshima Univ.; <sup>3</sup>Univ. Electro-Communications)

[*J. Am. Chem. Soc.* **127**, 5893–5901 (2005)]

Stable hypervalent carbon compounds (10-C-5) bearing a 2,6-bis(*p*-tolylloxymethyl)benzene ligand are synthesized and their structures are characterized by X-ray analysis and theoretical calculations. Among these, sterically flexible compounds bearing two O (*p*-Tol) groups or two O (*p*-CH<sub>3</sub>OC<sub>6</sub>H<sub>4</sub>) groups take symmetrical structures with two almost equal C–O distances. The electron density distribution analysis by accurate X-ray measurements and theoretical calculations show that the central carbon atom forms a weak and ionic hypervalent bond with the two oxygen atoms, as suggested by the small electron density ( $\rho(r)$ ) and small positive Laplacian ( $\nabla^2\rho(r)$ ) values at the bond critical points.

**I-A-19 Practical Performance Assessment of Accompanying Coordinate Expansion Recurrence Relation Algorithm for Computation of Electron Repulsion Integrals**

KATOUDA, Michio; KOBAYASHI, Masato<sup>1</sup>; NAKAI, Hiromi<sup>1</sup>; NAGASE, Shigeru

(<sup>1</sup>Waseda Univ.)

[*J. Theor. Comput. Chem.* **4**, 139–149 (2005)]

In the applications of molecular orbital and density functional methods, it is considerably time-consuming to calculate two-electron repulsion integrals for large molecular systems. A program code is developed to calculate effectively electron repulsion integrals based on the accompanying coordinate expansion recurrence relation (ACE-RR) algorithm. The present ACE-RR method is comparable to or at most 30% faster than the Pople–Hehre method. Furthermore, the ACE-RR method is drastically faster than the Dupuis–Rys–King method when the contraction of basis sets is high.

**I-A-20 2D NMR Characterization of the La@C<sub>82</sub> Anion**

TSUCHIYA, Takahiro<sup>1</sup>; WAKAHARA, Takatsugu<sup>1</sup>;

**MAEDA, Yutaka<sup>2</sup>; AKASAKA, Takeshi<sup>1</sup>;  
WAELECHLI, Markus<sup>3</sup>; KATO, Tatsuhisa<sup>4</sup>;  
OKUBO, Hiroshi<sup>5</sup>; MIZOROGI, Naomi;  
KOBAYASHI, Kaoru; NAGASE, Shigeru**  
(<sup>1</sup>Univ. Tsukuba; <sup>2</sup>Tokyo Gakugei Univ.; <sup>3</sup>Bruker  
Boispin, Co. Ltd.; <sup>4</sup>Josai Univ.; <sup>5</sup>Toyo Tanso Co. Ltd.)

[*Angew. Chem., Int. Ed.* **44**, 3282–3285 (2005)]

NMR spectroscopy has been very often employed as a powerful tool for elucidating the cage symmetry of endohedral metallofullerenes. However, it remains an important goal to verify the bond connectivity and assign the NMR lines, as this is essential for full structural characterization of endohedral metallofullerenes. As the first example for metallofullerenes, the mapping of the bond connectivity in the carbon cage of the La@C<sub>82</sub> anion and definitive assignment of the NMR lines are reported with the help of density functional calculations. It is suggested that the 2D INADEQUATE (incredible natural abundance double quantum transfer experiment) NMR measurement can be used as an alternative method to X crystallographic analysis for the structural characterization of endohedral metallofullerenes.

#### I-A-21 Open-Cage Fullerene Derivatives Suitable for the Encapsulation of a Hydrogen Molecule

**IWAMATSU, Sho-ichi<sup>1</sup>; MURATA, Shizuaki<sup>1</sup>;  
ANDOH, Yukihiko<sup>1</sup>; MINOURA, Masayuki<sup>1</sup>;  
KOBAYASHI, Kaoru; MIZOROGI, Naomi;  
NAGASE, Shigeru**  
(<sup>1</sup>Nagoya Univ.)

[*J. Org. Chem.* **70**, 4820–4825 (2005)]

The encapsulation of a hydrogen molecule into an open-cage fullerene having a 16-membered ring orifice is successfully performed. The efficiency of encapsulation depends strongly on both H<sub>2</sub> pressure and temperature. The encapsulated H<sub>2</sub> molecule is released by heating. The activation energy barriers for this process are determined to be 22–24 kcal/mol. From the differential scanning calorimetry measurement and density functional calculations, it is discussed whether the encapsulated H<sub>2</sub> molecule is stabilized or destabilized inside the open-cage fullerene.

#### I-A-22 Computed Structure and Energetics of La@C<sub>60</sub>

**SLANINA, Zdenek; LEE, Shyi-Long<sup>1</sup>;  
ADAMOWICZ, Ludwik<sup>2</sup>; UHLÍK, Filip<sup>3</sup>; NAGASE, Shigeru**  
(<sup>1</sup>Natl. Chung-Cheng Univ.; <sup>2</sup>Univ. Arizona; <sup>3</sup>Charles Univ.)

[*Int. J. Quantum. Chem.* **104**, 272–277 (2005)]

The molecular and electronic structures of La@C<sub>60</sub> are investigated by density functional calculations. The La atom is not located in the cage center, but is shifted

toward the wall. There is a substantial charge transfer from La to C<sub>60</sub>, at some levels of theory amounting roughly to three electrons. A larger binding energy is calculated for La@C<sub>60</sub>. However, the entropy term also influences the association equilibrium significantly, so that the standard Gibbs-energy change depends strongly on temperature. The reasons why La@C<sub>60</sub> could not be isolated yet are briefly discussed, as well as a possible relationship to superconductivity.

#### I-A-23 Metallic Phase in the Metal-Intercalated Higher Fullerene Rb<sub>8,8(7)</sub>C<sub>84</sub>

**RIKIISHI, Yoshie<sup>1</sup>; KASHINO, Yoko<sup>1</sup>; KUSAI, Haruka<sup>1</sup>; TAKABAYASHI, Yasuhiro<sup>1</sup>;  
KUWAHARA, Eiji<sup>1</sup>; KUBOZONO, Yoshihiro<sup>1,2</sup>;  
KAMBE, Takashi<sup>1</sup>; TAKENOBU, Taishi<sup>3</sup>; IWASA, Yoshihiro<sup>3</sup>; MIZOROGI, Naomi; NAGASE, Shigeru; OKADA, Susumu<sup>2</sup>**  
(<sup>1</sup>Okayama Univ.; <sup>2</sup>Univ. Tsukuba; <sup>3</sup>Tohoku Univ.)

[*Phys. Rev. B* **71**, 224118 (6 pages) (2005)]

A new material of higher fullerene, Rb<sub>x</sub>C<sub>84</sub>, is synthesized by intercalating Rb metals into C<sub>84</sub> crystals. The Rb<sub>x</sub>C<sub>84</sub> crystals show a simple cubic (sc) structure with lattice constants of 16.82(2) Å at 6.5 K and 16.87(2) Å at 295 K. The Rietveld refinements are achieved with the space group, *Pa*3, based on a model that the C<sub>2</sub> axis of D<sub>2d</sub>-C<sub>84</sub> aligned along [111]. The sample composition is determined to be Rb<sub>8,8(7)</sub>C<sub>84</sub>. The ESR spectrum at 303 K is composed of a broad peak with a peak-to-peak linewidth of Δ*H*<sub>pp</sub> = 220 G and a narrow peak with Δ*H*<sub>pp</sub> = 24 G. Temperature dependence of the broad peak clearly show a metallic behavior. The metallic behavior is discussed based on theoretical calculations.

#### I-A-24 Interplay of Single-Wall Carbon Nanotubes and Encapsulated La@C<sub>82</sub>, La<sub>2</sub>@C<sub>80</sub>, and Sc<sub>3</sub>N@C<sub>80</sub>

**LU, Jing<sup>1</sup>; NAGASE, Shigeru; RE, Suyong;  
ZHANG, Xinwei<sup>2</sup>; YU, Dapeng<sup>3</sup>; ZHANG, Jin<sup>3</sup>;  
HAN, Rushan<sup>3</sup>; GAO, Zhengxiang<sup>3</sup>; YE, Hengqiang<sup>3</sup>; ZHANG, Shuang<sup>3</sup>; PENG, Lianmao<sup>3</sup>**  
(<sup>1</sup>IMS and Peking Univ.; <sup>2</sup>Inst. Appl. Phys. Comput. Math.; <sup>3</sup>Peking Univ.)

[*Phys. Rev. B* **71**, 235417 (5 pages) (2005)]

Encapsulation of endohedral metallofullerenes (La@C<sub>82</sub>, La@C<sub>80</sub>, and Sc<sub>3</sub>N@C<sub>80</sub>) inside single-wall carbon nanotubes (SWNTs) is investigated by using first-principles calculations. It is found that La@C<sub>82</sub>, La<sub>2</sub>@C<sub>80</sub>, and Sc<sub>3</sub>N@C<sub>80</sub> are endothermically encapsulated inside (17,0) SWNT, while they are exothermically encapsulated inside the (14,7) and (19,0) SWNTs. Electron transfer takes place from SWNTs to strongly electrophilic La@C<sub>82</sub> and La<sub>2</sub>@C<sub>80</sub>. Dependent on the tube chirality, the Van Hove singularity positions of SWNT is significantly shifted by a local 3% radial strain induced by the insertion of metallofullerenes.

### I-A-25 Structural Evolution of [2+1] Cycloaddition Derivatives of Single-Wall Carbon Nanotubes: From Open Structure to Closed Three-Membered Ring Structure with Increasing Tube Diameter

LU, Jing<sup>1</sup>; NAGASE, Shigeru; ZHANG, Xinwei<sup>2</sup>; MAEDA, Yutaka<sup>3</sup>; WAKAHARA, Takatsugu<sup>4</sup>; NAKAHODO, Tsukasa<sup>4</sup>; TSUCHIYA, Takahiro<sup>4</sup>; AKASAKA, Takeshi<sup>4</sup>; YU, Dapeng<sup>5</sup>; GAO, Zhengxiang<sup>5</sup>; HAN, Rushan<sup>5</sup>; YE, Hengqiang<sup>5</sup>  
(<sup>1</sup>IMS and Peking Univ.; <sup>2</sup>Inst. Appl. Phys. Computational Math.; <sup>3</sup>Tokyo Gakugei Univ.; <sup>4</sup>Univ. Tsukuba; <sup>5</sup>Peking Univ.)

[THEOCHEM 725, 255–257 (2005)]

Sidewall functionalization of single-wall carbon nanotubes (SWNTs) is currently of considerable interest. By using density functional theory calculations, it is found that the [2+1] cycloaddition derivatives of the armchair (*m,m*) SWNTs evolve from an open structure to a closed three-membered ring structure when *m* > 11 for NH addition, *m* > 10 for O and CH<sub>2</sub> additions, and *m* > 5 for SiH<sub>2</sub> addition. The diameter upper limit of the opening of the sidewall of SWNTs upon [2+1] cycloaddition is predicted to be about 15 Å.

### I-A-26 Missing Metallofullerene La@C<sub>74</sub>

NIKAWA, Hidefumi<sup>1</sup>; KIKUCHI, Takashi<sup>1</sup>; WAKAHARA, Takatsugu<sup>1</sup>; HAKAHODO, Tsukasa<sup>1</sup>; TSUCHIYA, Takahiro<sup>1</sup>; RAHMAN, G. M. Aminur<sup>1</sup>; AKASAKA, Takeshi<sup>1</sup>; MAEDA, Yutaka<sup>2</sup>; YOZA, Kenji<sup>3</sup>; HORN, Ernst<sup>4</sup>; YAMAMOTO, Kazunori<sup>5</sup>; MIZOROGI, Naomi; NAGASE, Shigeru  
(<sup>1</sup>Univ. Tsukuba; <sup>2</sup>Tokyo Gakugei Univ.; <sup>3</sup>Bruker AXS K. K.; <sup>4</sup>Rikkyo Univ.; <sup>5</sup>Power Reactor Nuclear Fuel Development Co.)

[J. Am. Chem. Soc. 127, 9684–9685 (2005)]

Since the first extraction of La@C<sub>82</sub> in 1991, many soluble endohedral metallofullerenes have been separated and characterized. However, insoluble metallofullerenes such as La@C<sub>60</sub> and La@C<sub>74</sub> have not yet been isolated. The missing La@C<sub>74</sub> is isolated as a stable derivative, La@C<sub>74</sub> (C<sub>6</sub>H<sub>3</sub>Cl<sub>2</sub>). The structure is determined by X-ray crystallographic analysis and the properties are discussed on the basis of theoretical calculations. La@C<sub>74</sub> has considerable radical character on the C<sub>74</sub> (D<sub>3h</sub>) surface, and is trapped by the dichlorophenyl radical produced during extraction.

### I-A-27 Chemical Reactivity of Sc<sub>3</sub>N@C<sub>80</sub> and La<sub>2</sub>@C<sub>80</sub>

IIDUKA, Yuko<sup>1</sup>; IKENAGA, Ozora<sup>1</sup>; SAKURABA, Akihiro<sup>2</sup>; WAKAHARA, Takatsugu<sup>1</sup>; TSUCHIYA, Takahiro<sup>1</sup>; MAEDA, Yutaka<sup>3</sup>; NAKAHODO, Tsukasa<sup>1</sup>; AKASAKA, Takeshi<sup>1</sup>; KAKO, Masahiro<sup>4</sup>; MIZOROGI, Naomi; NAGASE, Shigeru

(<sup>1</sup>Univ. Tsukuba; <sup>2</sup>Niigata Univ.; <sup>3</sup>Tokyo Gakugei Univ.; <sup>4</sup>Univ. Electro-Communications)

[J. Am. Chem. Soc. 127, 9956–9957 (2005)]

For both Sc<sub>3</sub>N@C<sub>80</sub> and La<sub>2</sub>@C<sub>80</sub>, the carbon cage originates from the I<sub>h</sub> isomer of C<sub>80</sub> and has an electronic structure described as C<sub>80</sub><sup>6-</sup>. Despite this similarity, it is found that Sc<sub>3</sub>N@C<sub>80</sub> has a much lower thermal reactivity toward disilirane than La<sub>2</sub>@C<sub>80</sub>. This is the first example of reactivity difference caused by endohedral species. Theoretical calculations show that Sc<sub>3</sub>N@C<sub>80</sub> and La<sub>2</sub>@C<sub>80</sub> have almost the same HOMO levels. However, Sc<sub>3</sub>N@C<sub>80</sub> has a much higher LUMO level than La<sub>2</sub>@C<sub>80</sub>. The LUMO of Sc<sub>3</sub>N@C<sub>80</sub> is delocalized not only on the Sc<sub>3</sub>N cation but also on the C<sub>80</sub><sup>6-</sup> cage. In contrast, the LUMO of La<sub>2</sub>@C<sub>80</sub> is localized on the two La<sup>3+</sup> cation and is more suitable as an electron accommodation.

### I-A-28 Large-Scale Separation of Metallic and Semiconducting Single-Walled Carbon Nanotubes

MAEDA, Yutaka<sup>1</sup>; KIMURA, Shin-ichi<sup>2</sup>; KANDA, Makoto<sup>1</sup>; HIRASHIMA, Yuya<sup>1</sup>; HASEGAWA, Tadashi<sup>1</sup>; WAKAHARA, Takatsugu<sup>2</sup>; LIAN, Yongfu<sup>2</sup>; NAKAHODO, Tsukasa<sup>2</sup>; TSUCHIYA, Takahiro<sup>2</sup>; AKASAKA, Takeshi<sup>2</sup>; LU, Jing<sup>3</sup>; ZHANG, Xinwei<sup>3</sup>; GAO, Zhengxiang<sup>3</sup>; YU, Yapeng<sup>3</sup>; NAGASE, Shigeru; KAZAOUI, Said<sup>4</sup>; MINAMI, Nobutsugu<sup>4</sup>; SHIMIZU, Tetsuo<sup>4</sup>; TOKUMOTO, Hiroshi<sup>5</sup>; SAITO, Riichiro<sup>6</sup>  
(<sup>1</sup>Tokyo Gakugei Univ.; <sup>2</sup>Univ. Tsukuba; <sup>3</sup>Peking Univ.; <sup>4</sup>AIST; <sup>5</sup>Hokkaido Univ.; <sup>6</sup>Tohoku Univ.)

[J. Am. Chem. Soc. 127, 10287–10290 (2005)]

In the applications of single-walled carbon nanotubes (SWNTs), it is extremely important to separate semiconducting and metallic SWNTs. Although several methods have been reported for the separation, only low yields have been achieved at great expense. Theoretical calculations confirm that metallic SWNTs are more strongly adsorbed by amines than semiconducting SWNTs and the adsorbed amines are removable after separation because of the small absorption energies. Based on this confirmation, we have developed a separation method involving a dispersion-centrifugation process in a tetrahydrofuran solution of amine, which makes metallic SWNTs highly concentrated to 87% in a simple way.

### I-A-29 Encapsulation of La@C<sub>82</sub> and La<sub>2</sub>@C<sub>80</sub> inside Single-Walled Boron Nitride Nanotubes

SONG, Wei<sup>1</sup>; NI, Ming<sup>1</sup>; LU, Jing<sup>1</sup>; GAO, Zhengxiang<sup>1</sup>; NAGASE, Shigeru; YU, Dapeng<sup>1</sup>; YE, Hengqiang<sup>1</sup>; ZHANG, Xinwei<sup>2</sup>  
(<sup>1</sup>Peking Univ.; <sup>2</sup>Inst. Appl. Phys. Computational Math.)

[THEOCHEM 730, 119–122 (2005)]

As a new type of boron and nitrogen peapods, the possible encapsulation of endohedral metallofullerenes inside single-walled boron nitride nanotubes (BNNTs) is investigated by first-principle calculations, to make comparison with the corresponding carbon peapods. It is found that  $\text{La@C}_{82}$  and  $\text{La}_2\text{@C}_{80}$  can be exothermically encapsulated inside the (17,0) and (14,7) BNNTs. The minimum diameter for exothermic encapsulation is predicted to be 13.5 Å. The features of band structures are also discussed.

## I-B Prediction of Protein Tertiary Structures and Protein Folding Problem

Prediction of the three-dimensional structures of protein molecules by computer simulations is a very challenging problem in theoretical molecular science. The difficulty of the problem lies in two facts: (1) the inclusion of accurate solvent effects is non-trivial and time-consuming (2) there exist a huge number of local minima in the energy function, forcing conventional simulations to get trapped in states of energy local minima. We have been exploring the strategies that allow us to overcome these difficulties and to study the protein folding mechanism by directly folding proteins.

### I-B-1 Classification and Prediction of Low-Energy Membrane Protein Helix Configurations by Replica-Exchange Monte Carlo Method

KOKUBO, Hironori<sup>1</sup>; OKAMOTO, Yuko  
(<sup>1</sup>SOKENDAI)

[*J. Phys. Soc. Jpn.* **73**, 2571 (2004)]

The effectiveness of our classification and prediction method for transmembrane helix configurations of membrane proteins by replica-exchange simulations is tested with glycoporphin A transmembrane dimer. Replica-exchange simulations can sample wide configurational space without getting trapped in local-minimum free energy states and we can find stable structures at low temperatures. We classify low-energy configurations into clusters of similar structures by the principal component analysis. These clusters are identified as the global- and local-minimum free energy states. Our classifications revealed that there are only two major groups of similar structures in the case of the simulation with the dielectric constant  $\epsilon = 1.0$  and five such groups in the case of  $\epsilon = 4.0$ . The global-minimum free energy state in the case of  $\epsilon = 1.0$  is very close to the structure of the NMR experiments and the prediction was successful, while in the case of  $\epsilon = 4.0$  not the global-minimum but a local-minimum free energy state corresponds to the native structure. It is shown that the global-minimum free energy state at low temperatures is also the global-minimum potential energy state in both cases.

### I-B-2 Combination of the Replica-Exchange Monte Carlo Method and the Reference Interaction Site Model Theory for Simulating a Peptide Molecule in Aqueous Solution

MITSUTAKE, Ayori<sup>1</sup>; KINOSHITA, Masahiro<sup>2</sup>;  
OKAMOTO, Yuko; HIRATA, Fumio  
(<sup>1</sup>Keio Univ.; <sup>2</sup>Kyoto Univ.)

[*J. Phys. Chem. B* **108**, 19002 (2004)]

This article reports the first attempt to combine the replica-exchange Monte Carlo method and the reference interaction site model (RISM) theory for simulating a peptide molecule in aqueous solution. The energy function is the sum of the conformational energy and the solvation free energy. The solvation free energy for a fixed conformation of the peptide molecule is calculated

using the RISM theory. The replica-exchange method is modified so that the dependence of the energy function on the temperature can be incorporated. The effectiveness of the combined approach is demonstrated for Met-enkephalin in water. It is argued that the number of replicas required for a peptide molecule immersed in water is drastically reduced by employing the combined approach. Solvation properties of Met-enkephalin are discussed and the free energy surface in gas phase is compared with that in water.

### I-B-3 Multi-Overlap Molecular Dynamics Methods for Biomolecular Systems

ITOH, Satoru G.<sup>1</sup>; OKAMOTO, Yuko  
(<sup>1</sup>SOKENDAI)

[*Chem. Phys. Lett.* **400**, 308 (2004)]

We propose a molecular dynamics method for the multi-overlap algorithm. By utilizing a non-Boltzmann weight factor, this method realizes a random walk in the overlap space at a constant temperature and explores widely in the configurational space, where the overlap of a configuration with respect to a reference state is a measure for structural similarity. We can obtain detailed information about the free-energy landscape and the transition states among any specific reference conformations at that temperature. We also introduce a multi-dimensional extension of the multi-overlap algorithm. Applying this multi-dimensional method to a penta peptide, Met-enkephalin, we demonstrate its effectiveness.

### I-B-4 Secondary-Structure Preferences of Force Fields for Proteins Evaluated by Generalized-Ensemble Simulations

YODA, Takao<sup>1</sup>; SUGITA, Yuji<sup>2</sup>; OKAMOTO, Yuko  
(<sup>1</sup>Nagahama Inst. Bio-Sci. Tech.; <sup>2</sup>Univ. Tokyo)

[*Chem. Phys.* **307**, 269 (2004)]

Secondary-structure forming tendencies are examined for six well-known protein force fields: AMBER-94, AMBER96, AMBER99, CHARMM22, OPLS-AA/L, and GROMOS96. We performed generalized-ensemble molecular dynamics simulations of two peptides. One of these peptides is C-peptide of ribonuclease A, and the other is the C-terminal fragment from the B1 domain of streptococcal protein G. The former is known to form  $\alpha$ -helix structure and the latter  $\beta$ -hairpin struc-

ture by experiments. The simulation results revealed significant differences of the secondary-structure forming tendencies among the force fields. Of the six force fields, the results of AMBER99 and CHARMM22 were in accord with experiments for C-peptide. For G-peptide, on the other hand, the results of OPLS-AA/L

and GROMOS96 were most consistent with experiments. Therefore, further improvements on the force fields are necessary for studying the protein folding problem from the first principles, in which a single force field can be used for all cases.

## I-C Development of Simulation Algorithms for Complex Systems

Developing a powerful simulation algorithm that can alleviate the multiple-minima problem is important in many complex systems. We have been advocating the uses of the so-called generalized-ensemble algorithms such as multicanonical algorithm and replica-exchange method.

### I-C-1 Liquid-Gas Phase Transitions Studied by Multibaric-Multithermal Monte Carlo Simulations

OKUMURA, Hisashi; OKAMOTO, Yuko

[*J. Phys. Soc. Jpn.* **73**, 3304 (2004)]

We investigate the liquid-gas phase transition of a

Lennard-Jones 12-6 potential system by the multibaric-multithermal Monte Carlo algorithm. The advantage of this method is that one can sample configurational space both in the gas phase and in the liquid phase from only one simulation run. Our liquid-gas coexistence data agree well with those obtained previously by other methods. We also show that this method is efficient in investigation of the transition state, which is the saddle point of a free energy surface.

## I-D Other Results on Molecular Simulations

### I-D-1 Comparisons between a Molecular Dynamics and Hydrodynamics Treatment of Non-Stationary Thermal Processes in a Liquid

OKUMURA, Hisashi; HEYES, David M.<sup>1</sup>  
(<sup>1</sup>Univ. Surrey)

[*Phys. Rev. E* **70**, 061206 (2004)]

Molecular dynamics (MD) and Navier-Stokes hydrodynamics have been performed to model thermal relaxation processes arising from an initially established nonequilibrium stationary state. A nanoscale two-layer Lennard-Jones (LJ) liquid system was constructed in which the two parts were initially at a different temperature, with a narrow transitional zone between the two layers which was spatially linear in temperature. The highest temperature layer had widths of 5 or 20 LJ particle diameters. The hydrodynamics model used parameterized MD-derived transport coefficients and the LJ equation of state as input functions. The temporal and spatial temperature and density profiles produced by the two methods show good agreement, indicating that a hydrodynamics description is reliable even for non-stationary phenomena down to the scale of a few molecular diameters.

## I-E Applications of the Zhu-Nakamura Theory to Nonadiabatic Chemical Dynamics

### I-E-1 Nonadiabatic Transition and Chemical Dynamics: Multi-Dimensional Tunneling Theory and Applications of the Zhu-Nakamura Theory

NAKAMURA, Hiroki

[*J. Theor. Comput. Chem.* **4**, 127 (2005)]

Tunneling and nonadiabatic transition are the most important quantum mechanical effects in chemical dynamics. They are important not only for understanding the dynamics properly, but also for controlling molecular functions. The Zhu-Nakamura (ZN) theory can be combined with the quasi-classical trajectory method and with the IVR (Initial Value Representation)-type semiclassical theory to deal with large chemical systems. Laser control of molecular processes and control of molecular functions can also be realized by properly controlling nonadiabatic transitions. Furthermore, we have recently formulated an accurate theory for evaluating tunneling splitting and tunneling decay rate in multi-dimensional systems and also developed an efficient method to find caustics in multi-dimensional space. These methods combined with the ZN theory are expected to clarify various large scale chemical dynamics. This is a short review article on our recent activities mentioned above.

### I-E-2 Electron Transfer Rate to Cover the Whole Range from Adiabatic to Nonadiabatic Regime Based on the Zhu-Nakamura Theory

ZHAO, Yi<sup>1</sup>; NAKAMURA, Hiroki

(<sup>1</sup>IMS and Univ. Sci. Tech. China, China)

A new formula for electron transfer is formulated to bridge the gap between the adiabatic and nonadiabatic limits. The key point is to reformulate the prefactor of the famous Marcus formula by using the Zhu-Nakamura theory of nonadiabatic transition. It is shown that the new formula gives an excellent agreement with the quantum mechanical numerical results and can explain well the experimental data of Nelsen *et al.*

### I-E-3 Semiclassical Theory of Electron Transfer Beyond the Perturbation Theory

ZHAO, Yi<sup>1</sup>; LIANG, Wanzhen<sup>2</sup>; NAKAMURA, Hiroki

(<sup>1</sup>IMS and Univ. Sci. Tech. China, China; <sup>2</sup>Univ. Sci. Tech. China, China)

We consider a problem of evaluating electron transfer rate in the crossover region from nonadiabatic to adiabatic regime controlled by the electron coupling.

Based on the generalized nonadiabatic transition state theory<sup>1)</sup> proposed to overcome the quantitative deficiencies of the conventional transition state theory, the rate applicable to multi-dimensional systems in the linear response limit is expressed as a product of the well-known Marcus formula and a coefficient which represents the correction with respect to nonadiabatic transition across the seam surface. In the case of general multi-dimensional systems the Monte Carlo approach can be utilized to evaluate the effective probability and the effective free energy for any general Hamiltonian system expressed in Cartesian coordinates with nonlinear reaction coordinates and the non-Condon effect taken into account. Numerical demonstration is made by using a model system with a collection of harmonic oscillators. The rate obtained shows a good agreement with that evaluated from the Fermi Gordon rule in the weak electronic coupling limit; while the latter theory fails in the strong electronic coupling regime as expected. Numerical tests also show that a matching technique from multi-mode to an effective one mode gives a very good result in wide range of electronic coupling strength and temperature except in the deep tunneling regime.

#### Reference

1) Y. Zhao, G.V. Mil'nikov and H. Nakamura, *J. Chem. Phys.* **121**, 8854 (2004).

### I-E-4 Generalized Trajectory Surface Hopping Approach

OLOYEDE, Oluwaponmile<sup>1</sup>; MIL'NIKOV, Gennady V.; NAKAMURA, Hiroki  
(<sup>1</sup>SOKENDAI)

The TSH method is generalized so as to be applicable to high dimensional systems with use of the Zhu-Nakamura formulas. Not only the classically allowed transitions but also the classically forbidden ones can be treated uniformly. Furthermore the transition direction can be determined from the Hessian of potential energy surfaces, even if the nonadiabatic coupling vector is not available.

### I-E-5 Semiclassical Theory of Thermal Rate Constant for Multi-Surface Processes

CHIKAZUMI, Shinpei; MIL'NIKOV, Gennady V.; NAKAMURA, Hiroki

A semiclassical theory is formulated with use of the Zhu-Nakamura theory by extending the trace formula devised by Miller and co-workers. The statistical Monte Carlo method makes it possible to apply this theory to multi-dimensional systems.

## I-F Theory of Nonadiabatic Transition

### I-F-1 Rabi Dynamics of Coupled Atomic and Molecular Bose-Einstein Condensates

ISHKHANYAN, Artur<sup>1</sup>; CHERNIKOV, G. P.<sup>2</sup>; NAKAMURA, Hiroki

(<sup>1</sup>IMS and Engineering Cent. Armenian NAS, Armenia; <sup>2</sup>Russian Res. Cent. "Kurchatov Institute," Inst. Nuclear Fusion, Russia)

[*Phys. Rev. A* **70**, 053611 (2004)]

The dynamics of coherent Rabi oscillations in coupled atomic and molecular Bose-Einstein condensates is considered taking into account the atom-atom, atom-molecule and molecule-molecule elastic interactions. The exact solution for the molecule formation probability is derived in terms of the elliptic functions. The two-dimensional space of the involved parameters (intensity and detuning) is analyzed and divided into two regions where the Rabi oscillations show different characteristics. A resonance curve is found, on which the molecular formation probability monotonically increases as a function of time. The maximum value of the final transition probability on this curve is 1/2 (*i.e.*, total transition to the molecular state) and it is achieved at high field intensities starting from a minimal threshold defined by the interspecies interaction scattering lengths. The explicit form of the resonance curve is determined, and it is shown that the resonance frequency position reveals a nonlinear dependence on the Rabi frequency of the applied field. A singular point is found on the resonance curve, where a power-law time evolution of the system is observed.

### I-F-2 A Basic Two-State Model for Bosonic Field Theories with a Cubic Nonlinearity

ISHKHANYAN, Artur<sup>1</sup>; JAVANAINEN, Juha<sup>2</sup>; NAKAMURA, Hiroki

(<sup>1</sup>IMS and Engineering Cent. Armenian NAS, Armenia; <sup>2</sup>Univ. Connecticut, U.S.A.)

[*J. Phys. A: Math. Gen.* **38**, 3505–3516 (2005)]

A basic nonlinear two-state model generic in classical and bosonic field theories with a cubic nonlinearity is considered. For the class of models with constant external field amplitude a general strategy for attacking the problem is developed based on the reduction of the initial system of equations for the semiclassical atom-molecule amplitudes to a nonlinear Volterra integral equation for the molecular probability. A uniformly convergent series solution to the problem is constructed for the weak interaction limit. The Landau-Zener model is considered as a specific example. The first approximation term is derived and an asymptotic expression for the nonlinear transition probability is established in the weak interaction regime.

### I-F-3 Incorporation of Nonadiabatic Transition into Wave Packet Dynamics

MIL'NIKOV, Gennady V.; ZOU, Shiyang<sup>1</sup>; NAKAMURA, Hiroki

(<sup>1</sup>IMS and Univ. Bristol, U.K.)

Non-adiabatic wave packet dynamics is factorized into purely adiabatic propagation and instantaneous localized non-adiabatic transition. A general formula is derived for the quantum mechanical local non-adiabatic operator which is implemented within the framework of R-matrix method. The operator can be used for incorporating the nonadiabatic transition in semiclassical wave packets dynamics.

## I-G Theory of Multi-Dimensional Tunneling

### I-G-1 Instanton Theory for the Tunneling Splitting of Low Vibrationally Excited States

MIL'NIKOV, Gennady V.; NAKAMURA, Hiroki

[*J. Chem. Phys.* **122**, 124311 (2005)]

We develop the instanton theory for calculating the tunneling splitting of excited states. For the case of low vibrational quantum states we derive a canonically invariant formula which is applicable to a multidimensional system of arbitrary Riemannian metric. The effect of multidimensionality in relation to the vibrational excitation is explained in terms of the effective frequencies along the instanton trajectory. The theory is demonstrated to work well by taking HO<sub>2</sub> molecule as an example.

### I-G-2 Effect of Out-Of Plane Vibration on the Hydrogen Atom Transfer Reaction in Malonaldehyde

YAGI, Kiyoshi<sup>1</sup>; MIL'NIKOV, Gennady V.; TAKETSUGU, Tetsuya<sup>2</sup>; HIRAO, Kimihiko<sup>1</sup>; NAKAMURA, Hiroki

(<sup>1</sup>Univ. Tokyo; <sup>2</sup>Ochanomizu Univ.)

[*Chem. Phys. Lett.* **397**, 435–440 (2004)]

Tunneling splitting of the vibrational ground state is calculated for a planar model of malonaldehyde by the instanton method of Mil'nikov and Nakamura with use of *ab initio* potential energy surface. The planar model gives much larger tunneling splitting than the previous full dimensional calculations, indicating a strong effect

of the anharmonic coupling between the in-plane and out-of-plane modes. The anharmonicity is related to the Coriolis coupling between the OH stretching vibration and the pseudo-rotation of the hindered rotor. The present results suggest that the multidimensional effects should be carefully taken into account in the tunneling dynamics of polyatomic molecules.

### I-G-3 Ground State and Vibrationally Assisted Tunneling in the Formic Acid Dimer

MIL'NIKOV, Gennady V.; KÜHN, O.<sup>1</sup>;  
NAKAMURA, Hiroki

(<sup>1</sup>Freie Univ. Berlin, Germany)

[*J. Chem. Phys.* **123**, 074308 (2005)]

The previously developed instanton theory<sup>1)</sup> is applied to the calculation of vibrationally assisted tunneling splitting of the deuterated formic acid dimer (DCOOH)<sub>2</sub> with all the degrees of freedom taken into account. The ground state tunnel splitting is determined

by the density functional theory combined with coupled cluster level of quantum chemistry to be 0.0038 cm<sup>-1</sup> which is comparable to the experimental value 0.0029 cm<sup>-1</sup>. Further, the tunnel splittings of fundamental excitations are estimated for frequencies below 300 cm<sup>-1</sup>. In this energy range it is found that the excitation modes may either enhance or suppress tunneling as compared to the ground state. For the higher frequency modes a rapid growth of the tunnel splitting is observed. At frequencies above 1000 cm<sup>-1</sup> the semiclassical solution becomes unstable and no reliable tunneling splittings can be obtained. This is in vast contrast to the adiabatic approximation to the instanton theory in which the tunnel splittings can be retrieved up to 3000 cm<sup>-1</sup>. We discuss this disparity from the viewpoint of the multidimensional character of tunneling in hydrogen bonds and the adiabatic approximation is concluded to be inaccurate.

#### Reference

1) *J. Chem. Phys.* **122**, 124311 (2005).

## I-H Laser Control of Molecular Processes

### I-H-1 Laser Control of Electronic Transitions of Wave Packet by Using Quadratically Chirped Pulses

ZOU, Shiyang<sup>1</sup>; KONDORSKIY, Alexey;  
MIL'NIKOV, Gennady V.; NAKAMURA, Hiroki

(<sup>1</sup>IMS and Univ. Bristol, U.K.)

[*J. Chem. Phys.* **122**, 084112 (2005)]

An effective scheme is proposed for the laser control of wave packet dynamics. It is demonstrated that by using specially designed quadratically chirped pulses, fast and nearly complete excitation of wave packet can be achieved without significant distortion of its shape. The parameters of the laser pulse can be estimated analytically from the Zhu-Nakamura theory of nonadiabatic transition. If the wave packet is not too narrow or not too broad, then the scheme is expected to be utilizable for multidimensional systems. The scheme is applicable to various processes such as simple electronic excitation, pump-dump, and selective bond breaking,

and it is actually numerically demonstrated to work well by taking diatomic and triatomic molecules (LiH, NaK, H<sub>2</sub>O) as examples.

### I-H-2 Semiclassical Guided Optimal Control of Molecular Dynamics

KONDORSKIY, Alexey; MIL'NIKOV, Gennady V.;  
NAKAMURA, Hiroki

An efficient semiclassical optimal control theory applicable to multi-dimensional systems is formulated for controlling wave packet dynamics on a single adiabatic potential energy surface. The approach combines advantages of different formulations of optimal control theory: quantum and classical on one hand and global and local on the other. Numerical applications to the control of NCH-HNC isomerization demonstrate that this theory can provide an efficient tool to manipulate molecular dynamics of many degrees of freedom by laser pulses.

## I-I Development of New Molecular Functions

### I-I-1 A Theoretical Study of Cyclohexadiene/Hexatriene Photochemical Interconversion: Multireference Configuration Interaction Potential Energy Surfaces and Transition Probabilities for the Radiationless Decays

TAMURA, Hiroyuki; NANBU, Shinkoh<sup>1</sup>;  
NAKAMURA, Hiroki; ISHIDA, Toshimasa<sup>2</sup>  
(<sup>1</sup>IMS and Kyushu Univ.; <sup>2</sup>IMS and Kyoto Univ.)

[*Chem. Phys. Lett.* **401**, 487–491 (2005)]

The overall energetics and the feature of reactive potential energy surfaces for the photochemical interconversion between cyclohexadiene (CHD) and all-*cis*-hexatriene (cZc-HT) have been investigated using the multireference configuration interaction (MRCI) calculations. The adiabatic and the diabatic potential energy surfaces of the ground and the excited states have been calculated along the Jacobi coordinates. The conical intersections among the states are estimated and the corresponding non-adiabatic transition probabilities are calculated using the semiclassical Zhu-Nakamura formula. The  $1^1\text{B}-2^1\text{A}$  decay occurs by  $\text{C}_2$ -symmetry-breaking motion around the conical intersection. The non-adiabatic transition to  $1^1\text{A}$  occurs by the motion toward the 5-membered ring.

### I-I-2 Reaction Dynamics of Cyclohexadiene/Hexatriene Ultrafast Photoisomerization through Conical Intersections

TAMURA, Hiroyuki; NANBU, Shinkoh<sup>1</sup>; ISHIDA, Toshimasa<sup>2</sup>; NAKAMURA, Hiroki  
(<sup>1</sup>IMS and Kyushu Univ.; <sup>2</sup>IMS and Kyoto Univ.)

Fundamental mechanisms of photochromism applicable to molecular switches and memories are clarified using quantum mechanical wave-packet dynamics on the accurate *ab initio* potential energy surfaces. Cyclohexadiene/hexatriene ultrafast photoisomerization has been considered as a model system. The results are in agreement with the femtosecond time-resolution experiments. The overall reaction dynamics is revealed from photoexcitation to the ground state products *via* non-adiabatic transitions through conical intersections governing the excited state lifetime and the reaction yield. It is also found that the second excited state plays an important role in the dynamics and the efficiency of photochromism.

### I-I-3 Encapsulation of Hydrogen Atoms by Fullerenes and Carbon Nanotubes with the Use of Nonadiabatic Transition

NANBU, Shinkoh<sup>1</sup>; ISHIDA, Toshimasa<sup>2</sup>;  
NAKAMURA, Hiroki  
(<sup>1</sup>IMS and Kyushu Univ.; <sup>2</sup>IMS and Kyoto Univ.)

A probable mechanism is proposed to encapsulate hydrogen atoms into carbon nanotubes (CNTs) as well as fullerenes. In this mechanism, a non-adiabatic effect on nuclear dynamics, specifically the non-adiabatic tunneling effect, enables transmission of hydrogen atoms. A cap of CNTs or a pentagonal moiety (five-membered rings) of fullerenes is mimicked by corannulene molecule ( $\text{C}_{20}\text{H}_{10}$ ). The three-dimensional quantum mechanical wave packet dynamics calculations are carried out on the accurate *ab initio* potential energy surfaces of the ground and excited states. It is shown that a hydrogen atom can transmit through the five-membered ring of corannulene more than once out of four incidences when five carbon atoms in the second layer are replaced by borons. The result is interpreted in terms of the Zhu-Nakamura semiclassical theory of non-adiabatic transition.

## I-J Theoretical Studies of Electron Dynamics in Molecular Systems

Electron dynamics in molecular systems is an intrinsic process related to a number of interesting phenomena such as linear and nonlinear optical response, electric conduction, and also chemical reaction. Despite the importance, the electron dynamics has not been understood in detail. We have developed a computational method simulating the electron dynamics in real time, and investigated nonlinear optical response and multiple ionization of noble metal clusters.

### I-J-1 High-Order Harmonic Generation from Silver Clusters: Laser-Frequency Dependence and the Screening Effect of *d* Electrons

NOBUSADA, Katsuyuki; YABANA, Kazuhiro<sup>1</sup>  
(<sup>1</sup>Univ. Tsukuba)

[*Phys. Rev. A* **70**, 043411 (7 pages) (2004)]

We present time-dependent density functional studies of harmonic generation from Ag<sub>2</sub> and Ag<sub>8</sub> in pulsed laser fields. The harmonic generation is strongly dependent on the laser frequency. The harmonics are emitted from the clusters much more efficiently when the applied laser field is in tune with the dipole resonance frequency of the system. Such resonance frequency dependence is substantially equal to a resonance phenomenon in a forced oscillator in a sense that the valence *s*-electrons are shaken effectively at the tuned laser frequency and the induced dipole moment continues to oscillate even though the laser field is switched off. Furthermore, we have found that the polarizable core *d*-electrons significantly screen the valence *s*-electrons such that the electron density of the *s* electrons induced in the laser field is canceled out. The screening

effect of the *d* electrons becomes more important in the system of Ag<sub>8</sub> than Ag<sub>2</sub>.

### I-J-2 Multiple Ionization of a Silver Diatomic Molecule in an Intense Laser Field

SHIRATORI, Kazuya<sup>1</sup>; NOBUSADA, Katsuyuki;  
YABANA, Kazuhiro<sup>2</sup>  
(<sup>1</sup>Hokkaido Univ.; <sup>2</sup>Univ. Tsukuba)

[*Chem. Phys. Lett.* **404**, 365–369 (2005)]

Time-dependent density functional studies of multiple ionization of Ag<sub>2</sub> in an intense laser field 10<sup>14</sup> W/cm<sup>2</sup> are presented. Special emphasis is placed on elucidating frequency dependence and effects of the *d* electrons on the ionization processes. We have found that the *s* and *d* electrons move reciprocally toward the opposite directions in a manner such that the electric field induced by the *s*-electron polarization is cancelled out by the *d* electrons. This screening effect of the *d* electrons suppresses the multiple ionization in marked contrast to molecular systems such as alkali metal clusters which do not accompany inner *d*-electrons.

## I-K Electronic Structures and Photochemical Properties of Nanometer-Sized Metal Clusters

Nanometer-sized metal clusters provide significantly different physicochemical properties such as optical response, catalysis, and reactivity from corresponding bare metal clusters or bulk metals. We have investigated electronic structures and photochemical properties of monolayer-protected metal clusters with special emphasis on describing metal-molecule interactions.

### I-K-1 Electronic Structure and Photochemical Properties of a Monolayer-Protected Gold Cluster

NOBUSADA, Katsuyuki

[*J. Phys. Chem. B* **108**, 11904–11908 (2004)]

The electronic structure of a monolayer-protected gold cluster, [Au<sub>13</sub>(SCH<sub>3</sub>)<sub>8</sub>]<sup>3+</sup>, has been investigated by performing density functional calculations. The cluster

has a characteristic structure with *O<sub>h</sub>* molecular symmetry and eight (111) facets of a centered cuboctahedral Au<sub>13</sub> core cluster are fully passivated by eight methanethiolates. The bond distance between two neighboring gold atoms (= 3.673 Å) is much larger than that of the bare Au<sub>13</sub> cluster (= 2.929 Å), whereas the Au–S bond distance is 2.403 Å. These atomic rearrangement means that the methanethiolates stabilize the enlarged bare Au<sub>13</sub> cluster by bonding to the (111) hollow sites of the bare cluster. The absorption spectrum of the [Au<sub>13</sub>(SCH<sub>3</sub>)<sub>8</sub>]<sup>3+</sup> cluster is simulated within time-dependent

density functional theory. The spectrum shows clear absorption peaks and each peak is assigned to specific excitation processes.

also provides interesting photochemical properties which are rather different from those of similar-sized gold-methanethiolate clusters.

### **I-K-2 Glutathione-Protected Gold Clusters Revisited: Bridging the Gap between Gold(I)-Thiolate Complexes and Thiolate-Protected Gold Nanocrystals**

**NEGISHI, Yuichi; NOBUSADA, Katsuyuki; TSUKUDA, Tatsuya**

[*J. Am. Chem. Soc.* **127**, 5261–5270 (2005)]

Small gold clusters (~1 nm) protected by molecules of a tripeptide, glutathione (GSH), were prepared by reductive decomposition of Au(I)-SG polymers at a low temperature and separated into a number of fractions by polyacrylamide gel electrophoresis (PAGE). Chemical compositions of the fractionated clusters determined previously by electrospray ionization (ESI) mass spectrometry (Negishi, Y. *et al.*, *J. Am. Chem. Soc.* **126**, 6518 (2004)) were reassessed by taking advantage of freshly prepared samples, higher mass resolution, and more accurate mass calibration; the nine smallest components are reassigned to Au<sub>10</sub>(SG)<sub>10</sub>, Au<sub>15</sub>(SG)<sub>13</sub>, Au<sub>18</sub>(SG)<sub>14</sub>, Au<sub>22</sub>(SG)<sub>16</sub>, Au<sub>22</sub>(SG)<sub>17</sub>, Au<sub>25</sub>(SG)<sub>18</sub>, Au<sub>29</sub>(SG)<sub>20</sub>, Au<sub>33</sub>(SG)<sub>22</sub>, and Au<sub>39</sub>(SG)<sub>24</sub>. These assignments were further confirmed by measuring the mass spectra of the isolated Au:S(h-G) clusters, where h-GSH is a homoglutathione. It is proposed that a series of the isolated Au:SG clusters corresponds to kinetically trapped intermediates of the growing Au cores. The relative abundance of the isolated clusters was correlated well with the thermodynamic stabilities against unimolecular decomposition. The electronic structures of the isolated Au:SG clusters were probed by X-ray photoelectron spectroscopy (XPS) and optical spectroscopy. The Au(4f) XPS spectra illustrate substantial electron donation from the gold cores to the GS ligands in the Au:SG clusters. The optical absorption and photoluminescence spectra indicate that the electronic structures of the Au:SG clusters are well quantized; embryos of the sp band of the bulk gold evolve remarkably depending on the number of the gold atoms and GS ligands. The comparison of these spectral data with those of sodium Au(I) thiomalate and 1.8 nm Au:SG nanocrystals (NCs) reveals that the subnanometer-sized Au clusters thiolated constitute a distinct class of binary system which lies between the Au(I)-thiolate complexes and thiolate-protected Au NCs.

### **I-K-3 Gold-Thiolate Nanoring: Electronic Structure and Photochemical Properties**

**NOBUSADA, Katsuyuki**

We have studied electronic structure and photochemical properties of gold-methanethiolate complexes Au<sub>n</sub>(SCH<sub>3</sub>)<sub>n</sub>. The complexes have been found to be stable structures in the form of a circular ring. The characteristic Au–S interaction plays an important role in forming such a unique ring structure. The ring structure

## I-L Electronic Structure of a Molecule in Solution

Chemical reaction is undoubtedly the most important issue in the theoretical chemistry, and the electronic structure is a key to solve the problem. As long as molecules in the gas phase are concerned, the theory for the electronic structure has been enjoying its great success. However, when it comes to molecules in solution, the stage of theory is still an infant. About 15 years ago, we have proposed a method referred to as RISM-SCF based on the integral equation theory of molecular liquids (RISM) and the *ab initio* electronic structure theory (SCF).<sup>1)</sup> The method was applied successfully to a variety of chemical processes in solution including a number of different types of chemical reactions, S<sub>N</sub>2, acid-base, redox, and so on.

More recently, we have revised the theory so that the theory can account for the three dimensional distribution of solvent around solute.<sup>2)</sup> (3D-RISM) This revision turns out to be essential when one tries to treat the solvent distribution around the native state of protein. The new theory allows us to handle the electronic structure of protein in water with appropriate theories for quantum chemistry.

### References

- 1) S. Ten-no, F. Hirata and S. Kato, *Chem. Phys. Lett.* **214**, 391 (1993); *J. Chem. Phys.* **100**, 7443 (1994); H. Sato, F. Hirata and S. Kato, *J. Chem. Phys.* **105**, 1546 (1996).  
2) H. Sato, A. Kovalenko and F. Hirata, *J. Chem. Phys.* **112**, 9463 (2000).

### I-L-1 Electronic Structure Calculation of a Solvated Macro Molecule by Using Three-Dimensional Reference Interaction Site Model Combined with *Ab Initio* Molecular Orbital Theory

YOSHIDA, Norio; HIRATA, Fumio

[*J. Comput. Chem.* submitted]

The three dimensional reference interaction site model integral equation theory (3D-RISM) combined with the *ab initio* molecular orbital method (3D-RISM-SCF) is applied to a solvated macro molecular system.

The solvation structure around a solute molecule is obtained from the 3D-RISM integral equation under the electrostatic potential of the solute molecule, calculated by the *ab initio* molecular orbital theory.

The electrostatic potential should be calculated on each grid point in the three dimensional real space. Hence the solvated fock matrix are also prepared on each grid point. Therefore, the calculation of the electrostatic potential and the solvated fock matrix is the most time consuming part in this method. In this paper, we propose a new procedure to save the computational cost for calculating the electrostatic potential and the solvated fock matrix. The strategy of this procedure is to divide the space into three regions: (I) the inside of the repulsive cores, and (II) the region excluding (I), where the electron density is distributed, and (III) the remaining part in the super cell after applying the (I) and (II).

In the first region, it is possible to avoid the calculation of electrostatic potential and solvated Fock matrix

by assuming the potential to be infinity.

In the second region, the electrostatic potential is evaluated directly by integrating the molecular orbitals. In the outermost region, it is evaluated approximately by putting the effective point charge on each atomic site.

The electronic structure and the energy gradient of Methionine-Enkephalin and solvation structure are estimated by using this procedure in aqueous solution, and are compared with the results from other procedures. The results are compared also with those from the continuum model.

### I-L-2 New Theoretical Approach for the Diastereoselectivity of H/D Exchange Reaction on Methyl 3-Fluorobutanoate Anion

IKUTA, Yasuhiro; YOSHIDA, Norio; YAMAZAKI, Takeshi<sup>1</sup>; HIRATA, Fumio  
(<sup>1</sup>NINT, Canada)

[*Tetrahedron Lett.* submitted]

The origin of closed to *si*-face stereochemistry in the protonation of  $\beta$ -substituted ethyl butanoates in ethanol-*d*, which has been studied by Mohrig and co-workers, was examined with Me 3-fluoro butanoate anion as a computational model. It was found that the prediction of the selectivity was achieved with the solvent effect around substrate and the population of the ground state species. The transition state to *si*-face stereochemistry is found to be the most favorable process in ethanol.

## I-M Solvation Thermodynamics of Protein and Related Molecules

Concerning biomolecules such as protein, it is a final goal for the biochemistry and biophysics to explore the relation between conformations and biological functions. The first important step toward the goal would be to explain the conformational stability of biomolecules in terms of the microscopic structure of the molecules in solvent. It is an extremely difficult problem by any means due to the overwhelmingly large degrees of freedom to be handled, including protein and solvent.

In the past 10 years, we have been developing a method to attack the problem based on the statistical mechanics of liquids, especially, on the RISM theory.<sup>1)</sup> Recently, we put forward our effort to apply the three dimensional (3D) RISM theory to biomolecules, and have succeeded for the first time to obtain thermodynamic quantities of “real” protein, which is in agreement with experiments not only qualitatively but also quantitatively in case of the partial molar volume.<sup>2)</sup> The 3D-RISM theory turns out to be even more powerful to explore water molecules trapped in a cavity of protein.

### References

- 1) M. Kinoshita, Y. Okamoto and F. Hirata, *J. Am. Chem. Soc.* **120**, 1855 (1998).
- 2) T. Imai, A. Kovalenko and F. Hirata, *Chem. Phys. Lett.* **395**, 1 (2004).

### I-M-1 Hydrophobic Effects on Partial Molar Volume

**IMAI, Takashi<sup>1</sup>; HIRATA, Fumio**  
(<sup>1</sup>Ritsumeikan Univ.)

[*J. Chem. Phys.* **122**, 94509 (2005)]

The hydrophobic effects on partial molar volume (PMV) are investigated as a PMV change in the transfer of a benzene-like non-polar solute from the non-polar solvent to water, using an integral equation theory of liquids.

The volume change is divided into two effects. One is the “packing” effect in the transfer from the non-polar solvent to hypothetical “non-polar water” without hydrogen bonding networks. The other is the “iceberg” effect in the transfer from “non-polar water” to water. The results indicate that the “packing” effect is negative and a half compensated by the positive “iceberg” effect. The “packing” effect is explained by the difference in the solvent-compressibility. Further investigation shows that the sign and magnitude of the volume change depends on the solute-size and the solvent-compressibility. The finding gives a significant implication that the exposure of a hydrophobic residue caused by protein denaturation can either increase or decrease the PMV of protein depending on the size of the residue and the fluctuation of its surroundings. Possible applications of the method to problems related to the solvation thermodynamics of protein are discussed.

### I-M-2 Partial Molar Volume of Proteins Studied by the 3D-RISM Theory

**IMAI, Takashi<sup>1</sup>; KOVALENKO, Andriy<sup>2</sup>;  
HIRATA, Fumio**  
(<sup>1</sup>Ritsumeikan Univ.; <sup>2</sup>NINT, Canada)

[*J. Phys. Chem. B* **109**, 6658 (2005)]

The three-dimensional reference interaction site model (3D-RISM) theory is applied to the analysis of hydration effects on the partial molar volume of proteins. For the native structure of some proteins, the partial molar volume is decomposed into geometric and hydration contributions using the 3D-RISM theory combined with the geometric volume calculation.

The hydration contributions are correlated with the surface properties of protein. The thermal volume, which is the volume of voids around the protein induced by the thermal fluctuation of water molecules, is directly proportional to the accessible surface area of protein. The interaction volume, which is the contribution of electrostatic interactions between the protein and water molecules, is apparently governed by the charged atomic groups on the protein surface. The polar atomic groups does not make any contribution to the interaction volume. The volume differences between low- and high-pressure structures of lysozyme are also analyzed by the present method.

### I-M-3 Theoretical Study of Volume Changes Associated with the Helix-Coil Transition of an Alanine-Rich Peptide in Aqueous Solution

**IMAI, Takashi<sup>1</sup>; TAKEKIYO, Takahiro<sup>1</sup>;  
KOVALENKO, Andriy<sup>2</sup>; HIRATA, Fumio;  
TANIGUCHI, Yoshihiro<sup>1</sup>**  
(<sup>1</sup>Ritsumeikan Univ.; <sup>2</sup>NINT, Canada)

The changes in the partial molar volume (PMV) associated with the conformational transition of an alanine-rich peptide AK16 from the  $\alpha$ -helix structure to various random coil structures are calculated by the three-dimensional interaction site model (3D-RISM) theory coupled with the Kirkwood-Buff theory. The volume change is analyzed by decomposing it into contributions from geometry and hydration: the changes in the van der Waals, void, thermal, and interaction volume. The total change in the PMV is positive. This is primarily due to the growth of void space within the

peptide which is cancelled in part by the volume reduction resulting from the increase in the electrostatic interaction between the peptide and water molecules. The changes in the void and thermal volume of the coil structures are widely distributed and tend to compensate each other. Additionally, the relations between the hydration volume components and the surface properties are investigated. We categorize coil structures into extended coils with the PMV smaller than helix and general coils with the PMV larger than helix. The pressure therefore can both stabilize and destabilize the coil structures. The latter seems to be a more proper model of random coil structures of the peptide.

#### **I-M-4 Combination of the Replica-Exchange Monte Carlo Method and the Reference Interaction Site Model Theory for Simulating a Peptide Molecule in Aqueous Solution**

**MITSUTAKE, Ayori<sup>1</sup>; KINOSHITA, Masahiro<sup>2</sup>; OKAMOTO, Yuko<sup>3</sup>; HIRATA, Fumio**  
(<sup>1</sup>Keio Univ.; <sup>2</sup>Kyoto Univ.; <sup>3</sup>Nagoya Univ.)

[*J. Phys. Chem. B* **108**, 19002 (2004)]

This article reports the first attempt to combine the replica-exchange Monte Carlo method and the reference interaction site model (RISM) theory for simulating a peptide molecule in aqueous solution. The energy function is the sum of the conformational energy and the solvation free energy. The solvation free energy for a fixed conformation of the peptide molecule is calculated using the RISM theory. The replica-exchange method is modified so that the dependence of the energy function on the temperature can be incorporated. The effectiveness of the combined approach is demonstrated for Met-

enkephalin in water. It is argued that the number of replicas required for a peptide molecule immersed in water is drastically reduced by employing the combined approach. Solvation properties and free energy surfaces of Met-enkephalin in water are discussed.

#### **I-M-5 Water Molecules in a Protein Cavity Detected by a Statistical-Mechanical Theory**

**IMAI, Takashi<sup>1</sup>; HIRAOKA, Ryusuke<sup>1</sup>; KOVALENKO, Andriy<sup>2</sup>; HIRATA, Fumio**  
(<sup>1</sup>Ritsumeikan Univ.; <sup>2</sup>NINT, Canada)

[*J. Am. Chem. Soc. communication*, submitted]

Water molecules confined inside cavities in a protein are of great importance in understanding the structure, stability, and functions of the biomolecule. Considerable efforts have been devoted to observe such water molecules by experiments, but it is still a nontrivial task.

It is virtually impossible to “find” water molecules in a protein cavity by the ordinary molecular simulation, because they are most likely trapped in the biomolecule through a process of large conformational fluctuation or “folding.” The simulation of such water molecules is as difficult as the protein folding itself.

Surprisingly enough, in the present study, we could have detected water molecules in a protein cavity by means of a recently developed statistical mechanics of molecular solutions, or the three-dimensional reference interaction site model (3D-RISM) theory. This paper reports how the water molecules are detected by the 3D-RISM calculation.

The results may have great impact on biochemistry and biophysics including molecular recognition, enzymatic reaction, and so on.

## **I-N Collective Density Fluctuations in Polar Liquids and Their Response to Ion Dynamics**

As to the model for molecular diffusion in polar liquids, there are two quite different points of view. One is the conventional rot-translation model, and the other the interaction-site description which sees the diffusion of a molecule as a correlated motion of each atom (site).<sup>1)</sup> It is clearly advantageous to use the interaction-site description compared to the rot-translation model to account for chemical characteristics of solvent as well as solute dynamics. However, the interaction-site description has its own disadvantage in interpreting physical meaning of the results, since it does not give an explicit picture for the rotational relaxation of molecules, which can be directly probed by many experimental means including the dielectric and NMR relaxation. We have solved the problem by extracting collective modes of the density fluctuation from the site-site density correlation functions. In our recent study for dynamics of molecular liquids based on the interaction-site model, we have succeeded to abstract the collective excitations in liquids, which can be identified as optical and acoustic modes, by diagonalizing the collective frequency matrix appearing in the generalized Langevin equation. The two modes arise essentially from the rotational and translational motions of molecules.<sup>2)</sup> We applied the method to the ion dynamics in a dipolar liquid, and could have explained successfully the peculiar size dependence of friction of alkali and halide ions in terms of response of the collective excitations in solvent to the solute displacement.<sup>3)</sup>

In the past year, we have elaborated the memory kernel in our generalized Langevin equation base on the mode

coupling theory. We have also extended our treatment to dynamics of water and hydrated ions. Those studies as well as other related topics are reviewed below.

### References

- 1) F. Hirata, *J. Chem. Phys.* **96**, 4619 (1992).
- 2) S. Chong and F. Hirata, *Phys. Rev. E* **57**, 1691 (1998).
- 3) S. Chong and F. Hirata, *J. Chem. Phys.* **108**, 7339 (1998).

### I-N-1 Site-Site Memory Equation Approach in Study of Density/Pressure Dependence of Translational Diffusion Coefficient and Rotational Relaxation Time of Polar Molecular Solutions: Acetonitrile in Water, Methanol in Water, and Methanol in Acetonitrile

**KOBRYN, Alexander; YAMAGUCHI, Tsuyoshi<sup>1</sup>; HIRATA, Fumio**  
(<sup>1</sup>Nagoya Univ.)

[*J. Chem. Phys.* **122**, 184511 (2005)]

We present results of theoretical study and numerical calculation of the dynamics of molecular liquids based on combination of the memory equation formalism and the reference interaction site model—RISM. Memory equations for the site-site intermediate scattering functions are studied in the mode-coupling approximation for the first order memory kernels, while equilibrium properties such as site-site static structure factors are deduced from RISM. The results include the temperature-density (pressure) dependence of translational diffusion coefficients  $D$  and orientational relaxation times  $\tau$  for acetonitrile in water, methanol in water and methanol in acetonitrile, all in the limit of infinite dilution. Calculations are performed over the range of temperatures and densities employing the SPC/E model for water and optimized site-site potentials for acetonitrile and methanol. The theory is able to reproduce qualitatively all main features of temperature and density dependences of  $D$  and  $\tau$  observed in real and computer experiments. In particular, anomalous behavior, *i.e.* the increase in mobility with density, is observed for  $D$  and  $\tau$  of methanol in water, while acetonitrile in water and methanol in acetonitrile do not show deviations from the ordinary behavior. The variety exhibited by the different solute-solvent systems in the density dependence of the mobility is interpreted in terms of the two competing origins of friction, which interplay with each other as density increases: the collisional and dielectric frictions which, respectively increase and decrease with increasing density.

### I-N-2 Theoretical Study on the Dynamic Properties of Compressed Water and Water-Hydrophobic Solute Mixtures

**YAMAGUCHI, Tsuyoshi<sup>1</sup>; MATSUOKA, Tatsuro<sup>1</sup>; KODA, Shinobu<sup>1</sup>; CHONG, Song-Ho; HIRATA, Fumio**  
(<sup>1</sup>Nagoya Univ.)

The dynamic properties, including shear viscosity, self-diffusion coefficient, dielectric relaxation time and single-molecular reorientational relaxation time, of neat compressed water and model water-hydrophobic solute mixtures are calculated theoretically from the intermolecular interaction potentials. The reference interaction-site model integral equation theory is used to obtain the equilibrium structure of the liquid, which in turn is used as the input of the numerical calculation by the mode-coupling theory for molecular liquids based on the interaction-site model. For neat compressed water, the theory reproduced the increase in the molecular mobility with applying pressure qualitatively. The reorientational mobility is more enhanced by pressure than the translational one, which is in harmony with experiments. The retardation of the motion of water in the aqueous solution of hydrophobic solutes is also obtained by the theory. In a model system in which the electrostatic interaction between the solute and solvent is continuously varied, the mobility of solvent water has a maximum as the function of the hydrophobicity of the solute. This theoretical trend is in harmony with the transition from positive, *via* negative, to hydrophobic hydration regimes experimentally observed.

### I-N-3 Solvation Dynamics in Water Investigated by RISM/Mode-Coupling Theory

**NISHIYAMA, Katsura<sup>1</sup>; YAMAGUCHI, Tsuyoshi<sup>2</sup>; HIRATA, Fumio; OKADA, Tadashi<sup>1</sup>**  
(<sup>1</sup>Osaka Univ.; <sup>2</sup>Nagoya Univ.)

[*J. Mol. Liq.* **119**, 63 (2005)]

The reference interaction site model (RISM) theory combined with the generalized Langevin/mode-coupling theory (MCT) is applied to the investigation of solvation dynamics in water. The dynamic response function  $S_s(t)$  which measures the energy relaxation of the system is calculated with different model solutes. The RISM-MCT framework recently presented by Yamaguchi and coworkers [*J. Chem. Phys.* **117**, 2216 (2002); *Mol. Phys.* **101**, 1211 (2003)] is shown to be applicable well to the realistic description of solvation dynamics.  $S_s(t)$  initially relaxes with a Gaussian decay followed by an overdamping oscillation with the time period of 30 fs. As the multiplicity of the solute pole is increased, the magnitude of the  $S_s(t)$  damping becomes smaller and relaxation gets slower.

## I-O Statistical Mechanics of Interfacial Fluids

Microscopic structure of fluid interfaces has been drawing a lot of attention due to recent development in the experimental techniques devised particularly to probe the interface. However, there are many open questions remained unanswered. For example, how wide is the interfacial region, how does it depend on the chemical species consisting the solution? Is the interface more or less homogeneous in terms of density or concentration of the two fluids, or is it spatially inhomogeneous? If it is inhomogeneous, what is the spatial extent of the inhomogeneity? Answering those questions is the most difficult and challenging tasks for theoretical physics and chemistry, and not much progress has been made in the past, especially from a molecular view point. We have been developing statistical mechanics for two different types of interfacial fluids: fluid-fluid interface and fluids in porous media. Following are the latest achievement in that direction.

### I-O-1 A Molecular Theory of Liquid Interfaces

**KOVALENKO, Andriy<sup>1</sup>; HIRATA, Fumio**

(<sup>1</sup>NINT, Canada)

[*Phys. Chem. Chem. Phys.* **7**, 1785 (2005)]

We propose a site-site generalization of the Lovett-Mow-Buff-Wertheim integro-differential equation for the one-particle density distributions to polyatomic fluids. The method provides microscopic description of liquid interfaces of molecular fluids and solutions. It uses the inhomogeneous site-site direct correlation function of molecular fluid consistently constructed by nonlinear interpolation between the homogeneous ones. The site-site correlations of the coexisting bulk phases are obtained from the reference interaction site model (RISM) integral equation with our closure approximation. For illustration, we calculated the structure of the planar liquid-vapor as well as liquid-liquid interfaces of n-hexane and methanol at ambient conditions.

## I-P Photoinduced Phase Transitions in Molecular Materials

Photoirradiation may create electrons, holes or excitons, which are often accompanied by local structural deformation. Sometimes it causes spatially large structural transformations with the help of cooperativity possessed by interacting electrons and molecules. Thus, a nonequilibrium phase can be generated, which may not be reached by simply changing temperature or pressure because the energy of a photon is much higher than thermal energies. Such photoinduced phase transitions have been studied extensively, both experimentally and theoretically. Thanks to the great progress in laser spectroscopy techniques, charge and lattice dynamics are being clarified in many molecular materials on different time scales including ultrafast and/or coherent dynamics. We need to treat relevant itinerant-electron models, whose transfer integrals are off-diagonal elements giving transition amplitudes. This is in contrast to stochastic dynamics in classical statistical models, where transition probabilities are determined by the Boltzmann factors at finite temperatures.

### I-P-1 Photoinduced Dynamics and Nonequilibrium Characteristics in Quasi-One-Dimensional Electron Systems: Mott Insulators vs. Band Insulators

YONEMITSU, Kenji

[*J. Phys.: Conf. Series* **21**, 30–37 (2005)]

Electron-electron interactions play an important role in nonequilibrium properties of molecular materials. First, we show differences between photoinduced ionic-to-neutral and neutral-to-ionic transitions in quasi-one-dimensional extended Peierls Hubbard models with alternating potentials. Cooperative dynamics lead to nonlinear ionicity in the former, while uncooperative dynamics lead to quite linear ionicity in the latter, as a function of the energy supplied from the oscillating electric field. Interchain electron-electron interactions bring about initial competition among metastable and stable domains in neighboring chains, slowing down the phase transition. Interchain elastic couplings are necessary to form a ferroelectric long-range order. Second, we show differences between field-effect characteristics of Mott insulators and those of band insulators in one-dimensional Hubbard models, to which tight-binding models are attached for metallic electrodes and scalar potentials are added for interfacial barriers. Ambipolar characteristics are found in the former, while unipolar characteristics generally appear in the latter. In the former, charge transport is cooperative so that the drain current is insensitive to the difference between the work function of the channel and that of the electrodes, and thus insensitive to the polarity of the gate bias.

### I-P-2 Optical Responses of Photoexcited States in the One-Dimensional Ionic Hubbard Model

MAESHIMA, Nobuya<sup>1</sup>; YONEMITSU, Kenji  
(<sup>1</sup>IMS and Tohoku Univ..)

[*J. Phys.: Conf. Series* **21**, 183–188 (2005)]

Photoinduced optical responses are studied in the one-dimensional ionic Hubbard model with the nearest-neighbor repulsion  $V$ . For  $V = 0$ , carriers introduced by photoirradiation move freely both in the Mott insulator phase and in the band insulator phase, giving rise to a

Drude peak in the optical conductivity spectrum. The carriers in the Mott insulator phase remain conducting for  $0 < V < 2t$  because their kinetic energy overcomes the binding energy. By contrast, the electrons and the holes in the band insulator phase are bound to form excitons for  $V > 0$ , which do not contribute to the charge transport unless the excitation energy allows them to be separated. The dependence of the Drude weight in the lowest-energy photoexcited state on  $V$  and the system size is investigated for both phases. Implications to experimental studies of halogen-bridged metal-complex chains are discussed.

### I-P-3 Quantum Ising Model Coupled with Conducting Electrons

YAMASHITA, Yasufumi; YONEMITSU, Kenji

[*J. Phys.: Conf. Series* **21**, 232–236 (2005)]

The effect of photo-doping on the quantum paraelectric SrTiO<sub>3</sub> is studied by using the one-dimensional quantum Ising model, where the Ising spin describes the effective lattice polarization of an optical phonon. Two types of electron-phonon couplings are introduced through the modulation of transfer integral *via* lattice deformations. After the exact diagonalization and the perturbation studies, we find that photo-induced low-density carriers can drastically alter quantum fluctuations when the system locates near the quantum critical point between the quantum paraelectric and ferroelectric phases.

### I-P-4 Photoinduced Metallic Properties of One-Dimensional Strongly Correlated Electron Systems

MAESHIMA, Nobuya<sup>1</sup>; YONEMITSU, Kenji  
(<sup>1</sup>IMS and Tohoku Univ.)

[*J. Phys. Soc. Jpn.* **74**, 2671–2674 (2005)]

We study photoinduced optical responses of one-dimensional strongly correlated electron systems. Optical conductivity spectra are calculated for the ground and photoexcited states in a one-dimensional Hubbard model at half filling by the exact diagonalization method. It is found that, in the Mott insulator phase, the photoexcited state has large spectral weights including

the Drude weight below the optical gap. As a consequence, the spectral weight above the optical gap is markedly reduced. These results imply that a metallic state is induced by photoexcitation. A comparison between the photoexcited and hole-doped states shows that photoexcitation is similar to chemical doping.

### **I-P-5 Interchain-Coupling Effects on Photoinduced Neutral-Ionic Transition Dynamics in Mixed-Stack Charge-Transfer Complexes**

YONEMITSU, Kenji

[*J. Low Temp. Phys.* in press]

Effects of interchain electron-electron interactions on the photoinduced ionic-to-neutral and neutral-to-ionic transition dynamics are studied in a quasi-one-dimensional extended Peierls-Hubbard model with alternating potentials for mixed-stack charge-transfer complexes. The ionic-to-neutral transition dynamics depend on the strengths of interchain couplings. For weak couplings, the interchain coherence is destroyed. For strong couplings such as those corresponding to TTF-CA, once neutral domains are nucleated above an

increased absorption threshold, they grow spontaneously and cooperatively till the whole system is converted. In contrast, interchain couplings slightly enhance non-linearity of the otherwise uncooperative neutral-to-ionic transition dynamics.

### **I-P-6 Theory of Photoinduced Phase Transitions**

YONEMITSU, Kenji; NASU, Keiichiro<sup>1</sup>  
(<sup>1</sup>KEK)

[*J. Phys. Soc. Jpn.* in press]

Theories of photoinduced phase transitions have developed along with the progress in experimental studies, especially concerning their nonlinear characters and transition dynamics. At an early stage, stochastic dynamics are explained on the basis of statistical physics. Recently, a variety of dynamics observed in different electronic states are described by relevant electronic models. Especially, coherent motion of a macroscopic domain boundary needs appropriate interactions among electrons and lattice displacements. We describe the history of theories of photoinduced phase transitions and discuss a future perspective.

## **I-Q Collective Transport through Metal-Insulator Interfaces**

Molecular materials are used in many device structures. Charge transport is always through an interface between two materials with different electronic states and work functions. In field-effect transistors fabricated on an insulating material with coherent charge transport under electric fields, the insulator-(source/drain) electrode interface barrier potentials, known as Schottky barriers, play an important role. For band insulators, the Schottky barriers indeed govern the current-voltage characteristics. Because the work function of the electrodes is generally different from that of the material, the characteristics are generally very asymmetric with respect to the polarity of the gate bias and therefore unipolar. Quite recently, ambipolar characteristics are found in field-effect transistor device structures based on organic single crystals of a quasi-one-dimensional Mott insulator. The ambipolar characteristics imply very similar effects on electron and hole injections of the Schottky barriers when combined with electron correlation effects. We need to combine interacting electron models with electrostatic potentials that originate from the long-range Coulomb interaction and are responsible for the interface barrier potentials.

### **I-Q-1 Mechanism of Ambipolar Field-Effect Carrier Injections in One-Dimensional Mott Insulators**

YONEMITSU, Kenji

[*J. Phys. Soc. Jpn.* **74**, 2544–2553 (2005)]

To clarify the mechanism of recently reported, ambipolar carrier injections into quasi-one-dimensional Mott insulators on which field-effect transistors are fabricated, we employ the one-dimensional Hubbard model attached to a tight-binding model for source and drain electrodes. To take account of the formation of Schottky barriers, we add scalar and vector potentials,

which satisfy the Poisson equation with boundary values depending on the drain voltage, the gate bias, and the work-function difference. The current-voltage characteristics are obtained by solving the time-dependent Schrödinger equation in the unrestricted Hartree-Fock approximation. Its validity is discussed with the help of the Lanczos method applied to small systems. We find generally ambipolar carrier injections in Mott insulators even if the work function of the crystal is quite different from that of the electrodes. They result from balancing the correlation effect with the barrier effect. For the gate-bias polarity with higher Schottky barriers, the correlation effect is weakened accordingly, owing to collective transport in the one-dimensional correlated electron systems.

## I-R Strongly Correlated Electron Systems with Frustrations

Strongly correlated electron systems have produced many exotic phases. Especially in low dimensions, there are always subtle balances between the tendency toward a long-range order through instabilities and the tendency against it due to quantum fluctuations. Geometrical frustrations and/or orbital degrees of freedom enhance quantum fluctuations to lead to intriguing phenomena. Phase diagrams are clarified by paying special attentions to low-energy excitations near quantum critical points.

### I-R-1 Frustration-Induced $\eta$ Inversion in the $S = 1/2$ Bond-Alternating Spin Chain

MAESHIMA, Nobuya<sup>1</sup>; OKUNISHI, Kouichi<sup>2</sup>;  
OKAMOTO, Kiyomi<sup>3</sup>; SAKAI, Tôru<sup>4</sup>  
(<sup>1</sup>IMS and Tokyo Metropolitan Univ.; <sup>2</sup>Niigata Univ.;  
<sup>3</sup>Tokyo Inst. Tech.; <sup>4</sup>Tohoku Univ.)

[*Phys. Rev. Lett.* **93**, 127203 (4 pages) (2004)]

We study the frustration-induced enhancement of the incommensurate correlation for a bond-alternating quantum spin chain in a magnetic field, which is associated with a quasi-one-dimensional organic compound F<sub>5</sub>PNN. We investigate the temperature dependence of the staggered susceptibilities by using the density matrix renormalization group, and then find that the incommensurate correlation becomes dominant in a certain range of the magnetic field. We also discuss the mechanism of this enhancement on the basis of the mapping to the effective  $S = 1/2$  XXZ chain and a possibility of the field-induced incommensurate long-range order.

### I-R-2 Field-Induced Phase Transitions and Long-Range Orders in the $S = 1/2$ Spin Bond-Alternating Chain with Frustrating Interaction

MAESHIMA, Nobuya<sup>1</sup>; OKUNISHI, Kouichi<sup>2</sup>;  
OKAMOTO, Kiyomi<sup>3</sup>; SAKAI, Tôru<sup>4</sup>;  
YONEMITSU, Kenji  
(<sup>1</sup>IMS and Tohoku Univ.; <sup>2</sup>Niigata Univ.; <sup>3</sup>Tokyo Inst. Tech.; <sup>4</sup>Tohoku Univ.)

[*J. Phys. Soc. Jpn.* **74**, Suppl. 63–66 (2005)]

We study field-induced phase transitions and long-range orders in the  $S = 1/2$  spin bond-alternating chain with frustrating interaction. By using the inter-chain mean field theory combined with the finite temperature density matrix renormalization group, we investigate properties of field-induced long-range orders and phase transitions. We find that the inter-chain interaction strongly affects the realized phases of this system.

### I-R-3 Field-Induced Incommensurate Order in Frustrated Spin Chain

MAESHIMA, Nobuya<sup>1</sup>; OKUNISHI, Kouichi<sup>2</sup>;  
OKAMOTO, Kiyomi<sup>3</sup>; SAKAI, Tôru<sup>4</sup>;  
YONEMITSU, Kenji  
(<sup>1</sup>IMS and Tohoku Univ.; <sup>2</sup>Niigata Univ.; <sup>3</sup>Tokyo Inst. Tech.; <sup>4</sup>Tohoku Univ.)

[*Prog. Theor. Phys.* submitted]

A mechanism of the incommensurate long-range order induced by external magnetic field is considered to propose its possible realization in the bond-alternating spin chain F<sub>5</sub>PNN. Using the density matrix renormalization group analysis, we present several typical phase diagrams, depending on the interchain interaction and the frustration due to the next-nearest-neighbor coupling. A possible magnetization plateau at half the saturation moment is also discussed.

### I-R-4 Phase Diagram of the Excitonic Insulator

HÜLSEN, Björn<sup>1</sup>; BRONOLD, Franz X.<sup>2</sup>; FEHSKE, Holger<sup>2</sup>; YONEMITSU, Kenji  
(<sup>1</sup>Fritz-Haber-Inst.; <sup>2</sup>Ernst-Moritz-Arndt-Univ.)

[*Physica B* in press]

Motivated by recent experiments, which give strong evidence for an excitonic insulating phase in TmSe<sub>0.45</sub>Te<sub>0.55</sub>, we developed a scheme to quantitatively construct, for generic two-band models, the phase diagram of an excitonic insulator. As a first application of our approach, we calculated the phase diagram for an effective mass two-band model with long-range Coulomb interaction. The shielded potential approximation is used to derive a generalized gap equation controlling for positive (negative) energy gaps the transition from a semi-conducting (semi-metallic) phase to an insulating phase. Numerical results, obtained within the quasi-static approximation, show a steeple-like phase diagram in contrast to long-standing expectations.

### I-R-5 Effective Interaction between the Interpenetrating Kagome Lattices in Na<sub>x</sub>CoO<sub>2</sub>

INDERGAND, Martin<sup>1</sup>; YAMASHITA, Yasufumi;  
KUSUNOSE, Hiroaki<sup>2</sup>; SIGRIST, Manfred<sup>1</sup>  
(<sup>1</sup>ETH-Hönggerberg; <sup>2</sup>Tohoku Univ.)

[*Phys. Rev. B* **71**, 214414 (19 pages) (2005)]

A multiorbital model for a CoO<sub>2</sub> layer in Na<sub>x</sub>CoO<sub>2</sub> is derived. In this model, the kinetic energy for the degenerate  $t_{2g}$  orbitals is given by indirect hopping over oxygen, leading naturally to the concept of four interpenetrating Kagome lattices. Local Coulomb interaction couples the four lattices and an effective Hamiltonian for the interaction in the top band can be written in terms of fermionic operators with four different flavors. Focusing on charge- and spin-density instabilities, a big variety of possible metallic states with spontaneously broken symmetry are found. These states lead to different charge, orbital, spin, and angular momentum order-

ing patterns. The strong superstructure formation at  $x = 0.5$  is also discussed within this model.

### **I-R-6 Magnetism in Strongly Correlated and Frustrated Systems**

**UEDA, Kazuo<sup>1</sup>; YAMASHITA, Yasufumi**  
(<sup>1</sup>*Univ. Tokyo*)

[*Physica B* **359**, 626–632 (2005)]

In strongly correlated systems, some of the low-energy excitations are enhanced. In geometrically frustrated systems, due to the absence of long-range order, there remains (pseudo-) degeneracy associated with the low-energy excitations at low temperatures. Lifting of degeneracy in both Mott insulating systems and itinerant electron systems are discussed by considering the pyrochlore lattice as an example.

# I-S Theory and Applications of Relativistic Quantum-Chemical Methods to Molecular Properties of Compounds Containing Heavy Elements

In our project, we have been developing accurate quantum-chemical theories and methods, we applied these methods to calculations of circular dichroism (CD), magnetic circular dichroism (MCD), and nuclear magnetic resonance (NMR) spectra, in which magnetic interaction and/or electron-spin density play an important role, especially in compounds containing heavy elements. Our progresses in this period are as follows. (i) Excitation and CD spectra of dichalcogenide were calculated by the SAC-CI method and the trends of the observed CD spectra were reproduced, and then the mechanism of the well-known  $C_2$  rule and the quadrant rule in  $C_2$  molecules were clarified. (ii) MCD spectra of halogen molecules were calculated by the 2<sup>nd</sup>-order Douglas-Kroll relativistic method, and some relativistic effects in MCD were discussed. (iii)  $^{13}\text{C}$  NMR chemical shifts of CO in various metal complexes interacting with CO, which are models of metal enzymes in biological systems, were calculated and we found that the trend of  $^{13}\text{C}$  chemical shifts of CO interacting with various metals were classified by the electron configurations of metals.

## I-S-1 Theoretical Studies on Circular Dichroism Spectra of Linear and Cyclic Dichalcogenide Compounds (Chalcogen = S, Se, Te) by the SAC and SAC-CI Methods

SEINO, Junji<sup>1</sup>; HONDA, Yasushi<sup>1</sup>; HADA, Masahiko<sup>2</sup>; NAKATSUJI, Hiroshi<sup>3</sup>  
(<sup>1</sup>Tokyo Metropolitan Univ.; <sup>2</sup>IMS and Tokyo Metropolitan Univ.; <sup>3</sup>Kyoto Univ.)

[*J. Phys. Chem.* submitted]

We developed a method and a computer software to calculate circular dichroism (CD) intensity in a framework of the SAC/SAC-CI theory. Four chalcogen (Ch) compounds; dihydrogen dichalcogenide, dimethyl dichalcogenide, (+)-bis(2-methylbutyl) dichalcogenide, and 2,3-(R,R) dichalcogenadecalin (chalcogen = S, Se, Te) were treated. As shown in Figure 1, the calculated excitation spectra were in good agreement with the experimental ones, and the calculated CD intensities also reproduce the observed spectra in the low-energy region. In four compounds investigated here, the first and the second bands are assigned to the  $n\text{-}\sigma^*$  excitations between the Ch atoms, and the third and the fourth bands are assigned to the  $n\text{-}\sigma^*$  excitations between the chalcogen and carbon atoms, respectively. The change in the spectra against the R–Ch–Ch–R dihedral angle revealed the relation between the CD spectra and molecular structures of the dichalcogen compounds. These results were in accordance with the well-known experimental rules, namely the  $C_2$  rule and the quadrant rule. On the other hand, as the chalcogen is heavier, the lowest two bands were calculated to be in the low-energy region. This also agrees with the experimental trends.

The solvent and relativistic effects were not considered in this study, although they are expected to be important in fact. In particular, the treatment of the singlet-triplet coupling will be essential for ditellurides. These are interesting subjects for the study in the near future.

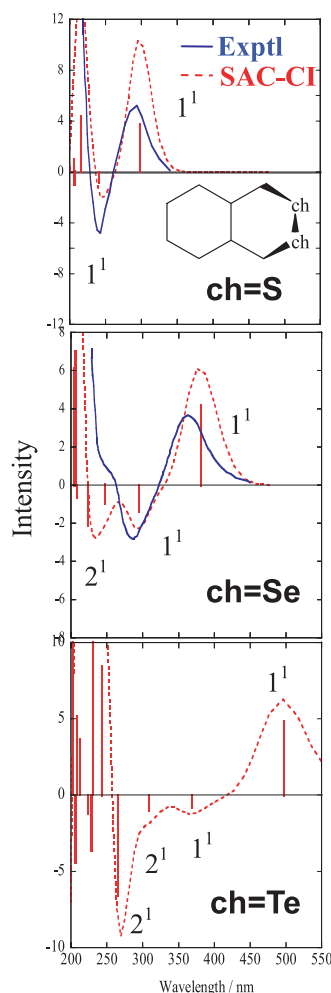


**Figure 1.** Calculated and observed circular dichroism (CD) spectra of 2,3-(R,R) dichalcogenadecalin (chalcogen = S, Se, Te). The observed spectra are shown by real lines and the calculated ones are shown by dotted lines.

### I-S-2 Theoretical Studies on Magnetic Circular Dichroism by the Finite Perturbation Method with Relativistic Corrections

HONDA, Yasushi<sup>1</sup>; HADA, Masahiko<sup>2</sup>; EHARA, Masahiro<sup>3</sup>; NAKATSUJI, Hiroshi<sup>3</sup>; MICHL, J.<sup>4</sup>

(<sup>1</sup>Tokyo Metropolitan Univ.; <sup>2</sup>IMS and Tokyo Metropolitan Univ.; <sup>3</sup>Kyoto Univ.; <sup>4</sup>Colorado Univ.)

[*J. Chem. Phys.* in press]

A theoretical method for calculating magnetic circular dichroism (MCD) of molecules was presented. We examined the numerical accuracy and the stability of the finite perturbation (FP) method and the sum-over-state (SOS) perturbation method. The relativistic effects were shown to be important for the MCD spectra of molecules containing heavy elements. Calculations using the FP and the SOS methods were carried out for ethylene, *para*- and *ortho*-benzoquinone (BQ), showing that the FP method was superior to the SOS method, as expected. The differences were not negligible, and even the signs of the terms obtained by the two methods were opposite for the lowest  $\pi$ - $\pi^*$  states of ethylene. The relativistic effect was examined using the second-order Douglas-Kroll Hamiltonians for the three  $n$ - $\pi^*$  states ( $^3\Pi_{1u}$ ,  $^3\Pi_{0u}$ , and  $^1\Pi_u$ ) of each of the halogen molecules I<sub>2</sub>, Br<sub>2</sub>, Cl<sub>2</sub>, and F<sub>2</sub>. The relativistic effects became important for the MCD spectra of heavy molecules: the Faraday terms of I<sub>2</sub> and Br<sub>2</sub> were strongly affected by the relativistic effects, while the effect was negligible for Cl<sub>2</sub> and F<sub>2</sub>. The spin-free relativistic Hamiltonian incorporating the one-electron spin-orbit term gave the results similar to the full relativistic case, indicating that the relativistic effects induced by the two-electron spin-orbit term in MCD are small. In all calculations, the signs of the Faraday terms agreed with those of the experimental values, although some of their absolute values were overestimated compared to the experiments. This was thought to be mainly due to a lack of electron correlation. A two-component quasi-relativistic theory based on the Douglas-Kroll-Hess transformation is developed in order to study a magnetic shielding constant. The Hamiltonian that is proposed in this study is considering the relativistic effect on magnetic vector potential with the Douglas-Kroll theory. The present Hamiltonian can be applied to calculation of magnetic shielding constants, without further expansion in powers of  $c^{-1}$ . The calculated results indicated that the relativistic corrections are essential to the theoretical treatments of MCD for molecules containing heavy atoms.

### I-S-3 <sup>13</sup>C NMR Chemical Shifts of Small Molecules Interacting with Metal Complexes in Heme Proteins and Metal Enzymes

HADA, Masahiko<sup>1</sup>; KUZUOKA, Chie<sup>2</sup>

(<sup>1</sup>IMS and Tokyo Metropolitan Univ.; <sup>2</sup>Tokyo Metropolitan Univ.)

[*J. Comput. Chem., Jpn.* to be submitted]

We treated (a) the paramagnetic <sup>13</sup>C NMR chemical shifts of CN anion interacting with model complexes of

ferric heme proteins and (b) diamagnetic <sup>13</sup>C NMR of CO interacting with various imidazole-metal complexes which act as a model of metal enzymes in various biological systems.

(a) The observed paramagnetic carbon-13 chemical shifts of cyanide in ferric porphyrin complexes were recently reported by Fujii. When the trans ligand is a cyanide anion, the shift is -2500 ppm from TMS. When replaced with an imidazole ligand, the shift becomes -4000 ppm. We can observe these chemical shifts over a very wide range. This wide variation of chemical shifts is essentially due to the spin density of the resonance carbon in these open-shell paramagnetic molecules. Therefore, we can use these cyanide-carbon NMR chemical shifts as a probe for testing various heme-protein environments. The trends of <sup>13</sup>C chemical shifts in these systems should be clarified by the theoretical methods. The objectives of this theme are followings. (i) Using an accurate quantum-chemical method, SAC/SAC-CI, we present accurate energy-levels for ferric ( $d_{xy}$ )<sup>2</sup>( $d_{xz,yz}$ )<sup>3</sup> and ( $d_{xy}$ )<sup>1</sup>( $d_{xz,yz}$ )<sup>4</sup> in bis(cyanide)porphyrinato Iron(III) [FeP(CN)<sub>2</sub>], bis(cyanide)(*meso*-tetraethyl) porphyrinato Iron(III) [FeTEP(CN)<sub>2</sub>], and (cyanide)(imidazole) porphyrinato-Iron(III) [FeP(CN-Im)]. (ii) We calculate the paramagnetic <sup>13</sup>C NMR chemical shifts of iron-bound <sup>13</sup>CN of the above three complexes, both in the ground and low-lying excited states including the ferric ( $d_{xy}$ )<sup>2</sup>( $d_{xz,yz}$ )<sup>3</sup> and ( $d_{xy}$ )<sup>1</sup>( $d_{xz,yz}$ )<sup>4</sup> configurations. Then we show the relations between the calculated <sup>13</sup>C chemical shifts, the electronic configurations, and the ruffling of the porphyrin rings.

First, we analyzed the <sup>13</sup>C chemical shifts of CO in some typical excited states. The temperature dependent Fermi contact term plays an important role to control the <sup>13</sup>C chemical shifts of CO by transferring the electron-spin density from the d-orbital of Fe to the CN ligand. This mechanism depends on the electronic configurations of Fe, and is affected sensitively by the trans-ligands.

Second, the effect of deviation of porphyrin ring. The D<sub>4h</sub> structure becomes the S<sub>4</sub> structure by replacing hydrogen atoms with methyl or ethyl groups. The electronic ground state is the B<sub>2</sub> state, though it is the E<sub>g</sub> state in the D<sub>4</sub> structure. We found that the ruffling of porphyrin ring drastically affect the chemical shifts of Fe-bounded CN. The total trend of the NMR shifts is controlled by both changing electronic states and ruffling of porphyrin ring.

(b) Various metal-imidazole complexes in metal enzymes interact with CO, were investigated by observing the NMR chemical shifts of <sup>13</sup>C of CO. MIm<sub>3</sub>(CO)<sub>2</sub> (M = Cr<sup>2+</sup>, Fe<sup>2+</sup>, Cu<sup>+</sup>, Zn<sup>2+</sup>; Im = Imidazole) were used as a model of metal-enzymes. The calculated NMR chemical shifts agree well with the downfield shift observed experimentally in Cu<sup>+</sup>. The trend of the <sup>13</sup>C NMR chemical shifts were explained by the d-d transition mechanism, namely by the 2<sup>nd</sup>-order perturbation theory for the paramagnetic term.

## I-T Polyamorphism in Molecular Liquids

So far the only quantity known as the order parameter that distinguishes liquids from gases is density. However, a recent experimental confirmation of the very existence of the pressure-induced “structural” transition between stable liquids of black phosphorus lends strong impetus to reconsideration on the concepts of liquids. As represented by amorphous ice, such polyamorphism in metastable states has been known for a long time. Very recently we found that the melting curve of the low-pressure crystalline phase of a molecular crystal  $\text{SnI}_4$ , which is known to undergo pressure-induced solid-state amorphization, has a maximum at around 2 GPa. This means that an abrupt change in liquid density takes place at that pressure, which is expected to be attributable to liquid-liquid phase transition. The purpose of the project is not only to experimentally reveal the transition but also to construct the statistical-mechanical model for the transition from which order parameters other than the density characterizing the polyamorphism can be extracted.

### I-T-1 Construction of an Interaction-Site Model for Molecular Systems

**FUCHIZAKI, Kazuhiro**  
(*IMS and Ehime Univ.*)

Our target substance is a molecular crystal  $\text{SnI}_4$ , which exhibits a variety of structural and electrical properties under high pressures.<sup>1)</sup> Although our model crystalline with octupole-octupole interactions entered as the first nonvanishing contribution to the perturbed part exhibited considerably higher melting points<sup>2)</sup> compared to the experimental results,<sup>3)</sup> investigations on the liquid state utilizing this model is still attractive, since no experimental information under high pressures has been as yet available. However, actual numerical computations are much time-consuming. Hence, to set up a new interactions-site model that can deal with molecular systems more efficiently in the simulations is by no means trivial.

Let us suppose molecular systems consisting of electrically neutral molecules with internal degrees of freedom. We assume that the intermolecular interactions are given by the sum of the interactions between the interaction sites within a molecule. The constituent interaction is proportional to the inverse power  $s$  of a distance between the interaction sites. Let  $\mathbf{r}_i$  be the center-of-mass position of the  $i$ th molecule. The position of the  $k$ th interaction site relative to  $\mathbf{r}_i$  is given by  $\alpha^k \mathbf{p}_i^k$ ,  $\mathbf{p}_i^k$  being fixed to the molecule. We locate a “charge” at the interactions site, which is denoted by  $\zeta_i^k(s)$ . The quotation marks are intended to mean that the charges are ordinary electric charges when  $s = 1$ , but otherwise, they are virtual whose magnitude yields the units of [energy]/[(length) <sup>$s$</sup> ] when multiplied with each other. This generalization of the concept of charges allows us to treat the interaction sites in a unified fashion without regarding the Coulombic interaction sites as being special. We then arrange these molecules in a  $p$ -dimensional computational cell, whose basis vectors are given by  $[\mathbf{u}_1, \mathbf{u}_2, \dots, \mathbf{u}_p] = \mathbf{h}$ . When the periodic boundary condition is imposed, the position of  $k$ th interaction site within  $i$ th molecule in  $m$ th image cell is given by  $\mathbf{r}_m + \mathbf{r}_i + \alpha^k \mathbf{p}_i^k = \mathbf{r}_m + \mathbf{r}_i^k(\alpha^k)$ . Here,  $\mathbf{r}_m = \mathbf{h}\mathbf{m}$ ,  $\mathbf{m}$  being the vector whose components are all integers. Then, total intermolecular interaction is given by  $\Phi = \sum_s \Phi(s;p)$  with

$$\Phi(s;p) = \frac{1}{2} \sum_m \sum_i \sum_{k \in i} \sum_j \sum_{l \in j} \frac{\zeta_i^k(s) \zeta_j^l(s)}{|\mathbf{r}_m + \mathbf{r}_i^k(\alpha^k(s); \alpha^l(s))|^s},$$

where  $\mathbf{r}_{ij}^{kl}(\alpha^k(s); \alpha^l(s)) = \mathbf{r}_i^k(\alpha^k) - \mathbf{r}_j^l(\alpha^l)$ . The lattice sums appearing in this expression corresponds to a special case of the generalized zeta function of  $p$ th order developed by the author.<sup>4)</sup> Derivation of the final expression for  $\Phi(s;p)$  together with some examples of its implementation will soon be reported.

#### References

- 1) N. Hamaya, K. Sato, K. Usui-Watanabe, K. Fuchizaki, Y. Fujii and Y. Ohishi, *Phys. Rev. Lett.* **79**, 4597–4600 (1997).
- 2) K. Fuchizaki and K. Nagai, *Solid State Commun.* **132**, 305–308 (2004).
- 3) K. Fuchizaki, Y. Fujii, Y. Ohishi, A. Ohmura, N. Hamaya, Y. Katayama and T. Okada, *J. Chem. Phys.* **120**, 11196–11199 (2004).
- 4) K. Fuchizaki, *J. Phys. Soc. Jpn.* **63**, 4051–4059 (1994).

## I-U Nonlinear Processes Induced by Ultrafast Laser Pulses

Recent technological progress on the generation of intense XUV pulses has opened up a new field on ultrafast and nonlinear optics. Commercial femtosecond Ti:Sapphire laser systems typically produce light pulses with pulse durations of tens of fs around the wavelength of 800 nm. Recalling that the optical cycle of the 800 nm light pulse is 2.7 fs, the pulse duration of tens of fs implies that tens of cycles are contained in a single pulse. When the number of the cycles decreases down to a few-cycle, new phenomena which are dependent on the carrier-envelope phase (absolute phase) emerge. In this project, we have carried out theoretical investigation related to the few-cycle pulse.

### I-U-1 Few-Cycle Effects in the Low Intensity Regime

NAKAJIMA, Takashi<sup>1</sup>; WATANABE, Shuntaro<sup>2</sup>  
(<sup>1</sup>IMS and Kyoto Univ.; <sup>2</sup>Univ. Tokyo)

One of the most fascinating features induced by few-cycle-pulses is that laser-induced dynamics such as ionization and high harmonic generation have a dependence on the carrier-envelope-phase (CEP). Naturally any kinds of CEP effects will be easily smeared out if the CEP is not stabilized on the shot-to-shot basis. Whether and how much CEP effects we can see depends on the number of cycles and pulse intensity, and the dependence is different for different systems even

with the same pulse conditions. In the intensity region where tunneling ionization plays a major role, the dynamics can be rather well described using a semi-classical theory, *i.e.*, quasi-static tunneling theory for ionization, with the help of classical mechanics after the electron ejection, and it was shown that photoelectron yields exhibit a clear CEP dependence. In the weaker intensity region, however, tunneling ionization hardly takes place and multiphoton ionization is the dominant process for ionization. It has not yet been clarified whether and how much CEP effects can be seen in the weaker intensity region. We have theoretically studied the CEP effects in this intensity regime and found significant CEP effects in terms of the total ionization yield and the bound state population of atomic systems.

## I-V Control of Photoionization Processes Using Lasers

Optical control of various photoexcitation processes are of great interest in recent years, which is termed "coherent control." In this project, we have theoretically explored the possibility to control spin-polarization and the ejection angle of photoelectrons.

### I-V-1 Control of the Spin-Polarization of Photoelectrons/Photoions Using Short Laser Pulses

NAKAJIMA, Takashi  
(IMS and Kyoto Univ.)

[*Appl. Phys. Lett.* **84**, 3786–3788 (2004)]

Since highly spin-polarized species such as electrons, ions, and nucleus, *etc.*, are very useful in various fields, developing a new method to control the spin degree of freedom is one of the most important issues in modern technology and science. Recently we have theoretically proposed a generic pump-probe scheme to control spin-polarization of photoelectrons/photoions by short laser pulses. The validity of the theoretical treatment, however, has been limited to the weak field in which a very small fraction of atoms are pumped to the excited states. For the maximum production of spin-polarized ions/electrons, it is desired to use strong pump/probe pulses. Based on the Schrödinger equation, we have developed a theory of spin-polarization so that the laser intensities can be arbitrarily strong. By numerically solving the derived equations for the realis-

tic scheme of Mg atom, we have found a intensity-dependent spin-polarization.

### I-V-2 Control of Photoelectron Angular Distributions Using a Dressing Laser

NAKAJIMA, Takashi<sup>1</sup>; BUICA, Gabriela<sup>2</sup>  
(<sup>1</sup>IMS and Kyoto Univ.; <sup>2</sup>Kyoto Univ.)

[*Phys. Rev. A* **71**, 013413 (2005)]

[*Phys. Rev. A* **72**, 053416 (2005)]

Strong dressing laser field can induce various interesting modification in laser-matter interactions. Among them, an interesting modification is observed in the photoionization spectra in the wavelength region at which two-photon near-resonance is satisfied for the initially occupied state by a probe laser and initially unoccupied state by a dressing laser. This is known as laser-induced continuum structure (LICS). Recently we have reported the theoretical analysis of LICS for the K atom in terms of the modification of photoelectron angular distribution, where the geometry of laser polarization has been limited to the case in which both probe and dressing lasers are linearly polarized and parallel.

We have obtained strong modifications, as a function of the two-photon laser detuning and the dressing laser intensity, in the photoelectron distribution and the branching ratios into different ionization continua.

We have further extended the analysis for the case with a variable polarization angle. Again, a significant polarization-angle dependence has been found in terms of the photoelectron angular distribution and the branching ratios into the different ionization continua.

## I-W Theoretical Studies on Dynamical Foundation of Chemical Reactions and Proteins

Recent experimental developments in single molecule spectroscopy have shed light on the distinct nonergodic features and the heterogeneity of the state space and non-Markovian process of biomolecules. This project focuses on the dynamical foundation of chemical reactions, *i.e.*, why and how do the reacting systems climb through the saddle? and on the developments of new time series analyses to extract the dynamical information regarding the underlying state space structure from single molecule time series.

### I-W-1 Phase Space Reaction Network on Multibasin Energy Landscapes

LI, Chun Bui<sup>1,2</sup>; MATSUNAGA, Yasuhiro<sup>1</sup>; TODA, Mikito<sup>3</sup>; KOMATSUZAKI, Tamiki<sup>1,2,4</sup>  
(<sup>1</sup>Kobe Univ.; <sup>2</sup>JST/CREST; <sup>3</sup>Nara Women's Univ.; <sup>4</sup>IMS)

[*J. Chem. Phys.* **123**, 184301 (13 pages) (2005)]

Recent theoretical developments<sup>1-4</sup> in chemical reactions have greatly improved our understanding of the definability of the no-return dividing hypersurface and the reaction path along which all reacting species follow. By using the HCN/CNH isomerization reaction as an illustrative vehicle of chemical reactions on multi-basin energy landscapes, we give explicit visualizations of molecular motions associated with straight-through reaction tube in the phase space inside which all reactive trajectories pass from one basin to another, with eliminating recrossing trajectories in the configuration space. This visualization provides us with a chemical intuition of how chemical species “walk along” the reaction rate slope in the multi-dimensional phase space compared with the intrinsic reaction path in the configuration space. The distinct nonergodic features in the two different HCN and CNH wells can be easily demonstrated by a section of Poincaré surface of section in those potential minima, which predicts *a priori* the pattern of trajectories residing in the potential well. We elucidate the global phase space structure which gives rise to non-Markovian dynamics or dynamical correlation of sequential multi-basin chemical reactions. The controllability of the product state in chemical reactions is also presented in terms of the phase space structure.

#### References

- 1) T. Komatsuzaki and R. S. Berry, *Proc. Natl. Acad. Sci. U.S.A.* **98**, 7666 (2001).
- 2) T. Komatsuzaki and R. S. Berry, *J. Chem. Phys.* **130**, 4105 (2001).
- 3) T. Komatsuzaki and R. S. Berry, *Adv. Chem. Phys.* **123**, 79 (2002).
- 4) M. Toda, T. Komatsuzaki, T. Konishi, R. S. Berry and S. A. Rice, Eds., “Geometrical Structures of Phase Space in Multidimensional Chaos: Applications to Chemical Reaction Dynamics in Complex Systems,” *Adv. Chem. Phys.* **130A,130B** (2005).

### I-W-2 A Construction of Multidimensional Free Energy Landscape from an Ensemble of Single Molecule Time Series

BABA, Akinori<sup>1,2</sup>; KOMATSUZAKI, Tamiki<sup>1,2,3</sup>  
(<sup>1</sup>Kobe Univ.; <sup>2</sup>JST/CREST; <sup>3</sup>IMS)

Recent experimental developments in single molecule spectroscopy hold great promise to shed light on the complexity of dynamics of biomolecules. However, without any knowledge about the potential energy function and the number of energy basins with the metric relation among them, what can we learn from an observed single molecule scalar time series about the multivariate free energy landscape or, in general, state space structure buried in the observations?

Using local ergodicity ansatz as a 0<sup>th</sup> order description, we developed a new empirical self-consistent scheme to elucidate the local ergodic state distribution function from an ensemble of short single molecule time series and construct an effective multidimensional free energy landscape where local ergodic states are located with preserving the “metric” relationship among them as possible in the projected space. We also proposed the transition sequence analysis to elucidate the degree of memory along each transition sequence path.

### I-W-3 A New Technique to Differentiate the Origin of Observed non-Brownian Dynamics in the Principal Component Space

MATSUNAGA, Yasuhiro<sup>1</sup>; LI, Chun Bui<sup>1,2</sup>; KOMATSUZAKI, Tamiki<sup>1,2,3</sup>  
(<sup>1</sup>Kobe Univ.; <sup>2</sup>JST/CREST; <sup>3</sup>IMS)

The dimensional reduction is crucial to focus on some important degrees of freedom in manybody protein dynamics. The principal component (PC) analysis is one of the most widely used methods and the projection of protein dynamics on the PC space have often shown large deviations from a simple normal Brownian picture, for example, in Crambin in crystal,<sup>1</sup> Cytochrome *c* in water,<sup>2</sup> Plastocyanin in water.<sup>3</sup> However, it was derived analytically<sup>4</sup> that multidimensional normal Brownian motion can also exhibit the regular behavior on the PC space deviated from normal Brownian motion. What can we learn from the projection of complex protein dynamics onto the PC space?

We developed a new diagnostic technique to differentiate the origin of the observed regular behavior in order to extract essential (rather than artifact) informa-

tion inherent to the dynamics of the protein by using finite size Liapunov exponent concept<sup>5),6)</sup> and the PC eigenvalue spectrum.<sup>7)</sup>

#### References

- 1) A. E. García, R. Blumenfeld, G. Hummer and J. A. Krumhansl, *Physica D* **107**, 225 (1997).
- 2) A. E. García and G. Hummer, *Proteins* **36**, 175 (1999).
- 3) P. Carlini, A. R. Bizzarri and S. Cannistraro, *Physica D* **165**, 242 (2002).
- 4) B. Hess, *J. Chem. Phys.* **62**, 8438 (1999).
- 5) G. Paladin, M. Serva and A. Vulpiani, *Phys. Rev. Lett.* **74**, 66 (1995).
- 6) T. Shibata and K. Kaneko, *Physica D* **124**, 177 (1998).
- 7) J. B. Gao, Y. Cao and J. -M. Lee, *Phys. Lett. A* **314**, 392 (2003).

#### I-W-4 Polypeptide in Water on the Lagrange Picture in Fluid Dynamics

**NODA, Satoshi<sup>1</sup>; BABA, Akinori<sup>1,2</sup>;**  
**KOMATSUZAKI, Tamiki<sup>1,2,3</sup>**  
 (<sup>1</sup>Kobe Univ.; <sup>2</sup>JST/CREST; <sup>3</sup>IMS)

The (overdamped) Langevin formulation has been one of the most utilized methods in describing complex dynamics of biomolecules in solution. This is based on an implicit assumption of the existence of separable time scales between the global dynamics of biomolecules and those of the surrounding solvents. However, recently, it was revealed for human Lysozyme in solution<sup>1),2)</sup> that the rotational diffusion of *local dipole field*, which is defined as a short time ensemble average of the dipole moment vectors of many individual water molecules at a solvent site through which they pass or visit, has dynamical memory up to 70 times longer than the rotational relaxation of the individual water molecules in the vicinity of human Lysozyme. This indicates that the time separability required for validating the Langevin formulation does not necessarily hold and water molecules may not necessarily retard the protein motions as "friction." We examined a dynamic inseparability of helix-coil transition of polyalanine and the surrounding water rearrangement by investigating the correlation between individual site dipole vector field and turn moiety dynamics of polyalanine. We found that, at the turn formation, the site-dipole field dynamics and turn formation is correlated more significant than those before and after the formation, that is consistent with the computational mechanics analysis for Leu-Enkephalin in solution.<sup>3)</sup>

#### References

- 1) J. Higo, *et al.*, *Proc. Natl. Acad. Sci. U.S.A.* **98**, 5961 (2001).
- 2) T. Yokomizo, S. Yagihara and J. Higo, *Chem. Phys. Lett.* **374**, 453 (2003).
- 3) D. Nerukh, G. Karvounis and R. C. Glen, *Complexity* **10**, 40 (2004).



## RESEARCH ACTIVITIES II

### Department of Molecular Structure

#### II-A Development of Dynamic Near-Field Spectroscopy and Application to Nanometric Systems

There is much demand for the study of local optical properties of molecular assemblies and materials, to understand mesoscopic phenomena and/or to construct optoelectronic devices in the nanometric scale. Scanning near-field optical microscopy (SNOM), which enables spatial resolution beyond the diffraction limit of light, shows remarkable progress in technology in these days. Combination of this advanced optical technology with ultrafast spectroscopic methods may offer a direct probe of molecular dynamical processes in mesoscopic systems. It may bring essential and basic knowledge for analyzing origins of characteristic features and functionalities of mesoscopic systems. We are constructing apparatuses for near-field dynamic spectroscopy with the femtosecond temporal resolution and the nanometer spatial resolution. Using the apparatuses developed, we have observed characteristic spatiotemporal behavior of various organic molecular systems and metal nanoparticles, for the purpose of understanding spatial coherence and dissipation of excitations and their dynamics. Outlines of the experimental results obtained are summarized here.

##### II-A-1 Morphological and Spectroscopic Properties of Thin Films of Self-Assembling Amphiphilic Porphyrins on Hydrophilic Surface as Revealed by Scanning Near-Field Optical Microscopy

NAGAHARA, Tetsuhiko; IMURA, Kohei;  
OKAMOTO, Hiromi; OGURO, Akane<sup>1</sup>; IMAHORI,  
Hiroshi<sup>1</sup>  
(<sup>1</sup>Kyoto Univ.)

[*J. Phys. Chem. B* **109**, 19839–19844 (2005)]

We fabricated porphyrin thin films on mica surfaces from acidic aqueous solutions of the pre-organized H-aggregates of amphiphilic porphyrins (5,10,15,20-tetrakis(4-(4-(trimethylammonio)butoxy)phenyl)porphyrin bromide, TABPP, and the related compounds) by simple spin-coating method. The morphological and spectroscopic properties of the film formed on mica substrate were investigated by atomic force microscopy and scanning near-field optical microscopy. The surface topographic image and the near-field transmission image taken at the wavelength of the H-aggregate band (Figures 1a and b) are negatively correlated very well each other. That is, the optical transmission at the position of higher topographic height (the bright part in the topographic image) is lower than that at the lower-height position. This indicates that the film of ~3 nm height consists mainly of the H-aggregate. The results obtained demonstrate that the pre-organized H-aggregate structure in solution can be transferred as a thin film with a thickness of monolayer level without losing their substantial structure and photophysical properties.

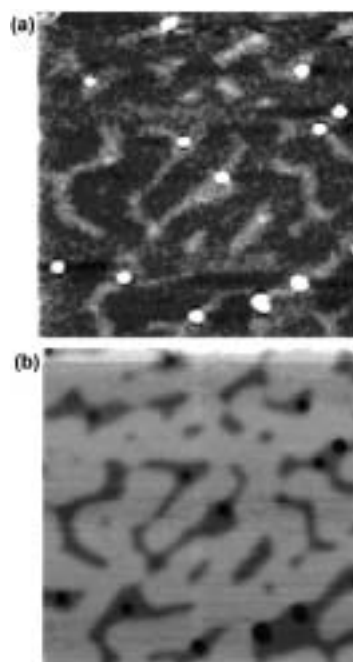


**Figure 1.** (a) Surface topography of the thin-film sample of TABPP on mica (scan area:  $10\ \mu\text{m} \times 10\ \mu\text{m} \times 3\ \text{nm}$ ). Bright and dark parts correspond to high and low parts of the sample surface, respectively. (b) Transmission image of the sample obtained at 430 nm. Bright and dark parts correspond to high and low transmission intensities, respectively.

##### II-A-2 Scanning Near-Field Optical Microscopic Study of Porphyrin Nanowire

NAGAHARA, Tetsuhiko; IMURA, Kohei;  
OKAMOTO, Hiromi; OZAWA, Hiroaki; OGAWA,  
Takuji

We studied optical properties of molecular nanowires of coupled zinc porphyrins with bulky dendric groups, by means of scanning near-field optical microscopy and spectroscopy. The topographic images and the

near-field-excited fluorescence images gave string-like structures, and correlated well to each other. We also performed polarization dependence measurements. The analysis of the obtained data is now in progress.

### II-A-3 Imaging of Plasmon Modes in Gold Nanorods

IMURA, Kohei; NAGAHARA, Tetsuhiko;  
OKAMOTO, Hiromi

[*J. Phys. Chem. B* **109**, 13214–13220 (2005)]

Surface plasmon resonances (SPRs) of noble metals have attracted much interest, since the SPR gives not only fundamental importance in science but also various applications in nanotechnology. Knowledge of the spatial characteristics of the surface plasmons, as well as the spectral and polarization characteristics, is essential for the control of electric field confinement in near-field and of plasmon properties. We investigate the spatial characteristics of plasmon-mode wavefunctions by a SNOM.

Gold nanorods were prepared in solutions using the seed-mediated methods. For SNOM measurements, gold nanorods were dispersed on cover-slips by spin-coating method. Figures 1(a,b) show two typical near-field two-photon induced photoluminescence (TPI-PL) images observed for single gold nanorods. The dotted squares indicate approximate shapes of the rods estimated from the topographic measurements. As can be seen in the figures, the PL intensities show characteristic spatial oscillations along the long axis. Figures 1(c,d) show calculated electromagnetic local density of states (LDOS) images for the corresponding nanorods. The good agreements between the observations and the calculated LDOS images indicate that oscillatory structures found in Figures 1(a,b) represent spatial characteristics of the plasmon modes of the nanorods at the excitation wavelength.

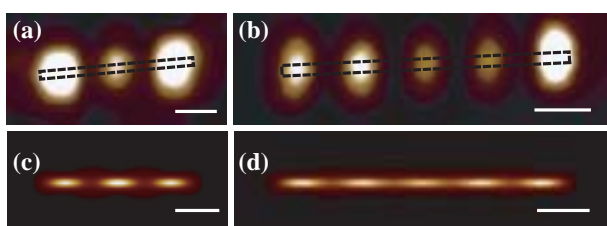


**Figure 1.** (a,b) TPI-PL images for single gold nanorods: (a)  $20 \pm 5$  nm  $\times$   $330 \pm 30$  nm, (b)  $20 \pm 5$  nm  $\times$   $540 \pm 40$  nm. (c,d) Calculated LDOS maps for the corresponding gold nanorods (a,b), respectively. Scale bars are 100 nm.

### II-A-4 Near-Field Two-Photon Induced Photoluminescence from Single Gold Nanorods

IMURA, Kohei; NAGAHARA, Tetsuhiko;  
OKAMOTO, Hiromi

[*J. Phys. Chem. B* **109**, 13214–13220 (2005)]

Studies of photoluminescence (PL) from the metal nanoparticles were limited because of very low quantum efficiencies. A strong enhancement of PL from gold nanorods upon single photon excitation was reported.<sup>1)</sup> The enhancement was ascribed to the local field enhancement due to the SPR of the gold nanorods. Two-photon optical processes involve an additional field enhancement, and thus a greater enhancement of PL efficiency is expected. We investigate two-photon induced PL (TPI-PL) from single gold nanorods of variety of lengths and diameters using an apertured SNOM, in order to characterize the emission mechanism and the optical features of the TPI-PL process.

Dependencies of the PL intensity on the polarizations of both the excitation (incoming) and the emitted (outgoing) photons are shown in Figure 1. The dependence of the PL intensity on the incident electric-field polarization [Figure 1(a)] indicates that TPI-PL is excited by the sequential one-photon process. Figures 1(c) and 1(d) show polarization characteristics of the emitted photons from the X (645–655 nm) and L (450–550 nm) regions, respectively. The emission from the X region shows an almost perfect polarization along the long axis while that from the L region is only partially polarized. The polarization characteristics obtained can be reasonably understood on the basis of the crystalline structure and the band structure of the gold nanorods.

### Reference

1) M. B. Mohamed, V. Volkov, S. Link and M. A. El-Sayed, *Chem. Phys. Lett.* **317**, 517 (2000).

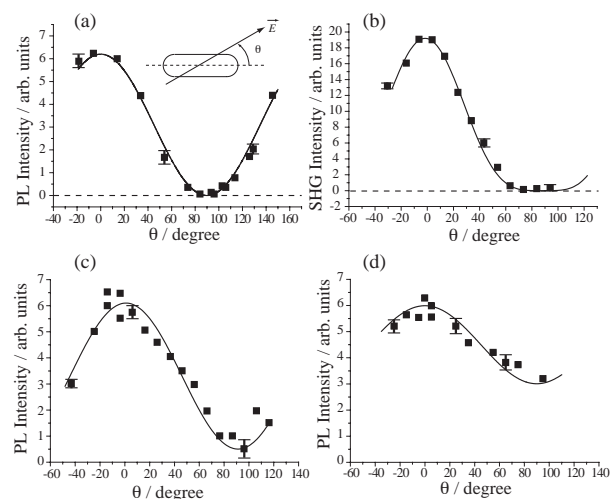


**Figure 1.** (a) Incident polarization dependence of the PL intensity. (b) Incident polarization dependence of the SHG intensity from the same nanorod. (c,d) Polarization characteristics of the detected photons in (c) the X region (645–655 nm) and (d) the L region (450–550 nm), respectively.

### II-A-5 Dispersion Relation of Plasmon Modes in the Gold Nanorods

IMURA, Kohei; NAGAHARA, Tetsuhiko;  
OKAMOTO, Hiromi

[*J. Chem. Phys.* **122**, 154701 (2005)]

Surface plasmon (SP) resonances of noble metal particles have recently attracted much interest, especially for their ability in local confinement of optical near-field. Imaging of electromagnetic local density of states (LDOS) inside single noble particles leads to direct optical observation of the SP modes. We study the optical-frequency dependent spatial characteristics of the LDOS inside the gold nanorods by the transmission-mode SNOM to obtain a dispersion relation of the SP modes.

By plotting the resonance frequencies of SP modes versus the wave vectors (which are directly obtained from the SP-mode images), the dispersion relation of the gold nanorod is obtained. The dispersion relation based on the DOS calculations for the rods is given in Figure 1 (triangles). The calculated points roughly follow a single dispersion curve, which is converging to the resonance frequency of the transverse SP mode at high wavenumber limit. We have also found that the near-field observations for various length nanorods with approximately the same diameter (closed circles) follow this curve. The results indicate that the resonance energies of multipolar SP modes in various rods of a given diameter can be estimated from the dispersion curve, even if the rod lengths are different.

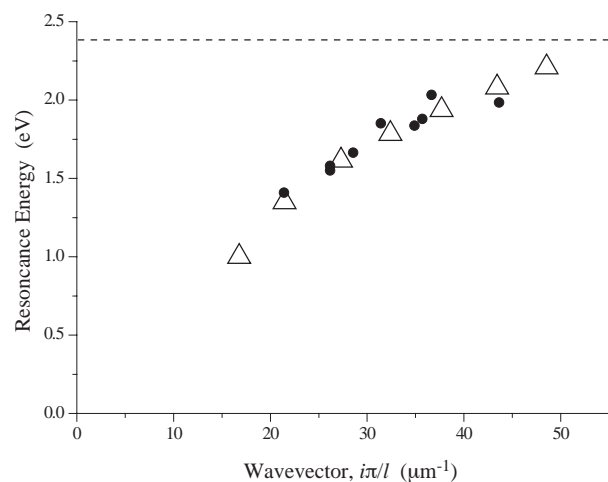


**Figure 1.** SP dispersion relation for gold nanorods. Closed circles: Observations. Open triangles: Calculations. Dashed horizontal line indicates the transverse SP resonance energy.

#### II-A-6 Imaging and Dispersion Relations of Surface Plasmon Modes in Silver Nanorods by Near-Field Spectroscopy

LIM, Jong Kuk<sup>1</sup>; IMURA, Kohei; NAGAHARA, Tetsuhiko; KIM, Seong Keun<sup>2</sup>; OKAMOTO, Hiromi (<sup>1</sup>IMS and Seoul Natl. Univ.; <sup>2</sup>Seoul Natl. Univ.)

[*Chem. Phys. Lett.* **412**, 41–45 (2005)]

Surface plasmons of silver nanorods were investigated by using scanning near-field optical microscopy. The silver nanorods were synthesized in water solution by reducing  $\text{AgNO}_3$  under existence of surfactant molecules. Near-field transmission images showed spatially oscillatory patterns in the silver nanorods. The oscillatory features of images are attributable to plasmon-

mode wavefunctions. As is similar to the gold nanorod cases, the spatial oscillation period depends on the wavelength of the observing light. From the near-field images and spectra, the wave vectors and the resonant frequencies of the plasmon modes observed were directly estimated. In this way the dispersion relations of the plasmon modes for various silver nanorods were obtained. It was found that dispersion relation of a nanorod is dependent on its diameter. The spectral features obtained are compared with those for gold nanorods.

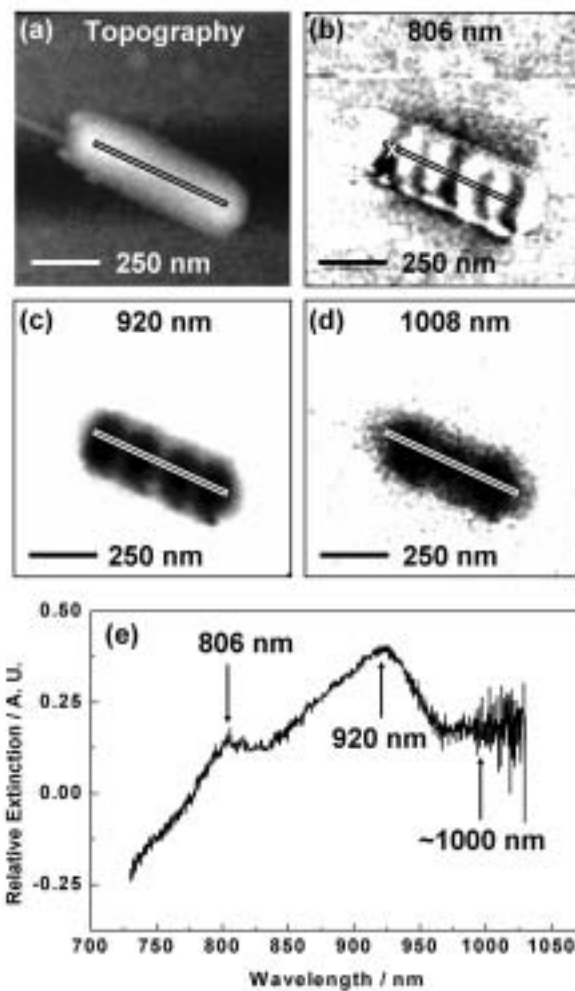


**Figure 1.** Representative images of nanorods and their near-field spectrum. (a) Topography of silver nanorod, *ca.* 20 nm in diameter and *ca.* 530 nm in length. (b)–(d) Near-field transmission images probed with an unpolarized light at 806, 920, and 1008 nm, respectively. (e) Near-field spectrum taken at the position marked “X” in the near-field transmission (b).

#### II-A-7 Ultrafast Near-Field Imaging of Single Gold Nanorods and Nanoplates

IMURA, Kohei; OKAMOTO, Hiromi

It is of fundamental importance to know how the electron-electron and electron-phonon scattering processes after photoexcitation depend upon size and shape of nanoparticles and how they proceed inside the particle. Dynamic spectroscopy of a single particle with

high temporal and spatial resolution must be informative for this purpose. Previously we performed ultrafast near-field pump-probe imaging of relatively short gold nanorods, and revealed the position dependent electron-phonon relaxation. In the present study, we have extended the study to longer nanorods and nanoparticles of other shapes, and investigated the dynamic behavior after photoexcitation in a space- and time-resolved manner.

A Ti:sapphire laser ( $\lambda = 780$  nm,  $< 100$  fs, 80 MHz) was used for time-resolved pump-probe measurements. From the near-field pump-probe measurements of various single gold nanorods and nanoplates, we found that the energy dissipation processes are dependent upon its size and shape, as well as upon the internal position of the nanoparticle.

### **II-A-8 Near-Field Spectroscopy of Close-Packed Self-Assembled Monolayer Films of Gold Nanoparticles**

**IMURA, Kohei; OKAMOTO, Hiromi; HOSSAIN, M. Kamal<sup>1</sup>; ISHIOKA, Kunie<sup>1</sup>; KITAJIMA, Masahiro<sup>1</sup>**

*(<sup>1</sup>Natl. Inst. Mater. Sci. and Univ. Tsukuba)*

Two-dimensional (2D) nanostructured materials of noble metal nanoparticles, in particular gold nanoparticles, have attracted much attention because of their unique optical properties. To characterize its optical properties as well as its potentiality in industry, we are studying the transmission, two-photon induced photoluminescence (TPI-PL), and surface enhanced Raman scattering (SERS) from the 2D structure by near-field spectroscopy and microscopy.

The 2D nanostructure of gold nanoparticles was fabricated by simply controlling the surface tension and the coverage area. The surface morphology of the fabricated 2D structure was examined by an atomic force microscope and a scanning electron microscope, and found to be a well-ordered close-packed monolayer, whose area is as large as several hundreds  $\mu\text{m}^2$  to  $\text{mm}^2$ .

In the near-field transmission spectra, it is found that the 2D structure exhibits several longitudinal surface plasmon resonances resulted from the localized plasmon coupling. In these regions, near-field TPI-PL and SERS intensities from the 2D structure are stronger than those from the isolated particles. These observations can be ascribed to the higher electric field enhancements in the ordered structure.

## II-B Spectroscopic Studies on Atoms and Ions in Liquid Helium

Atoms and ions in liquid helium are known to reside in bubble-like cavities due to the Pauli repulsive force between electrons. Physical properties of these exotic surroundings are determined by the potential energy of the impurity-He<sub>n</sub> system, the surface tension energy of the liquid helium, and the pressure-volume work. Spectroscopic studies of such impurity atoms and ions in liquid helium are expected not only to give interesting information on the structure and dynamics of the bubbles but also to contribute to the study on physical properties of superfluid liquid helium.

### II-B-1 Laser Spectroscopic Studies of Mg Atoms in Pressurized Liquid Helium

MORIWAKI, Yoshiaki<sup>1</sup>; MORITA, Norio  
(<sup>1</sup>Toyama Univ.)

We have measured excitation and emission spectra of the  $3s^2\ ^1S_0-3s3p\ ^1P_1$  transition of Mg atom in pressurized liquid helium-4 and helium-3. We have found that all these spectra show large spectral widths and large peak shifts with respect to the transition wavelength of free Mg atoms; while the excitation spectra are shifted toward the blue side, the emission spectra toward the red side. Although these are well-known spectral properties for impurity atoms in liquid He, we have also found that the peak wavelengths of the emission spectra, in particular, remain constant or slightly increase with the increasing liquid pressure. The latter is an interesting spectral property peculiar to this transition of Mg, because, for other atoms, such as Ba, Rb, Cs, Tm and Ca, and for other transitions of Mg, the increase of the liquid pressure always shifts their emission spectra toward shorter wavelength. Our bubble model calculation has successfully reproduced these properties of the Mg spectra, and has given a reasonable explanation to those peculiar properties. Moreover, further considerations based on the calculated results have suggested the possibility of the formation of a Mg( $3s3p\ ^1P_1$ )He<sub>n</sub> exciplex in a bubble.

## II-C Magnetic Structures of Magnetic Thin Films Studied by Using a Depth-Resolved XMCD Technique

Recently, we have developed a depth-resolved x-ray magnetic circular dichroism (XMCD) technique. In the soft x-ray region, an x-ray absorption spectrum is obtained generally by counting the Auger electrons emitted at the core hole relaxation, the number of which is proportional to the x-ray absorption intensity. The electron escape depth changes depending on the direction of emitted electrons. An imaging type microchannel plate is used as the electron detector, which enables us to collect the absorption spectra with various probing depths simultaneously. The XMCD spectra are obtained by reversing the sample magnetization direction at each incident helicity.

This simple technique can be applied to study the depth profile of magnetic structures of magnetic thin films.

### II-C-1 Direct Observation of an Oscillatory Behavior in the Surface Magnetization of Fe Thin Films Grown on a Ni/Cu(100) Film

AMEMIYA, Kenta<sup>1</sup>; MATSUMURA, Daiju<sup>1</sup>; ABE, Hitoshi<sup>1</sup>; KITAGAWA, Soichiro<sup>1</sup>; OHTA, Toshiaki<sup>2</sup>; YOKOYAMA, Toshihiko  
(<sup>1</sup>Univ. Tokyo; <sup>2</sup>IMS and Univ. Tokyo)

[*Phys. Rev. B* **70**, 195405 (2004)]

When a Fe film is deposited on a ferromagnetic (FM) substrate, the interface (bottom) of the Fe film should undergo some magnetic interaction with the substrate. Our aim is to study the magnetic coupling between the surface and interface for the Fe films on 6 ML Ni/Cu(100) as a function of the Fe film thickness with the depth-resolved XMCD technique. Figure 1 shows Fe L-edge XMCD spectra from 4–11 ML Fe films grown on a 6 ML Ni/Cu(100) taken at 200 K with various probing depths,  $\lambda_e$ . Each spectrum was normalized to the edge jump height, so that the XMCD intensity reflects the magnetic moments per atom as an average over the contribution from each Fe layer weighted with the electron attenuation factor. A series of the spectra from the 4 ML film (region I) show almost identical intensity regardless of  $\lambda_e$ , directly indicating a simple ferromagnetic structure. In contrast, the XMCD intensity from the 4.5 ML film is drastically reduced as  $\lambda_e$  increases. Moreover, the XMCD spectra exhibit a positive sign at L<sub>3</sub> edge, indicating that the Fe surface has an opposite magnetization direction with respect to the applied field. As the Fe thickness increases, the XMCD intensity decreases and almost vanishes around 6 ML, then grows up to 9 ML with an opposite sign. Finally, the XMCD signal almost disappears above 10 ML. These results clearly show that the Fe surface magnetization direction changes as a function of Fe thickness. Assuming that the magnetization of the Fe films consists of the contributions from (1) surface two layers, (2) inner layer and (3) interface layer, observed depth-resolved XMCD spectra were analyzed. The results show that the interface layer gives almost constant magnetization parallel with that of Ni, and the inner layer is almost nonmagnetic, and the surface two layers give the oscillatory magnetization depending on the Fe thickness. This apparent oscillation might come from the rotation of magnetic moment at the surface.

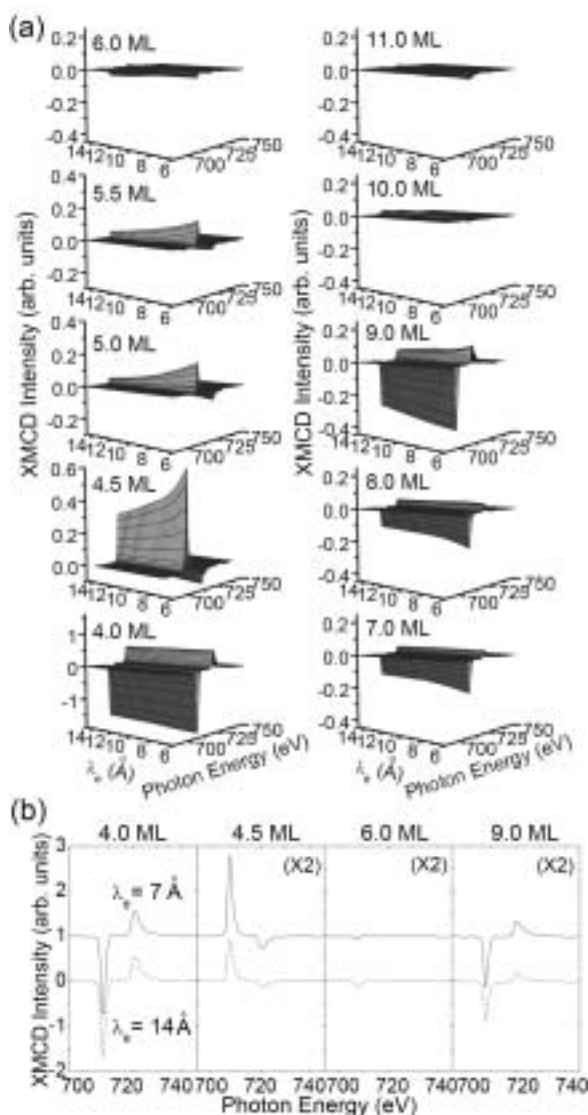


**Figure 1.** Fe L-edge XMCD spectra from Fe (4–11 ML)/Ni (6 ML)/Cu(100) films taken at 200 K with various probing depths,  $\lambda_e$  (a), together with the selected spectra at  $\lambda_e = 7$  and  $14 \text{ \AA}$  (b).

### II-C-2 Spin Reorientation Transition of Ni/Cu(100) and Co/Ni/Cu(100): Separation of the Surface and Bulk Components of the X-Ray Magnetic Circular Dichroism Spectrum

**AMEMIYA, Kenta<sup>1</sup>; SAKAI, Enju<sup>1</sup>;  
MATSUMURA, Daiju<sup>1</sup>; ABE, Hitoshi<sup>1</sup>; OHTA,  
Toshiaki<sup>2</sup>; YOKOYAMA, Toshihiko**  
(<sup>1</sup>Univ. Tokyo; <sup>2</sup>IMS and Univ. Tokyo)

[*Phys. Rev. B* **71**, 214420 (2005)]

The spin reorientation transition of Ni/Cu(100) and CO/Ni/Cu(100) films was investigated with the depth-resolved x-ray magnetic circular dichroism (XMCD) technique. The XMCD spectra from the surface and inner layers were separately extracted. As for the bare Ni films, the in-plane orbital magnetic moment in the surface layer is significantly enhanced. In contrast, the inner layers exhibit larger perpendicular orbital magnetic moment than the in-plane one. Upon CO adsorption, the surface magnetization is drastically reduced, while the inner layers are unaffected. These results directly explain the spin reorientation transition mechanism in Ni/Cu(100) and CO/Ni/Cu(100) systems.

## II-D Structure and Function of Metalloproteins and Its Molecular Design

Metal ion is a common cofactor that is crucial for active centers of proteins involved in many biologically important processes in cells, and a relatively small number of metal-based prosthetic groups are utilized to serve numerous and diverse chemical functions. A typical metal-based prosthetic group, which represents a fascinating example in this respect, is heme. Heme promotes a variety of functions, such as dioxygen storage, activation of small molecules, electron transfer reactions, and sensing gaseous molecule. In the field of protein design and engineering, hemoproteins also make particularly attractive targets. There are many reasons for this, including the exciting possibility of engineering protein-based molecules with useful catalytic, electronic or optoelectronic properties. Based on various kinds of spectroscopies, we have functionally and structurally characterized some hemoproteins including newly identified heme-regulated proteins, and designed hemoproteins showing improved activities and new functions.

### II-D-1 L358P Mutation on P450cam Simulates Structural Changes upon Putidaredoxin Binding. The Structural Changes Trigger Electron Transfer to Oxy-P450cam from Electron Donors

TOSHA, Takehiko<sup>1</sup>; YOSHIOKA, Shiro<sup>1</sup>; ISHIMORI, Koichiro<sup>2</sup>; MORISHIMA, Isao<sup>1</sup>  
(<sup>1</sup>Kyoto Univ.; <sup>2</sup>IMS and Kyoto Univ.)

[*J. Biol. Chem.* **279**, 42836–42843 (2004)]

To investigate the functional and structural characterization of a crucial cytochrome P450cam (P450cam)-putidaredoxin (Pdx) complex, we utilized a mutant whose spectroscopic property corresponds to the properties of the wild type P450cam in the presence of Pdx. The <sup>1</sup>H NMR spectrum of the carbonmonoxy adduct of the mutant, the Leu-358 3 Pro mutant (L358P), in the absence of Pdx showed that the ring current-shifted signals arising from D-camphor were upfield-shifted and observed as resolved signals, which are typical for the wild type enzyme in the presence of Pdx. Signals from the β-proton of the axial cysteine and the γ-methyl group of Thr-252 were also shifted upfield and downfield, respectively, in the L358P mutant as observed for Pdx-bound wild type P450cam. The close similarity in the NMR spectra suggests that the heme environment of the L358P mutant mimics that of the Pdx-bound enzyme. The functional analysis of the L358P mutant has revealed that the oxygen adduct of the L358P mutant can promote the oxygenation reaction for D-camphor with nonphysiological electron donors such as dithionite and ascorbic acid, showing that oxygenated L358P is “activated” to receive electron from the donor. Based on the structural and functional characterization of the L358P mutant, we conclude that the Pdx-induced structural changes in P450cam would facilitate the electron transfer from the electron donor, and the Pdx binding to P450cam would be a trigger for the electron transfer to oxygenated P450cam.

### II-D-2 Structural Diversities of Active Site in Clinical Azole Bound Forms between Sterol 14α-demethylases (CYP51) from Human and *Mycobacterium tuberculosis*

MATSUURA, Koji<sup>1</sup>; YOSHIOKA, Shiro; TOSHA, Takehiko; HORI, Hiroshi<sup>2</sup>; ISHIMORI, Koichiro<sup>3</sup>; KITAGAWA, Teizo; MORISHIMA, Isao<sup>1</sup>; KAGAWA, Norio<sup>4</sup>; WATERMAN, Michael R.<sup>4</sup>  
(<sup>1</sup>Kyoto Univ.; <sup>2</sup>Osaka Univ.; <sup>3</sup>IMS, Kyoto Univ. and Hokkaido Univ.; <sup>4</sup>Vanderbilt Univ.)

[*J. Biol. Chem.* **280**, 9088–9096 (2005)]

To gain insights into the molecular basis of the design for the selective azole anti-fungals, we compared the binding properties of azole-based inhibitors for cytochrome P450 sterol 14α-demethylase (CYP51) from human (HuCYP51) and *Mycobacterium tuberculosis* (MtCYP51). Spectroscopic titration of azoles to the CYP51s revealed that HuCYP51 has higher affinity for ketoconazole (KET), an azole derivative that has long lipophilic groups, than MtCYP51, but the affinity for fluconazole (FLU), which is a member of the anti-fungal armamentarium, was lower in HuCYP51. The affinity for 4-phenylimidazole (4-PhIm) to MtCYP51 was quite low compared with that to HuCYP51. In the resonance Raman spectra for HuCYP51, the FLU binding induced only minor spectral changes, whereas the prominent high frequency shift of the bending mode of the heme vinyl group was detected in the KET- or 4-PhIm-bound forms. On the other hand, the bending mode of the heme propionate group for the FLU-bound form of MtCYP51 was shifted to high frequency as found for the KET-bound form, but that for 4-PhIm was shifted to low frequency. The EPR spectra for 4-PhIm-bound MtCYP51 and FLU-bound HuCYP51 gave multiple *g* values, showing heterogeneous binding of the azoles, whereas the single *g<sub>x</sub>* and *g<sub>z</sub>* values were observed for other azole-bound forms. Together with the alignment of the amino acid sequence, these spectroscopic differences suggest that the region between the B' and C helices, particularly the hydrophobicity of the C helix, in CYP51s plays primary roles in determining strength of interactions with azoles; this differentiates the binding specificity of azoles to CYP51s.

### II-D-3 Two Heme Binding Sites Are Involved in the Regulated Degradation of the Bacterial Iron Response Regulator (Irr) Protein

YANG, Jianhua<sup>1</sup>; ISHIMORI, Koichiro<sup>2</sup>; O'BRIAN, Mark R.<sup>1</sup>

(<sup>1</sup>New York State Univ.; <sup>2</sup>IMS and Kyoto Univ.)

[*J. Biol. Chem.* **280**, 7671–7676 (2005)]

The iron response regulator (Irr) protein from *Bradyrhizobium japonicum* is a conditionally stable protein that degrades in response to cellular iron availability. This turnover is heme-dependent, and rapid degradation involves heme binding to a heme regulatory motif (HRM) of Irr. Here, we show that Irr confers iron-dependent instability on glutathione *S*-transferase (GST) when fused to it. Analysis of Irr-GST derivatives with C-terminal truncations of Irr implicated a second region necessary for degradation, other than the HRM, and showed that the HRM was not sufficient to confer instability on GST. The HRM-defective mutant IrrC29A degraded in the presence of iron but much more slowly than the wild-type protein. This slow turnover was heme-dependent, as discerned by the stability of Irr in a heme-defective mutant strain. Whereas the HRM of purified recombinant Irr binds ferric (oxidized) heme, a second site that binds ferrous (reduced) heme was identified based on spectral analysis of truncation and substitution mutants. A mutant in which histidines 117–119 were changed to alanines severely diminished ferrous, but not ferric, heme binding. Introduction of these substitutions in an Irr-GST fusion stabilized the protein *in vivo* in the presence of iron. We conclude that normal iron-dependent Irr degradation involves two heme binding sites and that both redox states of heme are required for rapid turnover.

### II-D-4 Involvement of Heme Regulatory Motif in Heme-Mediated Ubiquitination and Degradation of IRP2

ISHIKAWA, Haruto<sup>1</sup>; KATO, Michihiko<sup>2</sup>; HORI, Hiroshi<sup>3</sup>; ISHIMORI, Koichiro<sup>4</sup>; KIRISAKO, Takayoshi<sup>2</sup>; TOKUNAGA, Fuminori<sup>2</sup>; IWAI, Kozuhiro<sup>2</sup>

(<sup>1</sup>Osaka City Univ.; <sup>2</sup>Osaka City Univ. and CREST;

<sup>3</sup>Osaka Univ.; <sup>4</sup>IMS, Kyoto Univ., CREST and Hokkaido Univ.)

[*Mol. Cell.* **19**, 171–181 (2005)]

Iron regulatory protein 2 (IRP2), a regulator of iron metabolism, is modulated by ubiquitination and degradation. We have shown that IRP2 degradation is triggered by heme-mediated oxidation. We report here that not only Cys201, an invariant residue in the heme regulatory motif (HRM), but also His204 is critical for IRP2 degradation. Spectroscopic studies revealed that Cys201 binds ferric heme, whereas His204 is a ferrous heme binding site, indicating the involvement of these residues in sensing the redox state of the heme iron and in generating the oxidative modification. Moreover, the HRM in IRP2 has been suggested to play a critical role

in its recognition by the HOIL-1 ubiquitin ligase. Although HRMs are known to sense heme concentration by simply binding to heme, the HRM in IRP2 specifically contributes to its oxidative modification, its recognition by the ligase, and its sensing of iron concentration after iron is integrated into heme.

## II-E Structure and Energy Changes during Protein Reaction Dynamics

The thermodynamic properties (enthalpy, thermal expansion coefficient, compressibility, partial molar volume, etc.) as well as the transport property (diffusion coefficient) of proteins are of fundamental importance to understand the structural fluctuation and the dynamics of protein molecules. Traditional techniques that can access to these quantities are certainly useful and powerful to characterize the proteins. However, knowledge of these properties of time-dependent or unstable (intermediate) species during biological reactions is very limited. It is most desirable to develop and use a method that can measure these properties in time domain so that reaction intermediates can be characterized in a similar way. In this project, we try to construct a method to probe energies and conformational changes as well as the diffusion coefficients of biological proteins in time domain. One of interesting applications of this technique is to detect spectral silent kinetics in reactions of biological proteins.

### II-E-1 Hydrogen Bonding Dynamics During Protein Folding of Reduced Cytochrome *c*: Temperature and Denaturant Concentration Dependence

NISHIDA, Shinpei<sup>1</sup>; NADA, Tomokazu<sup>1</sup>;  
TERAZIMA, Masahide<sup>2</sup>

(<sup>1</sup>Kyoto Univ.; <sup>2</sup>IMS and Kyoto Univ.)

[*Biophys. J.* **89**, 2004–2010 (2005)]

Folding dynamics of reduced cytochrome *c* triggered by the laser induced reduction method is investigated from a view point of the intermolecular interaction change. Change of the diffusion coefficient of Cyt *c* during the refolding process is traced in time domain from the unfolded value to the native value continuously at various denaturant (guanidine hydrochloride (Gdn-HCl)) concentrations and temperatures. In the temperature range of 288 K–308 K and GdnHCl concentration range of 2.5 M–4.25 M, the diffusion change can be analyzed well by the two state model consistently. It was found that the  $m^\ddagger$ -value and the activation energy of the transition state from the unfolded state for the hydrogen bonding network change are surprisingly similar to that for the local structural change around the heme group monitored by the fluorescence quenching experiment. This agreement suggests the existence of common or similar fundamental dynamics including water molecular movement to control the refolding dynamics. The nature of the transition state is discussed.

### II-E-2 Conformational Dynamics of Phototropin 2 LOV2 Domain with the Linker upon Photoexcitation

EITOKU, Takeshi<sup>1</sup>; NAKASONE, Yusuke<sup>1</sup>;  
MATSUOKA, Daisuke<sup>2</sup>; TOKUTOMI, Satoru<sup>2</sup>;  
TERAZIMA, Masahide<sup>3</sup>

(<sup>1</sup>Kyoto Univ.; <sup>2</sup>Osaka Pref. Univ.; <sup>3</sup>IMS and Kyoto Univ.)

[*J. Am. Chem. Soc.* **127**, 13238–13244 (2005)]

Conformational dynamics of LOV2 domain of phototropin, a plant-blue-light photoreceptor, is studied by the pulsed laser induced transient grating (TG) technique. The TG signal of LOV2 without the linker

part to the kinase domain exhibits the thermal grating signal due to the heat releasing from the excited state and a weak population grating by the adduct formation. The diffusion coefficients of the adduct product after forming the chemical bond between the chromophore and Cys residue is found to be slightly smaller than that of the reactant, which fact implies that the core shrinks slightly on the adduct formation. After that change, no significant conformational change was observed. On the other hand, the signal of LOV2 with the linker part to the kinase domain clearly shows very different diffusion coefficients between the original and the adduct species. The large difference indicates significant global conformational change of the protein moiety upon the adduct formation. More interestingly, the diffusion coefficient is found to be time dependent in the observation time range. This dynamics representing the global conformational change is a clear indication of a spectral silent intermediate between the excited triplet state and the signaling product. From the temporal profile analysis of the signal, the rate of the conformational change is determined to be 2 ms.

## II-F Controllable Magnetic Properties of Ultrathin Magnetic Films Using Surface Chemical Techniques

Noble properties of magnetic thin films such as perpendicular magnetic anisotropy (PMA) and giant magnetoresistance (GMR) have extremely attracted scientific and technological interests. The origin of perpendicular magnetic anisotropy of ultrathin metal films is not fully understood and is an important subject in fundamental physics but is useful for high-density recording media. The GMR property is already utilized for read-heads of hard disk drives, although quantitative understanding of the GMR is still to be improved. We have been investigating drastic changes of magnetic properties of ultrathin metal films by using surface chemical modification such as atoms/molecules adsorption on the surface. Especially, the microscopic mechanism of spin reorientation transitions induced by gaseous adsorption on magnetic film surfaces have been investigated by means of the synchrotron radiation x-ray magnetic circular dichroism (XMCD), the visible-light magneto-optical Kerr effect (MOKE) and the magnetization induced second harmonic generation (MSHG) techniques. A goal of these works is spin engineering by which the magnetization of ultrathin metal films and nanowires can be controlled artificially.

### II-F-1 MOKE and XMCD Study on K Adsorption on Fe Ultrathin Films on Cu(001)

NAKAGAWA, Takeshi; WATANABE, Hirokazu;  
YOKOYAMA, Toshihiko

It is interesting to investigate whether electron donation to magnetic metal films induces the enhancement or suppression of magnetization. Especially, Fe could be a candidate whose magnetization is enhanced by electron donation. In the present work, we have studied the effect of K adsorption on *fcc* (face-centered-tetragonal) Fe and Co grown on Cu(001) by means of the polar MOKE and the XMCD methods.

Figure 1 shows the MOKE intensity from 3 ML Fe on Cu(001) as a function of K coverage, which was measured during K deposition. With the increase in the K coverage, the MOKE intensity increases and at 0.1 ML K deposition it is maximized. More deposition leads to the suppression. The K coverage of 0.1 ML roughly corresponds to the work function minimum. Although the MOKE intensity is usually proportional to the magnetization, it could not be the case if the electronic structure changes drastically. In order to confirm the enhanced magnetization and to obtain more direct information, we have performed XMCD measurements at BL4B of UVSOR-II. Figure 2(a) shows the Fe *L*-edge XMCD. A small increase in the XMCD signals is actually found at the K coverage of 0.1 ML. Table 1 summarizes the results of the quantitative analysis. In both the Fe and Co cases, the number of *3d* holes, which was estimated from the intensity of the white lines, is gradually reduced with the K coverage, this exemplifying the electron donation from K. In the Co case, the spin magnetic moment decreases monotonically with the K coverage. This finding is reasonable since the majority *3d* band of *fcc* Co is fully occupied and the donated electron is transferred to the minority *3d* bands, leading to the reduction of the spin magnetic moment of Co. On the contrary, the spin magnetic moment of Fe is maximized at 0.1 ML K. This verifies that the Fe spin magnetic moment is enhanced by a small amount of K deposition.

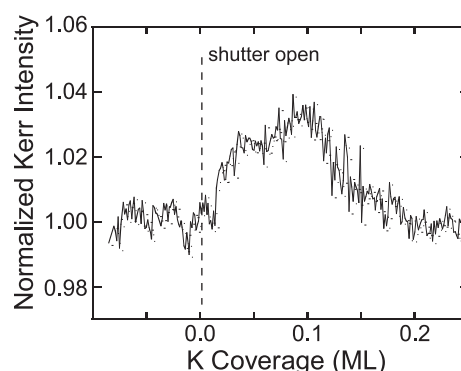


**Figure 1.** Polar MOKE intensity of 3 ML Fe/Cu(001) at 100 K as a function of K deposition.

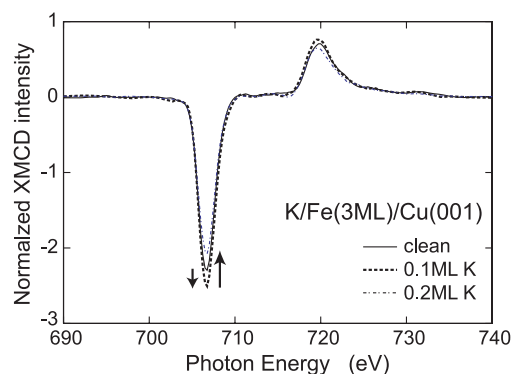


**Figure 2.** Fe *L*-edge XMCD of 3 ML Fe/Cu(001) (perpendicularly magnetized) at 100 K for the K coverages of 0.0, 0.1 and 0.2 ML.

**Table 1.** The results of the sum-rule analysis for 3 ML Fe and Co on Cu(001). *3d* hole numbers and spin ( $m_s$ ) and orbital ( $m_l$ ) magnetic moments of Fe and Co are given.

	K dep. (ML)	$3d_{\text{hole}}$ number	$m_s$ ( $\mu_B$ )	$m_l$ ( $\mu_B$ )
3 ML Fe /Cu(001)	0.0	3.40	2.29	0.24
	0.1	3.27	2.40	0.24
	0.2	3.00	1.91	0.17
3 ML Co /Cu(001)	0.0	2.50	1.67	0.26
	0.1	2.37	1.58	0.26
	0.2	2.27	1.50	0.29

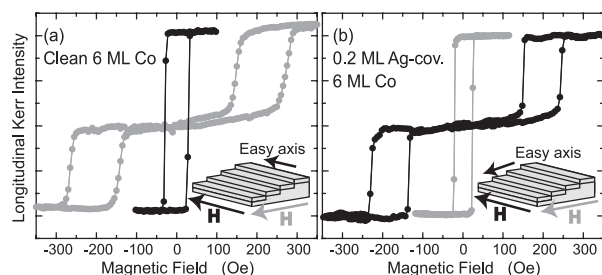
## II-F-2 Spin Reorientation Transition in Ag-Covered Co Films Grown on Vicinal Cu(001) Surface Studied by Means of XMCD

NAKAGAWA, Takeshi; WATANABE, Hirokazu; YOKOYAMA, Toshihiko

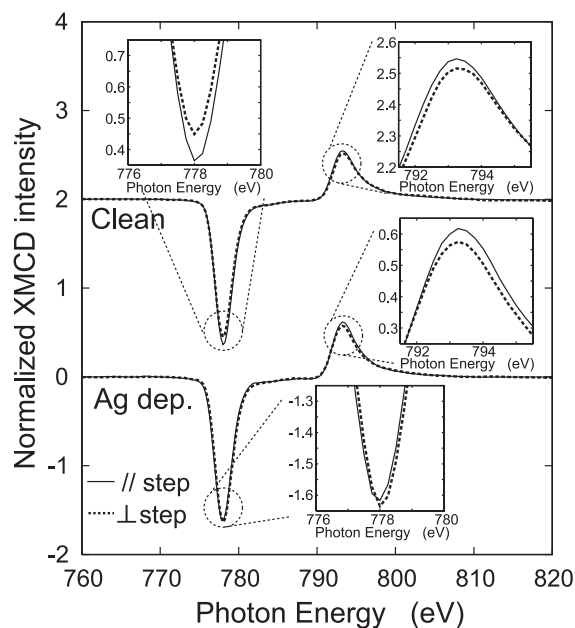
Magnetic thin films grown on vicinal surfaces exhibit strong uniaxial magnetic anisotropy; the magnetic property should be essentially different between the step-parallel and perpendicular directions. In this work, in order to obtain microscopic information on the spin reorientation transition in Ag-deposited Co films on Cu(1 1 17), we performed the longitudinal MOKE and XMCD experiments.

Figure 1 shows the magnetic hysteresis loops of MOKE. In the clean Co film, the magnetization curve along the //step direction exhibits normal rectangular shape, while that along the  $\perp$ step direction shows a double loop with zero remanence, this implying the easy axis of the //step direction. On the contrary, the reverse is true for the 0.2 ML Ag-deposited Co film; the magnetic easy axis changes from //step to  $\perp$ step, exhibiting clear spin reorientation transition. This results is identical with the previously reported work by Weber *et al.* [*Phys. Rev. B* **52**, R14400 (1995)].

Figure 2 shows the Co *L*-edge XMCD. The intensities of the  $L_{III}$ - and  $L_{II}$ -edge peaks exhibit clear difference between the clean and Ag-deposited Co films. Although the difference is rather small, one can find that larger orbital magnetic moments give the magnetic easy axis from the detailed sum-rule analysis: for clean Co,  $m_l^{\parallel} = 0.246 \mu_B$  and  $m_l^{\perp} = 0.225 \mu_B$ , while for Ag-deposited Co,  $m_l^{\parallel} = 0.200 \mu_B$  and  $m_l^{\perp} = 0.218 \mu_B$ . Moreover, we have determined the inclination angle of the easy axis. Figure 3 shows the results of the XMCD variation. The *x*-intercept corresponds to the easy axis, where  $0^\circ$  and  $-4.8^\circ$  respectively mean parallel to the physical plane and to the terrace plane. The present finding in Figure 3 concludes that the Ag deposition induces also the out-of-plane rotation of the easy axis from the physical surface plane ( $0^\circ$ ) to the terrace plane ( $-4.8^\circ$ ).



**Figure 1.** MOKE hysteresis loops of (a) clean and (b) Ag-deposited 6 ML Co/Cu(1 1 17) at 100 K.



**Figure 2.** Co *L*-edge XMCD of 6 ML Co/Cu(1 1 17) at 100 K before and after 0.2 ML Ag deposition.

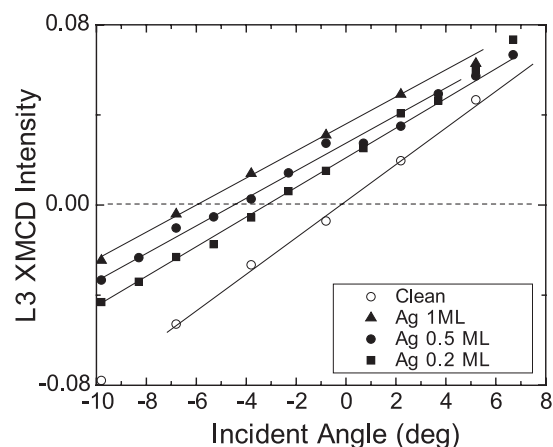


**Figure 3.** Angle dependence of Co  $L_{III}$ -edge XMCD intensity of 6 ML Co/Cu(1 1 17).

## II-F-3 Drastic Magnetization Change Observed in NO Adsorption on Co/Cu(1 1 17)

NAKAGAWA, Takeshi; WATANABE, Hirokazu; YOKOYAMA, Toshihiko

Magnetic thin films grown on vicinal surfaces exhibit strong uniaxial magnetic anisotropy and the anisotropy could be modified by surface chemical treatments. In this work, we have investigated the effect of NO adsorption on uniaxial Co films grown on Cu(1 1 17) by means of the longitudinal MOKE and the XMCD experiments.

Figure 1 shows the magnetic hysteresis loops of longitudinal MOKE. In the clean Co film, the magnetization curve along the //step direction exhibits normal rectangular shape, while that along the  $\perp$ step direction shows a double loop with zero remanence, this implying the presence of strong uniaxial magnetic anisotropy and the easy axis of the //step direction. However, drastic

changes can be seen after NO adsorption. The coercivity is reduced noticeably, and the //step and  $\perp$ step loops are completely identical, this indicating the disappearance of the inherent uniaxial anisotropy and the appearance of almost fourfold symmetric magnetic anisotropy. Such a change is much more drastic than the film on flat Cu(001).

Figure 2 shows the Co  $L$ -edge XMCD. The intensities of the  $L_{III}$ - and  $L_{II}$ -edge peaks exhibit clear difference between the clean and NO-adsorbed Co films. From the detailed sum-rule analysis, one can find that in a clean Co film a larger orbital magnetic moments give the magnetic easy axis (for clean Co,  $m_l^{\parallel} = 0.256 \mu_B$  and  $m_l^{\perp} = 0.224 \mu_B$ ), while the orbital magnetic moments are essentially the same between the //step and  $\perp$ step directions after NO adsorption ( $m_l^{\parallel} = 0.116 \mu_B$  and  $m_l^{\perp} = 0.123 \mu_B$ ). This is consistent with the longitudinal MOKE results.

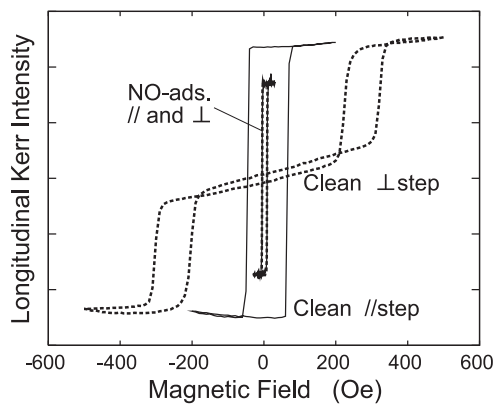


**Figure 1.** Longitudinal MOKE hysteresis loops of clean and NO-adsorbed 6 ML Co films on Cu(1 1 1 $\bar{7}$ ) at 100 K.

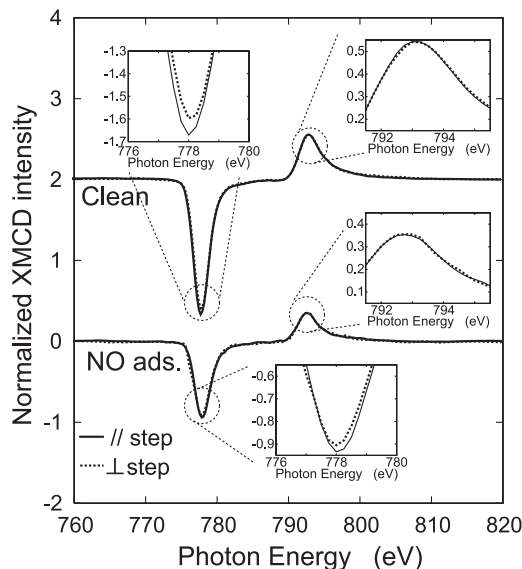


**Figure 2.** Co  $L$ -edge XMCD of 6 ML Co/Cu(1 1 1 $\bar{7}$ ) at 100 K before and after 0.5 ML NO adsorption.

## II-F-4 Direct Observation of Biquadratic Exchange Interaction in Fe/Ni/Cu(001) by Using MSHG

NAKAGAWA, Takeshi; YOKOYAMA, Toshihiko

Ultrathin  $fcc$  Fe films are known to exhibit various peculiar magnetic properties since  $fcc$  Fe shows ferromagnetism and antiferromagnetism depending on very small changes in the lattice constant. Very recently, Liu *et al.* [*Phys. Rev. B* **65** 224413 (2002)] observed an exchange bias in Fe/Ni/Cu(001) from their MOKE measurements and proposed that in there should exist biquadratic exchange interaction (perpendicular spin-spin interaction is stable). This observation is quite interesting since in the Fe/Ni system all the magnetic metal atoms are directly bonded with each other and Heisenberg exchange interaction is usually expected. In this work, we have obtained direct proof for the perpendicular magnetization in this system by using the MSHG technique exploited in this group.

Figure 1 shows the longitudinal MOKE and MSHG results. The curves of MOKE and MSHG Pin-Sout (S-polarization incidence and P-polarization reflection) give the magnetization along the magnetic field, while those of Pin-Pout and Sin-Pout the magnetization perpendicular to the magnetic field within the film plane. Actually, the perpendicular components are observed especially for 3.3 ML Fe. Figure 2 shows the remanent magnetization and the coercive field as a function of Fe coverage. Two minima at  $\sim 4$  and  $\sim 8$  ML Fe can be seen. We can recognize that each Fe layer interacts with the adjacent layer so that the magnetization directions are perpendicular with each other; 4 and 8 ML Fe films correspond to one and two periodic antiferromagnets, respectively. The presence of the biquadratic exchange interaction in this system is experimentally proved.

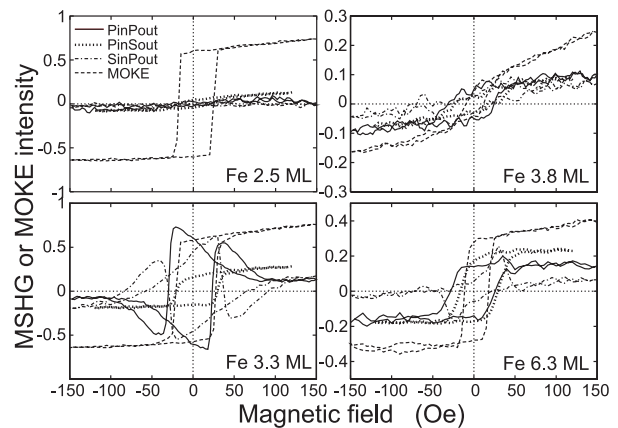


**Figure 1.** Magnetization curves given by the longitudinal MOKE and the MSHG (Pin-Pout, Sin-Pout and Pin-Sout) for Fe/Ni(7 ML)/Cu(001).

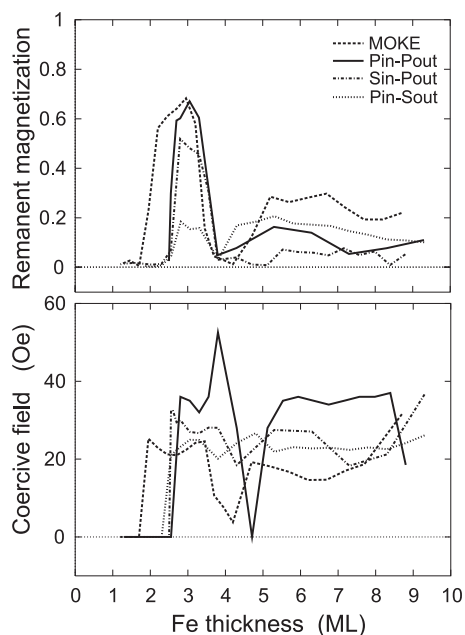


**Figure 2.** Remanent magnetization and the coercive field as a function of Fe coverage given by the longitudinal MOKE and the MSHG.

## II-G Local Structures of Molecular-Based Magnetic Materials Studied by X-Ray Absorption Fine Structure Spectroscopy

Molecular-based magnets provide noble properties such as quantum tunneling of magnetization, photoinduced magnetism *etc.* In order to understand fully the magnetic properties, structural information is indispensable. Although usually the X-ray diffraction analysis of single crystals is the most appropriate to determine the three-dimensional structure, there exist several cases when the X-ray diffraction analysis cannot be applied: the crystal structure is disordered, single crystals are hardly obtainable, and so forth. We have been studying local structures and electronic properties of interesting molecular magnets by means of X-ray absorption fine structure (XAFS) spectroscopy.

### II-G-1 Molecular Structure of Single-Molecule Magnet $\text{Mn}_{11}\text{Cr}$ , $\text{Mn}_{11}\text{Cr}^-$ and $\text{Mn}_{10}\text{Fe}_2$

YOKOYAMA, Toshihiko; HACHISUKA, Hidekazu<sup>1</sup>; AWAGA, Kunio<sup>1</sup>

(<sup>1</sup>Nagoya Univ.)

[*Phys. Rev. B* **70**, 104427 (2004)]

Single-molecular magnet of  $[\text{Mn}_{12}(\text{AcO})_{16}(\text{H}_2\text{O})_4]$  ( $\text{Ac} = \text{CH}_3\text{COO}$ ) has extensively been investigated because of its interesting properties such as stepwise magnetization due to the quantum tunneling effect. One of the outstanding features of molecular magnets is the ease of chemical modification. Recently, molecular magnets of  $\text{Mn}_{11}\text{Cr}$  ( $[\text{Mn}_{11}\text{CrO}_{12}(\text{AcO})_{16}(\text{H}_2\text{O})_4]$ )  $\text{Mn}_{10}\text{Fe}_2$  ( $[\text{Mn}_{10}\text{Fe}_2\text{O}_{12}(\text{AcO})_{16}(\text{H}_2\text{O})_4]$ ) and  $\text{Mn}_{11}\text{Cr}^-$  ( $[(\text{Ph})_4\text{P}][\text{Mn}_{11}\text{CrO}_{12}(\text{PhCOO})_{16}(\text{H}_2\text{O})_4]$ ) were synthesized. Although the single crystal x-ray diffraction analyses have been performed, the location of Cr or Fe cannot be determined because of the crystalline disorder of their positions. In such a case, EXAFS is the most

suitable technique to determine the molecular structure.

Figure 1 depicts the Fourier transforms of the EXAFS functions of  $\text{Mn}_{11}\text{Cr}$ . The x-ray molecular structure gives the average structure where Cr is not distinguished from Mn. There exist three types of Cr/Mn sites: Sites **1**, **2**, and **3**, as shown in Figure 2. Site **1** is occupied by  $\text{Mn}^{4+}$  ions, while Sites **2** and **3** are by  $\text{Mn}^{3+}$ . The Fourier transform of Cr is similar to the simulated one of Site **3**. It is thus concluded that, in  $\text{Mn}_{11}\text{Cr}$ ,  $\text{Cr}^{3+}$  exclusively occupies Site **3**, the tilted site for  $\text{Mn}^{3+}$  in the  $\text{Mn}_{12}$  skeleton. The magnitude of the experimental Cr–O peak is much stronger than that of the theoretical one of Site **3**, because the  $\text{Mn}^{3+}$  ion in Site **3** exhibits significantly distorted octahedron due to the Jahn-Teller effect, resulting in the suppression of the Mn–O contribution in the simulation. On the contrary, the  $\text{Cr}^{3+}$  ion shows no Jahn-Teller distortion, yielding more intense Cr–O contribution in the Fourier transform.

Essentially the same results are obtained for  $\text{Mn}_{10}\text{Fe}_2$  and  $\text{Mn}_{11}\text{Cr}^-$ , and in conclusion, the Cr/Fe ion locates exclusively at Site **3** with normal valency of Cr/Fe(III).

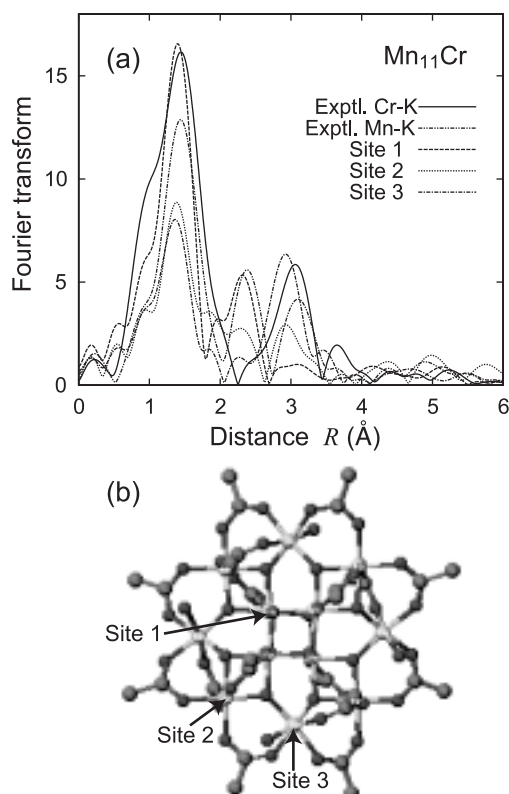


**Figure 1.** (a) Fourier transforms of the Cr (solid line) and Mn (dot-dot-dashed) K-edge EXAFS functions, together with the theoretical simulation results for Sites 1 (dotted), 2 (dot-dashed) and 3 (dashed). (b) Molecular structure of  $Mn_{12}$ . Mn atoms locate three inequivalent Sites 1, 2 and 3.

## II-G-2 Photoinduced Phase Transition of CuMo Cyanides Studied by XAFS Spectroscopy

MA, Xiao-Dong; YOKOYAMA, Toshihiko;  
HOZUMI, Toshiya<sup>1</sup>; HASHIMOTO, Kazuhito<sup>1</sup>;  
OHKOSHI, Shin-ichi<sup>1</sup>  
(<sup>1</sup>Univ. Tokyo)

[*Phys. Rev. B* **72**, 094107 (2005)]

Prussian-blue analogues often exhibit noble magnetic properties such as photoinduced magnetization. In this work, we have investigated the local structures and the electronic states mainly of the photoinduced phases of two CuMo cyanides of  $Cu_2Mo(CN)_8 \cdot 8H_2O$  (1) and  $Cs_{0.5}Cu_{1.75}Mo(CN)_8 \cdot 1.5H_2O$  (2) by means of XAFS. Usually, the photoinduced phase at low temperature is considered to be structurally identical to that of the corresponding high-temperature phase. However the photoinduced phase is an essentially new state for these two CuMo compounds because in the low-temperature phase even at room temperature they are likely to decompose with the temperature rise before thermally driven phase transition takes place.

Figure 1(a) shows the Cu K-edge spectra of samples (1) and (2) before and after photoirradiation, together with the reference spectra of  $Cu^{(I)}_2O$  and  $Cu^{(II)}O$ . One can immediately conclude that the Cu atoms in samples (1) and (2) are divalent before photoirradiation, and monovalent Cu appears after photoirradiation. Figure

1(b) shows the Mo and Cu K-edge EXAFS Fourier transforms of sample (2). Overall, one can find that the features of the initial low-temperature and photoinduced phases are almost identical. The interatomic distances are almost the same between the initial and the photoinduced phases. Differences between the low-temperature and the photoinduced phases can however be detected in the amplitude in the EXAFS oscillation. The coordination numbers of the Mo–N, Mo–Cu, and Cu–Mo shells are found reduced, while those of the Mo–C, Cu–N, and Cu–C shells as well as the first-nearest neighbor Mo–C and Cu–N shells are kept constant. The latter implies enhancement of the static Debye-Waller factors. The reduction of the coordination numbers for the Mo–N, Mo–Cu, and Cu–Mo shells may be ascribed not to the bond breaking but to the bond bending. One can qualitatively conclude that due to the photoirradiation the Mo–CN bond is bent, while the Cu–NC bond angle is kept unchanged.

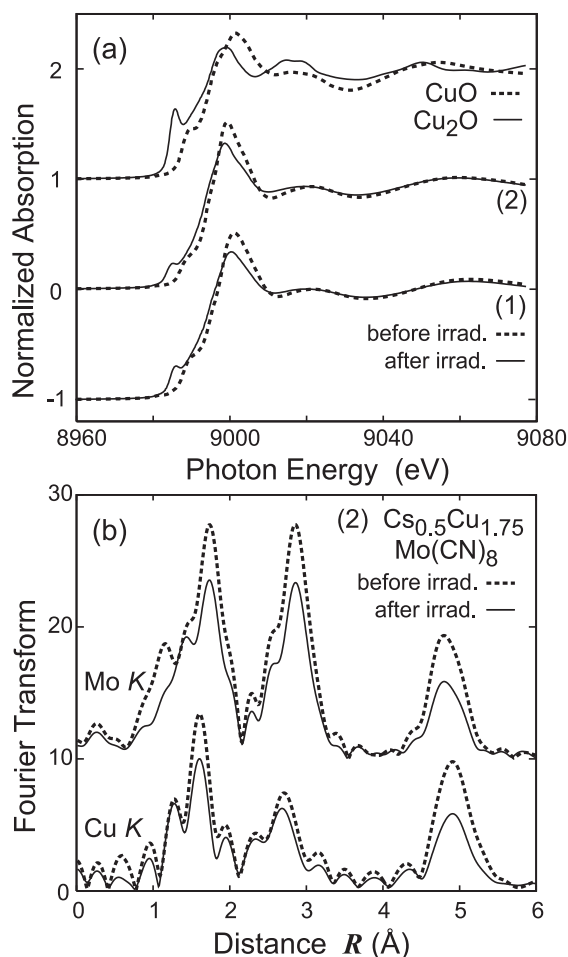


**Figure 1.** (a) Cu K-edge X-ray absorption spectra of samples (1) and (2), together with those of  $Cu_2O$  and  $CuO$ . (b) Fourier transforms of the Mo and Cu K-edge EXAFS oscillation functions of sample (2) at 30 K before and after photoirradiation.

## II-H Development of Fluorescent and Bioluminescent Proteins for Imaging Intracellular Molecular Dynamics

A current focus of biological researches is to quantify and image cellular events in living cells and animals. To probe the fundamental cellular events in living cells, we are exploring a new way for developing fluorescent and bioluminescent reporter proteins based on protein splicing. With these reporter proteins, analytical methods to detect protein-protein interactions, intracellular localization of proteins and their dynamics, enzyme activities, gene expression, and production of small bio-molecules are being actively under development. We are also investigating analytical techniques such as complementary DNA library screenings and proteome analysis.

### II-H-1 Quantitative Determination of Protein Nuclear Transport Induced by Phosphorylation or by Proteolysis

[*Anal. Chem.* **77**, 6588–6593 (2005)]

**KIM, Sung Bae<sup>1</sup>; TAKAO, Ryohei<sup>1</sup>; OZAWA, Takeaki; UMEZAWA, Yoshio<sup>1</sup>**  
(<sup>1</sup>Univ. Tokyo)

[*Anal. Chem.* **77**, 6928–6934 (2005)]

Nucleocytoplasmic transport of proteins in eukaryotic cells is a fundamental process for gene expression. The transport is regulated by post-translational modifications of the proteins such as ligand-binding, phosphorylation, and proteolysis. For monitoring the nuclear transport of proteins induced by a ligand binding, we have recently developed a genetically-encoded bioluminescent indicator based on reconstitution of split fragments of *Renilla reniformis* (Rluc) by protein splicing of a DnaE intein.<sup>1)</sup> We herein describe that the technique is used for detecting phosphorylation- or proteolysis-induced nuclear transports of a target protein. Two model proteins, signal transducer and activator of transcription 3 (STAT3) and sterol-regulatory element binding proteins-2 (SREBP-2), were exemplified as phosphorylation- and proteolysis-induced nuclear transport, respectively. Each STAT3 or SREBP-2 is connected with C-terminal halves of Rluc and DnaE. If the protein translocates into the nucleus, the C-terminal Rluc meets the N-terminal Rluc, and full-length Rluc is reconstituted by protein splicing in the nucleus. The indicator with SREBP-2 enabled to quantify the intracellular concentrations of cholesterol. The indicator with STAT3 quantified the extent of the nuclear transport induced by representative cytokines. This simple assay based on protein nuclear transports allows the selection of suitable drugs among candidates, and has significant potential for risk assessments such as carcinogenic chemical screening *in vitro* and *in vivo*.

#### Reference

1) S. B. Kim, T. Ozawa, S. Watanabe and Y. Umezawa, *Proc. Natl. Acad. Sci. U.S.A.* **101**, 11542–11547 (2004).

### II-H-2 A Stress Indicator for Noninvasively Imaging Endogenous Corticosterone in Living Mice

**KIM, Sung Bae<sup>1</sup>; OZAWA, Takeaki; UMEZAWA, Yoshio<sup>1</sup>**  
(<sup>1</sup>Univ. Tokyo)

The physical and emotional stress is one of the major controllers of physiological reactions and homeostasis in living animals. A stress hormone, corticosterone, is secreted from adrenal cortex into the blood vessel when animals sense the stress. The quantitative evaluation of corticosterone in living animals has been limited because of the unavailability of suitable methods *in vivo*. For a noninvasive molecular imaging of the stress, we developed a method for detecting physiological increases in the endogenous corticosterone caused by exo- and endogenous stress in living animals. We constructed a pair of genetically-encoded indicators composed of cDNAs of glucocorticoid receptor (GR), split *Renilla* luciferase (RLuc) and a *Synechocystis* sp. DnaE intein. The GR fused with C-terminal halves of RLuc and DnaE is localized in the cytosol, whereas a fusion protein of N-terminal halves of RLuc and DnaE is localized in the nucleus. If corticosterone induces GR translocation into the nucleus, the C-terminal RLuc meets the N-terminal one in the nucleus, and full-length RLuc is reconstituted by protein splicing with DnaE. Cell-based methods provided quantitative bioluminescence assay of the extent of GR translocation into the nucleus. We further demonstrated that the indicator enabled noninvasive imaging against two different types of imposed stress: a forced swimming and metabolic perturbation caused by 2-deoxy-D-glucose. This stress indicator should be valuable for screening pharmacological compounds and for tools to study the mechanism of physiological stress.

## RESEARCH ACTIVITIES III

### Department of Electronic Structure

### III-A Synthesis and Characterization of Exotic Molecule Based Nano-Crystals of Metal Acetylides: Toward Carbon Encapsulated Metal Dot Array, Metal Nano-Networks and Metal-Carbon Hybrid Systems

Metal-carbon binary junctions are expected to exhibit interesting properties, such as Shottoky barrier rectification, optical and tunneling devices, and chemical protector against oxidation. Metal acetylides have the ionic bond between the metallic cation and the acetylide anion. In the simplest case, divalent metal cations ( $M^{2+}$ ) form a fcc lattice structure with a  $C_2^{2-}$  anion between the two metal cations. The introduction of alkyl or aromatic group into the  $C_2$  unit, producing  $R-C\equiv C^-$ , can generate organometallic cluster compounds  $((R-C\equiv C^-)_a M^{a+})_n$ , ( $a = 1, 2$ ), some of which can be isolated as single crystals. These cluster compounds are soluble in organic solvent and provide solid films with nano-scale planarity by spin-coating method. Photoexcitation of metal-acetylides induces charge-neutralization reaction producing carbon-skinned metal particles, metallic nanowires or nano-sheets covered with organic polymer matrices. This property leads us to apply for photo-lithographical pattern generation of metallic circuits or magnetic arrays. On the other hand, the reaction mechanism of the photoreactions of the respective acetylide systems can be highly dependent on the electronic structure of metal atoms. We are also illuminating the mechanism of these reactions.

#### III-A-1 Self-Assembled Nanowire Synthesis of Highly-Anisotropic Copper Acetylide Molecules

JUDAI, Ken; NISHIJO, Junichi; OKABE, Chie;  
NISHI, Nobuyuki

Various methods have been suggested for metallic and semiconductive nanowire production, template based synthesis, vapor-liquid-solid growth, solution-liquid-solid process, oxide-assisted growth and so on. Above all, the production using a highly anisotropic crystal can be regarded as due to self-assembly of small molecules or atoms to a nanowire. The self-assembly method has potential advantage of relatively low cost, high purity, and large-scale production. However, only limited materials have anisotropic properties, for example, molybdenum chalcogenides, selenium, and tellurium. Besides, it is very hard to produce thin nanowires by only highly anisotropic properties. Here we report a new compound having a highly anisotropic crystal structure. Copper acetylide ( $C_2Cu_2$ ) molecules self-assemble into ultra thin nanowires under an extremely slow nucleation condition. Moreover, annealing of the  $C_2Cu_2$  nanowires converts to copper nanocables encapsulated in carbon outer layers. The copper nanocable core is extremely thin, in which only 8 Cu atoms can line up in the diameter.

One of the merits of self-assembly nanowire production is an extremely simple procedure of just preparing only a building block. The  $C_2Cu_2$  nanowire can be also generated facily. Figure 1 shows a scanning electron microscopy (SEM) image of  $C_2Cu_2$  products on silicon substrates, where the  $C_2Cu_2$  suspension in methanol has been dropped onto and air-dried. Nanowire morphology was observed when the  $C_2H_2$  exposing rate was kept extremely slow (0.05 mL/min). Although  $C_2Cu_2$  was

synthesized by chemical reaction of gram-order production in a flask, microscopic shape of the product is a nanoscale needle-like crystal. This indicates that  $C_2Cu_2$  molecules aggregate and self-assemble into nanowire morphology in an aqueous solution. On the contrary to the successful production of nanowires, a fast exposing rate of  $C_2H_2$  gas gave amorphous products. The key step of self-assembling for the nano-structure is just only the control of the nucleation rate of acetylide molecules.

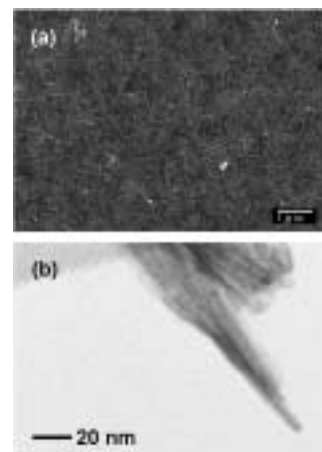


**Figure 1.** (a) SEM image of  $C_2Cu_2$  precipitate. Nanowire morphology can be obtained in the extremely slow nucleation condition. (b) TEM image of an end of a bundle of  $C_2Cu_2$  wires.

### III-A-2 Photochemical Conversion of $(\text{Cu}^+ \text{C}\equiv\text{C}^-t\text{-Butyl})_{24}$ Cluster Molecules to Cu Metallic Nano-Sheets Embedded in Polymer Nano-Film

NISHI, Nobuyuki; NISHIJO, Junichi; OKABE, Chie; OISHI, Osamu; JUDAI, Ken

Only a limited number of the cluster molecules with more than 20 metal atoms is known as structure-analyzed clusters. Olblich *et al.* reported the synthetic method and X-ray diffraction analysis of  $(\text{Cu}^+ \text{C}\equiv\text{C}^-t\text{-Butyl})_{24}$  in 1993. This molecule is soluble and shows red emission in *n*-hexane but its electronic absorption spectrum exhibits concentration dependence originated from molecular association. The association occurs in the concentration higher than  $1 \times 10^{-4}$  M. The spectral pattern of the thin film of this molecule is essentially the same as that of  $1 \times 10^{-3}$  M solution of *n*-hexane, showing a peak at 228 nm and a shoulder at 282 nm. The absorption threshold is seen at 510 nm. This absorption feature is essentially the same as those of monomer or dimer species of similar complex molecules. Cluster formation changes little of the electronic structure indicating very weak metal-metal interactions in these multinuclear cluster molecules. From the analogy of similar systems of various coordinated copper clusters, the emission is believed to originate from the triplet metal-ethynyl charge transfer state rather localized in a single pair. No emission is seen from the thin films and one can expect the presence of radiationless pathways for heat generation or reaction channel(s). The UV absorption spectrum of the spin-coated film shows a peak at 232 nm and a shoulder at 282 nm that is accompanied with the tail at 400 nm to 520 nm and the broad absorption (or background) down to near infrared region. The last broad extension is believed due to the optical scattering characteristics of the thin film. Thus, the photoexcitation of the film is expected to cause energy transfer in the triplet state. This molecule has 24 Cu-ethynyl groups and intracuster T-T annihilation can be induced. The infrared spectrum of the film also changes upon photoexcitation. The original cluster shows a doublet band at 1455 and 1474  $\text{cm}^{-1}$  characteristic of the coupled two  $-\text{C}\equiv\text{C}-$  bonds. On the photoillumination, new bands appear at higher frequencies, 1552 and 1573  $\text{cm}^{-1}$ . This indicates that the charge neutralization produces strong double bond networks around metallic copper fragments. Figure 1 shows the Transmission Electron Microscope (TEM) images of the film heated at 250 °C (left) and that irradiated with UV light from a 500W high pressure mercury lamp. The heating produces Cu nanoparticles with spherical or polyhedral shapes. The dominant sizes of the particles are 3.3 nm, 5.2 nm, 7 nm, 10.5 nm and 14 nm, suggesting the growth due to particle joining. On the other hand, photoexcitation causes growth of cubic crystals or planer copper sheets joining together and extending the metallic area wider and wider. Since the photoexcitation puts the energy into the metal atoms rather predominantly, the neutralized metal atoms are thought to cohere in the original crystal planes where the Cu cations are located. The heating may excite both metal

atoms and organic parts simultaneously and allow the metal atoms to cohere three dimensionally.

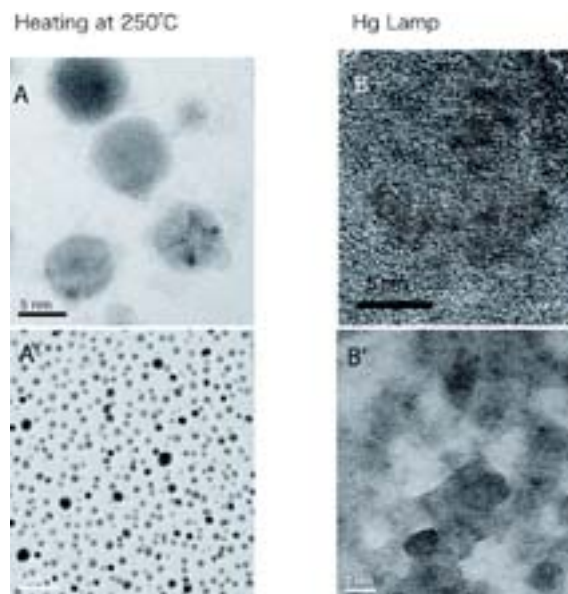


**Figure 1.** High resolution TEM images of heated (left; A and A') and photoexcited (right; B and B')  $(\text{Cu}^+ \text{C}\equiv\text{C}^-t\text{-Butyl})_{24}$  cluster films on collodion membranes.

### III-A-3 Guest Controlled Magnetism of $\text{CoC}_2$ Nanoparticles

NISHIJO, Junichi; JUDAI, Ken; NISHI, Nobuyuki

The structure of molecule-based magnets is often affected by gas or solvent absorption owing to their flexibility, and the flexibility opens up the way for controlling their magnetism by a chemical environment. We discovered that the molecule-based magnet  $\text{CoC}_2$  is an outstanding example of the "controllable magnet."

The as-prepared anhydrous  $\text{CoC}_2$  shows superparamagnetic behavior down to 2.5 K with the Curie constant of  $C = 2.5$  emu K/mol and saturation magnetization of  $M_s = 1.5 \mu_B$ . Below 2.5 K, a small part of anhydrous  $\text{CoC}_2$  shows ferromagnetic (FM) behavior, but the major part of anhydrous  $\text{CoC}_2$  are still superparamagnetic. The large Curie constant indicates the short range strong FM interaction between  $\text{Co}^{2+}$  cations. Though the existence of strong FM interactions, orientation disorder of the  $\text{C}_2^{2-}$  brings the weakening of the interaction in many places and prevents the FM transition. Once the material is exposed to ammonia gas, the  $\text{CoC}_2$  absorbs ammonia molecules accompanied by orientation ordering of the  $\text{C}_2^{2-}$ . The orientation ordering also means that the strength of the interaction between spins tend to be uniform. Indeed, the increase in the Curie constant from 2.5 to 3.5 emu K/mol by ammonia absorption suggests that the area of short range FM ordering is expanded by absorption, while the  $M_s$  keeps same value. The absorbed ammonia molecules are easily desorbed under ammonia-free condition. The desorption lowers the Curie constant from 3.5 to 2.7 emu K/mol. The decrease of the Curie constant is explained by the partial orientation disorder of  $\text{C}_2^{2-}$ ; that

is, desorption process disturbs the orientation of  $C_2^{2-}$  again, which reduces the range of the FM short range ordering. After the 1st absorption/desorption cycle, the Curie constant changes reversibly from 3.2 to 2.7 emu K/mol for ammonia absorbed and desorbed  $CoC_2$ , respectively.

The field-cooled (FC, 10 Oe) and zero field-cooled (ZFC) susceptibilities for ammonia absorbed and desorbed  $CoC_2$  are shown in figure 1. The 1st absorption raises both FC susceptibility and blocking temperature of  $T_B = 20$  K, which is indicated by the peak of ZFC susceptibility. Desorption lowers ZFC susceptibility and  $T_B$ , but the values are still larger than those of anhydrous  $CoC_2$ . After the 1st absorption/desorption cycle, though the ZFC susceptibility and  $T_B$  of ammonia absorbed  $CoC_2$  is little smaller than that of 1st cycle, the magnetism changes reversibly by absorption and desorption of ammonia. The  $T_B$  and the ZFC susceptibility at 1.8 K are raised from 5 K and 7.5 emu/mol to 10 K and 17 emu/mol, respectively, by ammonia absorption.

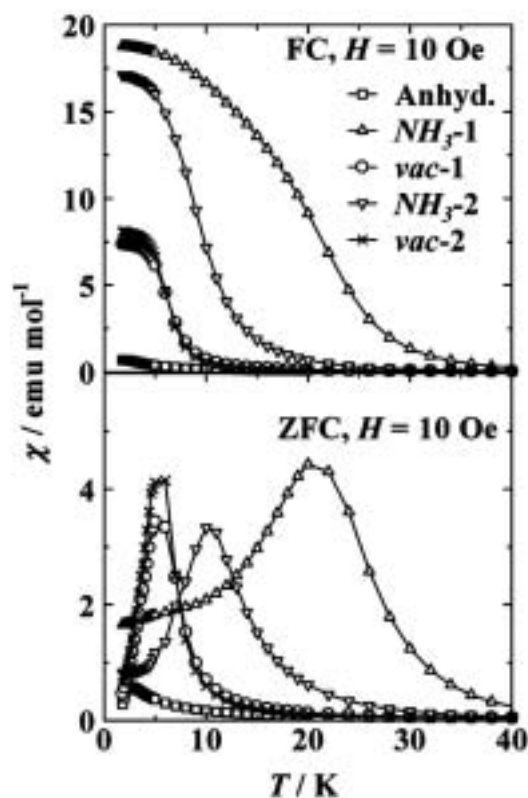


**Figure 1.** Field-cooled (FC) and zero field-cooled (ZFC) susceptibilities of ammonia absorbed/desorbed  $CoC_2$ . The legends  $NH_3$ -i and vac-i indicate the i-th times ammonia.

### III-A-4 Formation of Carbon-Encapsulated Metallic Nano-Particles from Metal Acetylides by Electron Beam Irradiation

**NISHIJO, Junichi; OKABE, Chie; BUSHIRI, Junaid M.; KOSUGI, Kentaroh; NISHI, Nobuyuki; SAWA, Hiroshi**

[*Eur. Phys. J. D* **34**, 219–222 (2005)]

Transition metal acetylides,  $MC_2$  ( $M = Fe, Co$  and  $Ni$ ), exhibit ferromagnetic behavior of which  $T_C$  is characteristic of their size and structure.  $CoC_2$  synthesized in anhydrous condition exhibited cubic structure with disordered  $C_2^{2-}$  orientation. Once being exposed to water (or air), the particles behave ferromagnetically due to the lengthening of the Co–Co distance by the coordination of water molecules to  $Co^{2+}$  cations. Heating of these particles induces segregation of metallic cores with carbon mantles. Electron beam or 193 nm laser beam can produce nanoparticles with metallic cores covered with carbon mantles.

### III-A-5 Reexamination of the Structures and Energies of $Li_2C_2$ and $Li_4C_4$

**LEE, Sang-Yeon<sup>1</sup>; BOO, Bong-Hyun<sup>2</sup>; KANG, Heun-Kag<sup>2</sup>; KANG, Dongeun<sup>2</sup>; JUDAI, Ken; NISHIJO, Junichi; NISHI, Nobuyuki**  
(<sup>1</sup>Kyungpook Natl. Univ.; <sup>2</sup>Chungnam Natl. Univ.)

[*Chem. Phys. Lett.* **411**, 484–491 (2005)]

The structures and energies of  $Li_2C_2$  and  $Li_4C_4$  have been reexamined by DFT and MP2 methods using a variety of basis sets of 6-311+G(3df) and cc-pVXZ ( $X = T, Q, 5$ ). Two low-lying isomers are found as the local minima on the potential energy surfaces of  $Li_4C_4$ . The lowest energy structure is shown to be multiply bridged  $D_{2h}$  form. A newly found quadruply bridged  $C_2$  form is found to be a local minimum, lying in energy above  $D_{2h}$  form by 22 kJ/mol in the energy. Also the energetics of high-lying isomers such as tetralithiotetrahydrene isomers were evaluated and discussed.

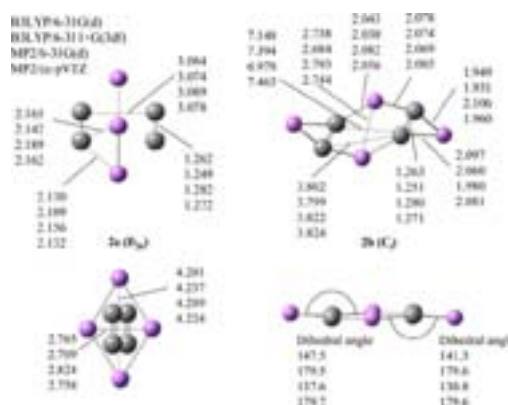


**Figure 1.** Geometries of low-lying isomers of  $Li_4C_4$  optimized by the various methods indicated herein.

## III-B Ultrafast Dynamics and Scanning Tunneling Microscopy

Proton transfer and geometrical isomerization processes in electronic excited states are investigated with our pico-femto dual wavelength valuable systems. For the study of molecules on metallic or crystalline surface, very low temperature Scanning Tunneling Microscope (LT STM) system are now in use for collaboration with users in universities.

### III-B-1 Excited-State Double-Proton Transfer in the 7-Azaindole Dimer in Gas Phase 3. Reaction Mechanism Studied by Picosecond Time-Resolved REMPI Spectroscopy

SAKOTA, Kenji<sup>1</sup>; OKABE, Chie; NISHI, Nobuyuki; SEKIYA, Hiroshi<sup>1</sup>  
(<sup>1</sup>Kyushu Univ.)

[*J. Phys. Chem. A* **109**, 5245–5247 (2005)]

The excited state double-proton transfer (ESDPT) reaction in the jet-cooled 7-azaindole dimer (7AI<sub>2</sub>) has been investigated with the picosecond time-resolved resonance-enhanced multiphoton ionization spectroscopy. The observed decay profiles of 7AI<sub>2</sub> by exciting the origin and the intermolecular stretch fundamental in the S<sub>1</sub> state are well reproduced by single exponential functions with time constants of 1.9±0.9 ps and 860±300 fs, respectively. This result provides a clear evidence of the concerted mechanism of ESDPT in 7AI<sub>2</sub>.

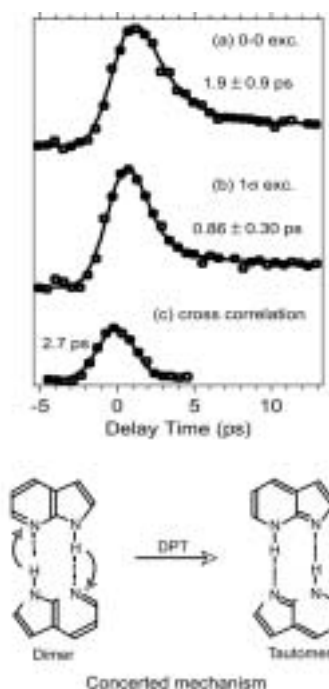


**Figure 1.** Top: Decay profiles of 7AI<sub>2</sub> pumped at (a) the origin and (b) the intermolecular stretching band, respectively. The wavelength of the probe laser was fixed at 620 nm in (a) and (b). The open circles are experimental data, while the solid curves are best-fitted curves obtained by biexponential functions. The cross correlation trace is also indicated in (c). The instrumental time resolution given by the fwhm of the cross-correlation trace is 2.7 ps. Bottom: Scheme of concerted mechanism.

### III-B-2 Ultrafast Excited-State Dynamics in Photochromic *N*-Salicylideneaniline Studied by Femtosecond Time-Resolved REMPI Spectroscopy

OKABE, Chie; NAKABAYASHI, Takakazu<sup>1</sup>; INOKUCHI, Yoshiya; NISHI, Nobuyuki; SEKIYA, Hiroshi<sup>2</sup>  
(<sup>1</sup>Hokkaido Univ.; <sup>2</sup>Kyushu Univ.)

[*J. Chem. Phys.* **121**, 9436–9422 (2004)]

Ultrafast processes in photoexcited *N*-salicylideneaniline have been investigated with femtosecond time-resolved resonance-enhanced multiphoton ionization spectroscopy. The ion signals *via* the S<sub>1</sub>(*n*,π\*) state of the enol form as well as the proton-transferred *cis*-keto form emerge within a few hundred femtoseconds after photoexcitation to the first S<sub>1</sub>(π,π\*) state of the enol form. This reveals that two ultrafast processes, excited-state intramolecular proton transfer (ESIPT) reaction and an internal conversion (IC) to the S<sub>1</sub>(*n*,π\*) state, occur on a time scale less than a few hundred femtoseconds from the S<sub>1</sub>(π,π\*) state of the enol form. The rise time of the transient corresponding to the production of the proton-transferred *cis*-keto form is within 750 fs when near the red edge of the absorption is excited, indicating that the ESIPT reaction occurs within 750 fs. The decay time of the S<sub>1</sub>(π,π\*) state of the *cis*-keto form is 8.9 ps by exciting the enol form at 370 nm, but it dramatically decreases to be 1.5–1.6 ps for the excitation at 365–320 nm. The decrease in the decay time has been attributed to the opening of an efficient nonradiative channel; an IC from S<sub>1</sub>(π,π\*) to S<sub>1</sub>(*n*,π\*) of the *cis*-keto form promotes the production of the *trans*-keto form as the final photochromic products. The two IC processes may provide opposite effect on the quantum yield of photochromic products: IC in the enol form may substantially reduce the quantum yield, but IC in the *cis*-keto form increase it.

### III-B-3 Orientation of Nitrous Oxide on Palladium(1 1 0) by STM

WATANABE, Kazuo<sup>1</sup>; KOKALJ, Anton<sup>2</sup>; INOKUCHI, Yoshiya<sup>1</sup>; RZEZNICKA, Izabela<sup>3</sup>; OHSHIMO, Keiji<sup>1</sup>; NISHI, Nobuyuki; MATSUSHIMA, Tatsuo<sup>3</sup>  
(<sup>1</sup>Univ. Tokyo; <sup>2</sup>J. Stefan Inst.; <sup>3</sup>Hokkaido Univ.)

[*Chem. Phys. Lett.* **406**, 474–478 (2005)]

The adsorption structure of N<sub>2</sub>O on Pd(110) was analyzed below 14 K by scanning-tunneling microscopy. The N<sub>2</sub>O monomer was oriented along the [001]

direction in the on-top form. Furthermore, the formation of small aggregates extending along the direction was observed. The observed images were well-simulated for two types of cluster structures optimized by density-

functional theory calculations. The components in the aggregates are proposed to be in a tilted form either on bridge sites or on-top sites.

## III-C Spectroscopic and Dynamical Studies of Molecular Cluster Ions

Electron deficiency of molecular cluster cations can attract electron rich groups or atoms exhibiting charge transfer or charge resonance interaction in the clusters. This causes dynamical structural change such as proton transfer or ion-core switching in hot cluster ions or clusters in solution.

### III-C-1 Infrared Photodissociation Spectra and Solvation Structure of $\text{Mg}^+(\text{CH}_3\text{OH})_n$ ( $n = 1-4$ )

MACHINAGA, Hironobu<sup>1</sup>; OHASHI, Kazuhiko<sup>1</sup>; INOKUCHI, Yoshiya<sup>2</sup>; NISHI, Nobuyuki; SEKIYA, Hiroshi<sup>1</sup>

(<sup>1</sup>Kyushu Univ.; <sup>2</sup>Univ. Tokyo)

[*Chem. Phys. Lett.* **391**, 85–90 (2004)]

The infrared photodissociation spectra of mass-selected  $\text{Mg}^+(\text{CH}_3\text{OH})_n$  ( $n = 1-4$ ) are measured and analyzed with the aid of density functional theory calculations. Hydrogen bonding between methanol molecules is found to be absent in  $\text{Mg}^+(\text{CH}_3\text{OH})_3$ , but detected in  $\text{Mg}^+(\text{CH}_3\text{OH})_4$  through characteristic frequency shifts of the OH stretch of methanol. The maximum number of the methanol molecules that can be directly bonded to the  $\text{Mg}^+$  ion is limited to three and the fourth molecule starts to fill the second solvation shell. The vibrational spectroscopy provides clear evidence for the closure of the first shell at  $n = 3$ .

### III-C-2 Infrared Photodissociation Spectroscopy of $\text{Mg}^+(\text{NH}_3)_n$ ( $n = 3-6$ ): Direct Coordination or Solvation through Hydrogen Bonding

OHASHI, Kazuhiko<sup>1</sup>; TERABARU, Kazutaka<sup>1</sup>; INOKUCHI, Yoshiya<sup>2</sup>; MUNE, Yutaka<sup>1</sup>; MACHINAGA, Hironobu<sup>1</sup>; NISHI, Nobuyuki; SEKIYA, Hiroshi<sup>1</sup>

(<sup>1</sup>Kyushu Univ.; <sup>2</sup>Univ. Tokyo)

[*Chem. Phys. Lett.* **393**, 264–270 (2004)]

The infrared photodissociation spectra of mass-selected  $\text{Mg}^+(\text{NH}_3)_n$  ( $n = 3-6$ ) are measured and analyzed with the aid of density functional theory calculations. No large frequency reduction is observed for the NH stretches of ammonia, suggesting that either all the ammonia molecules coordinate directly to the  $\text{Mg}^+$  ion or an additional ammonia in the second shell bridges two ammonias in the first shell through hydrogen bonds. Four or possibly five ammonia molecules are allowed to

occupy the first shell, in striking contrast to the closure of the first shell in  $\text{Mg}^+(\text{H}_2\text{O})_3$ .

### III-C-3 Electronic Spectra of Jet-Cooled 3-Methyl-7-Azaindole Dimer. Symmetry of the Lowest Excited Electronic State and Double-Proton Transfer

HARA, Akihiko<sup>1</sup>; KOMOTO, Yusuke<sup>1</sup>; SAKOTA, Kenji<sup>1</sup>; MIYOSHI, Riko<sup>1</sup>; INOKUCHI, Yoshiya; OHASHI, Kazuhiko<sup>1</sup>; KUBO, Kanji<sup>1</sup>; YAMAMOTO, Emi<sup>1</sup>; MORI, Akira<sup>1</sup>; NISHI, Nobuyuki; SEKIYA, Hiroshi<sup>1</sup>

(<sup>1</sup>Kyushu Univ.)

[*J. Phys. Chem. A* **108**, 10789–10793 (2004)]

The fluorescence excitation spectra are recorded for jet-cooled dual hydrogen-bonded 3-methyl-7-azaindole dimer ( $3\text{MAI})_2\text{-hh}$  and deuterated dimers ( $3\text{MAI})_2\text{-hd}$  and ( $3\text{MAI})_2\text{-dd}$  near the electronic origin region of the  $S_1-S_0$  transition, where *hd* and *dd* indicate the deuteration of an imino hydrogen and two imino hydrogens, respectively. A single origin is detected in the spectra of ( $3\text{MAI})_2\text{-hh}$  and ( $3\text{MAI})_2\text{-dd}$ , whereas two electronic origins separated by  $13\text{ cm}^{-1}$  are detected in the spectrum of ( $3\text{MAI})_2\text{-hd}$ . The excited-state double-proton transfer (ESDPT) occurs in ( $3\text{MAI})_2\text{-hh}$ , while ( $3\text{MAI})_2\text{-hd}$  and ( $3\text{MAI})_2\text{-dd}$  undergo excited-state proton/deuteron transfer and excited-state double deuteron transfer, respectively. In ( $3\text{MAI})_2\text{-hd}$ , the excitation is localized on either the  $3\text{MAI-h}$  or  $3\text{MAI-d}$  moiety. The localization of the excitation is explained by a weak coupling of the excitonic states of ( $3\text{MAI})_2\text{-hh}$  and ( $3\text{MAI})_2\text{-dd}$ . The effective symmetry of the lowest excited state of ( $3\text{MAI})_2\text{-hh}$  and ( $3\text{MAI})_2\text{-dd}$  belongs to the  $C_{2h}$  point group, while that of ( $3\text{MAI})_2\text{-hd}$  belongs to the  $C_s$  point group. The vibronic patterns in the excitation spectra of the ( $3\text{MAI})_2$  dimers is very similar to those of the 7-azaindole dimers, indicating that the methyl substitution provides little effect on the shape of the ESDPT potential.

**III-C-4 Structures of  $[(\text{CO}_2)_n(\text{H}_2\text{O})_m]^-$  ( $n = 1-4$ ,  $m = 1, 2$ ) Cluster Anions. I. Infrared Photodissociation Spectroscopy**

MURAOKA, Azusa<sup>1</sup>; INOKUCHI, Yoshiya<sup>1</sup>;  
NISHI, Nobuyuki; NAGATA, Takashi<sup>1</sup>  
(<sup>1</sup>Univ. Tokyo)

[*J. Chem. Phys.* **122**, 094303 (7 pages) (2004)]

The infrared photodissociation spectra of  $[(\text{CO}_2)_n(\text{H}_2\text{O})_m]^-$  ( $n = 1-4$ ,  $m = 1, 2$ ) are measured in the 3000–3800  $\text{cm}^{-1}$  range. The  $[(\text{CO}_2)_n(\text{H}_2\text{O})_1]^-$  spectra are characterized by a sharp band around 3570  $\text{cm}^{-1}$  except for  $n = 1$ ;  $[(\text{CO}_2)_1(\text{H}_2\text{O})_1]^-$  does not photodissociate in the spectral range studied. The  $[(\text{CO}_2)_n(\text{H}_2\text{O})_2]^-$  ( $n = 1, 2$ ) species have similar spectral features with a broadband at 3340  $\text{cm}^{-1}$ . A drastic change in the spectral features is observed for  $[(\text{CO}_2)_3(\text{H}_2\text{O})_2]^-$ , where sharp bands appear at 3224, 3321, 3364, 3438, and 3572  $\text{cm}^{-1}$ . *Ab initio* calculations are performed at the MP2/6-311++G\*\* level to provide structural information such as optimized structures, stabilization energies, and vibrational frequencies of the  $[(\text{CO}_2)_n(\text{H}_2\text{O})_m]^-$  species. Comparison between the experimental and theoretical results reveals rather size- and composition-specific hydration manner in  $[(\text{CO}_2)_n(\text{H}_2\text{O})_m]^-$ : (1) the incorporated  $\text{H}_2\text{O}$  is bonded to either  $\text{CO}_2^-$  or  $\text{C}_2\text{O}_4^-$  through two equivalent  $\text{OH}\cdots\text{O}$  hydrogen bonds to form a ring structure in  $[(\text{CO}_2)_n(\text{H}_2\text{O})_1]^-$ ; (2) two  $\text{H}_2\text{O}$  molecules are independently bound to the O atoms of  $\text{CO}_2^-$  in  $[(\text{CO}_2)_n(\text{H}_2\text{O})_2]^-$  ( $n = 1, 2$ ); (3) a cyclic structure composed of  $\text{CO}_2^-$  and two  $\text{H}_2\text{O}$  molecules is formed in  $[(\text{CO}_2)_3(\text{H}_2\text{O})_2]^-$ .

## III-D Development of High-Precision Coherent Control and Its Application

Coherent control is based on manipulation of quantum phases of wave functions. It is a basic scheme of controlling a variety of quantum systems from simple atoms to nanostructures with possible applications to novel quantum technologies such as bond-selective chemistry and quantum computation. Coherent control is thus currently one of the principal subjects of various fields of science and technology such as atomic and molecular physics, solid-state physics, quantum electronics, and information science and technology. One promising strategy to carry out coherent control is to use coherent light to modulate a matter wave with its optical phase. We have so far developed a high-precision wave-packet interferometry by stabilizing the relative quantum phase of the two molecular wave packets generated by a pair of fs laser pulses on the attosecond time scale. We will apply our high-precision quantum interferometry to gas, liquid, solid, and surface systems to explore and control various quantum phenomena.

### III-D-1 Space- and Time- Resolved Observation of Molecular Wave-Packet Interference on Femtosecond and Picometric Scales

**KATSUKI, Hiroyuki<sup>1</sup>; CHIBA, Hisashi<sup>1</sup>; OHMORI, Kenji<sup>1</sup>; GIRARD, Bertrand<sup>2</sup>; MEIER, Christophe<sup>2</sup>**  
(<sup>1</sup>IMS and CREST/JST; <sup>2</sup>Univ. Paul Sabatier)

We have developed a brand new method to observe molecular wave-packet interference in the time- and space-resolved fashion. It has been applied to the half revival of the vibrational wave packet in the iodine molecule. The observed temporal evolution of the interference has been well reproduced by the quantum mechanical calculation. We have succeeded in observing the quantum nodal structures which take place at a spatial resolution of less than 1 pm, and are created and dynamically changed on the femtosecond timescale. To our knowledge, this is for the first time that the dynamical matter-wave interferences are observed on the femtosecond time scale and picometric length scale.

### III-D-2 Real-Time Observation of Phase-Controlled Molecular Wave-Packet Interference

**KATSUKI, Hiroyuki<sup>1</sup>; HOSAKA, Kouichi<sup>1</sup>; CHIBA, Hisashi<sup>1</sup>; OHMORI, Kenji<sup>1</sup>; HONDA, Masahiro<sup>2,3</sup>; HAGIHARA, Yusuke<sup>2,3</sup>; FUJIWARA, Katsutoshi<sup>3</sup>; SATO, Yukinori<sup>2,3</sup>; UEDA, Kiyoshi<sup>2,3</sup>**  
(<sup>1</sup>IMS and CREST/JST; <sup>2</sup>CREST/JST; <sup>3</sup>Tohoku Univ.)

We have controlled quantum interference of vibrational wave packets (WP's) in the iodine molecule by using a pair of phase-locked fs pulses, and the real time evolution of that interference has been observed. The real-time evolution shows a clear dependence on the inter-pulse delay  $\tau_{\text{control}}$  between the locked pulses highly stabilized on attosecond time scale. We have also measured a population code, which is a population ratio among the vibrational eigenstates within a WP. The population code also shows a clear dependence on  $\tau_{\text{control}}$ . The ordinary frequency domain interpretation based on the spectral interference of locked pulses may be useful to elucidate population codes, but is no longer suitable for the present real-time observation. Moreover, the real-time evolution has allowed us to obtain additional phase information unable to be obtained from

population codes. The combination of a population code and real-time evolution is useful to obtain both phase and amplitude information stored in a WP, which is indispensable for developing novel quantum technologies such as atom- and molecule-based information processing. All these features provides basis for opening new perspective of coherent control in a wide variety of quantum systems.

### III-D-3 Development of Quantum Gate Operations with Vibrational Eigenstates of Molecules

**HOSAKA, Kouichi<sup>1</sup>; CHIBA, Hisashi<sup>1</sup>; KATSUKI, Hiroyuki<sup>1</sup>; OHMORI, Kenji<sup>1</sup>; TERANISHI, Yoshiaki<sup>2,3</sup>; OHTSUKI, Yukiyo<sup>2,3</sup>**  
(<sup>1</sup>IMS and CREST/JST; <sup>2</sup>CREST/JST; <sup>3</sup>Tohoku Univ.)

We have numerically studied quantum gate operations with the iodine molecule, based on the free temporal evolution of the vibrational wave packet and the high-precision wave-packet interferometer. The fidelities of the gate operations are found to be very high, and the proposed experimental scheme is feasible with our present experimental techniques.

## III-E Quantum-State Manipulation of Molecular Motions

Molecules in gas phase undergo translational, rotational and vibrational motions in a random manner, and the total molecular system is a statistical ensemble that contains a number of molecules in many different states of motions. This research group aims to establish methods to manipulate the quantum-state distribution pertinent to molecular motions, by utilizing the coherent interaction with laser lights. Three complement methods are now being explored for manipulation of molecular motions. The first one employs creation and detection of molecular wavepackets by fs pump-probe experiments. New experimental methods for probing vibrational and/or rotational wavepackets are developed and applied to jet-cooled polyatomic systems. The second method exploits an impulsive interaction with ultrafast intense laser light to transform the initial distribution into an arbitral non-equilibrium one. We are now constructing a vacuum chamber system for this purpose. The third one utilizes an adiabatic interaction to achieve the complete population transfer, by which all the molecules are launched into states with high excitation of vibrations or rotation. We are now constructing ns laser system with sufficiently high frequency resolution to drive the adiabatic coherent interaction. Along the development of the instrument, appropriate candidates for the quantum-state adiabatic manipulation are searched. Laser spectroscopic studies are carried out to explore energy-level structure of the intermolecular vibrations in molecular clusters containing benzene.

### III-E-1 Femtosecond Random-Phase Interferometry of Jet-Cooled Polyatomic Molecules

MIYAZAKI, Mitsuhiko<sup>1</sup>; HARUNA, Atsuyuki<sup>2</sup>; OHSHIMA, Yasuhiro  
(<sup>1</sup>IMS and Kyoto Univ.; <sup>2</sup>Kyoto Univ.)

Interferometric measurements with fs laser pulses have been extensively utilized to characterize coherent motion and decay of wavefunctions. The method, however, demands precise control of optical lengths, and it is a difficult task in particular for shorter laser wavelength. Recently, an alternative way for fs interferometry has been demonstrated,<sup>1),2)</sup> in which the relative optical phase between the two laser pulses is randomly modulated while the corresponding fluctuation in fluorescence is monitored. The method termed COIN (Coherence Observation by Interference Noise) is robust to turbulence in optical lengths and thus has vast applicability. Here we have applied COIN to several polyatomic molecules to investigate wavepacket dynamics and ultrafast nonradiative processes.

In the present setup, the third harmonic with ~200 fs duration of a 1 kHz Ti:Sapphire regenerative amplifier or an output of an optical parametric oscillator was sent to a Michelson interferometer, in which optical length of one arm was modulated by hot air stream from a blower. Two laser pulses with delay up to several hundred ps were colinearly introduced onto molecules, which were adiabatically cooled in a CW supersonic expansion. The resultant fluorescence was observed in a single shot basis, and more than 1000 laser pulses were subjected to the statistics giving the variance of fluorescence intensity at certain delay.

Rotational wavepacket dynamics has been studied by the COIN observation on the S<sub>1</sub>-S<sub>0</sub> 6<sub>0</sub><sup>1</sup> band of benzene. After the initial decay of coherence, weak (~5%) rotational revivals are observed in the range of 10–30 ps. The signals depend strongly on rotational temperature, and their feature is well reproduced by a model calculation with the known spectroscopic parameters. Such a sharp dependence on the rotational distribution is in pronounced contrast to the results from a related method, *i.e.*, rotational coherence spectroscopy,<sup>3)</sup> where gross shape of signals is not so sensitive to the temperature. The present study demonstrates the utility of COIN for monitoring the rotational distribution with high temporal resolution.

Electronic relaxation after the naphthalene S<sub>2</sub> excitation has also been examined by COIN. The initial coherence decays within the laser pulse duration due to the ultrafast (<< 100 fs) internal conversion from S<sub>2</sub> into S<sub>1</sub>. This observation is in accord with the results from fs photoelectron spectroscopy,<sup>4)</sup> indicating potentiality of COIN to studies on ultrafast relaxation dynamics after photoexcitation.

#### References

- 1) O. Kinrot, *et al.*, *Phys. Rev. Lett.* **75**, 3822 (1995).
- 2) Ch. Warmuth, *et al.*, *J. Chem. Phys.* **112**, 5060 (2000); **114**, 9901 (2001).
- 3) P. M. Felker, *J. Phys. Chem.* **96**, 7844 (1992).
- 4) M. Schmitt, *et al.*, *J. Chem. Phys.* **114**, 1206 (2001).

### III-E-2 Wavepacket Observation of Methyl Internal Rotation in *o*-Fluorotoluene

MIYAZAKI, Mitsuhiko<sup>1</sup>; HARUNA, Atsuyuki<sup>2</sup>; HASEGAWA, Hirokazu; OHSHIMA, Yasuhiro  
(<sup>1</sup>IMS and Kyoto Univ.; <sup>2</sup>Kyoto Univ.)

The S<sub>1</sub>-S<sub>0</sub> origin region of *o*-fluorotoluene has been examined to observe wavepacket dynamics associated with internal rotation of the methyl group. In addition to COIN observation, time-resolved fluorescence depletion (TRFD) is implemented in fs time domain for the first time. The experimental arrangement for TRFD is essentially the same with COIN: total fluorescence intensity is recorded in this case as a function of delay between two fs laser pulses. Here optical cycle interference is smeared out by the random modulation in optical length, so population change induced by pump-dump process is only monitored as fluorescence depletion. The laser beam is focused at the molecular jet and fluorescence from the central part of the irradiated region is only collected to observe depletion as large as possible.

The observed TRFD and COIN spectra are shown in Figure 1, and the corresponding power spectra after

Fourier transformation are indicated in Figure 2. In the case of methyl internal rotation, the ground and the lowest excited states are coupled with *ortho* and *para* nuclear spin wavefunctions, respectively, and thus both states are populated even in adiabatically cooled jet conditions. Accordingly, TRFD spectrum is a sum of independent beats between the vibronic levels in  $S_1$  that are optically connected with the two internal-rotation states in  $S_0$ . On the other hand, COIN spectrum exhibits all the interferences between the transitions from the two states, because it is given as the variance, *i.e.*, the average of the square of fluorescence fluctuation. The present study demonstrates the significance of the two complement experiments in extracting the energy-level structure of the internal rotation from the time-domain observation.

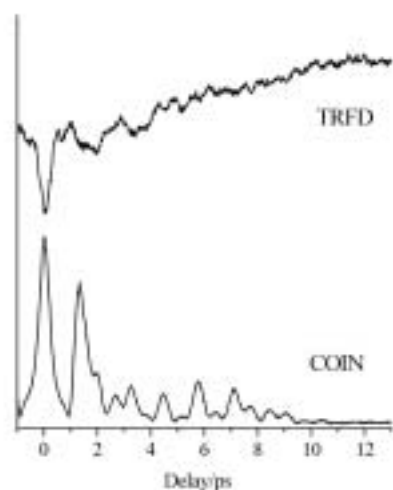


**Figure 1.** TRFD and COIN spectra observed by the excitation of the  $S_1$ - $S_0$  origin region of *o*-fluorotoluene.

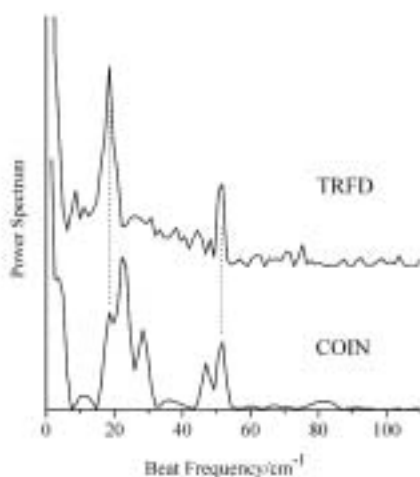


**Figure 2.** Power spectra obtained from the Fourier transformation of the time-domain TRFD and COIN spectra in Figure 1.

### III-E-3 Construction of an Experimental Apparatus for Nonadiabatic Quantum-State Manipulation of Molecular Motions

HASEGAWA, Hirokazu; OHSHIMA, Yasuhiro

A vacuum chamber system and a data acquisition system have been designed and constructed to achieve quantum-state manipulation of molecular motions, in particular nonadiabatic molecular alignment induced by laser fields in gas phase. Molecules aligned by the interaction of intense fs laser pulses with induced electric dipole are probed through ionization. Ionization is attained by field ionization using delayed-intense fs pulses or resonance enhanced multiphoton ionization using ns laser pulses. In the former approach, dynamics of transiently aligned molecules are probed in time domain, while the change in rotational-state distribution induced by impulsive interaction with intense fs light is monitored in the latter method.

The vacuum system, composed of three differentially pumped chambers, is designed so as to be coupled with continuous or pulsed supersonic molecular beam (Figure 1). Ions produced by the interaction of laser fields with jet-cooled molecules are detected by a time-of-flight mass spectrometer. The electrode for ion extraction is designated with a small pinhole ( $< 1$  mm), in order to ensure the detection of ions that are produced only in the region, where pump and probe laser pulses are overlapped. The integrated environment software for a data acquisition and laser control has been developed on the computer.

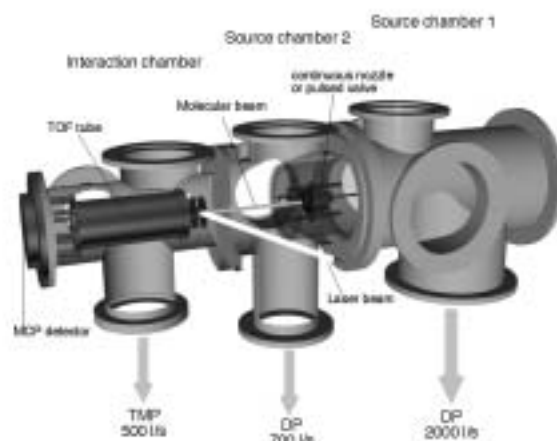


**Figure 1.** Vacuum chamber system for quantum-state manipulation of molecular motions.

### III-E-4 Development of High-Resolution Coherent Pulsed Laser

OHSHIMA, Yasuhiro

We are constructing an all solid-state single-mode pulsed laser with Fourier-transform limited resolution ( $\leq 0.01$   $\text{cm}^{-1}$ ), for quantum-state manipulation by coherent light-matter interaction, such as stimulated Raman adiabatic passage. In the system, the output from a cw extra-cavity diode laser or a Ti:Sapphire laser injection-seeds the optical parametric amplification by BBO nonlinear crystals excited by a single-mode Nd:YAG laser. At present, we routinely achieve the output power of 20 mJ/pulse, which reaches to 20% conversion efficiency, without injection seeding. Precise adjustment of optical layout is now under way for narrow band operation by the external seeding.

**III-E-5 Laser Spectroscopy of the van der Waals Vibrations of Benzene–Water****MIYAKE, Shin-ichiro<sup>1</sup>; MIYAZAKI, Mitsuhiro<sup>2</sup>; OHSHIMA, Yasuhiro***(<sup>1</sup>Kyoto Univ.; <sup>2</sup>IMS and Kyoto Univ.)*

Benzene-water has attracted much attention as a prototypical system containing the  $\pi$  hydrogen bond. Still, more experimental information should be accumulated for quantitative description of the intermolecular interaction in the complex. We have recently examined in detail the vibronic spectrum of the benzene–water 1:1 cluster pertaining to the  $S_1$ – $S_0$   $6_0^1$  transition of the benzene moiety, recorded by utilizing resonance two-photon ionization (R2PI) time-of-flight mass spectrometry. UV–UV hole-burning measurement has been performed to observe weak vibronic bands, which are buried in the R2PI excitation spectrum by background signals due to fragmentation of higher clusters. A dozen of bands associated to van der Waals (vdW) mode excitation are clearly seen in the region up to  $160\text{ cm}^{-1}$  from the  $6_0^1$  transition. The vdW structure cannot be assigned as a simple combination of a few normal modes, implying a substantial anharmonic coupling between the intermolecular vibrations. In particular, the appearance of an extremely low-frequency ( $\sim 8\text{ cm}^{-1}$ ) band, similar to the case in the  $S_0$  state, is considered to be the signature of the 3D hindered internal rotation of water in the cluster. Detailed analysis on the vdW structure is now under way with the aid of the results on isotopic variants.

## III-F Photophysics and Photochemistry of Aromatic Molecules in the Condensed Phase

Excited aromatic compounds generally release energy by various pathways such as photophysical processes and photochemical reactions. Electronically excited molecules are relaxed into a stable or metastable state through radiative and/or nonradiative processes as photophysical processes. It is well known that photochemical reactions occurring from excited state are bond dissociation, cyclization, isomerization, hydrogen abstraction, electron transfer, and so on. In addition, there exist relaxation processes and their quantum yields characteristic to each compound. It is very important to investigate dynamics of photoexcited molecules.

Intermediates such as excited states and radicals, which can be generated with laser irradiation, have been detected by laser flash photolysis as described. The shorter pulse width of a light source becomes, the shorter-lived intermediates can be detected. Furthermore, the properties of intermediates would be clarified. These information should be obtained from photophysical and photochemical dynamics of the intermediate that are interested.

On the other hand, it becomes difficult to elucidate nonradiative processes, such as internal conversion and intersystem crossing from the excited state, by laser flash photolysis. Time-resolved photothermal techniques, however, are powerful to study nonradiative processes because they can detect the released heat from excited molecules directly with high sensitivity. They should be described in detail. Combination of photoexcited and photothermal methods will give us detailed information on photophysical and photochemical dynamics of intermediates, as well as excited states.

### III-F-1 Excited-State Dynamics of 4-Thiothymidine with UVA Light Irradiation

HARADA, Yosuke<sup>1</sup>; SUZUKI, Tadashi<sup>1</sup>; ICHIMURA, Tejiro<sup>2</sup>  
(<sup>1</sup>Tokyo Inst. Tech.; <sup>2</sup>IMS and Tokyo Inst. Tech.)

Thionucleobases and thionucleosides have received renewed attention because of their distinct property, namely, high sensitivity to UVA light (320–400 nm) in which region normal DNA constituents are transparent. 4-Thiothymidine (4-TT), an analogue of the naturally occurring nucleoside thymidine, has strong absorption in the UVA region. Recently it was reported that 4-TT can be readily incorporated into cellular DNA and that low doses of UVA light can easily inflict lethal damage on the DNA containing 4-TT, causing cell death. The synergistic use of 4-TT and UVA light offers a novel approach to cancer treatment. Apparently, electronically excited state of 4-TT is at the initial and crucial stage of the UVA-induced cell killing, and thus photophysical and photochemical studies of 4-TT would be of great significance.

We have measured transient absorption spectrum of 4-TT in deaerated acetonitrile with the nanosecond 355 nm laser. Immediately after the laser shot, an intense bleaching at 335 nm and a broad absorption band at 380–600 nm (Abs. Max. 530 nm) were observed. The bleaching is ascribed to the depletion of the ground state molecules while the absorption band is assigned to the absorption of the lowest excited triplet ( $T_1$ ) state of 4-TT (T–T absorption). The T–T absorption decayed with the rate constant of  $1 \times 10^6 \text{ s}^{-1}$ . In triplet quenching experiments by KI, the absorption intensity of the photoproducts decreased correspondingly to shortening of triplet lifetime of 4-TT. Our experimental results suggest that photochemical process would take place *via* the  $T_1$  state of 4-TT and other several intermediate states. A good understanding of the photophysics and photochemistry of 4-TT could offer valuable insights to the mechanisms by which cancer cells are killed.

### III-F-2 Photochemical Reaction Dynamics of o-Quinones

HARADA, Yosuke<sup>1</sup>; WATANABE, Sadayuki<sup>1</sup>; SUZUKI, Tadashi<sup>1</sup>; ICHIMURA, Tejiro<sup>2</sup>  
(<sup>1</sup>Tokyo Inst. Tech.; <sup>2</sup>IMS and Tokyo Inst. Tech.)

[*J. Photochem. Photobiol., A* **170**, 161–167 (2005)]

Photoreaction dynamics of 9,10-phenanthrene-quinone (PQ) and 1,2-naphthoquinone (NQ) in solution has been studied by laser flash photolysis technique. The real-time transient absorption measurements found out; (1) by excitation at 355 nm in the presence of alcohol, absorption band characteristic to the quinone ketyl radical emerged as the triplet–triplet (T–T) absorption of the quinone submerged, (2) the rise of the absorption of the ketyl radical consisted of two components; the fast and slow ones, where the fast one had the rise rate constant corresponding to the decay rate of triplet quinone, while the slow one rose up much slowly. The experimental fact clearly revealed that the slow reaction should give rise to formation of the ketyl radical following the hydrogen abstraction of triplet PQ and NQ from alcohol, and should be attributed to the hydrogen atom transfer between the parent quinone in the ground state and counter  $\alpha$ -hydroxyalkyl radical produced from alcoholic molecule. In this study, we carried out the real-time measurement and clarified the reaction mechanism between the  $\alpha$ -hydroxyalkyl radicals and the ground state quinones.

Triplet PQ and NQ show remarkable high reactivity with benzene. The notable reactivity would result from their characteristic molecular conformation; namely, the existence of two adjacent carbonyl groups would cause the stabilized conformation in the transition state through doubly hydrogen bonding with the hydrogen donor.

### III-F-3 Evidence of Phenoxyethyl Radical Formation in Laser Photolysis of Anisole in Solution

ANDO, Mayaka<sup>1</sup>; YOSHIIKE, Shigeru<sup>1</sup>; SUZUKI, Tadashi<sup>1</sup>; ICHIMURA, Teijiro<sup>2</sup>; OKUTSU, Tetsuo<sup>3</sup>; UEDA, Minoru<sup>3</sup>; HORIUCHI, Hiroaki<sup>3</sup>; HIRATSUKA, Hiroshi<sup>3</sup>; KAWAI, Akio<sup>1</sup>; SHIBUYA, Kazuhiko<sup>1</sup>

(<sup>1</sup>Tokyo Inst. Tech.; <sup>2</sup>IMS and Tokyo Inst. Tech.; <sup>3</sup>Gunma Univ.)

[*J. Photochem. Photobiol., A* **174**, 194–198 (2005)]

Transient absorption spectrum of anisole in acetonitrile was observed by a 248-nm laser photolysis. In addition to the structured band observed at 400 nm, which was assigned to phenoxy radical, a broad absorption band appeared at around 440 nm. The lifetime of the unknown species was not affected by oxygen. By means of acetone photosensitization reaction, photolysis of 1,2-diphenoxyethane, and ESR measurements, the species was assigned to phenoxyethyl radical, produced with two-photon absorption through the S<sub>1</sub> state of anisole to form anisole cation and consecutive deprotonation of the cation.

### III-F-4 Production and Excited State Dynamics of the Photorearranged Isomer of Benzyl Chloride and Its Methyl Derivatives Studied by Stepwise Two-Color Laser Excitation Techniques

NAGANO, Mika<sup>1</sup>; SUZUKI, Tadashi<sup>1</sup>; ICHIMURA, Teijiro<sup>2</sup>; OKUTSU, Tetsuo<sup>3</sup>; HIRATSUKA, Hiroshi<sup>3</sup>; KAWAUCHI, Susumu<sup>1</sup>

(<sup>1</sup>Tokyo Inst. Tech.; <sup>2</sup>IMS and Tokyo Inst. Tech.; <sup>3</sup>Gunma Univ.)

[*J. Phys. Chem. A* **109**, 5825–5831 (2005)]

Production and photoexcited dynamics of reaction intermediates with photolyses of benzyl chloride (BzCl) and methyl-substituted benzyl chlorides (MeBzCl) were studied by using stepwise two-color laser excitation transient absorption (TC-TA) and two-color laser excitation time-resolved thermal lensing (TC-TRTL) measurements. With photoexcitation of BzCl the formation of transient photo-rearranged isomer was suggested in the previous paper.<sup>1)</sup> Such an isomer formation for MeBzCl was also observed in a 248 nm excitation. It was found that further photoexcitation of the isomers with the 308 nm light caused photodissociation to yield the corresponding benzyl radicals. The reaction quantum yield and the molar absorptivity of the photo-rearranged isomer of BzCl were estimated. The heat of reaction for the photodissociation of the isomer was successfully determined with the TC-TRTL measurement. These experimental results were consistent with MO calculations.

#### Reference

- 1) H. Hiratsuka, T. Okamoto, S. Kuroda, T. Okutsu, H. Maeoka, M. Taguchi and T. Yoshinaga, *Res. Chem. Intermed.* **27**, 137–153 (2001).

## III-G Spectroscopy and Excited State Dynamics of Jet-Cooled Aromatic Molecules

The phenomena of energy relaxation in isolated molecules have been central in chemical kinetics over many decades. An extensive subject has been followed by the application of supersonic jet techniques, which enabled the study of well isolated ultra-cold molecules. The jet-cooled molecules are isolated in gas phase, thus, the experiments are not subjected to interactions between molecules and solvents or to vibrational relaxation in condensed phases.

The large transition energy is reserved in optically electronic excited molecules where the idea of temperature for molecular internal energy is replaced by the excess energy, by which photodissociation is induced. Investigation of nonradiative electronic relaxation processes, *i.e.* internal conversion (IC) or intersystem crossing (ISC) between two electronic states of the same or different electron spin multiplicity of photoexcited molecules, respectively, has long been interest of the photochemical dynamics because of the important role of these processes in photochemical reaction system.

A triplet state serves as an important intermediate in nonradiative processes of excited molecules. The dynamics of the triplet state generation, *i.e.* ISC, plays an important role in photochemical processes. For instance, chlorinated benzene derivatives in the first excited singlet (S<sub>1</sub>) state have small values (10<sup>-2</sup>) of the fluorescence quantum yields, suggesting that the ISC process to excited triplet states takes place due to the large spin-orbit coupling induced by the heavy Cl atom effect. The excited triplet state molecules undergo the C–Cl dissociation whose quantum yield is almost unity. Accordingly, the investigation of the ISC process assists to understand the photochemical reactions.

The substituent of the CH<sub>3</sub> or OCH<sub>3</sub> group on the benzene ring should play an important role in their photoexcited states. When these molecules are excited to the singlet excited state, internal rotational bands of these groups are observed for lower frequency regions than 200 cm<sup>-1</sup> in the LIF excitation spectra. Measurements of these internal band intensities and their fluorescence lifetimes should give information on the relaxation dynamics of these molecules.

### III-G-1 Spectroscopy and Relaxation Dynamics of Photoexcited Anisole and Anisole-d<sub>3</sub> Molecules in a Supersonic Jet

MATSUMOTO, Ryu<sup>1</sup>; SAKEDA, Kosaku<sup>1</sup>;  
MATSUSHITA, Yoshihisa<sup>1</sup>; SUZUKI, Tadashi<sup>1</sup>;  
ICHIMURA, Teijiro<sup>2</sup>

(<sup>1</sup>Tokyo Inst. Tech.; <sup>2</sup>IMS and Tokyo Inst. Tech.)

[*J. Mol. Struct.* **735-736**, 153–167 (2005)]

The vibronic structures of the S<sub>1</sub>–S<sub>0</sub> electronic transitions of jet-cooled anisole and anisole-d<sub>3</sub> molecules have been investigated in detail using the laser induced fluorescence and single vibrational level dispersed fluorescence (DF) spectroscopy. Normal mode frequencies of the ground and excited states including the methyl and methoxy internal rotations were determined by analyses of dispersed fluorescence spectra and molecular orbital calculations. Strong vibrational mixing in the S<sub>1</sub> state was observed in several DF spectra. Duschinsky rotation between 6a and 6b modes prominently appeared for both molecules and it was found that methyl deuteration depressed the second-order vibronic coupling of these modes. Another explicit Duschinsky rotation was found in 10b and 16a modes of both molecules. However, in the case of the deuterated molecule the mixing cannot be explained by only Duschinsky rotation. A Fermi resonance due to level proximity should be involved in the mixing scheme. Vibronic bands in the higher frequency regions exhibit broadened and structureless fluorescence due to intramolecular vibrational energy redistribution (IVR). The onset of the IVR process inferred from the DF spectra was found to be increased by methyl deuteration on the contrary to general propensity rule. The deuteration effect is characteristic of anisole molecules and indicates considerable decrease in the interaction with the dark bath modes. Fluorescence lifetime measurements suggest the enhancement of intersystem crossing in the levels with out-of-plane vibrational components. The observed broadening of DF spectra corresponded to nonradiative decay rates from levels with the in-plane vibrational modes. This suggests that the energy flow into out-of-plane bath modes through the IVR process should dominate nonradiative rates on initially excited in-plane vibrational levels. Our analysis clarified that the out-of-plane vibrations accompanying the methoxy motion make large contribution to the relaxation dynamics.

### III-G-2 Internal Rotational Motion of the Chloromethyl Group of the Jet-Cooled Benzyl Chloride Molecule

MATSUMOTO, Ryu<sup>1</sup>; SUZUKI, Tadashi<sup>1</sup>;  
ICHIMURA, Teijiro<sup>2</sup>

(<sup>1</sup>Tokyo Inst. Tech.; <sup>2</sup>IMS and Tokyo Inst. Tech.)

[*J. Phys. Chem. A* **109**, 3331–3336 (2005)]

The mass-resolved resonance enhanced two-photon ionization spectra of jet-cooled benzyl chloride were measured. Some low-frequency vibronic bands around

the S<sub>1</sub>–S<sub>0</sub> origin band were assigned to transitions of the internal rotational mode of the chloromethyl group. The internal rotational motion was analyzed by using the one-dimensional free rotor approximation. The conformation in the S<sub>1</sub> state was found to be that in which the C–Cl bond lies in orthogonal to the benzene plane. For the species with *m/e* 126, the transition energy of the internal rotational bands corresponded well to the potential energy values of  $V_2 = 1900 \text{ cm}^{-1}$  and  $V_4 = 30 \text{ cm}^{-1}$  in the S<sub>1</sub> state and the reduced rotational constant *B* values 0.50 and 0.47 cm<sup>-1</sup> in the S<sub>0</sub> and S<sub>1</sub> states, respectively. The *B* values obtained for the chlorine isotopomer (*m/e* 128) were slightly different. The S<sub>1</sub> potential barrier height was found to be about 3 times larger than that for the S<sub>0</sub> state. Molecular orbital calculations suggest that the difference between energies of the HOMO and LUMO with respect to the rotation of the chloromethyl group correspond approximately to the potential energy curve obtained for the S<sub>1</sub> state.

### III-G-3 Molecular Structure and Excited State Dynamics of Jet-Cooled *o*-, *m*- and *p*-Fluoroanisole

ISOZAKI, Tasuku<sup>1</sup>; SAKEDA, Kosaku<sup>1</sup>; SUZUKI, Tadashi<sup>1</sup>; ICHIMURA, Teijiro<sup>2</sup>

(<sup>1</sup>Tokyo Inst. Tech.; <sup>2</sup>IMS and Tokyo Inst. Tech.)

Intramolecular isomerism plays a significant role in biologically relevant molecular systems such as the folding of proteins and molecular machines. In understanding the function of the complicated large biological molecules, it is important to know the conformational properties and excited state dynamics of their local units. In this point of view, the molecular structure and relaxation dynamics of anisole derivatives were studied. It is known that *meta*-substituted anisole has two stable *planar* conformers (*i.e.* *cis* and *trans*), which are raised from the orientation of the methoxy group with respect to the substituent. Our aim is to clarify fluorination effect against anisole on the electronic transitions, conformational structure, vibronic structure and relaxation dynamics of *o*-, *m*- and *p*-fluoroanisole (FA).

We measured the laser-induced fluorescence (LIF) excitation and single vibronic level (SVL) dispersed fluorescence spectra of jet-cooled *o*-, *m*- and *p*-FA. The SVL dispersed fluorescence spectra were also measured by pumping each vibronic band. The observed bands were assigned with the aid of the quantum chemical calculations. The SVL dispersed fluorescence spectra indicated that the vibrational band mixing should take place in the S<sub>1</sub> state, and the IVR process becomes more dominant with the higher excess energy. The vibrational band mixing and IVR process are characteristic for each isomer.

### III-G-4 Evidence for a Non-Planar Conformer and Conformational Isomerization of *o*-Fluoroanisole in a Low-Temperature Ar Matrix

ISOZAKI, Tasuku<sup>1</sup>; SAKEDA, Kosaku<sup>1</sup>; SUZUKI, Tadashi<sup>1</sup>; ICHIMURA, Teijiro<sup>2</sup>; TSUJI, Kazuhide<sup>1</sup>;  
SHIBUYA, Kazuhiko<sup>1</sup>

(<sup>1</sup>Tokyo Inst. Tech.; <sup>2</sup>IMS and Tokyo Inst. Tech.)

[Chem. Phys. Lett. **409**, 93–97 (2005)]

FT-IR spectra of *o*-fluoroanisole were measured in a low-temperature Ar matrix with and without UV irradiation. The observed bands, without irradiation, were assigned to the *trans* conformer with the aid of the quantum chemical calculations at the B3LYP/cc-pVTZ level. By comparing the IR spectrum, after irradiation, with the calculated spectra, the formation of a *non-planar* conformer was established. The *non-planar* conformer gradually decayed by a unimolecular process under dark conditions at 16 K, while the *trans* conformer increased. The back-reaction rate was estimated, and the reaction dynamics between the *trans* and *non-planar* conformers was discussed.

### III-G-5 Molecular Structure and Puckering Vibration of 1-Aminoindan in a Supersonic Jet

IGA, Hiroshi<sup>1</sup>; ISOZAKI, Tasuku<sup>1</sup>; SUZUKI, Tadashi<sup>1</sup>; ICHIMURA, Teijiro<sup>2</sup>

(<sup>1</sup>Tokyo Inst. Tech.; <sup>2</sup>IMS and Tokyo Inst. Tech.)

The laser-induced fluorescence (LIF) and single vibronic level dispersed fluorescence spectra of 1-aminoindan (1-AI) were measured in a supersonic jet. Two prominent intense bands observed at 36934 and 37062 cm<sup>-1</sup> in the LIF spectrum were assigned to the 0<sup>0</sup> bands of rotational isomers resulting from the orientation of the amino group. The low-frequency puckering vibration was compared with indan. The puckering frequency and transition intensity of 1-AI are the same as indan in the S<sub>0</sub> state and not in the S<sub>1</sub> state. The quantum chemical calculations suggest six possible isomers, however, only two stable rotational isomers were observed in the spectra. The intramolecular N–H···π hydrogen bond should play an important role in the stabilization of the rotational isomers.

## III-H Photochemical Reactions in Microreactors

Many chemical synthesis has been so far conducted by temperature controlled chemical reactions using specific catalyst. Utilization of characteristic catalyst, however, is restricted to some enantioselective synthetic reactions. Light is a powerful tool to excite molecules into electronically excited states selectively to give rise to specific reaction channel. Our proposal is application of laser light to elucidate the mechanism of photo-induced chemical reactions taken place in micro-region reaction vessel. Laser light has a couple of advantages to investigate the reaction mechanism, such as high power, time-resolved analysis, and polarization character (linear or circular dichroism), that is specifically related to characteristic properties of the enantiomer. Another feature of the laser light is a small beam divergence, of which diameter still can be focused into much smaller area such as micrometer region. Taking into account of these considerations, we have set up the laser photochemical synthesis system and photocatalytic reaction system with immobilized titanium dioxide. Both the laser irradiation system and the product analysis section can be processed on the same site of the microreactor. The products generated by the laser irradiation can be analyzed at the downstream site of the reactor using a second laser irradiation. If the product emits the detectable fluorescence, the LIF measurement can be applicable. In case of non-emitting substance an opto-acoustic and/or photothermal spectroscopy, or Raman spectroscopy should be employed. We have investigated enantioselective reaction of cyclooctene derivatives as a model system, and photocatalytic degradation of endocrine disruptors with immobilized titanium dioxide.

### III-H-1 Application of Microfabricated Reactors for Asymmetric Photoreaction

ICHIMURA, Teijiro<sup>1</sup>; KUMADA, Shinji<sup>2</sup>;  
WAKABAYASHI, Kazuhito<sup>2</sup>; SAKEDA, Kosaku<sup>2</sup>;  
MATSUSHITA, Yoshihisa<sup>2</sup>; SUZUKI, Tadashi<sup>2</sup>

(<sup>1</sup>IMS and Tokyo Inst. Tech.; <sup>2</sup>Tokyo Inst. Tech.)

[2<sup>nd</sup> International Conference on Green and Sustainable  
Chemistry (2005)]

We reinvestigated the asymmetric photoreaction of enantiodifferentiating *Z-E* photoisomerization of cyclooctene sensitized by aromatic esters in a microreactor. Effects of residence time, temperature, and laser power on the photoreaction were investigated. The results indicate that high ee value was obtained within the short residence time. In contrast, the longer residence time was required to achieve higher *E/Z* ratio. The higher

laser power and/or reputation rate becomes, the quicker the *E/Z* ratio should reach to the highest value. The ee value was quite sensitive to the temperature. The reaction mechanism will be discussed in terms of the conformational structure of excimer.

### III-H-2 Photocatalytic Reaction in Microfabricated Reactors

MATSUSHITA, Yoshihisa<sup>1</sup>; KUMADA, Shinji<sup>1</sup>;  
WAKABAYASHI, Kazuhito<sup>1</sup>; SAKEDA, Kosaku<sup>1</sup>;  
ICHIMURA, Teijiro<sup>2</sup>

(<sup>1</sup>Tokyo Inst. Tech.; <sup>2</sup>IMS and Tokyo Inst. Tech.)

[The Third International Workshop on Micro Chemical  
Plants (2005)]

Photocatalytic reaction in microspace was investigated by using a microreactor with immobilized tita-

nium dioxide. Since a photocatalytic reaction takes place on an irradiated titanium dioxide surface, a micro-fabricated reactor which has a large surface-to-volume ratio must prove its advantages on the reaction.

Photodegradation of endocrine disruptors was examined as a model reaction. The microreactors made of quartz with a cross-section of 0.5 mm width and 0.1–0.5 mm depth were coated with a photocatalytic titanium dioxide layer of approximately 1 micron thickness. Aqueous solutions of 3-chlorophenol, monochlorobenzene, bisphenol A, and *N,N*-dimethylformamide were introduced to the microreactor with a syringe pump then irradiated with a UV light source. The following light sources were employed for the excitation of photocatalytic titanium dioxide: XeCl (308 nm) excimer laser, YAG (355 nm) laser and OPO laser (300–400 nm) excited with the YAG laser, and UV-emitting diodes (UV-LED, 365, 375 and 385 nm).

The variation profiles of the concentration of endocrine disruptors as a function of irradiation time were examined. Degradation increased with increasing the residence time and reaches 30% for 3-chlorophenol and 13% for bisphenol A at a irradiation time of 5 seconds in the case of 385 nm UV-LED excitation with a microreactor of 0.1 mm depth. Higher degradation was obtained for lower concentrations of endocrine disruptors and smaller thickness of microspace. Degradation kinetics and photonic efficiencies dependent on the nature of the light source are further discussed.

Feasibility of photocatalytic reaction in microreactors was thus proven and optimization of excitation wavelength and photon density, design of the microreactor, and flow rate and irradiation time are under progress for the establishment of the photocatalytic microreaction system.

## III-I In-Situ Observation of Surface Reactions by Variable Temperature Scanning Tunneling Microscopy

Chemical reactions at a well-defined single crystal surface has been intensively investigated as a prototype for heterogeneous catalytic reaction, electrochemical reaction and corrosion. The surface chemical reactions are heterogeneous in nature reflecting the structural and electronic imperfections relevant to steps, vacancies and impurities. In addition, the surface reactions are significantly influenced by the presence of reactants and products which often form ordered arrays. Therefore, in order to get better understanding of the surface reactions, it is vital to unravel the nature of these local properties which are closely linked to catalytic activity. The advent of scanning tunneling microscopy (STM) has enabled us to tackle the challenge with the ability to image the surface reactions in both real-time and real-space with atomic resolution. We investigate the reactivity of novel one-dimensional (1D)  $\text{-Ag-O-Ag-O-}$  compounds formed upon the dissociative adsorption of oxygen molecule on Ag(110) using variable temperature STM (VT-STM). The 1D compounds are arranged periodically to form  $(n \times 1)$  ( $n = 2-7$ ) reconstructed structures. In addition, the 1D compounds show structural fluctuation in low O coverage regime reflecting the low dimensionality. These characteristics make them promising as a model system to explore physical and chemical properties of nano-structured materials.

### III-I-1 In-Situ Observation of CO Oxidation on Ag(110)(2x1)-O by Scanning Tunneling Microscopy: Structural Fluctuation and Catalytic Activity

NAKAGOE, Osamu<sup>1</sup>; WATANABE, Kazuya<sup>2</sup>; TAKAGI, Noriaki<sup>3</sup>; MATSUMOTO, Yoshiyasu<sup>2</sup>  
(<sup>1</sup>Hokkaido Univ.; <sup>2</sup>IMS and SOKENDAI; <sup>3</sup>IMS and Univ. Tokyo)

[*J. Phys. Chem. B* **109**, 14536–14543 (2005)]

On the added-row reconstructed Ag(110)( $n \times 1$ )-O surfaces where one-dimensional  $\text{-Ag-O-Ag-O-}$  chains arrange periodically, the clean-off reaction of O adatoms by CO was investigated using variable temperature scanning tunneling microscopy (VT-STM). Based on the *in-situ* STM observations of the surface structure variation in the course of the reaction at various temperatures, we found that the reaction kinetics are significantly affected by the structural transition of AgO chains from a solid straight line configuration to dynamically fluctuating configurations. Below 230 K where the chains are straight, the reaction takes place only at the end of the chains, so that the reaction progresses in the zeroth order kinetics with the reaction front propagating along the chain. The temperature dependence of the reaction rates yields the activation barrier of 41 kJ/mol and the pre-exponential factor of  $1.7 \times 10^3 \text{ cm}^{-2}\text{s}^{-1}$ . At room temperature, the reaction rate is drastically accelerated when almost half of O adatoms are eliminated and the chains start fluctuating. The dynamic formation of active sites equivalent to the end of chains upon the chain fluctuation results in the nonlinear increase of the reaction rate.

### III-I-2 Propagation of Reaction Front in the Disproportionate Reaction of H<sub>2</sub>O on Ag(110)(5x1)-O Surface: Role of Hydrogen Bonding Interaction

TAKAGI, Noriaki<sup>1</sup>; NAKAGOE, Osamu<sup>2</sup>; WATANABE, Kazuya<sup>3</sup>; MATSUMOTO, Yoshiyasu<sup>3</sup>

(<sup>1</sup>IMS and Univ. Tokyo; <sup>2</sup>Hokkaido Univ.; <sup>3</sup>IMS and SOKENDAI)

[*J. Phys. Chem. B* **109**, 14536–14543 (2005)]

The structural evolution in the course of the disproportionation of H<sub>2</sub>O with O adatoms in the added-row reconstructed Ag(110)-O surfaces was investigated by variable temperature scanning tunneling microscopy. Initially, the reaction takes place only at the ends of the added-rows, and then, after the induction period, the reaction progresses explosively with the reaction front propagating at the rate of 1 nm/s. The strong non-linearity can be explained by the autocatalytic reaction model where clustering of H<sub>2</sub>O by the hydration of OH makes both H<sub>2</sub>O coverage and reactivity of H<sub>2</sub>O sufficiently high that a new reaction pathway opens to drive the reaction front.

# RESEARCH ACTIVITIES IV

## Department of Molecular Assemblies

### IV-A Optical Study of Charge Ordering States in Organic Conductors

In the organic charge-transfer salts, the charge carriers in organic crystal is located at the boundary between localized and extended (delocalized) states, mainly because the interatomic distances between the neighboring molecules are much longer than the bond length within the molecule. Therefore, charge ordering (CO) originated from the localization of the charge carriers is widely found in organic conductors through the phase transition. Recently, CO has been found in several organic conductors, and the electronic phase diagrams of typical organic conductors are re-considered taking CO into account. The CO state is drawing attention, first because a CO phase is neighbored on a superconducting phase, wherein a new type of pairing mechanism for superconductivity is theoretically predicted, second because some compounds in a CO phase shows ferroelectric property. To detect CO states, we employ infrared and Raman spectroscopy. Some molecules have charge-sensitive intramolecular vibrational modes, the frequency of which shifts proportional to the molecular charge (oxidation state of molecule). The Raman and infrared spectra change dramatically at the CO phase-transition temperature, since CO is accompanied by an inhomogeneous distribution of molecular charge. The goal of this study is (1) the understanding of the unusual electronic state of the conducting phase above the CO phase transition, (2) the investigation of the optical properties related to the ferroelectric CO phase, and (3) the characterization of the insulating electronic state near the superconducting phase.

#### IV-A-1 Examination of the Charge-Sensitive Vibrational Modes in ET Molecule

YAMAMOTO, Takashi; YAKUSHI, Kyuya;  
URUICHI, Mikio; YAMAMOTO, Kaoru;  
KAWAMOTO, Atsushi<sup>1</sup>; TANIGUCHI, Hiromi<sup>2</sup>  
(<sup>1</sup>Hokkaido Univ.; <sup>2</sup>Saitama Univ.)

[*J. Phys. Chem. B* **109**, 15226 (2005)]

We re-investigated the two C=C stretching modes of the five-member rings of ET [ET = bis(ethylenedithio) tetrathiafulvalene], namely,  $\nu_2$  (in-phase mode) and  $\nu_{27}$  (out-of-phase mode). The frequency of the  $\nu_{27}$  mode of ET<sup>+</sup> was corrected to be  $\sim 1400\text{ cm}^{-1}$ , which was identified from the polarized infrared reflectance spectra of (ET)(ClO<sub>4</sub>), (ET)(AuBr<sub>2</sub>Cl<sub>2</sub>) and the deuterium- or <sup>13</sup>C-substituted compounds of (ET)(AuBr<sub>2</sub>Cl<sub>2</sub>). It was clarified from DFT calculations that the frequency of the  $\nu_{27}$  mode of the flat ET<sup>0</sup> molecule was significantly different from that of the boat-shaped ET<sup>0</sup> molecule. We obtained the linear relationship between the frequency and the charge on the molecule,  $\rho$ , for the flat ET molecule, which was shown to be  $\nu_{27}(\rho) = 1398 + 140(1-\rho)\text{ cm}^{-1}$ . The frequency shift due to oxidation is remarkably larger than reported in previous studies. The fractional charges of several ET salts in a charge-ordered state can be successfully estimated by applying this relationship. Therefore, the  $\nu_{27}$  mode is an efficient probe to detect  $\rho$  in the charge-transfer salts of ET. Similarly, the linear relationship for the  $\nu_2$  mode was obtained as  $\nu_2(\rho) = 1447 + 120(1-\rho)$ . This relationship was successfully applied to the charge-poor molecule of  $\theta$ -type ET salts in the charge-ordered state, but could not be applied to the charge-rich molecule. This discrepancy was semi-quantitatively explained by the hybridization between the  $\nu_2$  and  $\nu_3$  modes.

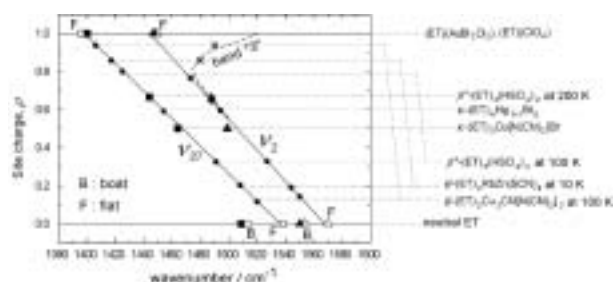


**Figure 1.** Frequencies of the  $\nu_{27}$  and  $\nu_2$  modes plotted as a function of the charge,  $\rho$ , on the ET molecule. Solid squares and solid triangles denote the experimental data, and open squares and open triangles denote the calculation data. The straight lines show the linear relationships between the frequencies and  $\rho$ , deduced from least-squares fitting. The  $\rho$  value of the ET salts is inversely estimated from the linear relation and the data points thus obtained are indicated by solid circles. The broken line shows the  $\rho$  dependence of the band “3”, and  $\times$  denotes the frequencies of the A-symmetry mode of the  $\theta$ -type ET salts.

#### IV-A-2 Infrared and Raman Studies of $\theta$ -(BEDT-TTF)<sub>2</sub>CsZn(SCN)<sub>4</sub>: Comparison with the Frozen State of $\theta$ -(BEDT-TTF)<sub>2</sub>RbZn(SCN)<sub>4</sub>

SUZUKI, Kenji<sup>1</sup>; YAMAMOTO, Kaoru;  
YAKUSHI, Kyuya; KAWAMOTO, Atsushi<sup>2</sup>  
(<sup>1</sup>SOKENDAI; <sup>2</sup>Hokkaido Univ.)

[*J. Phys. Soc. Jpn.* **74**, 2631–2639 (2005)]

We present the optical conductivity and Raman spectra of  $\theta$ -(BEDT-TTF)<sub>2</sub>CsZn(SCN)<sub>4</sub>. The vibrational and vibronic bands in the 1200–1600  $\text{cm}^{-1}$  region was assigned with the aid of the <sup>13</sup>C-substituted compound. The nearly uniform charge distribution was found in a

whole temperature range from 300 K to 6 K. However, the space group symmetry  $I222$  is locally broken already at room temperature. The broken symmetry suggests the resemblance to the high-temperature phase and frozen state of  $\theta$ -(BEDT-TTF)<sub>2</sub>RbZn(SCN)<sub>4</sub>, which consists of short-range ordered charge-ordering domains. The amplitude in the charge-ordering domain of  $\theta$ -(BEDT-TTF)<sub>2</sub>CsZn(SCN)<sub>4</sub> is extremely small in a whole temperature range. At room temperature, hydrostatic pressure narrows the bandwidth of  $\theta$ -(BEDT-TTF)<sub>2</sub>CsZn(SCN)<sub>4</sub> to enlarge the amplitude in short-ranged ordered domains. The long-range ordered charge ordering in  $\theta$ -(BEDT-TTF)<sub>2</sub>CsZn(SCN)<sub>4</sub> was found at 10 K under the hydrostatic pressure of 2.5 GPa.

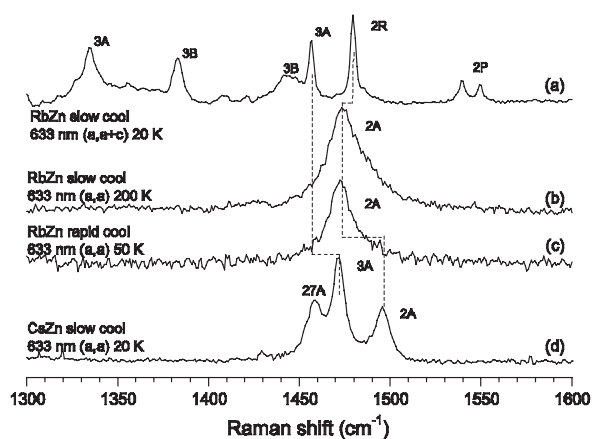


**Figure 1.** Comparison of the Raman spectra excited by 633 nm laser of slowly cooled RbZn measured at (a) 20 K (below  $T_{CO}$ ) and (b) 200 K (above  $T_{CO}$ ), (c) rapidly cooled RbZn measured at 50 K, and (d) slowly cooled CsZn measured at 20 K.  $\nu_{2P}$  and  $\nu_{2R}$  denote the  $\nu_2$  modes at charge-poor ( $\rho = 0.2$ ) site and charge-rich ( $\rho = 0.8$ ) site, respectively.

#### IV-A-3 Robust Superconducting State in the Low-Quasiparticle-Density Organic Metals $\beta''$ -(BEDT-TTF)<sub>4</sub>[(H<sub>3</sub>O)M(C<sub>2</sub>O<sub>4</sub>)<sub>3</sub>]-Y: Superconductivity due to Proximity to a Charge-Ordered State

BANGURA, A. F.<sup>1</sup>; COLDEA, A. I.<sup>1</sup>; SINGLETON, J.<sup>2</sup>; ARDAVAN, A.<sup>1</sup>; AKUTSU-SATO, A.<sup>3</sup>; AKUTSU, H.<sup>3</sup>; TURNER, S. S.<sup>3</sup>; DAY, P.<sup>3</sup>; YAMAMOTO, Takashi; YAKUSHI, Kyuya  
(<sup>1</sup>Oxford Univ.; <sup>2</sup>Los Alamos Natl. Lab.; <sup>3</sup>Royal Inst. GB)

[*Phys. Rev. B* **72**, 014543 (13 pages) (2005)]

We report magneto-transport measurements on the quasi-two-dimensional charge-transfer salts  $\beta''$ -(BEDT-TTF)<sub>4</sub>[(H<sub>3</sub>O)M(C<sub>2</sub>O<sub>4</sub>)<sub>3</sub>]-Y, with Y = C<sub>6</sub>H<sub>5</sub>NO and C<sub>6</sub>H<sub>5</sub>CN using magnetic fields of up to 45 T and temperature down to 0.5 K. A surprisingly robust superconducting state with an in-plane upper critical field  $B_{c2||} \approx 33$  T, comparable to the highest critical field of any BEDT-TTF superconductor, and critical temperature  $T_c \approx 7$  K is observed when M = Ga and Y = C<sub>6</sub>H<sub>5</sub>NO<sub>2</sub>. The presence of magnetic M ions reduces the in-plane upper critical field to  $\approx 18$  T for M = Cr and Y = C<sub>6</sub>H<sub>5</sub>NO<sub>2</sub> and M = Fe and Y = C<sub>6</sub>H<sub>5</sub>CN. Prominent

superconducting salts possess Fermi surfaces with one or two small quasi-two-dimensional pockets, their total area comprising  $\leq 6\%$  of the room-temperature Brillouin zone; the quasiparticle effective masses were found to be enhanced when the ion M was magnetic (Fe or Cr). The low effective masses and quasiparticle densities, and the systematic variation of the properties of the  $\beta''$ -(BEDT-TTF)<sub>4</sub>[(H<sub>3</sub>O)M(C<sub>2</sub>O<sub>4</sub>)<sub>3</sub>]-Y salts with unit-cell volume points to the possibility of a superconducting ground state with a charge-fluctuation-mediated superconductivity mechanism such as that proposed by Merino and McKenzie [*Phys. Rev. Lett.* **87**, 237002 (2001)] rather than the spin-fluctuation mechanism appropriate for the  $\kappa$ -(BEDT-TTF)<sub>2</sub>X salts.

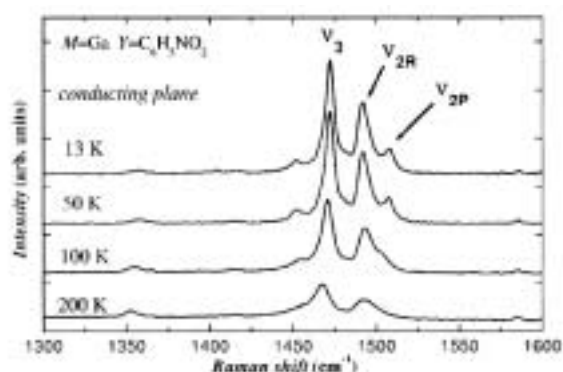


**Figure 1.** Raman spectra of  $\beta''$ -(BEDT-TTF)<sub>4</sub>[(H<sub>3</sub>O)Ga(C<sub>2</sub>O<sub>4</sub>)<sub>3</sub>]-C<sub>6</sub>H<sub>5</sub>NO<sub>2</sub> taken at fixed temperature in the range  $13 \leq T \leq 200$  K. Note that the charge-sensitive  $\nu_2$  band shows a clear splitting, which suggests the CO state below 50 K in this compound.

#### IV-A-4 Influence of the Cooling Rate on Low-Temperature Raman and Infrared-Reflection Spectra of Partially Deuterated $\kappa$ -(BEDT-TTF)<sub>2</sub>Cu(N(CN)<sub>2</sub>)Br

MAKSIMUK, M.; YAKUSHI, Kyuya; TANIGUCHI, H.<sup>1</sup>; KANODA, Kazushi<sup>1</sup>; KAWAMOTO, Atsushi<sup>2</sup>  
(<sup>1</sup>Univ. Tokyo; <sup>2</sup>Hokkaido Univ.)

[*Synth. Met.* **149**, 13–18 (2005)]

Raman and infrared-reflection spectra of  $\kappa$ -(BEDT-TTF)<sub>2</sub>Cu(N(CN)<sub>2</sub>)Br and its deuterated and partially deuterated analogues were measured at temperatures between 5 and 300 K and cooling rates from 1 to 20 K/min. It was found that, in partially deuterated samples, the interdimer electron-molecular vibration splitting of  $\nu_3$  mode in Raman spectra, and linewidths of some phonon peaks both in Raman and infrared spectra depend on the cooling rate. These observations were explained by disorder-related effects.

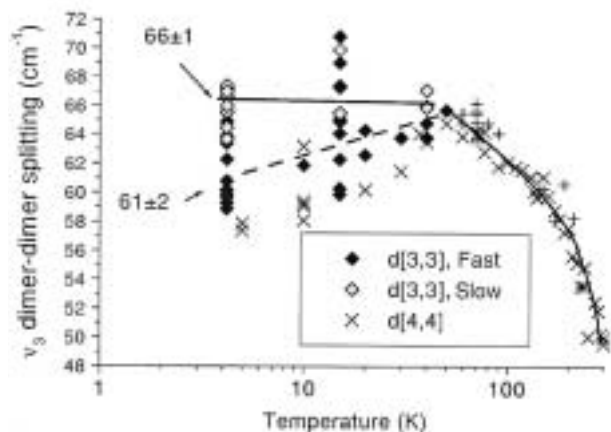


**Figure 1.** Temperature dependence of the dimer-dimer EMV (electron-molecular vibration) splitting of  $\nu_3$  for d(3,3) after “slow” cooling ( $\diamond$ ), “fast” cooling ( $\blacklozenge$ ), and above 50 K (crosses, +). The results for d(4,4) are also shown (crosses,  $\times$ ). Lines are guide to the eye.

#### IV-A-5 Optical Second Harmonic Generation in a Charge-Ordered Organic Conductor $\alpha$ -(BEDT-TTF) $_2$ I $_3$

YAMAMOTO, Kaoru; BOYKO, Sergiy; YAKUSHI, Kyuya; OKABE, Chie; NISHI, Nobuyuki; KASHIWAZAKI, Akimitsu<sup>1</sup>; HIRAMATSU, Fukiko<sup>1</sup>; IWAI, Shinichiro<sup>1</sup>  
(<sup>1</sup>Tohoku Univ.)

Charge ordering (CO) in highly correlated CT complexes induces large modulation in the charge distribution. Since the modulation causes strong local polarization, it is suggested that such a polar state may show special features in dielectric properties, as ionic crystals do. In the present study, we investigated the nonlinear optical property of the title compound by means of the observation of second-harmonic generation (SHG). Near-IR ultra-short laser pulses were irradiated to a filmy single crystal as the excitation light, and the generated SH signal was detected in a transmission geometry.

It is known that this compound transforms from a semiconductor to an insulator at  $T_{CO}$  (135 K) due to CO. As shown in (Figure 1), the SH signal emerges below  $T_{CO}$ , indicating that the inversion symmetry, existing at high temperatures, is broken by the spontaneous polarization induced by CO below  $T_{CO}$ . The prominent feature of the highly correlated system is in the competition of several electronic phases. Therefore, understanding of the mechanism of CO and then finding the way to connect it with the optical nonlinearity discovered here are important to explore the potential application of the correlated materials as a unique nonlinear optical media.

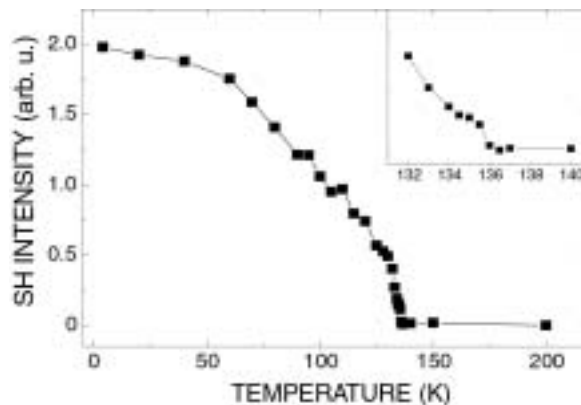


**Figure 1.** Temperature dependence of the intensity of second harmonic light from  $\alpha$ -(BEDT-TTF) $_2$ I $_3$ . Inset shows the close-up of the data around  $T_{CO}$ .

#### IV-A-6 Correlation between Structural Instabilities and Raman Shift and Width in $\beta$ -(ET) $_2$ I $_3$ and $\kappa$ -(ET) $_2$ Cu[N(CN) $_2$ ]I

DROZDOVA, Olga; TANATAR, Makariy<sup>1</sup>; YAKUSHI, Kyuya; KUSHCH, N. D.<sup>1</sup>  
(<sup>1</sup>Inst. Problems Chem. Phys., RAS)

Motivation of this study is to test the temperature dependence (Raman shift and width) of some selected intramolecular vibrations under the influence of both structural and electronic anomalies, in order to find a sensitive and reliable method to distinguish the nature clearly between such anomalies. For this purpose, we measured simultaneously the C=C modes of the ET molecule ( $\nu_2$  and  $\nu_3$ , these are sensitive to ET geometry and local charge, as well as transfer integral), and CN mode of the polymeric anion (sensitive to structural effects only). Here we report the results obtained on the titled compounds because of possibility to directly compare the data with the published low-temperature structural studies.

(a)  $\beta$ -(ET) $_2$ I $_3$ : Anomalies in the Raman shift of  $\nu_2$  were found at 100 and 170 K, where superstructures are known to appear.<sup>1)</sup> No abnormality was observed in the Raman shift of  $\nu_3$  nor in the line width of the modes of  $\nu_2$  and  $\nu_3$ .

(b)  $\kappa$ -(ET) $_2$ Cu[N(CN) $_2$ ]I: Discontinuous jumps in the Raman shift (clear deviations from  $T^2$  behavior) of both  $\nu_2$  and  $\nu_3$  ( $A_g$ ), as well as  $\nu$ (CN) were found at 155 and 220 K. These are characteristic temperatures where  $0.5c^*$  and  $0.38c^*$  superstructures are formed.<sup>2)</sup> In addition, a rapid increase in Raman shift of  $\nu_2$  was observed below 45 K. On the other hand,  $\nu_2$  ( $B_{2g}$ ) showed approximately linear temperature dependence of an opposite sign, with a change of slope at 50 K. Further studies of  $\kappa$ -(ET) $_2$ X compounds will be performed and compared with other physical properties.

#### References

- 1) T. Ishiguro, K. Yamaji, and G. Saito, *Organic Superconductors*, Springer 1998, and references therein.
- 2) M. A. Tanatar, V. S. Yefanov, S. Kagoshima, E. Ohmichi, T. Osada, N. D. Kushch and E. B. Yagubskii, *Phys. Rev. Lett.* submitted.

#### IV-A-7 Inhomogeneous Charge Distribution in (EDO-TTF)<sub>2</sub>X (X = ReO<sub>4</sub> and GaCl<sub>4</sub>)

DROZDOVA, Olga; YAKUSHI, Kyuya; URUICHI, Mikio; OTA, Akira<sup>1</sup>; YAMOCCHI, Hideki<sup>1</sup>; SAITO, Gunzi<sup>1</sup>

(<sup>1</sup>Kyoto Univ.)

Recently synthesized organic conductors (EDO-TTF)<sub>2</sub>X (where X = ReO<sub>4</sub> and GaCl<sub>4</sub>) have quasi-one-dimensional (Q1D) crystal structure formed by two differently packed columns (A and B) of EDO-TTF alternated with chains of inorganic anion. Each column involves non-equivalent EDO-TTF molecules A1, A2, B1, and B2. The infrared spectra showed a phase transition at  $T^* = 125$  K, where the Drude contribution disappeared, an optical gap opened, and a strong vibronic bands emerged. On the other hand, the Raman spectra were insensitive to  $T^*$ , and showed no essential change in the whole temperature region 300–4.2 K. The Raman-active C=C stretching vibrations of EDO-TTF, sensitive to the molecular charge, were split into several components (Figure 1). These were interpreted as an inhomogeneous charge distribution on the four sites in the unit cell. From the Raman shift frequencies, the respective site charge differences were found as  $A1 - A2 = 0.25e$ , and  $B1 - B2 = 0.1e$ . Charge localization was suggested as a driving force of the phase transition at 125 K.

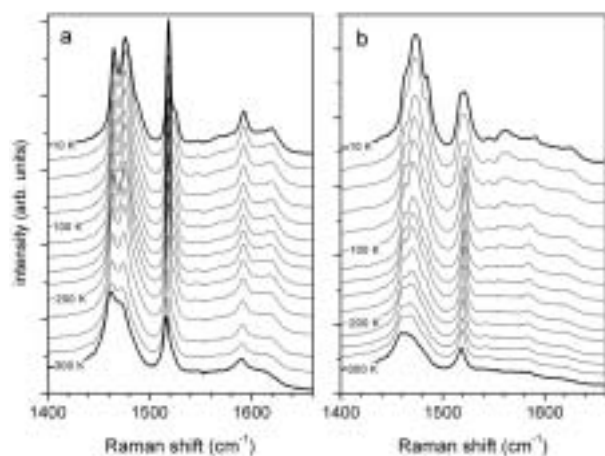


**Figure 1.** Temperature dependence of the Raman spectra of (a) (EDO-TTF)<sub>2</sub>ReO<sub>4</sub> and (b) (EDO-TTF)<sub>2</sub>GaCl<sub>4</sub>.

#### IV-A-8 Re-Examination of the Site Charge Difference in TEA(TCNQ)<sub>2</sub>

DROZDOVA, Olga; YAKUSHI, Kyuya

In 1/4-filled organic charge transfer salts (CTS) the charge ordered (CO) state is classified into  $4k_F(0101)$  and  $2k_F(0110)$  waves. The latter is further divided into  $2k_F$  BCDW-I ( $\circ \dots \circ = \bullet \dots \bullet = \circ \dots \circ$ ) and  $2k_F$  BCDW-II ( $\circ \dots \circ - \bullet \dots \bullet = \circ \dots \circ$ ), where the open circle has the charge of  $(1-\Delta q)/2$  and that at the solid circle has the charge of  $(1+\Delta q)/2$ . We have recently analyzed the  $2k_F$  BCDW-II state in (EDO-TTF)<sub>2</sub>X (X = PF<sub>6</sub>, AsF<sub>6</sub>).<sup>1</sup> TEA(TCNQ)<sub>2</sub> is regarded as a typical representative compound for  $2k_F$  BCDW-I based on the x-ray crystal

structure analysis. We analyzed the site charge distribution using vibrational analysis and determined  $\Delta q$ . The Raman-active (gerade) modes of TCNQ were perturbed by *emv* coupling. Therefore we employed the IR-active (ungerade) modes. Cs<sub>2</sub>(TCNQ)<sub>3</sub> compound was used as a reference. The results obtained at 300 K and 6 K are summarized in the Table 1.

**Table 1.** Estimation of the difference in site charge,  $\Delta q$ .

TCNQ Mode	shift (per 1e) $\Delta v$ cm <sup>-1</sup>	Cs <sub>2</sub> TCNQ <sub>3</sub>		TEA(TCNQ) <sub>2</sub>			
		obs. $\Delta v$ cm <sup>-1</sup>	charge difference $\Delta q$	300 K		6 K	
				$\Delta v$ cm <sup>-1</sup>	$\Delta q$	$\Delta v$ cm <sup>-1</sup>	$\Delta q$
b <sub>2u</sub> v <sub>34</sub> C=C	36	30	0.83	18	0.50	20	0.56
b <sub>2u</sub> v <sub>33</sub> C≡N	75	50	0.67	44	0.59	47	0.63
b <sub>1u</sub> v <sub>19</sub> C≡N	47	44	0.94	34	0.72	37	0.79
averaged site charge			0.78		0.61		0.66

#### Reference

1) O. Drozdova, K. Yakushi, K. Yamamoto, A. Ota, H. Yamochi, G. Saito, H. Tashiro and D. B. Tanner, *Phys. Rev. B* **70**, 075107 (2004).

#### IV-A-9 Spectroscopic Evidence for the Monovalent-to-Divalent Phase Transition of Biferrocenium (F<sub>1</sub>TCNQ)<sub>3</sub>

URUICHI, Mikio; YAKUSHI, Kyuya; MOCHIDA, Tomoyuki<sup>1</sup>

(<sup>1</sup>Toho Univ.)

[*J. Low Temp. Phys.* submitted]

The ionic crystal D<sup>+</sup>A<sub>3</sub><sup>-</sup> (D = dineopentylbiferrocene and A = F<sub>1</sub>TCNQ) undergoes a first-order phase transition, in which second ionization occurs to form a doubly ionized state, D<sup>2+</sup>A<sub>3</sub><sup>2-</sup>.<sup>1</sup> As shown in the left panel of Figure 1, we found a dramatic change in the optical transition in the near-infrared region. This optical transition is interpreted as the charge-transfer excitation within the F<sub>1</sub>TCNQ trimer. We simulated the optical transition employing a trimer model. First, the transfer integral and site energy within the F<sub>1</sub>TCNQ trimer, A<sup>3-</sup>, were estimated to reproduce the spectrum (oscillator strength and peak position) of 290 K. The site energy is introduced to take effectively the intra- and inter-trimer Coulomb interaction energy into account. Using the parameters thus obtained, the spectrum of A<sub>3</sub><sup>2-</sup> is simulated. As shown in the right panel of Figure 1, the change of this optical transition is quantitatively reproduced by the trimer model, in which the valence of the trimer changes from A<sub>3</sub><sup>-</sup> to A<sub>3</sub><sup>2-</sup>. This result strongly supports the valence change character of this phase transition.

#### Reference

1) T. Mochida, K. Takazawa, M. Takahashi, M. Takeda, Y. Nishio, M. Sato, K. Kajita, H. Mori, M. M. Matsushita and T. Sugawara, *J. Phys. Soc. Jpn.* **74**, 2214 (2005).

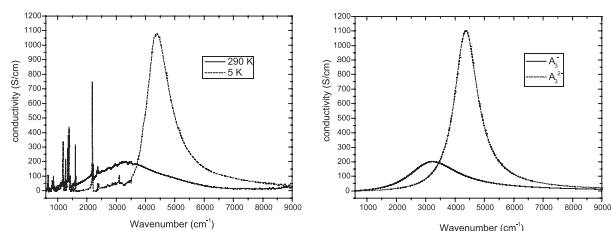


**Figure 1.** Optical conductivity spectra at 290 K and 5 K (left panel), and the Simulation based on a trimer model (right panel).

#### IV-A-10 Phase Separation in the Monovalent-to-Divalent Phase Transition of Biferrocenium-(F<sub>1</sub>TCNQ)<sub>3</sub>

URUICHI, Mikio; YAKUSHI, Kyuya; MOCHIDA, Tomoyuki<sup>1</sup>  
(<sup>1</sup>Toho Univ.)

The ionic crystal  $D^+A_3^-$  ( $D$  = dineopentylbiferrocene and  $A = F_1TCNQ$ ) undergoes a first-order phase transition, in which second ionization occurs to form a doubly ionized state,  $D^{2+}A_3^{2-}$ .<sup>1)</sup> This monovalent-to-divalent phase transition gradually occurs in a wide temperature range from 160 K to 100 K. X-ray diffraction experiments showed that the Bragg spots consist of pairs of spots between 160 K and 100 K. One set is assigned to the unit cell of high-temperature phase and another is assigned to the low-temperature phase. On decreasing temperature, the intensities of the spots of high-temperature phase decreased and those of low-temperature phase increased. This observation is strong evidence for the phase separation in the temperature range of 160 K–100 K.

The Raman spectrum above 160 K also showed a big change below 100 K. When the laser is focused on the area of 2  $\mu\text{m}$  diameter, the Raman spectrum shows position dependence: Only the monovalent peak (1446  $\text{cm}^{-1}$ ) is found in some area, while the divalent peak (1431  $\text{cm}^{-1}$ ) is found in other area, and both peaks are observed at the boundary of the two areas. The thickness of the boundary is estimated to be  $\sim 10\text{--}15 \mu\text{m}$ . In this boundary, the intensity ratio of the monovalent and divalent peaks changes gradually. The boundary area is so thick that may involve monovalent and divalent domains smaller than 2  $\mu\text{m}$ . We mapped the 100  $\mu\text{m} \times 200 \mu\text{m}$  area at the phase-separation temperature. In this area, we observed only macroscopic domains, the size of which changes depending on the temperature.

The Raman spectrum and X-ray diffraction experiments described above showed that macroscopic domains of the monovalent and divalent phases coexist between 160 K and 100 K and the volume fraction of the two phases continuously changes in this phase-separation temperature region.

#### Reference

- 1) T. Mochida, K. Takazawa, M. Takahashi, M. Takeda, Y. Nishio, M. Sato, K. Kajita, H. Mori, M. M. Matsushita and T. Sugawara, *J. Phys. Soc. Jpn.* **74**, 2214 (2005).

## IV-B Magnetic Resonance Studies for Molecular-Based Conductors

Molecular based conductors are one of the extensively studied materials. The development of the understanding of the electronic phases of these materials enables us systematic investigations of low-dimensional highly correlated electrons systems. Competition of the electronic phases in molecular based conductors has attracted much attention. Magnetic resonance investigations are powerful investigations to understand the fundamental electronic properties, because they are microscopic and also dynamical measurements. The investigations of such electronic phases by means of magnetic resonance measurements are important to understand the unsolved fundamental problems in the field of solid state physics.

In this project, we performed the multi-frequency- (X-, Q- and W-bands) and pulsed-ESR, and broad-line NMR measurements for molecular based conductors to understand the electron spin dynamics in the low temperature electronic phases.

### IV-B-1 Charge Disproportionation in (TMTTF)<sub>2</sub>SCN Observed by <sup>13</sup>C NMR

FUJIYAMA, Shigeki; NAKAMURA, Toshikazu

[*Phys. Rev. B* **70**, 045102 (6 pages) (2004)]

The results of the <sup>13</sup>C NMR spectra and nuclear spin-lattice relaxation rate  $1/T_1$  for the quasi-one-dimensional quarter-filled organic material (TMTTF)<sub>2</sub>SCN are presented. Below the anion ordering temperature ( $T_{AO}$ ), a new broad line appears in the NMR spectra and the intensity of the distinct line owing to the inner carbon site from the inversion center is almost halved. The remarkable difference in the temperature dependence of  $1/T_1$  below  $T_{AO}$  for the two sharp lines corresponding to outer and inner carbon sites shows the development of a local electronic state. Our simple model of a charge configuration based on the electrostatic interaction between the SCN anions and TMTTF molecules is consistent with our observation of a local gap for the spin excitation. Nevertheless, we reveal that only the electrostatic interaction is insufficient to reproduce the observed divergence of the frequency shift and the linewidth of the newly appearing broad line stemming from the charge-accepting inner site at a much lower temperature than  $T_{AO}$ .

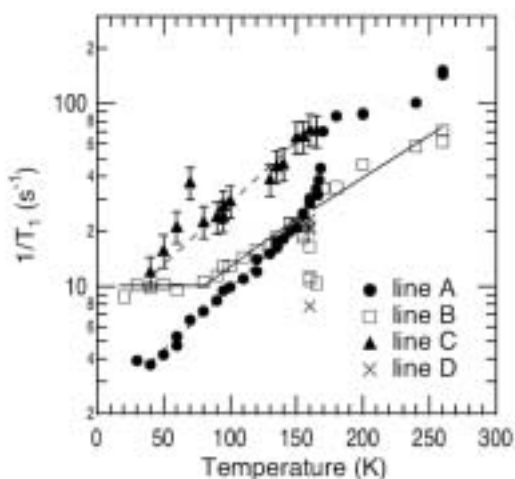


**Figure 1.** Nuclear spin-lattice relaxation rates for distinct lines. The solid and dashed lines are guides to the eye.

### IV-B-2 Redistribution of Electronic Charges in the Spin-Peierls State in (TMTTF)<sub>2</sub>AsF<sub>6</sub> Observed by <sup>13</sup>C NMR

FUJIYAMA, Shigeki; NAKAMURA, Toshikazu

[*J. Phys. Soc. Jpn.* in press]

We report the results of <sup>13</sup>C NMR spectra and nuclear spin lattice relaxation rate  $1/T_1$  for a quasi-one-dimensional quarter-filled organic material (TMTTF)<sub>2</sub>-AsF<sub>6</sub>, which undergoes charge ordering ( $T_{CO} = 102$  K) and spin-Peierls phase transitions ( $T_{SP} = 12$  K). The ratio of two  $1/T_1$  for the charge accepting and donating sites which grows from  $T_{CO}$  finally saturates in approaching  $T_{SP}$ , that indicates an opening of single gap for the spin excitation spectra. At  $T_{SP}$ , however, doubly split NMR lines from inequivalently charged molecules merge originated from the variation in charge densities. This shows a rearrangement of the charge configuration in the spin-Peierls state.

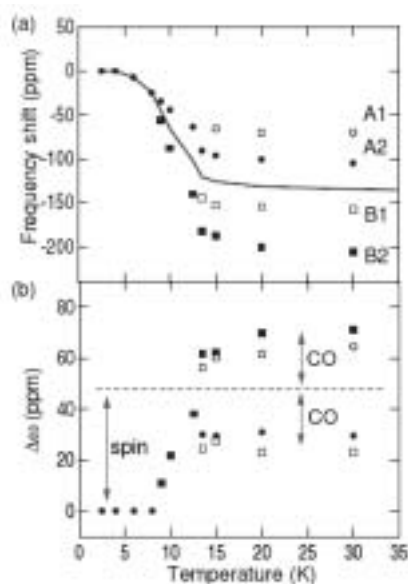


**Figure 1.** (a) The peak positions in the vicinity and below  $T_{SP}$ . (b) The gaps between the peak positions and the averaged frequency denoted as the solid line in (a). The dashed line shows the spin contribution to  $\Delta\omega$ .

### IV-B-3 Deuteration Effect and Possible Origin of the Charge-Ordering Transition of $(\text{TMTTF})_2\text{X}$

FURUKAWA, Ko; HARA, Toshifumi;  
NAKAMURA, Toshikazu

[*J. Phys. Soc. Jpn.* in press]

ESR, NMR and X-ray measurements were performed for pristine and fully perdeuterio-TMTTF,  $(\text{TMTTF}-d_{12})_2$  salts. Significant enhancement by deuteration of the charge-order phase transition temperature,  $T_{\text{CO}}$ , was observed in ESR measurements for all  $(\text{TMTTF})_2\text{X}$  salts measured. No obvious relation between the  $\text{SbF}_6$  anion motion and the TMTTF charge-order was found by  $^{19}\text{F}$  NMR. We also performed single crystal X-ray measurements to understand the deuteration effects and temperature dependence of the crystal structure. A possible relationship between the  $T_{\text{CO}}$ 's and crystallographical parameters is proposed. The deuteration effects and possible origin of the charge-ordering transition of TMTTF salts are discussed.

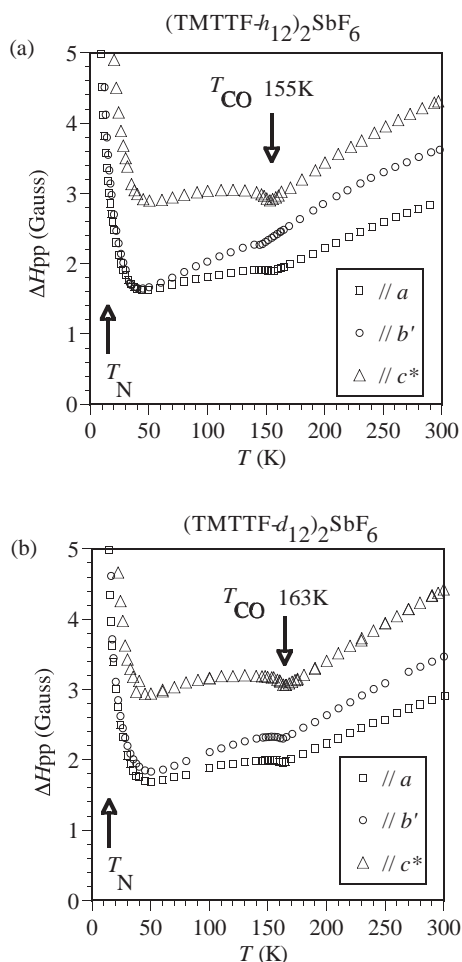


**Figure 1.** Temperature dependence of the ESR linewidth,  $\Delta H_{\text{pp}}$ , of (a) pristine,  $(\text{TMTTF}-h_{12})_2\text{SbF}_6$  and (b) deuterated,  $(\text{TMTTF}-d_{12})_2\text{SbF}_6$ .

### IV-B-4 Redistribution of Electronic Charge in $(\text{TMTTF})_2\text{ReO}_4$ : $^{13}\text{C}$ NMR Investigation

NAKAMURA, Toshikazu; HARA, Toshifumi;  
FURUKAWA, Ko

[*J. Low Temp. Phys.* in press]

$^{13}\text{C}$  NMR measurements were performed for a one-dimensional organic conductor,  $(\text{TMTTF})_2\text{ReO}_4$ . An intermediate charge-ordering (CO) phase has been found firstly for a TMTTF salt with a  $T_d$ -symmetry counter anion: The NMR parameters indicate two inequivalent molecules with unequal electron densities below 225 K. Moreover, the spin-singlet transition associated with  $\text{ReO}_4$  anion ordering was confirmed at around 158 K by  $^{13}\text{C}$  NMR measurements. A drastic change of NMR parameters below 158 K also indicates a redistribution of the electronic charge at the anion ordering temperature.

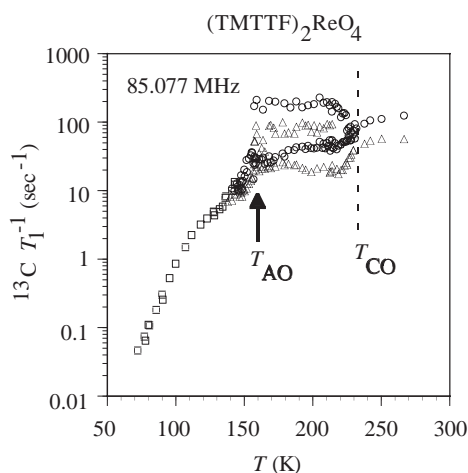


**Figure 1.** Temperature dependence of the  $^{13}\text{C}$  NMR spin-lattice relaxation rate,  $^{13}\text{C} T_1^{-1}$ , of  $(\text{TMTTF})_2\text{ReO}_4$ .

### IV-B-5 Spin Structure of Organic Conductors $(\text{TMTTF})_2\text{X}$

FURUKAWA, Ko; HARA, Toshifumi;  
NAKAMURA, Toshikazu

Organic conductors,  $(\text{TMTTF})_2\text{X}$  ( $X = \text{Br}, \text{SbF}_6$ , and  $\text{PF}_6$ ), are examined by electron spin resonance (ESR) spectroscopy, X-ray diffraction and theoretical calculation of  $g$ -tensor. In the case of the counter anions with octahedral symmetry, the anomalous change of the principal values and axes of the  $g$ -tensor, which were determined by the angular dependence of  $g$ -values, were observed in the temperature range from 20 K to the room temperature. However, the  $g$ -tensor was temperature independence in the Br salt. The temperature variation of the crystal structure for both salts is performed by X-ray diffraction. No obvious change of the molecular structure is observed in both salts. In the octahedral counter anion salts, the distance between the TMTTF molecules and the counter anion shrank due to the bulk counter anion as the temperature decreased. In order to interpret the anomalous  $g$ -shift, the theoretical calculation of the  $g$ -tensor based on the DFT-GIAO method is carried out. The relationship between the spin and the crystal structure will be discussed.

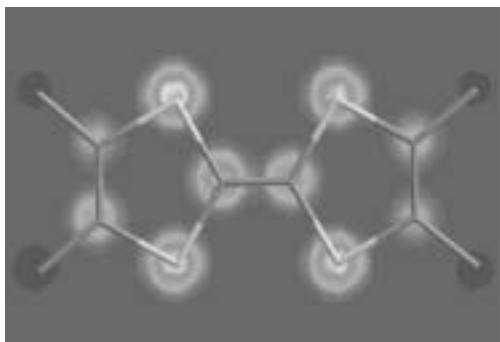


**Figure 1.** Spin density of the TMTTF radical determined by the DFT-GIAO method.

#### IV-B-6 Multi-Frequency ESR Measurements for (TMTTF)<sub>2</sub>X

HARA, Toshifumi; FURUKAWA, Ko;  
NAKAMURA, Toshikazu

TMTTF family salts are now attracted attention by the recent progress of the charge ordering (CO) investigations. Recently, we proposed the possible charge ordering configurations for each of (TMTTF)<sub>2</sub>X salts according to the difference of the ESR linewidth anisotropy at low temperatures. The CO configurations of (TMTTF)<sub>2</sub>X are roughly divided into three groups, and this classification is consistent with the results determined by other measurements. However the origin of the charge ordering phenomena is not clarified, and the quantitative understanding of the ESR linewidth is not succeeded so far. So we performed multi-frequency (X- [10GHz], Q- [30GHz], and W-bands [100GHz]) ESR measurements for one of typical TMTTF salts, (TMTTF)<sub>2</sub>SbF<sub>6</sub>, which shows the charge ordering transition at 154 K. The ESR linewidth determined by the W-band measurement is obviously larger than that by X-band below the charge ordering transition. We discuss the low temperature electron spin dynamics from the ESR point of view.

#### IV-B-7 Extremely Slow Charge Fluctuations in the Metallic State of the Two-Dimensional Molecular Conductor $\theta$ -(BEDT-TTF)<sub>2</sub>RbZn(SCN)<sub>4</sub>

CHIBA, Ryo<sup>1</sup>; HIRAKI, Ko-ichi<sup>1</sup>; TAKAHASHI,

Toshihiro<sup>1</sup>; YAMAMOTO, M. Hiroshi<sup>2</sup>;  
NAKAMURA, Toshikazu  
(<sup>1</sup>Gakushuin Univ.; <sup>2</sup>RIKEN)

[*Phys. Rev. Lett.* **93**, 216405 (4 pages) (2004)]

Large charge disproportionation has been confirmed in the metallic state of a 1/4-filled organic conductor  $\theta$ -(BEDT-TTF)<sub>2</sub>RbZn(SCN)<sub>4</sub> by means of <sup>13</sup>C-NMR analysis on a selectively <sup>13</sup>C-enriched single crystal sample. By comparing the homogeneous and inhomogeneous linewidths, the temperature dependence of the extremely slow dynamics of charge fluctuations has been determined first. The exotic nature of the metallic state of this salt is discussed.

#### IV-B-8 Sliding Spin-Density Wave of (TMTSF)<sub>2</sub>PF<sub>6</sub> Studied with Narrow-Band Noise

SEKINE, Tomoyuki<sup>1</sup>; SATOH, Norikazu<sup>1</sup>;  
NAKAZAWA, Mitsuhiko<sup>1</sup>; NAKAMURA,  
Toshikazu  
(<sup>1</sup>Sophia Univ.)

[*Phys. Rev. B* **70**, 214201 (13 pages) (2004)]

We report narrow-band noise (NBN) due to sliding motions of the spin-density wave (SDW) condensate at 2.0 K in three samples of (TMTSF)<sub>2</sub>PF<sub>6</sub> and the magnetic-field effects. Typical NBN spectra coming from the saw-toothed-wave current oscillations are clearly observed. The periodic peaks due to the 4k<sub>F</sub>-charge-density wave (CDW) collective excitation are found, together with the SDW moving with a faster velocity, revealing that the sliding mode of the SDW is coupled with 4k<sub>F</sub>-CDW fluctuations. Observation of the interference peaks gives evidence of spatially non-uniform dc current carried by the deformable SDW in domains. At large currents the NBN spectrum drastically changes with increasing current and depends on applied magnetic field, suggesting a dynamical phase transition from the plastic-flow phase to the moving-solid phase. In the moving-solid phase the frequencies of the periodic peaks decrease with increasing current because the spatial coherency grows rapidly. The current oscillations in this phase are interpreted in terms of the coexistence of the 2k<sub>F</sub>-CDW collective excitation with the phason.

## IV-C Synchrotron X-Ray Diffraction Experiments and MEM Analyses for Single Crystals of Organic Conductors

By recent development of aggressive experimental and theoretical researches, electronic phases of organic conductors have been clarified so far. The remarkable anisotropy (low-dimensionality), small band-width and flexibility of the lattice are the characteristics of organic conductors. In most cases, band-structures of organic conductors are deduced with frontier orbitals (the highest occupied molecular orbital: HOMO as for a donor molecule, for example) estimated by molecule orbit calculations applying the tight-binding approximation. The Fermi surfaces calculated above correspond very well with that estimated from quantum vibration and/or angular dependence magneto-resistance experiments. Consistency with first principle calculations is also good. These facts

indicate that most of physics phenomena can be explained within the framework that the frontier orbital can be treated as if one rigid atomic orbital in an alkaline metal. The main aims of this project are, 1) to study whether there is a change of symmetry of frontier orbitals (electric charge distribution in molecules), which is believed to be rigid so far, at phase transitions, and 2) to investigate possible relation between the detailed electric charge distribution in molecules and the electronic phases. Of course, the tight-binding approximation with a rigid frontier orbital is firm to be very good approximation. However, there are several experimental results which suggest a change of electric charge distribution in the molecule in some systems. We performed synchrotron X-ray diffraction experiments and MEM (The Maximum Entropy Method) analyses to investigate the electric charge distribution of molecules for such interesting systems.

This project is partially supported by Grant-in-Aid for Creative Scientific Research Collaboratory on Electron Correlation-Toward a New Research Network between Physics and Chemistry- (13NP0201) from the Ministry of Education, Culture, Sports, Science and Technology, Japan.

#### IV-C-1 Low-Temperature Charge-Ordering State of (TMTTF)<sub>2</sub>PF<sub>6</sub>

HARA, Toshifumi; FURUKAWA, Ko; KAKIUCHI, Toru<sup>1</sup>; SAWA, Hiroshi<sup>2</sup>; NAKAMURA, Toshikazu (<sup>1</sup>SOKENDAI; <sup>2</sup>KEK)

As for the charge-ordering problem which is one of the recent hot topics, electronic charge configurations at low temperatures are clarified so far by several groups containing us. The importance of the long-range Coulomb interaction is pointed out by theoretical researches. TMTTF family salts have been attracting attention due to observations of their charge-ordering (CO) phenomena. <sup>13</sup>C NMR indicates the existence of inequivalent TMTTF sites at low temperatures, and dielectric permittivity measurements show ferroelectric behaviors for (TMTTF)<sub>2</sub>MF<sub>6</sub> (*M* = P, As, Sb) salts. We also proposed that the variation of charge-ordering patterns such as -O-O-o-o- and -O-o-O-o- along the stacking axes for a series of TMTTF salts by ESR linewidth analyses. However, as for the research of the charge-ordering, the electric charge distribution in the molecule was ignored so far. Hence we performed synchrotron X-ray diffraction measurements and MEM analyses to investigate the electric charge distribution of molecules and to understand the low-temperature charge-ordering state of (TMTTF)<sub>2</sub>PF<sub>6</sub>. Figure shows the charge distribution of

(TMTTF)<sub>2</sub>PF<sub>6</sub> at R.T. Further investigations are now underway.

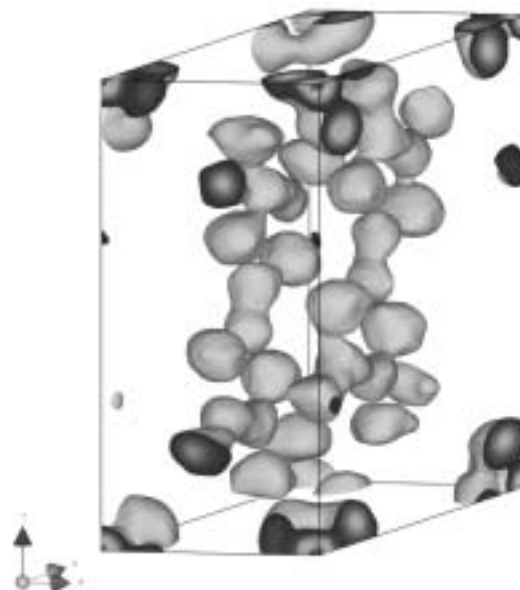


**Figure 1.** Charge distribution of (TMTTF)<sub>2</sub>PF<sub>6</sub> at R.T. determined by synchrotron X-ray diffraction measurements and MEM analyses.

### IV-D EPR Study toward Molecular Biology as Microscopic and Selective Probes Measurements

The structure analyses of the material related to fundamental biology are now hot topics. Especially synchrotron X-ray measurements attract much attention since they can provide detail of the structural information. However, X-ray measurements can be applied only for crystalline material, the resolution is not so good. On the other hand, EPR measurements are advantageous because they are microscopic and selective probes and they can provide dynamical information. Hence, we performed the multi-frequency- and pulsed-ESR for such kind of materials to understand the local structure and possible mechanism of several biological processes.

#### IV-D-1 First Detection of the Multiline Signal from the $S_2$ -State Manganese Cluster of Photosystem II by Single-Crystal W-Band EPR Spectroscopy

MATSUOKA, Hideto<sup>1</sup>; SHEN, Jian-Ren<sup>2</sup>; MINO, Hiroyuki<sup>3</sup>; FURUKAWA, Ko; KATO, Tatsuhisa<sup>4</sup>; KAWAMORI, Asako<sup>5</sup>

(<sup>1</sup>IMS and Free Univ. Berlin; <sup>2</sup>Okayama Univ.; <sup>3</sup>Nagoya Univ.; <sup>4</sup>IMS and Josai Univ.; <sup>5</sup>Kwansei Gakuin Univ. )

[*J. Phys. Chem. B* submitted]

The multiline signal from the  $S_2$ -state manganese cluster in the oxygen evolving complex of photosystem II (PSII) was observed in single crystals of a thermophilic cyanobacterium *Thermosynechococcus vulcanus* for the first time by W-band (95 GHz) electron paramagnetic resonance (EPR), as shown in the figure. The single-crystal spectra were reasonably interpreted by spectral simulation with the hfc parameters appropriate for a trimer-monomer structure of the cluster. The use of PSII single crystals allowed us to determine precisely the  $g$ -tensor of the cluster. The principal values of the tensor indicated that the Mn(III) ion in the cluster exists in an approximate axial symmetry. This work demonstrated that single-crystal experiments are crucial to detect the distinct resolved hfs of the  $S_2$  state at W-band.

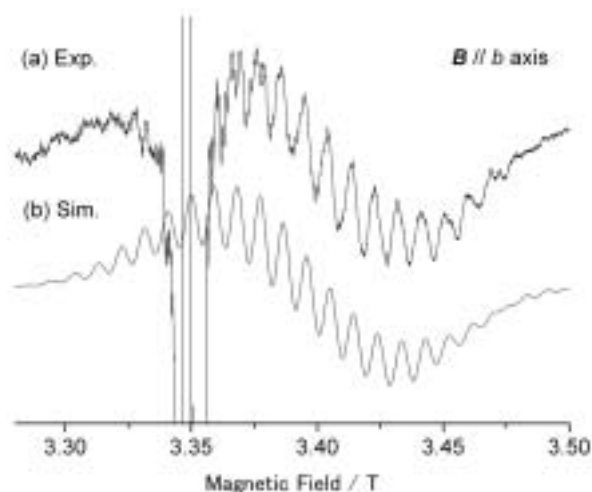


**Figure 1.** (a) Light-minus-dark W-band EPR spectra observed at 6 K for the  $S_2$  state in single crystals of PSII from *T. vulcanus*. (b) The best-fit simulation of (a). The crystallographic  $b$ -axis was approximately parallel to the direction of the magnetic field.

## IV-E Development of Multi-Functional Molecular Systems

Since the molecules tend to retain their independence even in the solid state, the molecular systems can be considered to be suitable systems to construct multi-functional systems by assembling various molecular building blocks with different characters. We are trying to develop various new functional molecular materials such as single-component molecular conductors, photo-controllable magnetic conductors and dielectrically active porous molecular systems.

Recently, “dual-action organic conductors” such as magnetic molecular conductors have attracted a considerable interest. We have discovered unprecedented conductors exhibiting “superconductor  $\rightarrow$  insulator transition,” ( $\lambda$ -(BETS) $_2$ Fe $_x$ Ga $_{1-x}$ Cl $_4$ , BETS = bis(ethylenedithio)tetraselenafulvalene) and the antiferromagnetic organic superconductors ( $\kappa$ -(BETS) $_2$ FeX $_4$  X = Br, Cl) and the field-induced organic superconductor ( $\lambda$ -(BETS) $_2$ FeCl $_4$ ,  $\lambda$ -(BETS) $_2$ Fe $_x$ Ga $_{1-x}$ Cl $_4$ ,  $\kappa$ -(BETS) $_2$ FeBr $_4$ ). However, except these systems, there have been only a few systems showing clear synergetic actions between conduction and magnetic parts. Very recently, we have discovered “constant resistivity state (CRS)” below  $T_c$  in the system exhibiting superconductor  $\rightarrow$  insulator transition at zero magnetic field ( $\lambda$ -(BETS) $_2$ Fe $_x$ Ga $_{1-x}$ Cl $_4$ ,  $x \approx 0.35$ ).

We have recently obtained a new  $\kappa$ -type BETS conductor with weakly ferromagnetic (canted antiferromagnetic) metal state and new molecular conductors exhibiting spin-crossover transition coupled with resistivity hysteresis and LIESST (Light-Induced Excited Spin State Trapping).

By utilizing weak host-guest interaction and polarizability of guest molecules, we have recently obtained new porous molecular systems with high-temperature polarizable and low-temperature unpolarizable states.

Besides these systems, we have recently developed the single-component molecular metals based on the transition metal with extended-TTF ligands. Au(tmdt) $_2$ , which is isostructural to the first single-component molecular metal Ni(tmdt) $_2$  is the first molecular conductor where  $\pi$  conduction electron and antiferromagnetic order coexist above 100 K.

### IV-E-1 Dielectric Properties of Porous Molecular Crystals Containing Polar Molecules

CUI, HengBo; TAKAHASHI, Kazuyuki; OKANO, Yoshinori; KOBAYASHI, Hayao; WANG, Zheming<sup>1</sup>; KOBAYASHI, Akiko<sup>2</sup>  
(<sup>1</sup>Peiking Univ.; <sup>2</sup>Univ. Tokyo)

[*Angew. Chem., Int. Ed.* **117**, 6666–6670 (2005)]

Recently molecular materials with porous coordination frameworks have aroused a considerable interest because of their various attractive properties arising from the synergy of the host lattice and guest molecules such as guest-switched spin crossover transition, gas sorption, molecular storage, and magnetic solvent sensor. However, to our knowledge, the reports on the dielectric properties of porous molecular materials seem to be very rare, though ferroelectric properties of molecular materials have recently attracted an increasing interest. We have recently obtained molecular systems exhibiting unprecedented dielectric properties by combining a porous ferrimagnetic molecular crystal, [Mn(HCOO) $_2$ ] and polar guest molecules, H $_2$ O and CH $_3$ OH. [Mn $_3$ (HCOO) $_6$ ](H $_2$ O)(CH $_3$ OH) showed characteristic temperature-dependent dielectric constant for  $E//a$ ,  $b$  but featureless behavior for  $E//c$ . It is very interesting that molecules confined in the narrow one-dimensional channel show a fairly sharp “transition-like behavior” because in general the system with strong one-dimensional nature hardly exhibits the phase transition.

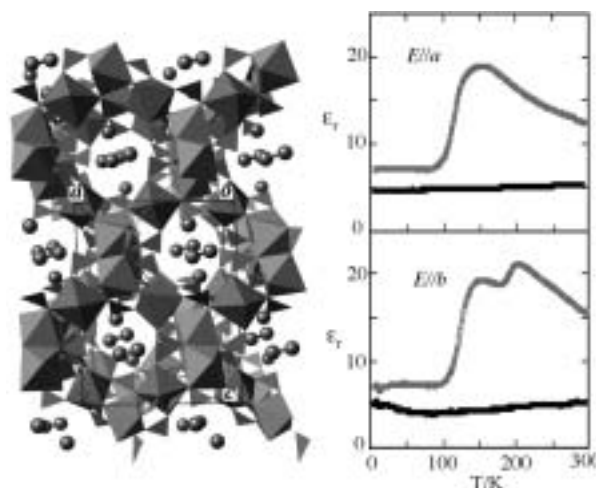


**Figure 1.** Crystal structure and dielectric constants of [Mn $_3$ (HCOO) $_6$ ](H $_2$ O)(CH $_3$ OH). The spheres in the channel are C and O atoms of the guest molecules. The black lines are the dielectric constants of the crystal without guest molecules.

### IV-E-2 Giant Dielectric Constants of Porous Molecular Crystal with Guest Water Cluster

CUI, HengBo; LONG, La-Sheng; TAKAHASHI, Kazuyuki; OKANO, Yoshinori; KOBAYASHI, Hayao; KOBAYASHI, J. Akiko<sup>1</sup>; KOBAYASHI, Akiko<sup>1</sup>  
(<sup>1</sup>Univ. Tokyo)

Except for the ferroelectric (or anti-ferroelectric) materials, the heavy metal compounds such as PbCl $_2$  ( $\epsilon_r = 33.5$  (20 °C)), PbO ( $\epsilon_r = 25.9$  (20 °C)), and TlBr ( $\epsilon_r = 30.3$  (25 °C)) are known to be typical materials with large dielectric constants. It will be desirable to find a way to develop such highly polarizable materials with-

out pernicious heavy metal atoms, especially molecular materials with dielectric properties switchable between high and low dielectric states. Since most molecules have no positional freedom in the crystalline state, the dielectric constants of molecular crystals are usually very small and almost temperature independent. On the other hand, there exist polar molecules with fairly large polarizabilities in the liquid state. Needless to say, the water is the exceptional system with very large dielectric constant, which becomes as high as 100 just above the freezing point (supercooled state). This value is about 40 times larger than that of benzene. We have examined the dielectric properties of water cluster formed in the channel of porous molecular crystal,  $\text{Cu}_3\text{La}_2(\text{NH}(\text{CH}_2\text{COO})_2)_6$  and found the extremely large enhancement of the dielectric constants around room temperature. To our surprise, the dielectric constant seems to exceed 200 at high temperature.

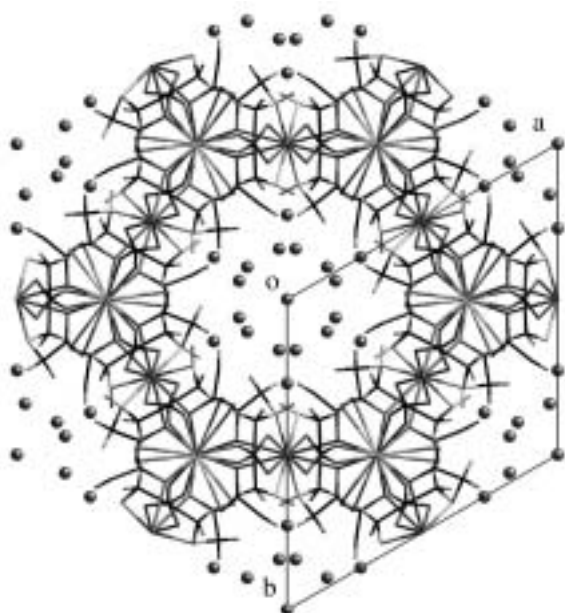


**Figure 1.** Crystal structure of  $\text{Cu}_3\text{La}_2(\text{NH}(\text{CH}_2\text{COO})_2)_6$  viewed along the  $c$  axis of the hexagonal porous crystal. The spheres in the channel are O atoms of water molecules forming one-dimensional water cluster.

#### IV-E-3 Synthesis and Characterization of a Porous Magnetic Diamond Framework Compound, $\text{Co}_3(\text{HCOO})_6$ , and Its $\text{N}_2$ Sorption Characteristic

WANG, Zheming<sup>1</sup>; ZHANG, Bin<sup>2</sup>; KURMOO, Mohamedally<sup>3</sup>; GREEN, Mark, A.<sup>4</sup>; OTSUKA, Takeo; KOBAYASHI, Hayao  
(<sup>1</sup>Peiking Univ.; <sup>2</sup>IC, CAS; <sup>3</sup>Univ. Louis Pasteur; <sup>4</sup>Royal Inst.)

[*Inorg. Chem.* **44**, 1230–1237 (2005)]

$[\text{Co}_3(\text{HCOO})_6](\text{CH}_3\text{OH})(\text{H}_2\text{O})$ , the iso-structural analogue of the porous magnet of coordination framework  $[\text{Mn}_3(\text{HCOO})_6](\text{CH}_3\text{OH})(\text{H}_2\text{O})$ , was prepared by slow diffusion technique and characterized by X-ray and neutron diffraction methods, IR, TGA-DSC and

BET and its magnetic properties measured. It crystallizes in the monoclinic system, space group  $P2_1/c$ ,  $a = 11.247(2)$ ,  $b = 9.812(2)$ ,  $c = 18.103(3)$  Å,  $\beta = 127.245(3)^\circ$ ,  $V = 1590.3(5)$  Å<sup>3</sup>,  $Z = 4$ ,  $R_1 = 0.0356$  (determined from single crystal data at 87 K) and it possesses a unit cell volume that is 10% smaller than  $[\text{Mn}_3(\text{HCOO})_6](\text{CH}_3\text{OH})(\text{H}_2\text{O})$  due to the smaller radius of  $\text{Co}^{2+}$  ion. The cell parameters, obtained from neutron powder data at 2 K, are  $a = 11.309(2)$ ,  $b = 9.869(1)$ ,  $c = 18.201(3)$  Å,  $\beta = 127.244(8)^\circ$ ,  $V = 1617.3(5)$  Å<sup>3</sup>. The pore volume also reduces from 33% to 29% by replacing Mn by Co. The material exhibits an interesting diamond framework based on Co-centered  $\text{CoCo}_4$  tetrahedral nodes, in which all metal ions have octahedral coordination geometry and all HCOO groups link the metal ions in *syn-syn/anti* modes. It displays high thermal stability up to 270 °C. The compound easily loses the guest molecules without loss of crystallinity and it partly re-absorbs water from the atmosphere. Significant  $\text{N}_2$  sorption was observed for the desolvated framework suggesting the material possesses permanent porosity. The magnetic properties show a tendency to a 3D long-range magnetic ordering, probably antiferromagnetic with a spin canting arrangement below 2 K.

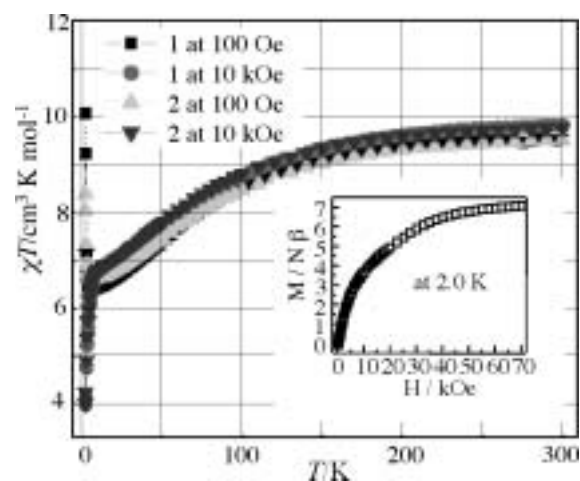


**Figure 1.** The temperature dependence of the magnetic susceptibility of **1** ( $[\text{Co}_3(\text{HCOO})_6](\text{CH}_3\text{OH})(\text{H}_2\text{O})$ ) and desolvated form **2** ( $[\text{Co}_3(\text{HCOO})_6]$ ) in applied field of 100 Oe and 10 kOe. Inset is the isothermal field dependent magnetization at 2.0 K for **1**. Magnetization at 70 kOe is 7.10  $N\beta$ .

#### IV-E-4 Superconductivity and Voltex Phases in the Two-Dimensional Organic Conductor $\lambda$ -(BETS)<sub>2</sub>Fe<sub>x</sub>Ga<sub>1-x</sub>Cl<sub>4</sub> ( $x = 0.45$ )

UJI, Shinya<sup>1</sup>; TERASHIMA, Taichi<sup>1</sup>; YASUZUKA, Shuma<sup>1</sup>; TOKUMOTO, Madoka<sup>2</sup>; TANAKA, Hisashi<sup>2</sup>; KOBAYASHI, Akiko<sup>3</sup>; KOBAYASHI, Hayao  
(<sup>1</sup>Natl. Inst. Mater. Sci.; <sup>2</sup>AIST; <sup>3</sup>Univ. Tokyo)

[*Phys. Rev. B* **71**, 104525 (7 pages) (2005)]

Resistance measurements have been performed in two-dimensional organic conductor  $\lambda$ -(BETS)<sub>2</sub>Fe<sub>x</sub>Ga<sub>1-x</sub>Cl<sub>4</sub> ( $x = 0.45$ ) to investigate the superconducting proper-

ties. In magnetic field parallel to the layers, the superconducting (S) phase is stabilized in a wide magnetic field range, which is qualitatively understood by Jaccarino-Peter compensation mechanism. Depending on the internal field produced by the Fe 3d moments, three vortex phases in the S phase appear with increasing field. The superconducting transitions show characteristic field dependence, which is correlated to the vortex phases. In field perpendicular to the layers, the S phase appear only near the antiferromagnetic phase. The results for  $x = 0.45$  are also compared with those for the isostructural nonmagnetic salt  $x = 0$ .

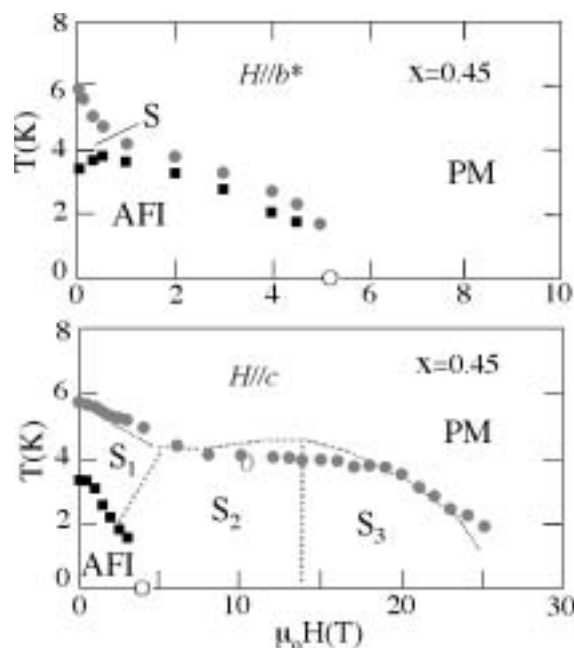


**Figure 1.**  $T$ - $H$  phase diagram of  $\lambda$ -(BETS) $_2$ Fe $_x$ Ga $_{1-x}$ Cl $_4$  ( $x = 0.45$ ) for  $H//b^*$  and  $H//c$ .

#### IV-E-5 Constant Resistivity State in the Field-Induced Organic Superconductor, $\lambda$ -(BETS) $_2$ Fe $_x$ Ga $_{1-x}$ Cl $_4$

CUI, HengBo; TAKAHASHI, Kazuyuki; KOBAYASHI, Hayao; KOBAYASHI, Akiko<sup>1</sup> (<sup>1</sup>Univ. Tokyo)

In 2001, Uji *et al.* have discovered the field-induced superconductivity (FISC) in two-dimensional organic conductor,  $\lambda$ -(BETS) $_2$ FeCl $_4$  with  $\pi$ -d coupled antiferromagnetic insulating ground state below 8.5 K. Balicas *et al.* have found the FISC to be most stabilized around 33 T. Similar FISC states were also observed in a series of mixed-anion systems,  $\lambda$ -(BETS) $_2$ Fe $_x$ Ga $_{1-x}$ Cl $_4$ . We have also reported the unprecedented resistivity switching between insulating, superconducting and metallic states in  $\lambda$ -(BETS) $_2$ Fe $_x$ Ga $_{1-x}$ Cl $_4$  ( $x \approx 0.4$ ). We have recently reexamined the resistivity of  $\lambda$ -(BETS) $_2$ Fe $_x$ Ga $_{1-x}$ Cl $_4$  ( $x \approx 0.4$ ) up to 15 T at the temperature range down to 1 K. The crystal with  $x = 0.37$  exhibited a superconducting transition at 4.6 K and superconductor-insulator transition around 2.3 K at zero magnetic field. But the superconducting state was changed to “the temperature- and field-independent resistivity state”

with increasing magnetic field applied parallel to  $ac$  conduction plane. This constant resistivity state (CRS) was also observed in the crystals with  $x \approx 0.39$ , 0.37 (other crystal) and 0.30. But three crystals with  $x$ -value higher than 0.43 did not show CRS. The ratio of the resistivity of CRS ( $\rho_c$ ) and the resistivity just above the superconducting transition ( $\rho_m$ ), that is,  $\rho_m/\rho_c$  is linearly dependent on  $x$ . To our knowledge,  $\lambda$ -(BETS) $_2$ Fe $_x$ Ga $_{1-x}$ Cl $_4$  ( $x \approx 0.35$ ) is the first superconductor showing CRS.

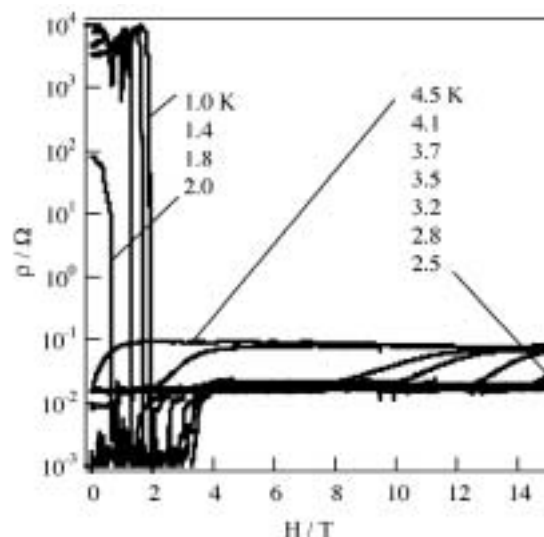


**Figure 1.** Low-temperature resistivity behavior of  $\lambda$ -(BETS) $_2$ Fe $_x$ Ga $_{1-x}$ Cl $_4$  ( $x = 0.37$ ) under the magnetic field applied parallel to the  $ac$  conduction plane.

#### IV-E-6 (Tetrathiafulvalene)[Fe<sup>III</sup>(C<sub>2</sub>O<sub>4</sub>)Cl<sub>2</sub>]: An Organic-Inorganic Hybrid Exhibiting Canted Antiferromagnetism

ZHANG, Bin<sup>1</sup>; WANG, Zheming<sup>2</sup>; FUJIWARA, Hideki; KOBAYASHI, Hayao; KURMOO, Mohamedally<sup>3</sup>; INOUE, Katsuya<sup>4</sup>; MORI, Takehiko<sup>5</sup>; GAO, Song<sup>2</sup>; ZHANG, Yan<sup>2</sup>; ZHU, Daoben<sup>1</sup> (<sup>1</sup>IC CAS; <sup>2</sup>Peiking Univ.; <sup>3</sup>Univ. Louis Pasteur; <sup>4</sup>Hiroshima Univ.; <sup>5</sup>TIT)

[*Adv. Mater.* **17**, 1988–1991 (2005)]

Over the past twenty years, the field of molecular materials has been decorated with a wide range of interesting compounds, based either on purely organic or inorganic molecules and organic-inorganic hybrids, exhibiting diverse electrical, magnetic and optical properties. While several electrical and magnetic ground states have been established and very well documented in the literature, the possibility of introducing novel properties with organic-inorganic hybrids remains a big challenge to date. The key feature of these hybrids is the interaction through space or through weak supra-molecular contacts. While this can be quite strong between nearest neighbours having strong  $\pi$ - $\pi$  overlap, especially those containing chalcogenides, the interactions between  $\pi$ -d are usually quite weak. To enhance the d-d super-exchange within the inorganic moiety, the use of 2D-polymeric anions containing oxalato bridges

has been very successful to produce magnetic systems. On the other hand, it appears that chalcogen-halogen contacts may be a good source for the  $\pi$ -d coupling in compounds containing isolated  $\text{MX}_4$  anions. The present work is an attempt to mixed oxalate and halogen at the metal site of the anions to introduce d-d superexchange and  $\pi$ -d interaction in charge-transfer complex. Recently, two coordination compounds with  $\text{C}_2\text{O}_4^{2-}$  and  $\text{Cl}^-$  have been reported and show ferromagnetic transition at 40 K and 70 K. We, therefore, present the first example of a TTF complex from a novel polymeric one-dimensional counter anion of iron that contains terminal chlorine and oxalate bridges. A new molecular-hybrid  $(\text{TTF})[\text{Fe}^{\text{III}}(\text{C}_2\text{O}_4)\text{Cl}_2]$  displaying canted antiferromagnetism has been prepared and characterized. It is the first salt of TTF or its derivatives to contain a one-dimensional magnetic coordination polymer as anion. Due to  $\pi$ -d interaction, through short  $\text{S}\cdots\text{Cl}$ ,  $\text{S}\cdots\text{O}$  contacts, a 3D-Néel state is stabilized at a rather high temperature of 20 K. It is a semiconductor with band gap of 1 eV.

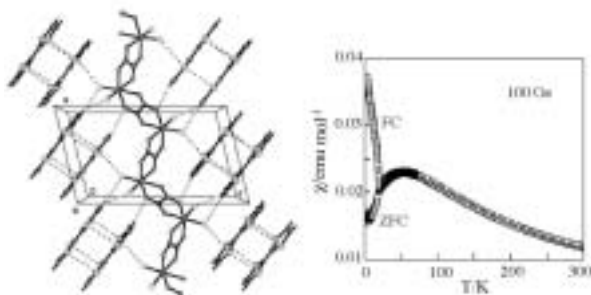


**Figure 1.** Crystal structure and zero-field cooling (ZFC) and field cooling (FC)  $M/H$  versus temperature curves of  $[\text{TTF}][\text{Fe}(\text{C}_2\text{O}_4)\text{Cl}_2]$ .

#### IV-E-7 Development of Single-Component Molecular Metals

**KOBAYASHI, Akiko<sup>1</sup>; ZHOU, Biao<sup>1</sup>;  
KOBAYASHI, Hayao**  
(<sup>1</sup>Univ. Tokyo)

[*J. Mater. Chem.* **15**, 3449–3451 (2005)]

Our recent studies on single-component molecular metals was introduced. The realization of molecular metal based on single-component molecules had been one of the long-standing challenges in the chemistry of molecular conductors since the discovery of semiconducting properties of molecular crystals around 1950. In contrast to typical inorganic metals composed of single elements, such as Na and Au, all of the molecular metals developed until 2000 are composed of more than two chemical species. However, we have proved that the metal electrons can be generated automatically by the self-assembling of the same kind of molecules. The novel nickel complex with the extended-TTF dithiolate ligand  $[\text{Ni}(\text{tmdt})_2]$  (tmdt = trimethylene-tetrathiafulvalenedithiolate) is the first three-dimensional single-component molecular metal with metallic state down to 0.6 K. The isostructural molecular conductor  $[\text{Au}(\text{tmdt})_2]$  exhibited an antiferromagnetic transition

around 110 K without loss of its high conductivity, which is extraordinarily high compared with the magnetic transition temperatures of the other molecular conductors ever developed. A brief description was also presented on “single-component alloy system”  $[\text{Ni}_x\text{Au}_{1-x}(\text{tmdt})_2]$ .

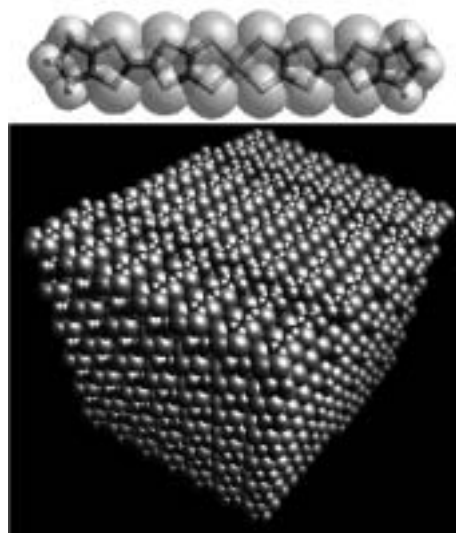


**Figure 1.** The molecular packing in single-component molecular metal  $[\text{Au}(\text{tmdt})_2]$  which is the first molecular system exhibiting the coexistence of  $\pi$  conduction electrons and magnetic order above 100 K.

#### IV-E-8 Crystal Structures and Physical Properties of Single-Component Molecular Conductors Consisting of Nickel and Gold Complexes with Bis(trifluoromethyl)-tetrathiafulvalenedithiolate Ligands

**SASA, Masaaki<sup>1</sup>; FUJIWARA, Emiko<sup>1</sup>;  
KOBAYASHI, Akiko<sup>1</sup>; ISHIBASHI, Shoji<sup>2</sup>;  
TERAKURA, Kiyoyuki<sup>4</sup>; OKANO, Yoshinori;  
FUJIWARA, Hideki; KOBAYASHI, Hayao**  
(<sup>1</sup>Univ Tokyo; <sup>2</sup>AIST; <sup>3</sup>Hokkaido Univ.)

[*J. Mater. Chem.* **15**, 155–163 (2005)]

The neutral nickel and gold complexes with bis-(trifluoromethyl)tetrathiafulvalenedithiolate ligands,  $[\text{M}(\text{hfdt})_2]$  ( $\text{M} = \text{Ni}, \text{Au}$ ) were prepared in order to examine the possibility of the development of single-component molecular conductors soluble to organic solvents. However, in contrast to the previous report, the crystals did not show any solubility to usual organic solvents. On the other hand, the crystal structure analysis showed unique two-dimensional layered structures, despite that the single-component molecular conductors usually tend to take compact three-dimensional molecular arrangement. Each layer is separated by the terminal  $\text{CF}_3$  groups to form the “ $\text{CF}_3$  bi-layer structure.” The shortest intermolecular  $\text{F}\cdots\text{F}$  distance (3.018 Å for  $[\text{Ni}(\text{hfdt})_2]$  and 2.862 Å for  $[\text{Au}(\text{hfdt})_2]$ ) is significantly longer than the van der Waals  $\text{F}\cdots\text{F}$  distance (2.70 Å) and the distribution of the frontier electrons is almost zero around the  $\text{CF}_3$  bi-layer region. This is due to the strong  $\text{F}\cdots\text{F}$  segregation effect, which will provide a

useful way to control the molecular aggregation in the single-component molecular conductors. The extended-Hückel tight-binding band structure calculations and the *ab-initio* local density approximation (LDA) band structure calculations were made for  $[\text{Ni}(\text{hfdt})_2]$ , which can explain the semiconducting and non-magnetic properties of the system. The extended-Hückel tight-binding band structure calculations were also made for  $[\text{Au}(\text{hfdt})_2]$ . The calculated band structure is consistent with weakly semiconducting and almost non-magnetic properties of  $[\text{Au}(\text{hfdt})_2]$ .

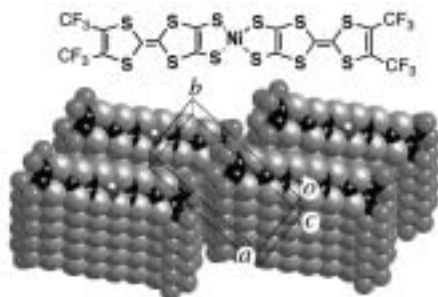


Figure 1. The molecular packing of  $[\text{Ni}(\text{hfdt})_2]$ .

#### IV-E-9 *Ab Initio* Electronic Structure Calculation of Single-Component Molecular Conductor $\text{Au}(\text{tmdt})_2$ (Tmdt = Trimethylenetetrafulvalenedithiolate)

ISHIBASHI, Shoji<sup>1</sup>; TANAKA, Hisashi<sup>1</sup>; TOKUMOTO, Madoka<sup>1</sup>; KOBAYASHI, Akiko<sup>2</sup>; KOBAYASHI, Hayao; TERAURA, Kiyoyuki<sup>3</sup> (<sup>1</sup>AIST.; <sup>2</sup>Univ. Tokyo; <sup>3</sup>Hokkaido Univ.)

[*J. Phys. Soc. Jpn.* **74**, 843–846 (2005)]

We have investigated the electronic structure of  $\text{Au}(\text{tmdt})_2$  (tmdt = trimethylenetetrafulvalenedithiolate), which is a single-component conductor showing a magnetic phase transition around 100 K, by *ab initio* plane-wave pseudopotential calculations. A single band crosses the Fermi level. This band and the next band below are a result of the strongly hybridization between the two neighbouring molecular levels near the Fermi level (SOMO and HOMO-1) and the system is more properly described as quarter-filled rather than half-filled in the strong correlation regime. The Fermi surface has corrugated-sheet-like parts nearly parallel to each other. Interband generalized susceptibility suggests the presence of a nesting vector  $a^*/2$ . Spin-polarized calculation on the doubled unit cell along the  $a$  axis results in an antiferromagnetic order. The nesting is not perfect and Fermi-surface pockets remain in the magnetic phase. The implications of the present calculations with regard to experimental results are discussed.

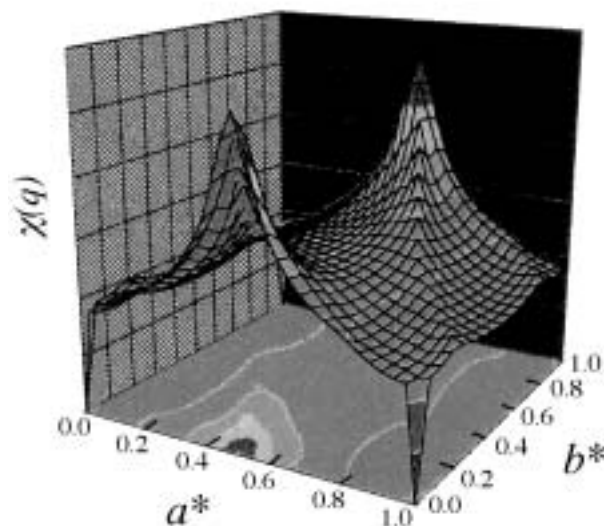


Figure 1. The interband generalized susceptibility of  $[\text{Au}(\text{tmdt})_2]$ .

#### IV-E-10 The Light-Induced Excited Spin State Trapping Effect on $\text{Ni}(\text{dmit})_2$ Salt with an Fe(III) Spin-Crossover Cation: $[\text{Fe}(\text{qsal})_2][\text{Ni}(\text{dmit})_2] \cdot 2\text{CH}_3\text{CN}$

TAKAHASHI, Kazuyuki; CUI, HengBo; KOBAYASHI, Hayao; EINAGA, Yasuaki<sup>1</sup>; SATO, Osamu<sup>2</sup> (<sup>1</sup>Keio Univ.; <sup>2</sup>Kyushu Univ.)

[*Chem. Lett.* **34**, 1240–1241 (2005)]

Recently spin-crossover (SC) complexes have aroused a considerable attention in molecular materials scientists. Since the spin conversion between the low-spin (LS) and high-spin (HS) states can be induced by external perturbations such as temperature, pressure, and light, the introduction of the SC component is expected to give a switching ability to a molecular solid. The number of the reports of the LIESST effect on Fe(III) complexes is very rare. Therefore, realization of the LIESST in an Fe(III) SC component may be the first step to develop various photo-switchable molecular materials. We have focused our attention on the Fe(III) spin crossover complex,  $[\text{Fe}(\text{qsal})_2][\text{Ni}(\text{dmit})_2] \cdot 2\text{CH}_3\text{CN}$  [qsalH = *N*-(8-quinoly)-salicylaldehyde, dmit = 4,5-dithiolato-1,3-dithiole-2-thione]. Temperature dependence of  $\chi_M T$  in  $[\text{Fe}(\text{qsal})_2][\text{Ni}(\text{dmit})_2] \cdot 2\text{CH}_3\text{CN}$  showed a cooperative spin transition (Figure 1a). On illumination with a diode laser (830 nm) at 5 K (Figure 1b), the magnetization of the complex gradually increased, indicating that the light-induced metastable HS state could be trapped. On heating after saturation of magnetization with light illumination, the relaxation from the metastable HS to the ground LS states was observed at around 40 K ( $T_{\text{LIESST}} = 46$  K). The magnetization curve of the annealing sample followed that before illumination. This indicates that the change by light is completely reversible. Furthermore, the decrease in magnetization by illuminating the metastable HS state with a diode laser (980 nm) suggests that the magnetism of the 1:1 complex can be controlled by light irradiation.

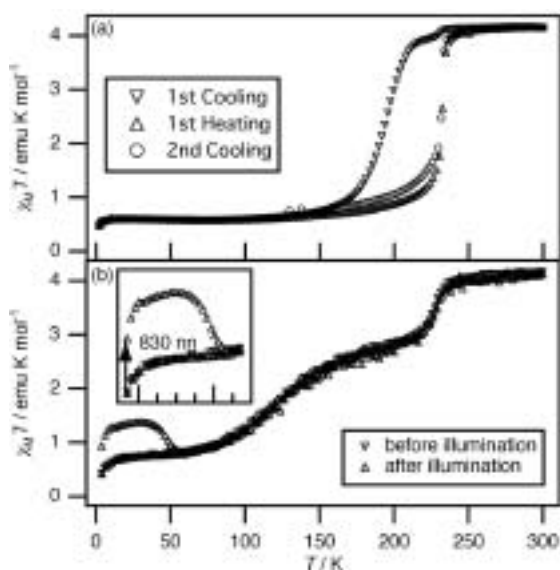


**Figure 1.**  $\chi_M T$  vs.  $T$  plot of  $[\text{Fe}(\text{qsal})_2][\text{Ni}(\text{dmit})_2] \cdot 2\text{CH}_3\text{CN}$ : (a) Bulk sample, (b) the LIESST experiment of ground sample with an adhesive tape by using a diode laser (830 nm).

#### IV-E-11 Synergic Behavior between Spin and Conducting Property in $\text{Ni}(\text{dmit})_2$ Salt with $\text{Fe}(\text{III})$ Spin-Crossover Cation

TAKAHASHI, Kazuyuki; CUI, HengBo; OKANO, Yoshinori; KOBAYASHI, Hayao; EINAGA, Yasuaki<sup>1</sup>; SATO, Osamu<sup>2</sup>  
(<sup>1</sup>Keio Univ.; <sup>2</sup>Kyushu Univ.)

Recently considerable interest has been attracted to the development of novel molecular-based conducting materials exhibiting the synergy between conductivity and magnetism. We have attempted to explore the possibility of “dynamic” and “reversible” control of electrical conducting state by external stimuli. It is well known that the conducting properties of molecular conductors are changed greatly by the small modification of their crystal structures. Since the spin transition between the low-spin (LS) and the high-spin (HS) states accompanies a remarkable structural change in coordination bond length and geometry, the electrical conductivity of conducting spin-crossover (SC) complex can be expected to be “dynamically” and “reversibly” controlled by a structural change involving the spin conversion. The conducting complex was prepared by electrocrystallization of  $[\text{Fe}(\text{qsal})_2][\text{Ni}(\text{dmit})_2] \cdot 2\text{CH}_3\text{CN}$  in acetonitrile. The crystal structure analyses revealed that the ratio of  $\text{Fe}(\text{qsal})_2$  and  $\text{Ni}(\text{dmit})_2$  proved to be 1 to 3.  $\text{Ni}(\text{dmit})_2$  anions formed one-dimensional columns along the  $b$  axis and were arranged in a herringbone manner along the side-by-side direction. Temperature dependence of magnetic moment and electrical resistivity of the 1:3 complex were shown in Figure 1. As a result of the cooling and heating processes, the magnetic behavior showed a narrow hysteresis loop with width of 8 K between 90 and 120 K. The change in  $\chi_M T$  value, which was larger than that estimated for the antiferromagnetic coupling of spins of  $\text{Ni}(\text{dmit})_2$ , seemed to derive from the spin transition. The crystal showed a semiconducting behavior ( $\sigma_{\text{RT}} = 0.1 \text{ S cm}^{-1}$ ;  $E_a = 0.2$

eV). Interestingly, a hysteresis loop of resistivity was observed in the temperature range of 90–120 K, which corresponds to the temperature range of the hysteresis of magnetic behavior. The relatively low resistivity in heating process is consistent with the compact molecular packing usually observed in the LS state. To our knowledge, this is the first observation of the resistivity anomaly coupled with spin transition.

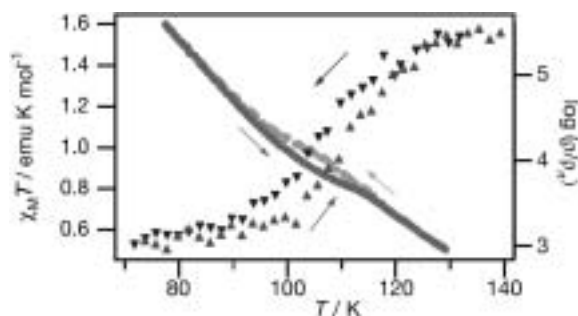


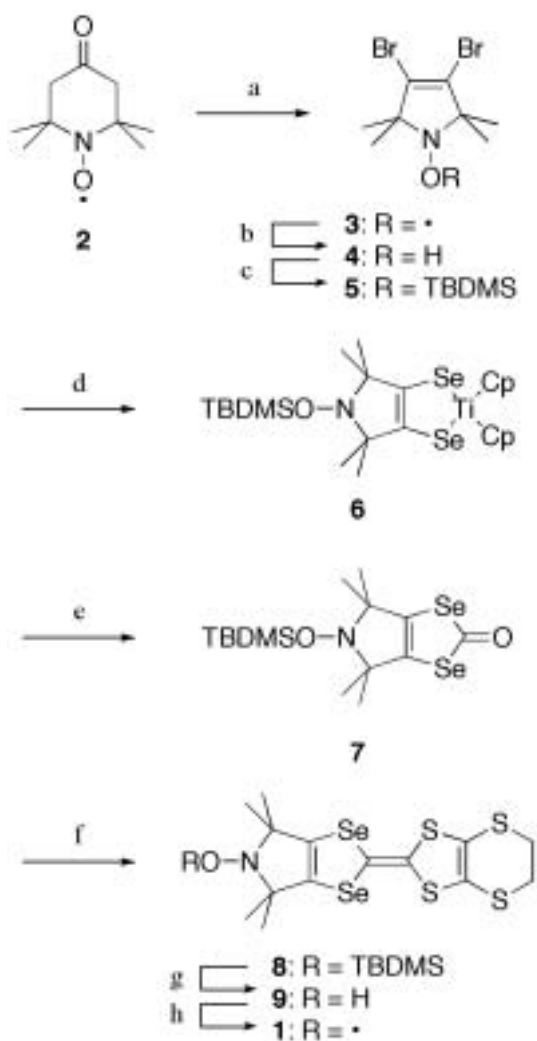
**Figure 1.**  $\chi_M T$  vs.  $T$  plot (triangle, scale: left) and  $\log(\rho/\rho_{\text{RT}})$  vs.  $T$  plot (circle, scale: right) of the 1:3 complex at the temperature range between 70 and 140 K.

#### IV-E-12 Synthesis and Molecular Structure of a Novel PROXYL-Fused $\pi$ -Electron Donor, PROXYL-ET-STF

TAKAHASHI, Kazuyuki; KOBAYASHI, Hayao

The development of novel magneto-electronic properties based on the interplay between conducting electrons and localized spins has aroused a great attention in molecular materials. To realize the coupling between conducting  $\pi$ -electrons and the spins on the stable organic radical in purely organic systems is one of the targets in this field. Despite several reports of syntheses and physical properties of  $\pi$ -electron donor or acceptor molecules with stable organic radicals and their conducting complexes, the number of metallic complexes based on these donors is rare. Probably since the organic stable radicals are usually bulky, it is difficult to construct the conduction path based on the overlap of  $\pi$ -donor parts. In order to decrease a hindrance to the formation of conduction path, we have designed and synthesized PROXYL-fused  $\pi$ -electron donor, PROXYL-ET-STF.

Synthesis of PROXYL-ET-STF is summarized in Scheme 1. The donor was isolated as fine needles and stable in air. X-ray structural analysis was performed on a single crystal of the neutral donor molecule. The molecular structure of PROXYL-ET-STF was a little bent, but the radical part was almost parallel to the 1,3-diselenol ring. Donor molecules were stacked in a head-to-tail manner to form one-dimensional columns. These observations suggest that PROXYL-ET-STF is a promising donor to afford conducting complexes with a stable organic radical. Physicochemical properties and preparation of the conducting complexes of this donor are now in progress.



**Scheme 1.** Synthesis of PROXYL-ET.

(a) NaOBr; (b) Diphenylhydrazine; (c) TBDMSOTf; (d) *t*-BuLi, Se, Cp<sub>2</sub>TiCl<sub>2</sub>, THF; (e) triphosgene, THF; (f) 4,5-ethylenedithio-1,3-dithol-2-thione, P(OMe)<sub>3</sub>, toluene; (g) TBAoF, THF; (h) Ag<sub>2</sub>O, THF.

## IV-F Electronic and Magnetic Properties of $\pi$ -Electron-Based Molecular Systems

$\pi$ -electrons are an interesting building block in architecting functionalized electronic and magnetic molecular systems. We have focused on nano-sized graphite and TTF-based organic charge transfer complexes, in which  $\pi$ -electrons play an important role, in developing new types of molecular electronic systems. In nanographene, single layer nanographite, which is defined as flat open  $\pi$ -electron system have edges and contrasted to closed  $\pi$ -electron systems of fullerenes and carbon nanotubes, non-bonding  $\pi$ -electronic state appearing around the Fermi level generates unconventional nanomagnetism. We have found an interesting electronic wave interference effect in finite-sized graphite with distortion-network structures and anisotropy of the Raman spectra of nanographite ribbons. A combination of TTF-based  $\pi$ -electron donor and counteranion having localized spins is a useful way in producing molecular magnetic conductors, which are expected to have properties different from traditional metal magnets featured with s-d interaction. Under this scheme, we have developed a new class of TTF-based organic magnetic conductors. The interaction between the conducting  $\pi$ -electrons of donors and the localized d-electrons of magnetic anions are found to show interesting interplay between magnetism and electron transport.

### IV-F-1 Metal-Insulator Transition in Iodinated Amorphous Conducting Carbon Films

KUMARU, Latha<sup>1</sup>; SUBRAMANYAM, S. V.<sup>1</sup>; ETO, Soichiro<sup>2</sup>; TAKAI, Kazuyuki<sup>2</sup>; ENOKI, Toshiaki  
(<sup>1</sup>Indian Inst. Sci.; <sup>2</sup>Tokyo Inst. Tech.)

[*Carbon* **42**, 2133–2137 (2004)]

In this work, the effect of iodine incorporation on the electrical conductivity, magnetic susceptibility ( $\chi$ ) and magnetoresistance (MR) of amorphous conducting carbon (a-C) films has been discussed. Variation in conductivity of a-C films depends on the sample preparation conditions and iodine concentration. Evidence of metal–insulator (M–I) transition as a function of pyrolysis temperature is observed for iodinated (a-C:I) samples. The temperature dependent magnetic susceptibility of a-C:I sample shows a Curie behavior at low temperatures. The positive magnetoresistance is observed for all the samples irrespective of the conduction regimes. This is accounted by the electron–electron interaction in the a-C:I system.

### IV-F-2 Magnetic Resonance Study of Nanodiamonds

SHAMES, Alexander I.<sup>1</sup>; PANICH, A. M.<sup>1</sup>; KEMPIŃSKI, W.<sup>2</sup>; BAIDAKOVA, M. V.<sup>3,4</sup>; OSIPOV, V. Yu.<sup>3</sup>; ENOKI, Toshiaki; VUL', A. Ya.<sup>3</sup>  
(<sup>1</sup>Ben-Guiron Univ. Negev.; <sup>2</sup>Polish Acad. Sci.; <sup>3</sup>Ioffe Phys.-Tech. Sci.; <sup>4</sup>Tokyo Inst. Tech.)

[NATO Science Sries, D. M. Gruen, O. A. Shenderova, A. Ya. Vul', Eds., Springer; Dordrecht/Boston/London, pp.271 (2005)]

Magnetic resonance techniques, namely Electron Paramagnetic Resonance (EPR) and solid state Nuclear Magnetic Resonance (NMR), are powerful non-destructive tools for studying electron-nuclear and crystalline structure, inherent electronic and magnetic properties and transitions in carbon-based nanomaterials. EPR allows to control purity of ultradispersed diamond (UDO) samples, to study the origin, location and spin-

lattice relaxation of radical-type carbon-inherited paramagnetic centers (RPC) as well as their transformation during the process of temperature driven diamond-to-graphite conversion. Solid state NMR on <sup>1</sup>H and <sup>13</sup>C nuclei provide one with information on the crystalline quality, allows quantitative estimation of the numbers of different allotropic forms, and reveals electron-nuclear interactions within the UDO samples under study. Results of recent EPR and <sup>13</sup>C NMR study of pure and transition metal doped UDD samples, obtained by detonation technique, are reported and discussed. In addition to characteristic EPR signals, originated from para- and ferromagnetic impurities and doping ions, the UDD samples show a high concentration of RPC (up to 10<sup>20</sup> spin/gram), which are due to structural defects (dangling C–C bonds) on the diamond cluster surface. *In-situ* EPR sample's vacuumization experiment in conjunction with precise SQUID magnetization measurements allowed concluding that each UDD particle carries a single spin (dangling bond) per each from 8 crystal (111) facets bounded the particle.

### IV-F-3 $d$ -Electron-Induced Negative Magnetoresistance of $\pi$ - $d$ Interaction System Including Brominated-TTF Donor

NISHIJO, Junichi<sup>1</sup>; MIYAZAKI, Akira<sup>1</sup>; ENOKI, Toshiaki; WATANABE, Ryoji<sup>2</sup>; KUWATANI, Yoshiyuki<sup>3</sup>; IYODA, Masahiko<sup>3</sup>  
(<sup>1</sup>Indian Inst. Sci.; <sup>2</sup>Tokyo Inst. Tech.; <sup>3</sup>Tokyo Metropolitan Univ.)

[*Inorg. Chem.* **44**, 2493–2506 (2005)]

A new  $\pi$ - $d$  interaction system (EDT-TTFBr<sub>2</sub>)<sub>2</sub>FeBr<sub>4</sub> (EDT-TTFBr<sub>2</sub> = 4,5-dibromo-4',5'-ethylenedithio-tetrathiafulvalene) and its nonmagnetic anion analogue (EDT-TTFBr<sub>2</sub>)<sub>2</sub>GaBr<sub>4</sub> based on a brominated TTF-type organic donor are investigated. The salts featured by quasi-1D  $\pi$ -electronic systems are metallic with metal-insulator transitions taking place at about 20 and 70 K for the FeBr<sub>4</sub><sup>-</sup> and GaBr<sub>4</sub><sup>-</sup> salts, respectively, where the low-temperature insulating state is associated with charge ordering or a Mott insulator followed by an anti-ferromagnetic transition at lower temperatures. The

$\text{FeBr}_4^-$  salt is featured with an antiferromagnetic transition of the anion d spins at a Néel temperature ( $T_N$ ) = 11 K, which is significantly high despite its long anion-anion Br-Br contact, suggesting the importance of the  $\pi$ -d interaction in the magnetism. The surprisingly strong  $\pi$ -d interaction, *ca.* -22.3 K estimated from the magnetization curve, evidences the usefulness of the chemical modification of the donor molecule with bromine substitution to achieve strong intermolecular interaction. The antiferromagnetic state of the anion d spins affects the transport of the conducting  $\pi$  electrons through the strong  $\pi$ -d interaction, as evidenced by the presence of a resistivity anomaly of the  $\text{FeBr}_4^-$  salt at  $T_N$ . Below  $T_N$ , the  $\text{FeBr}_4^-$  salt shows negative magnetoresistance that reaches -23% at the highest magnetic field investigated ( $B = 15$  T), whereas only a small positive magnetoresistance is observed in the  $\pi$ -electron-only  $\text{GaBr}_4^-$  salt. The mechanism of the negative magnetoresistance is explained by the stabilization of the insulating state of the  $\pi$  electrons by the periodic magnetic potential of the anion d spins in the  $\text{FeBr}_4^-$  salt, which is modified by applying the external magnetic field.

#### IV-F-4 Electronic and Magnetic Properties of $\pi$ -d Interaction System $(\text{EDTDM})_2\text{FeBr}_4$

OKABE, K.<sup>1</sup>; YAMAURA, J. -I.<sup>2</sup>; MIYAZAKI, Akira<sup>1</sup>; ENOKI, Toshiaki  
(<sup>1</sup>Tokyo Inst. Tech.; <sup>2</sup>Univ. Tokyo)

[*J. Phys. Soc. Jpn.* **74**, 1508–1520 (2005)]

The crystal structure and electronic and magnetic properties of magnetic molecular conductor  $(\text{EDTDM})_2\text{FeBr}_4$  are investigated. The material undergoes a SDW transition at  $T_{\text{MI}} \sim 11$  K and an antiferromagnetic transition of  $\text{Fe}^{3+}$  d-spins at  $T_N = 3$  K. In addition to the appearance of an anomaly in the resistivity around  $T_N$ , a large magnetoresistance is observed below  $T_N$ , which diverges at the critical pressure ( $P_c \sim 9.2$  kbar) of the MI transition. The perturbation potential from the antiferromagnetic  $\text{Fe}^{3+}$  spin arrangement stabilizes the SDW state, leading to the anomaly in the resistivity. The application of magnetic field reduces the potential of the  $\text{Fe}^{3+}$  spins, which leads to the large negative magnetoresistance. This indicates that the  $\pi$ -d interaction plays an important role in the interplay between the magnetism and the electron transport.

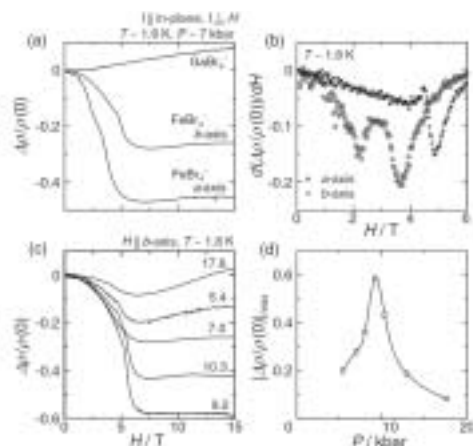


**Figure 1.** The field dependence of the magnetoresistance at  $T \sim 1.9$  K for  $(\text{EDTDM})_2\text{MBr}_4$  ( $M = \text{Fe}, \text{Ga}$ ) under the pressure of 7.0 kbar. (b) The field dependence of the magnetoresistance at  $T \sim 1.8$  K for  $(\text{EDTDM})_2\text{FeBr}_4$  under pressures of 5.4, 7.0, 9.2, 10.3 and 17.6 kbar. (c) The numerical derivatives of the intra-layer magnetoresistance of  $(\text{EDTDM})_2\text{FeBr}_4$  at  $P \sim 7.0$  kbar as a function of applied field. (d) The pressure dependence of the maximum of the absolute value of the negative magnetoresistance of  $(\text{EDTDM})_2\text{FeBr}_4$ .

#### IV-F-5 Observation of Zigzag- and Armchair-Edges of Graphite

KOBAYASHI, Yousuke<sup>1</sup>; KUSAKABE, Koichi<sup>2</sup>; FUKUI, Ken-ichi<sup>1</sup>; ENOKI, Toshiaki; KABURAGI, Yutaka<sup>3</sup>  
(<sup>1</sup>Tokyo Inst. Tech.; <sup>2</sup>Osaka Univ.; <sup>3</sup>Musashi Inst. Tech.)

[*Phys. Rev. B* **71**, 193406 (4 pages) (2005)]

The presence of structure-dependent edge states of graphite is revealed by both ambient and ultra high vacuum (UHV) scanning tunneling microscopy and scanning tunneling spectroscopy observations. On a hydrogenated zigzag (armchair) edge, bright spots are (are not) observed together with a  $(\sqrt{3} \times \sqrt{3}) R30^\circ$  superlattice near the Fermi level ( $V_S \sim -30$  mV for a peak of the local density of states) under UHV (Figure 1), demonstrating that a zigzag edge is responsible for the edge states, although there is no appreciable difference between as-prepared zigzag and armchair edges in air. Even in the hydrogenated armchair edge, however, bright spots are observed at defect points, at which partial zigzag edges are created in the armchair edge.

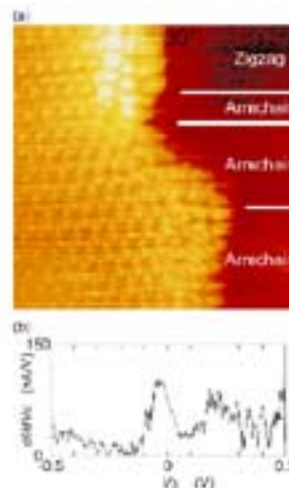


**Figure 1.** (Color) (a) An atomically resolved UHV STM image of zigzag and armchair edges ( $9 \times 9$  nm<sup>2</sup>). (b) Typical  $dI/dV_S$  curve from STS data at a zigzag edge.

## IV-G Progress of Conjugated Phenomena Coupled with Spin and Photon for Assembled Hetero-Molecular System

Intercalation of photochromic molecule into magnetic system provides fascinating multi-functionalities such as photo-magnetism, which gains much attention for their application to devices. The main subjects in this project are the development of photo-induced spin-crossover phenomena at room temperature by using the photo-isomerization of intercalated molecule, and the development of the transformation of magnetism for two-dimensional ferromagnetic system coupled with photochromic molecule.

### IV-G-1 Reversible Photomagnetism in a Cobalt Layered Compound Coupled with Photo-Chromic Diarylethene

OKUBO, Masashi<sup>1</sup>; ENOMOTO, Masaya<sup>1</sup>; KOJIMA, Norimichi<sup>2</sup>

(<sup>1</sup>Univ. Tokyo; <sup>2</sup>IMS and Univ. Tokyo)

[*Solid State Commun.* **135**, 777 (2005)]

Photomagnetism is one of the most attractive topics in recent research on molecular solids. In order to produce a photo-controllable magnet, we have synthesized a novel organic-inorganic hybrid system coupled with a photochromic diarylethene anion, 2,2'-dimethyl-3,3'-(perfluorocyclopentene-1,2-diyl)bis(benzo [b]thiophene-6-sulfonate) (**1a**) and cobalt LDHs (layered double hydroxides). The anion exchange reaction between the diarylethene anion, **1a**, and the layered double hydroxide,  $\text{Co}_2(\text{OH})_3(\text{CH}_3\text{COO})\cdot\text{H}_2\text{O}$  (**2**), takes place successfully (Figure 1), which was elucidated by powder X-ray diffraction analysis and IR spectra. Based on the elemental analysis, the title compound synthesized by the anion exchange reaction between **2** and **1a** has the chemical composition,  $\text{Co}_4(\text{OH})_7(\mathbf{1a})_{0.5}\cdot\text{H}_2\text{O}$  (**3**). Powder X-ray diffraction analysis revealed the interlayer distance of  $c = 27.8 \text{ \AA}$ . The magnetic susceptibility measurements elucidated the ferromagnetic intra- and inter-layer interactions and the Curie temperature of  $T_C = 9 \text{ K}$ .

In order to investigate the photo-irradiation effect on the magnetism, we carried out light irradiation on **3** spread thin on a glass plate in the dark at room temperature. After the irradiation, we measured the temperature dependence of the AC and DC susceptibilities and the hysteresis loop at 2 K. Although there is no light irradiation effect on the Curie temperature, the hysteresis loop shows a photomagnetic effect. The coercive field as well as the remnant magnetization decreases from 940 Gauss to 550 Gauss after light irradiation of 313 nm. The initial hard magnet is switched to a soft magnet by light irradiation of 313 nm. In addition, the soft magnet is almost reversibly returned to the initial hard magnet by the light irradiation of 550 nm. As plotted in Figure 2, both the coercive field and the remnant magnetization change almost reversibly by light irradiation of 313 nm and 550 nm. By UV irradiation of 313 nm, **3** shows the photo-isomerization of diarylethene anion from the open form to the closed one in solid state, which leads to the decreases in the coercive field and the remnant magnetization. Furthermore, the photo-excited state is returned to the initial state (open form) almost reversibly by

visible-light irradiation of 550 nm. In this manner, we have succeeded in controlling the magnetic properties reversibly by two kinds of photo-irradiation for the organic-inorganic hybrid system, **3**.<sup>1)</sup>

#### Reference

1) M. Okubo, M. Enomoto and N. Kojima, *Solid State Commun.* **134**, 777–782 (2005).



**Figure 1.** Schematic representation of the anion exchange reaction and the structure of **3**.

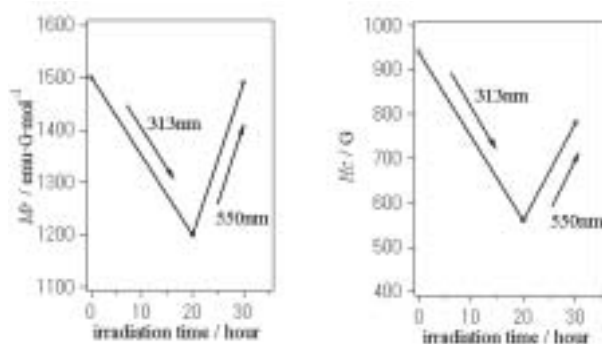


**Figure 2.** Photo-irradiation effects on the coercive field ( $H_c$ ) and the remnant magnetization ( $M_r$ ) of **3** at 2 K.

## IV-H Molecular Crystals toward Nano-Devices by Use of d- $\pi$ Interaction, Crystal Designing and Optical Doping

After some 30 years' intensive research on molecular charge transfer (CT) salts as potential functional materials, the research field has now gotten ready to examine how to make them into actual devices. Such efforts are concentrated on the developments of organic thin films for field effect transistors and light-emitting devices, both of which are carried out in a number of laboratories and groups with worldwide competitions. In order to examine the potential applicability of molecular materials from a different point of view, we are carrying out basic studies on development and physical properties of molecular CT single crystals. Major part of our study can be classified into three categories; the physical properties of the CT salts including localized spins, crystal designing using polycarboxylate anions, and device formation by optical doping method.

### IV-H-1 Light-Induced Transformation of Molecular Materials into Devices

NAITO, Toshio; INABE, Tamotsu<sup>1</sup>; NIIMI, Hironobu<sup>1</sup>; ASAKURA, Kiyotaka<sup>1</sup>  
(<sup>1</sup>Hokkaido Univ.)

[*Adv. Mater.* **16**, 1786–1790 (2004)]

Many kinds of molecular solids are now attracting a worldwide interest as promising candidates for advanced materials such as electronic/magnetic/optical devices and energy converters. In particular, semiconductor diodes based on photovoltaic effect appear one of the most effective ways to utilize molecular materials, if there is an appropriate doping method available. This work concerns a finding of a novel method of (persistent) carrier doping to molecular materials. The method is simple and versatile; just illuminating the desired part of material as long as it contains a photosensitive chemical species in addition to an electroactive one. Although various kinds of photo-excited states reported thus far have typical lifetimes of some hundreds of micro-seconds at longest in general, the doped state survived even several months after the illumination was finished. The experimental results demonstrate that one can control the conducting properties of an arbitrary part of a molecular material using appropriately focussed illumination. In other words, this method opens a new way for making devices and conducting nano-architectures from a wide variety of molecular solids, which have awaited for a space-resolved doping method under a mild condition.

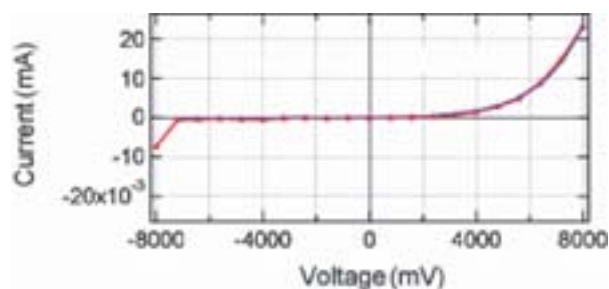


**Figure 1.** Current-Voltage property curve of the single crystal of Ag(DM)<sub>2</sub> after UV-VIS illumination upon only half of it for ~21 days.

### IV-H-2 Molecular Conductors Containing Photoreactive Species

NAITO, Toshio; INABE, Tamotsu<sup>1</sup>  
(<sup>1</sup>Hokkaido Univ.)

[*J. Phys. IV France* **114**, 553–555 (2004)]

In order to examine the possibility of (persistent) carrier doping to molecular crystals by light exposure, some different types of molecular crystals containing photoreactive species are synthesized and characterized. The [Ru(bpy)<sub>3</sub>]<sup>2+</sup> cation (bpy = 2,2'-bipyridyl) yielded two different new complexes with [Ni(dmit)<sub>2</sub>]<sup>-</sup> radical species, both of which were structurally characterized and turned out to be band insulators. Methy viologen (MV) has been found to yield a new phase of the complex with [Ni(dmit)<sub>2</sub>]<sup>-</sup>, MV[Ni(dmit)<sub>2</sub>]<sub>2</sub>. The temperature dependences of electrical resistivity (decreasing with lowering temperature down to 1.0 K) and magnetic susceptibility (Pauli paramagnetism from 300 K to 1.8 K with a hysteresis below ~100 K) clearly indicate that this phase is metallic. The thermoelectric power exhibited ~0  $\mu$ VK<sup>-1</sup> from 300 K–4.2 K. This phase turned out to be metastable, and the crystals gradually turned into insulating ones. The effects of UV-VIS light exposure to the conducting and magnetic properties of Ag(DMeDCNQI)<sub>2</sub> have been studied, and clear differences between the exposed and the pristine crystals were observed. The ESR signal at 3.7 K suggested that the exposed sample should include the Ag(0) species.

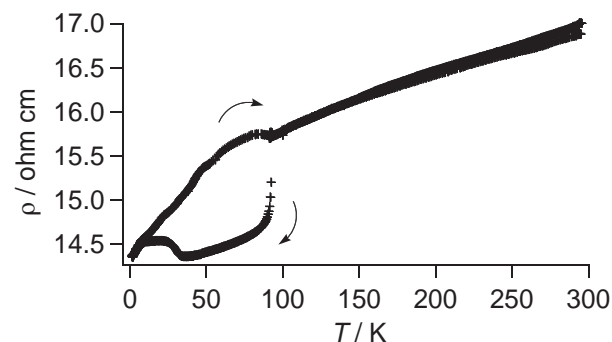


**Figure 1.** Temperature-dependent electrical resistivity of MV[Ni(dmit)<sub>2</sub>]<sub>2</sub>.

### IV-H-3 A New Optical Doping Method toward Molecular Electronics

NAITO, Toshio; INABE, Tamotsu<sup>1</sup>; NIIMI, Hironobu<sup>1</sup>; ASAKURA, Kiyotaka<sup>1</sup>  
(<sup>1</sup>Hokkaido Univ.)

[*Synth. Met.* **152**, 289–292 (2005)]

This work concerns a finding of a novel method of (persistent) carrier doping to molecular materials. The method is simple and versatile; just illuminating the material as long as it contains a photosensitive chemical species in addition to an electroactive one. Although various kinds of photo-excited states reported thus far have typical lifetimes of some hundreds of microseconds at longest in general, the doped state survived even a week after the illumination was finished. The experimental results demonstrate that one can control the conducting properties of an arbitrary part of a molecular material using appropriately focussed illumination. In other words, this method opens a new way for making devices and conducting nano-architectures from a wide variety of molecular solids, which have awaited for a space-resolved doping method.

### IV-H-4 Photochemical Method of Device Fabrication Starting from Molecular Crystals

NAITO, Toshio; SUGAWARA, Hideyuki<sup>1</sup>; INABE, Tamotsu<sup>1</sup>; MIYAMOTO, Takeshi<sup>1</sup>; NIIMI, Hironobu<sup>1</sup>; ASAKURA, Kiyotaka<sup>1</sup>  
(<sup>1</sup>Hokkaido Univ.)

[*Mol. Cryst. Liq. Cryst.* submitted]

The conductivity of a silver salt of *N,N'*-dicyanoquinonediimine irreversibly varied in approximate proportion to an illumination of a wide range of wavelengths. Depending on the illumination conditions, four different states ( $\beta$ ,  $\gamma$ ,  $\delta$ , and  $\epsilon$ ) were obtained with different structures. The  $\beta$  structure is in particular important, where the formal charge of the *N,N'*-dicyanoquinonediimine molecules continuously decreased to  $-0.4$ – $-0.35$  with retaining the crystal structure, when we kept the temperature  $< 155$  °C during the illumination. The non-illuminated area of the sample retained its original electrical property with a well-defined interface, which enabled a fabrication of a junction-structure in the single crystal.

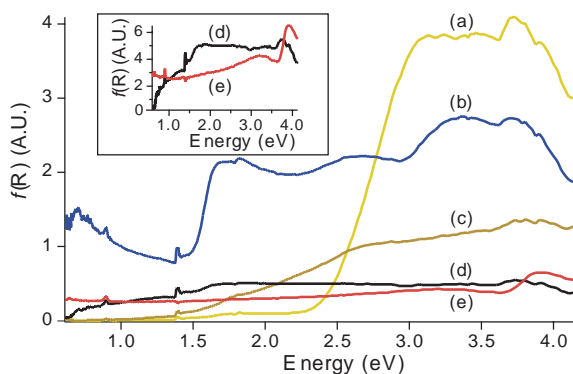


**Figure 1.** Diffuse scattering spectra of (a) isolated neutral DM species, (b)  $\alpha$ -, (c)  $\gamma$ -, (d)  $\delta$ -, and (e)  $\epsilon$ -Ag(DM)<sub>2</sub>, respectively. The inset shows (d) and (e) spectra with  $f(R)$  enlarged by 10 times.

### IV-H-5 Photochemical Control of Dark Conductivity—A New Approach to Devices Based on Molecular Crystals

NAITO, Toshio; SUGAWARA, Hideyuki<sup>1</sup>; INABE, Tamotsu<sup>1</sup>; KITAJIMA, Yoshinori<sup>2</sup>; MIYAMOTO, Takeshi<sup>1</sup>; NIIMI, Hironobu<sup>1</sup>; ASAKURA, Kiyotaka<sup>1</sup>  
(<sup>1</sup>Hokkaido Univ.; <sup>2</sup>KEK)

[*J. Low Temp. Phys.* submitted]

Thermal analysis of Ag(DM)<sub>2</sub>, where DM = 2,5-dimethyl-*N,N'*-dicyanoquinonediimine, clarified that the salt had an insulating amorphous phase ( $\geq 155$  °C). Characterization of this and related solid states of Ag(DM)<sub>2</sub> indicated that a photo-induced process should be essential in controlling the number of carriers and thus conduction behavior of the salt by illumination. In fact, while heating could do nothing but make the salt insulating when the sample temperature exceeded 155 °C, ultraviolet-visible light illumination ( $< 155$  °C) could gradually change the properties to be semi-conducting with retaining the crystal lattice (average structure).

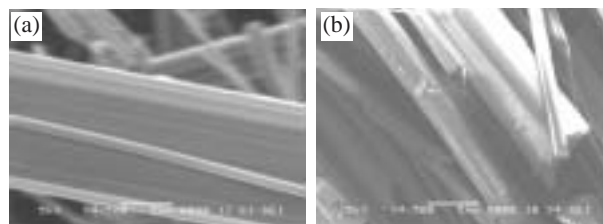


**Figure 1.** Scanning Electron Microprobe (SEM) photographs of different states after UV-Vis illumination on single crystals of Ag(DM)<sub>2</sub>; (a)  $\beta$ -, and (b)  $\gamma$ -states, respectively. The SEM photographs of the pristine ( $\alpha$ -) samples (not shown here) much resemble those of the  $\beta$ -state.

### IV-H-6 Molecular Unit Based on Metal Phthalocyanine; Designed for Molecular Electronics

MATSUDA, Masaki<sup>1</sup>; HANASAKI, Noriaki<sup>1</sup>; IKEDA, Shingo<sup>1</sup>; TAJIMA, Hiroyuki<sup>1</sup>; NAITO, Toshio; INABE, Tamotsu<sup>2</sup>  
(<sup>1</sup>Univ. Tokyo; <sup>2</sup>Hokkaido Univ.)

[*J. Phys. IV France* **114**, 541–543 (2004)]

We obtained three conducting crystals based on a [Fe<sup>III</sup>(Pc)(CN)<sub>2</sub>] molecular unit. All crystals showed a large anisotropic negative magnetoresistance arising from the  $\pi$ -d interaction self-contained in the [Fe<sup>III</sup>(Pc)(CN)<sub>2</sub>] unit. The anisotropy is attributable to the anisotropic *g*-tensor in the [Fe<sup>III</sup>(Pc)(CN)<sub>2</sub>] unit. We also obtained a thin film containing [Fe<sup>II</sup>(Pc)(CN)<sub>2</sub>]. The film exhibits photocurrent response for the UV irradiation. These features suggest [M(Pc)(CN)<sub>2</sub>] molecular

unit is a well-designed one for a building block of molecular devices.

#### IV-H-7 Anisotropic Giant Magnetoresistance Originating from the $\pi$ -d Interaction in a Molecule

MATSUDA, Masaki<sup>1</sup>; HANASAKI, Noriaki<sup>1</sup>;  
TAJIMA, Hiroyuki<sup>1</sup>; NAITO, Toshio; INABE,  
Tamotsu<sup>2</sup>

(<sup>1</sup>Univ. Tokyo; <sup>2</sup>Hokkaido Univ.)

[*J. Phys. Chem. Solids* **65**, 749–752 (2004)]

We synthesized  $\text{TPP}[\text{Fe}^{\text{III}}(\text{Pc})(\text{CN})_2]_2$ ,  $\text{PTMA}_x[\text{Fe}^{\text{III}}(\text{Pc})(\text{CN})_2]_y(\text{MeCN})$ , and  $\text{PXX}[\text{Fe}^{\text{III}}(\text{Pc})(\text{CN})_2]$ , a new series of charge-transfer salts containing the axially-substituted phthalocyanine (Pc),  $[\text{Fe}^{\text{III}}(\text{Pc})(\text{CN})_2]^-$ . In this molecular unit, the  $\pi$  conduction electron derived from the Pc-ring coexists with the d electron which is a potential source of a local magnetic moment. Therefore various phenomena associated with the interplay between local magnetic moments and conduction electrons are expected. We observed the giant negative magnetoresistance (GNMR) in all the three salts. The GNMR is highly anisotropic for the magnetic-field direction, and reflects the  $g$ -tensor anisotropy of the local magnetic moment in the  $[\text{Fe}^{\text{III}}(\text{Pc})(\text{CN})_2]^-$  unit. This indicates that the GNMR in these salts originates from the strong  $\pi$ -d interaction in the  $[\text{Fe}^{\text{III}}(\text{Pc})(\text{CN})_2]^-$  unit.

#### IV-H-8 Phthalocyanine-Pphthalocyanine Salt Crystal: A Unique Assembly Design

OHTSUKA, Yoshikazu<sup>1</sup>; NAITO, Toshio; INABE,  
Tamotsu<sup>1</sup>

(<sup>1</sup>Hokkaido Univ.)

[*J. Porphyrins Phthalocyanines* **9**, 68–71 (2005)]

A unique salt composed of cationic and anionic phthalocyanine complexes has been prepared and structurally characterized. The cationic component is di(pyridine)(phthalocyaninato)cobalt(III) and the anionic one is dicyano(phthalocyaninato)cobalt(III). They arrange alternately in the crystal, forming a two-dimensional sheet with partial  $\pi$ - $\pi$  overlaps.

#### IV-H-9 Physical Properties of Electrically Conducting and Stable Molecular Neutral Radical Solid $[\text{Co}(2,3\text{-Nc})(\text{CN})_2]\text{CH}_3\text{CN}$ (2,3-Nc = 2,3-Naphthalocyanine)

NAITO, Toshio; MATSUMURA, Naoko<sup>1</sup>; INABE,  
Tamotsu<sup>1</sup>; MATSUDA, Masaki<sup>2</sup>; TAJIMA,  
Hiroyuki<sup>2</sup>

(<sup>1</sup>Hokkaido Univ.; <sup>2</sup>Univ. Tokyo)

[*J. Porphyrins Phthalocyanines* **8**, 1258–1268 (2004)]

Solid state properties of dicyano(2,3-naphthalocyaninato)cobalt(III) neutral radical crystal,  $[\text{Co}(2,3\text{-Nc})(\text{CN})_2]\text{CH}_3\text{CN}$ , were characterized by the measure-

ments of the resistivity under high pressure and under uniaxial strain, thermoelectric power, magnetic susceptibility, ESR and polarized reflectance spectra. The title compound exhibited thermally activated-type electrical conductivity along the  $c$ -axis. The room temperature (RT) resistivity  $\rho_{\text{RT}}$  along the  $c$ -axis and activation energy  $E_a$  rapidly decreased with increasing pressure. The temperature-dependent thermoelectric power  $S$  was that of a typical one-dimensional (1D) semiconductor. However the high absolute value of  $S$  suggested that this electronic system should be strongly correlated. Although the electrical resistivity exhibited monotonical temperature-dependence, the magnetic susceptibility clearly indicated a Peierls-type transition and marked fluctuation from RT. Both of Peierls-type transitions and fluctuations are characteristic phenomena to 1D conductors. Furthermore ESR spectra manifested that the Peierls-type transition occurred at 100 K. The inconsistency between the electrical behaviour (without a phase-transition) and magnetic behaviour (with a phase-transition) indicates the separation of the degrees of freedom in spin and charge (spin-charge separation) of this material. Spin-charge separation is a theoretically predicted phenomenon peculiar to the 1D conductors with strong correlation. The reflectance spectra were quantitatively explained by a 1D Hubbard model, and manifested the existence of a structural fluctuation of this material from RT. Based on these observed physical properties it is concluded that  $[\text{Co}(2,3\text{-Nc})(\text{CN})_2]\text{CH}_3\text{CN}$  is a strongly correlated 1D semiconductor with a Mott-Hubbard type energy gap and characterised with a fluctuation and spin-charge separation.

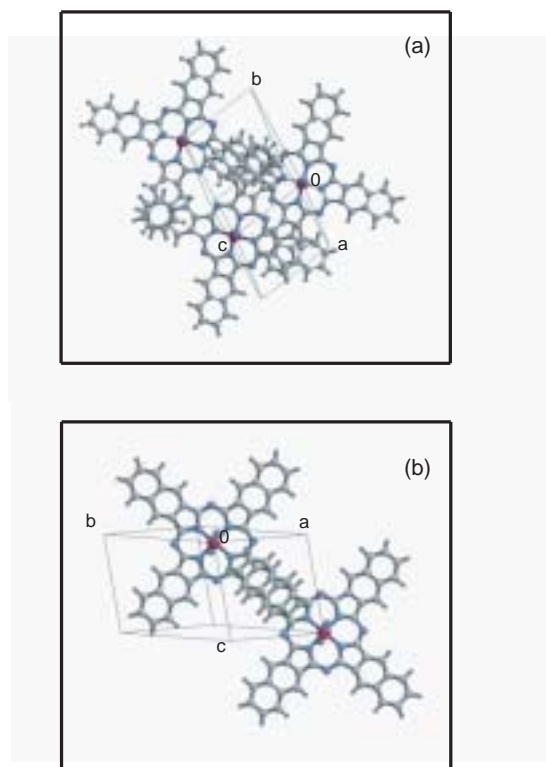


**Figure 1.** Crystal structure. For simplicity, (a) only three radical species at origin, [011] and [001], and (b) two radical species at origin and [101] are shown. The  $\text{CH}_3\text{CN}$  molecules are omitted for clarity.

#### IV-H-10 Charge Disproportionation and Anomalous Giant Magnetoresistance in a One-dimensional Conductor, $\text{TPP}[\text{Co}(\text{Pc})(\text{CN})_2]_2$

TAJIMA, Hiroyuki<sup>1</sup>; HANASAKI, Noriaki<sup>1</sup>; MASUDA, Kouki<sup>1</sup>; MATSUDA, Masaki<sup>1</sup>; KODAMA, Katsuaki<sup>1</sup>; TAKIGAWA, Masashi<sup>1</sup>; OHMACHI, Eiji<sup>1</sup>; OSADA, Toshihito<sup>1</sup>; NAITO, Toshio; INABE, Tamotsu<sup>2</sup>; HASEGAWA, Hiroyuki<sup>3</sup> (<sup>1</sup>Univ. Tokyo; <sup>2</sup>Hokkaido Univ.; <sup>3</sup>NICT)

[*Synth. Met.* in press]

Magnetoresistance study on the charge transfer salts of  $[\text{Fe}(\text{Pc})(\text{CN})_2]$  revealed various interesting phenomena, such as anisotropic giant negative magnetoresistance, weak ferromagnetism, and anisotropic Curie-Weiss magnetic susceptibility.<sup>1)</sup> These interesting phenomena originate from the orbital magnetic moment remaining in the  $[\text{Fe}(\text{Pc})(\text{CN})_2]$  unit, and the d- $\pi$  interaction inherently existing in this unit. Contrary to the  $[\text{Fe}(\text{Pc})(\text{CN})_2]$  salts, physical properties of the  $[\text{Co}(\text{Pc})(\text{CN})_2]$  salts have not been investigated in detail. In this paper, we report the magnetotransport and NQR studies on  $\text{TPP}[\text{Co}(\text{Pc})(\text{CN})_2]_2$  salts. This salt is a one-dimensional conductor, where the partially oxidized  $[\text{Co}(\text{Pc})(\text{CN})_2]$  units stack uniformly along the  $c$ -axis. The salt exhibits Pauli-paramagnetic susceptibility. The electrical resistivity is semiconducting with a very small activation energy less than 0.01 eV. Interestingly, this salt exhibits very large positive magnetoresistance at low-temperature ( $\Delta R(8 \text{ T})/R(0 \text{ T}) \sim 6$ ). Moreover, the field orientation dependence is quite small below 10 T. These facts indicate that the magnetoresistance in this salt is not an ordinary orbital effect. In order to examine the mechanism of the anomalous magnetoresistance, we have measured  $^{59}\text{Co}$  NQR spectra. We found a sign of charge disproportionation at 1.8 K. On the basis of magnetotransport ( $B < 38 \text{ T}$ ), NQR and NMR ( $B < 16 \text{ T}$ ) measurements, we will discuss the anomalous electronic state of this salt.

#### Reference

1) For example see, N. Hanasaki *et al.*, *Phys. Rev. B* **62**, 5839–5842 (2000).

#### IV-H-11 Structural, Electrical and Magnetic Properties of $\alpha\text{-(ET)}_7[\text{MnCl}_4]_2 \cdot (1,1,2\text{-C}_2\text{H}_3\text{Cl}_3)_2$ (ET = bis(ethylenedithio)tetrathiafulvalene)

NAITO, Toshio; INABE, Tamotsu<sup>1</sup> (<sup>1</sup>Hokkaido Univ.)

[*Bull. Chem. Soc. Jpn.* **77**, 1987–1995 (2004)]

A new charge-transfer salt of ET with a chloromanganate(II) complex anion has been synthesized and characterized by X-ray structural analysis, resistivity measurements, magnetic susceptibility, electron spin resonance (ESR) and extended Hückel tight binding band calculation. The crystal has a sheet structure comprised of  $\alpha$ -type two-dimensional (2D) donor arrangement in the  $bc$ -plane and insulating sheets of discrete  $[\text{MnCl}_4]^{2-}$  anions and 1,1,2- $\text{C}_2\text{H}_3\text{Cl}_3$  (TCE) molecules. Its con-

ducting property exhibits considerable anisotropy, which is effectively metallic along the  $b$ -axis down to 1.2 K under 2.9 kbar and higher pressure. The magnetic susceptibility is approximately reproduced by the Curie-Weiss law with the Weiss temperature  $\theta = -(1.35 \pm 0.07)$  K from 2–300 K. ESR measurements revealed that the  $\pi$ -electron system in this salt exhibits Pauli paramagnetism at least at 3.6– $\sim 50$  K. The band calculation suggests that the HOMO (the highest occupied molecular orbital) band has extremely small dispersion almost solely along the  $b^*$ -axis with a simple one-dimensional (1D) Fermi surface. Considering all the data above, it is concluded that this salt has unusually stable and narrow 1D metallic band structure, which is a rare example even in a great number of molecular conducting salts reported to date.

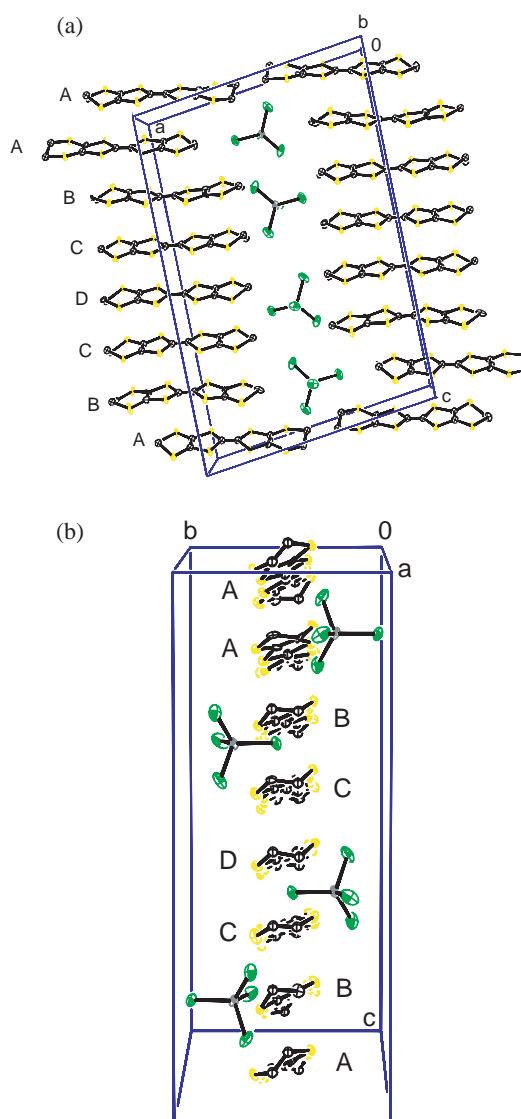


**Figure 1.** Unit cell; front view of (a)  $ac$ -, and (b)  $bc$ -planes. Hydrogen atoms are omitted for clarity.

#### IV-H-12 New Binuclear Copper Complexes $[(9\text{S}3)\text{Cu}(\text{CN})\text{Cu}(9\text{S}3)]\text{X}_n$ ( $\text{X} = \text{BF}_4$ , $n = 1$ ; $\text{X} = \text{TCNQ}$ , $n = 2$ ) (9S3 = 1,4,7-trithiacyclononane): Syntheses, Crystal Structures and Magnetic Properties

NAITO, Toshio; NISHIBE, Kunimasa<sup>1</sup>; INABE, Tamotsu<sup>1</sup>  
(<sup>1</sup>Hokkaido Univ.)

[Z. Anorg. Allg. Chem. **630**, 2725–2730 (2004)]

The binuclear Cu complexes of 1,4,7-trithiacyclononane (9S3) with an inorganic anion (BF<sub>4</sub><sup>-</sup>) and with an organic radical anion TCNQ<sup>-</sup> (7,7',8,8'-tetracyanoquinodimethanide) were synthesized and their molecular and crystal structures were examined in connection with each magnetic property. A new complex cation [Cu(9S3)CN(9S3)Cu] varied its charges and magnetic properties depending on the counter anions; [Cu(9S3)CN(9S3)Cu](BF<sub>4</sub>) (**1**) was obtained as diamagnetic colorless crystals, while [Cu(9S3)CN(9S3)Cu](TCNQ)<sub>2</sub> (**2**) was obtained as dark blue crystals with antiferromagnetic property. Complex **1** crystallized in the monoclinic space group C2/c with *a* = 26.863(2), *b* = 7.0878(5), *c* = 13.4864(8) Å, β = 116.318(2)°. Complex **2** crystallized in the triclinic space group P1̄ with *a* = 12.521(1), *b* = 20.2698(8), *c* = 8.0205(4) Å, α = 100.688(4), β = 93.846(5), γ = 94.953(4)°. Both complexes were comprised of cyano-bridged two Cu(9S3) ions with tetrahedral coordination geometry. The X-ray structural study revealed that **1** had two crystallographically equivalent Cu(I) centers, while **2** had two crystallographically independent Cu(I/II) sites. The two Cu(I/II) sites could not be distinguished from the X-ray structural study. As for **2** the IR spectra showed that both crystallographically independent TCNQ species were monoanions and were strongly dimerized due to pstacking, which well explained their diamagnetic contribution to the magnetic susceptibility and the highly insulating property of this salt. The temperature-dependent magnetic susceptibility of **2** showed a deviation from the Curie-Weiss behavior around 60 K, which indicated a strong antiferromagnetic intermolecular interaction between the copper complexes and that such intermolecular interaction should partly occur *via* the TCNQ radical anion dimer.

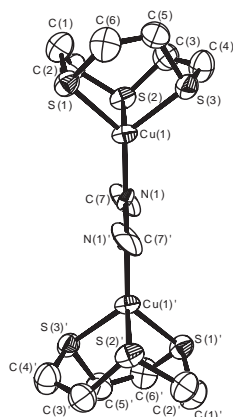


**Figure 1.** The molecular structure of the [Cu(9S3)CN(9S3)Cu]<sup>+</sup> cation (50% probability ellipsoids). The hydrogen atoms are omitted for clarity.

#### IV-H-13 Crystal Design of Cation-Radical Salts Based on the Supramolecular Self-Organizing Arrangement of Mellitate Anions

INABE, Tamotsu<sup>1</sup>; KOBAYASHI, Norihito<sup>1</sup>; NAITO, Toshio  
(<sup>1</sup>Hokkaido Univ.)

[J. Phys. IV France **114**, 449–453 (2004)]

Mellitate anions form hydrogen-bonding infinite networks in the salts with pyridinium cations. The network pattern depends on the number of deprotonation (*n*) from the mellitic acid; for *n* = 3, triangular hydrogen-bond units form a two-dimensional sheet, while for *n* = 2, dual hydrogen-bond units induce one-dimensional belts or two-dimensional grids. These self-organizing properties have been utilized for the crystal design of the TTF-type radical cation salts. Crystallization with TMTTF gave two kinds of crystals. One of the radical cation salt crystals consists of channel network of the anions and one-dimensional columns of TMTTF in the channels. In the other TMTTF salt, the anions with *n* = 1 form a two-dimensional sheet with methanol molecules. The TMTTF radicals are packed between the sheets with their molecular planes parallel to the anion planes.

#### IV-H-14 A Helical π-Radical Cation Column in the Double Helix of Mellitate Anions

KOBAYASHI, Norihito<sup>1</sup>; NAITO, Toshio; INABE, Tamotsu<sup>1</sup>  
(<sup>1</sup>Hokkaido Univ.)

[Adv. Mater. **16**, 1803–1806 (2004)]

Recent investigations of supramolecular network formation of mellitate anions in pyridinium salts have revealed that strong hydrogen bonds between the carboxy and carboxylate groups (the pair can be considered as dual hydrogen bond) predominantly form between neighboring anions, and its infinite sequence results in a chain, grid, or channel network. This self-organizing property is useful for aligning the cationic counterions. Herein, these anion structures have been utilized for the crystallization of π-radical cations. Electrochemical oxidation of TTF in the presence of mellitic acid and pyridine gave hexagonal platelets of [TTF]<sub>2</sub>[C<sub>6</sub>(COO)<sub>6</sub>H<sub>4</sub><sup>2-</sup>]. A TTF π-radical cation salt with a unique helical columnar structure has been successfully constructed within the supramolecular double helix of mellitate anions. The TTF radical tends to dimerize in a one-dimensional column; however, the twisting distortion induces a kink defect, which appears as orientational disorder. The absence of three-dimensionally correlated dimerization phase locking may arise from shielding of the one-dimensional column by the mellitate anions. This investigation indicates that combining charged functional molecules with a supramolecular network formed by their counterions is a promising approach to the crystal design of novel functional molecular materials. Indeed, it has recently been revealed that unique π-radical arrangements occurred in mellitate salts formed with other TTF-type molecules, in which mellitate anions formed a channel or sheet network by self-organization.

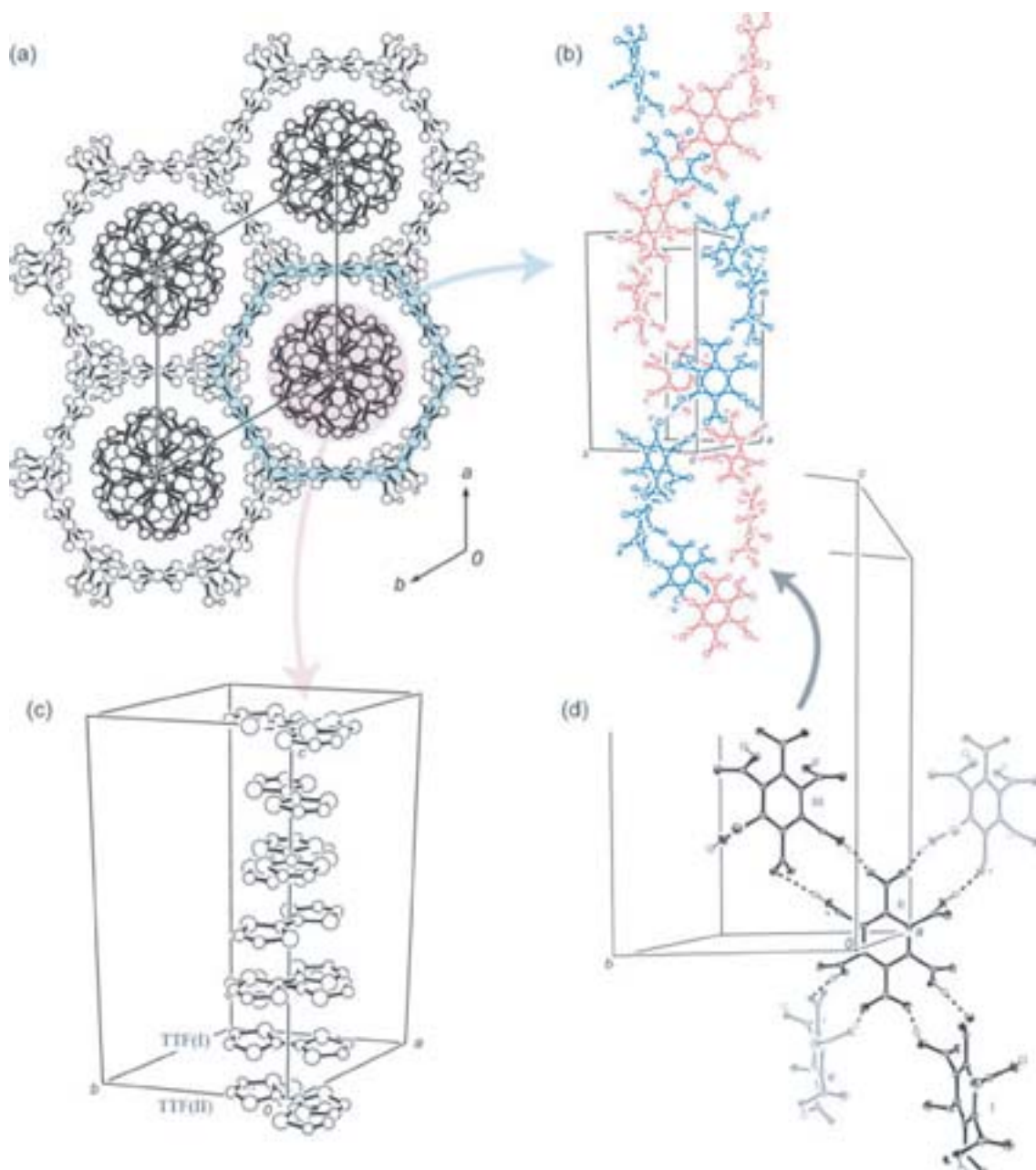


**Figure 1.** Molecular arrangement in  $[\text{TTF}^+]_2[\text{C}_6(\text{COO})_6\text{H}_4^{2-}]$ . a) Hexagonal channel structure of mellitate anions and the TTF columns viewed along the  $c$ -axis. b) Mellitate-anion double helix. c) Helical TTF column. d) Hydrogen bond in the mellitate network; anions **I**, **II**, and **III** are related by the  $6_2$  screw axis at  $(0,0,z)$ .

#### IV-H-15 Network Formation of Mellitate Anions $[\text{C}_6(\text{COO})_6\text{H}_{6-n}]^{n-}$ in the Salts with Piperidinium Derivatives and $\alpha$ -Phenylenediammonium

KOBAYASHI, Norihito<sup>1</sup>; INABE, Tamotsu<sup>1</sup>;  
NAITO, Toshio  
(<sup>1</sup>Hokkaido Univ.)

[*CrystEngComm* **6**, 189–196 (2004)]

Single crystals of mellitate anion  $[\text{C}_6(\text{COO})_6\text{H}_{6-n}]^{n-}$  with piperidinium  $[\text{C}_5\text{H}_{10}\text{NH}_2^+]_3[\text{C}_6(\text{COO})_6\text{H}_3^{3-}]$  (**1**) and  $[\text{C}_5\text{H}_{10}\text{NH}_2^+]_2[\text{C}_6(\text{COO})_6\text{H}_4^{2-}]\cdot\text{CH}_3\text{OH}\cdot 3\text{H}_2\text{O}$  (**2**), with 1-methylpiperidinium  $[\text{C}_5\text{H}_{10}\text{NHCH}_3^+]_2$

$[\text{C}_6(\text{COO})_6\text{H}_4^{2-}]\cdot 2\text{H}_2\text{O}$  (**3**), and with  $\alpha$ -phenylenediammonium  $[\text{C}_6\text{H}_4(\text{NH}_3)_2^{2+}]_2[\text{C}_6(\text{COO})_6\text{H}_2^{4+}]\cdot 2\text{CH}_3\text{OH}$  (**4**) have been prepared and structurally characterized. In all of the salts, two-dimensional (2D) networks of mellitate anions were formed due to the strong self-organization of the anion. In **1**, a 2D hexagon-type network of hydrogen-bond has been observed to form among the anions. This is characteristic of the mellitate anions with  $n = 3$  ( $n$ : deprotonation number from the acid). In other salts, a 2D anion network containing either water molecules or  $-\text{NH}_3$  groups commonly formed. Since the network pattern occurs with different cation species, this hydrogen-bonding unit was determined to be dominant in the  $n = 2$  anion with water and the  $n = 4$  anion with  $-\text{NH}_3$  species.

## IV-I Charge and Spin Dynamics of Organic Conductors

The spin and charge dynamics in organic conductors play important role in the emergence of the exotic properties in organic conductors, for example, superconductivity, magnetic ordering and charge ordering. It is important to reveal not only magnetic properties, but also the total picture of organic conductors. As known well,  $^{13}\text{C}$ -NMR is a one of the most powerful tool in the point of the magnetism. Since nuclear magnetic moment,  $I$ , is  $1/2$ ,  $^{13}\text{C}$ -NMR is not sensitive to the charge properties. On the other hand, optical studies, which are sensitive to the charge properties, are complementary to NMR study. In order to study both magnetic and charge properties, we performed  $^{13}\text{C}$ -NMR and optical works.

### IV-I-1 Electron Delocalization on $\kappa$ -(BEDT-TTF) $_2$ Cu $_2$ (CN) $_3$ under Pressure

KAWAMOTO, Atsushi<sup>1</sup>; HONMA, Yosuke<sup>2</sup>;  
KUMAGAI, Ken-ichi<sup>2</sup>; MATSUNAGA, Noriaki<sup>2</sup>;  
NOMURA, Kazushige<sup>2</sup>  
(<sup>1</sup>IMS and Hokkaido Univ.; <sup>2</sup>Hokkaido Univ.)

[Phys. Rev. B submitted]

$\kappa$ -(BEDT-TTF) $_2$ X is a system, whose bandwidth is comparable to the effective onsite coulomb repulsion. The phase diagram of this system has been considered to represent the competition between anti-ferromagnetic insulating behavior and superconductivity.

The  $\kappa$ -(BEDT-TTF) $_2$ X system have been well explained using a parameter,  $U/W$  as well as the high  $T_c$  cuprates. Although  $\kappa$ -(BEDT-TTF) $_2$ Cu $_2$ (CN) $_3$  exhibited the superconductivity under pressure, this salt behaves as an insulator without magnetic ordering under ambient pressure. Similar to the case of other salts, AF fluctuations intensified with a decrease in temperature. In addition to that, line broadenings, which suggested inhomogeneous electron localization, was observed.

We have proposed that the electron localization effect is significant in a relatively narrow bandwidth of the salt and the scenario in which, pressure application increases the bandwidth, suppresses the localization and produces the superconductivity.

In order to determine the relationship between the insulator phase and the superconductivity and confirm the proposed scenario, we measured the  $^{13}\text{C}$ -NMR of  $\kappa$ -(BEDT-TTF) $_2$ Cu $_2$ (CN) $_3$  under pressures. We observed a decrease in the spin susceptibility with an increase in pressure and the suppression of the line broadening above critical pressure.

The temperature dependences of  $(T_1T)^{-1}$  under pressures exhibited the same behavior as that of  $\kappa$ -(BEDT-TTF) $_2$ X, where X = Cu[N(CN) $_2$ ]Br and Cu(NCS) $_2$ .

These results suggested that the electronic structure of  $\kappa$ -(BEDT-TTF) $_2$ Cu $_2$ (CN) $_3$  under pressures is same as that of other  $\kappa$ -(BEDT-TTF) $_2$ X salts. Moreover, they supported our scenario of the emergence of the superconductivity.

### IV-I-2 Coherent-Incoherent Crossover Behavior of Electron on $\kappa$ -(BEDT-TTF) $_2$ Ag(CN) $_2$ ·H $_2$ O

KAWAMOTO, Atsushi<sup>1</sup>; KUMAGAI, Ken-ichi<sup>2</sup>;  
YAMAMOTO, Kaoru; YAKUSHI, Kyuya

(<sup>1</sup>IMS and Hokkaido Univ.; <sup>2</sup>Hokkaido Univ.)

[to be submitted]

$\kappa$ -(BEDT-TTF) $_2$ X system showed the variety electronic states, for example, superconductivity (SC), anti-ferromagnetic ordering (AF), etc. Experimentally, the most impressive aspects are an adjustment between the superconducting and the magnetic ordering state and the peak of  $(T_1T)^{-1}$  at  $T^*$  in NMR study as observed in high  $T_c$  cuprates. These result suggests the mechanism of superconductivity intermediated by magnetic fluctuations as same as high  $T_c$  cuprates.  $^{13}\text{C}$ -NMR is a one of the most powerful tool in the point of magnetic dynamics. On the other hand, optical studies, which are sensitive to the charge dynamics, are complementary to NMR study which detects the magnetism. We performed single crystal  $^{13}\text{C}$ -NMR and optical works. Many researchers paid the attention to mainly  $T_c = 10$  K class samples near the AF-SC boundary. However  $\kappa$ -(BEDT-TTF) $_2$ Ag(CN) $_2$ ·H $_2$ O, which is far from the boundary, should be paid the attention. Is there the peak structure in  $(T_1T)^{-1}$  in this sample and the relationship between  $T^*$  and SC?

We measured  $^{13}\text{C}$ -NMR and reflection spectrum in  $\kappa$ -(BEDT-TTF) $_2$ Ag(CN) $_2$ ·H $_2$ O. We could not observed the increase of the AF magnetic fluctuation as in  $\kappa$ -(BEDT-TTF) $_2$ Cu[N(CN) $_2$ ]Cl. Results of  $^{13}\text{C}$ -NMR suggested the emergence of superconductivity did not require the increase of the AF magnetic fluctuation but the crossover to the Fermi liquid regime. Optical studies suggested the crossover corresponds to the development of the coherency of conduction electron.

### IV-I-3 Charge Ordering State on (BEDT-TTF) $_3$ Cl $_2$ ·2H $_2$ O

KAWAMOTO, Atsushi<sup>1</sup>; OGURA, Takashi<sup>2</sup>;  
KUMAGAI, Ken-ichi<sup>2</sup>; TANIGUCHI, Hiromi<sup>3</sup>  
(<sup>1</sup>IMS and Hokkaido Univ.; <sup>2</sup>Hokkaido Univ.; <sup>3</sup>Saitama Univ.)

[to be submitted]

The organic superconductors, as represented by  $\kappa$ -(BEDT-TTF) $_2$ X, are attractive compound, because of the relationship between anti-ferromagnetic fluctuation and superconductivity well as High- $T_c$  cuprates. Since these  $\kappa$ -type salts are well known to have the nature of the strong dimerization, they can be considered as a half-filled electron system. Many experiments on  $\kappa$ -

(BEDT-TTF)<sub>2</sub>X have been well explained by the universal phase diagram using a parameter,  $U/W$ , where  $U$  is the effective on-site coulomb repulsive energy and  $W$  is the bandwidth.

On the other hand, if the dimerization is weak and the  $U$  is small, the system cannot be regarded as half-filled system. In addition to the  $U$ , the effective off-site Coulomb repulsive energy  $V$  makes the system form Charge Ordering (CO) state.

In some of organic conductors, such as  $\alpha$ -type,  $\theta$ -type salts, their insulator phase was said not to be antiferromagnetic ordering state. Since the dimerization in these salts is not so strong, the insulator phase of these salts is likely to form the CO state. Applying pressure, some of these salts show the superconductivity. Therefore we are also interested in the relationship between charge fluctuation and superconductivity. Quasi-two-dimensional (Q2D) organic conductor (BEDT-TTF)<sub>3</sub>Cl<sub>2</sub>·2H<sub>2</sub>O is metallic at 300 K and it undergoes metal-insulator transition (MIT) at  $T \sim 150$  K from magnetic susceptibility and electric conductivity measurements. The MIT has been believed to be connected with charge density wave (CDW) formation. However, the formation of the charge ordering (CO) in the insulator phase was also expected. Using <sup>13</sup>C-NMR measurement, we observed the split of the NMR spectrum which corresponded to the charge rich and poor sites below the MIT temperature and could conclude the insulator state is the CO state.

# RESEARCH ACTIVITIES V

## Department of Applied Molecular Science

### V-A Molecular Design and Functions of Photoactive and Spin-Active Supramolecular Assemblies

To achieve photosynthesis with a totally artificial system is a supreme challenge in science and a dream of molecular scientist. In nature, plants and photosynthetic bacteria depend on photosynthesis utilizing elaborate chromophore arrays to trap solar energy, followed by an efficient energy transfer to the reaction center. Although there have been many efforts to design molecular systems for light-harvesting, they usually suffer from inadequate energy transfer efficiency. Synthetic macromolecules have attracted attention as potential photosynthetic antennae, since they can be incorporated and organized. However, examples thus far reported are generally derived from linear-chain polymers, which, unlike biological macromolecules, can adopt ill-defined morphologies, many of which lead to complicated photochemical events associated with intra- and interchain interactions. Moreover, broad molecular weight distribution and uncontrolled structures inherent in linear chain synthetic polymers, make it difficult to develop meaningful correlation between their structures and photochemical functions.

In this project, we are focusing on development of novel nanomaterials for the exploitation of new functions and properties through molecular design and programmed self-assembly. Especially, creation of novel nanomaterials exhibiting high capability of controlling photoinduced energy transfer and photoinduced electron transfer is one of important missions.

In relation to the above project, we are intended to exploit spatially well-defined dendritic macromolecules for highly controlled arrays of supramolecular and macromolecular metallo-complexes with the goal of developing unique functions that are impossible with small molecules. In detail, we aim for demonstration of principles for molecular design of spin-active nanomaterials, realization of photo-induced spin transition and control of spin state in confined space, and creation of functional nanomaterials for future-generation spin devices.

#### V-A-1 Molecular Design of Light-Harvesting Antennae

JIANG, Donglin

[*Dendritic Polymers* (in Japanese), NTS, p. 2–21 (2005)]

In the present chapter, we highlight our recent efforts to construct several new bioinspired dendrimers and their self-organization by focusing attention on structure–function relationships.

## V-B Bioinorganic Chemistry and Structural Biology of Heme Proteins

One of research activities of my group is directed toward developing a rigorous, quantitative understanding of the biochemical function of heme proteins such as oxygenases, peroxidases and oxidases by characterization of their structural and functional properties. We use different experimental strategies including protein engineering, spectroscopic characterization of the molecular structure of the active centers, measurements of dynamics of substrates and inhibitor binding, and X-ray crystallography.

My current heme protein projects include (1) elucidation of the catalytic mechanism of heme oxygenase, one of the essential components of the heme catabolism and biosynthesis of carbon monoxide, a versatile physiological messenger molecule, (2) elucidation of the mechanism of controlling reactivity of hemoglobin and myoglobin, and (3) determination of heme sensing mechanism of Bach1, a heme-dependent transcription factor which regulates heme oxygenase gene expression. Effective clues to delineate the detailed active site structure have been obtained by X-ray crystallography, resonance Raman and magnetic resonance studies. The synergy of site-directed mutagenesis, structural biology, and spectroscopic techniques has revealed the specific roles of amino acids located in the active centers of heme proteins. Ligands and substrates binding measurements complement the structural data for our understanding functional properties displayed by heme proteins at the molecular level.

### V-B-1 Proton Transfer at Helium Temperatures during Dioxygen Activation by Heme Monooxygenases

(<sup>1</sup>Tohoku Univ.; <sup>2</sup>IMS and Tohoku Univ.)

DAVYDOV, Roman<sup>1</sup>; CHEMERISOV, Sergey<sup>2</sup>; WERST, David E.<sup>2</sup>; RAJH, Tijana<sup>2</sup>; MATSUI, Toshitaka<sup>3</sup>; IKEDA-SAITO, Masao<sup>4</sup>; HOFFMAN, Brian M.<sup>1</sup>

(<sup>1</sup>Northwestern Univ.; <sup>2</sup>Argonne Natl. Labs.; <sup>3</sup>Tohoku Univ.; <sup>4</sup>IMS and Tohoku Univ.)

[*J. Am. Chem. Soc.* **126**, 15960–15961 (2004)]

Heme oxygenase (HO) catalyzes the O<sub>2</sub> and NADPH/cytochrome P450 reductase-dependent conversion of heme to biliverdin, free iron ion, and CO through a process in which the heme participates both as dioxygen-activating prosthetic group and substrate. In the first measurement of enzymatic proton transfer at liquid helium temperatures, we examine protonation of the peroxo-ferriheme state HO produced by *in situ* radiolytic cryoreduction of oxy-HO in H<sub>2</sub>O and D<sub>2</sub>O solvents at *ca.* 4 K and above, and compare these findings with analogous measurements for oxy-P450cam and for oxy-Mb. Proton transfer in HO occurs at helium temperatures in both solvents; it occurs in P450cam at ~50 K and higher; in Mb it does not occur until *T* > 170 K. For Mb, this transfer at 180 K is biphasic, and the majority phase shows a solvent kinetic isotope effect of 3.8. We discuss these results in the context of the picture of environmentally coupled tunneling, which links proton transfer to two classes of protein motions: environmental reorganization (*i* in Marcus-like equations) and protein fluctuations (“active dynamics”; gating) which modulate the distance of proton transfer.

### V-B-2 Roles of Distal Asp in Heme Oxygenase from *Corynebacterium diphtheriae*, HmuO: A Water-Driven Oxygen Activation Mechanism

MATSUI, Toshitaka<sup>1</sup>; FURUKAWA, Momoko<sup>1</sup>; UNNO, Masaki<sup>1</sup>; TOMITA, Takeshi<sup>1</sup>; IKEDA-SAITO, Masao<sup>2</sup>

Heme oxygenases found in mammals, plants and bacteria catalyze degradation of heme using the same mechanism. Roles of distal Asp (Asp136) residue in HmuO, a heme oxygenase of *Corynebacterium diphtheriae*, have been investigated by site-directed mutagenesis, enzyme kinetics, resonance Raman spectroscopy and X-ray crystallography. Replacements of the Asp136 by Ala and Phe resulted in reduced heme degradation activity due to the formation of ferryl heme, showing that the distal Asp is critical in HmuO heme oxygenase activity. D136N HmuO catalyzed heme degradation at a similar efficiency to wild type and D136E HmuO, implying that the carboxylate moiety is not required for the heme catabolism by HmuO. Resonance Raman results suggest that the inactive ferryl heme formation in the HmuO mutants is induced by disruption of the interaction between a reactive Fe–OOH species and an adjacent distal pocket water molecule. Crystal structural analysis of the HmuO mutants confirms partial disappearance of this nearby water in D136A HmuO. Our results provide the first experimental evidence for the catalytic importance of the nearby water molecule that can be universally critical in heme oxygenase catalysis, and propose that the distal Asp helps in positioning the key water molecule at a position suitable for efficient activation of the Fe–OOH species.

### V-B-3 O<sub>2</sub>- and H<sub>2</sub>O<sub>2</sub>-Dependent Verdoheme Degradation by Heme Oxygenase: Reaction Mechanisms and Potential Physiological Roles of the Dual Pathway Degradation

MATSUI, Toshitaka<sup>1</sup>; NAKAJIMA, Aya<sup>1</sup>; FUJII, Hiroshi; MANSFIELD MATERA, Kathryn<sup>2</sup>; MIGITA, Catharina T.<sup>3</sup>; YOSHIDA, Tadashi<sup>4</sup>; IKEDA-SAITO, Masao<sup>5</sup>

(<sup>1</sup>Tohoku Univ.; <sup>2</sup>Baldwin-Wallace College; <sup>3</sup>Yamaguchi Univ.; <sup>4</sup>Yamagata Univ.; <sup>5</sup>IMS and Tohoku Univ.)

[*J. Biol. Chem.* **280**, in press (2005)]

Heme oxygenase (HO) catalyzes the catabolism of heme to biliverdin, CO and a free iron through three successive oxygenation steps. The third oxygenation, oxidative degradation of verdoheme to biliverdin, has been the least understood step in spite of its importance in regulating HO activity. We have examined in detail the degradation of a synthetic verdoheme IX $\alpha$  complexed with rat HO-1. Our findings include: (1) HO degrades verdoheme through a dual pathway using either O<sub>2</sub> or H<sub>2</sub>O<sub>2</sub>; (2) the verdoheme reactivity with O<sub>2</sub> is the lowest among the three O<sub>2</sub> reactions in the HO catalysis, and the newly found H<sub>2</sub>O<sub>2</sub> pathway is approximately 40-fold faster than the O<sub>2</sub>-dependent verdoheme degradation; (3) both reactions are initiated

by the binding of O<sub>2</sub> or H<sub>2</sub>O<sub>2</sub> to allow the first direct observation of degradation intermediates of verdoheme; and (4) Asp140 in HO-1 is critical for the verdoheme degradation regardless of the oxygen source. On the basis of these findings, we propose that the HO enzyme activates O<sub>2</sub> and H<sub>2</sub>O<sub>2</sub> on the verdoheme iron with the aid of a nearby water molecule linked with Asp140. These mechanisms are similar to the well-established mechanism of the first oxygenation, *meso*-hydroxylation of heme, and thus, HO can utilize a common architecture to promote the first and third oxygenation steps of the heme catabolism. In addition, our results infer the possible involvement of the H<sub>2</sub>O<sub>2</sub>-dependent verdoheme degradation *in vivo*, and potential roles of the dual pathway reaction of HO against oxidative stress are proposed.

## V-C Pro-Oxidants-Induced Iron Release from the Fe-S Cluster of Mitochondrial Aconitase and Its Prevention by Frataxin

Pro-oxidants, such as hydrogen peroxide and superoxide anion, are highly toxic for many living organisms. One of the adverse effects of pro-oxidants is modulation of mitochondrial respiration. Using EPR spectroscopy, we have identified that pro-oxidants deactivate mitochondrial aconitase, the key enzyme in citrate cycle, by releasing one of Fe from the 4Fe-4S cluster, and that mitochondria is surprisingly equipped a recovery mechanism to restore the active 4Fe-4S cluster. We have recently discovered that this restoration is achieved by an iron insertion from frataxin, an iron storage protein in mitochondria, which functions as an iron chaperon protein. We are in the process of elucidation of the inter protein iron transfer mechanism from frataxin to aconitase at molecular level.

### V-C-1 Reversible Redox-Dependent Modulation of Mitochondrial Aconitase and Proteolytic Activity during *In Vivo* Cardiac Ischemia/Reperfusion

**BULTEAU, Anne-Laure<sup>1</sup>; LUNDBERG, Kathleen C.<sup>1</sup>; IKEDA-SAITO, Masao<sup>2</sup>; ISAYA, Grazia<sup>3</sup>; SZWEDA, Luke I.<sup>1</sup>**

(<sup>1</sup>Case Western Reserve Univ.; <sup>2</sup>IMS and Tohoku Univ.; <sup>3</sup>Mayo Clinic College Med.)

[*Proc. Natl. Acad. Sci. U. S. A.* **102**, 5987–5991 (2005)]

Recent evidence indicates that mitochondrial aconitase can be reversibly inhibited or progress to irreversible inactivation and degradation in response to pro-oxidants. Cardiac ischemia/reperfusion is associated with an increase in mitochondrial free radical production. In the current study, the effects of reperfusion-induced production of pro-oxidants on mitochondrial aconitase and proteolytic activity were determined to assess whether alterations represented a regulated response to changes in redox status or oxidative damage. Evidence is provided that ATP-dependent proteolytic activity increased during early reperfusion followed by a time-dependent reduction in activity to control levels. These alterations in proteolytic activity paralleled an increase and subsequent decrease in the

level of oxidatively modified protein. *In vitro* data supports a role for pro-oxidants in the activation of ATP-dependent proteolytic activity. Despite inhibition during early periods of reperfusion, aconitase was not degraded under the conditions of these experiments. Aconitase activity exhibited a decline in activity followed by reactivation during cardiac reperfusion. Loss and regain in activity involved reversible sulfhydryl modification. Aconitase was found to associate with the iron binding protein frataxin exclusively during reperfusion. *In vitro*, frataxin has been shown to protect aconitase from [4Fe-4S]<sup>2+</sup> cluster disassembly, irreversible inactivation, and potentially degradation. Thus, the response of mitochondrial aconitase and ATP-dependent proteolytic activity to reperfusion-induced pro-oxidant production appears to be a regulated event that would be expected to reduce irreparable damage to the mitochondria.

## V-D Quantum Emissions from Solid in Femtosecond Intense Laser Field and Its Application to Dynamic Imaging

Quantum emissions, which are high-energy electron, ion and photon beams, generated by interaction of femtosecond intense laser field with matter has recently been attracting considerable attention because of interest in fundamental science and its potential applications in compact acceleration, proton therapy and materials sciences. We have studied a mechanism of quantum emissions from solid target and its application to dynamic imaging of materials.

### V-D-1 Picosecond Time-Resolved X-Ray Diffraction from a Laser-Shocked Germanium Crystal over Hugoniot Elastic Limit

NAKAMURA, Kazutaka<sup>1</sup>; KAWANO, Hidetaka<sup>2</sup>;  
KISHIMURA, Hiroaki<sup>2</sup>; OKANO, Yasuhisa<sup>2</sup>;  
HIRONAKA, Yoichiro<sup>2</sup>; KONDO, Ken-ichi<sup>2</sup>  
(<sup>1</sup>IMS and Tokyo Inst. Tech.; <sup>2</sup>Tokyo Inst. Tech.)

[*Jpn. J. Appl. Phys.* **43**, 5477–5479 (2004)]

Picosecond time-resolved X-ray diffraction has been performed on a 300-ps laser-irradiated germanium crystal at 1.2 GW/cm<sup>2</sup>. Lattice deformation due to shock compression and the propagation of shock waves are directly observed. The observed lattice compression is 4.3% at maximum, which is higher than that at the Hugoniot elastic limit (HEL). The data suggest that the germanium-crystal lattice behaves elastically under shock compression at 7.5 GPa (above HEL) for 27 ps.

### V-D-2 Enhanced Generation of Fast Protons from a Polymer-Coated Metal Foil by a Femtosecond Intense Laser Field

KISHIMURA, Hiroaki<sup>1</sup>; MORISHITA, Hiroto<sup>1</sup>;  
OKANO, Yasuaki<sup>1</sup>; OKANO, Yasuhisa<sup>1</sup>;  
HIRONAKA, Yoichiro<sup>1</sup>; KONDO, Ken-ichi<sup>1</sup>;  
NAKAMURA, Kazutaka<sup>2</sup>; OISHI, Yuji<sup>3</sup>;  
NEMOTO, Koshichi<sup>3</sup>  
(<sup>1</sup>Tokyo Inst. Tech.; <sup>2</sup>IMS and Tokyo Inst. Tech.;  
<sup>3</sup>CRIEP)

[*Appl. Phys. Lett.* **85**, 2736–2738 (2004)]

The results of generation of fast protons from 5- $\mu$ m-thick copper foil targets by 60fs laser irradiation at  $1.5 \times 10^{17}$  W/cm<sup>2</sup> are presented. Both polyvinylmethylether (PVME)-coated and uncoated copper foil targets are examined. Fast protons are measured using a Thomson mass spectrometer and maximum proton energies are 570 and 280 keV for the PVME-coated and the uncoated target, respectively. The intensity of fast protons with energy of 160 keV from the PVME-coated target is approximately 80-fold higher than that from the uncoated target.

### V-D-3 Electron Imaging of Charge Separated Field on a Copper Film Induced by Femtosecond Laser Irradiation

OKANO, Yasuaki<sup>1</sup>; HIRONAKA, Yoichiro<sup>1</sup>;

KONDO, Ken-ichi<sup>1</sup>; NAKAMURA, Kazutaka<sup>2</sup>  
(<sup>1</sup>Tokyo Inst. Tech.; <sup>2</sup>IMS and Tokyo Inst. Tech.)

[*Appl. Phys. Lett.* **86**, 141501–141503 (2005)]

An instantaneous charge-separated field, built up at the femtosecond-laser-irradiated surface of a copper film, was observed by time-resolved electron imaging using an energy-chirped electron probe-beam. The probe beams with effective energies of 170 keV were generated by intense femtosecond laser irradiation onto a molybdenum target at an intensity of  $10^{17}$  W/cm<sup>2</sup>. From the deflection of the probe electrons, the electric field was estimated to be 1.5 MV/m at a pump-laser intensity of  $10^{15}$  W/cm<sup>2</sup>.

# RESEARCH ACTIVITIES VI

## Department of Vacuum UV Photoscience

### VI-A Electronic Structure and Decay Mechanism of Inner-Shell Excited Molecules

In this project, we have two major subjects: (a) resonant photoelectron spectroscopy and (b) resonant inelastic soft X-ray emission spectroscopy following inner-shell excitations of simple molecules and clusters. We have succeeded in development of a next-generation soft X-ray emission spectrometer. In the spectral assignments, angle(symmetry)-resolved photoion yield techniques and R-matrix/MQDT theoretical approaches are essential.

#### VI-A-1 Development of a Transmission-Grating Spectrometer for Soft-X-Ray Emission Studies

HATSUI, Takaki; HORIGOME, Toshio; KOSUGI, Nobuhiro

Last year we reported our new design of a transmission-grating spectrometer (TGS) for high resolution soft X-ray emission studies. This spectrometer will realize a resolution  $E/\Delta E$  up to 5000 in the energy region of 50–600 eV. Here we report the first results using a prototype setup. The spectrometer has a Wolter type I mirror, a free-standing transmission grating, and a back-illuminated charge coupled device (CCD). A high collection angle up to  $1.5 \times 10^{-3}$  sr is achieved by introducing the Wolter mirror as a prefocusing system. The developed Wolter mirror<sup>1)</sup> shows a slope error less than 0.4 arcsec. A SiC transmission grating with a groove density of 6250 l/mm is also developed.<sup>2)</sup> The CCD is mounted at 1.5 m downstream of the grating on a Rowland torus mount with a radius of 0.75 m. Diffracted x-rays are detected in the normal incidence geometry, resulting in high detection efficiency. Ray-trace simulations indicate that aberrations do not practically degrade the energy resolution as high as 5000. It is limited by the figure errors of the optical elements and the spatial resolution of the detector. The energy resolution of TGS was examined by measuring the diffuse scattering of a tungsten wire with a diameter of 3  $\mu\text{m}$  illuminated. Figure 1 illustrates a line profile along dispersion direction of the CCD detector image. The results indicate that the energy resolving power is above 3100 at 110 eV. Further evaluation of the performance by introducing the entrance slit is now under progress.

#### References

- 1) In collaboration with A. Ohba *et al.* (Hamamatsu Photonics K.K.).
- 2) Manufactured by NTT-ATN.

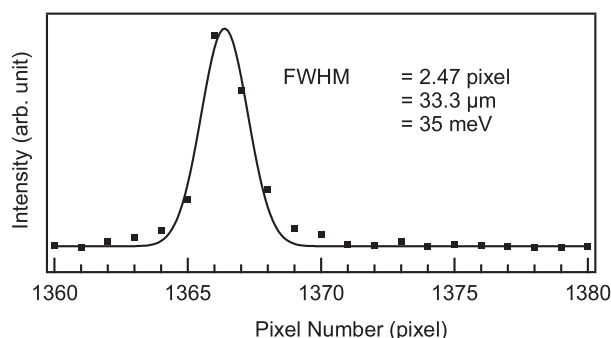


**Figure 1.** Line profile along dispersion direction of the CCD detector image. Full width at half maximum of 33.3  $\mu\text{m}$ , which corresponds to energy resolution of 35 meV ( $E/\Delta E = 3100$ ), has been obtained.

#### VI-A-2 Application of R Matrix/MQDT Method to both Valence and Core Excitations in NO

HIYAMA, Miyabi; KOSUGI, Nobuhiro

Both valence and core excitations of NO molecule are studied using the R matrix/Multi-channel Quantum Defect Theory<sup>1)</sup> program code, GSCF4R.<sup>2)</sup> In the case of valence excitation, the quantum defects and the coupling constant between  $\pi\text{-Rydberg}$  state and  ${}^2\Pi$  state of NO were calculated. The theoretical quantum defects for  ${}^2\Sigma$ ,  ${}^2\Pi$ , and  ${}^2\Delta$  are in good agreement with the experimental values. The theoretical coupling constants not only for B( ${}^2\Pi$ ) but also for L( ${}^3\Pi$ ) are also in good agreement with the experimental values. In the case of core excitation, the potential curves above the N 1s ionization threshold of NO were calculated. There may be six potential energy curves corresponding to the resonances around 412 eV. Finally, the twin local maxima near 412 eV in the absorption spectra of NO may be assigned to the resonances whose characters are  $\sigma^*$  excitation and the mixture of  $\sigma^{*-}$  and doubly excitations, respectively.

#### References

- 1) M. Hiyama and M. S. Child, *J. Phys. B* **35**, 1337–1351 (2002); **36**, 4547–4559 (2003).
- 2) M. Hiyama and N. Kosugi, *J. Theor. Comput. Chem.* **4**, 35–47 (2005).

## VI-B Soft X-Ray Photoelectron-Photoabsorption Spectroscopy and Electronic Structure of Molecular Solids and Clusters

This project has been carried out in collaboration with Wuerzburg University. We have two subprojects: (a) molecules and radicals in condensed phase and in rare gas matrix, and (b) ionic fragmentations of atomic and molecular clusters following the inner-shell resonance excitation. In (a), we have measured excitation spectra in some matrix phases at the bending-magnet beamline BL4B of the UVSOR facility. In (b), we have developed a new cluster source for photoelectron measurements on a newly constructed undulator beamline BL3U.

### VI-B-1 Photoionization of Small Krypton Clusters in the Kr 3d Regime: Evidence for Site-Specific Photoemission

HATSUI, Takaki; SETOYAMA, Hiroyuki;  
KOSUGI, Nobuhiro; WASSERMANN, Bernhard<sup>1</sup>;  
BRADEANU, Ioana<sup>2</sup>; RÜHL, Eckart<sup>2</sup>  
(<sup>1</sup>Berlin Frei Univ.; <sup>2</sup>Würzburg Univ.)

[*J. Chem. Phys.* in press]

Kr 3d ionization energies of small, variable size krypton clusters are investigated by photoelectron spectroscopy, where the size regime of clusters with an average size  $\langle N \rangle \leq 30$  is studied. Characteristic shifts in Kr 3d ionization energies to lower binding energies are found compared to the bare atom. These are also different from those of large krypton clusters. Moreover, we find evidence for photoionization of the krypton dimer. Its 3d ionization energy is barely shifted relative to the atomic value. Results from model calculations considering different isomers and cluster sizes as well as defect sites give evidence that the experimental results can be related to photoionization from different surface sites in variable size krypton clusters. This can be related to site-specific photoemission in small Kr clusters. The results are compared to size effects in Kr 3d near-edge features of variable size Kr clusters as well as recent results on Kr 3d photoionization of large Kr clusters.

### VI-B-2 Core Excitation in O<sub>3</sub> Localized to One of Two Symmetry-Equivalent Chemical Bonds – Molecular Alignment through Vibronic Coupling

WIESNER, Karoline<sup>1</sup>; NAVES DE BRITO, Arnaldo<sup>2</sup>; SORENSEN, Stacey<sup>3</sup>; KOSUGI, Nobuhiro; BJORNEHOLM, Olle<sup>1</sup>  
(<sup>1</sup>Uppsala Univ.; <sup>2</sup>LNLS; <sup>3</sup>Lund Univ.)

[*J. Chem. Phys.* **122**, 154303 (2005)]

Core excitation from terminal oxygen O<sub>T</sub> in O<sub>3</sub> is shown to be an excitation from a localized core orbital to a localized valence orbital. The valence orbital is localized to one of the two equivalent chemical bonds. We experimentally demonstrate this with the Auger Doppler effect which is observable when O<sub>3</sub> is core-excited to the highly dissociative O<sub>T</sub> 1s<sup>-1</sup>7a<sub>1</sub><sup>+1</sup> state. Auger electrons emitted from the atomic oxygen frag-

ment carry information about the molecular orientation relative to the electromagnetic field vector at the moment of excitation. The data together with analytical functions for the electron-peak profiles give clear evidence that the preferred molecular orientation for excitation only depends on the orientation of one bond, not on the total molecular orientation. The localization of the valence orbital “7a<sub>1</sub>” is caused by mixing of the valence orbital “5b<sub>2</sub>” through vibronic coupling of anti-symmetric stretching mode with b<sub>2</sub>-symmetry. To the best of our knowledge, it is the first discussion of the localization of a core excitation of O<sub>3</sub>. This result explains the success of the widely used assumption of localized core excitation in adsorbates and large molecules.

## VI-C Ultrafast Dynamics of Molecules in Intense Laser Fields

The behavior of molecules in an intense laser field ( $10^{12}$ – $10^{18}$  W/cm<sup>2</sup>) has been an attractive target of research for a deeper understanding of the light-matter interaction. In the present study, the characteristic nuclear dynamics occurring in intense laser fields, such as structural deformation and multiple breaking of chemical bonds, has been studied by a newly developed experimental method, called *coincidence momentum imaging* (CMI), which allows us to determine the momentum vectors of all the fragment ions ejected from a single parent molecule. By using the CMI technique combined with the pump-and-probe scheme, the real-time probing of the nuclear wavepacket evolution in the three-dimensional internal coordinate space is demonstrated. Based on this novel technique, it has been found that CS<sub>2</sub><sup>2+</sup> formed in intense laser fields ( $\sim 1.3 \times 10^{14}$  W/cm<sup>2</sup>) undergoes ultrafast dissociation along the symmetric stretching coordinate leading to simultaneous breaking of the two C–S bonds. A high temporal resolution pump-probe CMI measurement is under progress with sub-10 fs intense laser pulses.

### VI-C-1 Probing the Ultrafast Nuclear Motion in CS<sub>2</sub><sup>2+</sup> in Intense Laser Fields

HISHIKAWA, Akiyoshi; UEYAMA, Mazakuni<sup>1</sup>;  
YAMANOUCI, Kaoru<sup>1</sup>  
(<sup>1</sup>Univ. Tokyo)

[*J. Chem. Phys.* **122**, 151104 (4 pages) (2005)]

The nuclear dynamics of CS<sub>2</sub> exposed to an intense laser field (60 fs,  $1.3 \times 10^{14}$  W/cm<sup>2</sup>) is studied by the pump-probe coincidence momentum imaging of the Coulomb explosion process, CS<sub>2</sub><sup>3+</sup> → S<sup>+</sup> + C<sup>+</sup> + S<sup>+</sup>. From the dependence of momentum correlations among the fragment ions on the time delay between pump and probe pulses, the existence of the dissociation pathway along the symmetric stretching coordinate leading to concerted breaking of the two C–S bonds is identified in addition to the dissociation along the anti-symmetric stretching leading to S<sup>+</sup> + CS<sup>+</sup>. It is also shown that the S–C–S bending motion is largely excited when both of the two C–S bonds stretch by the coupling of two different light-dressed states.

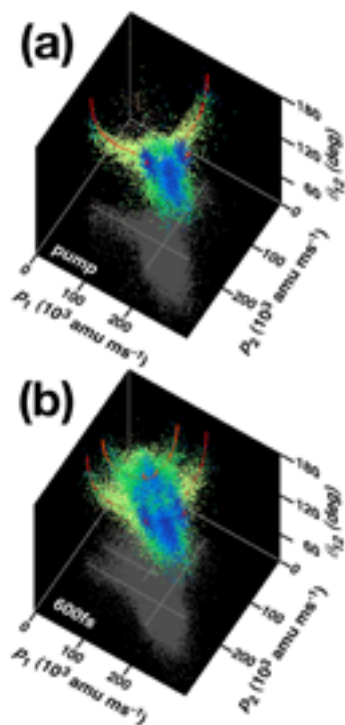


**Figure 1.** (a) Three-dimensional momentum correlation map for the Coulomb explosion process, CS<sub>2</sub><sup>3+</sup> → S<sup>+</sup> + C<sup>+</sup> + S<sup>+</sup>, obtained only with a pump pulse ( $1.3 \times 10^{14}$  W/cm<sup>2</sup>, 60 fs, 800 nm), where  $\theta_{12}$  represents the angle between the two momentum vectors  $p_1(S^+)$  and  $p_2(S^+)$  of the resultant S<sup>+</sup> ions, and  $p_1 = |p_1(S^+)|$  and  $p_2 = |p_2(S^+)|$ . Solid lines represent the result of the simulation based on the classical free-rotor model. (b) Momentum correlation map at a time delay of  $\Delta t = 600$  fs, exhibiting new features with a pair of wings in the low momentum region ( $p_1, p_2 < 150 \times 10^3$  amu m/s).

### VI-C-2 Concerted and Sequential Coulomb Explosion Processes of N<sub>2</sub>O in Intense Laser Fields by Coincidence Momentum Imaging

UEYAMA, Mazakuni<sup>1</sup>, HASEGAWA, Hirokazu<sup>1</sup>;  
HISHIKAWA, Akiyoshi; YAMANOUCI, Kaoru<sup>1</sup>  
(<sup>1</sup>Univ. Tokyo)

[*J. Chem. Phys.* **123**, 154305 (8 pages) (2005)]

The Coulomb explosion dynamics of N<sub>2</sub>O in intense laser fields (800 nm, 60 fs,  $\sim 1.6 \times 10^{14}$  W/cm<sup>2</sup>) is studied by the coincidence momentum imaging method. From the momentum correlation maps obtained for the three-body fragmentation pathway, N<sub>2</sub>O<sup>3+</sup> → N<sup>+</sup> + N<sup>+</sup> + O<sup>+</sup>, the ultrafast structural deformation dynamics of N<sub>2</sub>O prior to the Coulomb explosion is extracted. It is revealed that the internuclear N–N and N–O distances stretch simultaneously as the bond angle  $\angle$ N–N–O decreases. In addition, two curved thin distributions are identified in the momentum correlation maps, and are interpreted well as those originating from the sequential dissociation pathway, N<sub>2</sub>O<sup>3+</sup> → N<sup>+</sup> + NO<sup>2+</sup> → N<sup>+</sup> + N<sup>+</sup> + O<sup>+</sup>.

### VI-C-3 Development of an Intense Sub-10fs Laser Source with a Hollow Fiber/Chirped Mirror Compressor

TAKAHASHI, Eiji J.; HISHIKAWA, Akiyoshi

An intense ultrashort laser source was designed and developed to study the Coulomb explosion dynamics of molecules in a sub-10fs intense laser field. The output from a Ti:Sapphire laser system (800 nm, <40 fs, 1 kHz) was introduced to a hollow fiber placed on a V-shape block in a cell, filled with Ar at a pressure of  $\sim 0.1$  MPa. During the propagation of the laser through the fiber, the

spectral bandwidth was increased up to by the self-phase modulation effect (Figure 1(a)). The output from the hollow fiber was then collimated by a concave mirror and compressed by a pair of chirped mirrors. The pulse duration after the compression was measured to be 9.0 fs from the interferometric autocorrelation trace (Figure 1(b)). The output energy from the pulse compression system exceeds 0.4 mJ/pulse, which is sufficient to generate a field intensity of  $\sim 10^{16}$  W/cm<sup>2</sup> with an F/5 focusing optics.

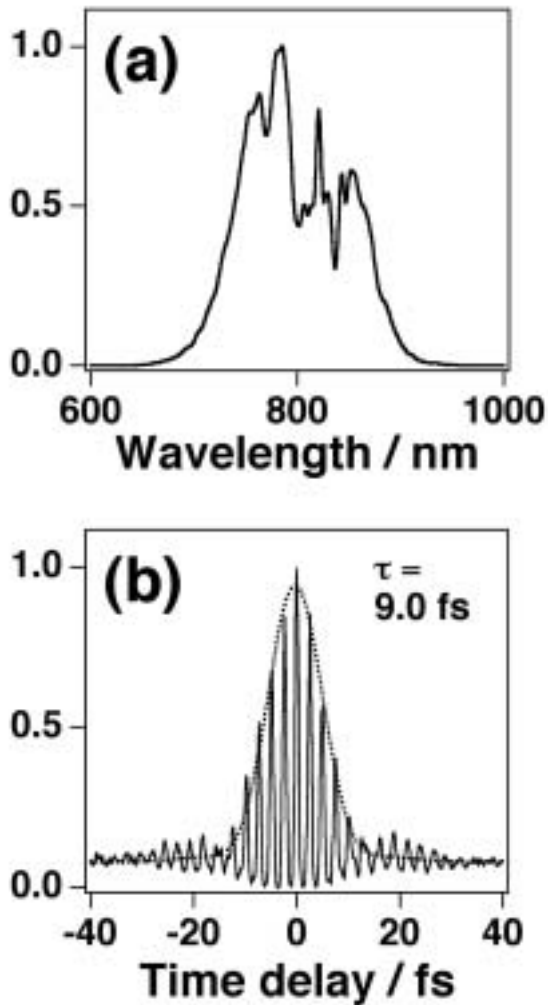


**Figure 1.** (a) The laser spectrum after the propagation through the hollow fiber. (b) The autocorrelation trace of the laser pulse after the compression by the chirped mirrors. The autocorrelation intensity profile obtained by Fourier transform of the spectrum (a) is plotted with a dotted curve. The pulse duration is determined to be 9.0 fs.

## VI-D Synchrotron Radiation Stimulated Surface Reaction and Nanoscience

Synchrotron radiation (SR) stimulated process (etching, CVD) has excellent characteristics of unique material selectivity, low damage, low contamination, high spatial resolution and high precision, *etc.* In this project, nanolevel controlled structures are created using the synchrotron radiation stimulated process, and the reaction mechanisms are investigated by scanning tunneling microscopy and atomic force microscopy. Concerning the SR etching, we are considering to apply this technique to the microfabrication of integrated protein transistor circuits. Electric property measurement of a supported lipid bilayer membrane was achieved using a  $\text{SiO}_2/\text{AgCl}/\text{Si}$  device which was fabricated by synchrotron irradiation etching.

### VI-D-1 Synchrotron Radiation Induced Si-H Dissociation on H-Si(111)-1x1 Surfaces Studied by In-Situ Monitoring in the Undulator-STM System

NONOGAKI, Youichi; URISU, Tsuneo

[*J. Vac. Sci. Technol., A* **23**, 1364–1366 (2005)]

Irradiation effects of the synchrotron radiation (SR) have been investigated on the hydrogen terminated- (H-) Si (111) surfaces by using the undulator beam and the in-situ scanning tunneling microscope (STM). The small protrusions (SPs) generated by the undulator beam irradiation were assigned to the rest-atoms with missing H (Figure 1). From the observed relation among the SP density, photon energy of the undulator beam and the total photon flux, it has been concluded that the main mechanism of the Si-H bond dissociation by the undulator beam irradiation is valence electron excitations of the Si-H bond by incident photons.

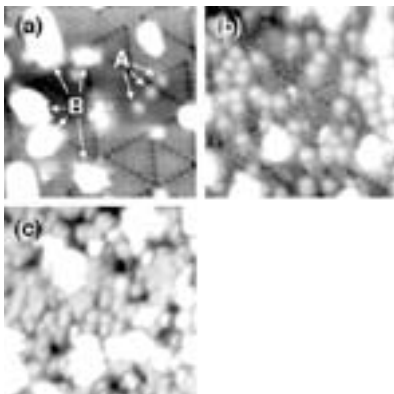


**Figure 1.** 10 nm × 10 nm STM images of H-Si(111) surfaces after the undulator beam irradiations with the exposure of (a) 0 mAs, (b) 5,000 mAs and (c) 10,000 mAs. The undulator gap height was fixed at 20 mm. In (a), small protrusions (SPs) and adatom islands (AIs) are indicated by A and B, respectively. It is observed that the SP density significantly increases with increasing irradiation dose. The appeared SPs are assigned to the rest-atoms with missing H.

### VI-D-2 Giant Vesicle Fusion on the Microelectrodes Fabricated by Femto-Second Laser Ablation Followed by Synchrotron Radiation Etching

RAHMAN, Md. Mashiur; NONOGAKI, Youichi; TERO, Ryugo; KIM, Yong-Hoon; UNO, Hidetaka; ZHANG, Zhen-Long; YANO, Takayuki; AOYAMA, Masaki; SASAKI, Ryuichiro<sup>1</sup>; NAGAI, Hiroyuki<sup>1</sup>; YOSHIDA, Makoto<sup>1</sup>; URISU, Tsuneo  
(<sup>1</sup>AISHIN SEIKI Co., Ltd.)

[*Jpn. J. Appl. Phys.* in press]

We have developed a new technique to fabricate the hole (well) with about 1 μm diameter for the microelectrode on the surface of  $\text{SiO}_2(600 \text{ nm})/\text{CoSi}_2(10 \text{ nm})/\text{Si}$  using synchrotron radiation (SR) stimulated etching. The Co photomask on the substrate was patterned by a femto-second-laser, and the  $\text{SiO}_2$  layer was SR-etched. This process enabled the fabrication of the electrode holes with keeping the original nano-level flatness ( $R_a \sim 0.8 \text{ nm}$ ) of the  $\text{SiO}_2$  surface. The lipid bilayer was formed by the giant vesicle fusion on these microelectrodes. Fluorescence microscopy, *in situ* AFM and electrical characteristics measurements showed that a single lipid bilayer with sufficiently high resistance (giga ohm seal) was successfully fabricated (Figure 1).

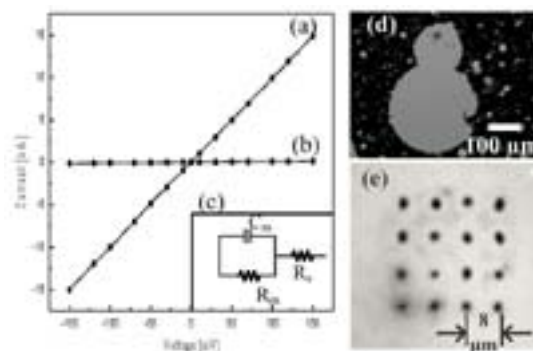


**Figure 1.** Current-voltage characteristics of the substrate measured under the KCl solution (10 mM), (a) before (■) and (b) after (●) the SPLB formation, and (c) the equivalent circuit of the system. The fluorescence microscopy image of the lipid bilayer formed by the rupture of the giant vesicle on (d)  $\text{SiO}_2/\text{CoSi}_2/\text{Si}$  surface and (e) the electrode area.

## VI-E Noble Semiconductor Surface Vibration Spectroscopy

As a new high sensitive and high resolution surface vibration spectroscopy technique, we are developing an infrared reflection absorption spectroscopy using buried metal layer substrate (BML-IRRAS), which have unique characteristics of high resolution and high sensitivity at finger print regions. Several Si surface chemical reactions are investigated using this BML-IRRAS. As a new fabrication technique of BML substrate, we have almost succeeded in developing the wafer bonding technique. It is considered that BML-IRRAS is also extremely useful in the research of bio-material integration on Si substrates.

### VI-E-1 Orientation of Avidin Molecules Immobilized on the COOH-Modified SiO<sub>2</sub>/Si(100) Surface

MISAWA, Nobuo; YAMAMURA, Shusaku; TERO, Ryugo; NONOGAKI, Youichi; URISU, Tsuneo

Avidin molecules were immobilized on COOH-modified SiO<sub>2</sub>/Si(100) surfaces with subnano-level flatness ( $R_a < 0.1$  nm) forming covalent bonds between COOH groups on the substrate surface and NH<sub>2</sub> groups of the avidin molecules. The avidin-immobilized surfaces were characterized by atomic force microscopy (AFM), infrared reflection absorption spectroscopy using buried metal layer substrate (BML-IRRAS), transmission infrared absorption spectroscopy (TIRAS), and ellipsometry. BML-IRRAS and TIRAS have the sensitivities to the perpendicular and the parallel (to the substrate surface) components of the dynamic dipole moment, respectively. In the  $\beta$ -sheet, the amide I transition dipole moment is oriented parallel to the C=O bond, which is oriented perpendicular to the axis of the  $\beta$ -strand which forms a  $\beta$ -barrel in avidin. Therefore, considering the molecular orientation dependence of the extended  $\beta$ -strand (1637 cm<sup>-1</sup>) peak intensity in avidin, it will be a minimum in BML-IRRAS and a maximum in TIRAS. It is concluded from these data that the avidin molecules are immobilized with the symmetry axis of the tetramer almost perpendicular to the substrate surface.

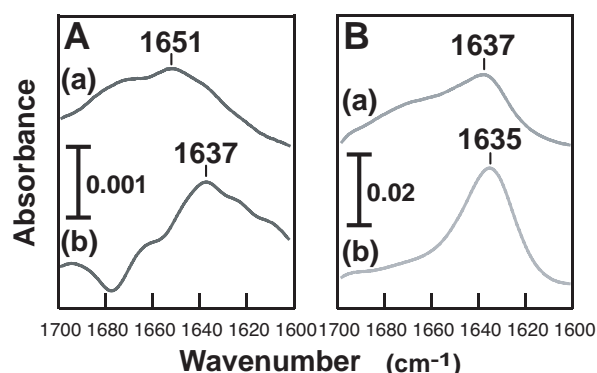


**Figure 1.** IR spectra of avidin molecules (A) covalently immobilized and (B) physisorbed on SiO<sub>2</sub>/Si surfaces. The spectra (a) and (b) are measured by BML-IRRAS and TIRAS, respectively.

### VI-E-2 Hydrogen-Atom-Induced Oxidation Reaction on Water-Terminated Si Surface, 2H+H<sub>2</sub>O/Si(100)-(2x1): A Theoretical Study

WATANABE, Hidekazu<sup>1</sup>; WANG, Zhi-Hong<sup>2</sup>; NANBU, Shinkoh; MAKI, Jun<sup>1</sup>; URISU, Tsuneo; AOYAGI, Mutsumi<sup>1</sup>; OOI, Kenta<sup>3</sup>  
(<sup>1</sup>Kyushu Univ.; <sup>2</sup>Nagoya Univ.; <sup>3</sup>AIST)

[Chem. Phys. Lett. **412**, 347–352 (2005)]

The reported oxidation reaction observed by BML-IRRAS spectra on the silicon surface system, 2H + H<sub>2</sub>O/Si(100) (Figure 1), has been studied by an *ab initio* molecular orbital method. The highest transition state is found at  $\approx +25$  kJ/mol from the reactant energy level, and the oxidation occurs easily under the experimental condition (Figure 2). The present study also accounts for the reactivity deduced from the absorption bands in the IR spectra. It is noted that the quenching of the reaction by thermal relaxation is impossible because the surface is not trapped into the metastable states located much lower in energy than the reactant.

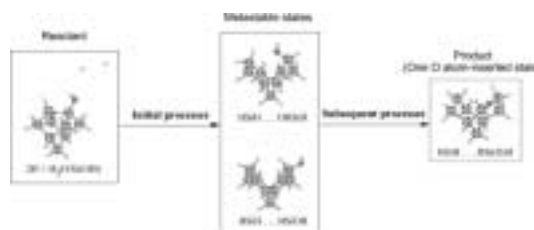


**Figure 1.** Reaction scheme of the H atom-induced oxidation on the H<sub>2</sub>O-terminated Si surface system 2H + H<sub>2</sub>O/Si(100)-(2x1), expressed by the actual conformation of the cluster model of the present work.

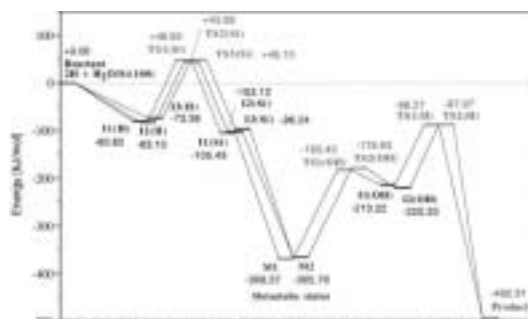


**Figure 2.** Energy diagram of the H atom-induced oxidation on the H<sub>2</sub>O-terminated Si surface system. The energies (in kJ/mol) are calculated with the HF/6-31+G\* method corrected for the ZPV.

## VI-F Integration and Characterization of Bio-Functional Materials on Silicon Surfaces

Integration of bio-functional materials on solid surfaces is an attractive research theme and important to the development of new biosensors and screening methods in which biological reactions are directly detected on electronic circuits. We have investigated the covalent immobilization of protein, lipid bilayer membrane deposition and have characterized the characteristics of these bio-functional materials using infrared absorption spectroscopy and atomic force microscopy. We also have developed a new compact fluorescence recovery after photobleaching apparatus using a semiconductor laser, which wavelength is tuned to the absorption maximum of the fluorescence dye molecules.

### VI-F-1 Fabrication of Avidin Single Molecular Layer on Silicon Oxide Surfaces and Formation of Tethered Lipid Bilayer Membranes

**TERO, Ryugo; MISAWA, Nobuo; WATANABE, Hidekazu<sup>1</sup>; YAMAMURA, Shusaku; NANBU, Shinkoh<sup>1</sup>; NONOGAKI, Youichi; URISU, Tsuneo**  
(<sup>1</sup>IMS and Kyushu Univ.)

[*e-J. Surf. Sci. Nanotech.* **3**, 237–243 (2005)]

Single molecular layer of avidin is fabricated on an atomically flat SiO<sub>2</sub> surface and characterized by atomic force microscopy (AFM) and infrared reflection absorption spectroscopy. Immobilization of avidin is performed as follows; i) ester-modification of the surface by silane-coupling agent, ii) carboxylation by hydrolysis in HCl and iii) amide bonding between the surface -COOH and -NH<sub>2</sub> in avidin molecules. Large dome structures (~60 nm height) are formed after the ester-modification, but an atomically flat surface is obtained after the hydrolysis reaction. AFM topographs and function-recognizing images (Figure 1) show that the each of avidin molecules adsorbs as a single molecule and retains the biotin-binding activity. Formation of a tethered bilayer membrane of a biotinylated phospholipid on the avidin layer is also described.

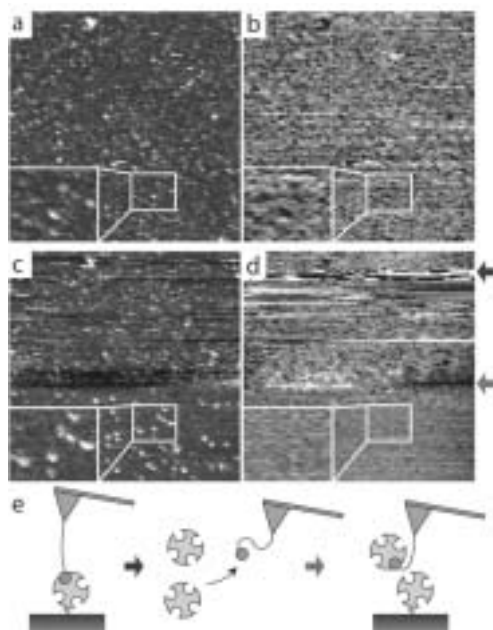


**Figure 1.** (a) AFM topograph ( $1.5 \times 1.5 \mu\text{m}^2$ ) and (b) function-recognizing image of the avidin on the SiO<sub>2</sub> surface obtained by biotinylated cantilever. (c, d) AFM topograph and function-recognizing image continuously observed after those in (a) and (b). Avidin solution was injected to the liquid phase (white arrow) and reached to the cantilever (black arrow). (e) Schematic illustration of the blocking experiment performed in (c) and (d). The size of the magnified images is  $0.28 \times 0.24 \mu\text{m}^2$ . All images are obtained in the buffer solution.

### VI-F-2 Deposition of Lipid Bilayers on OH-Density-Controlled Silicon Dioxide Surfaces

**TERO, Ryugo; URISU, Tsuneo; OKAWARA, Hiroshi<sup>1</sup>; NAGAYAMA, Kuniaki<sup>1</sup>**  
(<sup>1</sup>Okazaki Inst. Integrative Biosci.)

[*J. Vac. Sci. Technol., A* **23**, 751–754 (2005)]

We investigated the effect of the SiO<sub>2</sub> surface hydrophilicity on the formation of lipid bilayer membranes using the vesicle fusion method with atomic force microscopy, and applied the results to constructing membrane arrays. We obtained SiO<sub>2</sub> surfaces with different hydrophilicity by annealing chemically oxidized SiO<sub>2</sub> surfaces at various temperatures under an N<sub>2</sub> flow. The membrane formation rate is faster on less hydrophilic surfaces after depositing a 100-nm-filtered vesicle of dimyristoylphosphatidylcholine. Desorption of the surface hydroxyl groups causes a higher affinity between the lipid membrane and the substrate. We also describe a new method to fabricate membrane arrays using “chemical patterning.” When the surface hydroxyl groups are locally removed using a focused ion beam, a bilayer membrane selectively forms on the FIB-patterned region (Figure 1).

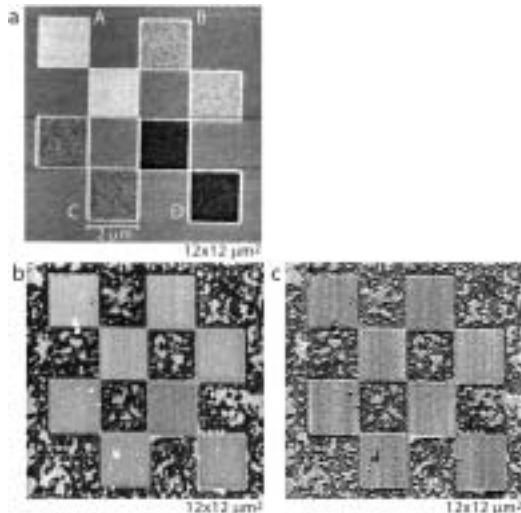


**Figure 1.** (a) AFM image ( $12 \times 12 \mu\text{m}^2$ ) and line profiles of  $2 \mu\text{m}$  square patterns made by FIB on the chemically oxidized  $\text{SiO}_2$  surface, observed in air. The  $\text{Ga}^+$  ion dosages in areas A-D were  $0.5, 1.5, 3$  and  $6 (\times 10^{15} \text{ atoms per cm}^2)$ , respectively. (b) AFM image ( $12 \times 12 \mu\text{m}^2$ ) and line profiles of the FIB-pattern (a) after deposition of DMPC bilayers, observed in a buffer solution. (c) Phase image ( $12 \times 12 \mu\text{m}^2$ ) obtained simultaneously with (b).

### VI-F-3 Supported Lipid Bilayer Formation by the Vesicle Fusion Induced by the Vesicle-Surface Electrostatic Attractive Interaction

**KIM, Yong-Hoon; RAHMAN, Md. Mashuur; ZHANG, Zhen-Long; TERO, Ryugo; URISU, Tsuneo**

The effect of the electrostatic attractive force between vesicles and the substrate surface on  $\text{Ca}^{2+}$  free supported lipid bilayer formation has been investigated by using atomic force microscopy and fluorescence microscopy. When negative-charged giant vesicles were incubated without  $\text{Ca}^{2+}$ , surface coverage of lipid bilayer was extremely low on the  $\text{SiO}_2$  surface (Figure 1a). It is well-known that the addition of  $\text{Ca}^{2+}$  induces the transformation from vesicle to the planar bilayer membrane on the solid surfaces (Figure 1b). On the other hand, in case of the positive-charged surface modified by aminopropyltrimethoxysilane, the high coverage of the lipid bilayer was obtained without adding  $\text{Ca}^{2+}$  (Figure 1c). The attractive force between the negative-charged giant vesicles and the positive-charged surface is essentially useful to induce the vesicle fusion without addition of  $\text{Ca}^{2+}$ .

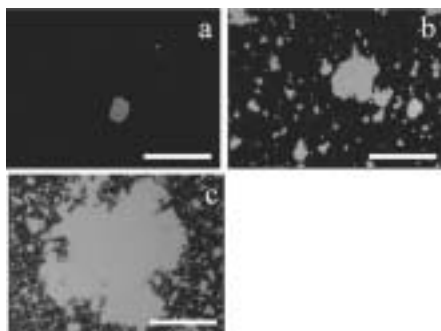


**Figure 1.** Fluorescence images of the lipid bilayer domain obtained under buffer solution: a) no addition of  $\text{Ca}^{2+}$  on the  $\text{SiO}_2$  surface, b) addition of  $\text{Ca}^{2+}$  on the  $\text{SiO}_2$  surface, and c) no addition of  $\text{Ca}^{2+}$  on the positive-charged surface. Scale bar is  $50 \mu\text{m}$ .

### VI-F-4 The Current Noise Characteristic of a Single Ion Channel

**UNO, Hidetaka; ZHANG, Zhen-Long; NAKAI, Naohito; TERO, Ryugo; NONOGAKI, Youichi; URISU, Tsuneo**

We are constructing an ion channel current measurement system using a patch clamp amplifier to investigate the lipid membrane formation, the protein reconstruction and the electrical property of membranes and proteins. The analysis of a membrane protein interaction is an important subject in the post-genome, and the development of highly efficient biosensors is demanded. We have designed a Si-based micro pore chip for ion channel current measurement (Figure 1). Teflon sheets have been generally used to make the pore, but the Si-based chip will achieve a high-speed and highly integrated biosensor.

The pore size is one of the important factors of the ion channel current measurement. The dependence of the current noise on the pore size was measured using pores with different sizes on Teflon films. The noise level single ion channel of gramicidin A in a diphytanoylphosphatidylcholine black membrane was measured in different bandwidths (Figure 2). The current noise increased with the pore size. This result shows that micronization of the pore size effectively reduce the noise level. Fabrication of Si-based chips to achieve the micron-order pore using micro-fabrication techniques is now under way.

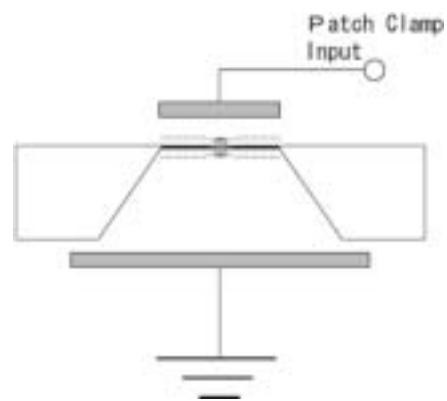


**Figure 1.** Schematic drawing of the Si-based micro pore chip for ion channel current measurement.

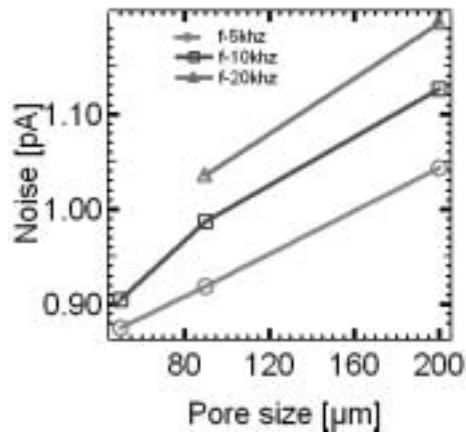


Figure 2. Channel current noise dependence on the pore size.

### VI-F-5 A New Type of Fluorescence Recovery After Photobleaching Apparatus Using both Illumination Arrangements of UV Lamp and 560 nm Laser

ZHANG, Zhen-Long; MO, Yu-Jun<sup>1</sup>; TERO, Ryugo; AOYAMA, Masaki; YOSHIDA, Hisashi; URISU, Tsuneo  
(<sup>1</sup>IMS and Henan Univ.)

A new fluorescence recovery after photobleaching (FRAP) setup was fabricated by which the FRAP curve could be directly obtained. Figure 1 shows the FRAP setup. There are two excitation light sources in the apparatus. One is an UV lamp. The other light source is a solid state laser with a wavelength of 560 nm for photobleaching and recording the fluorescence recovery process by a photomultiplier tube (PMT). In order to avoid photobleaching during the fluorescence recovery process and improve the ratio of signal to noise, a pulse-voltage generator was designed to control the laser. The pulse induced by the generator consists of two parts. Part I is continuous for photobleaching. And part II is periodic, in which the pulse width and period are 0.01 s and 1 s, respectively. The height and duration time of the two parts could be adjusted respectively according to varied samples. Two recording devices are equipped in the setup. One is a charge coupled device (CCD) connected to a computer, by which the fluorescence of the sample could be observed and the position of the photobleached spot could be confined. The other one is the photomultiplier tube (PMT) joined with an oscilloscope by which the FRAP curve could be obtained. A detection pinhole is employed to the confocal microscope before the PMT to reject the background of the fluorescence attained to PMT. Figure 2 shows the FRAP curve recorded directly by the PMT.

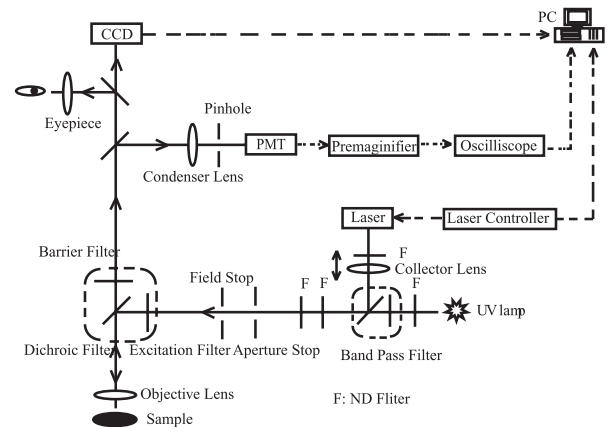


Figure 1. Schematic drawing of the new FRAP setup.

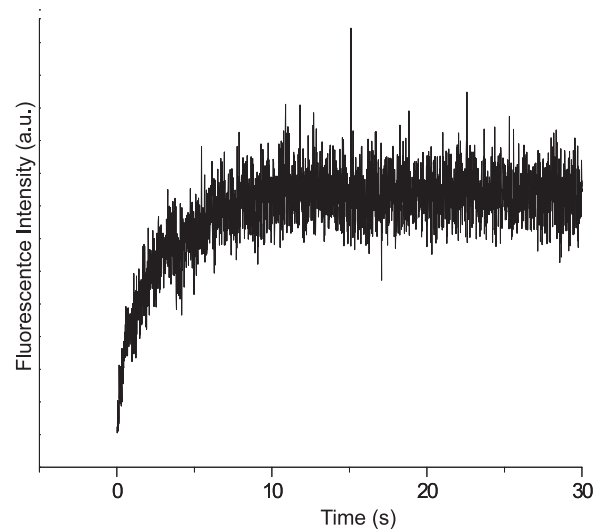


Figure 2. FRAP curve of the supported lipid bilayer (DPPC: POPS = 9:1, w/w) obtained by PMT.

## VI-G Photoionization and Photodissociation Dynamics Studied by Electron and Fluorescence Spectroscopy

Molecular photoionization is a major phenomenon in vacuum UV excitation and provides a large amount of information on fundamental electron-core interactions in molecules. Especially, neutral resonance states become of main interest, since they often dominate photoabsorption cross sections and lead to various vibronic states which are inaccessible in direct ionization. We have developed a versatile machine for two-dimensional photoelectron spectroscopy in order to elucidate dynamical aspects of superexcited states such as autoionization, resonance Auger decay, predissociation, vibronic couplings, and internal conversion. In a two-dimensional photoelectron spectrum (2D-PES), the photoelectron yield is measured as a function of both photon energy  $E_{h\nu}$  and electron kinetic energy  $E_k$  (binding energy). The spectrum, usually represented as a contour plot, contains rich information on photoionization dynamics.

Photofragmentation into ionic and/or neutral species is also one of the most important phenomena in the vacuum UV excitation. In some cases, the fragments possess sufficient internal energy to de-excite radiatively by emitting UV or visible fluorescence. It is widely accepted that fluorescence spectroscopy is an important tool to determine the fragments and to clarify the mechanisms governing the dissociation processes of diatomic and polyatomic molecules. For several years we have concentrated our energies on fluorescence spectroscopy of  $H_2O$  in the photon energy region of 15–55 eV.

### VI-G-1 Photofragmentation Mechanisms of $H_2O$ Studied by Ultraviolet Dispersed Spectroscopy

MITSUKE, Koichiro

[*J. Electron Spectrosc. Relat. Phenom.* **144-147**, 131–133 (2005)]

Fragmentation of  $H_2O$  has been studied by dispersed fluorescence spectroscopy at excitation photon energies above 20 eV.<sup>1)</sup> In dispersed spectra several vibrational bands begin to emerge below 320 nm with an appearance energy of  $h\nu \sim 30$  eV. We have assigned these peaks to  $OH(A^2\Sigma^+ \rightarrow X^2\Pi)$  transition, judging from characteristic peaks due to the  $R_1$  band heads for the  $\Delta v = v' - v'' = 0$  sequence at 306.4, 312.6, and 318.8 nm. The counter fragment of  $OH(A^2\Sigma^+)$  must be  $H^*(n)$  in the Rydberg state ( $n \geq 2$ ). The above appearance energy is much higher than the dissociation limits for the  $OH(A^2\Sigma^+) + H^*(n \geq 2)$  channels, but in good agreement with the vertical transition energies<sup>2)</sup> for the associated Rydberg states of  $H_2O$ . There exist salient hydrogen atomic lines at  $h\nu \geq 24.5$  eV constituting the Balmer series with  $n = 3-9$ , as indicated in Figure 1. The dispersed spectra reveal that there is no appreciable fluorescence signal from  $OH(A^2\Sigma^+)$  below 30 eV. Hence, the dissociation channel of  $OH(A^2\Sigma^+) + H^*(n)$  is not responsible for the Balmer emission at  $h\nu = 24.5-30$  eV. The most plausible process leading to this Balmer emis-

sion is the three-body dissociation to  $H^*(n \geq 3) + H(n = 1) + O(^3P_g)$ , which has the thermochemical threshold at 21.7 eV with  $n = 3$ .

#### References

- 1) K. Mitsuke, *J. Chem. Phys.* **117**, 8334–8340 (2002).
- 2) J. Appell and J. Durup, *Int. J. Mass Spectrom. Ion Phys.* **10**, 247–265 (1972/73).

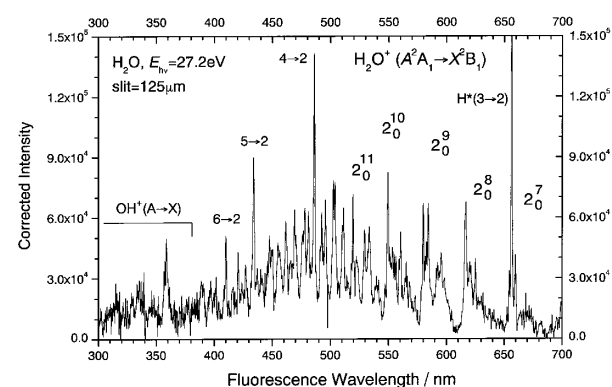


**Figure 1.** Dispersed fluorescence spectra of  $H_2O$  measured at  $h\nu = 27.2$  eV. The  $2^v_0$  symbols designate the vibrational progression in the bending mode  $\nu_2$  of the  $H_2O^+[A^2A_1(0, \nu_2', 0) \rightarrow \tilde{X}^2B_1(0, 0, 0)]$  transition. The hydrogen Balmer lines  $H^*[n^2L'_J \rightarrow 2^2L''_J]$  ( $n = 3-9$ ) are indicated by the  $(n \rightarrow 2)$  marks.

## VI-H Extreme UV Photoionization Studies of Fullerenes by Using a Grazing-Incidence Monochromator and High-Temperature Mass Spectrometer

On the beam line BL2B in UVSOR a grazing incidence monochromator has been constructed which supplies photons in the energy region from 20 to 200 eV [M. Ono, H. Yoshida, H. Hattori and K. Mitsuke, *Nucl. Instrum. Methods Phys. Res., Sect. A* **467-468**, 577–580 (2001)]. This monochromator has bridged the energy gap between

the beam lines BL3B and BL4B, thus providing for an accelerating demand for the high-resolution and high-flux photon beam from the research fields of photoexcitation of inner-valence electrons, *L*-shell electrons in the third-row atom, and *4d* electrons of the lanthanides.

Since 2001 we have tackled issues on photoabsorption and photofragmentation of fullerenes in the extreme UV. Geometrical structures and electronic properties of fullerenes have attracted widespread attention because of their novel structures, novel reactivity, and novel catalytic behaviors as typical nanometer-size materials. Moreover, it has been emphasized that the potential for the development of fullerenes to superconductors ( $T_c \sim 50$  K) and strong ferromagnetic substances is extremely high. In spite of such important species spectroscopic information is very limited in the extreme UV region, which has been probably due to difficulties in obtaining enough amount of sample. The situation has been rapidly changed in these few years, since the techniques of syntheses, isolation, and purification have been advanced so rapidly that appreciable amount of fullerenes is obtainable from several distributors in Japan.

### VI-H-1 Absolute Photoabsorption Cross Section of $C_{60}$ in the Extreme Ultraviolet

MORI, Takanori; KOU, Junkei; HARUYAMA, Yusuke<sup>1</sup>; KUBOZONO, Yoshihiro<sup>1</sup>; MITSUKE, Koichiro  
(<sup>1</sup>Okayama Univ.)

[*J. Electron Spectrosc. Relat. Phenom.* **144-147**, 243–246 (2005)]

The absolute photoabsorption cross section curve of  $C_{60}$  has been determined by means of mass spectrometry with the photon source of monochromatized synchrotron radiation of  $h\nu = 24.5\text{--}150$  eV. Description has been made on a high-temperature source of gaseous fullerenes and an efficient time-of-flight mass spectrometer. The absolute cross section curve is shown in Figure 1. The obtained cross sections were 762, 241 and 195 Mb at  $h\nu = 24.5, 90,$  and  $110$  eV, respectively with about 10% errors. The cross section curve was then normalized at  $h\nu = 25$  eV to the absolute photoabsorption cross section reported by Jaensch and Kamke,<sup>1)</sup> the most reliable data so far available in the valence excitation region of  $C_{60}$ . Accordingly, the present cross section data were altered to 407, 144 and 114 Mb at  $h\nu = 25, 90,$  and  $110$  eV, respectively.

#### Reference

1) R. Jaensch and W. Kamke, *Mol. Materials* **13**, 143 (2000).

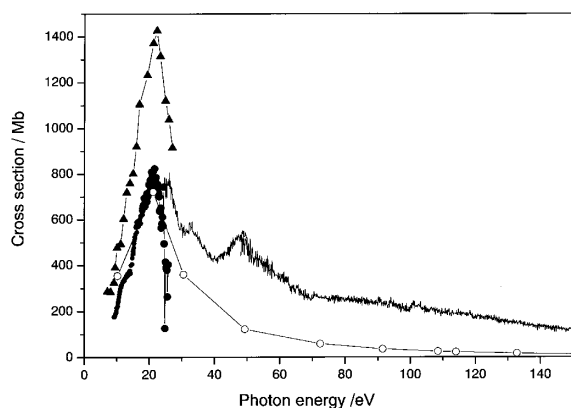


**Figure 1.** Absolute absorption cross section of  $C_{60}$  at  $h\nu = 24.5\text{--}150$  eV (solid line). The closed circles and triangles designate the previous data measured by Jaensch and Kamke and those compiled by Berkowitz, respectively. The open circles indicate the cross section of sixty carbon atoms.

### VI-H-2 Photofragmentation of $C_{60}$ in Valence Ionization

KOU, Junkei; MORI, Takanori; KUBOZONO, Yoshihiro<sup>1</sup>; MITSUKE, Koichiro  
(<sup>1</sup>Okayama Univ.)

[*J. Electron Spectrosc. Relat. Phenom.* **144-147**, 247–250 (2005)]

The yield curves for  $C_{60-2n}^+$  ( $n = 1\text{--}3$ ) produced by photoionization of  $C_{60}$  are measured in the  $h\nu$  range of 25–150 eV. The appearance energies increase with increasing  $n$ , as evidenced from Figure 1. Evaluation is made on the upper limits of the internal energies of the primary  $C_{60}^+$  above which  $C_{60-2n+2}^+$  fragments ( $n \geq 1$ ) cannot escape from further dissociating into  $C_{60-2n}^+ + C_2$ . These limits agree well with the theoretical internal energies of  $C_{60}^+$  corresponding to the threshold for the formation of  $C_{60-2n}^+$ , on the assumption that the binding energies of  $C_{60-2n+2}^+$  are equal to those proposed by Foltin *et al.*<sup>1)</sup>

#### Reference

1) M. Foltin, M. Lezius, P. Scheier and T. D. Märk, *J. Chem. Phys.* **98**, 9624 (1993).

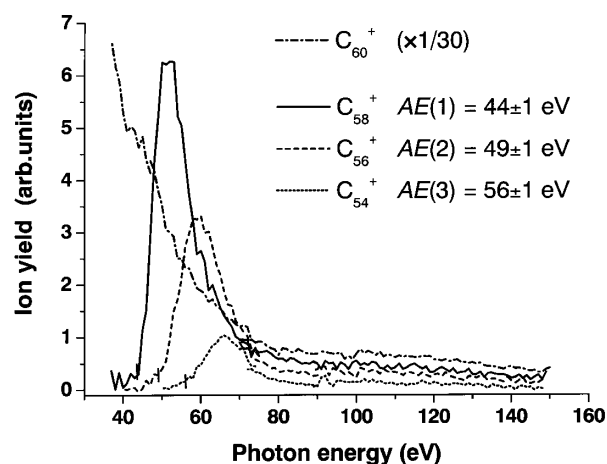


**Figure 1.** Ion yield curves of  $C_{60-2n}^+$  ( $n = 1\text{--}3$ ) and  $C_{60}^+$  ions. Every tic mark indicates the appearance energy  $AE(n)$  determined by, after subtracting an appropriate background, reading the photon energy at which the ion yield reaches 3% of the peak height of the curve.

### VI-H-3 Photofragmentation of C<sub>60</sub> in the Extreme Ultraviolet: Statistical Analysis on the Appearance Energies of C<sub>60-2n</sub><sup>z+</sup> (n ≥ 1, z = 1-3)

KOU, Junkei; MORI, Takanori; KUBOZONO, Yoshihiro<sup>1</sup>; MITSUKE, Koichiro  
(<sup>1</sup>Okayama Univ.)

[*Phys. Chem. Chem. Phys.* **7**, 119-123 (2005)]

The ion yield curves for C<sub>60-2n</sub><sup>z+</sup> (n = 1-5, z = 1-3) produced by photoionization of C<sub>60</sub> are measured in the photon energy (hν) range of 25-150 eV (see Figure 1). The appearance hν values are higher by 30-33 eV than the thermochemical thresholds for dissociative ionization of C<sub>60</sub> leading to C<sub>60-2n</sub><sup>z+</sup>. Evaluation is made on the upper limits of the internal energies of the primary C<sub>60</sub><sup>z+</sup> above which C<sub>60-2n+2</sub><sup>z+</sup> fragments (n ≥ 1) cannot escape from further dissociating into C<sub>60-2n</sub><sup>z+</sup> + C<sub>2</sub>. These upper limits agree well with the theoretical internal energies of C<sub>60</sub><sup>z+</sup> corresponding to the threshold for the formation of C<sub>60-2n</sub><sup>z+</sup> (see Figure 2). The photofragmentation of C<sub>60</sub><sup>z+</sup> is considered to be governed by the mechanism of internal conversion of the electronically excited states of C<sub>60</sub><sup>z+</sup>, statistical redistribution of the excess energy among a number of vibrational modes, and sequential ejection of the C<sub>2</sub> units.

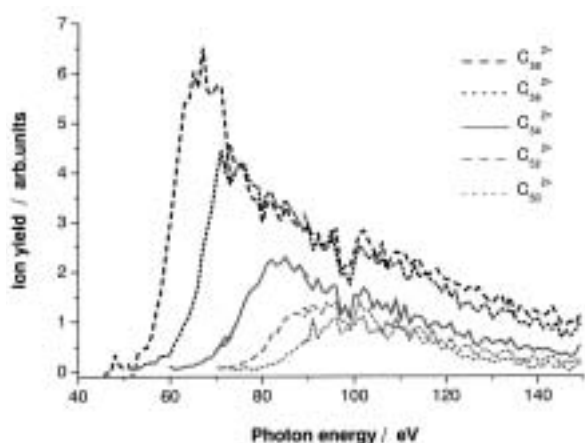


**Figure 1.** Ion yield curves of C<sub>60-2n</sub><sup>z+</sup> ions (n = 1-5) obtained from time-of-flight mass spectra.

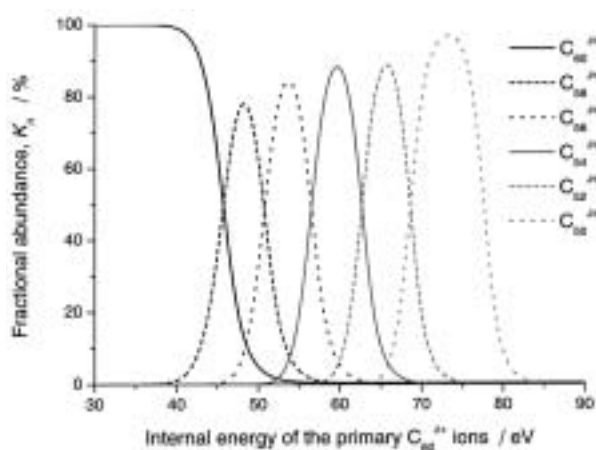


**Figure 2.** Fractional abundance curves of C<sub>60</sub><sup>z+</sup> and C<sub>60-2n</sub><sup>z+</sup> ions (n = 1-5) at 25 μs after photoionization of C<sub>60</sub> obtained by using the RRKM theory to calculate the rate constant for reaction C<sub>60-2n+2</sub><sup>z+</sup> (n ≥ 1) → C<sub>60-2n</sub><sup>z+</sup> + C<sub>2</sub>.

### VI-H-4 Fragmentation Mechanism of Highly Excited C<sub>70</sub> Cations in the Extreme Ultraviolet

MITSUKE, Koichiro; KATAYANAGI, Hideki; KOU, Junkei; MORI, Takanori; KUBOZONO, Yoshihiro<sup>1</sup>  
(<sup>1</sup>Okayama Univ.)

[*Am. Inst. Phys. Conf. Proc.* in press]

The ion yield curves for C<sub>70-2n</sub><sup>z+</sup> (n = 1-8, z = 2 and 3) produced by photoionization of C<sub>70</sub> were measured in the photon energy (hν) range of 25-150 eV. The appearance hν values were higher by ca. 34 eV than the thermochemical thresholds for dissociative ionization of C<sub>70</sub> leading to C<sub>70-2n</sub><sup>z+</sup>. Evaluation was made on the upper limits of the internal energies of the primary C<sub>70</sub><sup>z+</sup> above which C<sub>70-2n+2</sub><sup>z+</sup> fragments cannot escape from further dissociating into C<sub>70-2n</sub><sup>z+</sup> + C<sub>2</sub>. These critical internal energies agreed well with appearance internal energies of C<sub>70</sub><sup>z+</sup> theoretically obtained corresponding to the threshold for the formation of C<sub>70-2n</sub><sup>z+</sup> (see Figure 1). The photofragmentation of the parent C<sub>70</sub><sup>z+</sup> ions is considered to be governed by the mechanism of internal conversion of their electronically excited states, statistical redistribution of the excess energy among a number of vibrational modes, and sequential ejection of the C<sub>2</sub> units.

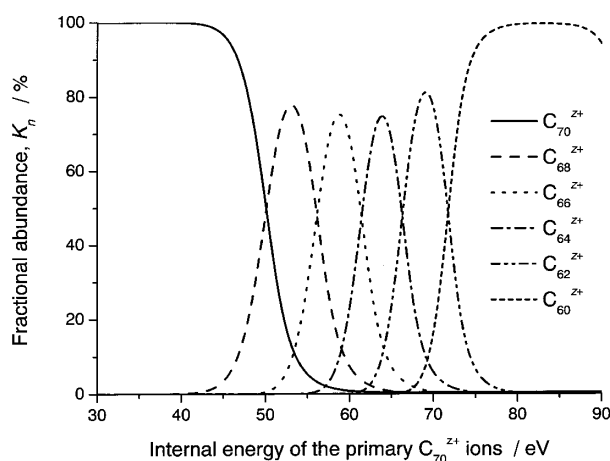


**Figure 1.** Fractional abundance curves of C<sub>70</sub><sup>z+</sup> and C<sub>70-2n</sub><sup>z+</sup> ions at 25 μs after photoionization of C<sub>70</sub> obtained by using the RRKM model to calculate the rate constants for reaction C<sub>70-2n+2</sub><sup>z+</sup> (n ≥ 1) → C<sub>70-2n</sub><sup>z+</sup> + C<sub>2</sub>.

### VI-H-5 4d → 4f Dipole Resonance of the Metal Atom Encapsulated in a Fullerene Cage: Ce@C<sub>82</sub>

MITSUKE, Koichiro; MORI, Takanori; KOU, Junkei; HARUYAMA, Yusuke<sup>1</sup>; KUBOZONO, Yoshihiro<sup>1</sup>  
(<sup>1</sup>Okayama Univ.)

[*J. Chem. Phys.* **122**, 064304 (5 pages) (2005)]

The yield curves for photoions from Ce@C<sub>82</sub> are measured by using synchrotron radiation in the photon energy range from 90 to 160 eV. Parent Ce@C<sub>82</sub><sup>z+</sup> and fragment ions C<sub>60</sub><sup>z+</sup> and C<sub>70</sub><sup>z+</sup> are observed in a mass spectrum ( $z = 1$  and  $2$ ) as shown in Figure 1. The yield curves for doubly-charged ionic species exhibit broad resonance in the photon energy region of from 120 to 140 eV which is ascribed to the  $4d \rightarrow 4f$  giant dipole resonance of the encapsulated Ce atom. The total photoabsorption cross section of Ce@C<sub>82</sub> was determined from partial photoionization cross sections for formation of the parent and fragment ions to be  $5.3^{+1.8}_{-1.1}$  and  $19.6^{+3.9}_{-3.5}$  Mb at photon energies of 110 and 130 eV, respectively.

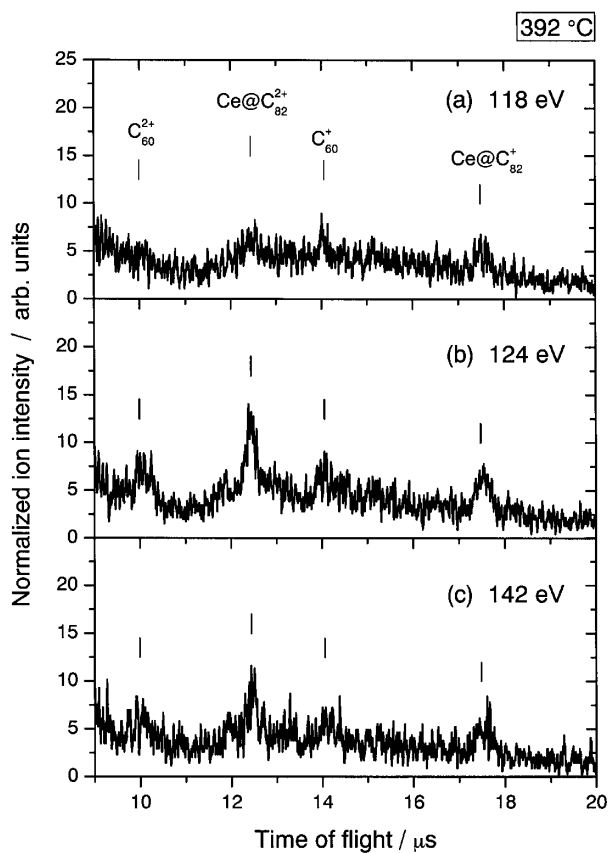


**Figure 1.** Time-of-flight mass spectra of the Ce@C<sub>82</sub><sup>z+</sup> ( $z = 1$  and  $2$ ) produced by photoionization of Ce@C<sub>82</sub> at  $h\nu = 118$ , 124, and 142 eV. The average temperature of the sample holder was set to 392 °C. Most of C<sub>60</sub><sup>z+</sup> ions arose from photoionization of C<sub>60</sub> neutrals which were desorbed from the surface of mass spectrometer.

#### VI-H-6 Photoion Yield Curves of Dy@C<sub>82</sub> in the Vacuum UV Region

MITSUKE, Koichiro; MORI, Takanori; KOU, Junkei; HARUYAMA, Yusuke<sup>1</sup>; TAKABAYASHI, Yasuhiro<sup>1</sup>; KUBOZONO, Yoshihiro<sup>1</sup>  
(<sup>1</sup>Okayama Univ.)

[*Int. J. Mass Spectrom.* **243**, 121–125 (2005)]

The photoion yield curves for Dy@C<sub>82</sub><sup>z+</sup> ( $z = 1$  and  $2$ ) from Dy@C<sub>82</sub> are measured by using synchrotron radiation in the photon energy range from 24.5 to 39.5 eV. Correction has been made to compensate the effect of transient change of the density of Dy@C<sub>82</sub> in the interaction region, with the help of the yield curve of C<sub>60</sub><sup>z+</sup> produced from C<sub>60</sub> remaining as a trace impurity in the sample. The yield of Dy@C<sub>82</sub><sup>+</sup> in Figure 1 exhibits a gradually descending curve with a flat region at 30–33 eV, similarly to the yield curve of C<sub>60</sub><sup>+</sup> from C<sub>60</sub>. The total photoabsorption cross section of Dy@C<sub>82</sub> was evaluated to be  $(1.2 \pm 0.4) \times 10^2$  Mb at the photon energy of 39.5 eV.

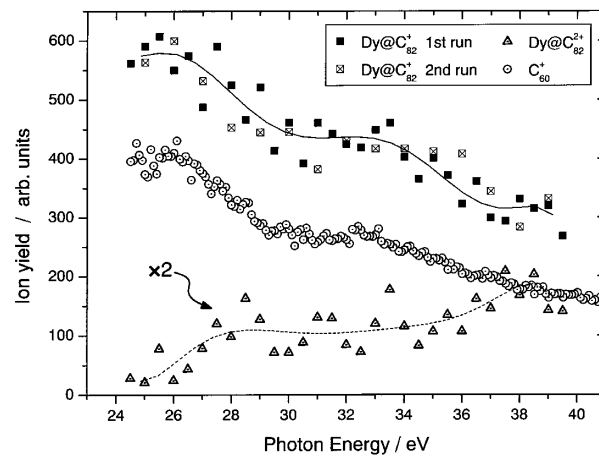


**Figure 1.** Yield curves of Dy@C<sub>82</sub><sup>+</sup> (solid square) and Dy@C<sub>82</sub><sup>2+</sup> (open triangle) produced from Dy@C<sub>82</sub> in the photon energy range of from 24.5–39.5 eV. The spectra are taken at photon energy intervals of 0.5 eV. The solid and dashed curves represent the results of the least-squares fitting to the data points of Dy@C<sub>82</sub><sup>+</sup> and Dy@C<sub>82</sub><sup>2+</sup>, respectively, using seventh order polynomial functions. The open circle symbols denote the yield curve of C<sub>60</sub><sup>+</sup> from C<sub>60</sub> measured by using the neat C<sub>60</sub> sample.

#### VI-H-7 4d–4f Dipole Resonance of the Pr Atom in an Endohedral Metallofullerene, Pr@C<sub>82</sub>

KATAYANAGI, Hideki; KAFLE, Bhim Prasad<sup>1</sup>; KOU, Junkei; MORI, Takanori; MITSUKE, Koichiro; TAKABAYASHI, Yasuhiro<sup>2</sup>; KUWAHARA, Eiji<sup>2</sup>; KUBOZONO, Yoshihiro<sup>2</sup>  
(<sup>1</sup>SOKENDAI; <sup>2</sup>Okayama Univ.)

Following our preceding paper on the photoion yield spectra of the endohedral metallofullerene, Ce@C<sub>82</sub>,<sup>1)</sup> photoion yield spectra of Pr@C<sub>82</sub> were measured in the photon energy range 100–150 eV with the help of time-of-flight mass spectrometry. Parent ions, Pr@C<sub>82</sub><sup>+</sup>, Pr@C<sub>82</sub><sup>2+</sup> and Pr@C<sub>82</sub><sup>3+</sup> were observed in the mass spectra. Photoion yield spectra of Pr@C<sub>82</sub><sup>+</sup> and Pr@C<sub>82</sub><sup>2+</sup> were obtained from the mass spectra and are shown in Figure 1. The photoion yield spectra of Pr@C<sub>82</sub><sup>2+</sup> showed a broad peak at 120–140 eV. The broad peak was assigned to the  $4d \rightarrow 4f$  giant dipole resonance of the encapsulated Pr atoms. Absolute photoabsorption cross sections of Pr@C<sub>82</sub> were evaluated from the photoion yield spectra and found to be  $23.6 \pm 6.7$  at 110 eV (off-resonance) and  $35.0 \pm 6.3$  Mb at 130 eV (on-resonance).

The enhancement of photoabsorption due to the giant resonance was comparable to that in Ce@C<sub>82</sub>. The shapes of the peaks in the Pr@C<sub>82</sub> spectra, which originated from interference effects induced by the fullerene cage, were, however, different from those in the Ce@C<sub>82</sub> spectra. This could be accounted for by that the interference effects depend on the interior metal atoms.

#### Reference

- 1) K. Mitsuke, T. Mori, J. Kou, Y. Haruyama and Y. Kubozono, *J. Chem. Phys.* **122**, 064304 (2005).

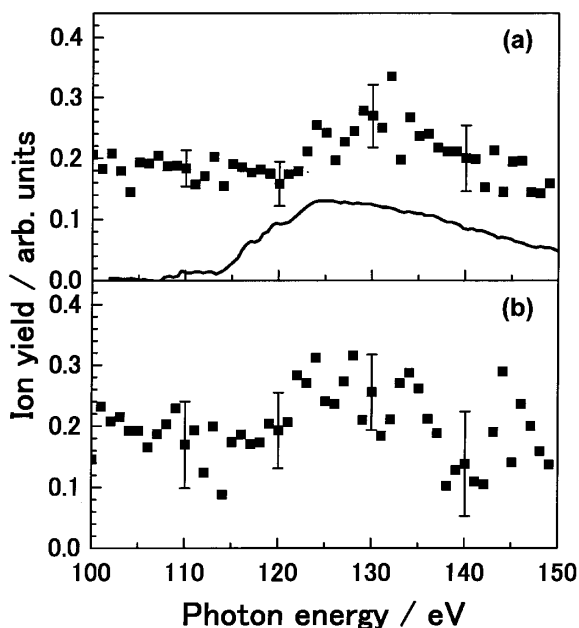


**Figure 1.** Ion yield curves of (a) Pr@C<sub>82</sub><sup>2+</sup> and (b) Pr@C<sub>82</sub><sup>+</sup>. Error bars correspond to 1 $\sigma$  of five experimental runs. Solid curve in (1) are the absorption spectra of Pr atoms. For each data, the vertical scaling is arbitrary.

## VI-I Kinetic Energy Analysis of the Fragment ions Produced from Fullerenes

When fullerenes gain enough amount of energy through photoionization processes, primarily formed ions are known to undergo decomposition into fragment ions with even numbered carbon atoms via sequential loss of C<sub>2</sub> units. We have measured the yield curves for C<sub>60-2n</sub><sup>z+</sup> from C<sub>60</sub> as a function of the internal energy of the parent C<sub>60</sub><sup>z+</sup> ions to study the mechanisms and kinetics of the sequential unimolecular reactions. These experimental yield curves have been compared with the theoretical fractional abundance curves which have been derived by employing the RRKM theory to every process of the sequential reactions: C<sub>60-2n+2</sub><sup>z+</sup> (n  $\geq$  1)  $\rightarrow$  C<sub>60-2n</sub><sup>z+</sup> + C<sub>2</sub>. To a first approximation the critical activation energies of the reactants C<sub>60-2n+2</sub><sup>z+</sup> were assumed to be equal to their binding energies for the above reactions. Indeed the experimental and theoretical curves provide almost the same appearance energies for the formation of C<sub>60-2n</sub><sup>z+</sup> (n  $\geq$  1). More reliable calculations of the rate constants of the individual reactions are needed before closer comparison between the two curves will be made. For such calculations we must know precise values of the activation energies for the reactions, together with the vibrational spectra of the transition states. This induced us to develop a new ion spectrometer for the fragment ions produced from C<sub>60</sub><sup>z+</sup> and C<sub>70</sub><sup>z+</sup>. We wish that the magnitude of the potential barriers of the reactions can be estimated from the average kinetic energy release measured by this spectrometer.

### VI-I-1 Development of the Photofragment Imaging Apparatus to Measure Scattering Distributions of the C<sub>60-2n</sub><sup>z+</sup> and C<sub>70-2n</sub><sup>z+</sup> Fragments Produced by Dissociative Photoionization of C<sub>60</sub> and C<sub>70</sub>

KAFLE, Bhim Prasad<sup>1</sup>; KATAYANAGI, Hideki;  
MITSUKE, Koichiro  
(<sup>1</sup>SOKENDAI)

In dissociative photoionization of solitary fullerenes (C<sub>60</sub>, C<sub>70</sub>), we have measured the photofragment (C<sub>60-2n</sub><sup>z+</sup>, C<sub>70-2n</sub><sup>z+</sup>) yield curves in the photon energy

range of 45–150 eV.<sup>1)</sup> From the results we concluded that the excess energy is statistically distributed among the internal degrees of freedom of the parent ions (C<sub>60</sub><sup>z+</sup>, C<sub>70</sub><sup>z+</sup>) and C<sub>2</sub> units are ejected sequentially. Moreover, the results imply that the dissociation has no barrier and that no resonant state participates in the dissociation. To clarify these implications, we designed the photofragment imaging apparatus on the basis of the time-of-flight mass spectrometer that we had constructed. From the photofragment images, we can extract the kinetic energy and angular distributions of the photofragments. These distributions reveal clearly whether there exist a barrier and/or resonance.

We adopted the Eppink-Parker type velocity focusing electrodes<sup>2)</sup> to achieve the energy resolution on the images to resolve less than 0.1 eV increase by the photofragmentation. To select a bunch of fragments having a desired mass from neighboring bunches, for example, selecting  $C_{66}^+$  from the consecutive masses such as  $C_{68}^+$ ,  $C_{66}^+$  and  $C_{64}^+$ , we designed a “mass gate” which consists of a potential switch and retarding electrodes. In order to optimize the dimensions of the setup, we performed ion trajectory simulations utilizing SIMION 7.0 software. The most suitable dimensions were obtained already and are schematically illustrated in Figure 1.

The operation principle of this setup is as follows. As long as the tube of the potential switch is kept grounded, all fragments are reflected back by the retarding electrode and do not hit an imaging detector. When an entire bunch of fragments having a desired mass enters inside the tube, the pulsed voltage is applied to the tube. The potential felt by the bunch are suddenly elevated and the bunch passes through the retarding electrode and thus hits the imaging detector.

Parts of this setup are being fabricated at the machine shop in IMS. The parts will be installed in the end-station at the beam line 2B in UVSOR. We are planning to examine the performance of the setup using  $SF_6$  as a standard sample.

#### References

- 1) J. Kou, T. Mori, Y. Kubozono and K. Mitsuke, *Phys. Chem. Chem. Phys.* **7**, 119 (2005).
- 2) A. T. J. B. Eppink and D. H. Parker, *Rev. Sci. Instrum.* **68**, 3477 (1997).

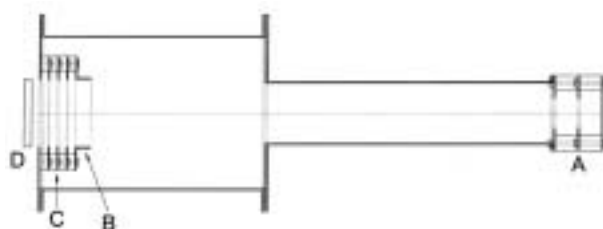


**Figure 1.** Schematic illustration of the photofragment imaging apparatus. A, repeller and extractor; B, potential switch; C, retarding electrodes; D, imaging detector.



# RESEARCH ACTIVITIES VII

## Department of Computational Molecular Science

### VII-A Computer Simulation of Quantum Systems in Condensed Phase

#### VII-A-1 A Study of Molecular Vibrational Relaxation Mechanism in Condensed Phase Based upon Mixed Quantum-Classical Molecular Dynamics: I. A Test of IBC Model for the Relaxation of a Nonpolar Solute in Nonpolar Solvent at High Density

SATO, Masahiro; OKAZAKI, Susumu

[*J. Chem. Phys.* **123**, 124508 (2005)]

In order to investigate vibrational relaxation mechanism in condensed phase, a series of mixed quantum-classical molecular dynamics calculations have been executed for non-polar solute in non-polar solvent and polar solute in polar solvent. In the first paper (Paper I), relaxation mechanism of I<sub>2</sub> in Ar, where Lennard-Jones force is predominant in the interaction, is investigated as a function of density and temperature, focusing our attention on the isolated binary collision (IBC) model. The model was originally established for the relaxation in gas phase. A key question, here, is "Can we apply the IBC model to the relaxation in the high-density fluid?" Analysing the trajectory of solvent molecule as well as its interaction with the solute, we found that collisions between them may be defined clearly even in the high-density fluid. Change of the survival probability of the vibrationally first excited state on collision was traced. The change caused by collisions with a particular solvent molecule was also traced together with the interaction between them. Each collision makes a contribution to the relaxation by a stepwise change in the probability. The analysis clearly shows that the relaxation is caused by collisions even in the high-density fluid. Difference between stepwise relaxation and continuous one found for the total relaxation in the low-density fluid and in the high-density one, respectively, was clarified to come from just the difference in frequency of the collision. The stronger the intensity of the collision is, the greater the relaxation caused by the collision is. Further, the shorter the collision time is, the greater the resultant relaxation is. The discussion is followed by the succeeding paper (Paper II), where we report that molecular mechanism of the relaxation of a polar molecule in supercritical water is significantly different from that assumed in the IBC model despite that the

density dependence of the relaxation rate showed a linear correlation with the local density of water around the solute, the linear correlation being apparently in good accordance with the IBC model. The puzzle will be solved in Paper II.

#### VII-A-2 A Study of Molecular Vibrational Relaxation Mechanism in Condensed Phase Based upon Mixed Quantum-Classical Molecular Dynamics: II. Non-Collisional Mechanism for the Relaxation of a Polar Solute in Supercritical Water

SATO, Masahiro; OKAZAKI, Susumu

[*J. Chem. Phys.* **123**, 124509 (2005)]

Mixed quantum-classical molecular dynamics method has been applied to vibrational relaxation of a hydrophilic model NO in supercritical water at various densities along an isotherm above the critical temperature. The relaxation rate was determined based on the Fermi's golden rule at each state point and showed an inverse S-shaped curve as a function of bulk density. The hydration number was also calculated as a function of bulk density based on the calculated radial distribution function, which showed a good correlation with the relaxation rate. Change of the survival probability of the solute vibrational state was analyzed as a function of time together with the trajectory of the solvent water and the interaction with it. We will show that the solvent molecule resides near the solute molecule for a while and the solvent contributes to the relaxation by the random-noise-like coulombic interaction only when it stays near the solute. After the solvent leaves the solute, it shows no contribution to the relaxation. The relaxation mechanism for this system is significantly different from the collisional one found for a nonpolar solute in nonpolar solvent in Paper I. Then, the relaxation rate is determined, on average, by the hydration number or local density of the solvent. Thus, the density dependence of the relaxation rate for the polar solute in supercritical water is apparently similar to that found for the nonpolar solute in nonpolar solvent, although the molecular process is quite different from each other.

## VII-B Molecular Dynamics Study of Classical Complex Systems

### VII-B-1 A Large-Scale Molecular Dynamics Study of Dynamic Structure Factor and Dispersion Relation of Acoustic Mode in Liquid and Supercritical Water

KOMATSU, Takahiro; YOSHII, Noriyuki; MIURA, Shinichi; OKAZAKI, Susumu

[*Fluid Phase Equilib.* **226**, 345–350 (2004)]

Large-scale and long-time molecular dynamics calculations have been performed using a fluctuating charge model TIP4P-FQ in order to investigate structure

and dynamics of supercritical water near the critical point. The calculated Ornstein-Zernike behavior of the structure factor  $S(k)$  in the small wave number region was in satisfactory agreement with experiment. The intermediate scattering function  $F(k,t)$  showed much slower decay in the supercritical water than that found in the ambient water. Further, the calculated dynamic structure factor  $S(k,\omega)$  clearly showed the existence of acoustic mode for both systems. The calculated dispersion relation for the liquid water is in good agreement with the IXS data. In the supercritical water near the critical point, the acoustic excitation propagates with a speed of about 420 m/s.

## VII-C Development of Simulation Algorithms for Quantum Many-Body Systems

### VII-C-1 Quantum Rotation of Carbonyl Sulfide Molecules in Superfluid Helium Clusters: A Path Integral Hybrid Monte Carlo Study

MIURA, Shinichi

[*J. Phys.: Condens. Matter* **17**, S3259 (2005)]

Carbonyl sulfide (OCS) molecules in superfluid helium-4 clusters have been studied by path integral hybrid Monte Carlo methods. A new technique was developed to treat quantum rotational degree of freedom of the molecules in the hybrid Monte Carlo methods, which is referred to be a “Legendre potential technique.” Then, our method was applied to the OCS-doped helium clusters. It was found that although the molecule is solvated inside the cluster, the calculated orientational correlation function exhibits free-rotor-type behavior. The estimated effective rotational constant was in good agreement with the experimental value.

## VII-D Theory of Sum Frequency Generation Spectroscopy

Visible-Infrared Sum Frequency Generation (SFG) spectroscopy has been recognized as a powerful experimental technique to optically probe a variety of interface structure. In spite of the recent technical progress in experimental measurement, its analysis remains a challenging issue in general, since experimental spectra are not often amenable to straightforward fitting or interpretation. We have proposed theoretical methods to compute SFG directly *via* molecular modeling and molecular dynamics simulation, without resorting to empirical parameterization. This work aims at developing our methods for practical applications.

### VII-D-1 Improved Computation of Sum Frequency Generation Spectrum of Water Surface

MORITA, Akihiro

The SFG spectrum of water surface was calculated with significantly improved accuracy *via* the time-

dependent formalism we have recently proposed. The revisions include molecular modeling of OH stretching region, sampling statistics, and treatment of boundary conditions. The computation was performed by fully exploiting the massive parallel environment of the NAREGI supercomputers. The calculated spectra show excellent agreement with the recent experiments, allowing us fairly detailed comparison and analysis.

## VII-E Theory of Mass Transfer Kinetics at Liquid-Vapor Interfaces

Mass transfer kinetics at liquid-vapor interfaces is of fundamental significance in atmospheric chemistry or fluid engineering, and accordingly it has been studied over a century. Understanding of the mass transfer kinetics ranges from phenomenological macroscopic or thermodynamic description to molecular-scale dynamics, and precise comparison between laboratory experiments and molecular-level simulation poses conflicting, unresolved problems. This study tries to obtain a unified picture of mass transfer kinetics, including bulk transport and surface accommodation.

### VII-E-1 Mass Accommodation Coefficient of Water

MORITA, Akihiro; SUGIYAMA, Masakazu<sup>1</sup>;  
KODA, Seiichiro<sup>2</sup>; HANSON, David R.<sup>3</sup>  
(<sup>1</sup>Univ. Tokyo; <sup>2</sup>Sophia Univ.; <sup>3</sup>NCAR)

[*J. Phys. Chem. B* **109**, 14747–14749 (2005)]

The mass accommodation coefficient  $\alpha$  of water into liquid water has been a controversial issue for a long time, whether  $\alpha$  is essentially unity or smaller than one. We have recently argued that the molecular dynamics study yield an  $\alpha$  value very close to one, and the droplet train experiments, which insists a significantly smaller than one, is in fact not inconsistent to the unit  $\alpha$ , after accurate analysis of the experimental uptake kinetics. This study strengthens our argument, and showing possible directions to resolve this conflict.

## VII-F Theoretical Studies on Electronic Structure and Dynamics of Electronically Excited States

### VII-F-1 Encapsulation of Hydrogen Atoms by Fullerenes and Carbon Nanotubes with the Use of Nonadiabatic Transition

NANBU, Shinkoh<sup>1</sup>; ISHIDA, Toshimasa<sup>2</sup>;  
NAKAMURA, Hiroki  
(<sup>1</sup>IMS and Kyushu Univ.; <sup>2</sup>Kyoto Univ.)

An aggressive usage of the non-adiabatic phenomenon is proposed. In this proposal, atomic hydrogen is encapsulated by the transmission through five-membered rings of fullerenes with the help of the non-adiabatic tunneling phenomenon. Cyclopentadienyl radical (C<sub>5</sub>H<sub>5</sub>) and corannulene (C<sub>20</sub>H<sub>10</sub>) are used to model a pentagonal moiety of fullerenes. To demonstrate the proposal, the first principles calculations are performed for the non-adiabatic dynamics on the potential energy surfaces determined by multi-reference configuration interaction (MRCI) method. The results show that the non-adiabatic transitions between ground and excited states essentially control the hydrogen atom transmission through the five-membered ring of corannulene. This transmission is found to occur more than once out of four incidences when the five carbons which surround the five-membered ring are replaced by borons. This phenomenon can be interpreted in terms of the Zhu-Nakamura semiclassical theory of non-adiabatic transition.

### VII-F-2 Ab Initio Calculated Structures of Conformers for 1,3-Dimethoxy-p-tert-Butylcalix[4] Crown-5-Ether Complexed with Potassium Cation

CHOE, Jong-In<sup>1</sup>; CHANG, Suk-Kyu<sup>1</sup>; LEE, Sik<sup>1</sup>;  
NANBU, Shinkoh<sup>2</sup>  
(<sup>1</sup>Chung-Ang Univ.; <sup>2</sup>IMS and Kyushu Univ.)

[THEOCHEM 722, 117–123 (2005)]

Stable molecular conformations were calculated for the 1,3-dimethyl ether of p-tert-butylcalix[4]crown-5-ether (**1**) in the various conformers and their potassium-ion complexes. The structures of three distinct conformation have been optimized using ab initio RHF/6-31G methods. After geometry optimizations, B3LYP/6-31+G(d,p) single point calculations of the final structures are done to include the effect of electron correlation and basis set with diffuse function and polarization function. Relative stability of free host **1** is in following order: cone (most stable) > partial-cone > 1,3-alternate conformer. For two different kinds of complexation mode, the potassium cation in the crown-5-ether moiety (*cr*) has much better complexation efficiency than in the benzene-rings (*bz*) pocket for all three kinds of conformation of host molecule **1**. The relative stability of complex (**1** + K<sup>+</sup>) in the *cr*-binding mode is in following order: cone ~ 1,3-alternate > partial-cone conformer.

### VII-F-3 Theoretical Transition Probabilities for the $\tilde{A}^2A_1-\tilde{X}^2B_1$ System of H<sub>2</sub>O<sup>+</sup> and D<sub>2</sub>O<sup>+</sup> and Related Franck-Condon Factors Based on Global Potential Energy Surfaces

TOKUE, Ikuo<sup>1</sup>; YAMASAKI, Katsuyoshi<sup>1</sup>; NANBU, Shinkoh<sup>2</sup>  
(<sup>1</sup>Niigata Univ.; <sup>2</sup>IMS and Kyushu Univ.)

[J. Theor. Comput. Chem. 4, 225–245 (2005)]

In order to elucidate the ionization dynamics, in particular the vibrational distribution, of H<sub>2</sub>O<sup>+</sup>( $\tilde{A}$ ) produced by the photoionization and the Penning ionization of H<sub>2</sub>O and D<sub>2</sub>O with He\*(2<sup>3</sup>S) atoms, the Franck-Condon factors (FCFs) were presented for the H<sub>2</sub>O( $\tilde{X}$ ) → H<sub>2</sub>O<sup>+</sup>( $\tilde{X}$ ,  $\tilde{A}$ ) ionization and the transition probabilities were presented for the H<sub>2</sub>O<sup>+</sup>( $\tilde{A}-\tilde{X}$ ) system. The FCFs were obtained by quantum vibrational calculations using the three-dimensional potential energy surfaces (PESs) of H<sub>2</sub>O( $\tilde{X}^1A_1$ ) and H<sub>2</sub>O<sup>+</sup>( $\tilde{X}^2B_1$ ,  $\tilde{A}^2A_1$ ,  $\tilde{B}^2B_2$ ) electronic states. The global PESs were determined by the multi-reference configuration interaction calculations with the Davidson correction and the interpolant moving least squares method combined with the Shepard interpolation. The obtained FCFs exhibit that the H<sub>2</sub>O<sup>+</sup>( $\tilde{X}$ ) state primarily populates the vibrational ground state since its equilibrium geometry is almost equal to that of H<sub>2</sub>O( $\tilde{X}$ ), while the bending mode ( $\nu_2$ ) is strongly enhanced for the H<sub>2</sub>O<sup>+</sup>( $\tilde{A}$ ) state; the maximums in the population of H<sub>2</sub>O<sup>+</sup> and D<sub>2</sub>O<sup>+</sup> are around  $\nu_2 = 11-12$  and  $15-17$ , respectively. These results are consistent with the distributions observed by photoelectron spectroscopy. Transition probabilities for the  $\tilde{A}-\tilde{X}$  system of H<sub>2</sub>O<sup>+</sup> and D<sub>2</sub>O<sup>+</sup> show that the bending progressions consist of the great part of the  $\tilde{A}-\tilde{X}$  emission and that combination bands from the (1,  $\nu_2' = 4-8$ , 0) state are next important.

### VII-F-4 Analysis of the Ultraviolet Absorption Cross Sections of Six Isotopically Substituted Nitrous Oxide Specie Using 3D Wavepacket Propagation

NANBU, Shinkoh<sup>1</sup>; JOHNSON, Matthew S.<sup>2</sup>  
(<sup>1</sup>IMS and Kyushu Univ.; <sup>2</sup>Univ. Copenhagen)

[J. Phys. Chem. A 108, 8905–8913 (2004)]

The ultraviolet absorption cross sections of six isotopically substituted nitrous oxide species (<sup>14</sup>N<sup>14</sup>N<sup>16</sup>O, <sup>14</sup>N<sup>14</sup>N<sup>17</sup>O, <sup>14</sup>N<sup>14</sup>N<sup>18</sup>O, <sup>14</sup>N<sup>15</sup>N<sup>16</sup>O, <sup>15</sup>N<sup>14</sup>N<sup>16</sup>O, and <sup>15</sup>N<sup>15</sup>N<sup>16</sup>O) were computed using the wavepacket propagation technique to explore the influence of excited state dynamics, transition dipole surface and initial vibrational state. Three-dimensional potential energy surfaces for the electronic states of N<sub>2</sub>O related to the experimentally observed photoabsorption between 170 and 220 nm were calculated using the *ab*

*ab initio* molecular orbital (MO) configuration interaction (CI) method. The transition dipole moment surfaces between these states were also calculated. Numerous wave packet simulations were carried out and used to calculate the temperature-dependent photodissociation cross sections of the six isotopically substituted species. The photolytic isotopic fractionation constants determined using the calculated cross sections are in good agreement with recent experiments. The results show that in addition to the effect of the changed shape of the ground state vibrational wavefunction with isotopic substitution, photodissociation dynamics play a central role in determining isotopic fractionation constants.

#### **VII-F-5 Theoretical Study of the Oxidation Reaction for the H Atom-Induced Water-Terminated Si Surface $2\text{H}+\text{H}_2\text{O}/\text{Si}(100)-(2\times 1)$**

**WATANABE, Hidekazu<sup>1</sup>; NANBU, Shinkoh<sup>1</sup>;  
WANG, Zhi-Hong<sup>2</sup>; MAKI, Jun<sup>1</sup>; URISU, Tsuneo;  
AOYAGI, Mutsumi<sup>1</sup>; OOL, Kenta<sup>3</sup>**  
(<sup>1</sup>IMS and Kyushu Univ.; <sup>2</sup>Nagoya Univ.; <sup>3</sup>AIST)

[*Chem. Phys. Lett.* **412**, 347–352 (2005)]

The reported oxidation reaction observed by BML-IRRAS spectra on the silicon surface system,  $2\text{H} + \text{H}_2\text{O}/\text{Si}(100)$ , has been studied by an *ab initio* molecular orbital method. The highest transition state is found at  $\approx +25$  kJ/mol from the reactant energy level, and the oxidation occurs easily under the experimental condition. The present study also accounts for the reactivity deduced from the absorption bands in the IR spectra. It is noted that the quenching of the reaction by thermal relaxation is impossible because the surface is not trapped into the meta-stable states located much lower in energy than the reactant.



# RESEARCH ACTIVITIES VIII

## Coordination Chemistry Laboratories

Prof. Youichi Ishii (Chuo Univ.) and Prof. Takashi Hayashi (Osaka Univ.) took the position of Laboratory of Coordination Bond from April 2005. Prof. Hiroyuki Matsuzaka (Osaka Prefecture Univ.) and Prof. Keiji Ueno (Gunma Univ.) finished their term as Adjunct Prof. of the Laboratory of Coordination Bond in March 2005. Their effort during their term is gratefully appreciated. Prof. Kazushi Mashima (Osaka Univ.) and Assoc. Prof. Masato Kurihara (Yamagata Univ.) continue the position of the Laboratory of Complex Catalyst.

### VIII-A Reduction of CO<sub>2</sub> and Oxidation of Organic Molecules Aiming at Energy Conversion between Chemical Energy and Electricity

Electro- and photochemical reduction of CO<sub>2</sub> affording methanol has become crucial issue in line with the progress of fuel energy cells using methanol. Carbon dioxide easily forms  $\eta^1$ - and  $\eta^2$ -CO<sub>2</sub> adducts by the reaction with coordinatively unsaturated low-valent metal complexes. Metal complexes with  $\eta^1$ -CO<sub>2</sub> in protic media are smoothly converted to the corresponding metal-CO ones, which undergo reductive cleavages of the M-CO bonds by accumulation of electrons at the metal centers under electrolysis conditions. A number of metal complexes have proven to catalyze reduction of CO<sub>2</sub> to CO, but the process prevents the CO ligand from hydrogenation leading to methanol formation. To achieve electrochemical reduction of the carbonyl ligand derived from CO<sub>2</sub>, we are designing new types of metal complexes that can provide electrons to carbonyl carbon through redox active ligands without increasing electron densities in the metal centers.

Metal complexes that have an ability to oxidize organic molecules at potentials more negative than the reduction potential of dioxygen enable the direct conversion from chemical energy of organic molecules to electricity. Metal-oxo complexes are possible candidates for the smooth oxidation of organic molecules, since metal-oxo species are believed to work as active centers in various metal enzymes, which oxidize various biological substrates under very mild conditions. Mechanistic understandings of the reactivity of metal-oxo species are limited because of the difficulty of selective formation of reactive M-O frameworks in artificial systems. On the other hand, high valent Ru=O complexes can be obtained by sequential electron and proton loss of the corresponding Ru-OH<sub>2</sub> ones, and have proven to work as oxidants of organic molecules. We have succeeded smooth and reversible conversion between aqua and oxo ligands on Ru-dioxolene frameworks without using any oxidants by taking advantage of dioxolene as a redox active ligand. Along this line, we have been preparing a variety of metal-aqua complexes bearing a dioxolene ligand aiming at oxidation of hydrocarbons by the corresponding metal-oxo forms.

#### VIII-A-1 Redox Behavior of New Ru-Dioxolene-Ammine Complexes and Catalytic Activity toward Electrochemical Oxidation of Alcohol under Mild Conditions

HINO, Takami; WADA, Tohru; FUJIWARA, Tetsunori; TANAKA, Koji

[*Chem. Lett.* **33**, 1596–1597 (2004)]

The new Ru-dioxolene-ammine complexes, [Ru<sup>II</sup>(NH<sub>3</sub>)(sq)(trpy)](ClO<sub>4</sub>) (**1**, sq = 3,5-di-tert-butyl-1,2-benzoquinone, trpy = 2,2':6',2''-terpyridine) and [Ru<sup>III</sup>(NH<sub>3</sub>)(sq)(trpy)](ClO<sub>4</sub>)<sub>2</sub> (**2**), were prepared. **2** is quantitatively reduced to **1** in CH<sub>3</sub>OH in the presence of base. Furthermore, both MeOH and *i*-PrOH are catalytically oxidized under the controlled potential electrolysis of **1** at 0 V (*vs.* SCE) in CH<sub>2</sub>Cl<sub>2</sub>. Both **1** and **2** lose the catalytic activity toward the oxidation of alcohols when the NH<sub>3</sub> ligand of the complexes was replaced by CH<sub>3</sub>O<sup>-</sup> during the electrolysis conditions.

#### VIII-A-2 Equilibrium of Low- and High-Spin States of Ni(II) Complexes Controlled by the Donor Ability of the Bidentate Ligands

OHTSU, Hideki; TANAKA, Koji

[*Inorg. Chem.* **43**, 3024–3030 (2004)]

Low-spin nickel(II) complexes containing bidentate ligands with modulated nitrogen donor ability, Py(Bz)<sub>2</sub> or MePy(Bz)<sub>2</sub> (Py(Bz)<sub>2</sub> = *N,N*-bis(benzyl)-*N*-[(2-pyridyl)methyl]amine, MePy(Bz)<sub>2</sub> = *N,N*-bis(benzyl)-*N*-[(6-methyl-2-pyridyl)methyl]amine), and a beta-diketonate derivative, *t*BuacacH (*t*BuacacH = 2,2,6,6-tetramethyl-3,5-heptanedione), represented as [Ni(Py(Bz)<sub>2</sub>)(*t*Buacac)](PF<sub>6</sub>) (**1**) and [Ni(MePy(Bz)<sub>2</sub>)(*t*Buacac)](PF<sub>6</sub>) (**2**) have been synthesized. In addition, the corresponding high-spin nickel(II) complexes having a nitrate ion, [Ni(Py(Bz)<sub>2</sub>)(*t*Buacac)(NO<sub>3</sub>)] (**3**) and [Ni(MePy(Bz)<sub>2</sub>)(*t*Buacac)(NO<sub>3</sub>)] (**4**), have also been synthesized for comparison. Complexes **1** and **2** have tetracoordinate low-spin square-planar structures, whereas the coordination environment of the nickel ion

in **4** is a hexacoordinate high-spin octahedral geometry. The absorption spectra of low-spin complexes **1** and **2** in a noncoordinating solvent, dichloromethane (CH<sub>2</sub>Cl<sub>2</sub>), display the characteristic absorption bands at 500 and 540 nm, respectively. On the other hand, the spectra of a CH<sub>2</sub>Cl<sub>2</sub> solution of high-spin complexes **3** and **4** exhibit the absorption bands centered at 610 and 620 nm, respectively. The absorption spectra of **1** and **2** in *N,N*-dimethylformamide (DMF), being a coordinating solvent, are quite different from those in CH<sub>2</sub>Cl<sub>2</sub>, which are nearly the same as those of **3** and **4** in CH<sub>2</sub>Cl<sub>2</sub>. This result indicates that the structures of **1** and **2** are converted from a low-spin square-planar to a high-spin octahedral configuration by the coordination of two DMF molecules to the nickel ion. Moreover, complex **1** shows thermochromic behavior resulting from the equilibrium between low-spin square-planar and high-spin octahedral structures in acetone, while complex **2** exists only as a high-spin octahedral configuration in acetone at any temperature. Such drastic differences in the binding constants and thermochromic properties can be ascribed to the enhancement of the acidity of the nickel ion of **2** by the steric effect of the *o*-methyl group in the MePy(Bz)<sub>2</sub> ligand in **2**, which weakens the Ni-N (pyridine) bond length compared with that of the non-substituted Py(Bz)<sub>2</sub> ligand in **1**.

#### VIII-A-3 A Platinum-Ruthenium Dinuclear Complex Bridged by Bis(terpyridyl)xanthene

OKAMURA, Rei; WADA, Tohru; AIKAWA, Katsuji; NAGATA, Toshi; TANAKA, Koji

[*Inorg. Chem.* **43**, 7210–7217 (2004)]

4,5-Bis(2,2':6',2''-terpyrid-4'-yl)-2,7-di-*tert*-butyl-9,9-dimethylxanthene (btpyxa) was prepared. to serve as a new bridging ligand *via* Suzuki coupling of terpyridin-4'-yl triflate and 2,7-di-*tert*-butyl-9,9-dimethylxanthene-4,5-diboronic acid. The reaction of btpyxa with either 1 equiv or an excess of PtCl<sub>2</sub>(cod) (cod = 1,5-cyclooctadiene) followed by anion exchange afforded mono- and dinuclear platinum complexes [(PtCl)(btpyxa)](PF<sub>6</sub>) (**1**)(PF<sub>6</sub>) and [(PtCl)<sub>2</sub>(btpyxa)](PF<sub>6</sub>)<sub>2</sub> (**2**)(PF<sub>6</sub>)<sub>2</sub>, respectively. The x-ray crystallography of **1**(PF<sub>6</sub>)-CHCl<sub>3</sub> revealed that the two terpyridine units in the ligand are nearly parallel to each other. Heterodinuclear [(PtCl){Ru(*t*Bu<sub>2</sub>SQ)(DMSO)}(btpyxa)](PF<sub>6</sub>)<sub>2</sub> (**4**)(PF<sub>6</sub>)<sub>2</sub>, *t*Bu<sub>2</sub>SQ = 3,5-di-*tert*-butyl-1,2-benzosemiquinone) and the monoruthenium complex [Ru(*t*Bu<sub>2</sub>SQ)(DMSO)(trpy)](PF<sub>6</sub>) (**5**)(PF<sub>6</sub>), trpy = 2,2':6',2''-terpyridine) were also synthesized. The CV of **2**<sup>2+</sup> suggests possible electronic interaction between the two Pt(trpy) groups, whereas such an electronic interaction was not suggested by the CV of **4**<sup>2+</sup> between Pt(trpy) and Ru(*t*Bu<sub>2</sub>SQ) frameworks.

#### VIII-A-4 Immobilization of a High-Valent Rhenium Complex on an Indium-Doped Tin-Oxide Electrode: Enhanced Catalytic Activity of a *trans*-Dioxorhenium(V) Complex in Electrochemical Oxidation of Alcohols

SUGIMOTO, Hideki<sup>1</sup>; TSUKUBE, Hiroshi<sup>1</sup>;

TANAKA, Koji  
(<sup>1</sup>Osaka City Univ.)

[*Eur. J. Inorg. Chem.* 4550–4553 (2004)]

A high-valent *trans*-dioxorhenium(V) complex containing pyridine ligands was successfully immobilized on an ITO (indium-doped tin-oxide) electrode. The complex formed a monolayer structure on the electrode surface and promoted electrochemical catalytic oxidation of 1-phenylethanol to acetophenone in CH<sub>2</sub>Cl<sub>2</sub>. Oxidation hardly occurred in CH<sub>2</sub>Cl<sub>2</sub> solution containing the free rhenium(V) complex. Immobilization of other high-valent metal complexes will present opportunities for design of functional electrodes with high activities.

#### VIII-A-5 Synthesis, Chemical- and Electrochemical Properties of Ruthenium(II) Complexes Bearing 2,6-Bis(2-naphthyridyl)pyridine

KOIZUMI, Take-aki; TANAKA, Koji

[*Inorg. Chim. Acta* **358**, 1999–2004 (2005)]

Ruthenium complexes with a terpyridine-analogous ligand, 2,6-bis(2-naphthyridyl)pyridine (**1**, bnp), were synthesized and their chem. and electrochemical properties studied. The structures of [Ru(bnp)(tpy)](PF<sub>6</sub>)<sub>2</sub> (**1**) and [Ru(bnp)<sub>2</sub>](PF<sub>6</sub>)<sub>2</sub> (**2**) were determined by x-ray structure analysis. The bnp localized redox potentials of **1** and **2** showed significant pos. shift by 260–290 mV relative to the analogous Ru-terpyridine complexes.

#### VIII-A-6 Synthesis, Structures and Electrochemical Properties of Ruthenium (II) Complexes Bearing Bidentate 1,8-Naphthyridine and Terpyridine Analogous (N,N,C)-Tridentate Ligands

KOIZUMI, Take-aki; TOMON, Takashi; TANAKA, Koji

[*J. Organomet. Chem.* **690**, 4272–4279 (2005)]

1,8-Naphthyridine (napy) and terpyridine-analogous (N,N,C) tridentate ligands coordinated ruthenium (II) complexes, [RuL(napy-*k*2 N,N') (dmsO)](PF<sub>6</sub>)<sub>2</sub> (**1**: L = L 1 = N''-methyl-4'-methylthio-2,2':6',4''-terpyridinium, **2**: L = L 2 = N''-methyl-4'-methylthio-2,2':6',3''-terpyridinium) were prepared and their chem. and electrochemical properties were characterized. The structure of complex **1** was determined. by X-ray crystallographic study, showing that it has a distorted octahedral coordination style. The cyclic voltammogram of **1** in DMF exhibited two reversible ligand-localized redox couples. On the other hand, the CV of **2** shows two irreversible cathodic peaks, due to the Ru–C bond of **2** containing the carbenic character. The IR spectra of **1** in CO<sub>2</sub>-saturated CH<sub>3</sub>CN showed the formation of Ru-(η<sup>1</sup>-CO<sub>2</sub>) and Ru-CO complexes under the controlled potential electrolysis of the solution at –1.44 V (*vs.* The electrochemical reduction of CO<sub>2</sub> catalyzed by **1** at

–1.54 V (vs. Fc/Fc<sup>+</sup>) in DMF –0.1 M Me<sub>4</sub>NBF<sub>4</sub> produced CO with a small amount of HCO<sub>2</sub>H.

#### VIII-A-7 Synthesis and Electrochemical Properties of Bis(bipyridine)ruthenium(II) Complexes Bearing Pyridinyl- and Pyridinylidene Ligands Induced by Cyclometalation of N'-Methylated Bipyridinium Analogs

KOIZUMI, Take-aki; TOMON, Takashi; TANAKA, Koji

[*J. Organomet. Chem.* **690**, 1258–1264 (2005)]

Ruthenium cyclometalated complexes with *N*-mono-methylated 2,4'- and 2,3'-bipyridine N,C-ligands were prepared and characterized. Reaction of [(bpy)<sub>2</sub>RuCl<sub>2</sub>] (bpy = 2,2'-bipyridine) with 1-methyl-4-(2-pyridinyl)pyridinium (HL1, PF<sub>6</sub>) and 1-methyl-3-(2-pyridinyl)pyridinium (HL<sub>2</sub>, PF<sub>6</sub>) hexafluorophosphates and AgPF<sub>6</sub> afforded cyclometalated complexes [(bpy)<sub>2</sub>Ru(L1-C3, N')][PF<sub>6</sub>]<sub>2</sub> (**1**) and carbenoid complex **I** (**2**), respectively. Structure of **2** was confirmed by low-field shift of the C4-carbon of the cyclometalated bipyridinium ligand and by x-ray structure determine. The ligand-localized redox potentials of **1** and **2** also revealed the substantial difference in the electron donating ability of both ligands.

#### VIII-A-8 Electronic Structural Changes Between Nickel(II)-Semiquinonato and Nickel(III)-Catecholato states Driven by Chemical and Physical Perturbation

OHTSU, Hideki; TANAKA, Koji

[*Chem. Eur. J.* **11**, 3420–3426 (2005)]

The selective synthesis of tetracoordinate square-planar low-spin nickel(II)-semiquinonato (NiII-SQ) and nickel(III)-catecholato (NiIII-Cat) complexes, [Ni(L)(SQ/CAT)](PF<sub>6</sub>) (L = dibenzyl(2-pyridylmethyl)amine, SQ = 3,5-di-*tert*-butylsemiquinonate, CAT = 3,5-di-*tert*-butylcatecholate), **1** and **2**, respectively, was achieved by using bidentate ligands with modulated nitrogen-donor ability to the nickel ion. The electronic structures of **1** and **2** were revealed by XPS and EPR measurements. The absorption spectra of **1** and **2** in a non-coordinating solvent, dichloromethane (CH<sub>2</sub>Cl<sub>2</sub>), are completely different from those in THF, being a coordinating solvent. As expected the gradual addition of DMF, which is also a coordinating solvent like THF, into a solution of **1** or **2** in CH<sub>2</sub>Cl<sub>2</sub> leads to color changes from blue (for **1**) and brown (for **2**) to light green, which is the same color observed for solutions of **1** or **2** in THF. Also, the same color changes are induced by varying the temp. Such spectral changes are attributable to the transformation from square-planar low-spin NiII-SQ and NiIII-Cat complexes to octahedral high-spin NiII-SQ ones, caused by the coordination of two solvent molecules to the nickel ion.

#### VIII-A-9 Synthesis and Crystal Structures of [W(3,6-Dichloro-1,2-Benzenedithiolate)<sub>3</sub>]<sup>n-</sup> (n = 1, 2) and [Mo(3,6-Dichloro-1,2-Benzenedithiolate)<sub>3</sub>]<sup>2-</sup>: Dependence of the Coordination Geometry on the Oxidation Number and Counter-Cation in Trigonal-Prismatic and Octahedral Structures

SUGIMOTO, Hideki<sup>1</sup>; FURUKAWA, Yuuki<sup>1</sup>; TARUMIZU, Makoto<sup>1</sup>; MIYAKE, Hiroyuki<sup>1</sup>; TANAKA, Koji; TSUKUBE, Hiroshi<sup>1</sup>  
(<sup>1</sup>Osaka City Univ.)

[*Eur. J. Inorg. Chem.* 3088–3092 (2005)]

The novel complexes (Et<sub>4</sub>N)<sub>2</sub>[W(bdtCl<sub>2</sub>)<sub>3</sub>] (**1a**), (Ph<sub>4</sub>P)<sub>2</sub>[W(bdtCl<sub>2</sub>)<sub>3</sub>] (**1b**), (Et<sub>4</sub>N)[W(bdtCl<sub>2</sub>)<sub>3</sub>] (**2a**), (Ph<sub>4</sub>P)[W(bdtCl<sub>2</sub>)<sub>3</sub>] (**2b**), (C<sub>5</sub>NH<sub>6</sub>)[W(bdtCl<sub>2</sub>)<sub>3</sub>] (**2c**), and (Et<sub>3</sub>NH)<sub>2</sub>[Mo(bdtCl<sub>2</sub>)<sub>3</sub>] (**3a**) (bdtCl<sub>2</sub> = 3,6-dichloro-1,2-benzenedithiolate) were prepared and characterized by X-ray crystallography, UV/Vis spectroscopic, and electrochemical methods. Versatile geometrical changes around the tungsten centers were observed. The trigonal-prismatic structure of the tungsten center in (Et<sub>4</sub>N)<sub>2</sub>[W(bdtCl<sub>2</sub>)<sub>3</sub>] (**1a**) is changed to an intermediate structure between trigonal prismatic and octahedral upon solid-state oxidation of the complex of (Et<sub>4</sub>N)[W(bdtCl<sub>2</sub>)<sub>3</sub>] (**2a**). Replacement of the counter-cation of (Et<sub>4</sub>N)<sub>2</sub>[W(bdtCl<sub>2</sub>)<sub>3</sub>] (**1a**) with Ph<sub>4</sub>P<sup>+</sup> also resulted in geometrical changes and somewhat of an octahedral contribution is included in (Ph<sub>4</sub>P)<sub>2</sub>[W(bdtCl<sub>2</sub>)<sub>3</sub>] (**1b**). However, almost the same coordination structures are present in the series of structures (Et<sub>4</sub>N)[W(bdtCl<sub>2</sub>)<sub>3</sub>] (**2a**), (Ph<sub>4</sub>P)[W(bdtCl<sub>2</sub>)<sub>3</sub>] (**2b**), and (C<sub>5</sub>NH<sub>6</sub>)[W(bdtCl<sub>2</sub>)<sub>3</sub>] (**2c**), with an oxidation no. of +5. These structures adopt an intermediate geometry between trigonal prismatic and octahedral. No geometrical change was observed upon changing the metal center from tungsten to molybdenum in [M(bdtCl<sub>2</sub>)<sub>3</sub>]<sup>2-</sup> (M = W and Mo).

#### VIII-A-10 Dioxo-Molybdenum(VI) and Mono-oxo-Molybdenum(IV) Complexes Supported by New Aliphatic Dithiolene Ligands: New Models with Weakened Mo=O Bond Characters for the Arsenite Oxidase Active Site

SUGIMOTO, Hideki<sup>1</sup>; HARIHARA, Makoto<sup>1</sup>; SHIRO, Motoo<sup>1</sup>; SUGIMOTO, Kunihisa<sup>1</sup>; TANAKA, Koji; MIYAKE, Hiroyuki<sup>1</sup>; TSUKUBE, Hiroshi<sup>1</sup>  
(<sup>1</sup>Osaka City Univ.)

[*Inorg. Chem.* **44**, 6386–6392 (2005)]

The *cis*-dioxo-molybdenum(VI) complexes, [MoO<sub>2</sub>(L(H))<sub>2</sub>]<sup>2-</sup> (**1b**), [MoO<sub>2</sub>(L(S))<sub>2</sub>]<sup>2-</sup> (**2b**), and [MoO<sub>2</sub>(L(O))<sub>2</sub>]<sup>2-</sup> (**3b**) (L(H) = cyclohexene-1,2-dithiolate, L(S) = 2,3-dihydro-2H-thiopyran-4,5-dithiolate, and L(O) = 2,3-dihydro-2H-pyran-4,5-dithiolate), with new aliphatic dithiolene ligands were prepared and investigated by infrared (IR) and UV-vis spectroscopic and electrochemical methods. The mono-oxo-molybdenum(IV) complexes, [MoO(L(H))<sub>2</sub>]<sup>2-</sup> (**1a**), [MoO(L(S))<sub>2</sub>]<sup>2-</sup> (**2a**), and [MoO(L(O))<sub>2</sub>]<sup>2-</sup> (**3a**), were further

characterized by X-ray crystal structural determinations. The IR and resonance Raman spectroscopic studies suggested that these *cis*-dioxo molybdenum(VI) complexes (**1b-3b**) had weaker Mo=O bonds than the common Mo(VI)O<sub>2</sub> complexes. Complexes **1b-3b** also exhibited strong absorption bands in the visible regions assigned as charge-transfer bands from the dithiolene ligands to the *cis*-MoO<sub>2</sub> cores. Because the oxygen atoms of the *cis*-Mo(VI)O<sub>2</sub> cores are relatively nucleophilic, these complexes were unstable in protic solvents and protonation might occur to produce Mo(VI)O(OH), as observed with the oxidized state of arsenite oxidase.

unusually large shift of the  $\nu(\text{C}=\text{O})$  band on going from [2]<sup>0</sup> (1950 cm<sup>-1</sup>) to [2]<sup>-</sup> (1587 cm<sup>-1</sup>) also supports a reversible cyclometalation driven by the bpyO-localized redox reaction.

#### VIII-A-11 Electrochemical Hydrogenation of [Ru(bpy)<sub>2</sub>(napy-*k*N)(CO)]<sup>2+</sup>: Inhibition of Reductive Ru–CO Bond Cleavage by a Ruthenacycle

TOMON, Takashi; KOIZUMI, Take-aki; TANAKA, Koji

[*Angew. Chem., Int. Ed.* **44**, 2229–2232 (2005)]

A 5-membered metallacycle (2+) hydrogenated at the 4-position of the naphthyridine ligand results from the reduction of [Ru(bpy)<sub>2</sub>(napy-*k*N)(CO)]<sup>2+</sup> (**1**<sup>2+</sup>; bpy = 2,2'-bipyridine, napy = 1,8-naphthyridine) at -1.40 V in H<sub>2</sub>O. Chemical or electrochemical oxidation of 2+ regenerates 1+ in almost quantitative yield.

#### VIII-A-12 Stabilization and Destabilization of the Ru–CO Bond During the 2,2'-Bipyridin-6-onato (bpyO)-Localized Redox Reaction of [Ru(terpy)(bpyO)(CO)](PF<sub>6</sub>)

TOMON, Takashi; KOIZUMI, Take-aki; TANAKA, Koji

[*Eur. J. Inorg. Chem.* 285–293 (2005)]

Two stereoisomers of [Ru(terpy)(bpyO)(CO)](PF<sub>6</sub>) (**1**<sup>+</sup> and **2**<sup>+</sup>; terpy = 2,2':6',2''-terpyridine, bpyO = 2,2'-bipyridin-6-onato) were prepared. The pyridonato moiety in the bpyO ligand of **1**<sup>+</sup> and **2**<sup>+</sup> is located *trans* and *cis*, respectively, to CO. Treatment of **1**<sup>+</sup> and **2**<sup>+</sup> with HPF<sub>6</sub> produced **1H**<sup>2+</sup> and **2H**<sup>2+</sup>, both of which contain bpyOH (bpyOH = 6-hydroxy-2,2'-bipyridine). The difference in the p*K*<sub>a</sub> values of **1H**<sup>2+</sup> (3.5) and **2H**<sup>2+</sup> (3.9) reflects the stronger electronic interaction between CO and the pyridonato moiety in the bpyO ligand in the *trans* position compared with that in the *cis* position. The molecular structures of **1**(PF<sub>6</sub>), **2**(PF<sub>6</sub>)H<sub>2</sub>O and **2H**(PF<sub>6</sub>)<sub>2</sub>H<sub>2</sub>O were detd. by x-ray structure analyses. **1**<sup>+</sup> and **2**<sup>+</sup> undergo one, reversible reduction at *E*<sub>1/2</sub> = -1.65 V and -1.51 V, respectively, and one irreversible reduction at *E*<sub>p,c</sub> = -2.07 and *E*<sub>p,c</sub> = -2.13 V, respectively. Both reductions are assigned to redox reactions localized at the terpy and bpyO ligands. Irreversible reduction of **1**<sup>0</sup> results from reductive cleavage of the Ru–CO bond of **1**<sup>-</sup>. However, a two-electron oxidation of **2**<sup>-</sup> almost regenerates **2**<sup>+</sup> because of the depression of the reductive Ru–CO bond cleavage of **2**<sup>-</sup> due to cyclometalation formed by an attack of O of bpyO to the C of the Ru–CO bond. An

## VIII-B Coordination Chemistry of Sterically Hindered Ligands and Multidentate Ligands, and Activation of Small Molecules

This project is focused on the design and synthesis of new ligands that are capable of supporting novel structural features and reactivity. Currently, we are investigating multidentate ligands based on aryloxy, thiolate, and amidinate. In addition, we set out to study metal complexes with sterically hindered arylthiolate ligands. Our recent efforts have been directed toward activation of small molecules.

### VIII-B-1 Synthesis of a Vanadium(III) Tris(arythiolato) Complex and Its Reactions with Azide and Azo Compounds; Formation of a Sulfenamide Complex *via* Cleavage of an Azo N=N Bond

KOMURO, Takashi; MATSUO, Tsukasa;  
KAWAGUCHI, Hiroyuki

[*Inorg. Chem.* **44**, 175–177 (2005)]

Thiolate complexes continue to attract considerable attention due to their unique chemical properties and structural diversity. Since thiolate groups meet the electronic and steric requirements necessary to stabilize a wide variety of metal complexes, they have been used as auxiliary ligands. On the other hand, thiolate complexes are known to undergo chemistry at the sulfur center, including oxidation/reduction and protonation/deprotonation, a complement to traditional chemistry for these complexes centered on the metal. In this study, we report the synthesis of a mononuclear vanadium(III) complex having the  $[\text{SC}_6\text{H}_3\text{-2,6-(SiMe}_3)_2]^- (= [\text{SAr}]^-)$  ligands.

The tris(arythiolate) vanadium(III) complex (**1**) has been synthesized in good yield. This complex is found to undergo CH activation across a V–S bond in the presence of TMEDA to give a cyclometalated species along with free arylthiol. Complex **1** behaves as a two-electron reductant toward  $\text{Ad-N}_3$ , yielding an imide complex. Treatment of **1** with azobenzene produces an imide-sulfenamide compound, in which an azo N=N bond cleavage takes place concomitant with formation of a V=N and an S–N bond. These results suggest that the reaction proceeds through a cooperative activation sequence involving both vanadium and sulfur centers.

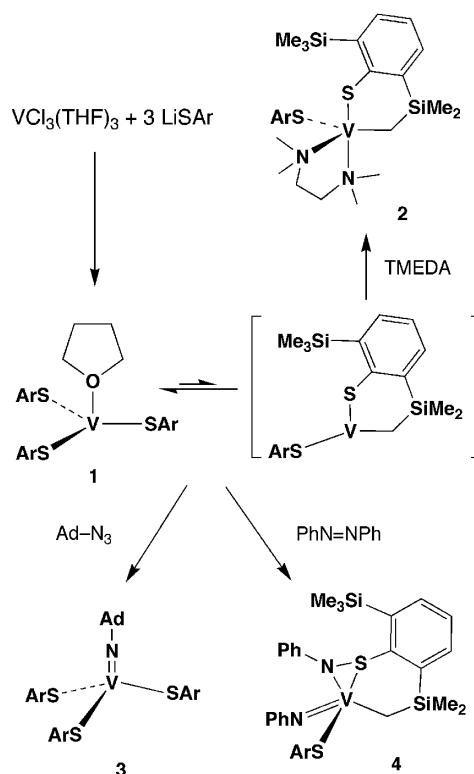


Figure 1.

### VIII-B-2 Titanium and Zirconium Complexes of Preorganized Tripodal Triaryloxy Ligands

AKAGI, Fumio; MATSUO, Tsukasa;  
KAWAGUCHI, Hiroyuki

[*J. Am. Chem. Soc.* **127**, 11936–11937 (2005)]

Multidentate ligands play an important role in coordination chemistry and catalyst design. An attractive multidentate ligand is a trianionic tetradentate ligand of the tripodal  $[\text{X}_3\text{E}]$  type ( $\text{X} = \text{N}, \text{O}, \text{S}$ ;  $\text{E} = \text{N}, \text{P}$ ), which had led to atrane molecules with unique structures and patterns of reactivity. The degree of interaction between the metal center and the neutral E atom can exert a profound influence on the reactivity of the resulting complexes. In this context, a tri(2-oxyphenyl)methane-derived system  $[\text{O}_3]^{3-}$  appears practically attractive. This ligand can coordinate to a metal in two forms, which differ mainly as a result of the relative stereochemistry at the methine carbon. Furthermore, intramolecular metalation of the somewhat acidic methine linkage in the  $[\text{O}_3]$  complexes is expected to occur quite readily, resulting in formation of 5-carbametalatranes

([O<sub>3</sub>C] complexes). In this study, tri(2-oxy-3,5-di-*tert*-butylphenyl)methane has been used to prepare titanium and zirconium complexes of the general formula [O<sub>3</sub>]MX (M = Ti, X = NEt<sub>2</sub>, Cl, CH<sub>2</sub>Ph; M = Zr, X = CH<sub>2</sub>Ph). The tripodal [O<sub>3</sub>] ligand in titanium complexes adopt the *syn*- and the *anti*-conformation, while the *syn* complex of zirconium undergoes facile C–H activation to give a 5-carbametalatrane [O<sub>3</sub>C]Zr(THF)<sub>3</sub>. Reactivity studies with these group 4 metal complexes are ongoing.

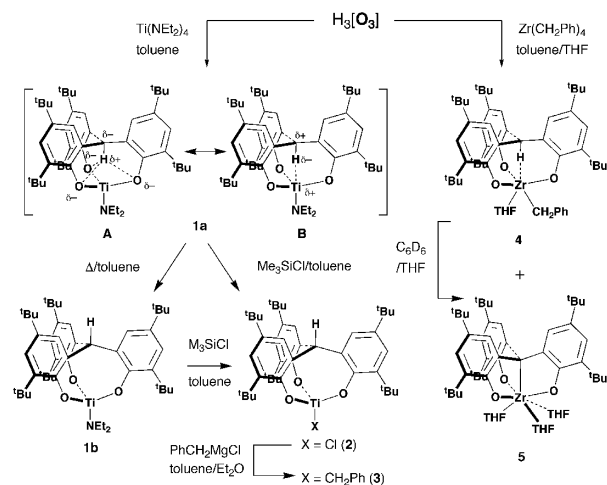


Figure 1.

## VIII-C Preparation and Properties of the Homo- and Heterometallic Clusters

This project focuses on the development of a systematic synthetic route to a series of the homo- and heterometallic clusters as templates or catalysts for new types of activation and transformation of organic, inorganic, and organometallic molecules at the well-defined multimetallic reaction sites. Especially, preparation and reactivity of dinuclear Ru(II) complexes having the bridging amido, imido, and alkoxido ligands has been extensively studied.

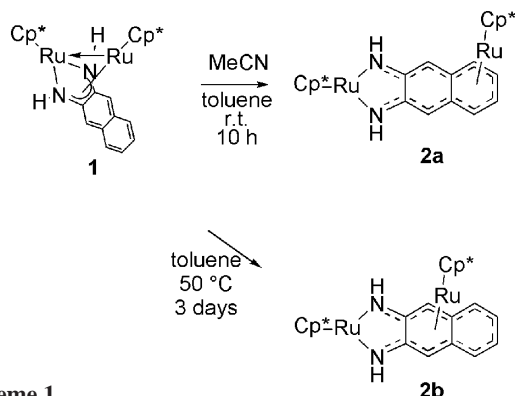
### VIII-C-1 A Dinuclear Ru(II) $\kappa^2$ -Diamido/ $\eta^6$ -Naphthalene Complex Featuring a Coordinatively Unsaturated Yet Highly $p$ -Basic ( $\eta^5$ -C<sub>5</sub>Me<sub>5</sub>)Ru Diamide Fragment

TAKEMOTO, Shin<sup>1</sup>; OSHIO, Shinya<sup>1</sup>;  
SHIROMOTO, Takayuki<sup>1</sup>; MATSUZAKA,  
Hiroyuki<sup>2</sup>

(<sup>1</sup>Osaka Pref. Univ.; <sup>2</sup>IMS and Osaka Pref. Univ.)

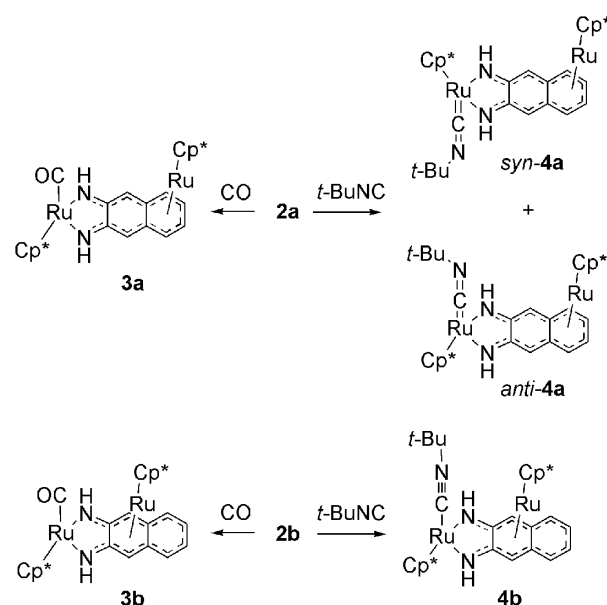
[*Organometallics* **24**, 801–804 (2005)]

Acetonitrile induced a clean isomerization of the amido-bridged diruthenium complex [(Cp\*<sub>2</sub>Ru)<sub>2</sub>{ $\mu_2$ - $\kappa^2$ : $\eta^4$ -2,3-naphthalenediamido}] (**1**) into a  $\kappa^2$ : $\eta^6$ -bonded dinuclear complex [Cp\*<sub>2</sub>Ru{ $\mu^2$ - $\kappa^2$ : $\eta^6$ -2,3-naphthalenediamido}RuCp\*] (**2a**) featuring a coordinatively unsaturated Cp\*<sub>2</sub>Ru terminal diamide fragment. Isomerization of **1** also took place on heating a solution of **1** in hexanes, toluene, or toluene-acetone at 50 °C to give another isomer **2b** selectively, in which the {Cp\*<sub>2</sub>Ru}<sup>+</sup> fragment is bound to the inner ring of the naphthalene moiety.



Scheme 1.

Structural and spectroscopic data of its carbon monoxide or *tert*-butyl isocyanide adducts indicated that the Cp\*<sub>2</sub>Ru diamide fragment can serve as a strong  $\pi$ -base.



Scheme 2.

### VIII-C-2 Dinuclear Ruthenium(II) Catecholato and 2,3-Naphthalenediolato Complexes Featuring $\kappa^2$ -Diaryloxo/ $\eta^6$ -Arene Coordination Mode

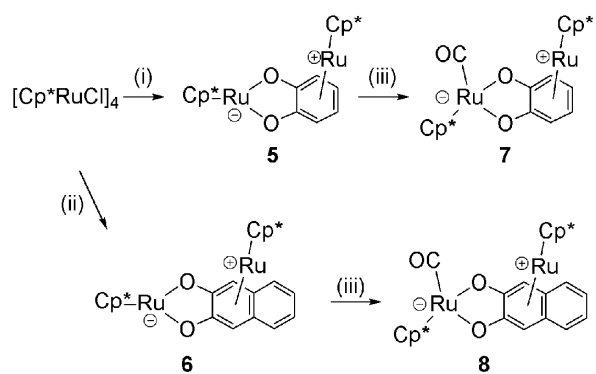
TAKEMOTO, Shin<sup>1</sup>; OGURA, Shin-ichiro<sup>1</sup>;  
KAMIKAWA, Ken<sup>1</sup>; MATSUZAKA, Hiroyuki<sup>2</sup>

(<sup>1</sup>Osaka Pref. Univ.; <sup>2</sup>IMS and Osaka Pref. Univ.)

[*Inorg. Chim. Acta* in press]

A new dinuclear ruthenium(II) catecholato complex [Cp\*<sub>2</sub>Ru( $\kappa^2$ : $\eta^6$ - $\mu_2$ -1,2-O<sub>2</sub>C<sub>6</sub>H<sub>4</sub>)RuCp\*] (**5**; Cp\* =  $\eta^5$ -C<sub>5</sub>Me<sub>5</sub>) has been prepared by the reaction of [Cp\*<sub>2</sub>RuCl]<sub>4</sub> with 2 equiv of disodium catecholate in THF. Complex **5** has a dinuclear structure, in which one of the Cp\*<sub>2</sub>Ru fragments is  $\kappa^2$ -bonded to the two oxygen atoms and the other is  $\eta^6$ -bonded to the aromatic ring. Similar treatment of [Cp\*<sub>2</sub>RuCl]<sub>4</sub> with disodium 2,3-naphthalenediolate affords an analogous  $\kappa^2$ : $\eta^6$ -bonded dinuclear complex [Cp\*<sub>2</sub>Ru( $\kappa^2$ : $\eta^6$ - $\mu_2$ -2,3-O<sub>2</sub>C<sub>10</sub>H<sub>6</sub>)RuCp\*] (**6**) with selective  $\pi$ -complexation at the oxygen-substituted naphthalene ring. The molecular structure of **6** has been determined by X-ray crystallography. The oxygen-bound ruthenium atoms in complexes **5** and **6** are coordinatively unsaturated and readily uptake 1 equiv of carbon monoxide to give the corresponding carbonyl adducts [Cp\*<sub>2</sub>Ru(CO)( $\kappa^2$ : $\eta^6$ - $\mu_2$ -1,2-O<sub>2</sub>C<sub>6</sub>H<sub>4</sub>)RuCp\*] (**7**)

and  $[\text{Cp}^*\text{Ru}(\text{CO})(\kappa^2:\eta^6-\mu_2-2,3-\text{O}_2\text{C}_{10}\text{H}_6)\text{RuCp}^*]$  (**8**), respectively.



**Scheme 1.** Preparation of Complexes. (i)  $\text{Na}_2[1,2-\text{O}_2\text{C}_6\text{H}_4]$ , (ii)  $\text{Na}_2[2,3-\text{O}_2\text{C}_{10}\text{H}_6]$ , (iii) CO (1 atm).

## VIII-D Modification of Myoglobin by Replacing the Native Heme with Metalloporphyrinoids

Functionalization of hemoproteins is one of the attractive subjects for creating a new biomaterial. Recently, we have prepared various artificial prosthetic groups and inserted them into apomyoglobin to obtain reconstituted myoglobins. For example, iron porphycene, a structural isomer of iron porphyrin, is a unique prosthetic group to modulate the myoglobin function, since the Lewis acidity of iron atom in the porphycene framework could be strong, and the  $dz^2$  orbital level of the iron atom is stabilized due to the decrease of the macrocycle symmetry compared to porphyrin framework. The physicochemical properties of iron porphycene suggest that the replacement of the native heme in myoglobin with metalloporphycene will improve or convert the myoglobin function. From this project, it is found that the reconstitution of myoglobin with an artificial prosthetic group serves as a new way to create a functionalized hemoprotein.

### VIII-D-1 Ligand Binding Properties of Myoglobin Reconstituted with Iron Porphycene: Unusual O<sub>2</sub> Binding Selectivity against CO Binding

MATSUO, Takashi<sup>1</sup>; DEJIMA, Hirohisa<sup>2</sup>; HIROTA, Shun<sup>3</sup>; MURATA, Dai<sup>2</sup>; SATO, Hideaki<sup>2</sup>; IKEGAMI, Takahiro<sup>2</sup>; HORI, Hiroshi<sup>1</sup>; HISAEDA, Yoshio<sup>2</sup>; HAYASHI, Takashi<sup>4</sup>  
(<sup>1</sup>Osaka Univ.; <sup>2</sup>Kyushu Univ.; <sup>3</sup>Kyoto Pharm. Univ.; <sup>4</sup>IMS and Osaka Univ.)

[*J. Am. Chem. Soc.* **126**, 16007–16017 (2004)]

Sperm whale myoglobin, an oxygen storage hemoprotein, was successfully reconstituted with the iron porphycene having two propionates, 2,7-diethyl-3,6,12,17-tetramethyl-13,16-bis(carboxyethyl)porphycenato-iron. The physicochemical properties and ligand binding events of the reconstituted myoglobin were investigated. The ferric reconstituted myoglobin shows the remarkable stability against acid denaturation and only a low-spin characteristic in its EPR spectrum. The Fe(III)/Fe(II) redox potential (–190 mV vs. NHE) determined by the spectroelectrochemical measurements was much lower than that of the wild-type. These results can be attributed to the strong coordination of His93 to the porphycene iron, which is induced by the nature of the porphycene ring symmetry. The O<sub>2</sub> affinity of the ferrous reconstituted myoglobin is higher by 2,600-fold than that of the wild-type, mainly due to the decrease in the O<sub>2</sub> dissociation rate, whereas the CO affinity is not so significantly enhanced. As a result, the O<sub>2</sub> affinity of the reconstituted myoglobin exceeds its CO affinity ( $M' = K_{CO}/K_{O_2} < 1$ ). The ligand binding studies on H64A mutant support the fact that the slow O<sub>2</sub> dissociation of the reconstituted myoglobin is primarily caused by the stabilization of the Fe–O<sub>2</sub>  $\sigma$ -bonding. The high O<sub>2</sub> affinity and the unique characteristics of the myoglobin with the iron porphycene indicate that the reconstitution with a synthesized heme is a useful method not only to understand the physiological function of myoglobin but also to create a tailor-made function on the protein.

### VIII-D-2 Unusual Ligand Discrimination by a Myoglobin Reconstituted with a Hydrophobic Domain-Linked Heme

SATO, Hideaki<sup>1</sup>; WATANABE, Masahito<sup>1</sup>; HISAEDA, Yoshio<sup>1</sup>; HAYASHI, Takashi<sup>2</sup>  
(<sup>1</sup>Kyushu Univ.; <sup>2</sup>IMS and Osaka Univ.)

[*J. Am. Chem. Soc.* **127**, 56–57 (2005)]

New reconstituted horse heart myoglobins possessing a hydrophobic domain at the terminal of the two heme-propionate side chains were constructed. The O<sub>2</sub> and CO bindings for the reconstituted deoxymyoglobins were examined in detail by laser flash photolysis and stopped-flow rapid mixing techniques. The artificially created domain worked as a barrier against exogenous ligand penetration into the heme pocket, whereas the bound O<sub>2</sub> was stabilized in the reconstituted myoglobin as well as in the native one. In contrast, the CO dissociation rate constant for the reconstituted myoglobin increased by 20-fold compared to the native protein, suggesting that the incorporation of the hydrophobic domain onto the heme pocket perturbs the distal site structure of the reconstituted myoglobin. As a result, the substantial ligand selectivity for the reconstituted myoglobin significantly increases in favor of O<sub>2</sub> over CO with the  $M'$  value ( $= K_{CO}/K_{O_2}$ ) of 0.88. The present work concludes that the O<sub>2</sub> selectivity of myoglobin over CO is markedly improved by chemically modifying the heme-propionates without any mutation of the amino acid residues in the distal site.

### VIII-D-3 Enhancement of Peroxidase Activity of Myoglobin Reconstituted with Iron Porphycene: Compound III Formation due to the Reaction of Ferric Myoglobin with Hydrogen Peroxide

HAYASHI, Takashi<sup>1</sup>; MURATA, Dai<sup>2</sup>; MATSUO, Takashi<sup>2</sup>; SATO, Hideaki<sup>3</sup>; HISAEDA, Yoshio<sup>3</sup>  
(<sup>1</sup>IMS and Osaka Univ.; <sup>2</sup>Osaka Univ.; <sup>3</sup>Kyushu Univ.)

[*Angew. Chem., Int. Ed.* submitted]

The replacement of native heme with an artificially created metal complex is one of the attractive studies in a series of hemoprotein modifications. However, the number of studies that demonstrate the conversion of myoglobin to peroxidase using the reconstitution by non-native prosthetic group have been quite limited. To enhance the peroxidase activity of myoglobin, we

focused on iron porphycene as a structural isomer of iron porphyrin. Reconstituted myoglobin with 2,7-diethyl-3,6,12,17-tetramethyl-13,16-dicarboxyethyl-porphycenatoiron(III) accelerated the  $\text{H}_2\text{O}_2$ -dependent oxidation of substrates such as guaiacol, thioanisole, and styrene. At pH 7.0, and 20 °C, the initial rate of the guaiacol oxidation is 10-fold faster than that observed for native myoglobin. This finding clearly suggests that the replacement of native heme with iron porphycene enhances the peroxidase activity. In addition, the guaiacol oxidation catalyzed by the reconstituted myoglobin was accelerated at the higher pH values. Moreover, the stopped-flow technique demonstrated that two reaction intermediates, the compound II-like species and compound III, formed from compound II with the excess amounts of  $\text{H}_2\text{O}_2$ , were detected in the absence of a substrate. It is the first example that compound III is formed *via* compound II in myoglobin chemistry. The enhancement of peroxidase activity and the formation of the stable compound III in myoglobin with iron porphycene could be due to the strong coordination of the Fe–His93 bond.

#### VIII-D-4 Preparation and $\text{O}_2$ Binding Study of Myoglobin Having a Cobalt Porphycene

MATSUO, Takashi<sup>1</sup>; TSURUTA, Takashi<sup>2</sup>;  
MAEHARA, Keiko<sup>2</sup>; SATO, Hideaki<sup>2</sup>; HISAEDA,  
Yoshio<sup>2</sup>; HAYASHI, Takashi<sup>3</sup>

(<sup>1</sup>Osaka Univ.; <sup>2</sup>Kyushu Univ.; <sup>3</sup>IMS and Osaka Univ.)

[*Inorg. Chem.* **44**, 9391–9396 (2005)]

Sperm whale myoglobin, an oxygen-storage hemo-protein, was reconstituted with 2,7-diethyl-3,6,12,17-tetramethyl-13,16-bis(carboxyethyl)porphycenato-cobalt(II) in order to investigate the reactivity of a cobalt porphycene in a protein matrix. Similar to the previously reported finding for the myoglobin with the iron porphycene, the reconstituted myoglobin with the cobalt porphycene was also found to have a higher  $\text{O}_2$  affinity by two orders of magnitude when compared to the myoglobin possessing cobalt protoporphyrin IX. The EPR spectra of the deoxy and oxy myoglobins having the cobalt porphycene at 77 K also have similar features to the myoglobin with cobalt protoporphyrin IX. These spectra suggest that the porphycene cobalt in the deoxy form is coordinated by one nitrogenous ligand postulated to be the imidazole ring of His93, and that the bond configuration of  $\text{Co}^{\text{II}}-\text{O}_2$  is regarded as the  $\text{Co}^{\text{III}}-\text{O}_2^{\bullet-}$  species.

## VIII-E Synthesis of Transition Metal Complexes Containing a Novel Metal-Silicon and Metal-Gallium Bonding

Synthesis of transition metal complexes with unprecedented bonds between a metal and a heavy main group element is one of current topics on inorganic chemistry. In this project, we have investigated the synthesis, structure, and reactivities of metal complexes containing organosilicon and -gallium ligands. We also synthesized a cofacial dimanganese complex, which shows catalytic activity for asymmetric oxidation of sulfides.

### VIII-E-1 Synthesis of a Cofacial Schiff-Base Dimanganese(III) Complex for Asymmetric Catalytic Oxidation of Sulfides

HIROTSU, Masakazu<sup>1</sup>; OHNO, Naoki<sup>2</sup>;  
NAKAJIMA, Takashi<sup>2</sup>; UENO, Keiji<sup>3</sup>  
(<sup>1</sup>Gunma Univ. and Osaka City Univ.; <sup>2</sup>Gunma Univ.;  
<sup>3</sup>IMS and Gunma Univ.)

[*Chem. Lett.* **34**, 848–849 (2005)]

Asymmetric oxidation of sulfides is a key reaction for synthesis of biologically active compounds with chiral sulfoxide centers. It has been reported that optically active salen-type Schiff base manganese(III) complexes are efficient catalysts for the asymmetric oxidation of sulfides. However, the enantioselectivity is not high enough for synthetic applications. Design of chiral macrocyclic dinuclear complexes would be a good approach to efficient asymmetric catalysts, because two metal centers are expected to behave cooperatively as an enantioselective Lewis acid center to catch a sulfide and an active oxidation site upon sulfoxidation, respectively. Among macrocyclic Schiff base complexes, face-to-face salen-type complex dimers have been limited to a few systems. In this work, we report a new catalyst, optically active Schiff base manganese(III) complex dimer **1** (Figure 1). The two Schiff base manganese(III) units in **1** are doubly bridged by two 9,9-dimethylxanthenediyl spacers to form a cofacial structure. The dimanganese complex catalyzed the asymmetric oxidation of methyl phenyl sulfide by iodosobenzene.

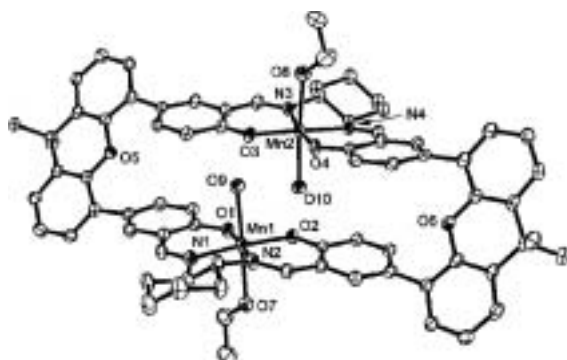


Figure 1. Molecular Structure of Dimanganese Complex 1.

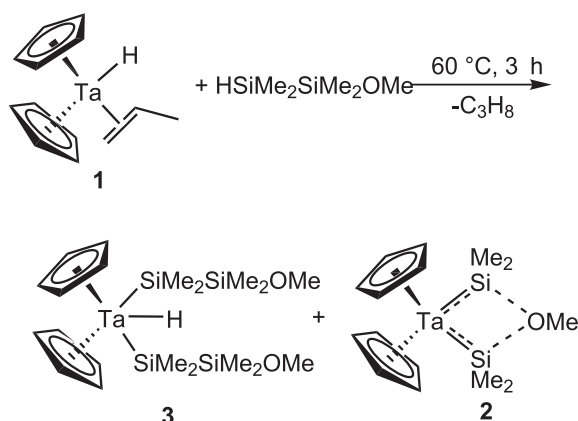
### VIII-E-2 Synthesis and Structure of a Base-Stabilized Silyl(silylene)tantalum Complex

KOSHIKAWA, Hidenori<sup>1</sup>; OKAZAKI, Masaaki<sup>2</sup>;  
MATSUMOTO, Shun-ichi<sup>1</sup>; UENO, Keiji<sup>3</sup>;

TOBITA, Hiromi<sup>1</sup>; OGINO, Hiroshi<sup>4</sup>  
(<sup>1</sup>Tohoku Univ.; <sup>2</sup>Kyoto Univ.; <sup>3</sup>IMS and Gunma Univ.;  
<sup>4</sup>Univ. Air)

[*Chem. Lett.* in press]

Over the past few decades, transition-metal silylene complexes with metal–silicon double bonds have attracted much interest as silicon analogues of carbene complexes, and as possible intermediates in various transformation reactions of organosilicon compounds. Until now, a wide variety of silylene complexes has been synthesized as not only a base-stabilized form but also a base-free form. To our best knowledge, all these examples are Fischer-type ones, in which the metal–silicon bond is polarized in a  $M^{\delta-}-Si^{\delta+}$  manner. Theoretical studies on early transition metal–silylene complexes revealed that the Schrock-type metal–silylene complex  $L_n Nb=SiR_2$  is more stable than the Fischer-type  $L_n M=SiR_2$  ( $M = Fe, Cr$ ), although silylene complexes of group 5 transition metals have not been prepared yet. We herein report the synthesis and structure of methoxy-bridged silyl(silylene)tantalum complex. Thermal reaction of  $Cp_2Ta(\eta^2-C_3H_6)$  (**1**) with  $HSiMe_2SiMe_2OMe$  in toluene at 60 °C gave  $Cp_2Ta\{SiMe_2\cdots O(Me)\cdots SiMe_2\}$  (**2**) (7%) and  $Cp_2TaH(SiMe_2SiMe_2OMe)_2$  (**3**) (8%). The former methoxy-stabilized silyl(silylene) complex was characterized by X-ray diffraction study.



### VIII-E-3 Synthesis and Structures of the First Titanium(IV) Complexes with Cyclic Tetrasiloxide Ligands: Incomplete and Complete Cage Titanosiloxanes

HIROTSU, Masakazu<sup>1</sup>; TARUNO, Shinsuke<sup>2</sup>;  
YOSHIMURA, Takashi<sup>2</sup>; UENO, Keiji<sup>3</sup>

(<sup>1</sup>Gunma Univ. and Osaka City Univ.; <sup>2</sup>Gunma Univ.;  
<sup>3</sup>IMS and Gunma Univ.)

[Submitted for publication]

Group 4 metal complexes immobilized on silica surfaces are industrially and commercially important catalysts. However, the improvement of the catalysts is hindered by the complicated surface structures, making the reaction processes unclear. Several types of siloxido complexes have been synthesized using mono-, di-, and trisiloxido ligands, which can be considered as model compounds for the heterogeneous catalysts. Cyclic tetrasiloxido ligands are also potentially useful as a silica surface model but few complexes with such ligands have been reported so far. Here we report the first titanium(IV) complexes with cyclic tetrasiloxido ligands,  $[\text{Ti}(\text{L}^1\text{H})(\text{OSiMe}_3)]_2(\text{H}_2\text{O})$  (**1**) and  $(\text{CpTiCl})_4(\text{L}^2)_2$  (**2**), which were synthesized using the all-*cis* isomer of cyclotetrasiloxanetetraols  $\text{R}_4(\text{SiO})_4(\text{OH})_4$  ( $\text{L}^1\text{H}_4$ :  $\text{R} = \text{Ph}$ ,  $\text{L}^2\text{H}_4$ :  $\text{R} = \textit{i}\text{Pr}$ ) as ligand precursors. X-ray analysis revealed that **1** is a binuclear complex with bridging siloxy and aqua ligands while **2** has a tetranuclear cage structure capped by two  $\text{L}^2$  ligands.

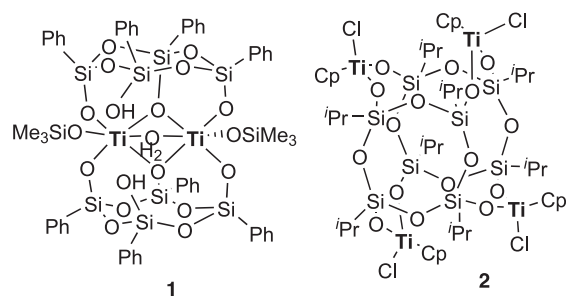


**Figure 1.** Molecular Structure of Titanium Complexes with Cyclic Tetrasiloxido Ligands.

## VIII-F Syntheses, Structures, and Reactivities of Multinuclear Transition Metal Complexes with O- and N-Donor Ligands

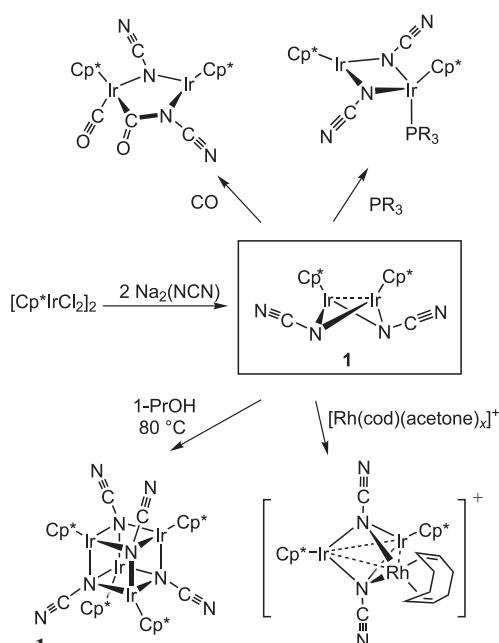
Organotransition metal complexes with O- and N-donor ligands have recently been attracting considerable attention, because they often show structures, reactivities, and physicochemical properties significantly different from those of the complexes with P- and S-donor ligands. In this project it has been disclosed that O- and N-donor ligands such as cyanamide ( $\text{NCN}^{2-}$ ) and cyclophosphate ( $\text{P}_3\text{O}_9^{3-}$ ,  $\text{P}_4\text{O}_{12}^{4-}$ ) ions act as effective bridges to form multinuclear complexes with characteristic structures. The newly synthesized diiridium complex  $[\text{Cp}^*\text{Ir}(\mu\text{-NCN-}N,N)]_2$  provides a versatile building block for the synthesis of a series of tri- and tetranuclear cyanamido clusters. On the other hand, di- and trinuclear Ti(IV) complexes built up with  $\text{Cp}^*\text{Ti}$  units and cyclophosphato ligand(s) possess novel three-dimensional structures and exhibit unique fluxional behavior in solution.

### VIII-F-1 A Cyanamido-Bridged Diiridium Complex: A Reactive Building Block for Polynuclear Cyanamido Complexes

KAJITANI, Hidenobu<sup>1</sup>; TANABE, Yoshiaki<sup>2</sup>;  
KUWATA, Shigeki<sup>3</sup>; ISHII, Youichi<sup>4</sup>  
(<sup>1</sup>Univ. Tokyo; <sup>2</sup>Chuo Univ.; <sup>3</sup>Tokyo Inst. Tech.; <sup>4</sup>IMS  
and Chuo Univ.)

[*Organometallics* **24**, 2251–2254 (2005)]

Treatment of diiridium complex  $[\text{Cp}^*\text{IrCl}_2]_2$  ( $\text{Cp}^* = \eta^5\text{-C}_5\text{Me}_5$ ) with 2 equiv of  $\text{Na}_2\text{NCN}$  has been found to afford the NCN-bridged diiridium complex  $[\text{Cp}^*\text{Ir}(\mu_2\text{-NCN-}N,N)]_2$  (**1**), which undergoes further reactions with donor molecules such as CO and phosphines. Complex **1** works as an excellent building block for the synthesis of NCN-capped multinuclear complexes: its reactions with cationic group 8–10 metal complexes such as  $[\text{Cp-Ru}(\text{MeCN})_3]^+$  ( $\text{Cp} = \eta^5\text{-C}_5\text{H}_5$ ),  $[\text{Rh}(\text{cod})(\text{acetone})_n]^+$  ( $\text{cod} = 1,5\text{-cyclooctadiene}$ ), and  $[\text{Pd}(\eta^3\text{-C}_3\text{H}_5)(\text{acetone})_n]^+$  give the heterotrimeric complexes  $[(\text{Cp}^*\text{Ir})_2(\text{ML})(\mu_3\text{-NCN})_2]^+$  ( $\text{ML} = \text{CpRu}, \text{Rh}(\text{cod}), \text{Pd}(\eta^3\text{-C}_3\text{H}_5)$ ), while the dimerization of **1** leads to the cubane-type tetrairidium complex  $[\text{Cp}^*\text{Ir}(\mu_3\text{-NCN})_4]$  (Scheme 1).



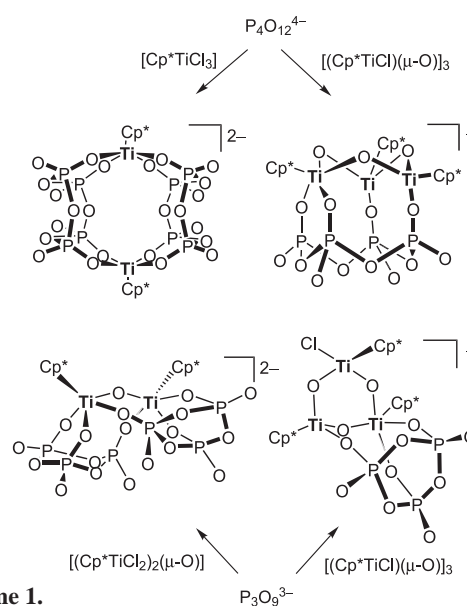
Scheme 1.

### VIII-F-2 Synthesis, Structures, and Solution Behavior of Di- and Trinuclear Titanium(IV)-Cyclophosphato Complexes

KAMIMURA, Sou<sup>1</sup>; MATSUNAGA, Tsukasa<sup>1</sup>;  
KUWATA, Shigeki<sup>2</sup>; IWASAKI, Masakazu<sup>3</sup>; ISHII,  
Youichi<sup>4</sup>  
(<sup>1</sup>Univ. Tokyo; <sup>2</sup>Tokyo Inst. Tech.; <sup>3</sup>Saitama Inst. Tech.;  
<sup>4</sup>IMS and Chuo Univ.)

[*Inorg. Chem.* **43**, 6127–6129 (2004)]

The reaction of the cyclotetraphosphate ion ( $\text{P}_4\text{O}_{12}^{4-}$ ) with  $[\text{Cp}^*\text{TiCl}_3]$  gives  $[(\text{Cp}^*\text{Ti})_2(\text{P}_4\text{O}_{12})_2]^{2-}$  where the  $\text{P}_4\text{O}_{12}$  ligands adopt a saddle conformation, while that with  $[(\text{Cp}^*\text{TiCl})_3(\mu\text{-O})_3]$  leads to  $[(\text{Cp}^*\text{Ti})_3(\mu\text{-O})_3(\text{P}_4\text{O}_{12})]^-$  containing a crown form  $\text{P}_4\text{O}_{12}$  ligand; both products feature their unique cage structures. The latter complex is fluxional in solution, and the variable temperature  $^1\text{H}$  NMR study has revealed that the  $\text{Ti}_3\text{O}_3$  unit is rotating on the  $\text{P}_4\text{O}_{12}$  platform. On the other hand, the reactions of the cyclotriphosphate ion ( $\text{P}_3\text{O}_9^{3-}$ ) with  $[(\text{Cp}^*\text{TiCl}_2)_2(\mu\text{-O})]$  and  $[(\text{Cp}^*\text{TiCl})_3(\mu\text{-O})_3]$  afford  $[(\text{Cp}^*\text{Ti})_2(\mu\text{-O})(\text{P}_3\text{O}_9)_2]^{2-}$  and  $[(\text{Cp}^*\text{Ti})_3(\mu\text{-O})_3\text{Cl}(\text{P}_3\text{O}_9)]^-$ , respectively, and in both cases the  $\text{P}_3\text{O}_9$  ligands bridge the two titanium centers with an  $\eta^2:\eta^1$  coordination mode (Scheme 1).



Scheme 1.

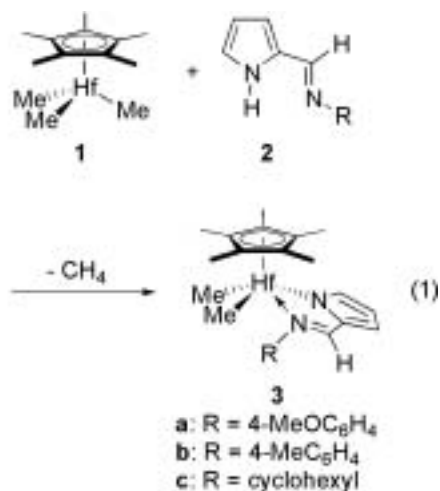
## VIII-G Organometallic Chemistry: Synthesis, Characterization, and Catalysts

### VIII-G-1 Living Polymerization of 1-Hexene Catalyzed by Half-Metallocene Dimethyl Complexes of Hafnium with Bidentate *N*-Substituted Iminopyrrolyl Ligands

MASHIMA, Kazushi<sup>1</sup>; YASUMOTO, Takahiro<sup>2</sup>;  
YAMAGATA, Tsuneaki<sup>2</sup>  
(<sup>1</sup>IMS and Osaka Univ.; <sup>2</sup>Osaka Univ.)

[*Organometallics* **24**, 3375–3377 (2005)]

We have been interested in iminopyrrolyl ligands as a unique unsymmetrical monoanionic ligand capable of supporting non-metallocene type group 4 metal complexes. As an extension of our continuous interest in the iminopyrrolyl ligand system. We here report the syntheses of half-metallocene type hafnium dimethyl complexes with iminopyrrolyl ligand and their catalytic performance for 1-hexene polymerization upon treated with  $[\text{Ph}_3\text{C}][\text{B}(\text{C}_6\text{F}_5)_4]$ , giving monodispersed poly(1-hexene) with high isotacticity (up to  $[\text{mmmm}] = 90\%$ ). These complexes were the first hafnium catalyst precursors for stereospecific living polymerization of  $\alpha$ -olefin. Non-bridged half-metallocene dimethyl hafnium complexes **3a-c** with *N*-substituted iminopyrrolyl ligands **2a-c** have been synthesized and characterized by NMR spectroscopy as well as X-ray analyses for **3a** and **3b**. These complexes were found to be active catalysts for isospecific living polymerization of 1-hexene upon treated with  $[\text{Ph}_3\text{C}][\text{B}(\text{C}_6\text{F}_5)_4]$  below 0 °C.

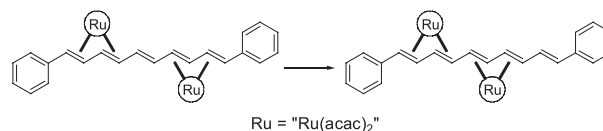


### VIII-G-2 Unique Preferential Conformation and Movement of Ru(acac)<sub>2</sub> Fragment(s) Coordinated in an $\eta^4$ -*s-trans* Fashion to All Diene Unit(s) of $\alpha,\omega$ -Diphenylpolyenes

MASHIMA, Kazushi<sup>1</sup>; FUKUMOTO, Hiroki<sup>2</sup>  
(<sup>1</sup>IMS and Osaka Univ.; <sup>2</sup>TITech)

[*Organometallics* **24**, 3932–3938 (2005)]

$\alpha,\omega$ -Diphenylpolyene complexes bearing bis(acetylacetonato)ruthenium(II) of general formula  $\text{Ru}_n(\text{acac})_{2n}$  (polyene) [**1**:  $n = 1$ , polyene = 1,4-diphenylbuta-1,3-diene; **2**:  $n = 1$ , polyene = 1,6-diphenylhexa-1,3,5-triene; **3**:  $n = 2$ , polyene = 1,8-diphenylocta-1,3,5,7-tetraene; **4** and **6**:  $n = 2$ , polyene = 1,10-diphenyldeca-1,3,5,7,9-pentaene; **5**:  $n = 3$ , polyene = 1,12-diphenyl-dodeca-1,3,5,7,9,11-hexaene] were prepared by reaction of  $\text{Ru}(\text{acac})_3$  with the corresponding polyene in the presence of excess amounts of zinc dust. The  $\text{Ru}(\text{acac})_2$  fragment(s) in **1–6** coordinated in an  $\eta^4$ -*s-trans* fashion to each diene unit of the polyene ligands. The  $\Delta$ - $\text{Ru}(\text{acac})_2$  unit and its counter part  $\Lambda$ - $\text{Ru}(\text{acac})_2$  were assigned to coordinate to the *re*-face and the *si*-face of the diene unit, respectively, on the basis of the crystal structure of complexes **1** and **2** together with the previously reported **3**. The hexaene complex **5** was assumed to have the structure of *anti,anti*- $\Delta,\Lambda,\Delta$ -**5a** and its enantiomer *anti,anti*- $\Lambda,\Delta,\Delta$ -**5b**. Pentaene complex **4**, in which two ' $\text{Ru}(\text{acac})_2$ ' fragments were bound to C(1)–C(4) and C(7)–C(10) of the pentaene ligand, was isolated. The  $\text{Ru}(\text{acac})_2$  fragment of **4** moved over the pentaene in  $\text{CHCl}_3$  to settle in the thermodynamically stable **6**, in which two ruthenium fragments located at adjacent positions. Metal migration process, as monitored by decrease of **4**, was found to be first-order for **4**, giving activation parameters ( $\Delta G^\ddagger$  (25 °C) =  $22.5 \pm 0.2$  kcal/mol;  $\Delta S^\ddagger$  (25 °C) =  $-14.2 \pm 0.8$  cal mol<sup>-1</sup> K<sup>-1</sup>). The negative value of  $\Delta S^\ddagger$  suggested that the migration of the  $\text{Ru}(\text{acac})_2$  fragment is an intramolecular process.



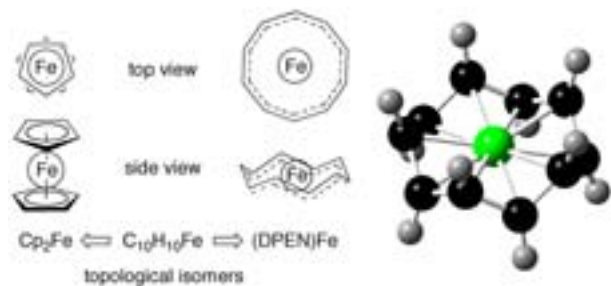
### VIII-G-3 A Topological Isomer of Ferrocene: Theoretical Approach for Transition Metal Complexes with Conjugated All Trans Cyclodecapentaene

MASHIMA, Kazushi<sup>1</sup>; OHSHIMA, Takashi<sup>2</sup>;  
NAKAMURA, Akira<sup>3</sup>  
(<sup>1</sup>IMS and Osaka Univ.; <sup>2</sup>Osaka Univ.; <sup>3</sup>OM Res.)

[*J. Organomet. Chem.* **690**, 4375–4377 (2005)]

Since the discovery of ferrocene in early 1950s, organometallic chemistry of transition metals has been developed extensively in terms of the fundamental bonding, physical properties, and attracting applications as catalysts as well as source for materials. We anticipate that it may be possible to create cyclic polyene coordinating systems, the smallest one being all-trans cyclodeca-1,3,5,7,9-pentaene (DPEN). Thus, by using DFT computation [B3LYP/6-311+G(2d,p) and BP86 level], we examined the capability of all-trans DPEN as a ligand for transition metals. We found that iron(0) and

some other transition metals coordinated by DPEN are stable molecules and unique topological isomers of the corresponding metallocene complexes.



At first, we calculated Fe(0)-DPEN complex. The shape and levels of some orbital interactions including HOMO and LUMO of the iron complex indicate the strong bonding interaction between Fe(0) and DPEN through the aromatic  $p\pi$ -electrons of DPEN. Thus, we found on the basis of DFT calculation that DPEN is a potential ligand to hold some transition metals in its center. These complexes are unique topological isomers of ferrocene,  $\text{Fe}(\text{C}_5\text{H}_5)_2$ , and metallocene derivatives. Computational estimation of general properties of the DPEN complexes is of our interest.

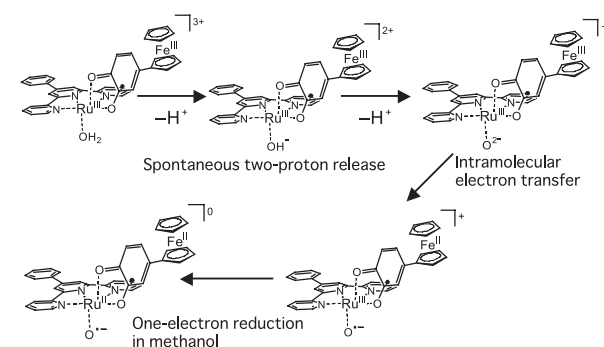
## VIII-H Development of Metal-Conjugated Multi-Electron Redox Systems in Metal-Dioxolene Complexes and Activation of Water Ligand

Dioxolenes act as a versatile electron-acceptor and/or -donor through the reversible two-electron redox reaction among three oxidation forms, catechol (Cat), semiquinone (SQ), and quinone (Q). The *o*-dioxolene ligands offer a wide range of the metal complexes showing a unique metal-conjugated intramolecular electron transfer, that is valence tautomerization. Development of the metal-conjugated multi-electron redox systems is one of the most essential in order to design electrocatalysts and electronic molecular devices. The ruthenium-dioxolene complexes exhibit the reversible two-electron redox behavior and each oxidation form has been recognized as the metal-conjugated resonance hybrids, on account of the accessible redox potentials between the metal center and the dioxolene ligands. A new three-electron redox system could be constructed in ruthenium complexes containing a ferrocene-attached dioxolene, leading to metal-conjugated resonance hybrids among the three redox sites, metal, dioxolene, and ferrocene. The ruthenium-dioxolene framework successfully activates its water ligand *via* the intramolecular electron transfer to produce  $\text{Ru}^{\text{II}}\text{-O}^{\bullet-}$  species, accompanied by compelling proton release from  $\text{Ru}^{\text{III}}\text{-OH}_2$  using an additive strong base. In this study, we prepared a similar  $\text{Ru}\text{-OH}_2$  complex bearing the ferrocene-attached dioxolene. In the three-electron redox system, the water molecule is activated through spontaneous two-proton release and the intramolecular electron transfer to the ruthenium-dioxolene-ferrocene framework.

### VIII-H-1 Synthesis of a $\text{Ru}\text{-OH}_2$ Complex Bearing a Ferrocene-Attached Catecholato Ligand and Its Spontaneous Proton Release

KURIHARA, Masato<sup>1</sup>; OHIZUMI, Tomohiro<sup>2</sup>;  
SAKAMOTO, Masatomi<sup>2</sup>; WADA, Tohru;  
TANAKA, Koji  
(<sup>1</sup>IMS and Yamagata Univ.; <sup>2</sup>Yamagata Univ.)

A ruthenium-acetato-terpyridine complex containing 4-ferrocenyl-1,2-benzoquinone,  $[\text{Ru}^{\text{II}}(\text{OAc})(\text{SQ-Fc})(\text{ph-terpy})]$  (**1**) was synthesized. Complex **1** showed the reversible three-electron redox behavior, derived from  $(\text{1}^-/\text{1})$ ,  $(\text{1}^+/\text{1})$ ,  $(\text{1}^+/1^{2+})$  redox couples. The one-electron oxidation form,  $[\text{Ru}^{\text{III}}(\text{OAc})(\text{SQ-Fc})(\text{ph-terpy})]\text{CF}_3\text{SO}_3$  (**1**<sup>+</sup>) was isolated as a blue precipitate from a dichloromethane solution of **1** on addition of 1 equivalent of  $\text{AgCF}_3\text{SO}_3$  in the yield of 78%. Our attempt to prepare the two-electron oxidation form,  $[\text{Ru}^{\text{III}}(\text{OAc})(\text{SQ-Fc}^+)(\text{ph-terpy})](\text{CF}_3\text{SO}_3)_2$  (**1**<sup>2+</sup>) has been unsuccessful, because **1**<sup>2+</sup> is labile under the synthetic conditions. The hydrolytic exchange of **1**<sup>+</sup> from the acetate to an aquo ligand was carried out using  $\text{HBF}_4$  in an acetone-water solution. The isolated hydrolysis form, **2** was characterized by ESI-mass and elemental analyses. On the basis of the elemental analysis, **2** consists of 90% of a  $\text{Ru}\text{-OH}$  form,  $[\text{Ru}^{\text{III}}(\text{OH})(\text{SQ-Fc}^+)(\text{ph-terpy})](\text{BF}_4)_2$  and 10% of a  $\text{Ru}\text{-O}$  form,  $[\text{Ru}^{\text{III}}(\text{O})(\text{SQ-Fc}^+)(\text{ph-terpy})](\text{BF}_4)$ . The mass signals due to the acetate complex completely disappeared in the ESI-mass spectrum of an acetone solution of **2**. The main signal at 719 *m/z* and the isotope pattern are ascribable to a  $[\text{Ru}^{\text{III}}(\text{O})(\text{SQ-Fc}^+)(\text{ph-terpy})]^+$ . These results suggest that the  $\text{Ru}\text{-OH}_2$  and  $\text{Ru}\text{-OH}$  forms are changed into the  $\text{Ru}\text{-O}$  form through spontaneous two-proton release as an only stable state in the solution, because of the strong electron attraction of  $\text{Ru}^{\text{III}}\text{-SQ-Fc}^+$  framework (Scheme 1). The  $\text{Ru}\text{-O}$  complex,  $[\text{Ru}^{\text{III}}(\text{O})(\text{SQ-Fc}^+)(\text{ph-terpy})]^+$  underwent one-electron reduction in a methanol solution to generate  $[\text{Ru}^{\text{II}}(\text{O}^{\bullet-})(\text{SQ-Fc})(\text{ph-terpy})]$ , according to the electronic spectral change (Scheme 1).



Scheme 1.

# RESEARCH ACTIVITIES IX

## Research Center for Molecular-Scale Nanoscience

### IX-A Nano-Science and Nano-Technology toward Molecular Scale Electronics

Molecular electronics is a fairly new and fascinating area of research that is firing the imagination of scientists. However, most single organic molecules are not conductive in a classical sense, long range electronic transport through single molecules can not be so effective to realize practical electronic circuits. Our group is interested in (1) construction of nano-structures made from conductive materials such as carbon nanotubes, metal particles or rods, with functional organic molecules, (2) measurements of electric or photonic properties of individual nano-structures while observing their nanometric images, and (3) conductance change of single molecules by external stimulation such as electric field, photon irradiation or chemical species.

#### IX-A-1 Photo Precursor for Pentacene

UNO, Hidemitsu<sup>1</sup>; YAMASHITA, Yuko<sup>2</sup>;  
KIKUCHI, Makoto<sup>2</sup>; WATANABE, Hikaru<sup>2</sup>;  
YAMADA, Hiroko<sup>2</sup>; OKUJIMA, Tetsuo<sup>2</sup>; OGAWA,  
Takuji<sup>3</sup>; ONO, Noboru<sup>2</sup>  
(<sup>1</sup>Ehime Univ., JST; <sup>2</sup>Ehime Univ.; <sup>3</sup>IMS, JST)

[*Tetrahedron Lett.* **46**, 1981–1983 (2005)]

Pentacene is one of the most sensational polycyclic hydrocarbons, which draws attention from many fields due to its high electron mobility. Many efforts have been focused on the device preparation of not only pentacene itself but also its derivatives. For the application of pentacene and its derivatives, one of the biggest problem is the low solubility in common solvents. Difficulties are often encountered in the purification of its derivatives, and several manipulations of a high vacuum sublimation are required. In the final stage of pentacene based devices, the vapor deposition technique under high vacuum is usually employed. In order to overcome the problem, precursors, which give pentacene or its derivatives by thermal decomposition, namely retro Diels-Alder reaction, were developed and their applications for field effect transistors (FET) and organic thin film transistors (OTFT) were recently reported. In these cases, retro Diels-Alder reaction of the precursors was designed to proceed at rather low temperatures by extrusion of tetrachlorobenzene and *N*-sulfinylacetamide. The requisite for such leaving molecules is sufficiently small and inert not to affect the property of pentacene devices. For these precursor methods, there is an inevitable drawback that the high vacuum sublimation technique, one of the most reliable and successful device preparation methods, cannot be applied, because the trigger of the precursors to pentacene is heat. We thought that not only this shortcoming of the precursor method but also property of the leaving molecules can be dramatically improved if the alternative physical decomposition method, namely light, is applied. In this communication, we report preparation of the first photo-convertible precursor to pentacene and its fundamental properties.

#### IX-A-2 Synthesis and Self-Assembly of Novel Porphyrin Molecular Wires

KAWAO, Masahiro<sup>1</sup>; OZAWA, Hiroaki<sup>2</sup>;  
TANAKA, Hirofumi<sup>3</sup>; OGAWA, Takuji<sup>3</sup>  
(<sup>1</sup>Ehime Univ., JST; <sup>2</sup>SOKENDAI, JST; <sup>4</sup>IMS, JST)

[*Thin Solid Films* in press (2005)]

Sub-micrometer long butadiyne-linked porphyrin wires were synthesized by oxidative coupling of diethynylporphyrin. The porphyrin wires were analyzed by analytical gel permeation chromatography, absorption spectroscopy and matrix-assisted laser desorption/ionization time of flight mass spectroscopy. Observations of the wire were performed by atomic force microscopy. Self-assembled structures of the wires were observed on highly oriented pyrolytic graphite. Self-assembling features of the porphyrin wires depended on the length of the porphyrin wires and the concentration of the depositing solution.

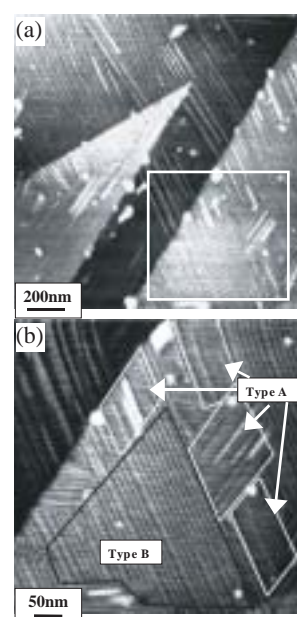


Figure 1.

### IX-A-3 Molecular Junctions Composed of Oligothiophene Dithiol Bridged Gold Nanoparticles Exhibiting Photoresponsive Properties

HUANG, Wei<sup>1</sup>; MASUDA, Gou<sup>2</sup>; MAEDA, Seisuke<sup>2</sup>; TANAKA, Hirofumi<sup>3</sup>; OGAWA, Takuji<sup>3</sup>  
(<sup>1</sup>Nanjing Univ.; <sup>2</sup>Ehime Univ.; <sup>3</sup>IMS, JST)

[Chem. Eur. J. 12, 607 (2006)]

Three oligothiophene dithiols with different number of thiophene rings (3, 6 or 9) were synthesized and characterized. X-ray single crystal structures of compounds 3',4'-dibutyl-5'5''-dithiocyanato-2,2':5',2''-terthiophene (**2**) and 5,5''''-dithiocyanato-tetrabutyl-2,2':5',2''':5'',2''':5''''-hexathiophene (**5**) were involved herein to show the exact molecular lengths as well as the difference between their UV-vis spectra arising from the different packing modes. These dithiols with different chain lengths were then treated with *t*-dodecanethiol protected active gold nano-particles (Au-NPs) *via* in situ thiol-to-thiol ligand exchange in the presence of 1 μm gap Au-electrodes. Thus the molecular junctions composed of self-assembled films were prepared, where oligothiophene dithiol bridged Au-NPs were attached to two electrodes by means of Au-S bonded contacts. The morphologies and *I-V* characteristics of these films were studied by SEM and AFM approaches, which suggest the thickness of the films varied within the size of one isolated Au-NPs and typical distance dependent semiconductor properties could be observed. Current-voltage (*I-V*) measurements for these devices were performed where the films served as active elements in the temperature range 6 ~ 300 K and classical Arrhenius plots and their linear fittings were carried out to give the activation energies ( $\Delta E$ ). Furthermore, preliminary studies on the photoresponsive properties of these junctions were explored at 80, 160 and 300 K, respectively. Physical and photochemical mechanisms were used to explain the possible processes. To the best of our knowledge, this is the first report where oligothiophene dithiols act as bridging units to link Au-NPs, and also the first report about functionalized Au-NPs exhibiting photo response properties in the solid state.

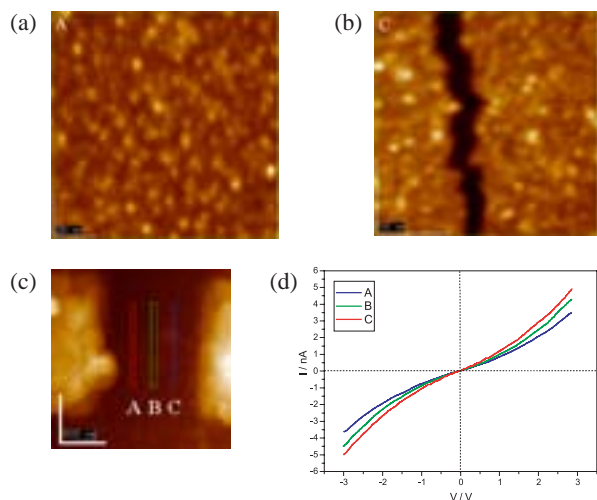


**Figure 1.** (a) and (b) Tapping mode AFM topographies of the self-assembled film of **14** on the micro-gap gold electrodes corresponding to the areas marked in (c). (d) *I-V* curves with different separations between cantilever and brass substrate by using contacting mode AFM.

### IX-A-4 Simple Preparation Method for Supramolecular Porphyrin Arrays on Mica Using Air/Water Interface

SATO, Hirokazu<sup>1</sup>; TSUTSUMI, Osamu<sup>1</sup>; TAKEDA, Kazuyoshi<sup>1</sup>; TANAKA, Hirofumi<sup>2</sup>; OGAWA, Takuji<sup>2</sup>  
(<sup>1</sup>Ebara Research Co.; <sup>2</sup>IMS, JST)

[Jpn. J. Appl. Phys. in press (2005)]

The fabrication of supramolecular porphyrin arrays on the surface of a mica substrate is demonstrated. The supramolecular structures are prepared at the air/water interface from a dilute solution of porphyrin dimer and bidentate ligand and then transferred to mica by using the conventional Langmuir-Blodgett method. Isolated wire-like structures and networks of structures are observed by atomic force microscopy. From the analysis of the height histogram and average width, these structures are considered to be side-by-side arrangements of supramolecular chains of porphyrin dimer and bidentate ligand. By changing the ligand molecule, we demonstrate that the configuration of the supramolecular structure can be controlled.

### IX-A-5 Novel Photochemical Synthesis of Pentacene and Its Derivatives

YAMADA, Hiroko<sup>1</sup>; YAMASHITA, Yuko<sup>1</sup>; KIKUCHI, Makoto<sup>1</sup>; WATANABE, Hikaru<sup>1</sup>; OKUJIMA, Tetsuo<sup>1</sup>; UNO, Hidemitsu<sup>2</sup>; OGAWA, Takuji<sup>3</sup>; OHARA, Keishi<sup>1</sup>; MUKAI, Kazuo<sup>1</sup>; ONO, Noboru<sup>1</sup>  
(<sup>1</sup>Ehime Univ.; <sup>2</sup>Ehime Univ., JST; <sup>3</sup>IMS, JST)

[Chem. Eur. J. 11, 6212 (2005)]

A novel -diketone precursor of pentacene, 6,13-dihydro-6,13-ethanopentacene-15,16-dione, was prepared and converted successfully to pentacene in 74% yield by photolysis of the precursor in toluene: Irradiation of the diketone solution in toluene with light of 460 nm under an Ar atmosphere caused the solution to change from yellow to fluorescent orange-pink within a few minutes, after which, purple precipitates appeared. After 35 min, the solution changed to colorless and the purple precipitates were filtered to give pentacene in 74% yield. By contrast, in the presence of oxygen, the color of the solution changed from yellow to pale yellow, and only 6,13-endoperoxide of pentacene was quantitatively obtained. The rate of the reaction upon photolysis was measured by observing the decay of *n*-\* absorption of the precursor at 460 nm, and was found to be similar in both the presence and absence of oxygen. Therefore, the photoreaction of the -diketone precursor seemed to occur *via* the singlet excited state. Because the T-T absorption of pentacene was observed upon

photolysis of the precursor in the nanosecond transient absorption measurement under an Ar atmosphere, the excited triplet state of the pentacene generated singlet oxygen by sensitization, and it reacted with the ground-state pentacene to give the 6,13-endoperoxide. The diketone deposited on glass was also converted successfully to pentacene film by photoirradiation. In addition, diketone precursors of a mixture of 2,8- and 2,9-dibromopentacene and 2,6-trianthrylene were also prepared and their photoconversion was performed.

### IX-A-6 Porphyrin Molecules Working as Nanodevice on Single-Walled Carbon Nanotube Wiring

TANAKA, Hirofumi<sup>1</sup>; YAJIMA, Takashi;  
MATSUMOTO, Takuya<sup>2</sup>; OTSUKA, Yoichi<sup>2</sup>;  
OGAWA, Takuji<sup>1</sup>  
(<sup>1</sup>IMS, JST; <sup>2</sup>Osaka Univ., JST)

[*Adv. Mater.* in press]

For the future development of molecular electronics, we should construct nanosized molecular devices placed on nanowiring. To obtain high-quality devices composed of a few molecules, the wiring and the device should be connected well to maintain a constant interface. For this purpose, a single-walled carbon nanotube (SWNT)/porphyrin complex was prepared and then its electronic property was investigated while observing a topographic image using point-contact current imaging atomic force microscopy (PCI-AFM). Using PCI-AFM, we can measure the current along the long axis of the wiring by which the quality of the device in the circuit can be determined. The *I-V* curves were asymmetric with respect to the origin where an aggregate of several porphyrin molecules was absorbed, while they were symmetric without them. This means the porphyrin aggregation works as a rectification device on SWNT wiring. This is the first study which proves the electron property of a few porphyrin molecules absorbed on SWNT.

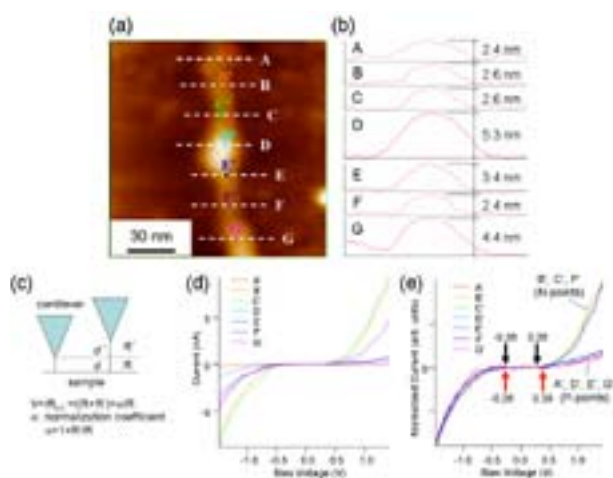


**Figure 1.** (a) Topographic image of **BPP-Zn** absorbed on SWNT electrode. The *I-V* measurement was performed at points A'-G'. (b) Cross section of each line in (a). (c) Relation between a tunnel resistance and a distance of sample and cantilever. (d) *I-V* curves obtained at each point. (e) The *I-V* curves were normalized at  $-1.5$  V. All curves are coincident below  $0$  V. *I-V* curves are classified into two types over  $0$  V. One is symmetrical with respect to the origin where porphyrin is absorbed and another is asymmetrical where no porphyrin is absorbed. Two types of arrow indicate the band edges (BE) of the objects. Black and red arrows indicate the BE of the object for N-points and P-points, respectively.

### IX-A-7 Electronic Properties of Single-Walled Carbon Nanotube/Porphyrin Polymer Complex Measured by Point-Contact Current Imaging Atomic Force Microscopy

TANAKA, Hirofumi<sup>1</sup>; YAJIMA, Takashi; KAWAO, Masahiro<sup>2</sup>; OGAWA, Takuji<sup>1</sup>  
(<sup>1</sup>IMS, JST; <sup>2</sup>SOKENDAI, IMS)

[*J. Nanosci. Nanotechnol.* in press]

The electronic properties of a porphyrin polymer wire absorbed on a single-walled carbon nanotube (SWNT) were investigated. Current-voltage (*I-V*) curves were measured simultaneously along with topographic observations using point-contact current imaging atomic force microscopy (PCI-AFM). *I-V* curves taken at the location of porphyrin polymer wire absorption were asymmetric with respect to the origin, while they were symmetric in the absence of a porphyrin polymer wire. The electron conduction mechanism of the porphyrin on the SWNT was similar to the case of SWNT/ 5,15-Bis-pentylporphyrinato zinc(II) complex in our recent work.

### IX-A-8 Preparation of Very Reactive Thiol-Protected Gold Nanoparticles: Revisiting the Brust-Schiffrin Method

ARAKI, Koiti<sup>1</sup>; MIZUGUCHI, Eisuke<sup>2</sup>; TANAKA, Hirofumi; OGAWA, Takuji  
(<sup>1</sup>SaoPaulo Univ.; <sup>2</sup>Ehime Univ.)

[*J. Nanosci. Nanotechnol.* in press]

Metal nanoparticles have attracted great interest in nanoscience and nanotechnology because of the many possibilities envisaged by the bottom-up approach since they possess unique optical, electrical, bonding and catalytic properties. Among them, the gold clusters are the most stable and extensively studied materials, and have been proposed for applications such as in photoelectrochemical devices, drug delivery systems and chemical and immunosensors. In all these cases, the properties of the materials should be adjusted by anchoring molecular species with suitable properties on the surface. In this sense, the availability of easily functionalizable and stable starting materials is an important aspect since there is a myriad of molecular species and other materials that can be combined with for the development of new inorganic-organic hybrid nanomaterials and applications.

The higher stability and possibility to isolate a solid that can be repeatedly isolated and redissolved in common organic solvents without decomposition and the possibility to treat them just as another organic molecular species is very convenient. However, there is a drawback for the widespread use of such a thiol protected materials: the sluggishness of the functionalization reaction by substitution of the protecting species, which can take more than a day to proceed until completion. The use of conventional organic chemistry on  $\omega$ -functionalized protecting molecules is also tedious and hampers the preparation of organic-inorganic hybrid nanomaterials, for example by coordinative layer-by-layer assembly. Accordingly, we revisited the Brust-Schiffrin method envisaging the preparation of substitutionally reactive but stable enough thiol protected gold nanoparticles to isolate them as a solid.

## IX-B Development of Organic Semiconductors for Molecular Thin-Film Devices

Organic light-emitting diodes (OLEDs) and organic field-effect transistors (OFETs) based on  $\pi$ -conjugated oligomers have been extensively studied as molecular thin-film devices. Organic semiconductors with low injection barriers and high mobilities are required for highly efficient OLEDs and OFETs. Radical cations or anions of an organic semiconductor have to be generated easily at the interface with an electrode (or a dielectric), and holes or electrons must move fast in the semiconducting layer. Compared with organic p-type semiconductors, organic n-type semiconductors for practical use are few and rather difficult to develop. Recently, we found that perfluorinated aromatic compounds are efficient n-type semiconductors for OLEDs and OFETs.

### IX-B-1 Organic Thin-Film Transistors with High Electron Mobility Based on Perfluoropentacene

INOUE, Youji<sup>1</sup>; SAKAMOTO, Youichi; SUZUKI, Toshiyasu; KOBAYASHI, Masafumi<sup>2</sup>; GAO, Yuan<sup>2</sup>; TOKITO, Shizuo<sup>1</sup>

(<sup>1</sup>NHK Sci. Tech. Res. Labs.; <sup>2</sup>Kanto Denka Kogyo)

[*Jpn. J. Appl. Phys., Part 1* **44**, 3663–3668 (2005)]

We report on n-channel organic thin-film transistors (OTFTs) based on the novel n-type organic semiconductor, perfluoropentacene. The transistor exhibits excellent electrical characteristics, with a high electron mobility of  $0.22 \text{ cm}^2/(\text{V s})$  and a good current on/off ratio of  $10^5$ . The electron mobility is comparable to the hole mobility of a pentacene OTFT. By combining the n-type perfluoropentacene and the p-type pentacene, we have fabricated ambipolar OTFTs and complementary inverter circuits. The OTFTs with heterostructures of the p- and n-type organic semiconductors can operate as an ambipolar device with high electron and hole mobilities of  $0.042$  and  $0.041 \text{ cm}^2/(\text{V s})$ . The complementary inverter using an n-channel perfluoropentacene OTFT and a p-channel pentacene OTFT exhibits excellent transfer characteristics with a voltage gain of 45. A complementary inverter using the ambipolar OTFTs is also demonstrated.

### IX-B-2 Organic Light-Emitting Diodes Using Multifunctional Phosphorescent with Iridium-Complex Core and Charge-Transporting Dendrons

TSUZUKI, Toshimitsu<sup>1</sup>; SHIRASAWA, Nobuhiko; SUZUKI, Toshiyasu; TOKITO, Shizuo<sup>1</sup>

(<sup>1</sup>NHK Sci. Tech. Res. Labs.)

[*Jpn. J. Appl. Phys., Part 1* **44**, 4151–4154 (2005)]

We report a novel class of light-emitting materials for use in organic light-emitting diodes (OLEDs): multifunctional phosphorescent dendrimers that have a phosphorescent core and dendrons based on charge-transporting building blocks. We synthesized first-generation and second-generation dendrimers consisting of a fac-tris(2-phenylpyridine)iridium [Ir(ppy)<sub>3</sub>] core and hole-transporting phenylcarbazole-based dendrons. Smooth amorphous films of these dendrimers were formed by spin-coating them from solutions. The OLEDs using the

dendrimer exhibited bright green or yellowish-green emission from the Ir(ppy)<sub>3</sub> core. The OLEDs using the film containing a mixture of the dendrimer and an electron-transporting material exhibited higher efficiency than those using the neat dendrimer film. The external quantum efficiency of OLEDs using the film containing a mixture of the first-generation dendrimer and an electron-transporting material was as high as 7.6%.

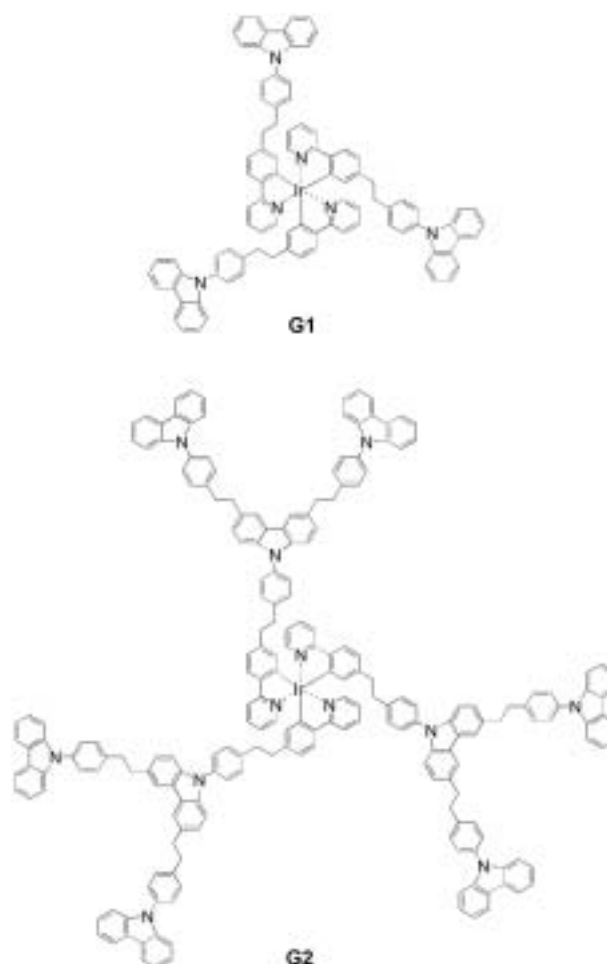


Figure 1. Structures of iridium complexes.

## IX-C Field-Effect Transistors with Organic Semiconductors

Considerable attention has recently focused on organic field-effect transistors (OFET) because of their potential use in low-cost flexible electronic devices. We have studied output characteristics of OFET devices based on newly synthesized organic compounds with novel device structures.

### IX-C-1 Preparation of Organic Light-Emitting Field-Effect Transistors with Asymmetric Electrodes

SAKANOUE, Tomo<sup>1</sup>; FUJIWARA, Eiichi;  
YAMADA, Ryo; TADA, Hirokazu  
(<sup>1</sup>SOKENDAI)

[*Chem. Lett.* **34**, 494–495 (2005)]

Light-emitting field-effect transistors (LEFET) based on poly [2-methoxy-5-(2-ethylhexoxy)-1,4-phenylenevinylene](MEH-PPV) were prepared with asymmetric electrodes of a Au/Cr source and an Al drain on a SiO<sub>2</sub> gate insulator (600 nm) through twice of photolithography and lift-off techniques (see Figure 1). The light emission was observed when the gate voltages increased above -40 V at the drain voltage of -100 V. The luminous efficiency of the devices was significantly improved comparing to those with conventional electrodes of Au/Cr.

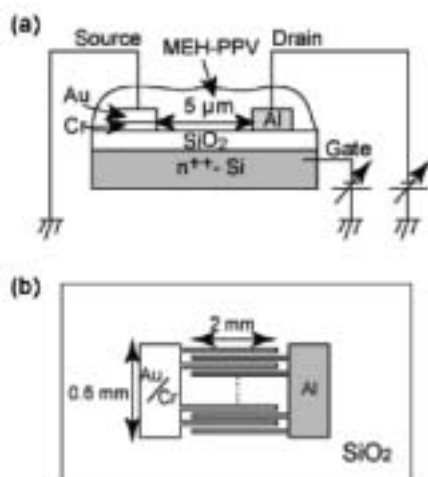


**Figure 1.** Schematic views of the LEFET with asymmetric Au/Cr-Al electrodes. (a) Side view of the device. (b) Top view of the FET substrate.

### IX-C-2 Field-Effect Transistors Based on Single-Crystalline Wires of Bis-(1, 2, 5-Thiadiazolo)-p-Quinobis(1, 3-Dithiole)

FUJIWARA, Eiichi; TAKADA, Masaki<sup>1</sup>;  
YAMASHITA, Yoshiro<sup>2</sup>; TADA, Hirokazu  
(<sup>1</sup>SOKENDAI; <sup>2</sup>Tokyo Inst. Tech.)

[*Jpn. J. Appl. Phys.* **44**, L82–L84 (2005)]

We prepared single-crystalline wires of bis(1, 2, 5-thiadiazolo)-p-quinobis(1, 3-dithiole), whose ends were anchored to the drain and source electrodes of bottom-contact-type field-effect transistors. Figure 1 shows the temperature dependence of carrier mobility in the range from 5 K to 330 K. The tunnel transport was found to be dominant at  $T < 30$  K. Thermally activated hopping behavior was observed in the temperature range from 30 K to 200 K. The mobility decreased with increasing temperature at  $T > 200$  K, indicating that phonon scattering governs carrier transport in single-crystalline wires.

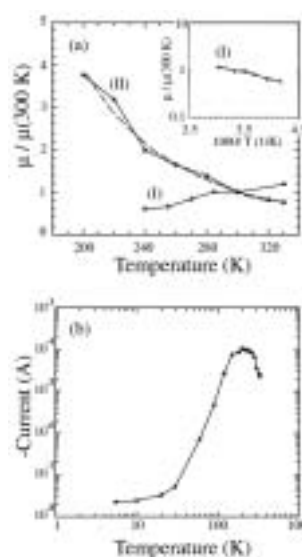


**Figure 1.** (a) Temperature dependences of the field-effect mobilities of densely packed grains (I) and crystalline wires (II). Each curve is normalized by the mobility at 300 K. Dashed line shows the  $T^{-x}$  fitting curve for  $x = 3$ . Inset shows Arrhenius's plot of curve (I). (b) Temperature dependence of the drain current of BTQBT wires. The drain and gate voltages were -50 V and -30 V, respectively.

## IX-D Molecular Assemblies on Silicon Surfaces via Silicon–Carbon Covalent Bonds

Preparation of molecular assemblies on inorganic semiconductors such as silicon and germanium has received a growing interest because of their potential application to stable resist for nano-patterning. We have prepared organic monolayers on silicon by wet process and studied film structures with IR.

### IX-D-1 Characterization of Molecular Assemblies on Silicon Surfaces by Attenuated Total Reflectance Infrared Spectroscopy

ARA, Masato<sup>1</sup>; YAMADA, Ryo; TADA, Hirokazu  
(<sup>1</sup>SOKENDAI)

[*Thin Solid Films* in press]

Alkyl monolayers anchored to Si(111) were prepared in diluted and neat 1-alkene by thermal reaction. Monolayers prepared were investigated by attenuated total reflectance infrared spectroscopy. It was found that alkyl chains in the monolayers anchored to Si(111) had an all-trans conformation. The rate of reaction between 1-alkene and hydrogen-terminated silicon remarkably depended on the concentration of 1-alkene as shown in Figure 1. However, monolayers prepared in diluted 1-

alkene were identical with that prepared in neat 1-alkene.

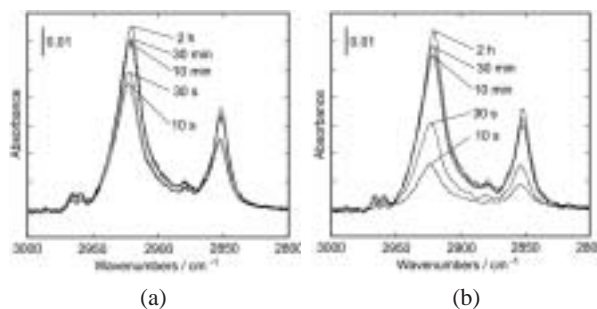


**Figure 1.** ATR spectra of C12 monolayers prepared in neat 1-dodecene (a) and those prepared in diluted 1-dodecene (b) with a p-polarized configuration, respectively. Reaction was carried out for 10 s, 30 s, 10 min, 30 min, and 2 h.

## IX-E Low Temperature Scanning Tunneling Microscopy and Spectroscopy of Organic Molecules on Metal Surfaces

The electronic structure of molecules adsorbed by metal surfaces is of growing interest in the field not only of surface science but also of molecular-scale electronic devices. Scanning tunneling microscopy and spectroscopy are useful to investigate molecular arrangements and electronic structure with atomic resolution. We have prepared epitaxial films of phthalocyanine molecules on clean metal surfaces and studies their structures by scanning tunneling microscopy and spectroscopy at low temperature.

### IX-E-1 Scanning Tunneling Microscopy and Spectroscopy of Phthalocyanine Molecules on Metal Surfaces

TAKADA, Masaki<sup>1</sup>; TADA, Hirokazu  
(<sup>1</sup>SOKENDAI)

[*Jpn. J. Appl. Phys.* **44**, 5332–5335 (2005)]

We studied the electronic structure of cobalt-phthalocyanine (CoPc) molecules on Au(111) and Cu(100) surfaces by scanning tunneling microscopy and

spectroscopy at 5 K. In the differential conductance ( $dI/dV$ ) spectra as shown in Figure 1, there were some peaks related to the highest occupied molecular orbital (HOMO), the lowest unoccupied MO (LUMO) and the d-orbitals of the Co atom. CoPc molecules on the Cu(100) surface had new electronic states between the peaks related to HOMO and LUMO, while those on the Au(111) surface did not show additional peaks. A  $dI/dV$  image indicated that the new states were generated by the hybridization between the LUMO of molecules and the electronic states of the Cu(100) surface.

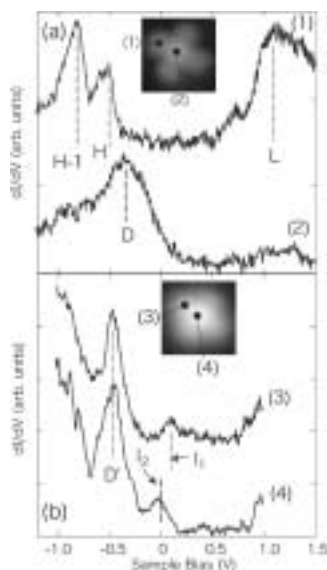


**Figure 1.** (a)  $dI/dV$  spectra of a single CoPc molecule on Au(111) surface at 5 K. (b)  $dI/dV$  spectra of a single CoPc molecule on Cu(100) surface at 5 K. Spectra (1)–(4) were measured at indicated spots on the inset images.

## IX-F Ratchet Motions of a Droplet Caused by Electrochemical Reaction of Monolayers

Control of droplet motions on small spaces is of growing interest since it leads to non-mechanical pumping systems in micro-fluidic devices. By introducing asymmetric characteristics to the surface, the droplet moves because of the imbalance of surface tensions. We found that electrochemical reactions of monolayers were used to dynamically control the surface property and the motion of the droplet.

### IX-F-1 Electrochemically Generated Wetting Gradient and Its Application for the Transport of Droplets

YAMADA, Ryo; TADA, Hirokazu

[*Langmuir* **21**, 4254–4256 (2005)]

The reversible transportation of droplets was realized by spatiotemporal control of the wetting gradient. The surface wetting was reversibly regulated by using electrochemical reactions of the ferrocenyl (Fc) alkanethiol monolayer and application of the in-plane bias voltage to the substrate as shown in Figure 1. The back-and-forth motion of the wetting boundary, where the surface changed from wetting to repulsive, sequentially caused a droplet unidirectional spreading and shrinking on the surface. These unidirectional motions resulted in the net transport of the droplet in inchworm-like manner as shown in Figure 2. The droplet moved backward when the direction of the in-plane bias voltage was reversed.

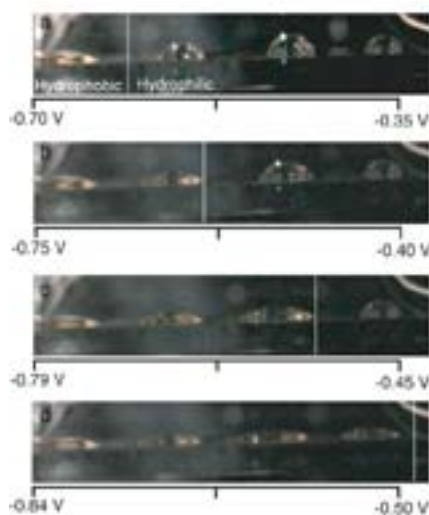


**Figure 1.** Photographs of nitrobenzene droplets.  $V_{bias}$  was fixed at 0.35 V and  $E_{offset}$  was shifted (a–d). Line in the photograph represents the position of the wetting boundary estimated from the shape of the droplets. Note that the current peak for  $Fc^+/Fc$  reaction was observed at *ca.*  $-0.5$  V in cyclic voltammogram.

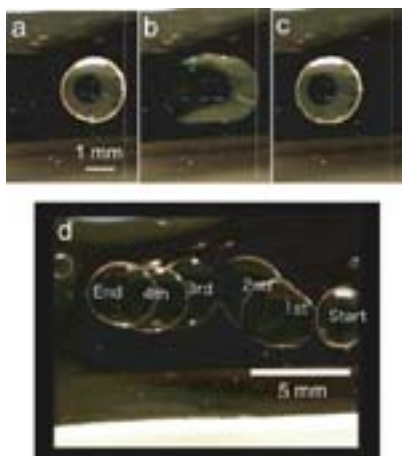


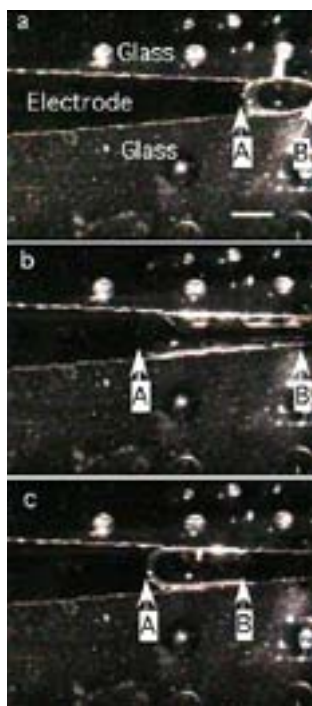
**Figure 1.** Directional deformations of the nitrobenzene droplet. The length of the scale bar in (a) is 3 mm. When the surface was changed from repulsive to wetting (a–b), the left side of the droplet (A) spread. When the surface was back to repulsive (bc), the right side of the droplet (B) shrank. These directional deformations resulted in a net transport of the droplet.

**Figure 2.** Photographs of inchworm motion of the droplet in the solution.  $E_{BIAS} = 0.5$  V.  $E_{offset} = -300$  mV (a),  $-340$  mV (b) and  $-300$  mV (c). (d) Trace of the multi-step inchworm motions of the droplet. Six photographs were superimposed.

### IX-F-2 Transport of a Droplet by Directional Deformations with Asymmetric Electrode

YAMADA, Ryo; TADA, Hirokazu

Ratchet motions of a droplet were realized by the repeated deformations of it on an asymmetric V-shaped electrode. The surface wetting of the electrode was reversibly regulated by electrochemical reactions of the ferrocenyl-alkane-thiol monolayer. When the surface was changed from repulsive to wetting, the contact line of the droplet facing to the wider side advanced while the other side was almost pinned. The contact line facing to the narrower side retracted when the surface was changed from wetting to repulsive. The directional deformations of the droplet resulted in a net transport of it.



## IX-G Development of Multi-Function Integrated Macromolecules and Their Organization on Substrate Surfaces for Planar Molecular-Scale Electronics Circuits

The concept of molecular-scale electronics is now realized for individual components such as wire, diode, switch, and memory cell, but the fabrication of complete molecular-scale circuits remains challenging because of the difficulty of connecting molecular modules to one another. Molecular monolithic technology, which integrates the wiring, transistors and the required passive elements on a single macromolecule, has been proposed as a promising solution to this problem. In this project we have been trying to establish both the architecture of this novel class of macromolecules and the protocols for their purposive organization on metal/semiconductor substrate surfaces.

### IX-G-1 Step-Wised Synthesis of Multifunctional Molecular Wires for Planar Metal-Molecule-Metal Junctions

TANAKA, Shoji

A series of 1–10 nm long building blocks (**1-4**) have been prepared. We have already developed i) “insulated molecular modules,” ii) “energy-gap tuning modules,” iii) “molecule-anchor modules,” and iv) “molecular junction modules” as the basic elements for multi-function integrated  $\pi$ -conjugated macromolecules. The building blocks **1-4** are widely applicable to assemble these functional modules in a single molecule. For example, a series of linear macromolecules (**5-6**), specifically designed for the systematic investigation of electron conduction in molecular wires, have been prepared easily from these blocks and modules in a few steps.

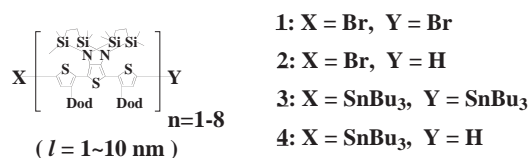


**Figure 1.** Molecular structure of 1–10 nm long building blocks.

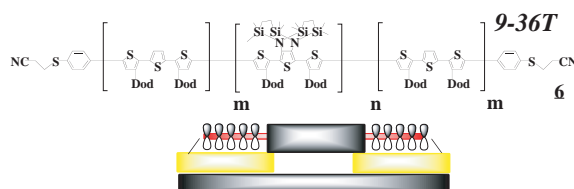
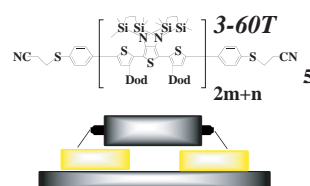


**Figure 2.** Molecular structure of insulated molecular wires with anchor units.

## IX-H Heterogeneous Aquacatalysis

Catalytic organic transformations under mild, safe, and green conditions is an important goal in synthetic organic chemistry. We recently reported that several palladium- and rhodium-catalyzed reactions, including  $\pi$ -allylic substitution, carbonylation, the Heck reaction, Suzuki-Miyaura cross-coupling, hydroformylation, cyclotrimerization of alkynes, and Michael-type addition of arylboronic acids, *etc.*, took place in water by use of metal-phosphine complexes anchored on to an amphiphilic polystyrene-poly(ethylene glycol) graft copolymer (PS-PEG) resin where the advantages of both aqueous- and heterogeneous-switching of a given catalytic transformation were combined in one system. Here we wish to report our progress in this subject.

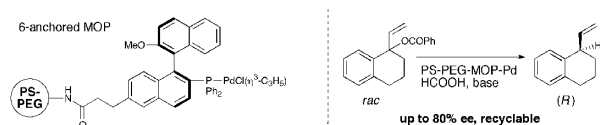
### IX-H-1 PS-PEG Resin-Supported Palladium-MOP Complexes. Application in Asymmetric $\pi$ -Allylic Reduction

[*Org. Lett.* 7, 291–293 (2005)]

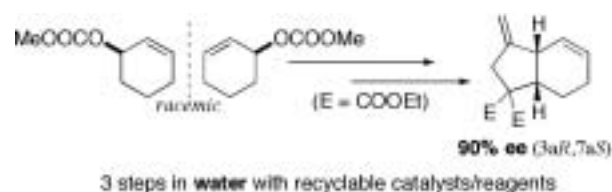
UOZUMI, Yasuhiro; HOCKE, Heiko

[*Tetrahedron* 60, 9297–9306 (2004)]

Homochiral palladium complexes of polymeric 2', 6-, and 6'-anchored 2-diphenylphosphino-1,1'-binaphthyl (MOP) ligands were prepared on polystyrene-poly(ethylene glycol) (PS-PEG) resin. The PS-PEG resin-supported palladium-MOP complexes exhibited high catalytic activity, stereoselectivity (up to 80% *ee*), and recyclability (6 times) in the asymmetric allylic reduction of 1-vinyl-1,2,3,4-tetrahydronaphth-1-yl benzoate to give 1-vinyl-1,2,3,4-tetrahydronaphthalene.



Cycloisomerization of 1,6-enynes proceeded smoothly in water under heterogeneous conditions in the presence of a palladium complex supported on polystyrene-poly(ethylene glycol) copolymer resin to give the corresponding cyclopentanes with high level of chemical greenness. Multi-step asymmetric synthesis of a hydrindane framework was achieved via palladium-catalyzed asymmetric  $\pi$ -allylic alkylation, propargylation, and cycloisomerization of 1,6-enynes, where all three steps were performed in water with recyclable polymeric catalysts.



### IX-H-2 Hydrogenation and Dehalogenation under Aqueous Conditions with an Amphiphilic Polymer-Supported Nanopalladium Catalyst

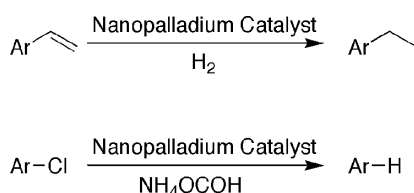
### IX-H-4 Controlled Monoarylation of Dibromoarenes in Water with a Polymeric Palladium Catalyst

NAKAO, Ryu; RHEE, Hakjune; UOZUMI, Yasuhiro

UOZUMI, Yasuhiro; KIKUCHI, Makoto

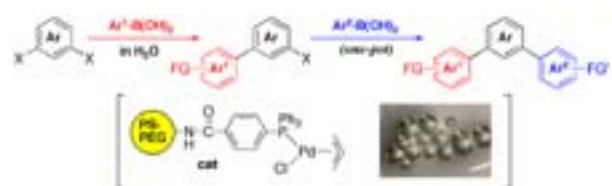
[*Org. Lett.* 7, 163–165 (2005)][*Synlett* 1775–1778 (2005)]

An amphiphilic polystyrene-poly(ethylene glycol) resin-supported nanopalladium particle catalyzed hydrogenation of olefins and hydrodechlorination of chloroarenes under aqueous conditions.



### IX-H-3 Cycloisomerization of 1,6-Enynes: Asymmetric Multi-Step Preparation of a Hydrindane Framework in Water with Polymeric Catalysts

A highly selective monoarylation of dibromoarenes was performed via the Suzuki-Miyaura cross-coupling with arylboronic acids with an amphiphilic polystyrene-poly(ethylene glycol) (PS-PEG) resin-supported phosphine-palladium complex in water under heterogeneous conditions to give bromobiaryls in high yields. Introduction of two different aryl groups on a aromatic moiety was achieved in a one-pot reaction by successive addition of two kinds of arylboronic acids under similar conditions. The polymeric palladium catalyst can be readily recovered and recycled.



NAKAI, Yasushi; UOZUMI, Yasuhiro

## IX-I Development of New Nanomaterials as Components in Advanced Molecular Systems

Nanometer-sized materials exhibit unique electronic behavior. In the quest of advanced redox catalysis, we are currently interested in combining nanometer-sized materials into molecular redox systems. As a basic architecture, composites of organic molecules and gold nanoparticles were synthesized and molecular dynamic simulations were carried out to predict the solution structures.

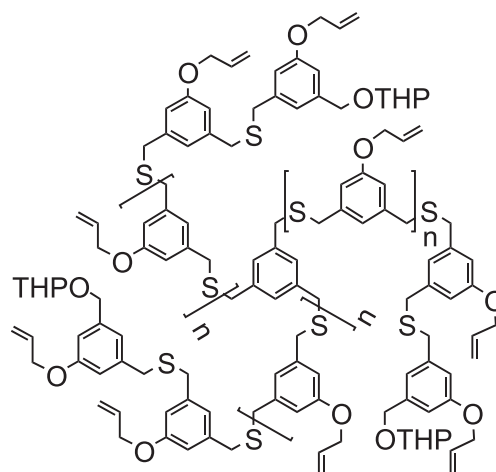
### IX-I-1 Gold Nanoparticles Stabilized by Tripod Thioether Oligomers: Synthesis and Molecular Dynamics Studies

HOSOKAWA, Youichi; MAKI, Suguru; NAGATA, Toshi

[*Bull. Chem. Soc. Jpn.* in press (2005)]

Gold nanoparticles (1.5–1.7 nm) were prepared by use of three tripod thioether oligomers (TTOs) as stabilizing molecules shown in Figure 1. The ICP-AES analyses of these TTO/Au<sub>n</sub> composites revealed the number of protecting molecules per nanoparticles as 25±19, 23±21, and 10±6. On the other hand, the molecular models suggested that the TTOs were of comparable sizes with the sizes of nanoparticles. In order to account for this discrepancy, we carried out molecular dynamic simulations of the TTO/Au<sub>n</sub> composites. The interaction parameters between organic molecules and the gold surface were newly developed so that they reproduced the adsorption enthalpies of small sulfur-containing molecules on the Au(111) surface. By use of these parameters, the self-assembly process of TTO molecules on the Au<sub>147</sub> surface was simulated in chloroform solvent. Figure 2 shows the typical results from a single run, in which 16 TTO molecules (**1a**) and an Au<sub>147</sub> nanoparticle (a cuboctahedral structure; diameter 1.7 nm) were placed in a box of CHCl<sub>3</sub> with dimensions 112.2×96.3×97.7 Å<sup>3</sup>. The surface of the gold nanoparticle was completely covered with three TTO molecules. Although it is not impossible to accommodate more than 20 **1a**'s around the surface of a gold nanoparticle, the more appropriate model would be coexistence of free, unbound **1a** molecules and gold nanoparticles covered with a small number of **1a**. The free and bound **1a** molecules should be in dynamic equilibrium in CHCl<sub>3</sub> solutions, as suggested

by the <sup>1</sup>H NMR spectra which showed only one set of slightly broadened signals.



**1a**: n = 1, **1b**: n = 3, **1c**: n = 5

**Figure 1.** The tripod thioether oligomers used in this study.

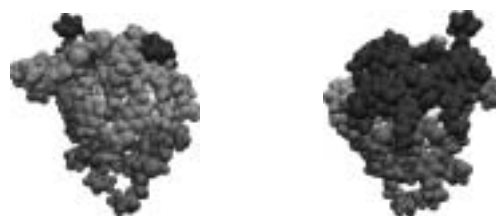


**Figure 2.** A snapshot structure from the **1a**<sub>16</sub>/Au<sub>147</sub> simulation, in which three **1a** molecules are adsorbed on the Au<sub>147</sub> surface. The space-filling views from two opposite directions are shown. The gold nanoparticle and the three different **1a** molecules are denoted in white color and three different levels of gray colors, respectively.

## IX-J Designing Artificial Photosynthesis at Molecular Dimensions

Photosynthesis is one of the finest piece of molecular machinery that Nature has ever created. Its ultrafast electron transfer and following well-organized sequence of chemical transformation have been, and will continue to be, challenging goals for molecular scientists. Our ultimate goal is to design artificial molecular systems that effect multiple chemical reactions triggered by light on the basis of molecular rationale.

## IX-J-1 Electrochemical Properties of Ferrocene-Dendrimer-Porphyrins

KIKUZAWA, Yoshihiro; NAGATA, Toshi

Synthesis of the ferrocene-dendrimer-porphyrins (Figure 1) was already reported in previous Annual Reviews. Figure 2 shows the differential pulse voltammograms (DPV) of  $G_n(\text{Fc})_m\text{-ZnP}$ , together with the reference compounds **Bn-ZnP** and **Fc-ZnP**, in  $\text{CH}_2\text{Cl}_2/0.1 \text{ mol/dm}^3 \text{ Bu}_4\text{NClO}_4$ . The ferrocene-dendrimer-porphyrin compounds showed three oxidation peaks at 0.2, 0.5 and 0.7 V (vs  $\text{FcCp}_2/\text{FcCp}_2^+$ ), which were assigned as the oxidation of the ferrocenyl groups, and the first and second oxidation of the porphyrin. Figure 3 shows the plots of  $i_{\text{max}}$  (the peak height) versus  $\Delta t^{-1/2}$  ( $\Delta t$  is the pulse width) for the first two oxidation peaks of **G3(Fc)<sub>14</sub>-ZnP**. The values for peak II showed good linearity, whereas those for peak I showed pronounced deviation from linearity. These results indicate that the electron transfer for the first oxidation (peak I) is slow in the electrochemical timescale. This slow kinetics can be attributed to the reorganization of the supporting electrolyte during the multiple electron transfer of the ferrocene-dendrimer redox pool.

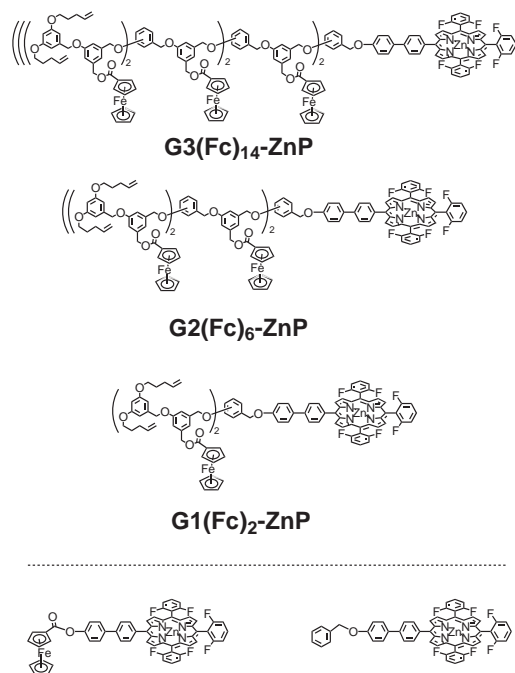


**Figure 1.** The structure of the ferrocene-dendrimer-linked porphyrins.

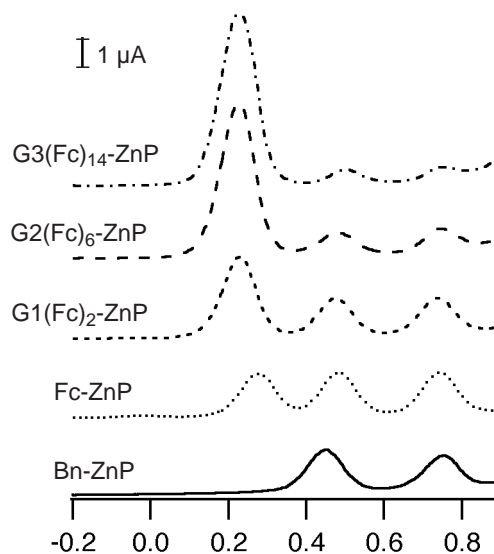


**Figure 2.** The differential pulse voltammograms of the ferrocene-dendrimer-porphyrins.

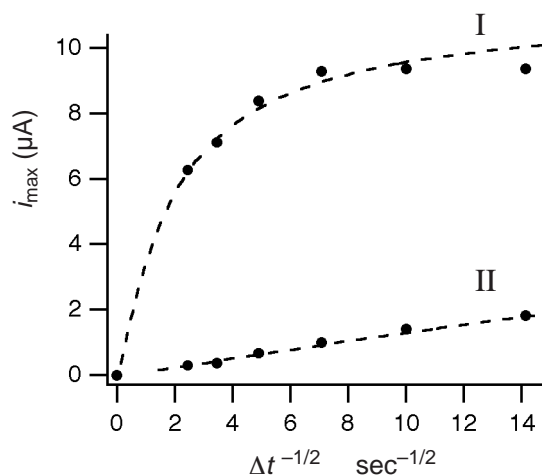


**Figure 3.** The  $i_{\text{max}}-\Delta t^{-1/2}$  plots of the first two oxidation peaks of **G3(Fc)<sub>14</sub>-ZnP**.

## IX-K Development of New Metal Complexes as Redox Catalysts

Redox catalysis is an important field of chemistry which translates a flow of electron into chemical transformation. It is also one of the requisites for artificial photosynthesis. This project of ours aims at developing new metal complexes that perform redox catalysis at low overpotential. Currently we are focusing our attention to the development of a series of cobalt phosphine complexes as possible catalysts for electrochemical reductions.

### IX-K-1 Synthesis, Structure and Electrochemistry of New Cobalt Complexes with Cyclopentadienyl and Bidentate Ligands

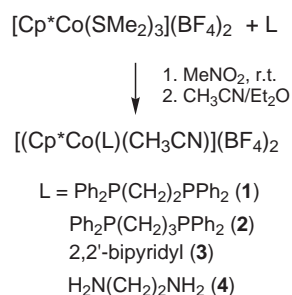
NAGASAWA, Takayuki; NAGATA, Toshi

Low-valent cobalt complexes are interesting candidates for electrocatalytic reductions. Herein we report the synthesis, structure, and electrochemistry a series of cobalt complexes with general formula  $[\text{Cp}^*\text{Co}(\text{L})(\text{S})]^{2+}$ , where  $\text{Cp}^*$  is pentamethylcyclopentadienyl anion, L is a bidentate ligand and S is an exchangeable monodentate ligand.

The key intermediate compound,  $[\text{Cp}^*\text{Co}(\text{SMe}_2)_3](\text{BF}_4)_2$ , was prepared from  $\text{Cp}^*\text{Co}(\text{CO})_2$  by a similar method as the Cp analog reported by Kuhn. The reaction of this compound with a bidentate ligand in  $\text{CH}_3\text{NO}_2$ , followed by treatment with  $\text{CH}_3\text{CN}/\text{Et}_2\text{O}$ , gave a crystalline product  $[\text{Cp}^*\text{Co}(\text{L})(\text{CH}_3\text{CN})](\text{BF}_4)_2$  in 80–90% yield (Scheme 1). The X-ray structure of **2** (L = dppp) is shown in Figure 1, which shows typical octahedral coordination of the Co(III) center. The cyclic voltammograms in  $\text{CH}_3\text{CN}$  showed two reversible waves corresponding to the Co(III)/Co(II) and Co(II)/Co(I) redox couples (Table 1).

**Table 1.** The reversible half-wave potentials of **1-4** in  $\text{CH}_3\text{CN}/\text{Bu}_4\text{NClO}_4$ .

	$E_{1/2}(\text{V vs. Cp}_2\text{Fe/Cp}_2\text{Fe}^+)$	
	Co(III)/Co(II)	Co(II)/Co(I)
<b>1</b>	-0.61	-1.13
<b>2</b>	-0.56	-1.26
<b>3</b>	-0.82	-1.15
<b>4</b>	-0.98	-2.25



**Scheme 1.** Synthesis of the cobalt complexes.

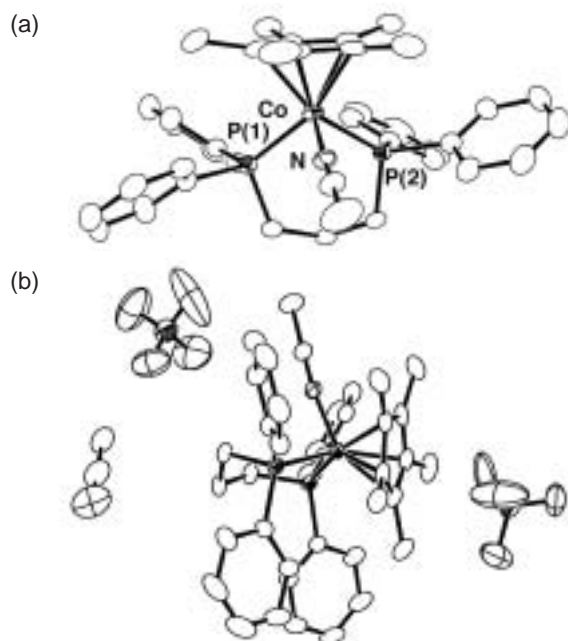


**Figure 1.** The ORTEP drawings of (a) the cationic part, and (b) the asymmetric unit of **2**.

## IX-L Photochemistry on Well-Defined Surfaces

Upon the irradiation of light in the wavelength range from visible to ultraviolet, a number of adsorbed molecules on metal surfaces reveal variety of photochemical processes, including photo-stimulated desorption, rearrangement of adsorbed states, photodissociation, and photo-initiated reactions with coadsorbates. A central and fundamental question in the surface photochemistry is to clarify how adsorbate-substrate systems are excited by photon irradiation. In addition, since photo-initiated reactions can be induced without any thermal activation of reactants, they may provide good opportunities for studying a new class of surface reactions that may not be induced thermally. We have studied photochemistry of various adsorption systems on well-defined metal and semiconductor surfaces mainly by temperature-programmed desorption (TPD), infrared reflection absorption spectroscopy (IRAS), x-ray photoelectron spectroscopy (XPS), work function measurements, and angular-resolved time-of-flight (TOF) mass spectrometry of photodesorbed species associated with pulsed laser irradiation. In this year, the photochemistry of cyclic alkane on Pt(111) and Cu(111) surfaces was studied mainly by TPD, XPS, and IRAS.

### IX-L-1 Photochemistry of Cyclohexane on Cu(111)

**YAMAGUCHI, Dai; MATSUMOTO, Taketoshi;**  
**WATANABE, Kazuya; TAKAGI, Noriaki<sup>1</sup>;**  
**MATSUMOTO, Yoshiyasu**  
 (<sup>1</sup>SOKENDAI and Univ. Tokyo)

[*Phys. Chem. Chem. Phys.* submitted]

The photochemistry of cyclohexane on Cu(111) and its excitation mechanism have been studied by temperature-programmed desorption, ultraviolet and X-ray photoelectron spectroscopy. Cyclohexane weakly adsorbed on Cu(111) has been known to show a broadened and redshifted CH stretching band, *i.e.*, CH vibrational mode softening. Although no dehydrogenation takes place thermally on this surface and by the irradiation

of photons at 5.0 eV, adsorbed cyclohexane is dissociated to cyclohexyl and hydrogen by the irradiation of photons at 6.4 eV. This is a marked contrast to cyclohexane in the gas phase where the onset of absorption is located at 7 eV. When the surface irradiated by 6.4-eV photons is further annealed, cyclohexyl is dehydrogenated to form cyclohexene that desorbs at 230 K. The systematic measurements of photochemical cross sections at 6.4 eV with linearly polarized light as a function of incident angle indicate that the electronic transition from the highest occupied band of cyclohexane to a partially occupied hybridized band near the Fermi level is responsible for the photochemistry. The hybridized band is formed by the interactions between the electronic states of cyclohexane and the metal substrate. The role of the hybridized band in the photochemistry and the CH vibrational mode softening is discussed.

## IX-M Ultrafast Dynamics at Well-Defined Surfaces

To understand the mechanism of surface photochemistry, it is vital to know how photoinduced electronic excitation induces adsorbate nuclear motions that ultimately lead to chemical reactions. We demonstrate the real-time observations of surface phonons and adsorbate-substrate vibrational modes by fs time-resolved second harmonics generation (TRSHG). If an excitation light pulse has a duration sufficiently shorter than a period of a vibrational mode or a phonon mode, it can excite the mode with a high degree of temporal and spatial coherence. This coherent nuclear motion modulates the second-order susceptibility  $\chi^{(2)}$ . Thus, by monitoring the intensity modulation of the second harmonics (SH) generation of a probe pulse, we can observe the evolution of the coherent nuclear motion subsequent to the electronic excitation at the surfaces. This year, in particular, we have demonstrated that coherent phonon modes can be selectively excited by tailored pulse trains.

### IX-M-1 Femtosecond Wavepacket Dynamics of Cs Adsorbates on Pt(111): Coverage and Temperature Dependences

**WATANABE, Kazuya; TAKAGI, Noriaki<sup>1</sup>;**  
**MATSUMOTO, Yoshiyasu**  
 (<sup>1</sup>Univ. Tokyo)

[*Phys. Rev. B* **71**, 085414 (9 pages) (2005)]

Femtosecond time-resolved second harmonic generation has been used to observe vibrational wavepacket

dynamics at a Cs-covered Pt(111) surface. The creation and dephasing of vibrational coherence are monitored *via* the intensity modulations in the second harmonic of probe pulses as a function of pump-probe delay. The TRSHG trace obtained from the clean surface shows an instantaneous sharp rise right after the excitation. This is followed by a fast decaying component ( $t < 1$  ps) and a slowly decaying one persistent to the longest delay ( $t = 6$  ps) of the measurements. When the surface is covered with Cs, SH signals are enhanced by about 70 times and strongly modulated waveforms are superimposed on the TRSHG traces. The oscillatory signals are found in

TRSHG signals upon the excitations at 580 and 800 nm, which are the manifestation of nuclear wavepacket dynamics on the surface. The Cs-coverage dependence studied in detail indicates that the wavepacket dynamics of Cs–Pt stretching modes and Pt surface phonon modes are responsible for the TRSHG signals. The cos-like initial phase of the oscillatory signals and the coverage dependence of the initial amplitude suggest that the vibrational coherence is associated with the resonant excitation between Cs-derived states in the quantum well of the Cs overlayer. The rate of Cs–Pt vibrational dephasing increases with the surface temperature. This behavior cannot be accounted for by the increasing contribution from hot bands of low frequency modes. Instead, pure dephasing caused by anharmonic coupling between Cs–Pt stretching and parallel modes in the Cs overlayer is likely the dominant mechanism for the vibrational dephasing.

### IX-M-2 Mode Selective Excitation of Coherent Surface Phonons on Alkali-Covered Metal Surfaces

WATANABE, Kazuya; TAKAGI, Noriaki<sup>1</sup>; MATSUMOTO, Yoshiyasu  
(<sup>1</sup>Univ. Tokyo)

[*Phys. Chem. Chem. Phys.* **7**, 2697–2700 (2005)]

We demonstrate the mode selective excitation of coherent phonons at Pt(111) surfaces covered with submonolayer cesium atoms. A burst of 150-fs laser

pulses with the repetition rate of 2.0 ~ 2.9 THz was synthesized by using a spatial-light modulator, and used for the coherent surface phonon excitation. The coherent nuclear motion was monitored by time-resolved second harmonic generation. By tuning the repetition rate, we succeeded in controlling the relative amplitude of the vibrational coherence of the Cs–Pt stretching mode (2.3 ~ 2.4 THz) to that of the Pt surface Rayleigh phonon mode (2.6 or 2.9 THz, depending on the Cs coverage).

### IX-M-3 Excitation Mechanism of Coherent Surface Phonons on Alkali-Metal Covered Surfaces

FUYUKI, Masanori<sup>1</sup>; WATANABE, Kazuya; MATSUMOTO, Taketoshi; MATSUMOTO, Yoshiyasu  
(<sup>1</sup>SOKENDAI)

We observed time-resolved second harmonic signals from the Cu(111) surface with a full monolayer of Na in ultra-high vacuum and investigated the excitation-wave-length dependence of the wave packet dynamics of the coherently excited Na–Cu stretching mode. Changing the photon energy of the pump pulse (25 fs) from 2.0 to 2.5 eV, the oscillation amplitude derived from the Na–Cu stretching motion is enhanced when the photon energy is resonant to the transitions from the ground state to image states. Thus, these measurements clearly indicate that the resonant excitation of electronic state of the adsorbate is essential for creation of the coherent surface phonons.

## IX-N Multiphoton Photoelectron Spectroscopy of Electronic States of Nano-Structured Materials on Surfaces

Electronic structure and excited state dynamics of nano-structured materials on surfaces are very important for exploring their properties, thermal reactivity and nonthermal processes including photochemistry and photo-induced charge transfer. For this purpose, we performed multiphoton photoelectron spectroscopy with the fs time resolution. In this year we applied this method to thin films of tris-(8-hydroxyquinoline) aluminum (Alq<sub>3</sub>).

### IX-N-1 The Electronic Structure and Femtosecond Electron Transfer Dynamics at Noble Metal/tris-(8-hydroxyquinoline) Aluminum Interfaces

INO, Daisuke<sup>1</sup>; WATANABE, Kazuya; TAKAGI, Noriaki<sup>2</sup>; MATSUMOTO, Yoshiyasu  
(<sup>1</sup>SOKENDAI; <sup>2</sup>Univ. Tokyo)

[*Phys. Rev. B* **71**, 115427 (10 pages) (2005)]

The electronic structures of tris-(8-hydroxyquinoline) aluminum (Alq<sub>3</sub>) on Cu(111) and Au(111) surfaces are studied by using ultraviolet photoelectron spectroscopy and two-photon photoelectron (2PPE) spectroscopy.

The work function decreases with increase of the coverage due to surface dipole of 5.1 D along the surface normal. The ionization potential from the highest occupied state 6.38 eV does not depend on the metal substrates used in this study. The anion states of Alq<sub>3</sub> adsorbed is created by photoinduced electron transfer from the metal substrates and are located at 2.85 and 3.71 eV above the Fermi level on Cu(111) and Au(111) surfaces, respectively. The full width at half maximum of the anion states is 0.2 eV on both the surfaces. Time-resolved 2PPE measurements show that the anion state created by electron transfer from the metal decays with the lifetime of 31±2 fs on Cu(111) and about three times shorter on Au(111). The angle-resolved 2PPE and the coverage dependence of the lifetime of the anion state

indicate that the electron transferred from the metal surface is localized at a molecule in the first layer. Thus, the ultrafast electron back transfer from the anion state

of  $\text{Alq}_3$  in the first layer dominates over the electron hopping to the second layer.

## IX-O Chemistry of One-Dimensional Nano-Surface Compounds Studied by Scanning Tunneling Microscopy

The fluctuating configurations of low-dimensional structures can be thermodynamically favorable at finite temperatures, because the energy gain overcomes the energy cost that accompanies local structural fluctuation. In particular, one-dimensional (1D) systems have a propensity to be sensitive to these fluctuations as described by one of the maxims of condensed matter physics, *i.e.*, one chain does not make a crystal. Thus, the dynamical formation of active species and sites by these fluctuations is a key factor in establishing a microscopic model for chemical reactions at surfaces and nano-structured compounds.

### IX-O-1 In-Situ Observation of CO Oxidation on $\text{Ag}(110)(2 \times 1)\text{-O}$ by Scanning Tunneling Microscopy: Structural Fluctuation and Catalytic Activity

NAKAGOE, Osamu<sup>1</sup>; WATANABE, Kazuya;  
TAKAGI, Noriaki<sup>2</sup>; MATSUMOTO, Yoshiyasu  
(<sup>1</sup>SOKENDAI; <sup>2</sup>Univ. Tokyo)

[*J. Phys. Chem. B* **109**, 14536–14543 (2005)]

It is well known that the adsorption of O on  $\text{Ag}(110)$  results in the formation of quasi-1D structures, AgO chains, accompanied by the mass transfer of substrate atoms.

AgO chains arrange periodically to form  $(n \times 1)$  ( $n = 2 \sim 7$ ) depending on the fractional O coverage due to repulsive inter-chain interactions. On the added-row reconstructed  $\text{Ag}(110)(n \times 1)\text{-O}$  surfaces where one-dimensional  $\text{-Ag-O-Ag-O-}$  chains arrange periodically, the clean-off reaction of O adatoms by CO was investigated using variable temperature scanning tunneling microscopy (VT-STM). Based on the in situ STM observations of the surface structure variation in the course of the reaction at various temperatures, we found that the reaction kinetics are significantly affected by the structural transition of AgO chains from a solid straight line configuration to dynamically fluctuating configurations. Below 230 K where the chains are straight, the reaction takes place only at the end of the chains, so that the reaction progresses in the zero-order kinetics with the reaction front propagating along the chain. The temperature dependence of the reaction rates yields the activation barrier of 41 kJ/mol and the pre-exponential factor of  $1.7 \times 10^3 \text{ cm}^{-2} \text{ s}^{-1}$ . At room temperature, the reaction rate is drastically accelerated when almost half of the O adatoms are eliminated and the chains start fluctuating. The dynamic formation of active sites equivalent to the end of chains upon the chain fluctuation results in the nonlinear increase of the reaction rate.

## IX-P Structures, Stabilities and Physicochemical Properties of Organometallic Hybrid Clusters

Recently, metal clusters have gained much attention because they exhibit novel physicochemical properties that are beyond the prediction made by a dimensional scaling of those of the corresponding bulk. In this regard, metal clusters protected by thiolates or stabilized by polymers are promising candidates for elementary units of nano-scale devices. Our interests are focused on the following issues on the organometallic hybrid clusters: (1) a large-scale preparation of the subnanometer-sized clusters, (2) development of size-selection method, (3) determination of chemical compositions of size-selected clusters (*i.e.* the numbers of metal atoms and organic molecules), and (4) elucidation of effect of the core size, core shape, and interaction with organic molecules on stabilities, electronic structures, and chemical properties.

### IX-P-1 Glutathione-Protected Gold Clusters Revisited: Bridging the Gap between Gold(I)-Thiolate Complexes and Thiolate-Protected Gold Nanocrystals

NEGISHI, Yuichi; NOBUSADA, Katsuyuki;  
TSUKUDA, Tatsuya

[*J. Am. Chem. Soc.* **127**, 5261–5270 (2005)]

Small gold clusters (~1 nm) protected by molecules of a tripeptide, glutathione (GSH), were prepared by reductive decomposition of Au(I)-SG polymers at a low temperature and separated into a number of fractions by polyacrylamide gel electrophoresis (PAGE). Chemical compositions of the fractionated clusters determined previously by electrospray ionization (ESI) mass spectrometry<sup>1)</sup> were reassessed by taking advantage of freshly-prepared samples, higher mass resolution and more accurate mass calibration; the nine smallest components are reassigned to Au<sub>10</sub>(SG)<sub>10</sub>, Au<sub>15</sub>(SG)<sub>13</sub>, Au<sub>18</sub>(SG)<sub>14</sub>, Au<sub>22</sub>(SG)<sub>16</sub>, Au<sub>22</sub>(SG)<sub>17</sub>, Au<sub>25</sub>(SG)<sub>18</sub>, Au<sub>29</sub>(SG)<sub>20</sub>, Au<sub>33</sub>(SG)<sub>22</sub>, and Au<sub>39</sub>(SG)<sub>24</sub>. These assignments were further confirmed by measuring the mass spectra of the isolated Au:S(*h*-G) clusters, where *h*-GSH is a *homo*-glutathione. It is proposed that a series of the isolated Au:SG clusters corresponds to kinetically trapped intermediates of the growing Au cores. The relative abundance of the isolated clusters was correlated well with the thermodynamic stabilities against unimolecular decomposition. The electronic structures of the isolated Au:SG clusters were probed by X-ray photoelectron spectroscopy (XPS) and optical spectroscopy. The Au(4f) XPS spectra illustrate substantial electron donation from the gold cores to the GS ligands in the Au:SG clusters. The optical absorption and photoluminescence spectra indicate that the electronic structures of the Au:SG clusters are well quantized: embryos of the sp band of the bulk gold evolve remarkably depending on the numbers of the gold atoms and GS ligands. The comparison of these spectral data with those of sodium Au(I) thiomalate and 1.8-nm Au:SG nanocrystals (NCs) reveals that the subnanometer-sized Au clusters thiolated constitute a distinct class of binary system which lies between the Au(I)-thiolate complexes and thiolate-protected Au NCs.

#### Reference

1) Y. Negishi *et al.*, *J. Am. Chem. Soc.* **126**, 6518 (2004).

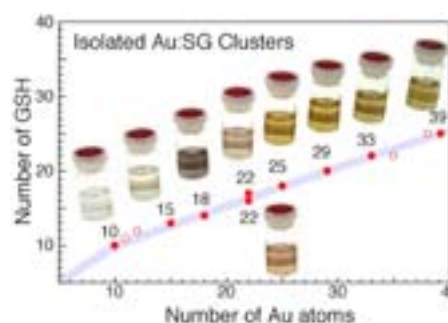


**Figure 1.** Chemical compositions of the Au:SG clusters isolated in the present study.

### IX-P-2 Large-Scale Synthesis of Thiolated Au<sub>25</sub> Clusters via Ligand Exchange Reactions of Phosphine-Stabilized Au<sub>11</sub> Clusters

SHICHIBU, Yukatsu<sup>1</sup>; NEGISHI, Yuichi;  
TSUKUDA, Tatsuya; TERANISHI, Toshiharu<sup>2</sup>  
(<sup>1</sup>JAIST; <sup>2</sup>Univ. Tsukuba)

[*J. Am. Chem. Soc.* **127**, 13464–13465 (2005)]

Phosphine-stabilized Au<sub>11</sub> clusters in chloroform were reacted with glutathione (GSH) in water under a nitrogen atmosphere. The resulting Au:SG clusters exhibit an optical absorption spectrum similar to that of Au<sub>25</sub>(SG)<sub>18</sub>, which was isolated as the major product from chemically prepared Au:SG clusters.<sup>1)</sup> Rigorous characterization by optical spectroscopy, electrospray ionization mass spectrometry, and polyacrylamide gel electrophoresis confirms that the Au<sub>25</sub>(SG)<sub>18</sub> clusters were selectively obtained on the sub-100-mg scale by ligand exchange reaction under aerobic conditions. The ligand exchange strategy offers a practical and convenient method of synthesizing thiolated Au<sub>25</sub> clusters on a large scale.

#### Reference

1) Y. Negishi *et al.*, *J. Am. Chem. Soc.* **127**, 5261 (2005).



**Figure 1.** Large-scale synthesis of the Au<sub>25</sub>(SG)<sub>18</sub> clusters via ligand exchange reactions.

### IX-P-3 Subnanometer-Sized Gold Clusters with Dual Molecular Receptors: Synthesis and Assembly in One-Dimensional Arrangements

NEGISHI, Yuichi; TSUNOYAMA, Hironori;  
YANAGIMOTO, Yasushi<sup>1</sup>; TSUKUDA, Tatsuya  
(<sup>1</sup>Okayama Univ.)

[*Chem. Lett.* **34**, 1638–1639 (2005)]

The gold (Au:S- $\beta$ -CD) clusters modified by thiolated  $\beta$ -cyclodextrin (HS- $\beta$ -CD) were prepared by reduction of AuCl<sub>4</sub><sup>-</sup> with NaBH<sub>4</sub> in DMSO solution: the concentration ratio, [HS- $\beta$ -CD]/[AuCl<sub>4</sub><sup>-</sup>], was fixed at 1. Interestingly, the core size distribution of the Au:S- $\beta$ -CD clusters determined by TEM measurements exhibits bimodal core-size distribution centered at *ca.* 1.1 and 2.4 nm. These two components were successfully separated by using polyacrylamide gel electrophoresis (PAGE). The low-mobility clusters contain the Au cores with the average diameter of 2.3 $\pm$ 0.4 nm whose optical absorption spectrum exhibits the surface plasmon band peaked at *ca.* 520 nm. In contrast, the Au clusters with the sizes of  $\sim$ 1 nm are barely discernible in the TEM image of the high-mobility clusters (**Au-1**). The optical spectroscopy and the thermogravimetric measurement suggest that fraction **Au-1** is composed of the Au<sub>12–15</sub> cores protected by two  $\beta$ -CD ligands. Since the diameter of the circle made by seven sulfurs of the S- $\beta$ -CD is comparable to the Au core size, this result inevitably implies that two S- $\beta$ -CD ligands are attached to the Au core so that the hydrophobic cavities are pointed toward the opposite side. This structural hypothesis was confirmed by the formation of one-dimensional assemblies of **Au-1** through binding interaction with ferrocene dimers (see structure in Figure 1). By use of tailor-made molecules as linkers, the **Au-1** clusters may be assembled in well-ordered arrangements with desired symmetry and interparticle distance.

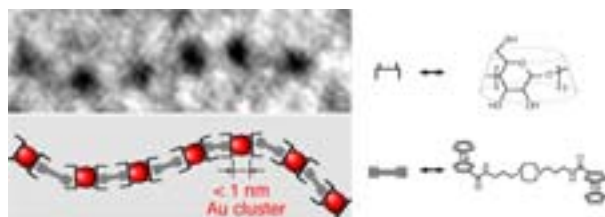


**Figure 1.** One-dimensional arrangements of **Au-1** formed by host-guest interaction with ferrocene dimers.

### IX-P-4 Size-Specific Catalytic Activity of Polymer-Stabilized Gold Nanoclusters for Aerobic Alcohol Oxidation in Water

TSUNOYAMA, Hironori; SAKURAI, Hidehiro;  
NEGISHI, Yuichi; TSUKUDA, Tatsuya<sup>1</sup>  
(<sup>1</sup>IMS, CREST)

[*J. Am. Chem. Soc.* **127**, 9374–9375 (2005)]

Gold nanoclusters ( $\phi$  = 1.3 nm) stabilized by poly(*N*-vinyl-2-pyrrolidone) (Au:PVP NCs) readily oxidize benzylic alcohols to the corresponding aldehydes and/or

carboxylic acids under ambient temperature in water. Kinetic measurement revealed that smaller Au:PVP NCs exhibit higher catalytic activity than larger (9.5 nm) homologues and, more surprisingly, than Pd:PVP NCs of comparable size (1.5 and 2.2 nm). On the basis of the marked difference in the kinetic isotope effect and activation energy between Au:PVP and Pd:PVP NCs, a reaction mechanism for alcohol oxidation catalyzed by Au:PVP NCs is proposed in which a superoxo-like molecular oxygen species adsorbed on the surface of the small Au NCs abstracts a hydrogen atom from the alkoxide.

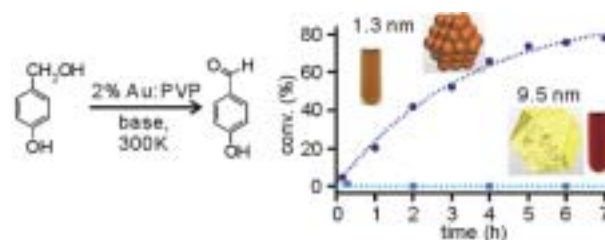


**Figure 1.** Time-course of conversion of *p*-hydroxyl benzyl alcohol by Au:PVP NCs ( $\phi$  = 1.3 and 9.5 nm).

### IX-P-5 Fabrication of Two dimensional Arrays of Size-Selected Gold Clusters

TSUNOYAMA, Hironori; NEGISHI, Yuichi;  
TSUKUDA, Tatsuya<sup>1</sup>  
(<sup>1</sup>IMS, CREST)

Alkanethiolate-protected gold (Au:SR) clusters of the size range of 1 ~ 5 nm were prepared by a ligand exchange of polymer-stabilized gold clusters (Au:PVP)<sup>1</sup> dispersed in water and subsequent heat treatment.<sup>2</sup> The Au:SR clusters thus obtained were size selected by using gel permeation chromatography (GPC).<sup>3</sup> The mass spectrometric characterization of the fractionated samples has revealed that the magic-numbered gold clusters with core masses of 8 kDa (1.1 nm), 14 kDa (1.3 nm), 22 kDa (1.5 nm), and 28 kDa (1.7 nm)<sup>4</sup> can be isolated by the GPC in a recycled operation. As for the Au:SR clusters of > 2 nm, the GPC separation yielded the sized selected clusters with a resolution of one atomic shell (0.5 nm in diameter). Two-dimensional arrays of the size-selected Au:SR clusters were fabricated by Langmuir-Brodgett technique. The structures of the films transferred to the amorphous carbon and other substrates (graphite and titania) were characterized by TEM, AFM, and SEM. Fabrication of model catalytic systems by using the cluster film thus prepared is now underway in collaboration with the groups of Profs. Al-Shamery (Oldenburg Univ.) and Matsumoto (IMS).

#### References

- 1) H. Tsunoyama *et al.*, *Langmuir* **20**, 11293 (2004).
- 2) T. Shimizu *et al.*, *J. Phys. Chem. B* **107**, 2719 (2003).
- 3) H. Murayama *et al.*, *J. Phys. Chem. B* **108**, 3496 (2004).
- 4) T. G. Schaaff *et al.*, *J. Phys. Chem. B* **101**, 7885 (1997).

## IX-Q Structural Analyses of Biological Macromolecules by Ultra-High Field NMR Spectroscopy

Our research seeks the underlying molecular basis for the function of biological macromolecules. In particular, we are interested in the function of molecular machines that work in the cellular processes involving protein folding, transport and degradation, and of glycoproteins playing important roles in the humoral and cellular immune systems. By use of ultra-high field NMR spectroscopy, we aim to elucidate the three-dimensional structure, dynamics, and interactions of proteins and glycoconjugates at the atomic level. A knowledge gained in this project will provide the structural basis for the rational design of drugs and biomolecular engineering that contribute towards a detailed understanding of biological systems.

### IX-Q-1 Ultra-High Field NMR Study of Carbohydrate-Protein Interactions

KAMIYA, Yukiko<sup>1</sup>; YAMAGUCHI, Yoshiki<sup>2</sup>;  
SASAKAWA, Hiroaki<sup>1</sup>; KATO, Koichi<sup>1</sup>  
(<sup>1</sup>IMS and Nagoya City Univ.; <sup>2</sup>Nagoya City Univ.)

NMR analyses of glycans have been hampered by spectral overlap and low sensitivity. It is obviously advantageous to measure NMR spectra of these molecules at an ultra-high magnetic field because of high resolution and high sensitivity. We demonstrate that the 920 MHz NMR spectra provide us with atomic information on complicated glycoconjugates.

The vesicular integral protein of 36 kDa (VIP36) is an intracellular animal lectin, which act as a putative cargo receptor recycling between the Golgi and the endoplasmic reticulum. Although VIP36 has been reported to recognize glycoproteins carrying high mannose-type oligosaccharides, very little has been known about structural aspects of the sugar-binding modes of this cargo receptor. We have therefore analyzed the interactions between a recombinant carbohydrate recognition domain of VIP36 (VIP36-CRD) and chemically synthesized oligosaccharides by use of nuclear magnetic resonance spectroscopy.

Figure 1a shows the anomeric regions of the 500 MHz <sup>1</sup>H NMR spectra of Man<sub>9</sub>GlcNAc<sub>2</sub>. The signals derived from Man-D1, Man-D2 and Man-D3 are severely degenerated. In contrast, these peaks are perfectly separated in the 920 MHz NMR spectrum (Figure 1b).

The one-dimensional <sup>1</sup>H NMR spectra of Man<sub>9</sub>GlcNAc<sub>2</sub> titrated with VIP36-CRD were observed for identification of sugar residues involved in binding to this lectin domain. Upon titration with VIP36-CRD, selective line broadening was observed for the signals originating from the mannose residues at positions 4, C, and D1, which correspond to the D1 arm of the Man<sub>9</sub>GlcNAc<sub>2</sub> (Figure 1c,d). On the basis of these data, we conclude that VIP36-CRD interacts predominantly with the D1 arm of high-mannose oligosaccharides.

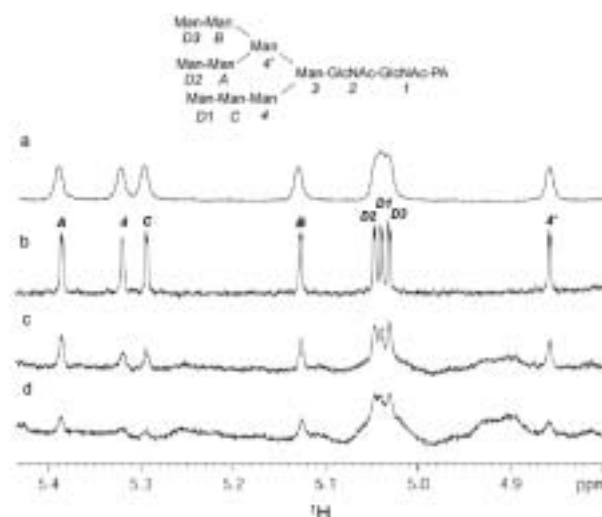


**Figure 1.** <sup>1</sup>H NMR spectra of oligosaccharide, Man<sub>9</sub>GlcNAc<sub>2</sub> (anomeric region). These spectra were recorded at the <sup>1</sup>H frequency of 500 MHz(a) and 920 MHz(b–d) in the absence (a, b) and presence of 0.2 equiv.(c) and 0.5 equiv.(d) of VIP36-CRD.

### IX-Q-2 Ultra-High Field NMR Study of Glycoproteins

NAGANO, Mayumi<sup>1</sup>; YAMAGUCHI, Yoshiki<sup>2</sup>;  
SASAKAWA, Hiroaki<sup>1</sup>; KATO, Koichi<sup>1</sup>  
(<sup>1</sup>IMS and Nagoya City Univ.; <sup>2</sup>Nagoya City Univ.)

Many of the proteins in the living systems express carbohydrate moieties. Although the biological importance of oligosaccharides covalently linked to proteins has been widely recognized, little is known about their specific roles from the structural aspect. This deficiency in our knowledge is largely due to the lack of an appropriate methodology to deal with glycoproteins as targets of structural biology. The carbohydrate moieties of glycoproteins generally exhibit microheterogeneities and possess a significant degree of freedom in internal motion, which hampers crystallization or interpretation of electron density. NMR spectroscopy can potentially provide us with information on structure and dynamics of glycoproteins in solution. However, there are few reports of structural determination of glycoproteins by NMR spectroscopy. In this situation, we have been developing NMR techniques for structural analyses at atomic resolution of glycoproteins in solution. In this methodology, the glycans and/or polypeptides of glyco-

proteins are uniformly or selectively labeled with stable isotopes ( $^{13}\text{C}$ ,  $^{15}\text{N}$ , and  $^2\text{H}$ ) by metabolic or enzymatic manners. We demonstrate our strategy using the Fc portion of immunoglobulin G (IgG) as a model system. A series of double and triple resonance experiments were performed for the uniformly  $^{13}\text{C}/^{15}\text{N}$ -labeled IgG-Fc. Figure 1 shows the 2D HSQC spectrum of IgG-Fc recorded on a 920 MHz NMR spectrometer. These spectra enabled us to assign the signals originating from the polypeptide backbone and the carbohydrate moieties. The NMR spectral data provide us with the basis for elucidation of structure and dynamics of the carbohydrate moieties as well as the polypeptide chains of the Fc glycoprotein in solution.

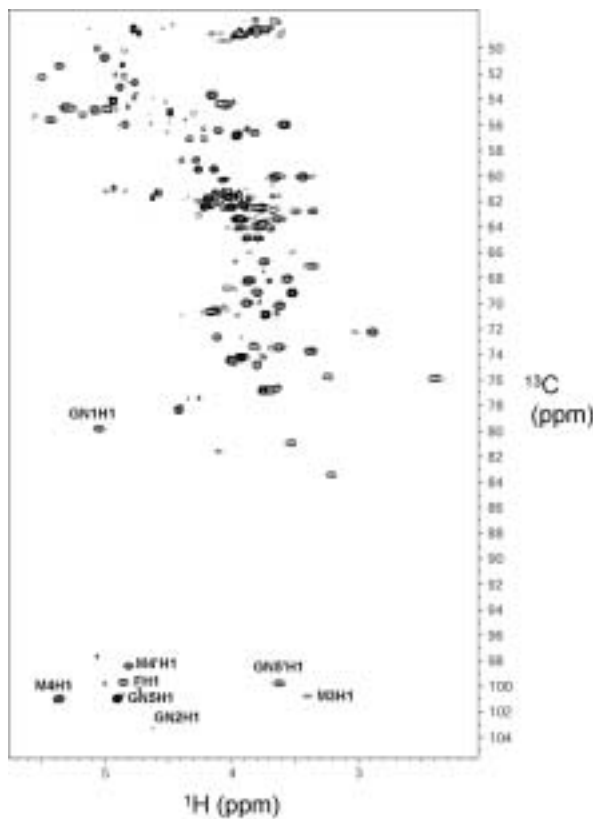


**Figure 1.**  $^1\text{H}$ - $^{13}\text{C}$  HSQC spectrum of the carbohydrate moieties of isotopically labeled IgG-Fc. The assignments of anomeric peaks are indicated in the spectrum.

## IX-R Electronic Structure and Collision Dynamics of Atoms and Molecules Studied by Electron Impact at Large Momentum Transfer

Binary ( $e,2e$ ) or electron momentum spectroscopy (EMS) is a high-energy electron-impact ionization experiment at large momentum transfer. The method involves coincident detection of the two outgoing electrons, allowing one to measure electron momentum densities for individual transitions or to look at molecular orbitals in momentum space. For molecular targets, however, EMS has long been plagued by the fact that the conventional ( $e,2e$ ) experiments measure averages over all orientations of gaseous targets; the spherical averaging results in enormous loss of versatile information on the target electronic structure, anisotropy of the target wavefunction in particular. To overcome the historical experimental difficulty, we have proposed the ( $e,2e+M$ ) method based on axial recoil fragmentation of the residual molecular ion and molecular frame ( $e,2e$ ) cross sections have been successfully measured for the first time. Further attempts along this line are now in progress, opening the door for detailed studies of bound electronic wavefunctions of molecules as well as of stereodynamics of electron-molecule collisions.

### IX-R-1 Development and Use of a Multichannel ( $e,2e$ ) Spectrometer for Electron Momentum Densities of Molecules

TAKAHASHI, Masahiko<sup>1</sup>; UDAGAWA, Yasuo<sup>1</sup>  
(<sup>1</sup>IMS and Tohoku Univ.)

[*J. Phys. Chem. Solids* **65**, 2055–2059 (2004)]

We have developed an ( $e,2e$ ) spectrometer with the introduction of modern multiparameter techniques. In particular, the high sensitivity achieved by simultaneous detection in energy and momentum is remarkable, opening up the possibilities of more precise and more advanced studies on the electronic structure of atoms and molecules. To illustrate some of the features, an overview of our recent results is presented. Highlights are applications to collision dynamics of H<sub>2</sub> and development of a method for a complete three-dimensional mapping of electron momentum densities in gaseous molecules. Both of these studies are based on the high sensitivity of the spectrometer.

### IX-R-2 Observation of Molecular Frame ( $e,2e$ ) Cross Section Using an Electron-Electron-Fragment Ion Triple Coincidence Apparatus

TAKAHASHI, Masahiko<sup>1</sup>; WATANABE, Noboru<sup>1</sup>;  
KHAJURIA, Yugal<sup>2</sup>; NAKAYAMA, Kazuya<sup>3</sup>;  
UDAGAWA, Yasuo<sup>1</sup>; ELAND, John H. D.<sup>4</sup>  
(<sup>1</sup>IMS and Tohoku Univ.; <sup>2</sup>IMS and IIT Madras;  
<sup>3</sup>Tohoku Univ.; <sup>4</sup>IMS and Oxford Univ.)

[*J. Electron Spectrosc. Relat. Phenom.* **141**, 83–93  
(2004)]

An apparatus for electron-electron-fragment ion triple coincidence experiments has been developed to examine binary ( $e,2e$ ) scattering reaction in the molecular frame. In the axial recoil limit of fragmentation of the residual ion, measurements of vector correlations among the three charged particles are equivalent to ( $e,2e$ ) experiments with fixed-in-space molecules. Details and performance of the apparatus are reported, together with preliminary result of collision dynamics

study on ionization-excitation processes of fixed-in-space H<sub>2</sub> molecules. We believe that this is the first observation of molecular frame ( $e,2e$ ) cross sections.

### IX-R-3 ( $e,3e$ ) Collisions on Mg in the Impulsive Regime Studied by Second Born Approximation

WATANABE, Noboru<sup>1</sup>; COOPER, John W.<sup>2</sup>; VAN  
BOEYEN, Roger W.<sup>3</sup>; DOERING, John P.<sup>3</sup>;  
MOORE, John H.<sup>2</sup>; COPLAN, Michael A.<sup>2</sup>  
(<sup>1</sup>IMS and Tohoku Univ.; <sup>2</sup>Univ. Maryland; <sup>3</sup>Johns  
Hopkins Univ.)

[*J. Phys. B: At., Mol. Opt. Phys.* **37**, 4551–4560 (2004)]

Five-fold differential cross sections for electron-impact double ionization of the 3s electrons of magnesium have been calculated in the second Born approximation in the impulsive regime. Comparing these results with calculations carried out in the first Born approximation demonstrates the dominant contribution of the second Born term. The second Born calculation shows that contribution of the two-step 2 (TS2) process becomes large under the condition where sequential binary collisions on the Bethe ridge can occur. The effect of electron correlation in the initial target state is also examined by using a configuration interaction wavefunction.

### IX-R-4 Electron Momentum Spectroscopy of Valence Satellites of Neon

WATANABE, Noboru<sup>1</sup>; KHAJURIA, Yugal<sup>2</sup>;  
TAKAHASHI, Masahiko<sup>1</sup>; UDAGAWA, Yasuo<sup>1</sup>  
(<sup>1</sup>IMS and Tohoku Univ.; <sup>2</sup>IMS and IIT Madras)

[*J. Electron Spectrosc. Relat. Phenom.* **142**, 325–334  
(2005)]

Electron momentum spectroscopy (EMS) study of the neon valence satellites is reported. The experiments were performed at impact energies of 1250, 1450 and 1670 eV using a multichannel spectrometer that features high sensitivity. Binding energy spectra up to 100 eV

and momentum profiles for the  $2p^{-1}$  and  $2s^{-1}$  primary transitions as well as the satellites are presented. The results are used to examine impact energy dependence of the relative intensities and shapes of the satellite momentum profiles. The results are also used to determine symmetries and spectroscopic factors of the satellites, and are compared with the previous experiments by EMS and photoelectron spectroscopy and sophisticated theoretical calculations. The present study has largely resolved controversies in the previous studies.

#### IX-R-5 Theoretical Fine Spectroscopy with Symmetry-Adapted-Cluster Configuration-Interaction Method: Outer- and Inner-Valence Ionization Spectra of Furan, Pyrrole, and Thiophene

EHARA, Masahiro<sup>1</sup>; OHTSUKA, Yuhki<sup>1</sup>;  
NAKATSUJI, Hiroshi<sup>1</sup>; TAKAHASHI, Masahiko<sup>2</sup>;  
UDAGAWA, Yasuo<sup>2</sup>

(<sup>1</sup>Kyoto Univ.; <sup>2</sup>IMS and Tohoku Univ.)

[*J. Chem. Phys.* **122**, 234319 (10 pages) (2005)]

Theoretical fine spectroscopy has been performed for the valence ionization spectra of furan, pyrrole, and thiophene with the symmetry-adapted-cluster configuration-interaction general-*R* method. The present method described that the  $\pi^1$  state interacts with the  $\pi_3^{-2}\pi^*$ ,  $\pi_2^{-2}\pi^*$ , and  $\pi_2^{-1}\pi_3^{-1}\pi^*$  shake-up states providing the split peaks and the outer-valence satellites, both of which are in agreement with the experiments. The intensity distributions were analyzed in detail for the inner-valence-region. In particular, for furan, theoretical intensities were successfully compared with the intensity measured by the electron momentum spectroscopy. The interactions of the  $3b_2$  and  $5a_1$  states with the shake-up states were remarkable for furan and pyrrole, while the  $4b_2$  state of thiophene had relatively large intensity.

#### IX-R-6 Observation of a Molecular Frame (*e,2e*) Cross Section: An (*e,2e+M*) Triple Coincidence Study on H<sub>2</sub>

TAKAHASHI, Masahiko<sup>1</sup>; WATANABE, Noboru<sup>1</sup>;  
KHAJURIA, Yugal<sup>2</sup>; UDAGAWA, Yasuo<sup>1</sup>; ELAND,  
John H. D.<sup>3</sup>

(<sup>1</sup>IMS and Tohoku Univ.; <sup>2</sup>IMS and IIT Madras; <sup>3</sup>IMS and Oxford Univ.)

[*Phys. Rev. Lett.* **94**, 213202 (4 pages) (2005)]

We report the first experimental results showing transition-specific anisotropy of molecular frame (*e,2e*) cross sections. Vector correlations between the two outgoing electrons and the fragment ion have been measured for specific ionization-excitation processes of H<sub>2</sub>. The results enable us to obtain molecular frame (*e,2e*) cross sections for transitions to the  $2s\sigma_g$  and  $2p\sigma_u$  excited states of H<sub>2</sub><sup>+</sup>, thereby making stereodynamics of the electron-molecule collisions directly visible.

#### IX-R-7 (*e,2e*) and (*e,3-1e*) Studies on Double Processes of He at Large Momentum Transfer

WATANABE, Noboru<sup>1</sup>; KHAJURIA, Yugal<sup>2</sup>;  
TAKAHASHI, Masahiko<sup>1</sup>; UDAGAWA, Yasuo<sup>1</sup>;  
VINITSKY, Pavel S.<sup>3</sup>; POPOV, Yuri V.<sup>3</sup>;  
CHULUUNBAATAR, Ochbadrakh<sup>4</sup>; KOZAKOV,  
Konstantin A.<sup>3</sup>

(<sup>1</sup>IMS and Tohoku Univ.; <sup>2</sup>IMS and IIT Madras;  
<sup>3</sup>Moscow State Univ.; <sup>4</sup>JINR)

[*Phys. Rev. A* **72**, 32705 (11 pages) (2005)]

The double processes of He in electron-impact ionization, single-ionization with simultaneous excitation and double-ionization, have been studied at large momentum transfer using an energy- and momentum-dispersive binary (*e,2e*) spectrometer. The experiment has been performed at an impact energy of 2080 eV in the symmetric noncoplanar geometry. In this way we have achieved a large momentum transfer of 9 a.u., a value that has never been realized so far for the study on double-ionization. The measured (*e,2e*) and (*e,3-1e*) cross sections for transitions to the  $n = 2$  excited state of He<sup>+</sup> and to doubly ionized He<sup>2+</sup> are presented as normalized intensities relative to that to the  $n = 1$  ground state of He<sup>+</sup>. The results are compared with first-order plane-wave impulse approximation (PWIA) calculations using various He ground-state wavefunctions. It is shown that shapes of the momentum-dependent (*e,2e*) and (*e,3-1e*) cross sections are well reproduced by the PWIA calculations only when highly correlated wavefunctions are employed. However, noticeable discrepancies between experiment and theory remain in magnitude for both the double processes, suggesting importance of higher-order effects under the experimental conditions examined as well as of acquiring more complete knowledge of electron correlation in the target.

#### IX-R-8 Electron Momentum Spectroscopy of the HOMO of Acetone

CHO, Tegyon<sup>1</sup>; TAKAHASHI, Masahiko<sup>2</sup>;  
UDAGAWA, Yasuo<sup>2</sup>

(<sup>1</sup>Tohoku Univ.; <sup>2</sup>IMS and Tohoku Univ.)

[*J. Photochem. Photobiol.* in press]

Electron momentum profiles of the HOMO of acetone have been measured under experimental conditions where a use of the plane-wave impulse approximation is justified. A double peak is observed in the experimental profile and it was found that calculated profiles by the use of the standard basis set always underestimate the magnitude of the low momentum peak. Possible origins of the discrepancies between the calculated and measured profiles are examined, leading to an improved agreement by modifying the exponents of diffuse functions employed.

**IX-R-9 ( $e,3-1e$ ) Reactions at Large Momentum Transfer: The Plane-Wave Second Born Approximation**

VINITSKY, Pavel S.<sup>1</sup>; POPOV, Yuri V.<sup>1</sup>;  
KOZAKOV, Konstantin A.<sup>1</sup>; WATANABE,  
Noboru<sup>2</sup>; TAKAHASHI, Masahiko<sup>2</sup>  
(<sup>1</sup>Moscow State Univ.; <sup>2</sup>IMS and Tohoku Univ.)

[*Phys. Rev. A* to be submitted]

We consider theoretically symmetric ( $e,3-1e$ ) reactions of He atom at large momentum transfer. For evaluating the corresponding four-fold differential cross sections, a theory based on the re-normalized plane-wave second Born approximation (SBA) is developed. The numerical SBA calculations for both coplanar and non-coplanar symmetric geometries are performed and compared with experiments.

**IX-R-10 Binary ( $e,2e$ ) Study on Xe: Momentum Profile for the 4d Orbital Revisited**

KHAJURIA, Yugal<sup>1</sup>; TAKAHASHI, Masahiko<sup>2</sup>;  
WATANABE, Noboru<sup>2</sup>; UDAGAWA, Yasuo<sup>2</sup>;  
YOSHINO, Tae<sup>3</sup>; SAKAI, Yasuhiro<sup>3</sup>;  
MUKOYAMA, Takeshi<sup>4</sup>  
(<sup>1</sup>IMS and IIT Madras; <sup>2</sup>IMS and Tohoku Univ.; <sup>3</sup>Toho Univ.; <sup>4</sup>Kansai Gaidai Univ.)

[*J. Phys. B: At. Mol. Opt. Phys.* to be submitted]

Binary ( $e,2e$ ) cross sections have been measured for Xe using an energy- and momentum-dispersive multi-channel spectrometer at impact energy of 2055 eV. Assuming that the Xe 5p ionization process can be described by the distorted-wave Born approximation (DWBA), the experimental momentum profile for the 4d orbital was placed on an absolute scale. The absolute-scale Xe 4d experiment has been compared with DWBA calculations using the Hartree-Fock and Dirac-Fock wavefunctions, in order to exploit relativistic effects in both shape and intensity of momentum profile. Although DWBA/DF has been found to give better description than DWBA/HF, noticeable discrepancies between experiment and theory still remain.

**IX-R-11 Binary ( $e,2e$ ) Study on Inner Shell Orbitals of Ar and Xe**

MIYAKE, Yusuke<sup>1</sup>; SHIBUYA, Masahiro<sup>1</sup>;  
TAKAHASHI, Masahiko<sup>2</sup>; WATANABE, Noboru<sup>2</sup>;

UDAGAWA, Yasuo<sup>2</sup>; SAKAI, Yasuhiro<sup>3</sup>;  
MUKOYAMA, Takeshi<sup>4</sup>  
(<sup>1</sup>Tohoku Univ.; <sup>2</sup>IMS and Tohoku Univ.; <sup>3</sup>Toho Univ.;  
<sup>4</sup>Kansai Gaidai Univ.)

[*J. Phys. B: At. Mol. Opt. Phys.* to be submitted]

Binary ( $e,2e$ ) experiments were performed on Xe 4p, 4s and Ar 2p, 2s orbitals. The results are compared with distorted-wave Born approximation calculations using the Hartree-Fock and Dirac-Fock wavefunctions, in order to exploit relativistic effects in momentum profile. Furthermore, for Xe the experiments have revealed a broad band at around 100 eV, which has not been found by photoelectron spectroscopy. The band has been assigned as giant resonance of Xe 4d in the sequential two collisions of the projectile with the target electrons.

**IX-R-12 Construction of a New ( $e,2e+M$ ) Apparatus for Complete Imaging of Molecular Orbitals**

TAKAHASHI, Masahiko<sup>1</sup>; WATANABE, Noboru<sup>1</sup>;  
SHIBUYA, Masahiro<sup>2</sup>; MIYAKE, Yusuke<sup>2</sup>;  
UDAGAWA, Yasuo<sup>1</sup>; MIZUTANI, Nobuo; SUZUI,  
Mitsukazu; MIURA, Kazuhiro<sup>2</sup>; YANAGIDA,  
Satomi<sup>2</sup>; MINEGISHI, Kouji<sup>2</sup>; JAGUTZKI,  
Ottmar<sup>3</sup>; DÖRNER, Reinhard<sup>3</sup>  
(<sup>1</sup>IMS and Tohoku Univ.; <sup>2</sup>Tohoku Univ.; <sup>3</sup>Univ.  
Frankfurt)

We have constructed a new electron-electron-fragment ion triple coincidence apparatus for complete imaging of molecular orbitals. The major sections of the apparatus are a chamber equipped with a 2300 L/s turbo molecular pump, an electron gun, a spherical analyzer followed by a hexagonal delay-line position-sensitive detector which covers the full  $2\pi$  azimuth of the two outgoing electrons emerging at the scattering angle of  $45^\circ$ , a velocity imaging system to detect all of parent and fragment ions from the  $4\pi$  solid angle, and data gathering electronics. The electron gun and spherical analyzer have been developed at the machine shop of the Tohoku University, while the chamber and the data gathering electronics have been developed at the equipment development center of IMS. This project aims at fully extending our preliminary ( $e,2e+M$ ) studies [M. Takahashi *et al.*, *J. Phys. Chem. Solids* **65**, 2055 (2004); *J. Electron Spectrosc. Relat. Phenom.* **141**, 83 (2004); *Phys. Rev. Lett.* **94**, 213202 (2005)], which have made it possible to perform molecular frame ( $e,2e$ ) spectroscopy for the first time.

**IX-S Electronic Structure and Collision Dynamics of Atoms and Molecules Studied by Photon Impact**

The group takes another, photon-impact, approach to issues of electronic structure and collision dynamics, since photon-impact and electron-impact or photoelectric effects and Compton scattering are complementary to each other.

### IX-S-1 Inner-Shell Photoelectron Angular Distributions from Fixed-in-Space OCS Molecules

GOLOVIN, Alexander V.<sup>1,2</sup>; ADACHI, Junichi<sup>1,3,4</sup>; MOTOKI, Souhei<sup>1</sup>; TAKAHASHI, Masahiko<sup>5</sup>; YAGISHITA, Akira<sup>1,3</sup>

(<sup>1</sup>KEK-PF; <sup>2</sup>St. Petersburg State Univ.; <sup>3</sup>Univ. Tokyo; <sup>4</sup>IMS; <sup>5</sup>IMS and Tohoku Univ.)

[*J. Phys. B: At. Mol. Opt. Phys.* **38**, L63–L68 (2005)]

The photoelectron angular distributions (PADs) for the OCS O 1s, C 1s and S 2p<sub>1/2</sub>, 2p<sub>3/2</sub> ionization have been measured in the shape resonance region. The experimental results have been compared with multiple scattering X $\alpha$  calculations. It is found that the position of an ionized atom plays a significant role. For a central position (C 1s ionization) the PAD is relatively symmetric. In the case of S 2p and O 1s ionization, electrons are emitted highly preferentially in a solid cone directed from the molecular centre to the respective S or O atom. For the OCS O 1s ionization the S–C fragment plays a very effective role as a ‘scatterer’ in the shape resonance region nearly all intensity in PAD is concentrated in the lobe between  $\theta = 50^\circ$  and  $80^\circ$ , but not along the molecular axis.

### IX-S-2 Coincidence Velocity Imaging Apparatus for the Study of Angular Correlations between Photoelectrons and Photofragments

HOSAKA, Kouichi<sup>1</sup>; ADACHI, Junichi<sup>1,2,3</sup>; GOLOVIN, Alexander V.<sup>2,4</sup>; TAKAHASHI, Masahiko<sup>5</sup>; WATANABE, Noboru<sup>5</sup>; YAGISHITA, Akira<sup>1,2</sup>

(<sup>1</sup>Univ. Tokyo; <sup>2</sup>KEK-PF; <sup>3</sup>IMS; <sup>4</sup>St. Petersburg State Univ.; <sup>5</sup>IMS and Tohoku Univ.)

[*J. Electron Spectrosc. Relat. Phenom.* submitted]

A new apparatus of coincidence velocity mapping has been developed for studies on inner-shell photoionization dynamics of molecules. It achieves velocity imaging for electrons and ions simultaneously, and keeps the time focusing. To demonstrate the performance of the new apparatus, some examples, photoelectron angular distributions from Ne atoms and randomly oriented NO molecules, photoion angular distributions from CO molecules, and photoelectron angular distributions from fixed-in-space CO and NO molecules, are reported.

### IX-S-3 Non-Dipole Effects in the Angular Distribution of Photoelectrons from the K-Shell of N<sub>2</sub> Molecule

HOSAKA, Kouichi<sup>1</sup>; ADACHI, Junichi<sup>1,2,3</sup>; GOLOVIN, Alexander V.<sup>2,4</sup>; TAKAHASHI, Masahiko<sup>5</sup>; TERAMOTO, Takahiro<sup>1</sup>; WATANABE, Noboru<sup>5</sup>; YAGISHITA, Akira<sup>1,2</sup>; SEMENOV, Sergei K.<sup>6</sup>; CHEREPKOV, Nikolai A.<sup>6</sup>

(<sup>1</sup>Univ. Tokyo; <sup>2</sup>KEK-PF; <sup>3</sup>IMS; <sup>4</sup>St. Petersburg State

Univ.; <sup>5</sup>IMS and Tohoku Univ.; <sup>6</sup>State Univ. Aerospace Instrum.)

[*J. Phys. B: At. Mol. Opt. Phys.* submitted]

Measurements and calculations of contribution of the non-dipole terms in the angular distribution of photoelectrons from the K-shell of randomly oriented N<sub>2</sub> molecules are reported. The angular distributions have been measured in the plane containing the photon polarization and the photon momentum vectors of linearly polarized radiation. Calculations have been performed in the relaxed core Hartree-Fock approximation with a fractional charge, and many-electron correlations were taken into account in the random phase approximation. Both theory and experiment show that the non-dipole terms are rather small in the photon energy region from the ionization threshold of the K-shell up to about 70 eV above it. From the theory it follows that the non-dipole terms for the individual shells of 1 $\sigma_g$  and 1 $\sigma_u$  are considerably large, therefore measurements resolving the contributions of the 1 $\sigma_g$  and 1 $\sigma_u$  shells are desirable.

### IX-S-4 Direct Observation of a Symmetry Lowering in Core-Electron Ionization for Highly Symmetric Molecules

HOSAKA, Kouichi<sup>1</sup>; ADACHI, Junichi<sup>1,2,3</sup>; GOLOVIN, Alexander V.<sup>2,4</sup>; TAKAHASHI, Masahiko<sup>5</sup>; TERAMOTO, Takahiro<sup>1</sup>; WATANABE, Noboru<sup>5</sup>; YAGISHITA, Akira<sup>1,2</sup>

(<sup>1</sup>Univ. Tokyo; <sup>2</sup>KEK-PF; <sup>3</sup>IMS; <sup>4</sup>St. Petersburg State Univ.; <sup>5</sup>IMS and Tohoku Univ.)

The symmetry lowering occurs quite often in the ionization of a core electron of equivalent constituent-atoms for highly symmetric molecules since the core-hole states of those molecules are generally quasi-degenerate and therefore couple over non-totally symmetric vibrational modes. Such couplings, referred as quasi-Jahn-Teller couplings, have been clearly investigated for the most basic example of CO<sub>2</sub>; the relation between the symmetry lowering and core-hole localization has been proved. The symmetry lowering which removes the equivalence of two oxygen atoms causes a fundamental quantum mechanical question; is it possible to decide whether the core hole is localized on the right oxygen atom or on the left? Here we report the direct observation of the symmetry lowering of the CO<sub>2</sub> induced by O1s photoionization.

## IX-T Study of Electronic Structure of Organic Thin Film and Organic/Inorganic Interface

Organic semiconductors have attracted much interest due to their highly potential, flexibility, electronic and optical properties, and their considerable promise in molecular device technologies. To clarify the electronic properties at the organic/organic and organic/metal interface, various characterization techniques such as high-resolution ultraviolet photoemission spectroscopy (UPS) and near-edge x-ray absorption fine structure (NEXAFS) have been performed for organic thin film systems, because origin of the energy position, band shape and band width of UPS spectra are keys to understand the interface properties such as the energy level alignment at the interface, intermolecular or molecule-substrate interactions, and carrier transfer/transport process. Especially, vibronic coupling and lifetime of a hole created in the highest occupied molecular orbital (HOMO) state in the organic thin film play a crucial role in the hole transport through the film and the electron injection from an electrode to the ionized molecule. The HOMO band in UPS spectra in principle involves such information about the hole, and thus offers a variety of key information that is necessary to unravel fundamental mechanism in carrier dynamics in organic devices.

### IX-T-1 Deep Insight into a Valence Hole in Organic Semiconductors: High-Resolution Ultraviolet Photoemission Study

**KERA, Satoshi; UENO, Nobuo<sup>1</sup>**  
(<sup>1</sup>Chiba Univ.)

[*IPAP Conf. Ser.* **6**, 51–56 (2005)]

We have succeeded to observe a very sharp highest occupied molecular orbital (HOMO) band for oriented thin films of various phthalocyanines prepared on graphite *via* high-resolution ultraviolet photoelectron spectroscopy. Hole-vibration couplings can be resolved even for films of large  $\pi$ -conjugated molecules. The fine structure would give us lots information on “hidden” properties in organic-based devices, such as molecular-vibration related carrier dynamics, intermolecular interaction, and molecule-substrate interaction. Moreover, it was found that the observed binding energy position is much affected by inhomogeneity of the film with different molecular orientations, leading to a broadening of the HOMO bandwidth.

### IX-T-2 UPS Fine Structures of Highest Occupied Band in Vanadyl-Phthalocyanine Ultrathin Film

**FUKAGAWA, Hirohiko<sup>1</sup>; YAMANE, Hiroyuki<sup>1</sup>;  
KERA, Satoshi; OKUDAIRA, K. Koji<sup>1</sup>; UENO,  
Nobuo<sup>1</sup>**  
(<sup>1</sup>Chiba Univ.)

[*J. Electron Spectrosc.* **144-147**, 475–478 (2005)]

Ultraviolet photoelectron spectra were measured for vanadyl phthalocyanine (VOPc) ultrathin films prepared on graphite to study effects of the molecular orientation and the electric dipole layer on the organic electronic states. VOPc has a permanent electric dipole perpendicular to the molecular plane, hence a well-defined electric dipole layer could be intentionally prepared by using the oriented monolayer. The observed binding-energy difference of the highest occupied molecular orbital (HOMO) bands between the oriented monolayer

and the double layer was found to agree with the vacuum level shift, leading to a conclusion that the molecular energy level with respect to the substrate Fermi level is changed when the molecule is in the electric dipole layer.

### IX-T-3 Fine Structure of the Highest Occupied Band in OTi-Phthalocyanine Monolayer

**YAMANE, Hiroyuki<sup>1</sup>; FUKAGAWA, Hirohiko<sup>1</sup>;  
HONDA, Hiroyuki<sup>1</sup>; KERA, Satoshi; OKUDAIRA,  
K. Koji<sup>1</sup>; UENO, Nobuo<sup>1</sup>**  
(<sup>1</sup>Chiba Univ.)

[*Synth. Met.* **152**, 297–300 (2005)]

Ultraviolet photoelectron spectra were measured for ultrathin films of OTi-phthalocyanine (OTiPc), which has an electric dipole perpendicular to the molecular plane, prepared on highly oriented pyrolytic graphite in order to study effects of the molecular orientation and the electric dipole layer on the organic electronic states. For the as-grown films, the observed highest occupied molecular orbital (HOMO) band consists of two prominent peaks that can be assigned to different molecular orientations. For the oriented monolayer obtained by annealing the as-grown film, we detected a very sharp HOMO band at 290 K. The binding-energy ( $E_B$ ) difference between the HOMO bands of the as-grown and annealed films was found to agree with the shift in the vacuum level. For the oriented monolayer, the observed sharp HOMO band involves at least four components that are ascribed to the coupling between the HOMO hole and the molecular vibration. Upon cooling the sample to 95 K, the HOMO bandwidth became sharper than that at 290 K. From the peak fitting using Voigt function, additional components are expected in the HOMO band at 95 K. Moreover, we detected the  $E_B$  shift in the HOMO band for the oriented monolayer upon cooling, which can be originated from decrease in the HOMO-hole screening due to the change in the film structure and/or the molecule-substrate interaction.

### IX-T-4 Hole/Vibration Coupling of the Highest Occupied Band in Pentacene Thin Film

**YAMANE, Hiroyuki<sup>1</sup>; NAGAMATSU, Shin-ichi<sup>1</sup>;  
FUKAGAWA, Hirohiko<sup>1</sup>; KERA, Satoshi;  
FRIEDLEIN, Rainer<sup>2</sup>; OKUDAIRA, K. Koji<sup>1</sup>;  
UENO, Nobuo<sup>1</sup>**  
(<sup>1</sup>Chiba Univ.; <sup>2</sup>Linköping Univ.)

[*Phys. Rev. B* **72**, 153412 (4 pages) (2005)]

The hole-vibration coupling of the highest occupied state in pentacene thin films on graphite is studied by high-resolution ultraviolet photoelectron spectroscopy. Vibration satellites in the film show a take-off-angle dependence, indicating that the Frank-Condon principle is not strictly satisfied in this system. They are more intense than in the gas phase and the vibrational energy in the film is slightly lower than that in the gas phase. This demonstrates that the reorganization energy in pentacene thin films is slightly larger than that estimated from the photoelectron spectrum of free pentacene molecules. Furthermore, it is pointed out that the electron hopping in the low-temperature film may occur in the femtosecond scale before the electronic polarization of the surrounding medium is completed.

#### **IX-T-5 Quantitative Analysis of Photoelectron Angular Distribution of a Single Domain Organic Monolayer Film: NTCDA on GeS(001)**

**KERA, Satoshi; TANAKA, Shinji<sup>1</sup>; YAMANE, Hiroyuki<sup>1</sup>; YOSHIMURA, Daisuke<sup>2</sup>; OKUDAIRA, K. Koji<sup>1</sup>; SEKI, Kazuhiko<sup>3</sup>; UENO, Nobuo<sup>1</sup>**  
(<sup>1</sup>Chiba Univ.; <sup>2</sup>IMS and Nagoya Univ.; <sup>3</sup>Nagoya Univ.)

[*Chem. Phys.* in press]

Angle-resolved photoelectron spectra were measured for a single-crystal monolayer film of naphthalene-1,4,5,8-tetracarboxylic dianhydride (NTCDA) prepared on a cleaved GeS(001) surface using synchrotron radiation. The observed photoelectron angular distributions were analyzed by a calculation using the single-scattering approximation combined with molecular orbital calculation. With the help of the low-energy electron diffraction pattern, the structure of the NTCDA monolayer on GeS(001) was estimated quantitatively.

#### **IX-T-6 UPS Study of VUV-Photodegradation of Polytetrafluoroethylene (PTFE) Ultrathin Film by Using Synchrotron Radiation**

**ONO, Masaki<sup>1</sup>; YAMANE, Hiroyuki<sup>1</sup>;  
FUKAGAWA, Hirohiko<sup>1</sup>; KERA, Satoshi;  
YOSHIMURA, Daisuke<sup>2</sup>; OKUDAIRA, K. Koji<sup>1</sup>;  
MORIKAWA, Eiji<sup>3</sup>; SEKI, Kazuhiko<sup>4</sup>; UENO, Nobuo<sup>1</sup>**  
(<sup>1</sup>Chiba Univ.; <sup>2</sup>IMS and Nagoya Univ.; <sup>3</sup>CAMD;  
<sup>4</sup>Nagoya Univ.)

[*Nucl. Instrum. Methods Phys. Res., Sect. B* **236**, 377–382 (2005)]

The VUV-photodegradation of polytetrafluoroethylene (PTFE) ultra-thin film was studied by ultraviolet photoelectron spectroscopy and quadrupole mass

spectrometry. These results were compared with the previous photodegradation studies of the polyvinylidene fluoride (PVDF) and polyethylene (PE). Generation of new peak,  $\pi$ -band originated from the C=C bond, was observed in the low binding energy region of the UPS spectra in both PVDF and PE during the photodegradation. In contrast, no new peak generation was observed in the UPS of the photodegraded PTFE. Mass spectrometry analysis also suggested that the C=C bond generation is not a major mechanism in the VUV photodegradation of PTFE.

#### **IX-T-7 Site-Specific Ion Desorption of Fluorinated Phthalocyanine Studied with Electron-Ion Coincidence Spectroscopy**

**OKUDAIRA, K. Koji<sup>1</sup>; WATANABE, Takahiro<sup>1</sup>;  
KERA, Satoshi; KOBAYASHI, Eiichi<sup>2</sup>; MASE, Kazuhiko<sup>2</sup>; UENO, Nobuo<sup>1</sup>**  
(<sup>1</sup>Chiba Univ.; <sup>2</sup>AIST)

[*J. Electron Spectrosc.* **144-147**, 464–464 (2005)]

Auger electron photo-ion coincidence (AEPICO) and Auger spectra of fluorinated copper phthalocyanine (F<sub>16</sub>CuPc) were observed to study the mechanism of the site-specific ion desorption. From the photon energy dependence of Auger electron spectra at fluorine (F) K-edge region, it is found that the spectator-Auger shift at  $h\nu = 691.4$  eV is about 2 eV. To estimate the contribution of spectator-Auger component to the Auger spectra, the difference Auger spectra were obtained by subtracting the Auger spectrum above F 1s ionization energy from observed Auger spectra. AEPICO yield spectra for F<sup>+</sup> at  $h\nu = 691.4$  eV gives a large intensity at  $E_{\text{kin}} = 650$  eV. The electron kinetic energy position of this intense F<sup>+</sup> AEPICO peak agrees with that of the difference Auger spectra, indicating that the most probable mechanism for F<sup>+</sup> ion desorption induced by the transition from F<sub>1s</sub> to  $\sigma(\text{C-F})^*$  is the spectator-Auger-stimulated ion desorption.

#### **IX-T-8 Polarized Near-Edge X-Ray-Absorption Fine Structure Spectroscopy of C<sub>60</sub>-Functionalized 11-Amino-1-Undecane Thiol Self-Assembled Monolayer: Molecular Orientation and Evidence for C<sub>60</sub> Aggregation**

**PATNAIK, Archita<sup>1</sup>; OKUDAIRA, K. Koji<sup>1</sup>; KERA, Satoshi; SETOYAMA, Hiroyuki<sup>1</sup>; MASE, Kazuhiko<sup>2</sup>; UENO, Nobuo<sup>1</sup>**  
(<sup>1</sup>Chiba Univ.; <sup>2</sup>AIST)

[*J. Chem. Phys.* **122**, 154703 (9 pages) (2005)]

Near-edge x-ray-absorption fine structure (NEXAFS) spectroscopy was adopted to probe the unoccupied electronic states of C<sub>60</sub> anchored onto an organized assembly of 11-amino-1-undecane thiol on Au(111). The polarization dependence of the intensity of  $\pi^*$  resonance associated with C<sub>60</sub>  $\pi$  network revealed the self-assembled monolayer (SAM) system to be oriented with an average molecular tilt angle of 57° with respect to the surface normal. Invoking the absence of solid-state band

dispersion effects and in comparison to solid C<sub>60</sub> and/or 1-ML C<sub>60</sub>/Au(111), the electronic structure of the resulting assembly was found dominated by spectral position shift and linewidth and intensity changes of the lowest unoccupied molecular orbital (LUMO), LUMO +1, and LUMO+2 orbitals. The latter implied hybridization between N *P<sub>z</sub>* of -NH<sub>2</sub> group of thiolate SAM and  $\pi$  levels of C<sub>60</sub>, resulting in a nucleophilic addition with a change in the symmetry of C<sub>60</sub> from *I<sub>h</sub>* to *C<sub>1</sub>* in the SAM. Occurrence of a new feature at 285.3 eV in the NEXAFS spectrum, assigned previously to  $\pi^*$  graphitic LUMO, signified the formation of aggregated clusters, (C<sub>60</sub>)<sub>*n*</sub> of C<sub>60</sub> monomer. Low tunneling current scanning tunneling microscopy confirmed them to be spherical and stable aggregates with *n* ~ 5.

# UVSOR Facility

## IX-U Development of the UVSOR Light Source

### IX-U-1 Successful Commissioning of New RF Cavity

MOCHIIHASHI, Akira; KATOH, Masahiro;  
HOSAKA, Masahito; YAMAZAKI, Jun-ichiro;  
HAYASHI, Kenji; TAKASHIMA, Yoshifumi<sup>1</sup>  
(<sup>1</sup>Nagoya Univ.)

We have built a new main RF accelerating cavity for the UVSOR-II electron storage ring. The new cavity can generate RF voltage of 150 kV without replacing the high power RF transmitter whose maximum output power is 20 kW. The cavity was installed in a short straight section in the spring 2005. The design RF voltage of 150 kV was soon achieved in the high-power test operation without electron beam. After the high power test operation, the test operation with electron beam was started. By carefully observing the pressure rise in the cavity, we have decided to start the user operation with a moderately high RF accelerating RF voltage of 100 kV, which is twice higher than before. After the vacuum is completely recovered, the operation with the design voltage of 150 kV will be started. These high values of the accelerating voltage have made the low emittance operation possible without reducing the

beam lifetime. Since May 2005, the UVSOR-II electron storage ring has been operated with a small emittance of 27 nm-rad for users.

### IX-U-2 Ion Trapping Phenomena at UVSOR-II

MOCHIIHASHI, Akira; KATOH, Masahiro;  
HOSAKA, Masahito; YAMAZAKI, Jun-ichiro;  
HAYASHI, Kenji; TAKASHIMA, Yoshifumi<sup>1</sup>;  
HORI, Yoichiro<sup>2</sup>  
(<sup>1</sup>Nagoya Univ.; <sup>2</sup>KEK)

We have observed the dependence of the vertical betatron tune on the vacuum condition on the UVSOR-II electron storage ring. We changed the vacuum condition artificially by turning off the vacuum pumps. The betatron tune was measured by RF-KO method. During the experiment, the storage ring was operated in multi-bunch filling mode, in which successive twelve RF buckets were filled with electrons and other four buckets were kept empty. This result strongly suggested that the non-linear electric field produced by the ions trapped by the electron beam caused the betatron tune shift. We have observed betatron tune shifts were consistent with the theoretical predictions.

## IX-V Researches by the Use of UVSOR

### IX-V-1 Development of Velocity Imaging Spectrometer for Observing Negative Fragment Ions

HIKOSAKA, Yasumasa; SHIGEMASA, Eiji

[*J. Electron Spectrosc. Relat. Phenom.* **148**, 5 (2005)]

A velocity imaging spectrometer has been developed to observe negative ions from molecular ion-pair dissociation. The imaging spectrometer furnishes with a pair of permanent magnets. The formed magnetic field effectively prevents the electrons' arrivals to the detector, without seriously affecting negative ions' flights. The performance of the imaging spectrometer is demonstrated in the observations of photoelectrons from O<sub>2</sub> and He, and O<sup>-</sup> from O<sub>2</sub>. Sample results on negative ion formation from O<sub>2</sub> and N<sub>2</sub>O, prove that the present imaging method provides useful information on the assignments of superexcited states and the dynamical properties of ion-pair dissociation.

### IX-V-2 Dynamics of Double Photoionization near the Ar 2p Threshold Investigated by Threshold Electron-Auger Electron Coincidence Spectroscopy

LABLANQUIE, Pascal<sup>1</sup>; SEINERMAN, Sergei<sup>2</sup>;  
PENENT, Francis<sup>3</sup>; AOTO, Tomohiro<sup>4</sup>;  
HIKOSAKA, Yasumasa; ITO, Kenji<sup>4</sup>  
(<sup>1</sup>LURE; <sup>2</sup>St. Petersburg State Maritime Tech. Univ.;  
<sup>3</sup>LCPMR; <sup>4</sup>KEK)

[*J. Phys. B* **38**, L9 (2005)]

Threshold electron-Auger electron coincidence spectroscopy measurements were carried out near the Ar 2p thresholds. Such a method allows us, for the first time, to observe the threshold electron yields associated with the selected final states of the Ar<sup>2+</sup> ion: 3p<sup>4</sup>(<sup>1</sup>D<sub>2</sub>), 3p<sup>4</sup>(<sup>1</sup>S<sub>0</sub>), 3p<sup>4</sup>(<sup>3</sup>P) resulting from the 2p hole Auger decay. All the spectra reveal strong PCI distortion. Comparison with calculations carried out in the framework of a quantum-mechanical PCI model allows us to clarify the mechanisms and the dynamics of threshold electron production. In the 3p<sup>4</sup>(<sup>1</sup>D<sub>2</sub>) and 3p<sup>4</sup>(<sup>1</sup>S<sub>0</sub>) channels, contribution to the threshold electron yield comes essentially from the PCI retardation of slow photoelectrons. In the 3p<sup>4</sup>(<sup>3</sup>P) final state channel, an additional process of valence multiplet decay of the 3p<sup>4</sup>(<sup>1</sup>D<sub>2</sub>)6d state plays a role at and below the L<sub>2</sub>, L<sub>3</sub> thresholds.

### IX-V-3 Origin of Threshold Electrons Produced in Decay of the Xe $4d^{-1}np$ Resonance

AOTO, Tomohiro<sup>1</sup>; HIKOSAKA, Yasumasa;  
HALL, Richard<sup>2</sup>; PENENT, Francis<sup>2</sup>;  
LABLANQUIE, Pascal<sup>3</sup>; ITO, Kenji<sup>1</sup>  
(<sup>1</sup>KEK; <sup>2</sup>DIAM; <sup>3</sup>LURE)

[*J. Electron Spectrosc. Relat. Phenom.* **142**, 319 (2005)]

Coincidence spectra of energetic electrons with threshold electrons were measured following photo-excitation of the Xe  $4d_{3/2,5/2} \rightarrow np$  resonances, in order to investigate the origin of threshold electrons, and the mechanism leading to formation of the Xe<sup>2+</sup>  $5p^{-2}$  and  $5s^{-1}5p^{-1}$  final states. A two-step decay process was observed in the production of Xe<sup>2+</sup>  $5p^{-2}(^1D)$  following decay of the  $7p$  resonance, where the intermediate state is Xe<sup>++</sup>  $5p^{-2}(^1S)8p$  that autoionizes emitting a pseudo-threshold electron. This process was confirmed in a time-of-flight analysis of the coincidence spectra of the energetic electrons with the threshold photoelectrons. It is suggested that a similar two-step process also contributes to the population of excited Xe<sup>2+</sup> states and is the main origin for the production of threshold electrons in decay of the  $4d^{-1} np$  resonances.

### IX-V-4 Coincidence Auger Spectroscopy

PENENT, Francis<sup>1,2</sup>; LABLANQUIE, Pascal<sup>3</sup>;  
HALL, Richard<sup>2</sup>; PALAUDOUX, Jerome<sup>1</sup>; ITO,  
Kenji<sup>4</sup>; HIKOSAKA, Yasumasa; AOTO,  
Tomohiro<sup>4</sup>; ELAND, John H. D.<sup>5</sup>  
(<sup>1</sup>LCPMR; <sup>2</sup>DIAM; <sup>3</sup>LURE; <sup>4</sup>KEK; <sup>5</sup>PTCL)

[*J. Electron Spectrosc. Relat. Phenom.* **144-147**, 7  
(2005)]

Auger electron spectroscopy (AES) and photoelectron spectroscopy (PES) are (with X-ray emission spectroscopy, XES) powerful analytical tools for material science and gas phase studies. However, the interpretation of Auger spectra can be very difficult due to the number and complexity of the involved processes. A deeper analysis, that allows a better understanding of relaxation processes following inner shell ionization, is possible with coincidence Auger spectroscopy. This method gives a new insight into electron correlation and allows disentangling of complex Auger electron spectra. In this paper, we present some examples related to gas phase coincidence Auger electron spectroscopy using synchrotron radiation. The detection in coincidence of an Auger electron with a threshold photoelectron presents two main advantages which are good energy resolution and high coincidence count rates. This technique has also provided new results on double Auger decay processes. A further qualitative breakthrough has been made with the development of a new experimental setup based on a magnetic bottle time-of-flight electron spectrometer. This opens up the field of multi-electron coincidence spectroscopy and allows a most detailed analysis with characterization of all possible decay pathways following inner shell ionization.

### IX-V-5 Collision Dynamics of the Kr<sup>8+</sup> + N<sub>2</sub> System Studied by a Multi-Coincidence Technique

KANEYASU, Tatsuo; AZUMA, Toshiyuki<sup>1</sup>;  
OKUNO, Kazuhiko<sup>1</sup>  
(<sup>1</sup>Tokyo Metropolitan Univ.)

[*J. Phys. B* **38**, 1341 (2005)]

We have developed a multi-coincidence technique to study MCI-molecule collisions. Using this technique, complicated reaction processes and collision dynamics in Kr<sup>8+</sup> + N<sub>2</sub> collisions have been successfully revealed in the energy region below 200 eV/u. The reaction processes in the single-, double-, triple- and quadruple-charge changing collisions are resolved and three low-energy collision phenomena, 'peak-shifting' of molecular ions, 'peak-splitting' and 'anisotropic fragmentation' of fragment ion pairs, are found in the time-of-flight spectra of target ions. By careful analysis of kinematics of all the products, it is concluded that the charge transfer in the Kr<sup>8+</sup> + N<sub>2</sub> collisions is dominated by multi-electron capture processes followed by electron emission and the collision dynamics is characterized by the transverse momentum transfer from the ion to the molecule and the appearance of the 'anisotropic fragmentation.'

### IX-V-6 Collision Dynamics of MCI-Molecule Systems Studied by Multi-Coincidence Technique

KANEYASU, Tatsuo; AZUMA, Toshiyuki<sup>1</sup>;  
OKUNO, Kazuhiko<sup>1</sup>  
(<sup>1</sup>Tokyo Metropolitan Univ.)

[*Nucl. Instrum. Methods Phys. Res., Sect. B* **235**, 352  
(2005)]

Collision dynamics and reaction processes in charge transfer collisions of Kr<sup>8+</sup> + N<sub>2</sub> below 200 eV/u have been studied. We used a multi-coincidence technique which enables us to obtain kinematic information for both the fragment ions and the scattered projectile. The collision phenomena observed in the time-of-flight spectra of target ions are well clarified in consideration of the kinematics in colliding particles. We found an anisotropy in charge-unbalanced fragmentation channels at lower collision energy. The anisotropic behavior becomes significant not only with decreasing the collision energy but also with increasing the charge imbalance of the fragment ion-pair. The collision dynamics in the Kr<sup>8+</sup> + N<sub>2</sub> system is characterized by the transverse recoil momentum and the anisotropic fragmentation.

### IX-V-7 Optical Investigations of the Clathrate $\alpha$ -Eu<sub>8</sub>Ga<sub>16</sub>Ge<sub>30</sub>

SICHELSCHMIDT, Joerg<sup>1</sup>; VOEVODIN,  
Vladimir<sup>1</sup>; PACHECO, J.<sup>1</sup>; GRIN, Yuri<sup>1</sup>;  
STEGLICH, Frank<sup>1</sup>; NISHI, Tatsuhiko<sup>2</sup>; KIMURA,  
Shin-ichi

(<sup>1</sup>Max-Planck Inst.; <sup>2</sup>SOKENDAI)

[*Eur. Phys. J. B* **46**, 363–366 (2005)]

We performed measurements of the optical reflectivity in the energy range 0.007–30 eV on the clathrate-VIII type compound  $\alpha$ -Eu<sub>8</sub>Ga<sub>16-x</sub>Ge<sub>30-x</sub> in order to investigate its electronic band structure. The very low charge carrier concentration as well as ferromagnetic ordering of the divalent Eu ions below 10.5 K characterize the spectra at photon energies below ~0.4 eV in accordance with the results of band structure calculations. Disorder induced bound states have been identified to affect the optical conductivity at energies between 10 and 100 meV.

#### IX-V-8 Influence of Cage Distortions on the Electronic Structure and Optical Properties of Ba<sub>6</sub>Ge<sub>25</sub>

ZEREC, Ivica<sup>1</sup>; CARRILLO-CABRERA, Wilder<sup>1</sup>; VOEVODIN, Vladimir<sup>1</sup>; SICHELSCHMIDT, Joerg<sup>1</sup>; STEGLICH, Frank<sup>1</sup>; GRIN, Yuri<sup>1</sup>; YARESKO, Alexander<sup>1</sup>; KIMURA, Shin-ichi (<sup>1</sup>Max-Planck Inst.)

[*Phys. Rev. B* **72**, 045122 (7 pages) (2005)]

Measurements of the optical conductivity on Ba<sub>6</sub>Ge<sub>25</sub> reveal a shift of optical spectral weights towards higher energies, as temperature is lowered below the structural phase transition. This behavior may be understood from the structural modifications revealed from the new structure refinements of x-ray diffraction data from high quality single crystals. Apart from Ba atoms, some Ge cage atoms are also shifted into distant split sites below the phase transition. In this way one covalent bond is broken between the corresponding Ge atoms and they become threefold bonded. Electronic band structure calculations for the low symmetry ordered model show that the bond breaking causes a shifting of three bands from the conduction to the valence region. This leads to a shifting of optical spectral weights towards higher energies, which is in agreement with the experimental data.

#### IX-V-9 Indirect and Direct Energy Gaps in Kondo Semiconductor YbB<sub>12</sub>

OKAMURA, Hidekazu<sup>1</sup>; MICHIZAWA, Takahiro<sup>1</sup>; NANBA, Takao<sup>1</sup>; KIMURA, Shin-ichi; IGA, Fumitoshi<sup>2</sup>; TAKABATAKE, Toshiro<sup>2</sup> (<sup>1</sup>Kobe Univ.; <sup>2</sup>Hiroshima Univ.)

[*J. Phys. Soc. Jpn.* **74**, 1954–1957 (2005)]

The optical conductivity [ $\sigma(\omega)$ ] of the Kondo semiconductor YbB<sub>12</sub> has been measured over wide ranges of temperature ( $T = 8$ –690 K) and photon energy ( $h\nu \geq 1.3$  meV). The  $\sigma(\omega)$  data reveal the entire crossover of YbB<sub>12</sub> from a metallic electronic structure at high  $T$ 's to a semiconducting one at low  $T$ 's. Associated with the gap development in  $\sigma(\omega)$ , a clear onset is newly found at  $h\nu = 15$  meV for  $T \leq 20$  K. The onset energy is

identified as the gap magnitude of YbB<sub>12</sub> appearing in  $\sigma(\omega)$ . This gap in  $\sigma(\omega)$  is interpreted as the indirect gap, which has been predicted by the renormalized-band model of the Kondo semiconductor. On the other hand, the strong mid-infrared (mIR) peak observed in  $\sigma(\omega)$  is interpreted as arising from the direct gap. The absorption coefficient around the onset and the mIR peak indeed show the characteristic energy dependences expected for indirect and direct optical transitions in conventional semiconductors.

#### IX-V-10 Kondo Ground States and Non-Fermi-Liquid Behavior in CeNi<sub>1-x</sub>Co<sub>x</sub>Ge<sub>2</sub>

LEE, B. K.<sup>1</sup>; HONG, J. B.<sup>1</sup>; KIM, J. W.<sup>1</sup>; JANG, K.-H.<sup>1</sup>; MUN, E. D.<sup>1</sup>; JUNG, M. H.<sup>2</sup>; KIMURA, Shin-ichi; PARK, T.<sup>3</sup>; PARK, J. -G.<sup>1</sup>; KWON, Yong-seung<sup>1</sup> (<sup>1</sup>Sungkyunkwan Univ., Korea; <sup>2</sup>BKSI, Korea; <sup>3</sup>LANL, U.S.A.)

[*Phys. Rev. B* **71**, 214433 (9 pages) (2005)]

We report measurements of the magnetic susceptibility, specific heat, and electrical resistivity of the heavy fermion alloy series CeNi<sub>1-x</sub>Co<sub>x</sub>Ge<sub>2</sub>. With increasing  $x$ , hybridization between the localized 4*f* and conduction band electrons is enhanced. The magnetic order observed at  $x = 0$  is completely suppressed at  $x = 0.3$  and non-Fermi-liquid behavior appears at the critical concentration, which is analyzed in terms of two-dimensional antiferromagnetic quantum fluctuations. Specific heat and magnetic susceptibility data are quantitatively explained by the Coqblin-Schrieffer model with degenerate impurity spin  $j = 1/2, 3/2, \text{ and } 5/2$  for Co concentration range of  $x \leq 0.6, 0.7 \leq x \leq 0.8, \text{ and } x \geq 0.9$ , respectively.

#### IX-V-11 Infrared Spectroscopy under Multiextreme Conditions: Direct Observation of Pseudogap Formation and Collapse in CeSb

NISHI, Tatsuhiko<sup>1</sup>; KIMURA, Shin-ichi; TAKAHASHI, Toshiharu<sup>2</sup>; MORI, Yoshihisa<sup>3</sup>; KWON, Yong-seung<sup>4</sup>; IM, Hojun<sup>1</sup>; KITAZAWA, Hideaki<sup>5</sup> (<sup>1</sup>SOKENDAI; <sup>2</sup>Kyoto Univ.; <sup>3</sup>Okayama Univ. Sci.; <sup>4</sup>Sungkyunkwan Univ., Korea; <sup>5</sup>NIMS)

[*Phys. Rev. B* **71**, 220401(R) (4 pages) (2005)]

Infrared reflectivity measurements of CeSb under multiextreme conditions (low temperatures, high pressures, and high magnetic fields) were performed. A pseudogap structure, which originates from the magnetic band folding effect, responsible for the large enhancement in the electrical resistivity in the single-layered antiferromagnetic structure (AF-1 phase) was found at a pressure of 4 GPa and at temperatures of 35–50 K. The optical spectrum of the pseudogap changes to that of a metallic structure with increasing magnetic field strength and increasing temperature. This change is the result of the magnetic phase transition from the AF-1 phase to other phases as a function of the

magnetic field strength and temperature. This result is an important optical observation of the formation and collapse of a pseudogap under multiextreme conditions.

#### IX-V-12 Infrared Study on CeSb under High Pressures

**KIMURA, Shin-ichi; NISHI, Tatsuhiko<sup>1</sup>; MORI, Yoshihisa<sup>2</sup>; SUMIDA, Yukitsune<sup>2</sup>; TAKAHASHI, Toshiharu<sup>3</sup>; KWON, Yong-seung<sup>4</sup>; IM, Hojun<sup>1</sup>; KITAZAWA, Hideaki<sup>4</sup>**

(<sup>1</sup>SOKENDAI; <sup>2</sup>Okayama Univ. Sci.; <sup>3</sup>Kyoto Univ.; <sup>4</sup>Sungkyunkwan Univ., Korea; <sup>5</sup>NIMS)

[*Physica B* **359-361**, 190–192 (2005)]

The optical reflectivity spectra ( $R(\omega)$ ) of CeSb have been measured at high pressures to investigate the origin of the physical properties appearing under pressures. At 300 K, the pressure dependence of  $R(\omega)$  revealed that the carrier density proportionally increases with increasing pressure up to 2.5 GPa. At lower temperature, the  $R(\omega)$  spectrum drastically changes with both temperature and pressure due to the complex magnetic phase diagram. Especially, at 2.5 GPa and 30 K, the  $R(\omega)$  intensity below 0.2 eV decreases, on the contrary that at around 0.3 eV increases. This result suggests that the density of states near the Fermi level decreases and shifts to the high-energy side.

#### IX-V-13 Electronic Structure of Bulk Metallic Glass $Zr_{55}Al_{10}Cu_{30}Ni_5$

**SODA, Kazuo<sup>1</sup>; SHIMBA, Kurando<sup>1</sup>; YAGI, Shinya<sup>1</sup>; KATO, Masahiko<sup>1</sup>; TAKEUCHI, Tsunehiro<sup>1</sup>; MIZUTANI, Uichiro<sup>1</sup>; ZHANG, T.<sup>2</sup>; HASEGARA, M.<sup>2</sup>; INOUE, Akihisa<sup>2</sup>; OTO, Takahiro; KIMURA, Shin-ichi**

(<sup>1</sup>Nagoya Univ.; <sup>2</sup>Tohoku Univ.)

[*J. Electron Spectrosc. Relat. Phenom.* **144-147**, 585–587 (2005)]

The electronic structure of a bulk metallic glass  $Zr_{55}Al_{10}Cu_{30}Ni_5$  has been studied by means of photoelectron spectroscopy in order to understand the origins of its large glass formation ability and unique mechanical properties from the microscopic point of view. The valence-band photoelectron spectra show three bands ascribed to the Zr 4d, Ni 3d, and Cu 3d states. A remarkable feature of these bands is the highly symmetric spectral shape with the high-binding energy and narrow width in comparison with the d bands of the crystalline transition metals. This is attributed to the lack of the crystalline periodicity in the metallic glass as well as the reduction in the neighbouring atoms to hybridize with those transition metals. A high-resolution valence-band spectrum also reveals the intensity reduction near the Fermi level, which implies that the pseudo-gap in the electronic structure may be one of the important factors for the glass formation.

#### IX-V-14 Carrier-Induced Infrared Magnetic Circular Dichroism in the Magnetoresistive Pyrochlore $Tl_2Mn_2O_7$

**OKAMURA, Hidekazu<sup>1</sup>; KORETSUNE, Toshihisa<sup>1</sup>; KIMURA, Shin-ichi; NANBA, Takao<sup>1</sup>; IMAI, Hideto<sup>2</sup>; SHIMAKAWA, Yuichi<sup>2</sup>; KUBO, Yoshimi<sup>2</sup>**  
(<sup>1</sup>Kobe Univ.; <sup>2</sup>NEC Corp.)

[*J. Phys. Soc. Jpn.* **74**, 970–974 (2005)]

Infrared magnetic circular dichroism (MCD), or equivalently magneto-optical Kerr effect, has been measured on the  $Tl_2Mn_2O_7$  pyrochlore, which is well known for exhibiting a large magnetoresistance around the Curie temperature  $T_C \sim 120$  K. A circularly polarized, infrared synchrotron radiation is used as the light source. A pronounced MCD signal is observed exactly at the plasma edge of the reflectivity near and below  $T_C$ . However, contrary to the conventional behavior of MCD for ferromagnets, the observed MCD of  $Tl_2Mn_2O_7$  grows with the applied magnetic field, and not scaled with the internal magnetization. It is shown that these results can be basically understood in terms of a classical magnetoplasma resonance. The absence of a magnetization-scaled MCD indicates a weak spin-orbit coupling of the carriers in  $Tl_2Mn_2O_7$ . We discuss the present results in terms of the microscopic electronic structures of  $Tl_2Mn_2O_7$ .

#### IX-V-15 Magnetic Ordering in Frustrated $Ce_5Ni_2Si_3$

**LEE, B. K.<sup>1</sup>; RYU, D. H.<sup>1</sup>; KIM, D. Y.<sup>1</sup>; HONG, J. B.<sup>1</sup>; JUNG, M. H.<sup>2</sup>; KITAZAWA, Hideaki<sup>3</sup>; SUZUKI, Osamu<sup>3</sup>; KIMURA, Shin-ichi; KWON, Yong-seung<sup>1</sup>**

(<sup>1</sup>Sungkyunkwan Univ., Korea; <sup>2</sup>BKSI, Korea; <sup>3</sup>NIMS)

[*Phys. Rev. B* **70**, 224409 (5 pages) (2004)]

The transport, magnetic, and thermal properties are studied on an antiferromagnetic compound  $Ce_5Ni_2Si_3$  with  $T_N = 7.3$  K. We find signatures of spin fluctuation in this geometrically frustrated magnet. The Curie-Weiss fit gives a large value of the paramagnetic Curie temperature, yielding a frustration parameter  $f = 8.4$ . The electronic specific heat coefficient  $\gamma = 300$  mJ/Ce mol  $K^2$  is strongly enhanced, leading to residual entropy at low temperatures. The spin fluctuation is suppressed as the magnetic field exceeds the metamagnetic transition field  $H_m = 1$  T, where the magnetoresistance decreases steeply. The steady increase of magnetic susceptibility below  $T_N$  is likely to be associated with the presence of paramagnetic Ce ions. For  $La_5Ni_2Si_3$ , a superconducting transition is observed at  $T_C = 1.8$  K.

#### IX-V-16 Features of Fluorescence Spectra of Polyethylene Terephthalate Films

**OUCHI, Isume<sup>1</sup>; NAKAI, Ikuo<sup>2</sup>; ONO, Mitsumasa<sup>3</sup>; KIMURA, Shin-ichi**

(<sup>1</sup>Tokushima Bunri Univ.; <sup>2</sup>Tottori Univ.; <sup>3</sup>Teijin DuPont Films Japan Ltd.)

[*Jpn. J. Appl. Phys.* **43**, 8107–8114 (2004)]

Out of two species of fluorescence of polyethylene terephthalate (PET), intrinsic fluorescence (I), which was caused by short-wavelength ( $< 320$  nm) excitation, was dominant for very thin films (less than a few microns), while, trap fluorescence (II), excited at longer wavelengths ( $> 320$  nm), was much more intense for thick films. This fact was confirmed, and explained by an elementary formula. Effects of polymerization catalysts onto the fluorescence spectra were found to be indirect; namely, peak positions of the fluorescence were not affected by catalyst systems, while fluorescence intensity was sensitive not only to catalyst systems but also to minute differences in local surroundings. Effects of catalyst systems on the weak absorption bands at 338 nm and 354 nm were examined. Integrated excitation spectra were resolved; therein, a hidden  $n \rightarrow \pi^*$  state was found. Most likely, this is related with the weak absorptions at 338 nm and 354 nm, which are the major origins of fluorescence (II).

#### IX-V-17 Anomalous Magnetic Properties and Non-Fermi-Liquid Behavior in Single Crystals of the Kondo Lattice $\text{CeNiGe}_{2-x}\text{Si}_x$

KIM, D. Y.<sup>1</sup>; RYU, D. H.<sup>1</sup>; HONG, J. B.<sup>1</sup>; PARK, J.-G.<sup>1</sup>; KWON, Yong-seung<sup>1</sup>; JUNG, M. A.<sup>1</sup>; JUNG, M. H.<sup>2</sup>; TAKEDA, Naoya<sup>3</sup>; ISHIKAWA, Masakazu<sup>3</sup>; KIMURA, Shin-ichi  
(<sup>1</sup>*Sungkyunkwan Univ., Korea*; <sup>2</sup>*KBSI, Korea*; <sup>3</sup>*Univ. Tokyo*)

[*J. Phys.: Condens. Matter* **16**, 8323–8334 (2004)]

We report on the magnetic susceptibility, specific heat and electrical resistivity of the heavy fermion compounds  $\text{CeNiGe}_{2-x}\text{Si}_x$  ( $0 \leq x \leq 1$ ). Compounds with  $x < 1$  show antiferromagnetic order, which with increasing  $x$  shifts toward lower temperature owing to increased exchange coupling between the localized 4f magnetic moments and conduction electrons. Eventually, the magnetic order almost becomes absent, for  $x = 1$ . An anomaly observed in the specific heat is well interpreted by the Kondo model for a degenerate impurity spin  $J = 1/2$  in the Coqblin–Schrieffer limit. A coherence peak indicative of the formation of a Kondo lattice is found in the electrical resistivity, whose features are consistent with the results for the specific heat. Interestingly, there is a significant deviation from Fermi-liquid behaviour at the critical concentration  $x = 1$ . This deviation is attributed to a quantum phase transition in a model with two-dimensional antiferromagnetic fluctuations.

#### IX-V-18 Sub-Natural Linewidth Auger Electron Spectroscopy of the 2s Hole Decay in HCl

ITO, Kenji; HIKOSAKA, Yasumasa; KANEYASU, Tatsuo; SHIGEMASA, Eiji

Auger-photoelectron coincidence spectroscopy, in which Auger electrons are measured in coincidence with the corresponding photoelectrons, can be a power-

ful tool to elucidate the decay dynamics of the core-hole states followed by the productions of doubly charged atomic and molecular ions. In our coincidence method, we measure threshold photoelectrons as photoelectrons to attain high detection efficiency. We have applied the coincidence method to the 2s hole decay in HCl. We tuned photon energy at the Cl 2s ionization threshold of HCl, and recorded the Auger electron spectrum in coincidence with the threshold photoelectrons. We have observed the Auger lines associated with the formations of  $\text{HCl}^{++}[(\text{Cl } 2p)^{-1}(\text{V})^{-1}]$  states via the  $L_1L_{2,3}V$  Coster-Kronig transitions, which are much faster than other Auger decay processes such as the LVV transitions. Ordinary Auger spectrum measured without any coincidences shows only broad structures due to the wide natural linewidth of the 2s hole states (1.8 eV FWHM). In contrast, several peaks appear on the coincidence spectrum we obtained, thanks to the sub-natural linewidth regime which is achieved by the coincidence observation using the high resolution spectrometers.

# Laser Research Center for Molecular Science

## IX-W Developments and Researches of New Laser Materials

Although development of lasers is remarkable, there are no lasers which lase in ultraviolet and far infrared regions. However, it is expected that these kinds of lasers break out a great revolution in not only the molecular science but also in the industrial world.

In this project we research characters of new materials for ultraviolet and far infrared lasers, and develop new lasers by using these laser materials.

### IX-W-1 Growth and Scintillation Properties of Yb Doped Aluminate, Vanadate and Silicate Single Crystals

**YOSHIKAWA, Akira<sup>1</sup>; OGINO, Hiraku<sup>1</sup>; SHIM, Jan Bo<sup>1</sup>; KOCHURIKIN, V. V.<sup>2</sup>; NIKL, M.<sup>3</sup>; SOLOVIEVA, N.<sup>3</sup>; ONO, Shingo; SARUKURA, Nobuhiko; KIKUCHI, M.<sup>4</sup>; FUKUDA, Tsuguo<sup>1</sup>**  
(<sup>1</sup>Tohoku Univ.; <sup>2</sup>GPI; <sup>3</sup>Inst. Phys. AS CR; <sup>4</sup>Tohoku Fukushi Univ.)

[*Opt. Mater.* **26**, 529 (2004)]

For the purpose of quick screening for charge transfer (CT) transitions of Yb<sub>3</sub> in various hosts, (Lu<sub>1-x</sub>Yb<sub>x</sub>)<sub>3</sub>Al<sub>5</sub>O<sub>12</sub> (Yb:LuAG) with  $x = 0.05, 0.15, 0.30$  and (Y<sub>1-x</sub>Yb<sub>x</sub>)AlO<sub>3</sub> (Yb:YAP) with  $x = 0.05, 0.10, 0.30$  were grown by the micro-pulling-down method. (Y,Yb)VO<sub>4</sub> with strong wetting was grown by edge defined film-fed growth method and materials, which require moderate temperature gradient, such as Ca<sub>8</sub>(La,Yb)<sub>2</sub>(PO<sub>4</sub>)<sub>6</sub>O<sub>2</sub> and (Gd,Yb)<sub>2</sub>SiO<sub>5</sub> were grown by Czochralski method. Strong dependence of the CT luminescence decay time and intensity on temperature was observed for Yb-doped LuAG and YAP. Super fast decay with 0.85 ns decay time was observed in Yb(30%) doped YAP at room temperature. Though the emission intensity is weak at room temperature, it exceeds several times that of PbWO<sub>4</sub>. In addition, CT luminescence of Yb:YAP occurs at longer wavelength than in BaF<sub>2</sub>, which enables the usage of glass-based photomultiplier for the detection. In addition, higher stopping power will be expected due to the higher density host compared with BaF<sub>2</sub>.

### IX-W-2 Onset Detection of Solid-State Phase Transition in Estrogen-Like Chemical via Terahertz Transmission Spectroscopy

**QUEMA, Alex; GOTO, Masahiro; SAKAI, Masahiro; JANAIRO, Gerardo<sup>1</sup>; OENZERFI, Riadh; TAKAHASHI, Hiroshi; ONO, Shingo; SARUKURA, Nobuhiko**  
(<sup>1</sup>De La Salle Univ.)

[*Appl. Phys. Lett.* **85**, 3914 (2004)]

Solid-state phase transition onset in an endocrine-disrupting estrogen-like chemical (1,4-naphthol) is detected using terahertz transmission spectroscopy. The appearance of two absorption peaks and the sudden

upsurge of terahertz-radiation power at 210 K indicate the onset of the solid-state phase transition. Differential scanning microscopy reveals a first-order phase transition at around 240 K while temperature-dependent x-ray diffraction analysis shows the occurrence of such phenomenon also at around 240 K. This demonstrates the sensitivity of the terahertz spectroscopic technique to phase transition since it provides a signal before such phenomenon actually occurs.

### IX-W-3 Design Principle of Wide-Gap Fluoride Hetero-Structures for Deep Ultraviolet Optical Devices

**OENZERFI, Riadh; ONO, Shingo; QUEMA, Alex; GOTO, Masahiro; SAKAI, Masahiro; SARUKURA, Nobuhiko; NISHIMATSU, Takeshi<sup>1</sup>; TERAKUBO, Noriaki<sup>1</sup>; MIZUSEKI, Hiroshi<sup>1</sup>; KAWAZOE, Yoshiyuki<sup>1</sup>; SATO, Hiroki<sup>1</sup>; YOSHIKAWA, Akira<sup>1</sup>; FUKUDA, Tsuguo<sup>1</sup>**  
(<sup>1</sup>Tohoku Univ.)

[*J. Appl. Phys.* **96**, 7655 (2004)]

The design of fluoride-based optical devices for deep ultraviolet applications is discussed. Variations in the band-gap energy and band structure with respect to composition are investigated for Li<sub>(1-x)</sub>K<sub>x</sub>Ba<sub>(1-y)</sub>Mg<sub>y</sub>F<sub>3</sub> perovskites. The band-gap energy, lattice constant, and band structure of perovskitelike fluorides are estimated based on *ab initio* calculations within the local-density approximation. The lattice-matched double hetero-structure with direct band-gap compounds (Li<sub>(1-x)</sub>K<sub>x</sub>Ba<sub>(1-y)</sub>Mg<sub>y</sub>F<sub>3</sub> on either LiBaF<sub>3</sub> or KMgF<sub>3</sub> substrates) is promising for fabrication.

### IX-W-4 Terahertz Time-Domain Spectroscopy of Amino Acids and Polypeptides

**YAMAMOTO, Koji<sup>1</sup>; TOMINAGA, Keisuke<sup>1</sup>; SASAKAWA, Hiroaki<sup>1</sup>; TAMURA, Atsuo<sup>1</sup>; MURAKAMI, Hidetoshi; OHTAKE, Hideyuki; SARUKURA, Nobuhiko**  
(<sup>1</sup>Kobe Univ.)

[*Biophys. J.* **L22** (2005)]

Frequency-dependent absorption coefficients and refractive indices of amino acids (glycine and L-alanine) and polypeptides (polyglycine and poly-L-alanine) in the wavenumber region from 7 to 55 cm<sup>-1</sup>

were measured by terahertz timedomain spectroscopy. A vibrational band was observed at  $45.5\text{ cm}^{-1}$  for polyglycine, which was assigned as an interchain mode. The reduced absorption cross sections of the amino acids and polypeptides show power-law behavior. The exponents are different between the monomers and polymers, and those of the two polypeptides suggest that the time dependences of the total dipole moments are similar in the timescale of subpico- to picoseconds.

## IX-X Development and Research of Advanced Tunable Solid State Lasers

Diode-pumped solid-state lasers can provide excellent spatial mode quality and narrow linewidths. The high spectral power brightness of these lasers has allowed high efficiency frequency extension by nonlinear frequency conversion. Moreover, the availability of new and improved nonlinear optical crystals makes these techniques more practical. Additionally, quasi phase matching (QPM) is a new technique instead of conventional birefringent phase matching for compensating phase velocity dispersion in frequency conversion. These kinds of advanced tunable solid-state light sources, so to speak "Chroma Chip Lasers," will assist the research of molecular science.

In this projects we are developing Chroma Chip Lasers based on diode-pumped-microchip-solid-state lasers and advanced nonlinear frequency conversion technique.

### IX-X-1 Spectroscopic Properties of Yb:GdVO<sub>4</sub> Single Crystal: Stark Levels, Selection Rules, and Polarized Cross Sections

SATO, Yoichi; TAIRA, Takunori; NAKAMURA, Osamu<sup>1</sup>; FURUKAWA, Yasunori<sup>1</sup>  
(<sup>1</sup>OXIDE)

[OSA Topical Meeting of Advanced Solid State Photonics MF8 (2005)]

Spectroscopic properties Yb:GdVO<sub>4</sub> single crystals were investigated. We determined the stark levels and discussed about the selection rules. We found that the 1030.7-nm transition from the lowest level in upper manifold to the highest level in lower manifold was forbidden transition in  $\pi$ -polarization. The absorption cross section, stimulated emission cross section, and radiative lifetime were also evaluated.  $\sigma_{ab}$  and  $\sigma_{em}$  at 948-nm were  $6.1$  and  $6.7 \times 10^{-20}$ -cm<sup>2</sup>, respectively. The calculated radiative lifetime of Yb:GdVO<sub>4</sub> was 313- $\mu$ s, and was consistent to the reported fluorescence lifetime of 320- $\mu$ s. From the wave-profiles of  $\sigma_{em}$  and polarized decay rate, the averaged wavelength of fluorescence was estimated to be 991-nm. If the pumping wavelength is set to 1000-nm, the absorption coefficient of 15 at.% Yb:GdVO<sub>4</sub> is still 9.8-cm<sup>-1</sup>, and laser cooling effect should be observed. Obtained spectroscopic parameters in this work were consistent with the previous report of laser oscillation. Authors also indicate that Yb:GdVO<sub>4</sub> has enough absorption at pumping wavelength for laser cooling.

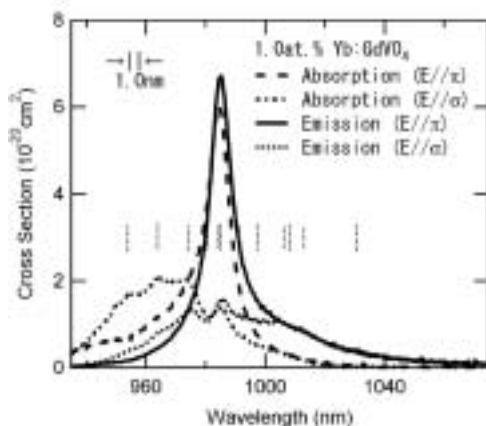


Figure 1. Polarized absorption and stimulated emission cross sections of Yb:GdVO<sub>4</sub>.

### IX-X-2 Spectroscopic Properties of All-Ceramic Composite with Layer-by-Layer of Nd:Y<sub>3</sub>Al<sub>5</sub>O<sub>12</sub> and Nd:Y<sub>3</sub>ScAl<sub>4</sub>O<sub>12</sub>

SATO, Yoichi; TAIRA, Takunori; IKESUE, Akio<sup>1</sup>  
(<sup>1</sup>JFCC)

[Conf. Lasers Electro-Optics JTuC28 (2005)]

The ceramic laser materials have been greatly interested because of their possibility for advanced lasers. The technique of composite ceramics has been especially considered to be the most important in the ceramics. Recently, this new ceramics technology about composite ceramics has been realized. In this work, we fabricated the all-ceramic composite with layer-by-layer of Nd:Y<sub>3</sub>ScAl<sub>4</sub>O<sub>12</sub> (YSAG) and Nd:Y<sub>3</sub>Al<sub>5</sub>O<sub>12</sub> (YAG).

The wide emission bandwidth of 5.5 nm in Nd:YSAG is composed of three transitions ( $R_1$ - $Y_1$ ,  $R_1$ - $Y_2$ ,  $R_2$ - $Y_3$ ), and contains the valley in its profile. The ratio of peak-to-valley is almost 50%, which reaches 93% in Nd:YAG. Fortunately, the valley in the emission band of Nd:YSAG overlaps the peak in the emission band of Nd:YAG. When we pumped from YSAG side with 809.0 nm pumping source, this peak-to-valley improved to 43%. If we fabricate the three-layered composite of YAG, YSAG, and Y<sub>3</sub>Sc<sub>2</sub>Al<sub>3</sub>O<sub>12</sub>, this specimen will perform more flat emission band. These profiles of fluorescence in Figure 1 are related to the effective emission cross-section, thus we can design the gain profile of this layered composite material. Even in the case of diode-pumping, we can control the spectroscopic properties by tuning the temperature of laser diode.

As a result, we found that the tuning of the pumping wavelength made the spectral profile of fluorescence from the composite ceramics more even than that from single-layered Nd:Y<sub>3</sub>Sc<sub>x</sub>Al<sub>5-x</sub>O<sub>12</sub> ceramics. The technique of composite ceramics is proved to be useful because it can provide not only the compositional tuning but also a new controllability by the selection of the pump source.

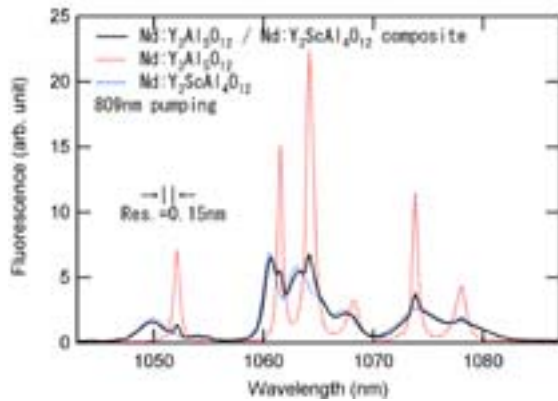


**Figure 1.** Fluorescence profiles of 1.0at.% Nd:YAG, Nd:YSAG, and their composite.

### IX-X-3 Hybrid Process for Measurement of Spectroscopic Properties of Nd:GdVO<sub>4</sub>

SATO, Yoichi; TAIRA, Takunori

[*Pac. Rim Conf. Lasers Electro-Optics CWI2-5* (2005)]

In order to construct highly performing solid-state lasers, laser materials should be able to absorb efficiently the pump radiation. The request of high pump absorption efficiency is more important for the case in microchip laser scheme, or under direct pumping into the emitting levels. Rare-earth doped vanadate crystals are the promised candidates solid-state lasers with high-performance because of their desirable properties of high optical absorption. However, there are many reports for an absorption cross section of the transition between  $^4I_{9/2}$  and  $^4F_{5/2}$  in Nd:GdVO<sub>4</sub>. In this paper, authors discussed how to evaluate the spectroscopic properties of Nd- and Yb-doped GdVO<sub>4</sub> crystals.

We propose the “Hybrid Process” which is shown in Figure 1 as a technique for the spectroscopic evaluation in order to avoid overlooking the influences of emission in absorption and the influences of absorption in emission by simultaneous evaluation. This process also gives the radiative quantum efficiency ( $\eta_r$ ). We studied Nd:GdVO<sub>4</sub> (Shandong Newphotonics) and Nd:YVO<sub>4</sub> (ITI) according to the Hybrid Process.

As a result, rare-earth doped vanadate crystals are the promised candidates solid-state lasers due to their large cross sections and relatively high thermal conductivity. In order to perform these superior characteristics, we have to notice that heavy heat generation under non-lasing condition and the difference in the thermal conductivity depending on the crystal-axis.

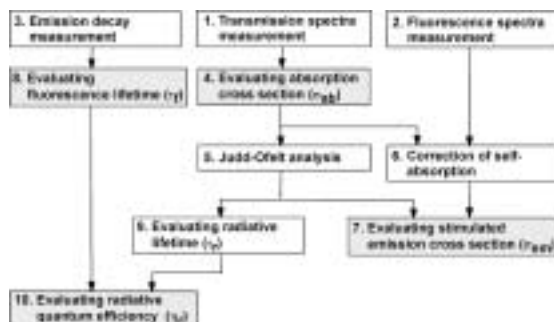


**Figure 1.** The flow-chart of “Hybrid Process” for measurement of the spectroscopic properties in Nd:vanadate.

### IV-X-4 Absorption, Emission Spectrum Properties and Efficient Laser Performances of Yb:Y<sub>3</sub>ScAl<sub>4</sub>O<sub>12</sub> Ceramics

SAIKAWA, Jiro; SATO, Yoichi; TAIRA, Takunori; IKESUE, Akio<sup>1</sup>  
(<sup>1</sup>JFCC)

[*Appl. Phys. Lett.* **85**, 1898 (2004)]

We report on the continuous-wave laser performances of Yb<sup>3+</sup>-doped disordered Y<sub>3</sub>Al<sub>5</sub>O<sub>12</sub>/Y<sub>3</sub>Sc<sub>2</sub>Al<sub>4</sub>O<sub>12</sub> (YAG/YSAG) ceramics fabricated by sintering method. These new materials exhibit relatively low minimum pump intensity ( $I_{\min}$ ) and broad emission bandwidth even in the yttrium aluminum garnet systems. The value of  $I_{\min}$  in the Yb:Y<sub>3</sub>ScAl<sub>4</sub>O<sub>12</sub> ceramics was found to be 2/3 compared with the Yb:YAG single crystal under 970-nm zero-line pumping. Efficient laser oscillation of 72% slope efficiency was obtained for input pump power. These materials attract great interest for high power femtosecond microchip lasers and amplifier applications.

### IX-X-5 Passive Mode Locking of a Mixed Garnet Yb:Y<sub>3</sub>ScAl<sub>4</sub>O<sub>12</sub> Ceramic Laser

SAIKAWA, Jiro; SATO, Yoichi; TAIRA, Takunori; IKESUE, Akio<sup>1</sup>  
(<sup>1</sup>JFCC)

[*Appl. Phys. Lett.* **85**, 5845 (2004)]

We have demonstrated a passively mode-locked Yb<sup>3+</sup>-doped Y<sub>3</sub>ScAl<sub>4</sub>O<sub>12</sub> ceramic laser, which is a solid solution of Y<sub>3</sub>Al<sub>5</sub>O<sub>12</sub> (YAG) and Y<sub>3</sub>Sc<sub>2</sub>Al<sub>4</sub>O<sub>12</sub> (YSAG), by using a semiconductor saturable-absorber mirror (SESAM). The maximum average output power was as high as 150 mW with a pulse duration of 500 fs. With a 0.5% output coupler, pulses as short as 280 fs having an average output power of 62 mW at 1035.8 nm were obtained.

### IX-X-6 High-Power Operation of Diode Edge-Pumped, Glue-Bonded, Composite Yb:Y<sub>3</sub>Al<sub>5</sub>O<sub>12</sub> Microchip Laser with Ceramic, Undoped YAG Pump Light-Guide

TSUNEKANE, Masaki; TAIRA, Takunori

[*Jpn. J. Appl. Phys.* in press]

The high-power operation of a diode edge-pumped, composite Yb<sup>3+</sup>-doped Y<sub>3</sub>Al<sub>5</sub>O<sub>12</sub> (Yb:YAG) microchip laser has been demonstrated. The novel composite microchip has a 5-mm-diameter, 300- $\mu$ m-thickness, single-crystal Yb:YAG core and a transparent ceramic, undoped YAG pump light-guide surrounding the core with the same thickness. The high-reflection coated face of the microchip was bonded to a water-cooled heat-sink by a thermally conductive glue for efficient con-

ductive cooling. The pump light from a fourfold diode stack directly coupled to the light-guide and maximum output powers of 410 W (peak) and 285 W have been successfully obtained at an input pump power of 866 W in quasi-continuous-wave (10 ms, 10 Hz) and continuous-wave operations, respectively, at room temperature.

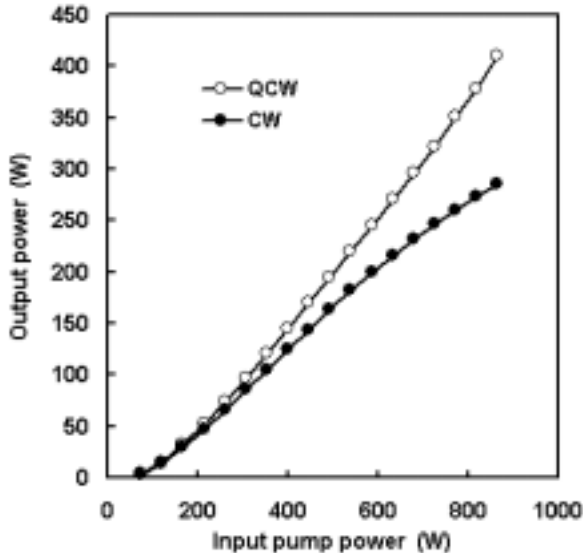


**Figure 1.** Input pump power versus laser output power of diode edge-pumped, composite Yb:YAG microchip laser in QCW and CW operations at room temperature.

#### IX-X-7 Continuous-Wave Deep Blue Generation in a Periodically Poled MgO:LiNbO<sub>3</sub> Crystal by Single-Pass Frequency Doubling of a 912-nm Nd:GdVO<sub>4</sub> Laser

MIZUUCHI, Kiminori<sup>1</sup>; MORIKAWA, Akihiro<sup>1</sup>; SUGITA, Tomoya<sup>1</sup>; YAMAMOTO, Kazuhisa<sup>1</sup>; PAVEL, Nicolaie<sup>2</sup>; TAIRA, Takunori  
(<sup>1</sup>Matsushita Co., Ltd.; <sup>2</sup>IAP-NILPRP, Romania)

[*Jpn. J. Appl. Phys.* **43**, L1293 (2004)]

We report blue emission at 456 nm by single-pass second-harmonic generation in a bulk periodically-poled MgO:LiNbO<sub>3</sub> crystal, for the first time to our best knowledge. Using as a pumping source a continuous-wave Nd:GdVO<sub>4</sub> laser operating at 912 nm, blue power of 167 mW with 8.3% infrared-to-blue conversion efficiency and 4.2%/W normalized conversion efficiency was obtained. The present data, combined with our previous results on green generation, supports the prospect of obtaining compact and high power visible sources based on bulk periodically poled MgO:LiNbO<sub>3</sub>.

#### IX-X-8 Continuous-Wave Ultraviolet Generation at 354-nm in a Periodically Poled MgO:LiNbO<sub>3</sub> by Frequency Tripling of a Diode End-Pumped Nd:GdVO<sub>4</sub> Microlaser

MIZUUCHI, Kiminori<sup>1</sup>; MORIKAWA, Akihiro<sup>1</sup>; SUGITA, Tomoya<sup>1</sup>; YAMAMOTO, Kazuhisa<sup>1</sup>; PAVEL, Nicolaie<sup>2</sup>; TAIRA, Takunori  
(<sup>1</sup>Matsushita Co., Ltd.; <sup>2</sup>IAP-NILPRP, Romania)

[*Appl. Phys. Lett.* **85**, 3959 (2004)]

Irregular side spread of polarization inversion was suppressed in PPMgLN up to 2-mm thickness by using a multipulse poling method. Cascaded THG was performed by employing a first-order SHG-QPM PPMgLN followed by a SFG-QPM PPMgLN stage, and a 1063 nm Nd:GdVO<sub>4</sub> laser as a pumping source. CW power of 47 mW at 354 nm with 3.9%/W/cm normalized conversion efficiency was obtained. To our knowledge this is the first demonstration in PPMgLN of such a system and the highest UV power at 354 nm reported by CW single-pass process in a QPM structure. The present result supports the prospect of obtaining compact and high power UV source based on bulk periodically poled MgO:LiNbO<sub>3</sub>.

#### IX-X-9 High-Power Continuous-Wave Intracavity Frequency-Doubled Nd:GdVO<sub>4</sub>-LBO Laser under Diode Pumping into the Emitting Level

PAVEL, Nicolaie<sup>1</sup>; TAIRA, Takunori  
(<sup>1</sup>IAP-NILPRP, Romania)

[*IEEE J. Sel. Top. Quantum Electron.* **11**, 631 (2005)]

Continuous-wave emission in Nd:GdVO<sub>4</sub> at the 1- $\mu$ m fundamental wavelength and 531-nm second harmonic, which was obtained by intracavity frequency-doubling with LBO, is investigated under end-pumping with high-power diode laser at 808 and 879 nm. The maximum green power of 5.1 W with 0.31 overall optical-to-optical efficiency in a beam of  $M^2 = 1.46$  was obtained under 879-nm pumping, directly into the <sup>4</sup>F<sub>3/2</sub> emitting level. To the authors best knowledge this is the highest CW green power obtained for the Nd:GdVO<sub>4</sub> laser material.

#### IX-X-10 Deep Blue Generation at 456 nm in a Periodically Poled MgO:LiNbO<sub>3</sub> Ridge-Type Waveguide by Single-Pass Frequency Doubling of a Nd:GdVO<sub>4</sub> Micro-Laser

PAVEL, Nicolaie<sup>1</sup>; TAIRA, Takunori; IWAI, Makato<sup>2</sup>; YOSHINO, Takeshi<sup>2</sup>; IMAEDA, Minoru<sup>2</sup>  
(<sup>1</sup>IAP-NILPRP, Romania; <sup>2</sup>NGK)

[*Conf. Lasers Electro-Optics CTuC30* (2005)]

This paper reports on our work toward scaling deep blue light by SHG-QPM process in a PPMgLN ridge-type waveguide: 93 mW power at 456 nm was achieved by single-pass SHG of a 912-nm Nd:GdVO<sub>4</sub> laser.

#### IX-X-11 Efficient 1.06 and 1.34- $\mu$ m Laser Emission of Highly-Doped Nd:YAG under 885-nm Diode Pumping into the Emitting Level

PAVEL, Nicolaie<sup>1</sup>; TAIRA, Takunori  
(<sup>1</sup>IAP-NILPRP, Romania)

[*European Conf. Lasers Electro-Optics CA-19-MON* (2005)]

This work reports on 1.34- $\mu\text{m}$  emission in Nd:YAG under direct pumping into the emitting level, at 885 nm, the first demonstration of such a system to the best of our knowledge. CW output power of 3.8 W at 1.34  $\mu\text{m}$  with overall optical-to-optical efficiency of 0.26 is obtained from a 2.5-at.% Nd:YAG single crystal pumped into the  $^4F_{3/2}$  level with a high-brightness 885-nm diode laser. The influence of the lasing wavelength and medium concentration on the thermal effects induced by optical pumping into the active component is discussed. It is shown that laser emission at 1.3  $\mu\text{m}$  increases the thermal effects in medium only under a certain value of  $C_{Nd}$ . This behavior was checked by mapping the temperature of the output surface of the Nd:YAG crystals. These results demonstrate that diode laser pumping into the emitting level of concentrated Nd-based laser materials is a solution for construction of efficient micro-lasers and for scaling to high power.

### **IX-X-12 High-Power Multi-Pass Pumped Microchip Nd:GdVO<sub>4</sub> Laser**

**PAVEL, Nicolaie<sup>1</sup>; TAIRA, Takunori**  
(<sup>1</sup>IAP-NILPRP, Romania)

[*Pacific Rim Conf. Lasers Electro-Optics* CTuI3-5  
(2005)]

We describe a continuous-wave thin-disk Nd:GdVO<sub>4</sub> laser in a multi-pass pumping scheme. Employing a 250- $\mu\text{m}$  thick, 0.5-at.% Nd:GdVO<sub>4</sub> crystal, a maximum output power of 13.9 W was obtained for 22 W absorbed power; the slope efficiency in absorbed power was 0.65. Pumping at 879 nm, directly into the  $^4F_{3/2}$  emitting level, resulted in laser operation with slope efficiency in absorbed power of 0.69; the laser output power was 3.6 W at an absorbed pump power of 6.2 W. We appreciate that with an improved heat transfer between the Nd:GdVO<sub>4</sub> and the cooling system, a Nd:GdVO<sub>4</sub> medium of lower doping and an increased number of passes of the pump radiation, this geometry could be also a good solution for efficient laser emission at 912 nm.

### **IX-X-13 Highly Efficient New Pumping Configuration for Microchip Solid State Laser**

**DASCALU, Traian<sup>1</sup>; TAIRA, Takunori**  
(<sup>1</sup>IAP-NILPRP, Romania)

[*European Conf. Lasers Electro-Optics* CThu4-2  
(2005)]

We propose a new pumping scheme which allows 94% absorption efficiency in Yb:YAG 15 at.% with 200  $\mu\text{m}$  thickness with uniform pump distribution. This configuration can be scaled up and it is very attractive especially for high power quasi-4-levels lasers where the reabsorption losses are important.

### **IX-X-14 High Energy Quasi-Phase-Matched Optical Parametric Oscillation in a 3-mm-Thick Periodically Poled MgO:LiNbO<sub>3</sub> Device**

**ISHIZUKI, Hideki; SHOJI, Ichiro; TAIRA, Takunori**

[*Opt. Lett.* **29**, 2527 (2004)]

We presented high energy optical parametric oscillation (OPO) using 3-mm-thick periodically poled MgO:LN (PPMgLN) device. The maximum total output energy of 22 mJ at the pump energy of 46 mJ was obtained using a Q-switched Nd:YAG laser of 30 Hz repetition rate with 15 ns pulse duration. The large-aperture PPMgLN devices would enable us to realize high-energy wavelength conversion, short pulse amplification, and pulse compression.

# Equipment Development Center

## IX-Y Development of New Instruments and Experimental Devices

The technical staff of the Equipment Development Center is partly engaged in planning, researching, designing and constructing high technology experimental instruments in collaboration with the scientific staff. And these experimental instruments are incorporated with new manufacturing technology and new mechanical idea.

### IX-Y-1 Development of a High-Precision Slit Blade for the Transmission-Grating Spectrometer

**KONDO, Takuhiko; SUZUI, Mitsukazu; TORII, Tatsuharu<sup>1</sup>; MASUDA, Tadashi<sup>1</sup>; HORIGOME, Toshio; HATSUI, Takaki**  
 (<sup>1</sup>Nagoya Univ.)

Development of the transmission-grating spectrometer for soft X-ray emission spectroscopy has been carried out by the Department Vacuum UV PhotoScience.

In order to improve further the energy resolution of the spectrometer, an entrance slit with the minimum slit opening of 1mm has been developed. In order to maintain the spectrometer efficiency, the distance between the sample and the slit is designed to be less than 1 mm. Accordingly, the slit blades are to be smaller than  $13 \times 10 \times 2.5 \text{ mm}^3$ . These requirements demanded a development of slit blades with a roughness of less than  $0.3 \mu\text{m}$  using a high-precision polishing process.

The blades were polished first on the side A and B (Figure 1). The resulting roughness was less than  $R_a 7 \text{ nm}$ . The edge surfaces were polished by using a clamp as shown in Figure 2. The four blades were pressed by the two plates via two screws (M4) so as to minimize the gap between the blades. The pressure was optimized so that the pile up did not occur during the polishing process. The resulting slit blade is shown in Figure 3. Figure 4 is the top view of the slit blade from A side. The edge roughness was about  $0.3 \mu\text{m}$ .

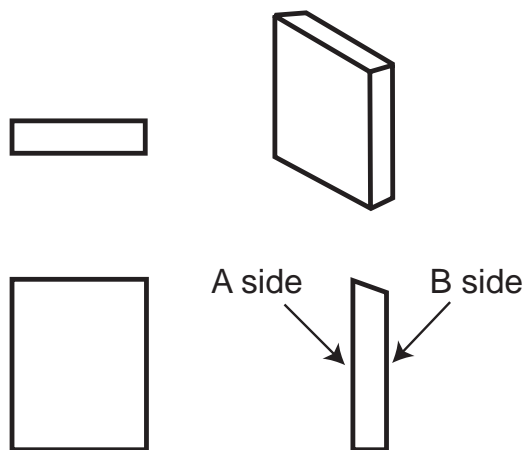


Figure 1. Schematic view of the slit blade.

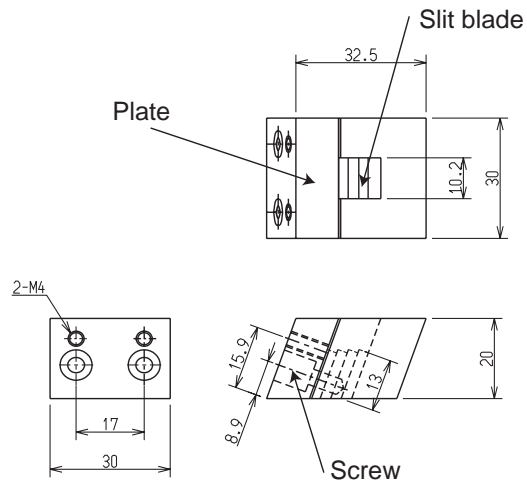


Figure 2. The clamp for the polishing of the edge surfaces.



Figure 3. Photograph of the slit.

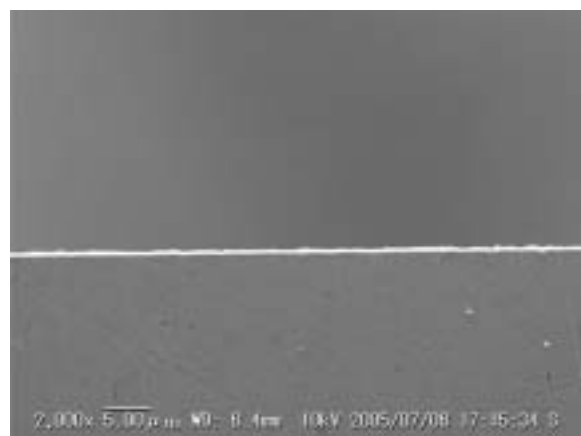


Figure 4. Top view of the slit blade observed by SEM.

## IX-Y-2 Manufacture of Glass Microreactor Chips

AOYAMA, Masaki; SUZUI, Mitsukazu;  
FUKUYAMA, Naoshi; YAMADA, Yoichi M. A.;  
UOZUMI, Yasuhiro

Glass microreactor chips used for catalyst research in Research Center for Molecular-scale Nanoscience were manufactured.

Although glass chips are usually manufactured by photolithography and wet etching, it takes expense and time to manufacture many arbitrary flow patterns. Then, we attached the diamond grinding tool in the general machine tool, and processed flow patterns into it.

The SEM photograph of flow patterns of a chip is shown in Figure 1. The quality of the material was PYREX glass, and the slot width and depth were 100  $\mu\text{m}$  and 40  $\mu\text{m}$ , respectively. Although generating of the deficit of a detailed crack and edge could become a problem in processing of a brittle material, it was processed by spindle speed 50,000 rpm, feed rate 1.0 mm/min, the depth of cut 5  $\mu\text{m}$ , and diamond tool particle size #1000, and good flow patterns whose processing side coarseness were about 1.5  $\mu\text{m}$  were obtained.

Such processing technology is applied to processing of brittle material such as silicone in addition to glass, and is useful also to manufacture of the micro parts for Department of Vacuum UV Photoscience.

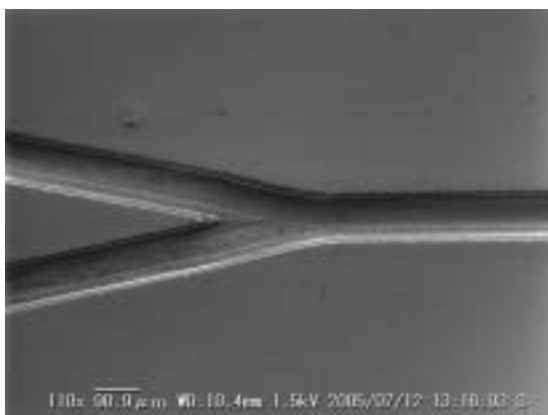


Figure 1. Flow patterns of a chip.

## IX-Y-3 Micro Processing by a Femto-Second Laser

AOYAMA, Masaki; YANO, Takayuki; SUZUI, Mitsukazu; SASAKI, Ryuichiro<sup>1</sup>; NAGAI, Hiroyuki<sup>1</sup>; YOSHIDA, Makoto<sup>1</sup>; TAKAHASHI, Kazuyuki; KOBAYASHI, Hayao; RAHMAN, Md. Mashiur; URISU, Tsuneo  
(<sup>1</sup>AISHIN Seiki Co., Ltd.)

Micro fabrication processing was done by using the femto-second fiber laser (FCPμJewel B-250) manufactured by IMRA in laboratory of AISHIN Seiki Co., Ltd.

Processing conditions are center wavelength 1560 nm, pulse width 900 fs, and repetition frequency 256

kHz. The main two cases are described in the following.

Diamond Anvil Cell for the high pressure experiment will be used by Department of Molecular Assemblies. In order to draw four probes out of the sample cavity of Diamond Anvil Cell, the groove for the wiring on the metal gasket of Diamond Anvil Cell is necessary. Schematic view of the metal gasket for the high pressure experiment is shown in Figure 1. The hole is at the center of gasket plate (8 × 8 × 0.3 mm<sup>3</sup> Inconel 625) and a diameter of 0.4 mm. Prepressing between both sides of the plate by Diamond Anvil resulted in the basin-like plastic deformation of the whole plate and a height of about 20  $\mu\text{m}$  of the swelling around the central hole. In order to pass through the wiring with a diameter of 10  $\mu\text{m}$ , the required groove width and depth are considered to be about 50  $\mu\text{m}$  and 30  $\mu\text{m}$ , respectively.

Excellent groove processing was attained in a short term with no heat effect on the sharpness of the edge and no deposition by melting. This result is shown in Figure 2.

It was applied to hole processing for the biosensor device used in Department of Vacuum UV Photoscience. An AFM measurement after hole processing is shown in Figure 3. Drilling of the Cobalt layer on SiO<sub>2</sub> with a diameter of about 1.5  $\mu\text{m}$  could be achieved by adjusting laser power and an exposure time.

A trial of the partial removal of a gold thin film from a circuit pattern on the SiO<sub>2</sub>-covered silicon substrate by the femto-second laser is now in progress.

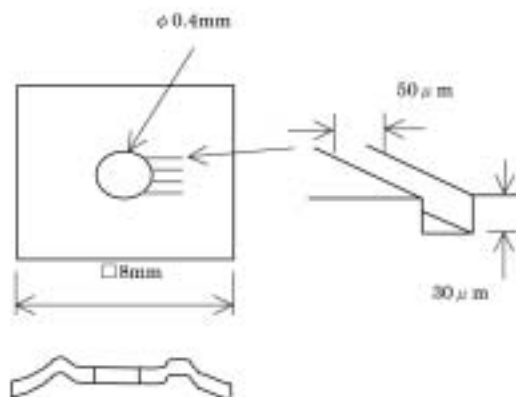


Figure 1. Schematic view of the metal gasket.

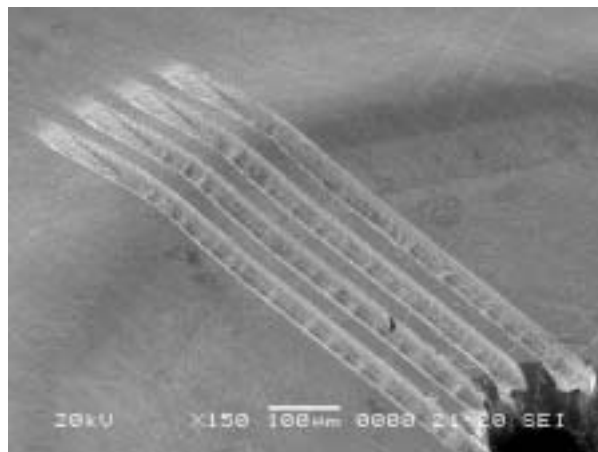


Figure 2.

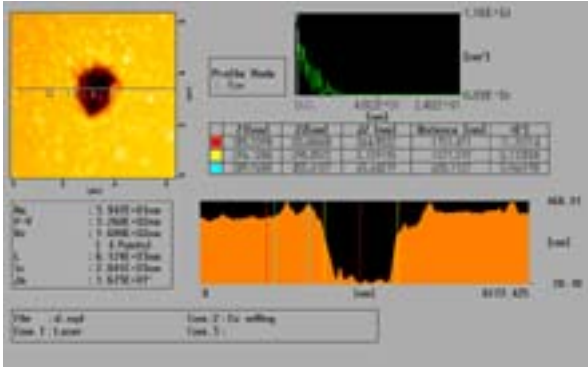


Figure 3. The measurement result of the cross section profile of a hole.

**IX-Y-4 Development of Electrical Control System of Fluorescence Recovery after Photobleaching Apparatus Using Semiconductor Laser for Illumination**

YOSHIDA, Hisashi; URISU, Tsuneo

We have developed the electrical control system of the fluorescence recovery after photobleaching (FRAP) apparatus as schematically shown in Figure 1. Two recording devices are equipped in the setup. One is a charge coupled device (CCD) by which the sample surface image and the photobleached spot image are monitored. The other one is photo-multiplier (PMT) by which the time dependence of the fluorescence intensity at the photobleaching spot can be monitored. A pinhole with 100 μm diameter is set at the confocal point of the microscope before the PMT. Two neutral density filters with different transmission coefficients are inserted to the filter holder to attenuate the UV lamp and laser intensities, respectively. The UV lamp illumination was used mainly for sample setting and was turned off during the photobleaching and the fluorescence recovery process. The photo-multiplier recording, which gives the time dependence of the fluorescence recovery directly, is very convenient in the calculation of the diffusion constant. The block diagram of a laser driving and the photo-multiplier detection system is shown in Figure 2. The semiconductor laser is drove by the bleaching pulse and succeeding pulse train of the sampling pulse.

The drive voltage 1.25 V correspond to the second harmonic output of ~5 mW. The fluorescence recovery can be monitored by the weak sampling pulse train without giving damage to dye molecules. The relation between the laser driving pulses and the photo-multiplier output monitoring pulse are shown also in Figure 2.

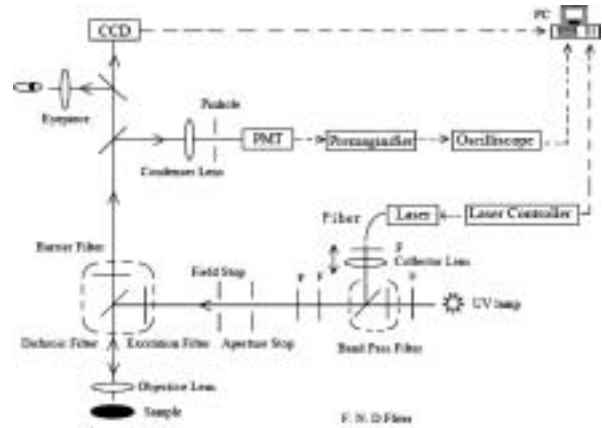


Figure 1.

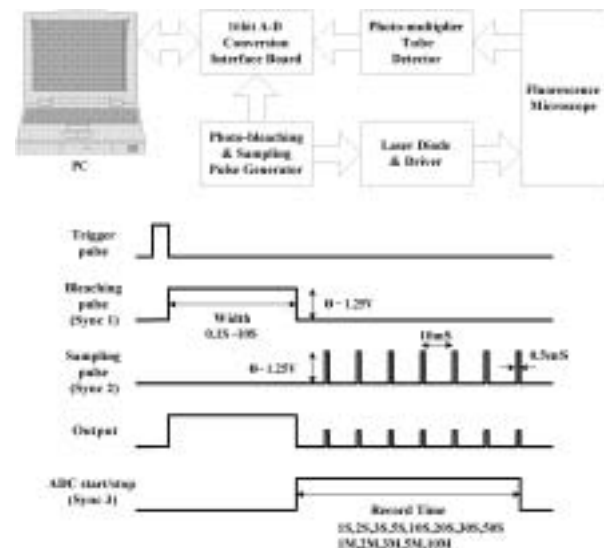


Figure 2.

## Safety Office

### IX-Z Development of Novel Heterocyclic Compounds and Their Molecular Assemblies for Advanced Materials

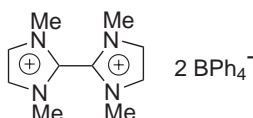
Heterocycles containing sulfur and/or nitrogen atoms are useful as components of functional materials since heteroatoms in their rings are helpful to stabilize ions or ion-radical species, and extended  $\pi$ -conjugation decreases Coulombic repulsion. In addition intermolecular interactions caused by heteroatom contacts can be expected to form novel molecular assemblies. In this project new electron acceptors, donors, and donor-acceptor compounds based on heterocycles such as 1,2,5-thiadiazole and 1,3-dithiole were synthesized and their properties including those of the charge-transfer complexes or ion-radical salts were investigated. Unique crystal structures were constructed by using weak intermolecular interactions such as hydrogen bonding or heteroatom contacts.

#### IX-Z-1 Molecular Arrangement in the Crystals of 1,1',3,3'-Tetramethyl-2,2'-bi-1*H*-imidazolium Bis(tetraphenylborate) with Ketone, Aldehyde, and Nitrile as Guest Molecules

ONO, Katsuhiko<sup>1</sup>; IWAO, Takeshi<sup>1</sup>; UCHIUMI, Hideki<sup>1</sup>; SUZUKI, Takahisa<sup>1</sup>; TOMURA, Masaaki<sup>1</sup>; OHKITA, Masakazu<sup>1</sup>; SAITO, Katsuhiko<sup>1</sup>  
(<sup>1</sup>Nagoya Inst. Tech.)

[*Bull. Chem. Soc. Jpn.* **78**, 867–872 (2005)]

1,1',3,3'-Tetramethyl-2,2'-bi-1*H*-imidazolium bis(tetraphenylborate), an ion-association compound, afforded inclusion crystals with a variety of guest molecules, such as ketone, aldehyde, and nitrile. X-ray crystallographic analyses revealed intermolecular interactions between the biimidazolium dication and the guest molecules in the inclusion crystals. Their contact modes depended on the molecular structures of the guest molecules, resulting in various molecular arrangements.



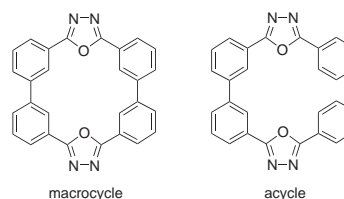
#### IX-Z-2 Macrocyclic and Acyclic Bis(2,5-diphenyl-1,3,4-oxadiazole)s with Electron-Transporting and Hole-Blocking Ability in Organic Electroluminescent Devices

ONO, Katsuhiko<sup>1</sup>; EZAKA, Seiichi<sup>1</sup>; HIGASHIBATA, Akinori<sup>1</sup>; HOSOKAWA, Ryohei<sup>1</sup>; OHKITA, Masakazu<sup>1</sup>; SAITO, Katsuhiko<sup>1</sup>; SUTO, Michitaka<sup>2</sup>; TOMURA, Masaaki<sup>1</sup>; MATSUSHITA, Yosuke<sup>3</sup>; NAKA, Shigeki<sup>3</sup>; OKADA, Hiroyuki<sup>3</sup>; ONNAGAWA, Hiroyoshi<sup>3</sup>  
(<sup>1</sup>Nagoya Inst. Tech.; <sup>2</sup>Dow Corning Asia Ltd.; <sup>3</sup>Toyama Univ.)

[*Macromol. Chem. Phys.* **206**, 1576–1582 (2005)]

Two types of bis(2,5-diphenyl-1,3,4-oxadiazole)s, macrocyclic and acyclic, were prepared and evaluated as electron-transporting and hole-blocking materials in

phosphorescent EL devices. Maximum efficiencies of  $\eta_{\text{ext}} = 10.4\%$  at  $J = 0.11 \text{ mA}\cdot\text{cm}^{-2}$  for the macrocycle and  $\eta_{\text{ext}} = 14.1\%$  at  $J = 3.01 \text{ mA}\cdot\text{cm}^{-2}$  for the acycle were observed. X-ray crystallographic analysis and DSC measurements revealed a strong intermolecular interaction between the macrocycles and weaker intermolecular interactions between the acycles. The EL characteristics depend on the intermolecular interactions.

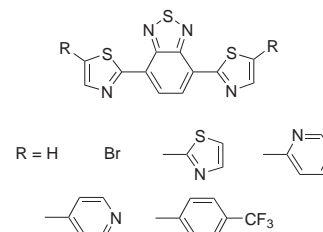


#### IX-Z-3 Synthesis, Characterization and FET Properties of Novel Dithiazolylbenzothiadiazole Derivatives

AKHTARUZZAMAN, Md.<sup>1</sup>; KAMATA, Naoto<sup>1</sup>; NISHIDA, Jun-ichi<sup>1</sup>; ANDO, Shinji<sup>1</sup>; TADA, Hirokazu<sup>2</sup>; TOMURA, Masaaki<sup>1</sup>; YAMASHITA, Yoshiro<sup>3</sup>  
(<sup>1</sup>Tokyo Inst. Tech.; <sup>2</sup>IMS and Osaka Univ.; <sup>3</sup>IMS and Tokyo Inst. Tech.)

[*Chem. Commun.* 3183–3185 (2005)]

Novel dithiazolylbenzothiadiazole derivatives easily obtained show efficient fluorescence with high electron affinity. The FET device of a trifluoromethylphenyl derivative exhibited a good n-type performance with high electron mobility. Since substituents can be easily introduced to the  $\alpha$ -position of thiazole, the dithiazolylbenzothiadiazole unit would be useful as a core for unique electron-accepting  $\pi$ -conjugated molecules.





# RESEARCH ACTIVITIES X

## Okazaki Institute for Integrative Bioscience

### X-A Single-Molecule Physiology

A single molecule of protein (or RNA) enzyme acts as a machine which carries out a unique function in cellular activities. To elucidate the mechanisms of various molecular machines, we need to observe closely the behavior of individual molecules, because these machines, unlike man-made machines, operate stochastically and thus cannot be synchronized with each other. By attaching a tag that is huge compared to the size of a molecular machine, or a small tag such as a single fluorophore, we have been able to image the individual behaviors in real time under an optical microscope. Stepping rotation of the central subunit in a single molecule of  $F_1$ -ATPase has been videotaped, and now we can discuss its detailed mechanism. RNA polymerase has been shown to be a helical motor that rotates DNA during transcription. Myosin V and VI are also helical motors that move as a left- or right-handed spiral on the right-handed actin helix. Single-molecule physiology is an emerging field of science in which one closely watches individual, 'live' protein/RNA machines at work and examines their responses to external perturbations such as pulling and twisting. I personally believe that molecular machines operate by changing their conformations. Thus, detection of the conformational changes during function is our prime goal. Complementary use of huge and small tags is our major strategy towards this end.

<http://www.k2.ims.ac.jp/>

#### X-A-1 One Rotary Mechanism for $F_1$ -ATPase over ATP Concentrations from Millimolar down to Nanomolar

SAKAKI, Naoyoshi; SHIMO-KON, Rieko; ADACHI, Kengo; ITOH, Hiroyasu<sup>1,2</sup>; FURUIKE, Shou; MUNHEYUKI, Eiro<sup>3</sup>; YOSHIDA, Masasuke<sup>3,4</sup>; KINOSITA, Kazuhiko, Jr.  
(<sup>1</sup>Hamamatsu Photonics; <sup>2</sup>CREST; <sup>3</sup>Tokyo Inst. Tech.; <sup>4</sup>ERATO)

[*Biophys. J.* **88**, 2047–2056 (2005)]

$F_1$ -ATPase is a rotary molecular motor in which the central  $\gamma$ -subunit rotates inside a cylinder made of  $\alpha_3\beta_3$ -subunits. The rotation is driven by ATP hydrolysis in three catalytic sites on the  $\beta$ -subunits. How many of the three catalytic sites are filled with a nucleotide during the course of rotation is an important yet unsettled question. Here we inquire whether  $F_1$  rotates at extremely low ATP concentrations where the site occupancy is expected to be low. We observed under an optical microscope rotation of individual  $F_1$  molecules that carried a bead duplex on the  $\gamma$ -subunit. Time-averaged rotation rate was proportional to the ATP concentration down to 200 pM, giving an apparent rate constant for ATP binding of  $2 \times 10^7 \text{ M}^{-1}\text{s}^{-1}$ . A similar rate constant characterized bulk ATP hydrolysis in solution, which obeyed a simple Michaelis-Menten scheme between 6 mM and 60 nM ATP.  $F_1$  produced the same torque of ~40 pN·nm at 2 mM, 60 nM, and 2 nM ATP. These results point to one rotary mechanism governing the entire range of nanomolar to millimolar ATP, although a switchover between two mechanisms cannot be dismissed. Below 1 nM ATP, we observed less regular rotations, indicative of the appearance of another reaction scheme.

#### X-A-2 ATP-Driven Stepwise Rotation of $F_0F_1$ -ATP Synthase

UENO, Hiroshi<sup>1</sup>; SUZUKI, Toshiharu<sup>1,2</sup>; KINOSITA, Kazuhiko, Jr.; YOSHIDA, Masasuke<sup>1,2</sup>  
(<sup>1</sup>Tokyo Inst. Tech.; <sup>2</sup>ERATO)

[*Proc. Natl. Acad. Sci. U.S.A.* **102**, 1333–1338 (2005)]

$F_0F_1$ -ATP synthase ( $F_0F_1$ ) is a motor enzyme that couples ATP synthesis/hydrolysis with a transmembrane proton translocation.  $F_1$ , a water-soluble ATPase portion of  $F_0F_1$ , rotates by repeating ATP-waiting dwell, 80° substep rotation, catalytic dwell, and 40°-substep rotation. Compared with  $F_1$ , rotation of  $F_0F_1$  has yet been poorly understood, and, here, we analyzed ATP-driven rotations of  $F_0F_1$ . Rotation was probed with an 80-nm bead attached to the ring of c subunits in the immobilized  $F_0F_1$  and recorded with a submillisecond fast camera. The rotation rates at various ATP concentrations obeyed the curve defined by a  $K_m$  of  $\approx 30 \mu\text{M}$  and a  $V_{\max}$  of  $\approx 350$  revolutions per second (at 37 °C). At low ATP, ATP-waiting dwell was seen and the  $k_{\text{on-ATP}}$  was estimated to be  $3.6 \times 10^7 \text{ M}^{-1}\text{s}^{-1}$ . At high ATP, fast, poorly defined stepwise motions were observed that probably reflect the catalytic dwells. When a slowly hydrolyzable substrate, adenosine 5'-[ $\gamma$ -thio]triphosphate, was used, the catalytic dwells consisting of two events were seen more clearly at the angular position of  $\approx 80^\circ$ . The rotational behavior of  $F_0F_1$  resembles that of  $F_1$ . This finding indicates that "friction" in  $F_0$  motor is negligible during the ATP-driven rotation. Tributyltin chloride, a specific inhibitor of proton translocation, slowed the rotation rate by 96%. However, dwells at clearly defined angular positions were not observed under these conditions, indicating that inhibition by tributyltin chloride is complex.

#### X-A-3 Activation of Pausing $F_1$ Motor by External Force

ONO-HARA, Yoko<sup>1</sup>; ISHIZUKA, Koji<sup>2</sup>; KINOSITA, Kazuhiko, Jr.; YOSHIDA, Masasuke<sup>2</sup>;

**NOJI, Hiroyuki<sup>1</sup>***(<sup>1</sup>Tokyo Inst. Tech.; <sup>2</sup>Univ. Tokyo)**[Proc. Natl. Acad. Sci. U.S.A. **102**, 4288–4293 (2005)]*

A rotary motor  $F_1$ , a catalytic part of ATP synthase, makes a  $120^\circ$  step rotation driven by hydrolysis of one ATP, which consists of  $80^\circ$  and  $40^\circ$  substeps initiated by ATP binding and probably by ADP and/or  $P_i$  dissociation, respectively. During active rotations,  $F_1$  spontaneously fails in ADP release and pauses after a  $80^\circ$  substep, which is called the ADP-inhibited form. In the present work, we found that, when pushed  $>+40^\circ$  with magnetic tweezers, the pausing  $F_1$  resumes its active rotation after releasing inhibitory ADP. The rate constant of the mechanical activation exponentially increased with the pushed angle, implying that  $F_1$  weakens the affinity of its catalytic site for ADP as the angle goes forward. This finding explains not only its unidirectional nature of rotation, but also its physiological function in ATP synthesis; it would readily bind ADP from solution when rotated backward by an  $F_o$  motor in the ATP synthase. Furthermore, the mechanical work for the forced rotation was efficiently converted into work for expelling ADP from the catalytic site, supporting the tight coupling between the rotation and catalytic event.

## X-B Bioinorganic Chemistry of Heme-Based Sensor Proteins

Heme-based sensor proteins show a novel function of the heme prosthetic group, in which the heme acts as an active site for sensing the external environmental signal such as diatomic gas molecules and redox change. Heme-based O<sub>2</sub>, NO, and CO sensor proteins have now been found in which these gas molecules act as a signaling factor that regulates the functional activity of the sensor proteins. Our research interest focuses on the elucidation of structure-function relationships of CO sensor protein (CooA), O<sub>2</sub> sensor protein (HemAT), and redox sensor protein (DcrA).

### X-B-1 Spectroscopic and Redox Properties of a CooA Homologue from *Carboxydotherrmus hydrogenoformans*

INAGAKI, Sayaka; MASUDA, Chiaki<sup>1</sup>; AKAISHI, Tetsuhiro<sup>1</sup>; NAKAJIMA, Hiroshi; YOSHIOKA, Shiro; OHTA, Takehiro; KITAGAWA, Teizo; AONO, Shigetoshi  
(<sup>1</sup>JAIST)

[*J. Biol. Chem.* **280**, 3269–3274 (2005)]

CooA is a CO-sensing transcriptional activator that contains a b-type heme as the active site for sensing its physiological effector, CO. In this study, the spectroscopic and redox properties of a new CooA homologue from *Carboxydotherrmus hydrogenoformans* (Ch-CooA) were studied. Spectroscopic and mutagenesis studies revealed that His-82 and the N-terminal -amino group were the axial ligands of the Fe(III) and Fe(II) hemes in Ch-CooA and that the N-terminal -amino group was replaced by CO upon CO binding. Two neutral ligands, His-82 and the N-terminal -amino group, are coordinated to the Fe(III) heme in Ch-CooA, whereas two negatively charged ligands, a thiolate from Cys-75 and the nitrogen atom of the N-terminal Pro, are the axial ligands of the Fe(III) heme in Rr-CooA. The difference in the coordination structure of the Fe(III) heme resulted in a large positive shift of redox potentials of Ch-CooA compared with Rr-CooA. Comparing the properties of Ch-CooA and Rr-CooA demonstrates that the essential elements for CooA function will be: (i) the heme is six-coordinate in the Fe(III), Fe(II), and Fe(II)-CO forms; (ii) the N-terminal is coordinated to the heme as an axial ligand, and (iii) CO replaces the N-terminal bound to the heme upon CO binding.

### X-B-2 Oxygen Sensing Mechanism of HemAT from *B. subtilis*: A Resonance Raman Spectroscopic Study

OHTA, Takehiro; YOSHIMURA, Hideaki; YOSHIOKA, Shiro; AONO, Shigetoshi; KITAGAWA, Teizo

[*J. Am. Chem. Soc.* **126**, 15000–15001 (2004)]

*HemAT-Bs* is a heme-containing signal transducer protein responsible for aerotaxis of *Bacillus subtilis*,

where the heme acts as an oxygen sensor. We have characterized the recombinant *HemAT-Bs* to elucidate the mechanisms of oxygen-sensing and signal transduction by *HemAT-Bs*. *HemAT-Bs* shows similar uv/vis spectra to those of myoglobin (Mb). Site-directed mutagenesis reveals that His123 is the proximal ligand of the heme in *HemAT-Bs*.

Resonance Raman (RR) evidence for structural linkage between the distal side of heme pocket and the signaling domain of an oxygen sensing hemoprotein, *HemAT-Bs*, is reported. The band-fitting analyses of the RR spectra in the Fe–O<sub>2</sub> stretching ( $\nu(\text{Fe}-\text{O}_2)$ ) region revealed the presence of three conformers with  $\nu(\text{Fe}-\text{O}_2)$  at 554, 566, and 572 cm<sup>-1</sup>, which reflect different H-bond strengths on the bound O<sub>2</sub> molecule. While recent X-ray analysis for CN<sup>-</sup>-bound *HemAT-Bs* suggested the importance of Thr95 and Tyr70, the species with the strongest H-bond (554 cm<sup>-1</sup>) was deleted in the T95A mutant and also by removal of the linker and signal domains; however, the Y70F mutant maintained the same three conformers. A scheme for specific O<sub>2</sub> sensing and signaling mechanism is discussed.

### X-B-3 Structure and Function of a Novel Redox Sensor DcrA Containing a C-Type Heme

YOSHIOKA, Shiro; AONO, Shigetoshi

Chemotaxis signal transducer protein DcrA from a sulfate-reducing bacterium *Desulfovibrio vulgaris* Hildenborough contains a c-type heme in its periplasmic domain (DcrA-N), which is the first example of a heme-based sensor protein containing a c-type heme as a prosthetic group. Optical absorption and resonance Raman spectroscopy indicates that the heme c in DcrA-N shows a redox-dependent ligand exchange. Upon reduction, a water molecule that may be the sixth ligand of the ferric heme c is replaced by an endogenous amino acid. Although the reduced heme in DcrA-N is six-coordinated with two endogenous axial ligands, CO can easily bind to the reduced heme to form CO-bound DcrA-N. Reaction of the reduced DcrA-N with molecular oxygen results in autoxidation to form a ferric state without forming any stable oxygen-bound form, probably due to the extremely low redox potential of DcrA-N (–250 mV). DcrA will act as a redox sensor, where the ligand exchange between water and an endogenous amino acid would be a trigger for signal transduction.

## X-C Bioinorganic Chemistry of a Novel Heme Enzyme that Catalyzes the Dehydration Reaction

Phenylacetaldoxime dehydratase from *Bacillus* sp. Oxd-1 (OxdB) catalyzes the dehydration reaction of Z-phenylacetaldoxime (PAOx) to produce phenylacetonitrile under mild conditions. OxdB exists in a monomer of a 40-kDa polypeptide containing a protoheme. The heme in OxdB is thought to be the active site for the dehydration reaction. OxdB is the first example of a hemeprotein catalyzing the dehydration reaction physiologically, although many functions of hemeproteins have been elucidated, including oxygen storage/transport, electron transfer, gas molecule sensor, and redox catalysis of various substrates. We are working on OxdB to elucidate the structure-function relationships of this novel heme enzyme.

### X-C-1 Regulation of Aldoxime Dehydratase Activity by Redox-Dependent Change in the Coordination Structure of the Aldoxime-Heme Complex

KOBAYASHI, Katsuaki; YOSHIOKA, Shiro;  
KATO, Yasuo<sup>1</sup>; ASANO, Yasuhisa<sup>1</sup>; AONO,  
Shigetoshi  
(<sup>1</sup>Toyama Pref. Univ.)

[*J. Biol. Chem.* **280**, 5486–5490 (2005)]

Phenylacetaldoxime dehydratase from *Bacillus* sp. strain OxB-1 (OxdB) catalyzes the dehydration of Z-phenylacetaldoxime (PAOx) to produce phenylacetonitrile. OxdB contains a protoheme that works as the active center of the dehydration reaction. The enzymatic activity of ferrous OxdB was 1150-fold higher than that of ferric OxdB, indicating that the ferrous heme was the active state in OxdB catalysis. Although ferric OxdB was inactive, the substrate was bound to the ferric heme iron. Electron paramagnetic resonance spectroscopy revealed that the oxygen atom of PAOx was bound to the ferric heme, whereas PAOx was bound to the ferrous heme in OxdB *via* the nitrogen atom of PAOx. These results show a novel mechanism by which the activity of a heme enzyme is regulated; that is, the oxidation state of the heme controls the coordination structure of a substrate-heme complex, which regulates enzymatic activity. Rapid scanning spectroscopy using stopped-flow apparatus revealed that a reaction intermediate (the PAOx-ferrous OxdB complex) showed Soret,  $\alpha$  and  $\beta$  bands at 415, 555, and 524 nm, respectively. The formation of this intermediate complex was very fast, finishing within the dead time of the stopped-flow mixer (3 ms). Site-directed mutagenesis revealed that His-306 was the catalytic residue responsible for assisting the elimination of the hydrogen atom of PAOx. The pH dependence of OxdB activity suggested that another amino acid residue that assists the elimination of the OH group of PAOx would work as a catalytic residue along with His-306.

## X-D Reaction Mechanism of Metalloenzymes Related to Oxygen Activation

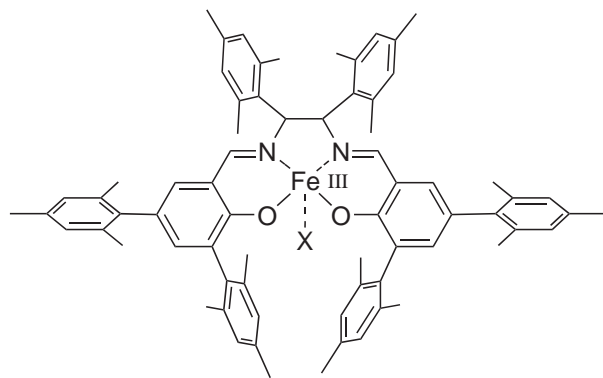
Oxygen is quite important molecule for most organisms. Oxygen is utilized for various physiological functions such as ATP synthesis, defense mechanism, oxidation reactions, and signal transduction. These diverse functions are realized by many metalloenzymes. In this project, we are studying molecular mechanisms of these metalloenzymes.

### X-D-1 Oxidizing Intermediates from the Sterically Hindered Salen Iron Complexes Related to the Oxygen Activation by Nonheme Iron Enzymes

KURAHASHI, Takuya; KOBAYASHI, Yoshio<sup>1</sup>;  
NAGATOMO, Shigenori; TOSHA, Takehiko;  
KITAGAWA, Teizo; FUJII, Hiroshi  
(<sup>1</sup>RIKEN)

[*Inorg. Chem.* in press]

Oxidizing intermediates are generated from non-heme iron(III) complexes to investigate the electronic structure and the reactivity, in comparison with the oxoiron(IV) porphyrin  $\pi$ -cation radical (compound I) as a heme enzyme model. Sterically hindered salen iron complexes, bearing a fifth ligand Cl (**1**), OH<sub>2</sub> (**2**), OEt (**3**) and OH (**4**), are oxidized both electrochemically and chemically. Stepwise one-electron oxidation of **1** and **2** generates iron(III)-mono- and diphenoxyl radicals, as revealed by detailed spectroscopic investigations, including UV-Vis, EPR, Mössbauer, resonance Raman, and ESIMS spectroscopies. In contrast to the oxoiron(IV) formation from the hydroxoiron(III) porphyrin upon one-electron oxidation, the hydroxo complex **4** does not generate oxoiron(IV) species. Reaction of **2** with *m*CPBA also results in the formation of the iron(III)-phenoxyl radical. One-electron oxidation of **3** leads to oxidative degradation of the fifth EtO ligand to liberate acetaldehyde even at 203 K. The iron(III)-phenoxyl radical shows high reactivity for alcoxide on iron(III), but exhibits virtually no reactivity for alcohols including even benzyl alcohol without a base to remove an alcohol proton. The present study explains unique properties of mononuclear nonheme enzymes with Tyr residues, and also a poor epoxidation activity of Fe salen compared to Mn and Cr salens.



X = Cl (**1**), OH<sub>2</sub> (**2**), OEt (**3**), OH (**4**)

**Figure 1.** Structure of Sterically Hindered Salen Complexes prepared in this study.

### X-D-2 Synthesis of Sterically Hidered Tris(4-imidazolyl)carbinol Ligands and their Copper(I) Complexes Related to Metalloenzymes

KUJIME, Masato; FUJII, Hiroshi

[*Tetrahedron Lett.* **46**, 2809–2812 (2005)]

In non-heme metalloenzymes, imidazole rings of histidine residues often form part of the metal-binding site. For examples, in the active sites of hemocyanin (Cu), nitrite reductase (Cu), and carbonic anhydrase (Zn), three imidazoles coordinate to one metal ion (Figure 1a). Because the coordination environment with three histidine imidazoles are generally occurred in many non-heme metalloenzymes, tripodal N-donor ligands such as hydrotris(2-pyrazolyl)borate and triaza-cyclononane have been used for synthetic model studies to mimic the active centers. For biomimetic studies, ligands with imidazolyl units are more desirable to understand the nature of metalloenzymes. Especially, a tripodal ligand with three 4-imidazolyl units, *e.g.*, tris(4-imidazolyl)carbinol, is better suited because the coordination environment of this ligand is close to the active sites of metalloenzymes. Therefore, it is desirable the synthesis of tris(4-imidazolyl)carbinol with stable NH protecting group and sterically hindered substituent to mimic the reactive intermediates. Here, we report the synthesis of tris(4-imidazolyl)carbinol ligands having chemically stable methyl group as the NH protective group and bulky substituent (isopropyl or phenyl) for stabilizing reactive species bound to metal center. The copper complexes prepared from these ligands can reproduce the metal active site of copper enzymes and are suitable for biomimetic studies.

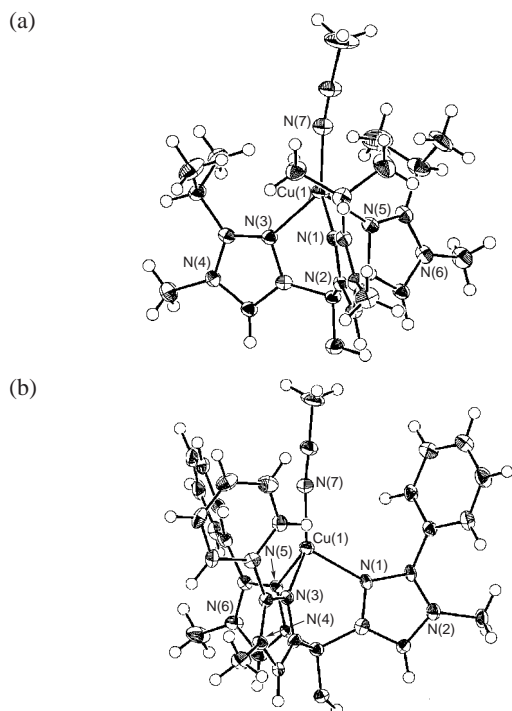


**Figure 1.** X-ray crystal structures of copper(I) acetonitrile complexes prepared in this study.

### X-D-3 O<sub>2</sub>- and H<sub>2</sub>O<sub>2</sub>-Dependent Verdoheme Degradation by Heme Oxygenase: Reaction Mechanisms and Potential Physiological Roles of the Dual Pathway Degradation

MATSUI, Toshitaka<sup>1</sup>; NAKAJIMA, Aya<sup>1</sup>; FUJII, Hiroshi; YOSHIDA, Tadashi<sup>2</sup>; IKEDA-SAITO, Masao<sup>3</sup>  
 (<sup>1</sup>Tohoku Univ.; <sup>2</sup>Yamagata Univ.; <sup>3</sup>IMS and Tohoku Univ.)

[*J. Biol. Chem.* in press]

Heme oxygenase (HO) catalyzes catabolism of heme to biliverdin, CO and a free iron through three successive oxygenation steps. The third oxygenation, oxidative degradation of verdoheme to biliverdin, has been the least understood step in spite of its importance to regulate the HO activity. We have thoroughly examined degradation of a synthetic verdoheme IXa complexed with rat HO-1. Our major findings include: (1) HO degrades verdoheme through a dual pathway using either O<sub>2</sub> or H<sub>2</sub>O<sub>2</sub>; (2) the newly found H<sub>2</sub>O<sub>2</sub> pathway is approximately 40-fold faster than the O<sub>2</sub>-dependent degradation; (3) both reactions are initiated by the binding of O<sub>2</sub> or H<sub>2</sub>O<sub>2</sub> to allow the first direct observation of degradation intermediates of verdoheme; and (4) Asp140 in HO-1 is critical for the verdoheme degradation regardless of the oxygen source. On the basis of these findings, we propose that the HO enzyme activates O<sub>2</sub> and H<sub>2</sub>O<sub>2</sub> on the verdoheme iron with the aid of a nearby water molecule linked with Asp140. These mechanisms are similar to a well-established mechanism of the first oxygenation, *meso*-hydroxylation of heme, and thus, HO can utilize a common architecture to promote the first and third oxygenation steps of the heme catabolism. We also point out a possible involvement of the H<sub>2</sub>O<sub>2</sub>-dependent verdoheme degradation *in vivo*, and propose potential roles of the dual pathway reaction of HO against oxidative stress.

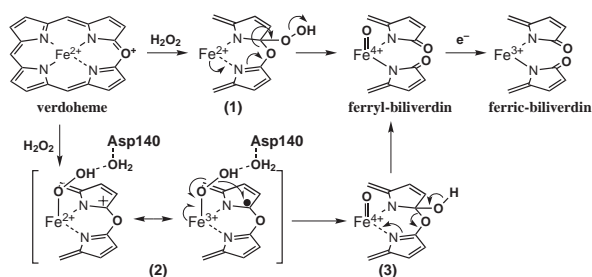


**Figure 1.** Proposed reaction mechanism of verdoheme in this study.

## X-E Reaction Mechanism of Metalloenzymes related to Global Nitrogen Cycle

For all organisms, organic nitrogen and ammonia are required as a constituent part of the cell. In order to keep the environment of the earth constant, the organic nitrogen, fixed nitrogen, must be completely reconverted into dinitrogen gas. The reverse process of the nitrogen fixing is called denitrification process. In this process, nitrate or nitrite ion is reduced to nitrogen gas via nitric oxide and nitrous oxide by many metalloenzymes, nitrate reductase, nitrite reductase, nitric oxide reductase, and nitrous oxide reductase. In this project, we are studying the molecular mechanism of these metalloenzymes relating to the denitrification process.

### X-E-1 Spectroscopic Characterization of Reaction Intermediates in a Model for Copper Nitrite Reductase

KUJIME, Masato; FUJII, Hiroshi

[*Angew. Chem., Int. Ed.* in press]

Reduction of nitrite (NO<sub>2</sub><sup>-</sup>) to gaseous nitric oxide (NO) is one of key processes in the global nitrogen cycle and carried out by bacterial copper-containing nitrite reductases (NiR). The enzymes contain two copper ion centers: the type 1 copper site for electron transfer and the type 2 copper site for the catalytic nitrite reduction. Crystallographic and spectroscopic

studies of NiR have proposed the mechanism of the nitrite reduction at the type 2 copper site. The enzyme reaction is initiated by the binding of the nitrite to the reduced form of the type 2 copper site to yield a copper(I) nitrite complex. Subsequently, the copper bound nitrite is reduced to NO and water with intramolecular one electron transfer from the type 2 copper(I) ion and two protons from a conserved aspartic acid placed near the type 2 site. During the course of synthetic study of the copper(I) nitrite complexes, we found that the rapid mixing of copper(I) nitrite complex with trifluoroacetic acid (TFA) with stopped flow at low temperature allows to detect new reaction intermediates in the reduction process. Here, we report detection and characterization of new reaction intermediates in the nitrite reduction. This study shows a new reaction mechanism, in which two protons required for the reaction are not provided to the copper bound nitrite simultaneously but stepwise and that the intramolecular electron transfer from the copper(I) ion to the copper bound nitrite occurs in the second protonation step (Figure 1).

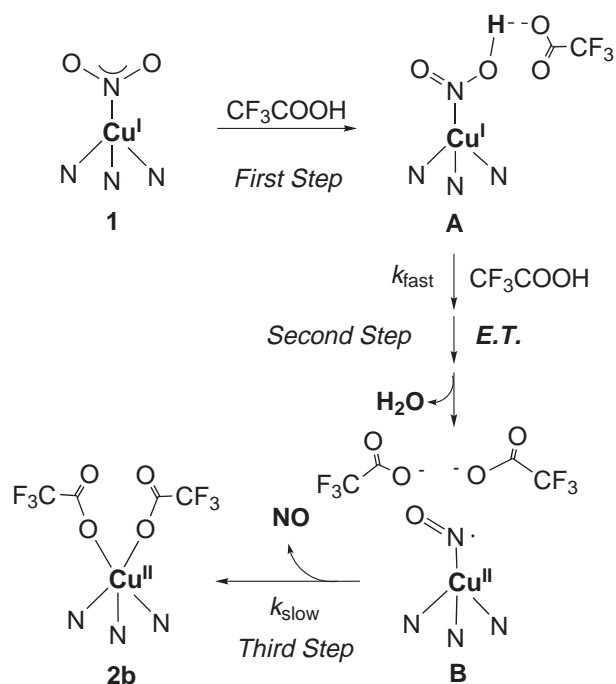


**Figure 1.** A proposed reaction mechanism of NiR in this study.

## X-F Biomolecular Science

Elucidation of a structure-function relationship of metalloproteins and structural chemistry of amyloid fibril are current subjects of this group. The primary technique used for the first project is the stationary and time-resolved resonance Raman spectroscopy excited by visible and UV lasers. Various model compounds of active site of enzymes are also examined with the same technique. IR-microscope dichroism analysis and AFM are the main techniques for the second project. The practical themes that we want to explore for the first project are (1) mechanism of oxygen activation by enzymes, (2) mechanism of active proton translocation and its coupling with electron transfer, (3) structural mechanism of signal sensing and transduction by heme-based sensory proteins, (4) higher order protein structures and their dynamics, and (5) reactions of biological NO. In category (1), we have examined a variety of terminal oxidases, cytochrome P450s (including AOS), and peroxidases, and also treated their reaction intermediates by using the mixed flow transient Raman apparatus and the Raman/absorption simultaneous measurement device. For (2) the third-generation UV resonance Raman (UVRR) spectrometer was constructed and we are applying it to a giant protein like cytochrome *c* oxidase with  $M_r = 210,000$ , particularly to explore the oxidation state of Tyr244 in the  $P_M$  intermediate. Recently, we succeeded in pursuing protein folding of apomyoglobin by combining the UV time-resolved Raman and rapid mixing techniques. With IR spectroscopy we determined the spectrum of carboxylic side chains of bovine cytochrome oxidase which undergo protonation/deprotonation changes and hydrogen-bonding status changes in response with electron transfers between metal centers or ligand dissociation from heme  $a_3$ . In (3) we are interested in a mechanism of ligand recognition specific to CO, NO or  $O_2$  and a communication pathway of the ligand binding information to the functional part of the protein. Several gas sensor heme proteins were extensively treated in this year. For (4) we developed a novel technique for UV resonance Raman measurements based on the combination of the first/second order dispersions of gratings and applied it successfully to 235-nm excited RR spectra of several proteins including mutant hemoglobins and myoglobins. Nowadays we can carry out time-resolved UVRR experiments with nanosecond resolution to discuss protein dynamics. With the system, we have succeeded in isolating the spectrum of tyrosinate in ferric Hb M Iwate, which was protonated in the ferrous state, and the deprotonated state of Tyr244 of bovine cytochrome *c* oxidase. The study is extended to a model of Tyr244, that is, imidazole-bound *para*-cresol coordinated to a metal ion, was synthesized and its UV resonance Raman was investigated. For (5) we purified soluble guanylate cyclase from bovine lung and observed its RR spectra in the presence of allosteric effector, YC-1. The CO and NO adducts in the presence of YC-1 were examined. To further investigate it, we are developing an expression system of this protein. For the amyloid study, we examined FTIR spectra of  $\beta_2$ -microglobulin and its fragment peptides of #11-21, K3, and K3-K7 which form a core part of amyloid fibril of  $\beta_2$ -microglobulin. The effect of seed upon the formation of the fibril was focused this year.

### X-F-1 Resonance Raman Characterization of the P Intermediate in the Reaction of Bovine Cytochrome *c* Oxidase

OGURA, Takashi<sup>1</sup>; KITAGAWA, Teizo  
(<sup>1</sup>IMS and Univ. Hyogo)

[*Biochim. Biophys. Acta* **1655**, 290–297 (2004)]

Reduced cytochrome *c* oxidase binds molecular oxygen, yielding an oxygenated intermediate first (Oxy) and then converts it to water *via* the reaction intermediates of P, F, and O in the order of appearance. We have determined the iron-oxygen stretching frequencies for all the intermediates by using time-resolved resonance Raman spectroscopy. The bound dioxygen in Oxy does not form a bridged structure with  $Cu_B$  and the rate of the reaction from Oxy to P ( $P_R$ ) is slower at higher pH in the pH range between 6.8 and 8.0. It was established that the P intermediate has an oxo-heme and definitely not the  $Fe_{a_3}-O-O-Cu_B$  peroxy bridged structure. The  $Fe_{a_3}=O$  stretching frequency ( $\nu_{Fe=O}$ ) of the  $P_R$  intermediate, 804/764  $cm^{-1}$  for  $^{16}O/^{18}O$ , is distinctly higher than that of F intermediate, 785/750  $cm^{-1}$ . The rate of reaction from P to F is quite different between  $H_2O$  and  $D_2O$  solutions, implicating the coupling of the electron transfer with vector proton transfer in this process. The P intermediate (607 nm form) generated in the reaction

of oxidized enzyme with  $H_2O_2$  gave the  $\nu_{Fe=O}$  band at 803/769  $cm^{-1}$  and the simultaneously measured absorption spectrum exhibited the difference peak at 607 nm. Reaction of the mixed valence CO adduct with  $O_2$  provided the P intermediate ( $P_M$ ) giving rise to an absorption peak at 607 nm and the  $\nu_{Fe=O}$  bands at 804/768  $cm^{-1}$ . Thus, three kinds of P intermediates are considered to have the same oxo-heme  $a_3$  structure. The  $\nu_4$  and  $\nu_2$  modes of heme  $a_3$  of the P intermediate were identified at 1377 and 1591  $cm^{-1}$ , respectively, and Raman excitation profiles were different between P and F. These observations may mean the formation of a  $\pi$  cation radical of porphyrin macrocycle in P.

### X-F-2 Core Structure of Amyloid Fibril Proposed from IR-Microscope Linear Dichroism

HIRAMATSU, Hirotsugu; GOTO, Yuji<sup>1</sup>; NAIKI, Hironobu<sup>2</sup>; KITAGAWA, Teizo  
(<sup>1</sup>Osaka Univ.; <sup>2</sup>Fukui Univ.)

[*J. Am. Chem. Soc.* **126**, 3008–3009 (2004)]

A new approach for studying a peptide conformation of amyloid fibril has been developed. It is based on infrared linear dichroism analysis using an IR-microscope for aligned amyloid fibril. The polarization direc-

tions of amide I and II bands were perpendicular similarly for  $\beta_2$ -microglobulin and its #21-31 peptide. Furthermore, this approach has shown that the #21-31 peptide consists of two C=O bonds in the  $\beta$ -sheet that makes  $0^\circ$  with the fibril axis, three C=O bonds in the  $\beta$ -sheet inclined by  $27^\circ$  with respect to the fibril axis, four residues in the random coil by  $47^\circ$ , and two residues in possible  $\beta$ -bulge structure by  $32^\circ$ . Plausible structures of the amyloid core in the fibril are proposed by taking account of these results.

### X-F-3 Activation of Heme-Regulated Eukaryotic Initiation Factor 2 $\alpha$ Kinase (HRI) Activation by Nitric Oxide Is Induced by the Formation of a Five-Coordinate NO-Heme Complex: Optical Absorption, Electron Spin Resonance and Resonance Raman Spectral Studies

IGARASHI, Jotaro<sup>1</sup>; SATO, Akira<sup>2</sup>; KITAGAWA, Teizo; YOSHIMURA, Tetsuhiko<sup>3</sup>; YAMAUCHI, Seigo<sup>1</sup>; SAGAMI, Ikuko<sup>4</sup>; SHIMIZU, Toru<sup>1</sup>  
(<sup>1</sup>Tohoku Univ.; <sup>2</sup>SOKENDAI; <sup>3</sup>Inst. Life Support Tec.; <sup>4</sup>Kyoto Pref. Univ.)

[*J. Biol. Chem.* **279**, 15752–15762 (2004)]

Heme-regulated eukaryotic initiation factor 2 $\alpha$  kinase (HRI) regulates the synthesis of hemoglobin in reticulocytes in response to heme availability. HRI contains a tightly bound heme at the N-terminal domain. Earlier reports show that nitric oxide (NO) regulates HRI catalysis. However, the mechanism of this process remains unclear. In the present study, we utilize *in vitro* kinase assays, optical absorption, electron spin resonance (ESR), and resonance Raman spectra of purified full-length HRI for the first time to elucidate the regulation mechanism of NO. HRI was activated *via* heme upon NO binding, and the Fe(II)-HRI(NO) complex displayed 5-fold greater eukaryotic initiation factor 2 $\alpha$  kinase activity than the Fe(III)-HRI complex. The Fe(III)-HRI complex exhibited a Soret peak at 418 nm and a rhombic ESR signal with g values of 2.49, 2.28, and 1.87, suggesting coordination with Cys as an axial ligand. Interestingly, optical absorption, ESR, and resonance Raman spectra of the Fe(II)-NO complex were characteristic of five-coordinate NO-heme. Spectral findings on the coordination structure of full-length HRI were distinct from those obtained for the isolated N-terminal heme-binding domain. Specifically, six-coordinate NO-Fe(II)-His was observed but not Cys-Fe(III) coordination. It is suggested that significant conformational change(s) in the protein induced by NO binding to the heme lead to HRI activation. We discuss the role of NO and heme in catalysis by HRI, focusing on heme-based sensor proteins.

### X-F-4 Steric and Hydrogen-Bonding Effects on the Stability of Copper Complexes with Small Molecules

WADA, Akira<sup>1</sup>; HONDA, Yasutaka<sup>1</sup>; YAMAGUCHI, Syuhei<sup>1</sup>; NAGATOMO, Shigenori; KITAGAWA, Teizo; JITSUKAWA, Koichiro<sup>1</sup>; MASUDA, Hideki<sup>2</sup>

(<sup>1</sup>Nagoya Inst. Tech.; <sup>2</sup>IMS and Nagoya Inst. Tech.)

[*Inorg. Chem.* **43**, 5725–5735 (2004)]

A series of the copper(II) complexes with tripodal tetradentate tris(pyridyl 2-methyl)amine-based ligands possessing the hydrogen-bonding 6-aminopyridine units (tapa, three amino groups; bapa, two amino groups; mapa, one amino group) have been synthesized, and their copper(II) complexes with a small molecule such as dioxygen and azide have been studied spectroscopically and structurally. The reaction of their Cu(II) complexes with NaN<sub>3</sub> have given the mononuclear copper complexes with azide in an end-on mode, [Cu(tapa)(N<sub>3</sub>)]ClO<sub>4</sub> (**1a**), [Cu(bapa)(N<sub>3</sub>)]ClO<sub>4</sub> (**2a**), [Cu(mapa)(N<sub>3</sub>)]ClO<sub>4</sub> (**3a**), and [Cu(tpa)(N<sub>3</sub>)]ClO<sub>4</sub> (**4a**) (tpa, no amino group). The crystal structures have revealed that the coordination geometries around the metal centers are almost a trigonal-bipyramidal rather than a square-planar except for **1a** with an intermediate between them. The UV-vis and ESR spectral data indicate that the increase of NH<sub>2</sub> groups of ligands causes the structural change from trigonal-bipyramidal to square-pyramidal geometry, which is regulated by a combination of steric repulsion and hydrogen bond. The steric repulsion of amino groups with the azide nitrogen gives rise to elongation of the Cu–N<sub>py</sub> bonds, which leads to the positive shift of the redox potentials of the complexes. The hydrogen bonds between the coordinated azide and amino nitrogens (2.84–3.05 Å) contribute clearly to the fixation of azide. The Cu(I) complexes with bapa and mapa ligands have been obtained as a precipitate, although that with tapa was not isolated. The reactions of the Cu(I) complexes with dioxygen in MeOH at  $-75^\circ\text{C}$  have given the *trans*- $\mu$ -1,2 peroxo dinuclear Cu(II) complexes formulated as [Cu(tapa)<sub>2</sub>(O<sub>2</sub>)]<sup>2+</sup> (**1c**), [Cu(bapa)<sub>2</sub>(O<sub>2</sub>)]<sup>2+</sup> (**2c**), and [Cu(mapa)<sub>2</sub>(O<sub>2</sub>)]<sup>2+</sup> (**3c**), whose characterizations were confirmed by UV-vis, ESR, and resonance Raman spectroscopies. UV-vis spectra of **1c**, **2c**, and **3c** exhibited intense bands assignable to  $\pi^*(\text{O}_2^{2-})$ -to-d(Cu) charge transfer (CT) transitions at  $\lambda_{\text{max}}/\text{nm}$  ( $\epsilon/\text{M}^{-1}\text{cm}^{-1}$ ) = 449 (4620), 474 (6860), and 500 (9680), respectively. The series of the peroxo adducts generated was ESR silent. The resonance Raman spectra exhibited the enhanced features assignable to two stretching vibrations  $\nu(^{16}\text{O}-^{16}\text{O}/^{18}\text{O}-^{18}\text{O})/\text{cm}^{-1}$  and  $\nu(\text{Cu}-^{16}\text{O}/\text{Cu}-^{18}\text{O})/\text{cm}^{-1}$  at 853/807 (**1c**), 858/812 (**2c**), 847/800 (**3c**), and at 547/522 (**2c**), 544/518 (**3c**), respectively. The thermal stability of the peroxo-copper species has increased with increase in the number of the hydrogen-bonding interactions between the peroxide and amino groups.

### X-F-5 Identification of Crucial Histidines Involved in Carbon-Nitrogen Triple Bond Synthesis by Aldoxime Dehydratase

KONISHI, Kazunobu<sup>1</sup>; ISHIDA, Kyoko<sup>1</sup>; OINUMA, Ken-Ichi<sup>1</sup>; OHTA, Takehiro; HASHIMOTO, Yoshiteru<sup>1</sup>; HIGASHIBATA, Hiroki<sup>1</sup>; KITAGAWA, Teizo; KOBAYASHI, Michihiko<sup>1</sup>  
(<sup>1</sup>Univ. Tsukuba)

[*J. Biol. Chem.* **279**, 47619–47625 (2004)]

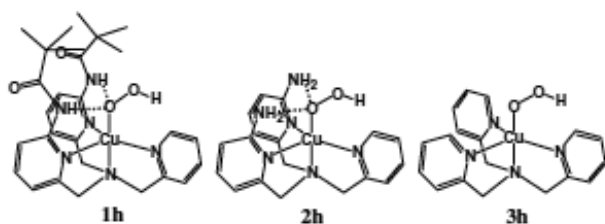
Aldoxime dehydratase (OxdA), which is a novel heme protein, catalyzes the dehydration of an aldoxime to a nitrile even in the presence of water in the reaction mixture. The combination of site-directed mutagenesis of OxdA (mutation of all conserved histidines in the aldoxime dehydratase superfamily), estimation of the heme contents and specific activities of the mutants, and CD and resonance Raman spectroscopic analyses led to the identification of the proximal and distal histidines in this unique enzyme. The heme contents and CD spectra in the far-UV region of all mutants except for the H299A one were almost identical to those of the wild-type OxdA, whereas the H299A mutant lost the ability of binding heme, demonstrating that His<sup>299</sup> is the proximal histidine. On the other hand, substitution of alanine for His<sup>320</sup> did not affect the overall structure of OxdA but caused loss of its ability of carbon-nitrogen triple bond synthesis and a lower shift of the Fe–C stretching band in the resonance Raman spectrum for the CO-bound form. Furthermore, the pH dependence of the wild-type OxdA closely followed the His protonation curves observed for other proteins. These findings suggest that His<sup>320</sup> is located in the distal heme pocket of OxdA and would donate a proton to the substrate in the aldoxime dehydration mechanism.

#### X-F-6 Thermal Stability of Mononuclear Hydroperoxocopper(II) Species. Effects of Hydrogen Bonding and Hydrophobic Field

YAMAGUCHI, Syuhei<sup>1</sup>; WADA, Akira<sup>1</sup>; NAGATOMO, Shigenori; KITAGAWA, Teizo; JITSUKAWA, Koichiro<sup>1</sup>; MASUDA, Hideki<sup>2</sup>  
(<sup>1</sup>Nagoya Inst. Tech.; <sup>2</sup>IMS and Nagoya Inst. Tech.)

[*Chem. Lett.* **33**, 1556–1557 (2004)]

The effects of hydrogen bonding and hydrophobic field on the thermal stabilities of Cu(II)–OOH complexes have been studied using tripodal tetradentate ligands with their functional groups on the basis of UV-vis, ESR, ESI-mass, and resonance Raman spectroscopies.



Scheme 1.

We succeeded in obtaining a stable hydroperoxocopper(II) complex with a tripodal tetradentate ligand, bis(6-pivalamido-2-pyridylmethyl)(2-pyridylmethyl)amine (BPPA) (**1h**)<sup>5</sup> for which the crystal structure and spectroscopic characterization of the hydroperoxocopper(II) complex were provided. Raman spectrum of **2h** in acetonitrile measured at –40 °C (using 406.7 nm laser excitation) gave a resonance-enhanced Raman band at 850 cm<sup>–1</sup>, which shifted to 801 cm<sup>–1</sup> ( $\Delta\nu = 49$  cm<sup>–1</sup>) when <sup>18</sup>O-labeled H<sub>2</sub>O<sub>2</sub> was used. That of **2h** in

methanol measured at –80 °C (using 406.7 nm laser excitation) gave Raman bands at 854 and 492 cm<sup>–1</sup>, assignable to  $\nu(\text{O–O})$  and  $\nu(\text{Cu–O})$ , respectively. The formation of **2h** was also confirmed from ESI mass spectrum measured in acetonitrile at –20 °C. The resonance Raman spectra of methanol solution of **3h** measured at –80 °C (using 406.7 nm laser excitation) showed a resonance-enhanced Raman band at 847 and 512 cm<sup>–1</sup>, which are assigned to  $\nu(\text{O–O})$  and  $\nu(\text{Cu–O})$ , the former of which shifted to 792 cm<sup>–1</sup> ( $\Delta\nu = 55$  cm<sup>–1</sup>) when <sup>18</sup>O-labeled H<sub>2</sub>O<sub>2</sub> was employed. The formation of **3h** was also confirmed from ESI mass spectrum measured in acetonitrile at –40 °C. Interestingly, the effects of hydrogen bonding and hydrophobic field on the thermal stabilities of Cu–OOH species, when their decomposition rates were followed using decrease in the absorption intensities of LMCT bands, was dramatically found out in the stability of these hydroperoxocopper(II) complexes.

#### X-F-7 Energy Funneling of IR Photons Captured by Dendritic Antennae and Acceptor Mode Specificity: Anti-Stokes Resonance Raman Studies on Iron(III) Porphyrin Complexes with a Poly(Aryl Ether) Dendrimer Framework

MO, Yu-Jun<sup>1</sup>; JIANG, Donglin<sup>2</sup>; UYEMURA, Makoto<sup>2</sup>; AIDA, Takuzo<sup>2</sup>; KITAGAWA, Teizo  
(<sup>1</sup>IMS and Henan Univ.; <sup>2</sup>Univ. Tokyo)

[*J. Am. Chem. Soc.* **127**, 10020–10027 (2005)]

A series of poly(aryl ether) dendrimer chloro-iron(III)porphyrin complexes ( $L_n\text{TPP}$ )Fe(III)Cl (number of aryl layers [ $n$ ] = 3 to 5) were synthesized and their Boltzman temperatures under IR irradiation were evaluated from ratios of Stokes to anti-Stokes intensities of resonance Raman bands. While the Boltzman temperature of neat solvent was unaltered by IR irradiation, ( $L_n\text{TPP}$ )Fe(III)Cl ( $n = 3$ –5) all showed a temperature rise that was larger than that of the solvent and greater as the dendrimer framework was larger. Among vibrational modes of the metalloporphyrin core, the temperature rise of an axial Fe–Cl stretching mode at 355 cm<sup>–1</sup> was larger than that for a porphyrin in-plane mode at 390 cm<sup>–1</sup>. Although the most of IR energy is captured by the phenyl  $\nu_8$  mode at 1597 cm<sup>–1</sup> of the dendrimer framework, an anti-Stokes Raman band of the phenyl  $\nu_8$  mode was not detected, suggesting the extremely fast vibrational relaxation of the phenyl mode. From these observations, it is proposed that the energy of IR photons captured by the aryl dendrimer framework is transferred to the axial Fe–Cl bond of ironporphyrin core and then relaxed to the porphyrin macrocycle.

#### X-F-8 Structural Model of the Amyloid Fibril Formed by $\beta_2$ -Microglobulin #21-31 Fragment Based on Vibrational Spectroscopy

HIRAMATSU, Hirotsugu; GOTO, Yuji<sup>1</sup>; NAIKI, Hironobu<sup>2</sup>; KITAGAWA, Teizo  
(<sup>1</sup>Osaka Univ.; <sup>2</sup>Fukui Univ.)

[*J. Am. Chem. Soc.* **127**, 7988–7989 (2005)]

A structural model of amyloid fibril formed by the #21-31 fragment of  $\beta_2$ -microglobulin is proposed from microscope IR measurements on specifically  $^{13}\text{C}$ -labeled peptide fibrils and Raman spectra of the dispersed fibril solution. The  $^{13}\text{C}$ -shifted amide frequency indicated the secondary structure of the labeled residues. The IR spectra have demonstrated that the region between F22 and V27 forms the core part with the extended  $\beta$ -sheet structure. Raman spectra indicated the formation of a dimer with a disulfide bridge between C25 residues.

### X-F-9 Excited State Property of Hardly Photodissociable Heme-CO Adduct Studied by Time-Dependent Density Functional Theory

OHTA, Takehiro; PAL, Biswajit; KITAGAWA, Teizo

[*J. Phys. Chem.* in press]

While most of CO-bound hemes are easily photodissociated with a quantum yield of nearly unity, we occasionally encounter a CO-heme which appears hardly photodissociable under ordinary measurement conditions of resonance Raman spectra using CW laser excitation and a spinning cell. This study aims to understand such hemes theoretically, that is, the excited state properties of the five-coordinate heme-CO adduct (5cH) as well as the 6c heme-CO adduct (6cH) with a weak axial ligand. Using a hybrid density functional theory we scrutinized the properties of the ground and excited spin states of the computational models of a 5cH and a water ligated 6cH (6cH-H<sub>2</sub>O), and compared these properties with those of a photodissociable imidazole ligated 6cH (6cH-Im). Jahn-Teller softening for the Fe-C-O bending potential in the  $a_1-e$  excited state was suggested. The excited state properties of 6cH-Im and 5cH were further studied with time-dependent DFT theory. The reaction products of the 6cH-Im and 5cH were assumed to be quintet and triplet states, respectively. According to the TD-DFT calculations, the Q excited state of 6cH-Im which is initially a pure  $\pi-\pi^*$  state, crosses the Fe-CO dissociative state ( $2A'$ ) without large elongation of the Fe-CO bond. In contrast, the Q state of the 5cH does not cross the Fe-CO dissociative state but results in the formation of the excited spin state with a bent Fe-C-O. Consequently, photodisomerization from linear to bent Fe-C-O in the 5cH is a likely mechanism for apparent unphotodissociation.

### X-F-10 Mechanism for Transduction of the Ligand-Binding Signal in Heme-Based Gas Sensory Proteins Revealed by Resonance Raman Spectroscopy

UCHIDA, Takeshi; KITAGAWA, Teizo

[*Acc. Chem. Res.* **38**, 662–670 (2005)]

Gene analysis has revealed a variety of new heme-containing gas sensory proteins in organisms ranging

from bacteria to mammals. These proteins are composed of sensor, communication, and functional domains. The sensor domain contains a heme that binds effector molecules such as NO, O<sub>2</sub>, or CO. Ligand binding by the sensor domain modulates the physiological role of the protein, such as DNA binding in the case of transcriptional factors or the catalytic reaction rate in the case of enzymes. This review summarizes resonance Raman (RR) studies, including static and time-resolved measurements, which have enabled elucidation of the mechanisms by which binding of specific target molecule by the sensor domain is transduced to alteration of the functional domain. These studies have shown that signals can be conveyed from the heme to the functional domain *via* three different pathways: i) a distal pathway, ii) a proximal pathway, and iii) a heme peripheral pathway.

### X-F-11 UV Resonance Raman Study of Model Complexes of the Cu<sub>B</sub> Site of Cytochrome c Oxidase

NAGANO, Yasutomo; LIU, Jin-Gang<sup>1</sup>; NARUTA, Yoshinori<sup>1</sup>; KITAGAWA, Teizo  
(<sup>1</sup>Kyushu Univ.)

[*J. Mol. Struct.* **735-736**, 279–291 (2005)]

A newly designed model complex for the Cu<sub>B</sub> site of cytochrome *c* oxidase (CcO), that is, Cu coordinated by two free imidazoles and an imidazole covalently linked to *p*-cresol [Cu<sup>II</sup>BIAIPBr]Br, (BIAIP = 2-[4-[[Bis(1-methyl-1*H*-imidazol-2-ylmethyl)amino]methyl]-1*H*-imidazol-1-yl]-4-methylphenol), and related molecules have been investigated with absorption and ultraviolet resonance Raman (UVR) spectroscopy employing the excitation wavelengths between 220 and 290 nm. Attention was focused on the electron delocalization through the cross-linkage between the phenol and imidazole rings, and the influences by the coordination of Cu<sup>II</sup> to imidazole. In addition to the  $\nu_{8a}$  and  $\nu_{8b}$  modes of *p*-cresol, a number of Raman bands involving vibrations of the imidazole moiety have been intensity-enhanced despite Raman excitation in resonance with the  $\pi-\pi^*$  transition of phenol, indicating appreciable mixing of the  $\pi$  systems of imidazole and phenol rings. Furthermore, two kinds of imidazoles seem to be differential; one is the imidazole linked to *p*-cresol which yielded Raman bands at 1249, 1191, and 1141 cm<sup>-1</sup> for protonated Cu<sup>II</sup>-BIAIP, and the other is one not linked to *p*-cresol, which yielded an intense band at 1488 cm<sup>-1</sup> band. Raman enhancement of the latter mode seems to be caused by preresonance to the lowest  $\pi-\pi^*$  transition of imidazole *via* the A-term mechanism. The Raman excitation profile (REP) of  $\nu_{8a}$  mode for the deprotonated phenol of the Cu<sup>II</sup>-complex revealed a weak local maximum corresponding to the L<sub>a</sub> band around 240 nm. Raman enhancement by the L<sub>a</sub> band was relatively weaker for the Cu<sup>II</sup>-complex than for the Zn<sup>II</sup>-complex and metal-free ligand, suggesting the more extensive mixing of  $\pi$  systems of *p*-cresol-imidazole through the cross-linkage for the Cu<sup>II</sup>-complex.

**X-F-12 Resonance Raman Investigation on the Specific Sensing Mechanism of a Target Molecule by Gas Sensory Proteins**

OHTA, Takehiro; KITAGAWA, Teizo

[*Inorg. Chem.* **44**, 758–769 (2005)]

Specific sensing of gas molecules such as CO, NO, and O<sub>2</sub> is a unique function of gas sensory hemoproteins, while hemoproteins carry out a wide variety of functions such as oxygen storage/transport, electron transfer, and catalysis as enzymes. It is important in the gas sensory proteins that the heme domain not only recognizes their target molecule, but also discriminates against other gases having similar molecular structures. Coordination of a target molecule to the heme is supposed to alter the protein conformation in the vicinity of heme, and the conformation change is propagated to the effector domain where substrate turnover, DNA binding, or interaction with a signal transduction protein will be performed in a way different from the case in binding of other gases. To understand the appearance of such a specificity, we focus our attention on the ligand-protein interactions in the distal side of heme here. Practically, the metal ligand vibrations as well as internal modes of ligand and heme are measured with resonance Raman spectroscopy for wild-type and some mutant proteins with full-length or limited sensory region. On the basis of such observations together with the knowledge currently available, we will discuss the mechanism of specific sensing of a diatomic molecule in gas sensory proteins.

**X-F-13 Communication Pathway between Heme and Protein in Myoglobin**GAO, Ying<sup>1</sup>; EL-MASHTOLY, Samir F.; PAL, Biswajit; HAYASHI, Takashi<sup>2</sup>; HARADA, Katsuyoshi<sup>3</sup>; NAKAGAWA, Tomoyuki<sup>3</sup>; KITAGAWA, Teizo(<sup>1</sup>SOKENDAI; <sup>2</sup>IMS and Osaka Univ.; <sup>3</sup>Kyushu Univ.)[*J. Am. Chem. Soc.* submitted]

We investigated the communication pathway between heme and protein with sperm whale myoglobin as a model. It is known that Trp7 and Tyr151 exhibit UVR spectral changes upon ligand binding to heme, we monitored their UVR spectral changes for three kinds of proteins in which the plausible pathway was removed (*i.e.*, *via* His93, propionate-6, or propionate-7). The UVR results demonstrate that the absence of the H-bonds between propionate-7 and both Ser92 and His97 significantly perturbs the transduction of a structural change in heme to Trp7, but the cleavage of the Fe–His(93) covalent bond eliminates the communication to Tyr151. Thus the H-bonds between the propionate-7 and the F-helix regulate the conformational changes of the A helix, while the Fe–His bond is responsible for a change in the C-terminus but not for the A helix.

**X-F-14 FT-IR Approaches on Amyloid Fibril Structure**

HIRAMATSU, Hirotsugu; KITAGAWA, Teizo

[*Biochim. Biophys. Acta* in press]

This review treats recent achievements of Fourier-transform infrared absorption spectroscopy on protein science, especially on amyloid fibril structure. It includes the brief explanation of theoretical background, description of related techniques, and recent applications to analysis of fibril structure. Concerns to theoretical background, successful analysis of Amide I in terms of transition dipole coupling between the C=O oscillators in peptide main chain has been described. The theory enables us to estimate a content of secondary structure in a protein. Related experimental techniques such as linear dichroism measurement, application of microscope, and isotope labeling, are introduced. The linear-dichroism measurement brings direct information on molecular orientation, microscope enables to treat a well-prepared particle, and isotope-label technique allows our structural discussion with one-residue resolution. Application of IR absorption spectroscopy and related techniques on amyloid fibril structure is reviewed. The model obtained is compared with protein native structure.

**X-F-15 Structural and Spectroscopic Characterization of (μ-Hydroxo or μ-Oxo)(μ-Peroxo)Diiron(III) Complexes: Models for Peroxo Intermediates of Non-Heme Diiron Proteins Structural and Spectroscopic Characterization of (μ-Hydroxo or μ-Oxo)(μ-Peroxo)Diiron(III) Complexes: Models for Peroxo Intermediates of Non-Heme Diiron Proteins**ZHANG, Xi<sup>1</sup>; FURUTACHI, Hideki<sup>1</sup>; FUJINAMI, Shuhei<sup>1</sup>; NAGATOMO, Shigenori; MAEDA, Yonezo<sup>2</sup>; WATANABE, Yoshihito<sup>3</sup>; KITAGAWA, Teizo; SUZUKI, Masatatsu<sup>1</sup>(<sup>1</sup>Kanazawa Univ.; <sup>2</sup>Kyushu Univ.; <sup>3</sup>IMS and Nagoya Univ.)[*J. Am. Chem. Soc.* **127**, 826–827 (2005)]

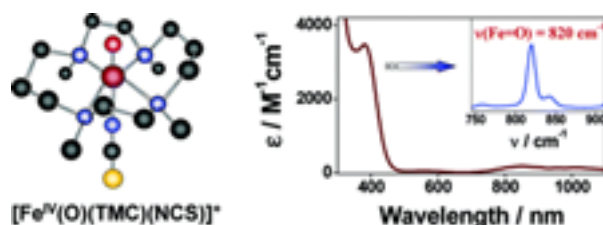
(μ-Hydroxo or oxo)(μ-1,2-peroxo)diiron(III) complexes having a tetradentate tripodal ligand (L) containing a carboxylate sidearm [Fe<sub>2</sub>(μ-OH or μ-O)(μ-O<sub>2</sub>)(L)<sub>2</sub>]<sup>n+</sup> were synthesized as models for peroxo-intermediates of non-heme diiron proteins and characterized by various physicochemical measurements including X-ray analysis, which provide fundamental structural and spectroscopic insights into the peroxodiiron(III) complexes.

**X-F-16 Axial Ligand Substituted Nonheme Fe<sup>IV</sup>=O complexes: Observation of Near-UV LMCT Bands and Fe=O Raman Vibrations**SASTRI, Chivukula V.<sup>1</sup>; PARK, Mi Joo<sup>1</sup>; OHTA, Takehiro; JACKSON, Timothy A.<sup>2</sup>; STUBNA,

Audria<sup>3</sup>; SEO, Mi Sook<sup>1</sup>; LEE, Jimin<sup>1</sup>; KIM, Jinheung<sup>1</sup>; KITAGAWA, Teizo; MUNCK, Eckard<sup>3</sup>; QUE, Lawrence Jr.<sup>2</sup>; NAM, Wonwoo<sup>1</sup>  
(<sup>1</sup>Ewha Womans Univ.; <sup>2</sup>Univ. Minnesota; <sup>3</sup>Carnegie Mellon Univ.)

[*J. Am. Chem. Soc.* **127**, 12494–12495 (2005)]

Axial ligand substitution of a mononuclear nonheme oxoiron(IV) complex,  $[\text{Fe}^{\text{IV}}(\text{O})(\text{TMC})(\text{NCCH}_3)]^{2+}$  (**1**) (TMC = 1,4,8,11-tetramethyl-1,4,8,11-tetraazacyclotetradecane), leads to the formation of new  $\text{Fe}^{\text{IV}}=\text{O}$  species with relatively intense electronic absorption features in the near-UV region. The presence of these near-UV features allowed us to make the first observation of  $\text{Fe}=\text{O}$  vibrations of  $S = 1$  mononuclear nonheme oxoiron(IV) complexes by resonance Raman spectroscopy. We have also demonstrated that the reactivity of nonheme oxoiron(IV) intermediates is markedly influenced by the axial ligands.



#### X-F-17 Reversible O–O Bond Cleavage and Formation of a Peroxo Moiety of a Peroxocarbonate Ligand Mediated by an Iron(III) Complex

FURUTACHI, Hideki<sup>1</sup>; HASHIMOTO, Koji<sup>1</sup>; NAGATOMO, Shigenori; ENDO, Taichi<sup>1</sup>; FUJINAMI, Shuhei<sup>1</sup>; WATANABE, Yoshihito<sup>2</sup>; KITAGAWA, Teizo; SUZUKI, Masatatsu<sup>1</sup>  
(<sup>1</sup>Kanazawa Univ.; <sup>2</sup>IMS and Nagoya Univ.)

[*J. Am. Chem. Soc.* **127**, 4550–4551 (2005)]

A mononuclear iron(III) complex containing a peroxocarbonate ligand,  $[\text{Fe}(\text{qn})_2(\text{O}_2\text{C}(\text{O})\text{O})]^-$  (qn = quinaldinate), underwent the reversible O–O bond cleavage and reformation of the peroxo group *via* the formation of  $\text{Fe}^{\text{IV}}=\text{O}$  or  $\text{Fe}^{\text{V}}=\text{O}$  species, which was confirmed by the resonance Raman and ESI-TOF/MS measurements.

#### X-F-18 Synthesis and Reactivity of a ( $\mu$ -1,1-Hydroperoxo)( $\mu$ -Hydroxo)Dicopper(II) Complex: Ligand Hydroxylation by a Bridging Hydroperoxo Ligand

ITOH, Kyosuke<sup>1</sup>; HAYASHI, Hideo<sup>1</sup>; FURUTACHI, Hideki<sup>1</sup>; MATSUMOTO, Takahiro<sup>1</sup>; NAGATOMO, Shigenori; TOSHA, Takehiko; TERADA, Shoichi<sup>1</sup>; FUJINAMI, Shuhei<sup>1</sup>; SUZUKI, Masatatsu<sup>1</sup>; KITAGAWA, Teizo  
(<sup>1</sup>Kanazawa Univ.)

[*J. Am. Chem. Soc.* **127**, 5212–5223 (2005)]

A new tetradentate tripodal ligand (L3) containing sterically bulky imidazolyl groups was synthesized, where L3 is tris(1-methyl-2-phenyl-4-imidazolylmethyl) amine. Reaction of a bis( $\mu$ -hydroxo)dicopper(II) complex,  $[\text{Cu}_2(\text{L3})_2(\text{OH})_2]^{2+}$  (**1**), with  $\text{H}_2\text{O}_2$  in acetonitrile at  $-40^\circ\text{C}$  generated a ( $\mu$ -1,1-hydroperoxo)dicopper(II) complex  $[\text{Cu}_2(\text{L3})_2(\text{OOH})(\text{OH})]^{2+}$  (**2**), which was characterized by various physicochemical measurements including X-ray crystallography. The crystal structure of **2** revealed that the complex cation has a  $\text{Cu}_2(\mu$ -1,1-OOH)( $\mu$ -OH) core and each copper has a square pyramidal structure having an  $\text{N}_3\text{O}_2$  donor set with a weak ligation of a tertiary amine nitrogen in the apex. Consequently, one pendant arm of L3 in **2** is free from coordination, which produces a hydrophobic cavity around the  $\text{Cu}_2(\mu$ -1,1-OOH)( $\mu$ -OH) core. The hydrophobic cavity is preserved by hydrogen bondings between the hydroperoxide and the imidazole nitrogen of an uncoordinated pendant arm in one side and the hydroxide and the imidazole nitrogen of an uncoordinated pendant arm in the other side. The hydrophobic cavity significantly suppresses the H/D and  $^{16}\text{O}/^{18}\text{O}$  exchange reactions in **2** compared to that in **1** and stabilizes the  $\text{Cu}_2(\mu$ -1,1-OOH)( $\mu$ -OH) core against decomposition. Decomposition of **2** in acetonitrile at  $0^\circ\text{C}$  proceeded mainly *via* disproportionation of the hydroperoxo ligand and reduction of **2** to  $[\text{Cu}(\text{L3})]^+$  by hydroperoxo ligand. In contrast, decomposition of a solid sample of **2** at  $60^\circ\text{C}$  gave a complex having a hydroxylated ligand  $[\text{Cu}_2(\text{L3})(\text{L3-OH})(\text{OH})_2]^{2+}$  (**2-(L3-OH)**) as a main product, where L3-OH is an oxidized ligand in which one of the methylene groups of the pendant arms is hydroxylated. ESI-TOF/MS measurement showed that complex **2-(L3-OH)** is stable in acetonitrile at  $-40^\circ\text{C}$ , whereas warming **2-(L3-OH)** at room temperature resulted in the *N*-dealkylation from L3-OH to give an *N*-dealkylated ligand, bis(1-methyl-2-phenyl-4-imidazolylmethyl)amine (L2) in  $\sim 80\%$  yield based on **2**, and 1-methyl-2-phenyl-4-formylimidazole (Phim-CHO). Isotope labeling experiments confirmed that the oxygen atom in both L3-OH and Phim-CHO come from OOH. This aliphatic hydroxylation performed by **2** is in marked contrast to the arene hydroxylation reported for some ( $\mu$ -1,1-hydroperoxo)dicopper(II) complexes with a xylyl linker.

#### X-F-19 Spectroscopic and Redox Properties of a CoxA Homologue from *Carboxydotherrmus hydrogenofmans*

INAGAKI, Sayaka<sup>1</sup>; MASUDA, Chiaki<sup>2</sup>; AKAISHI, Tetsuhiro<sup>2</sup>; NAKAJIMA, Hiroshi<sup>3</sup>; YOSHIOKA, Shiro; OHTA, Takehiro; PAL, Biswajit; KITAGAWA, Teizo; AONO, Shigetoshi  
(<sup>1</sup>SOKENDAI; <sup>2</sup>JAIST; <sup>3</sup>IMS and JAIST)

[*J. Biol. Chem.* **280**, 3269–3274 (2005)]

CooA is a CO-sensing transcriptional activator that contains a b-type heme as the active site for sensing its physiological effector, CO. In this study, the spectroscopic and redox properties of a new CoxA homologue from *Carboxydotherrmus hydrogenofmans* (Ch-CooA) were studied. Spectroscopic and mutagenesis studies revealed that His-82 and the N-terminal  $\alpha$ -amino group

were the axial ligands of the Fe(III) and Fe(II) hemes in Ch-CooA and that the N-terminal  $\alpha$ -amino group was replaced by CO upon CO binding. Two neutral ligands, His-82 and the N-terminal  $\alpha$ -amino group, are coordinated to the Fe(III) heme in Ch-CooA, whereas two negatively charged ligands, a thiolate from Cys-75 and the nitrogen atom of the N-terminal Pro, are the axial ligands of the Fe(III) heme in Rr-CooA. The difference in the coordination structure of the Fe(III) heme resulted in a large positive shift of redox potentials of Ch-CooA compared with Rr-CooA. Comparing the properties of Ch-CooA and Rr-CooA demonstrates that the essential elements for CooA function will be: (i) the heme is six-coordinate in the Fe(III), Fe(II), and Fe(II)-CO forms; (ii) the N-terminal is coordinated to the heme as an axial ligand, and (iii) CO replaces the N-terminal bound to the heme upon CO binding.

#### **X-F-20 Structural Diversities of Active Site in Clinical Azole-Bound Forms between Sterol 14 $\alpha$ -Demethylases (CYP51s) from Human and *Mycobacterium tuberculosis***

MATSUURA, Koji<sup>1</sup>; YOSHIOKA, Shiro<sup>2</sup>; TOSHA, Takehiko; HORI, Hiroshi<sup>3</sup>; ISHIMORI, Koichiro<sup>4</sup>; KITAGAWA, Teizo; MORISHIMA, Isao<sup>1</sup>; KAGAWA, Norio<sup>5</sup>; WATERMAN, Michael R.<sup>5</sup>  
(<sup>1</sup>Kyoto Univ.; <sup>2</sup>IMS and Vandervilt Univ.; <sup>3</sup>Osaka Univ.; <sup>4</sup>IMS and Kyoto Univ.; <sup>5</sup>Vandervilt Univ.)

[*J. Biol. Chem.* **280**, 9088–9096 (2005)]

To gain insights into the molecular basis of the design for the selective azole anti-fungals, we compared the binding properties of azole-based inhibitors for cytochrome P450 sterol 14 $\alpha$ -demethylase (CYP51) from human (HuCYP51) and *Mycobacterium tuberculosis* (MtCYP51). Spectroscopic titration of azoles to the CYP51s revealed that HuCYP51 has higher affinity for ketoconazole (KET), an azole derivative that has long lipophilic groups, than MtCYP51, but the affinity for fluconazole (FLU), which is a member of the anti-fungal armamentarium, was lower in HuCYP51. The affinity for 4-phenylimidazole (4-PhIm) to MtCYP51 was quite low compared with that to HuCYP51. In the resonance Raman spectra for HuCYP51, the FLU binding induced only minor spectral changes, whereas the prominent high frequency shift of the bending mode of the heme vinyl group was detected in the KET- or 4-PhIm-bound forms. On the other hand, the bending mode of the heme propionate group for the FLU-bound form of MtCYP51 was shifted to high frequency as found for the KET-bound form, but that for 4-PhIm was shifted to low frequency. The EPR spectra for 4-PhIm-bound MtCYP51 and FLU-bound HuCYP51 gave multiple  $g$  values, showing heterogeneous binding of the azoles, whereas the single  $g_x$  and  $g_z$  values were observed for other azole-bound forms. Together with the alignment of the amino acid sequence, these spectroscopic differences suggest that the region between the B' and C helices, particularly the hydrophobicity of the C helix, in CYP51s plays primary roles in determining strength of interactions with azoles; this differentiates the binding specificity of azoles to CYP51s.

#### **X-F-21 Stopped-Flow Spectrophotometric and Resonance Raman Analyses of Aldoxime Dehydratase Involved in Carbon-Nitrogen Triple Bond Synthesis**

OINUMA, Ken-Ichi<sup>1</sup>; KUMITA, Hideyuki<sup>1</sup>; OHTA, Takehiro; KONISHI, Kazunobu<sup>1</sup>; HASHIMOTO, Yoshiteru<sup>1</sup>; HIGASHIBATA, Hiroki<sup>1</sup>; KITAGAWA, Teizo; SHIRO, Yoshitsugu<sup>2</sup>; KOBAYASHI, Michihiko<sup>1</sup>  
(<sup>1</sup>Univ. Tsukuba; <sup>2</sup>RIKEN Harima Inst./Spring-8)

[*FEBS Lett.* **579**, 1394–1398 (2005)]

On stopped-flow analysis of aliphatic aldoxime dehydratase (OxdA), a novel hemoprotein, a spectrum derived from a reaction intermediate was detected on mixing ferrous OxdA with butyraldoxime; it gradually changed into that of ferrous OxdA with an isosbestic point at 421 nm. The spectral change on the addition of butyraldoxime to the ferrous H320A mutant showed the formation of a substrate-coordinated mutant, the absorption spectrum of which closely resembled that of the above intermediate. These observations and the resonance Raman investigation revealed that the substrate actually binds to the heme in OxdA, forming a hexa-coordinate low-spin heme.

#### **X-F-22 Synthesis, Characterization, and Thermal Stability of New Mononuclear Hydrogenperoxocopper(II) Complexes with N<sub>3</sub>O-Type Tripodal Ligands Bearing Hydrogen-Bonding Interaction Sites**

YAMAGUCHI, Syuhei<sup>1</sup>; KUMAGAI, Akinori<sup>1</sup>; NAGATOMO, Shigenori; KITAGAWA, Teizo; FUNAHASHI, Yasuhiro<sup>2</sup>; OZAWA, Tomohiro<sup>1</sup>; JITSUKAWA, Koichiro<sup>1</sup>; MASUDA, Hideki<sup>2</sup>  
(<sup>1</sup>Nagoya Inst. Tech.; <sup>2</sup>IMS and Nagoya Inst. Tech.)

[*Bull. Chem. Soc. Jpn.* **78**, 116–124 (2005)]

In order to understand the effect of an oxygen-containing ligand on the physico-chemical properties and reactivities of hydrogenperoxocopper complexes, new copper(II) complexes with the N<sub>3</sub>O-type tripodal ligand bearing pivalamido groups, *N,N*-bis(6-pivalamido-2-pyridylmethyl)glycine (Hbpga), and *N,N*-bis(6-pivalamido-2-pyridylmethyl)- $\beta$ -alanine (Hbpaa), have been designed and synthesized. Copper(II) complexes without any external ligand and those with a monodentate ligand, such as azido and chloro, have been prepared and characterized with the aid of electronic absorption and ESR spectroscopic, cyclic voltammetric, and X-ray structure analytical methods. The redox potential values of the Cu(II) complexes, when they were compared with the Cu(II) complex of bis(6-pivalamido-2-pyridylmethyl)(2-pyridylmethyl)amine (bppa), reported previously, shifted toward the negative side upon the introduction of a carboxylate group in the place of one pyridine of bppa. Reactions of [Cu(bpga)]ClO<sub>4</sub> (**1a**) and [Cu(bpaa)]PF<sub>6</sub> (**2a**) with hydrogen peroxide in the presence of triethylamine in both MeCN and MeOH solutions gave mononuclear copper(II) com-

plexes with hydrogenperoxide(1-), Cu–bpga–OOH (**1d**) and Cu–bpaa–OOH (**2d**) systems, respectively. The intense absorption bands, assignable to LMCT (HOO<sup>-</sup> → Cu(II)) and d–d bands, and ESR and resonance Raman spectra have revealed that they form trigonal bipyramidal copper complexes with OOH<sup>-</sup> in an end-on fashion. The thermal stabilities of **1d** and **2d** have also been studied by following the reduction rate of the LMCT bands at 283 K. Those of copper(II) complexes with hydrogenperoxide(1-) have been reduced in the order **1d** > **2d** >> [Cu(bppa)(OOH)]<sup>+</sup> (**3d**), all of which are rather stable compared with that of Cu(II)–tpa–OOH (tpa = tris(2-pyridylmethyl)amine). These findings indicate that the hydrogenperoxocopper(II) complexes are activated by introducing carboxylate coordination, although they are stabilized by hydrogen-bonding interactions.

### X-F-23 Spectroscopic Characterization of the Isolated Heme-Bound PAS-B Domain of Neuronal PAS Domain Protein 2 (NPAS2) Associated with Circadian Rhythms

KOUDO, Ryoji<sup>1</sup>; KUROKAWA, Hirofumi<sup>1</sup>; SATO, Emiko<sup>1</sup>; IGARASHI, Jotaro<sup>1</sup>; UCHIDA, Takeshi; SAGAMI, Ikuko<sup>2</sup>; KITAGAWA, Teizo; SHIMIZU, Toru<sup>1</sup>

(<sup>1</sup>Tohoku Univ.; <sup>2</sup>Kyoto Pref. Univ.)

[*FEBS J.* **272**, 4153–4162 (2005)]

Neuronal PAS domain protein 2 (NPAS2) is an important transcription factor associated with circadian rhythms. This protein forms a heterodimer with BMAL1, which binds to the E-box sequence to mediate circadian rhythm-regulated transcription. NPAS2 has two PAS domains with heme-binding sites in the N-terminal portion. In this study, we overexpressed wild-type and His mutants of the PAS-B domain (residues 241–416) of mouse NPAS2 and then purified and characterized the isolated homebound proteins. Optical absorption spectra of the wild-type protein showed that the Fe(III), Fe(II) and Fe(II)–CO complexes are 6-coordinated lowspin complexes. On the other hand, resonance Raman spectra indicated that both the Fe(III) and Fe(II) complexes contain mixtures of 5-coordinated high-spin and 6-coordinated low-spin complexes. Based on inverse correlation between  $\nu_{\text{Fe-CO}}$  and  $\nu_{\text{C-O}}$  of the resonance Raman spectra, it appeared that the axial ligand trans to CO of the heme-bound PAS-B is His. Six His mutants (His266Ala, His289Ala, His300Ala, His302Ala, His329Ala, and His335Ala) were generated, and their optical absorption spectra were compared. The spectrum of the His335Ala mutant indicated that its Fe(III) complex is the 5-coordinated high-spin complex, whereas, like the wild-type, the complexes for the five other His mutants were 6-coordinated low-spin complexes. Thus, our results suggest that one of the axial ligands of Fe(III) in PAS-B is His335. Also, binding kinetics suggest that heme binding to the PAS-B domain of NPAS2 is relatively weak compared with that of sperm whale myoglobin.

### X-F-24 Covalent Cofactor Attachment to Proteins: Cytochrome *c* Biogenesis

STEVENS, Julie M.<sup>1</sup>; UCHIDA, Takeshi; DALTROP, Oliver<sup>1</sup>; FERGUSON, Stuart J.<sup>1</sup>

(<sup>1</sup>Univ. Oxford)

[*Biochem. Soc. Trans.* **33**, 792–795 (2005)]

Haem (Fe-protoporphyrin IX) is a cofactor found in a wide variety of proteins. It confers diverse functions, including electron transfer, the binding and sensing of gases, and many types of catalysis. The majority of cofactors are non-covalently attached to proteins. There are, however, some proteins in which the cofactor binds covalently and one of the major protein classes characterized by covalent cofactor attachment is the *c*-type cytochromes. The characteristic haem-binding mode of *c*-type cytochromes requires the formation of two covalent bonds between two cysteine residues in the protein and the two vinyl groups of haem. Haem attachment is a complex post-translational process that, in bacteria such as *Escherichia coli*, occurs in the periplasmic space and involves the participation of many proteins. Unexpectedly, it has been found that the haem chaperone CcmE (cytochrome *c* maturation), which is an essential intermediate in the process, also binds haem covalently before transferring the haem to apocytochromes. A single covalent bond is involved and occurs between a haem vinyl group and a histidine residue of CcmE. Several *in vitro* and *in vivo* studies have provided insight into the function of this protein and into the overall process of cytochrome *c* biogenesis.

### X-F-25 Structure and Dioxygen-Reactivity of Copper(I) Complexes Supported by Bis(6-methylpyridin-2-yl-methyl)amine Tridentate Ligands

OSAKO, Takao<sup>1</sup>; TERADA, Shohei<sup>2</sup>; TOSHA, Takehiko; NAGATOMO, Shigenori; FURUTACHI, Hideki<sup>2</sup>; FUJINAMI, Shuhei<sup>2</sup>; KITAGAWA, Teizo; SUZUKI, Masatatsu<sup>2</sup>; ITO, Shinobu<sup>1</sup>

(<sup>1</sup>Osaka City Univ.; <sup>2</sup>Kanazawa Univ.)

[*Dalton Trans.* in press]

Structure and dioxygen-reactivity of copper(I) complexes **2<sup>R</sup>** supported by *N,N*-bis(6-methylpyridin-2-yl-methyl)amine tridentate ligands L2<sup>R</sup> [R (*N*-alkyl substituent) = –CH<sub>2</sub>Ph (Bn), –CH<sub>2</sub>CH<sub>2</sub>Ph (Phe) and –CH<sub>2</sub>CHPh<sub>2</sub> (PhePh)] have been examined in comparison with those of copper(I) complex **1<sup>Phe</sup>** of *N,N*-bis[2-(pyridin-2-yl)ethyl]amine tridentate ligand L1<sup>Phe</sup> and copper(I) complex **3<sup>Phe</sup>** of *N,N*-bis(pyridin-2-yl-methyl)amine tridentate ligand L3<sup>Phe</sup>. Copper(I) complexes **2<sup>Phe</sup>** and **2<sup>PhePh</sup>** exhibit a distorted trigonal pyramidal structure involving a d–π interaction with an η<sup>1</sup>-binding mode between the metal ion and one of the *ortho*-carbon atoms of the phenyl group of the ligand side arm [–CH<sub>2</sub>CH<sub>2</sub>Ph (Phe) and –CH<sub>2</sub>CHPh<sub>2</sub> (PhePh)]. Strength of the d–π interaction in **2<sup>Phe</sup>** and **2<sup>PhePh</sup>** is weaker than that of the d–π interaction with an η<sup>2</sup>-binding mode in **1<sup>Phe</sup>** but stronger than that of the η<sup>1</sup> d–π interaction in

**3<sup>Phe</sup>**. Existence of a weak d- $\pi$  interaction in **2<sup>Bn</sup>** in solution was also suggested, but its binding mode was not clear. Redox potential of copper(I) is also affected by the supporting ligand; **L3<sup>Phe</sup>** with the highest donor ability among the ligands gave the lowest  $E_{1/2}$  value of the copper(I) complex, while **L1<sup>Phe</sup>** with the lowest donor ability showed the highest  $E_{1/2}$  value. The redox potentials of **2<sup>R</sup>** were found between them, indicating that the electron-donor ability of **L2<sup>R</sup>** is between those of **L1<sup>Phe</sup>** and **L3<sup>Phe</sup>**. This was reflected in the copper(I)-dioxxygen reactivity, where the reaction rate of copper(I) complex toward O<sub>2</sub> dramatically increases in the order of **1<sup>R</sup>** < **2<sup>R</sup>** < **3<sup>R</sup>**. Structure of the resulting Cu<sub>2</sub>/O<sub>2</sub> intermediate was also altered by the supporting ligand. Oxygenation of copper(I) complex **2<sup>R</sup>** at a low temperature gave a ( $\mu$ - $\eta^2$ : $\eta^2$ -peroxo)dycopper(II) complex as in the case of **1<sup>Phe</sup>**, but its O–O bond is relatively weakened as compared to the peroxo complex derived from **1<sup>Phe</sup>**, and a small amount of a bis( $\mu$ -oxo)dycopper(III) complex co-existed. These results can be attributed to the higher electron-donor ability of **L2<sup>R</sup>** as compared to **L1<sup>Phe</sup>**. On the other hand, the fact that **3<sup>Phe</sup>** mainly afforded a bis( $\mu$ -oxo)dycopper(III) complex suggests that the electron-donor ability of **L2<sup>R</sup>** is not high enough to support the higher oxidation state of copper(III) of the bis( $\mu$ -oxo) complex.

#### X-F-26 Resonance Raman and FT-IR Studies on Proximal and Distal Histidine Environment of Cytochrome c and Neuroglobin

SAWAI, Hitomi<sup>1</sup>; MAKINO, Masatomo<sup>1</sup>; MIZUTANI, Yasuhisa<sup>2</sup>; OHTA, Takehiro; SUGIMOTO, Hiroshi<sup>3</sup>; UNO, Tadayuki<sup>4</sup>; KAWADA, Norifumi<sup>1</sup>; YOSHIKATO, Katsutoshi<sup>1</sup>; KITAGAWA, Teizo; SHIRO, Yoshitsugu<sup>3</sup>  
(<sup>1</sup>Univ. Hyogo; <sup>2</sup>IMS and Kobe Univ.; <sup>3</sup>RIKEN Harima Inst./Spring8; <sup>4</sup>Osaka Univ.)

[Biochemistry in press]

Cytochrome c (Cgb) and neuroglobin (Ngb) are first examples of hexa-coordinated globins of humans and other vertebrates, where a histidine (His) residue is an endogenous ligand at the sixth position of the heme iron in both the ferric and the ferrous forms. The static and time-resolved resonance Raman and FT-IR spectroscopic techniques were applied to examine the structures in the heme environment of these globins. Using the picosecond time-resolved resonance Raman (ps-TR<sup>3</sup>) spectroscopy, the Fe–His stretching ( $\nu_{\text{Fe-His}}$ ) bands of transient five-coordinate heme species for Cgb and Ngb, yielded upon photolysis of the carbon monoxide (CO) adducts, were observed at 229 and 221 cm<sup>-1</sup>, respectively. The  $\nu_{\text{Fe-His}}$  band of Cgb and Ngb did not exhibit any time-dependent shift in the 20–1000 ps time domain, being contrasted to the case of Mb. In combination of the present spectroscopic data with the crystallographic ones reported so far, it was likely suggested that the structure of Cgb and Ngb in the heme pocket would be altered upon the CO binding, and the altered structures are different from that of Mb, but the scales of the structural alteration are different between Cgb and Ngb. To investigate the structural property of the heme distal

side for the ligand-bound forms, the sets of ( $\nu_{\text{Fe-CO}}$ ,  $\nu_{\text{C-O}}$ ,  $\delta_{\text{Fe-C-O}}$ ) and ( $\nu_{\text{Fe-NO}}$ ,  $\nu_{\text{N-O}}$ ,  $\delta_{\text{Fe-N-O}}$ ) for the CO and NO complexes of Cgb and Ngb were observed. On the basis of the spectral comparison of some distal mutants for Cgb (H81A, H81V, R84A, R84K, R84T) and Ngb (H64A, H64V, K67A, K67R, K67T), it was found that three conformers were present in their CO complexes, and the distal His (His81 in Cgb and His64 in Ngb), which were replaced by the exogenous CO ligand, mainly contributes to the inter-conversion of the conformers. These structural characteristics of Cgb and Ngb were discussed in relation to their ligand binding and physiological properties.

#### X-F-27 Dynamic Ligation Properties of the *Escherichia coli* Heme Chaperone CcmE to Non-Covalently Bound Heme

STEVENS, Julie M.<sup>1</sup>; UCHIDA, Takeshi; DALTRUP, Oliver<sup>1</sup>; KITAGAWA, Teizo; FERGUSON, Stuart J.<sup>1</sup>  
(<sup>1</sup>Univ. Oxford)

[J. Biol. Chem. submitted]

The cytochrome *c* maturation protein CcmE is an essential membrane-anchored heme chaperone involved in the post-translational covalent attachment of heme to *c*-type cytochromes in Gram-negative bacteria such as *Escherichia coli*. Previous *in vitro* studies have shown that CcmE can bind heme both covalently (*via* a histidine residue) and non-covalently. In this work we present results on the latter form of heme binding to a soluble form of CcmE. Examination of a number of site-directed mutants of *E. coli* CcmE by resonance Raman spectroscopy has identified ligands of the heme iron and provided insight into the initial steps of heme binding by CcmE before it binds the heme covalently. The heme-binding histidine (H130) appears to ligate the heme iron in the ferric oxidation state but two other residues ligate the iron in the ferrous form, thereby freeing H130 to undergo covalent attachment to a heme vinyl group. It appears that the heme ligation in the non-covalent form is different from that in the holo-form, suggesting that a change in ligation could act as a trigger for the formation of the covalent bond.

## X-G Collaborative Research with FANTOM Consortium

The collaboration with Okazaki Institute for Integrative Bioscience has focused with the interaction of the Fantom Consortium. In this context, the group of Dr. Seto has focused on the analysis of the Ubiquitin protein within the Fantom-3 dataset, and to analyze the function.

### **X-G-1 The international Consortium, FANTOM\*, Discovered UBL Domains Interspersed over Mammalian Genomes**

**HAYASHIZAKI, Yoshihide**  
(*IMS and RIKEN GSC*)

Ubiquitin is a protein that has been well investigated in the fields of protein degradation and transport systems. Several proteins are reported that they have ubiquitin-like sequence, UBL domains. These proteins were named UBL-containing proteins, and comparative analyses of all UBL-containing proteins were performed among various species, including humans, mice, flies, worms, and yeast in this report.

We compared human UBL-containing proteins with mouse UBL-containing proteins, and found 43 orthologous pairs (74% in human UBL-containing proteins). The UBL-containing proteins were divergent protein family. We found two human UBL-containing proteins whose mouse orthologs did not possess a UBL domain. We also found three mouse UBL-containing proteins whose human orthologs did not possess a UBL domain. Moreover, 12 human UBL-containing proteins had no orthologs in the mouse genome, and 8 mouse UBL-containing proteins had no human orthologs. About 60% of the conserved UBL-containing proteins between human and mouse were expressed in the nervous system in FANTOM3 dataset. By using the phylogenic analysis of all UBL domains in humans, mice, flies, worms, and yeast, we found that 33% of UBL domains were species-specific, and that 40% of UBL domains were found in the human/mouse conserved group. Therefore, this study on the UBL-containing proteins show a tendency to diversify their amino acid sequences during the evolution.

\* FANTOM: Functional Annotation Of Mouse



## RESEARCH FACILITIES

The Institute for Molecular Science includes five research facilities. This section describes their latest equipment and activities. For further information please refer to older IMS Annual Review issues (1978–2004).

### Research Center for Molecular-scale Nanoscience

This center was established in April 2002 after reorganization including the Research Center for Molecular Materials, the Department of Electronic Structure and the Department of Molecular Assemblies. The Center is supposed to play a principal role to integrate the innovative progress that IMS has achieved in the fields of molecular science and material science. Its mission is to develop a new field of science systematizing new finding in physical and chemical properties of new molecular materials and nano structures, by elucidation and controlling the structure and function of the materials at the atom/molecular level. In addition, the center promote coloboration with internal and external researchers by providing technical services of common research facilities which are indispensable for nano science research.

The center is comprised of four divisions: (A) Molecular-scale electronics, (B) Nanocatalysis and biomolecular devices, (C) Nano-scale photoscience, and (D) Advanced molecular science, where the last division consists of visiting faculty members. The respective research activities of each divisions are reported in other sections in this Review. Technical staffs are also important members of the center, who manage the common equipments and facilities of the center, provide liquid nitrogen and helium, and take care of the elemental analyses.

### UVSOR Facility

The UVSOR accelerator complex consists of a 15 MeV injector linac, a 600 MeV booster synchrotron, and a 750 MeV storage ring. The magnet lattice of the storage ring is the so-called double-bend achromat. The double RF system is routinely operated for the user beam time, and the lifetime of the electron beam has been improved to around 6 hours at 200 mA. The storage ring is normally operated under multi-bunch mode with partial filling. The single bunch operation is also conducted about two weeks per year, which provides pulsed synchrotron radiation (SR) for time-resolved experiments. Initial beam currents stored under multi-bunch and single-bunch modes are 300 mA and 70 mA, respectively.

Eight bending magnets and two insertion devices are available for utilizing SR. The bending magnet with its radius of 2.2 m provides SR, whose critical energy is 425 eV. After completing the upgrade project, there are 16 beamlines operational at UVSOR, which can be classified into two categories. 9 of them are so-called "Open beamlines," which are open to scientists of universities and research institutes belonging to the government, public organizations, private enterprises and those of foreign countries. The rest of the 7 beamlines are so-called "In-house beamlines," which are dedicated to the use of the research groups within IMS. We have 1 soft X-rays (SX) station equipped with a double-crystal monochromator, 7 EUV and SX stations with a grazing incidence monochromator, 3 VUV stations with a normal incidence monochromator, 1 (far) infrared station equipped with FT interferometers, 1 station with a multi-layer monochromator, and 3 non-monochromatized stations for the irradiation of white-light.

Discussion with users, concerning the improvements and upgrades of the beamlines at UVSOR, has been continuously held as series of UVSOR workshops. The upgrade project of the UVSOR storage ring, in which the creation of four new straight sections and the achievement of much smaller emittance (27 nm-rad) were planned, has been approved in the fiscal year of 2002 and has been accomplished on schedule. Keeping pace with this project, a new in-vacuum undulator and high performance monochromator for BL3, and a new high-resolution photoelectron energy analyzer for the end station at BL5U, have been successfully installed. The renewal of the vacuum duct at BL6 has been completed during the regular shutdown in the spring of 2004. In coincidence with this, a so-called magic mirror has been installed as the first mirror for a new IR beamline, BL6B. It has been confirmed that the highest intensity in the world, has been achieved in the wavelength range from sub-milli to near IR region. Two vacant lots are left at BL2A and BL6A for constructing novel beamlines. A new RF cavity has been installed to the short straight section between B01 and B02 before the end of March 2005; BL2A will be a bending-magnet beamline while BL6A is to be an undulator one, which will be called BL6U. Regarding the utilization for the long straight section between B06 and B07, a UVSOR workshop has been held in March 2005. On the basis of the review and evaluation report on the present status of UVSOR in 2004, a high resolution and high flux variable polarization beamline BL7U for spectroscopy in the VUV range has been proposed, and possible scientific cases performed on this beamline have been discussed. Further serious discussion toward utilizing the available straight sections most effectively and formulating a basic plan on the beamline construction, will be continued.

All users are required to refer to the beam-line manuals and the UVSOR guidebook (latest revision in 1999), on the occasion of conducting actual experimental procedures. Those wishing to use the open and in-house beamlines are recommended to contact with the stationmaster/supervisor and the representative, respectively. For updated information of UVSOR, <http://www.uvsor.ims.ac.jp/>.

### Laser Research Center for Molecular Science

This center was established in 1997 by reorganization of a part of the Instrument Center. The new Center is composed of three research groups which are asked to develop new lasers suitable for pioneering researches in the new field of molecular science. The three groups are

1. Advanced Lasers for Chemical Reaction Studies,
2. Advanced Lasers for Synchrotron Radiation Applications,  
and
3. Advanced UV and IR Tunable Lasers.

The Laser Research Center is equipped with excimer lasers and solid-state light sources in various temporal and spectral regions, including femtosecond optical parametric oscillators (OPO). The synchronously pumped femtosecond (OPO) (OPAL; Spectra Physics) is tunable from 1.1  $\mu\text{m}$  up to 1.6  $\mu\text{m}$ .

The Laser Center also has general instruments and spectrophotometers. A fluorescence spectrophotometer (Fluorolog II; Spex) is composed of a xenon lamp house for excitation, double and single monochromators for spectroscopy, and changeable detectors (CCD and photomultiplier tube). Other instruments are UV-VIS and IR spectrophotometers, circular dichroism dispersion photometer, and general-purpose electronic instruments. Using these instruments, researchers can carry out various experiments not only in the ultrafast temporal region but also in the steady state regime.

### Equipment Development Center

Design and fabrication of the instruments, and research and developments of the new instruments necessary for the molecular science research are the mission of this center, which consists of the mechanical, electronic and glass work sections.

As a new attempt, we are going to expand our service to the outside researchers of universities and research institutes since October 2005. The main aims of this new attempt are to contribute to the molecular science community and to improve the technology level of the center staffs.

#### *Design and fabrication works of this fiscal year*

- Diebonding system for laser crystal
- TOF lens unit
- Reflection chamber
- Cooling heat sink DMCH-material
- Micro-manipulator
- Flexure stage
- 22Poles ion trap
- PMT housing
- Poling instrument
- Water-cooled jacket for a lens holder
- Electron yield detector with adjustment of Z-axis

#### *Research and developments of the new instruments*

- High-Precision slit blade
- Microreactor chip
- Micro processing by a femto-second laser
- Electrical Control System of FRAP
- Activities are described in detail in the section "RESEARCH ACTIVITIES"

### Safety Office

The Safety Office was established in April 2004. The Office is supposed to play a principal role in the institute to secure the safety and health of the staffs by achieving a comfortable workplace environment, and improvement of the working conditions. In concrete terms, it carries out planning, work instructions, fact-findings, and other services for safety and health in the institute. The office is comprised of the following staffs: the director of the office, safety and health administrators, safety and health office personnel, operational chiefs, and other staff members appointed by the Director General.

### Okazaki Research Facilities (related to IMS) Research Center for Computational Science

Research Center for Computational Science, Okazaki Research Facilities, National Institutes of National Sciences, provides up-to-date computational resources to academic researchers in molecular science and related fields. As of March 2005, this facility is used by 598 scientists in 154 project groups.

The computer systems, currently consisting of Fujitsu VPP5000, SGI SGI2800/Origin3800, NEC SX-7, NEC

TX-7 and Hitachi SR8000, cover a wide range of computational requests in quantum chemistry, molecular simulation, chemical reaction dynamics and solid state physics. These systems are linked to international networks through Super Science Information Network (super SINET). Detailed information on the hardware and software of the Center is available on the web site (<http://ccinfo.ims.ac.jp/>).

The Center provides a number of program suites, including Gaussian 03, GAMESS, Molpro2002, Hondo2003, AMBER, *etc.*, which are installed to the computer systems and kept updated for immediate use of the users. The Center also maintains and offers the Quantum Chemistry Literature Database (QCLDB, <http://qcldb2.ims.ac.jp/>), which has been developed by the Quantum Chemistry Data Base Group in collaboration with staff members of the Center. The latest release, QCLDB Release 2004, contains 68,308 data of quantum chemical studies.

In addition to offering computer resources to a wide range of molecular scientists, another vital aspect of the Center is to perform leading computational researches with massive computations. Since 2003 the Center is participating in the National Research Grid Initiative (NAREGI) project, a five-year national project by National Institute of Informatics (NII) and IMS. This joint project aims at developing grid computing system (NII) and thereby realizing extremely large-scale computational studies in the frontier of nanoscience (IMS). For these purposes, two supercomputer systems, Hitachi SR11000 and HA8000, were introduced to the Center in 2004, with combined performance exceeding 10 TFlops. Further information on the NAREGI project and the computer systems at the Center is found on the web site (<http://nanogrid.ims.ac.jp/nanogrid/>).



## SPECIAL RESEARCH PROJECTS

IMS has special research projects supported by national funds. Three projects in progress are:

- (a) Chemical Reaction Dynamics
- (b) Molecular Photophysics and Science
- (c) Novel Materials Science

These three projects are being carried out with close collaboration between research divisions and facilities. Collaborations from outside also make important contributions. Research fellows join these projects.

### (a) Chemical Reaction Dynamics

#### Folding Mechanism of Protein Molecules Studied by Generalized-Ensemble Algorithms

**OKAMOTO, Yuko; OKUMURA, Hisashi; KAWASHIMA, Yukio; ONO, Yuriko; KOKUBO, Hironori; ITOH, Satoru G.<sup>1</sup>**  
(<sup>1</sup>SOKENDAI)

Proteins are the most complicated molecules that exist in nature. Since protein structures are closely related to their biological functions, the understanding of their folding mechanism from the first principles is not only very challenging but also very important. To be more specific, it is widely believed that three-dimensional structures of proteins are determined by their amino-acid sequence information. However, nobody has completely succeeded in predicting it solely from the amino-acid-sequence information (prediction from the first principles).

There are two elements for the difficulty. One element is that the inclusion of accurate solvent effects is non-trivial because the number of solvent molecules that have to be taken into account is very large. The other element for the difficulty is that there exist a huge number of local minima in the energy function, and simulations by conventional techniques will necessarily get trapped in one of the local minima without ever finding the energy global minimum. Generalized-ensemble algorithms are new simulation algorithms that can alleviate this second difficulty (for reviews, see Refs.1-3). We have been developing new generalised-ensemble algorithms. We found that the combination of multi-canonical algorithm and replica-exchange method is particularly promising.

The goal of the present project is to further develop and test the effectiveness of generalize-ensemble algorithms in the protein folding problem and to succeed eventually in the prediction of tertiary structures of proteins from the first principles.

#### References

- 1) A. Mitsutake, Y. Sugita and Y. Okamoto, *Biopolymers (Pept. Sci.)* **60**, 96–123 (2001).
- 2) Y. Sugita and Y. Okamoto, *Lecture Notes in Computational Science and Engineering*, T. Schlick and H. H. Gan, Eds., Springer-Verlag, pp. 304–332 (2002).
- 3) Y. Okamoto, *J. Mol. Graphics Modell.* **22**, 425–439 (2004).

#### Electronic Structure and Decay Mechanism of Inner-Shell Excited Molecules

**KOSUGI, Nobuhiro; HATSUI, Takaki; HIYAMA, Miyabi**

This project is being carried out at the Beamlines 4B and 3U on the UVSOR-II ring. We have three sub-projects: (A) spin-orbit, exchange, and molecular field splittings in S 2p and P 2p excited states, (B) molecules in free clusters, in condensed phase, and in rare gas matrix, and (C) ionic fragmentations following the inner-shell resonance excitation. In (A), we have found some spin-forbidden ionized and excited states in non-radiative (photoelectron emission) and radiative (photon emission) deexcitation spectra. We have succeeded in development of a next-generation soft X-ray emission spectrometer. In (B), we have discussed blueshift and redshift in inner-shell excitation energy by relating to exchange repulsion and polarization stabilization from surrounding molecules. In (C), we are concentrating on theoretical interpretation, based on the R-matrix/MQDT method, of our experimental data measured for recent several years.

#### Computational Study of Quantum Dynamics of a Solute in Solution

**OKAZAKI, Susumu; MIURA, Shinichi; MIKAMI, Taiji; SATO, Masahiro**

Vibrational relaxation mechanism in condensed phase has been investigated based upon a series of mixed quantum-classical molecular dynamics calculations for non-polar solute in non-polar solvent and polar solute in polar solvent.

First, relaxation mechanism of I<sub>2</sub> in Ar, where Lennard-Jones force is predominant in the interaction, is investigated as a function of density and temperature, focusing our attention on the isolated binary collision (IBC) model. The model was originally established for the relaxation in gas phase. A key question, here, is “Can we apply the IBC model to the relaxation in the high-density fluid?” Analysing the trajectory of solvent molecule as well as its interaction with the solute, we found that collisions between them may be defined clearly even in the high-density fluid. Change of the survival probability of the vibrationally first excited state on collision was traced. The change caused by

collisions with a particular solvent molecule was also traced together with the interaction between them. Each collision makes a contribution to the relaxation by a stepwise change in the probability. The analysis clearly shows that the relaxation is caused by collisions even in the high-density fluid. Difference between stepwise relaxation and continuous one found for the total relaxation in the low-density fluid and in the high-density one, respectively, was clarified to come from just the difference in frequency of the collision. The stronger the intensity of the collision is, the greater the relaxation caused by the collision is. Further, the shorter the collision time is, the greater the resultant relaxation is.

Second, we found that molecular mechanism of the relaxation of a polar molecule in supercritical water is significantly different from that assumed in the IBC model despite that the density dependence of the relaxation rate showed a linear correlation with the local density of water around the solute, the linear correlation being apparently in good accordance with the IBC model. The puzzle has been solved by this project.

### Chemical Reactions at Surfaces and Nano-Structured Materials Studied by Spatio-Temporally Resolved Spectroscopy

**MATSUMOTO, Yoshiyasu; WATANABE, Kazuya; MATSUMOTO, Taketoshi**

Chemical reactions on solid surfaces are typical heterogeneous reactions. Studies in the time domain such as kinetics are useful to understand reaction mechanisms, but these are not enough to have a full understanding of the reaction mechanisms because reactions depend on local environment of reactants. Therefore, it is necessary to perform studies both in the time and spatial domains. This project aims for developing spatio-temporally resolved methods to probe various processes at surfaces. In the time domain, we perform fs time-resolved nonlinear spectroscopy including multiphoton photoelectron spectroscopy (MPS), second harmonic generation (SHG), and sum frequency generation (SFG). MPS is very suitable to investigate the unoccupied states of adsorbates and how they decay. This method is applied to ultrafast electron transfer at surfaces and interfaces. SHG is used for monitoring the dephasing processes of coherent vibrational motions at surfaces. This is a first step toward coherent control of surface processes. SFG provides time-resolved vibrational spectra of adsorbates, which is useful to detect reaction intermediates. On the other hand, in the spatial domain we perform scanning tunneling microscopy (STM) in ultrahigh vacuum conditions. Observations of temporal progresses in STM images while surface reactions take place make it possible to confirm active sites of the reactions. Furthermore, a variable temperature STM allows us to monitor changes in surface geometry with the atomic resolution during surface reactions. This capability is extremely useful to monitor spatial propagation of surface reactions, in particular, autocatalytic reactions.

### Towards Complete Imaging of Molecular Orbital Patterns: Development of Molecular Frame ( $e,2e$ ) Spectroscopy

**TAKAHASHI, Masahiko<sup>1</sup>; WATANABE, Noboru<sup>1</sup>; KHAJURIA, Yugal<sup>2</sup>; UDAGAWA, Yasuo<sup>1</sup>; ELAND, John H. D.<sup>3</sup>; JAGUTZKI, Ottmar<sup>4</sup>; DÖRNER, Reinhard<sup>4</sup>**

(<sup>1</sup>IMS and Tohoku Univ.; <sup>2</sup>IMS and IIT Madras; <sup>3</sup>IMS and Oxford Univ.; <sup>4</sup>Univ. Frankfurt)

The use of the ( $e,2e$ ) technique for measurement of electron momentum density in matter was first accomplished by Amaldi *et al.* on a thin carbon film in 1969.<sup>1</sup> Since then, a number of studies were conducted and have established the attempts as so-called binary ( $e,2e$ ) spectroscopy or electron momentum spectroscopy (EMS). The success of EMS with simple systems has led to its rapid expansion into various targets involving laser excited oriented atoms, biomolecules and solids. For molecules, however, EMS has long been plagued by the fact that the experiments measure averages over all orientations of gaseous targets. The spherical averaging results in enormous loss of versatile information on collision dynamics and target electronic structure; intrinsically anisotropic or three-dimensional character of the ( $e,2e$ ) scattering deteriorates into the one-dimensional momentum distribution. If it were possible to fix a molecule in space, the experiment would remove ambiguities inherent in the spherically averaged ( $e,2e$ ) cross sections.

To resolve the historical issue, we have proposed a method for complete imaging of electron momentum densities<sup>2</sup>; in the axial recoil limit of fragmentation of the residual ion measurements of vector correlations among the two outgoing electrons and the fragment ion are equivalent to ( $e,2e$ ) experiments with fixed-in-space molecules, which should be designated as ( $e,2e+M$ ) spectroscopy. Furthermore, we have observed, for the first time, transition-specific anisotropy of molecular frame ( $e,2e$ ) cross section,<sup>3,4</sup> a phenomenon for which detailed theoretical explanations are eagerly awaited. This project aims at establishing molecular frame ( $e,2e$ ) spectroscopy by extending the pioneering work<sup>2-4</sup> with introduction and/or development of latest multichannel techniques. We believe that the project would exploit a new area for studies on stereodynamics of electron-molecule collisions as well as on bound electronic wavefunctions of molecules, directly providing information important to atomic physics and momentum space chemistry.

#### References

- 1) U. Amaldi, A. Egiri, R. Marconero and P. Pizzella, *Rev. Sci. Instrum.* **40**, 1001–1004 (1969).
- 2) M. Takahashi, N. Watanabe, Y. Khajuria, K. Nakayama, Y. Udagawa and J. H. D. Eland, *J. Electron Spectrosc. Relat. Phenom.* **141**, 83–93 (2004).
- 3) M. Takahashi and Y. Udagawa, *J. Phys. Chem. Solids* **65**, 2055–2059 (2004).
- 4) M. Takahashi, N. Watanabe, Y. Khajuria, Y. Udagawa and J. H. D. Eland, *Phys. Rev. Lett.* **94**, 213202 (4 pages) (2005).

## (b) Molecular Photophysics and Science

### Theoretical Studies of Quantum Many-Particle Dynamics in Open Systems

**NOBUSADA, Katsuyuki; YABANA, Kazuhiro<sup>1</sup>;  
SHIRATORI, Kazuya<sup>2</sup>**  
(<sup>1</sup>Univ. Tsukuba; <sup>2</sup>Hokkaido Univ.)

This research project is aimed to develop new theoretical and numerical methods describing dynamics in quantum many-particle systems such as (i) electron dynamics (not explicitly taking account of spin degrees of freedom), (ii) exciton dynamics, (iii) spin dynamics, and also (iv) photon dynamics. For example, the electron dynamics in molecular systems is an intrinsic process related to a number of interesting phenomena such as linear and nonlinear optical response, electric conduction, and also chemical reaction. Despite the importance, the electron dynamics has not been understood in detail. Very recently, we have developed a computational method simulating the electron dynamics in real time, and investigated nonlinear optical response and multiple ionization of noble metal clusters.

Our goal of this project is to further elucidate the quantum dynamics even in open quantum systems where quantum dissipation is indispensable.

#### References

- 1) K. Nobusada and K. Yabana, "High-Order Harmonic Generation from Silver Clusters: Laser-Frequency Dependence and the Screening Effect of *d* Electrons," *Phys. Rev. A* **70**, 043411 (7 pages) (2004).
- 2) K. Shiratori, K. Nobusada and K. Yabana, "Multiple Ionization of a Silver Diatomic Molecule in an Intense Laser Field," *Chem. Phys. Lett.* **404**, 365–369 (2005).

### Spatiotemporal Dynamics in Nanometric Molecular Assemblies by Near-Field Spectroscopy

**OKAMOTO, Hiromi; IMURA, Kohei;  
NAGAHARA, Tetsuhiko; LIM, Jong Kuk;  
HORIMOTO, Noriko**

Recent technological progress in scanning near-field optical microscope (SNOM) has made it possible to perform optical measurements with very high spatial resolution beyond the diffraction limit. We have constructed apparatus for space- and time-resolved spectroscopic measurements, by combining SNOM and ultra-fast time-resolved pump-probe technique. With the apparatus, we have achieved ~50 nm spatial and ~100 fs temporal resolution at the same time. The continuum generation in photonic crystal fibers have enabled near-field pump-probe experiments in wide-range probe wavelengths. Various photophysical phenomena probed under such extremely high space and time resolution can be of considerable significance not only in physics and chemistry but also in biology, and thus will open a new research activity. We make use of this experimental methodology to investigate basic problems on physical and chemical processes in nanometric systems. Right

now we have performed measurements to understand basic local optical properties of porphyrin nanoassemblies and metal nanoparticles. On porphyrin assemblies, we have obtained morphological information of thin films on substrates. On metal nanoparticles, we have succeeded in direct imaging of resonant plasmon modes. The details of the apparatus and experimental results are reported in II-A.

### Studies on Laser Cooling and Trapping of Metastable Helium Atoms and Laser Spectroscopic Studies of Atoms and Ions in Liquid Helium

**MORITA, Norio; MORIWAKI, Yoshiki<sup>1</sup>**  
(<sup>1</sup>Toyama Univ.)

Concerning "studies on laser cooling and trapping of metastable helium atoms," we have added small improvements to our cooling and trapping apparatus for He atoms. On the other hand, as for "laser spectroscopic studies of atoms and ions in liquid helium," emission and excitation spectra of the  $3s^2\ ^1S_0-3s3p\ ^1P_1$  transition of Mg atom in pressurized liquid helium-4 and helium-3 have been measured. In the emission spectra we have found that their transition wavelengths, which are significantly red shifted, remain constant or slightly increase with increasing the liquid He pressure, whereas for other alkali-earth atoms the increase of the liquid pressure always shifts their emission spectra toward shorter wavelength. Our theoretical calculations based on a bubble model have successfully reproduced this unique spectral property, and have suggested the possibility of the formation of a  $Mg(3s3p\ ^1P_1)He_n$  exciplex in a bubble. (see II-B-1).

### Methods of Analysis for Protein Dynamics in Living Cells

**OZAWA, Takeaki**

Protein-protein interactions and protein localization have key roles in many essential biological processes in living cells. To investigate the biological processes, fluorescent and bioluminescent proteins, which are called reporters, are now being used as readout. One of the most useful reporters is a green fluorescent protein (GFP) derived from *Aequorea victoria* and its spectral variants. It is particularly valuable due to its structural stability and the fact that its chromophore is spontaneously formed in an autocatalytic cyclization that does not require any cofactors.

We have developed novel reporter proteins with general applicability for detecting protein-protein interactions and protein localization in living cells and animals. The principle is based on reconstitution of split reporter proteins by protein splicing, which involves a self-catalyzed excision of a protein splicing element, intein, from flanking polypeptide sequences, exteins, leading to ligation of the flanking exteins by a peptide bond. As the exteins, N- and C-terminal fragments of

rationally-dissected GFP was used. The N- and C-terminal reporters connected respectively with a pair of interacting proteins worked as indicators for protein-protein interactions. The split-GFP reporter provided a genetic method for identifying mitochondrial proteins from large-scale cDNA libraries. This basic concept of split reporter reconstitution by protein splicing provides a wide variety of applications for fundamental biological studies.

This research project aims to develop novel fluorescent and bioluminescent reporters with various spectral properties based on protein splicing. Using the reporters, I will develop methods of analysis for the gene expression, intracellular protein dynamics, enzyme activities, and protein-protein interactions in living subjects. To identify a key molecule in the biological processes, I am also investigating analytical techniques such as cDNA library screenings with fluorescence-activated cell sorting.

### **Development of Attosecond Coherent Control and Its Application**

**OHMORI, Kenji**

Coherent control is based on manipulation of quantum phases of wave functions. It is a basic scheme of controlling a variety of quantum systems from simple atoms to nanostructures with possible applications to novel quantum technologies such as bond-selective chemistry and quantum computation. Coherent control is also expected to serve as an effective tool for the fundamental test of quantum theory. We have developed an "attosecond phase modulator (APM)," which we have applied to vibrational wave packets in molecules to realize an unprecedented high-precision quantum interferometry. In this research project, we utilize our present APM as a sensitive decoherence detector for the fundamental test of quantum theory. Also the APM will be developed to a more flexible quantum-phase modulator. And they will be applied to (1) fundamental test and control of decoherence, (2) high-precision reaction control, (3) control of highly-nonlinear processes in intense laser fields, and (4) molecule-based quantum information processing.

### **Laser Manipulation of Molecular Motions and Its Application to Reaction Dynamics Studies**

**OHSHIMA, Yasuhiro; HASEGAWA, Hirokazu; MIYAZAKI, Mitsuhiro**

This special research program aims to establish methods for manipulating molecular motions in a quantum mechanical manner by utilizing the coherent interaction with laser lights, and to exploit the methods to detailed studies in chemical reaction dynamics. Three complement approaches are adopted. The first one employs fs pump-probe techniques to create and detect vibrational and/or rotational wavepackets of molecules. Time-resolved fluorescence depletion and random phase interferometry in fs regime have been applied for the first time to jet-cooled polyatomic systems. Observation of wavepacket dynamics has demonstrated for over-all

rotation of benzene and methyl internal rotation of *o*-fluorotoluene. The second method exploits an impulsive interaction with ultrafast intense laser light to transform the initial distribution into non-equilibrium one. New vacuum chamber system has been constructed for this purpose. The third one utilizes an adiabatic interaction to achieve the complete transfer in molecular quantum states, by which all the molecules are launched into states with high excitation of vibrations or rotation. A single-mode ns laser system is now under construction to realize the adiabatic interaction with coherent laser light. Along the instrumental development, an initial search for appropriate candidates for the quantum-state adiabatic manipulation has been started: energy-level structure of the intermolecular vibrations in the 1:1 benzene-water cluster is studied by mass-analyzed resonance enhanced two-photon ionization coupled with laser double-resonance technique.

### **Probing Ultrafast Molecular Dynamics by Extremely Short Laser Pulses**

**TAKAHASHI, Eiji J.; HISHIKAWA, Akiyoshi**

Highly excited molecules formed in intense laser fields often undergo ultrafast nuclear dynamics with a time scale shorter than 100 fs. This special research project is aimed to trace the evolution of such ultrafast nuclear motion in real time by extremely short laser pulses with the duration less than 10 fs. For this purpose, a pulse compression system consisting of a hollow fiber filled with Ar gas and a chirp mirror compressor was developed. The duration of the output pulse is typically 9 fs with an energy of 0.4 mJ/pulse. The pump-and-probe experiments combined with the coincidence momentum imaging technique are under progress.

### **Photoionization and Photodissociation of Fullerenes and Metal Encapsulated Fullerenes, Their Mechanisms, Kinetics, and Dynamics**

**MITSUKE, Koichiro; KATAYANAGI, Hideki; KOU, Junkei; MORI, Takanori**

Fullerenes are characterized by their unique geometric and electronic structures, and have attracted wide attention because they provide possibilities of applications toward materials of novel functionalities. Nevertheless, only a few experimental works have been made on photoabsorption spectroscopy of solitary fullerenes, particularly above their ionization thresholds. Hence, there is little information on their oscillator strength distributions, dielectric functions, and dynamics of highly-excited states.

We have observed for the first time the giant dipole resonance in the photoionization yield curves of isolated endohedral metallofullerenes. The yield curves for the singly- and doubly-charged parent ions from Ce@C<sub>82</sub> and Pr@C<sub>82</sub> were measured by using mass spectrometry. The curves of Ce@C<sub>82</sub><sup>2+</sup> and Pr@C<sub>82</sub><sup>2+</sup> exhibit broad resonances between  $h\nu = 120$  and 150 eV which were ascribed to the shape resonance arising from the  $4d \rightarrow 4f$  dipole transition in the encapsulated metal atom.

Analogous giant resonances are well known phenomena for the isolated atoms of Xe, Ba and various lanthanide metals. They are interpreted on the basis of favorable overlap between the wave functions of  $4d$  and  $4f$  atomic orbitals whose amplitudes are concentrated inside the associated centrifugal barriers generated on the effective potential that acts upon the ionized electron. Our results clearly show that such a resonance does not collapse even inside the fullerene cage, in a qualitative agreement with the theoretical prediction from previous *ab initio* TDLDA calculations made by Wendin and Wästberg in 1993.

### Theoretical Development of Interfacial Sum Frequency Generation Spectroscopy

MORITA, Akihiro; ISHIDA, Tateki; ISHIYAMA, Tatsuya

The visible-infrared Sum Frequency Generation spectroscopy has a wide applicability for interface characterization, including surfaces in ambient conditions and various liquid (liquid-gas, liquid-liquid, liquid-solid) interfaces. Although the spectra provides intramolecular vibrational spectroscopy specific to the interface region, it is not straightforward to extract unique information on the interface structure in a molecular level. This project develops theoretical methods to compute the SFG spectra by molecular dynamics simulation.

To apply our computational methods to a variety of systems, a general scheme of molecular modeling is a key ingredient. The molecular model should be polarizable and flexible, and in addition it should be capable of describing dipole and polarizability as a function of molecular conformation. To meet these requirements we are developing a new molecular model based on the Charge Response Kernel theory, which was proposed by us in 1997. While the original theory was based on the Hartree-Fock wavefunction, it is extended to the density functional theory to take account of the electron correlation effects.

The non-empirical computation of SFG spectroscopy needs a large computational cost, and therefore effective computation by a large-scale massive parallel environment is also critical. We are trying to establish an efficient computational scheme for the SFG calculations by utilizing the supercomputer resources in the IMS computer center.

### Decay and Dissociation Dynamics of Core Excited Molecules

SHIGEMASA, Eiji; HIKOSAKA, Yasumasa; KANEYASU, Tatsuo

Multielectron processes in inner-shell photoabsorption, in which more than two electrons are promoted by the absorption of a single photon, have long drawn special attention. This is because such processes are due entirely to correlation effects among the electrons in a system and consequently their investigation covers fundamental aspects of atomic and molecular physics. The ejection of a second electron into unoccupied bound and continuum states, accompanying the ionization of

the inner-shell electron, are often observed as shake-up and shake-off satellite structures in the corresponding photoelectron spectra. Another important example for the multielectron processes is the formation of neutral states embedded in the ionization continuum, which is generally referred to as the multiple excitations. The multielectron processes due to the electron correlation are known to happen not only in the primary inner-shell hole creation processes, but also in their relaxation processes.

The double toroidal analyzer (DTA) at UVSOR, which has been originally developed by a French group, has been under conditioning. The imaging detection without any exit slit enables us to observe electrons within an energy range more than 10% of the pass energy, and their angular distributions simultaneously. Recently it was confirmed that the performance of the analyzer has been improved considerably, after re-assembling of DTA and its careful tuning. The introduction of an ion time-of-flight spectrometer with a two dimensional detector is in the planning stage, to perform energy-selected-electron-ion coincidence experiments.

Parallel to the research and development of new experimental setups, some trial experiments have been made for observing minor products, such as highly excited neutral species and anions after the molecular inner-shell excitations. A strong enhancement due to the  $N^*$  formation has been observed around the  $1s$  threshold of  $N_2$  molecules. It has been found that the highly excited  $N_2^{+*}$  states leading to the  $N^*$  formation are populated by spectator Auger decay from the core-excited states, as well as by the recapture of slow photoelectrons into the Rydberg orbitals. It turns out that the metastable observation is a new and sensitive tool to study the decay dynamics of core-excited states and the photoelectron recapture due to the post-collision interaction. Concerning the anion imaging detection after the molecular inner-shell excitations, we have confronted difficulty in eliminating a large background noise by electrons, which may be fixed by performing time-resolved experiments.

## (c) Novel Materials Science

### Quantum Chemistry Calculations of Large Molecular Systems

ISHIMURA, Kazuya; NAGASE, Shigeru

Density functional theory (DFT) is currently the most widely used method to calculate larger molecular systems. However, the generally used DFT methods fail to describe weak non-covalent interactions that play an important role in host-guest chemistry, molecular recognition, and self-assembly. An efficient method to calculate non-covalent interactions in a reliable way is second order Møller-Plesset perturbation theory (MP2). To make MP2 calculations applicable to large molecular systems, we have developed a new parallel algorithm with two-step parallelization and dynamic load-balancing. This developed algorithm has been implemented in the freely distributed quantum chemistry program package GAMESS. The parallel efficiency is tested for two relatively large molecules, taxol ( $C_{47}H_{51}NO_{14}$ ) and luciferin ( $C_{11}H_8N_2O_3S_2$ ), with the 6-311G(d,p) basis set (1484 basis functions and 164 correlated electrons) and the aug-cc-pVTZ basis set (1198 basis functions and 46 correlated electrons), respectively. The cost of MP2 calculations is comparable to that of Hartree-Fock SCF calculations. The CPU efficiency of the present algorithm is high; the elapsed time is only slightly longer than the CPU time. An MP2 energy calculation on a carbon nanotube,  $C_{130}H_{10}$  (1970 basis functions), completes in less than 2 hours on 128 processors. Therefore, it is entirely practical to calculate the MP2 energies of relatively large molecular systems. We are now developing a parallel algorithm of MP2 energy gradient calculations to determine effectively the structures of large molecules.

### Theory for Equilibrium and Non-Equilibrium Properties of Low-Dimensional Molecular Materials with Strong Correlation

YONEMITSU, Kenji; YAMASHITA, Yasufumi; MAESHIMA, Nobuya; MIYASHITA, Satoshi

In low-dimensional molecular materials, effects of different interactions appear not only in their equilibrium phases but also in their non-equilibrium states. i) Ambipolar field-effect characteristics are recently found by an experimental group in metal-insulator-semiconductor field-effect transistor device structures based on organic single crystals of the quasi-one-dimensional Mott insulator (BEDT-TTF)( $F_2TCNQ$ ). For coherent charge transport, the insulator-(source and drain) electrode interface barrier (Schottky barrier) potentials are important. In FET devices based on band insulators, the Schottky barriers govern the IV characteristics. When the work function of the electrodes is different from that of the channel, the IV characteristics are generally very asymmetric with respect to the polarity of the gate bias and therefore unipolar. The ambipolar characteristics of the organic Mott insulator imply very similar effects of insulator-electrode interface bar-

rier potentials, when combined with electron correlation effects, for electron and hole injections. In order to understand its mechanism, we perform model calculations to show rather symmetric IV characteristics for Mott insulators only. Scalar potentials are included, which originate from the long-range Coulomb interaction and produce the Schottky barriers. The time-dependent Schrödinger equation is numerically solved for both the mean-field and many-body electronic wave functions to obtain the current density. We find ambipolar carrier injections in Mott insulators only, even if the work function of the crystal is quite different from that of the electrodes. They result from balancing the correlation effect with the barrier effect. For the gate-bias polarity with higher Schottky barriers, the correlation effect is weakened accordingly, owing to collective transport in the one-dimensional correlated electron systems. ii) Effects of interchain electron-electron interactions on the photoinduced ionic-to-neutral and neutral-to-ionic transition dynamics are studied in a quasi-one-dimensional extended Peierls-Hubbard model with alternating potentials for mixed-stack charge-transfer complexes. The ionic-to-neutral transition dynamics depend on the strengths of interchain couplings. For strong interchain couplings such as those corresponding to TTF-CA, once neutral domains are nucleated above an increased absorption threshold, they grow spontaneously and cooperatively till the whole system is converted. In contrast, interchain couplings slightly enhance nonlinearity of the otherwise uncooperative neutral-to-ionic transition dynamics. These results are consistent with the latest experimental results including coherent motion of the macroscopic neutral-ionic domain boundary during the photoinduced ionic-to-neutral transition.

### UHV Systems for MOKE, MSHG, XMCD and STM Measurements

NAKAGAWA, Takeshi; YOKOYAMA, Toshihiko; WATANABE, Hirokazu; MARUYAMA, Koichi

In order to investigate magnetic properties of ultrathin metal films, we have been so far constructing three ultrahigh vacuum chambers equipped with standard surface analysis apparatus and magnets. The first one is operated for the magneto-optical Kerr effect (MOKE) that is usually the most suitable method to characterize magnetic properties of ultrathin films. A UHV-compatible electromagnet (max. 3000 G, static) is installed. While information from the MOKE is basically attributed to the whole films, information only on surfaces and interfaces can be given by the magnetic second harmonic generation (MSHG) technique. We have installed a Ti:sapphire laser (800 nm) and the detection system in the same chamber. Both the MOKE and the MSHG data can now be taken with high quality. The second one is for X-ray magnetic circular dichroism (XMCD) that provides information on element-specific magnetization and on the orbital magnetic moment because of its importance for discussion on magnetic

anisotropy. This experiment can usually be done at Beamline 4B in UVSOR-II. In order to measure XMCD a similar UHV-compatible electromagnet is installed. X-ray absorption fine structure (XAFS) spectra of adsorbates are also obtainable in the same chamber for the determination of the surface structure. Furthermore, we will reconstruct this chamber at the end of this year and install a superconducting magnet (up to 7 T) with a sample cryostat (down to  $\sim 2$  K). The third one is for scanning tunneling microscopy (STM) to characterize surface structure. The chamber is now also being operated.

### Development and Characterization of Metal/Carbon Hybrid Nano-Systems

**NISHI, Nobuyuki; JUDAI, Ken; NISHIJO, Junichi**

Nanometals, such as wires, dots, sheets, or wheels, are expected to show quantum electronic properties. When nanometals with countable numbers of metallic atoms are aligned with interfacial  $\pi$  electron spacers through d- $\pi$  junctions, the electrons originally localized in metal atoms could transfer through  $\pi^*$  orbitals of the carbon spacers. The probability of this tunneling process is a function of carbon spacer distances and the applied electric field strength. Magnetic field is also expected to work on the tunneling processes.

We are developing new metal/carbon systems with transition metal acetylides. The acetylides are composed of ionic bonds between metal cations and ethynyl anions. The low lying electronic excited states of the acetylides are characterized as metal-ethynyl charge transfer states and the excitation induces charge neutralization reaction of the cation-anion pairs resulting in the production of metal clusters bonded with  $\pi$  electron systems of conjugated carbons. In the case of iron acetylide, FeC<sub>2</sub>, the produced iron nanocrystalline core wears graphitic skin with Fe-C direct chemical bonds.

We have succeeded to synthesize Cu<sub>2</sub>C<sub>2</sub> nanowires with diameters of 10–20 nm and lengths of approximately 1  $\mu$ m. The acetylide nanowires are converted to metallic copper nanowires with outside carbon layers by moderate heating or other excitations. The interface is composed of copper-carbon bonds, that is charge polarized in nature and forms Schottky-barrier like Fe nanocrystals with graphitic skins (3.5 nm thick) controlling the electron transfer directions under appropriate conditions.

Dissolving organometallic clusters in organic solvents allow us to make films as thin as 10 nm or less. A copper 24-mer with *t*-butyl-ethynyl groups, (*t*-butyl-C $\equiv$ C-Cu)<sub>24</sub>, is soluble in *n*-hexane and can provide thin films on various plates. We have succeeded to prepare metallic copper nano-films sandwiched in conjugated organic polymer thin layers just like nano-pies by photo-segregation of the original films. On the other hand, heating of the films provides nano-dots of metallic Cu particles embedded in organic polymers. Electronic properties of these new materials, such as conductivity and quantum tunneling effect, are now in progress.

### Charge ordering in Organic Conductors

**YAKUSHI, Kyuya; YAMAMOTO, Kaoru; URUICHI, Miki; YAMAMOTO, Takashi; DROZDOVA, Olga**

The charge ordering is originated from the localization of charge driven by the on-site and inter-site Coulomb interaction which is slightly stronger than the kinetic energy gain. In organic conductors, these competing energies are comparable with each other. Therefore, many organic conductors are situated in the boundary between delocalized and localized states. Organic conductors exhibits various electronic ground states such as charge-density wave (CDW), spin-density wave (SCW), antiferromagnetic state (AF), spin-Peierls state (SP), and superconducting state (SC) *etc.* through the electron-phonon, Coulomb, and exchange interactions. Recently, the charge-ordered state (CO) is recognized as the new ground state, and drawing attention. For example, the CO state shows ferroelectric property in some organic compounds, and the superconducting state neighbored on a CO state is considered to have a charge-fluctuation-mediated superconducting mechanism. We are investigating the CO system in organic conductors employing the technique of infrared and Raman spectroscopy, and obtained the following achievements. (1) We have examined more precisely the relationship between the charge on ET molecule and the frequency shift of  $\nu_{27}$  and  $\nu_2$ . Based on the isotope substituted ET compounds (<sup>13</sup>C and <sup>2</sup>H) and DFT calculation, we obtained the linear relationship,  $\nu_{27}(\rho) = 1398 + 140(1-\rho)$  cm<sup>-1</sup>, for the flat ET molecule. The frequency shift due to oxidation is remarkably larger than reported in previous studies. The fractional charges of several ET salts in a charge-ordered state can be successfully estimated by applying this relationship. Similarly, the linear relationship for the  $\nu_2$  mode was obtained as  $\nu_2(\rho) = 1447 + 120(1-\rho)$  in the region of  $0 < \rho < 0.8$ . (IV-A-1) (2) We examined the electronic states of  $\theta$ -(BEDT-TTF)<sub>2</sub>CsZn(SCN)<sub>4</sub> and the high-temperature and frozen states of  $\theta$ -(BEDT-TTF)<sub>2</sub>RbZn(SCN)<sub>4</sub>. The charge distribution is inhomogeneous with a large amplitude in the high-temperature and frozen states of  $\theta$ -(BEDT-TTF)<sub>2</sub>RbZn(SCN)<sub>4</sub>, whereas the amplitude of charge-density wave in  $\theta$ -(BEDT-TTF)<sub>2</sub>CsZn(SCN)<sub>4</sub> is very small. Although the charge distribution of the latter compound is nearly homogeneous, the indication of the weakly localized nature is found in the Raman spectrum and optical conductivity spectrum. This weakly localized nature is frozen below 20 K, which may be related to the non-linear conductivity. (IV-A-2) (3) In some compounds, the CO phase is considered to be neighbored on superconducting phase. We examined the Raman spectrum of  $\beta''$ -(BEDT-TTF)<sub>4</sub>[(H<sub>3</sub>O)Ga(C<sub>2</sub>O<sub>4</sub>)<sub>3</sub>] $\cdot$ C<sub>6</sub>H<sub>5</sub>NO<sub>2</sub>, wherein the electrical resistivity increases on lowering temperature and shows superconductivity at 5 K. We found a clear splitting in the  $\nu_2$  mode of this compound below 50 K. This observation suggests the possibility of a superconducting ground state with a charge-fluctuation-mediated superconductivity mechanism rather than the spin-fluctuation mechanism. (IV-A-3) (4) The CO state of some compound shows ferroelectricity. We discovered second

harmonic generation (SHG) in  $\alpha$ -(BEDT-TTF)<sub>2</sub>I<sub>3</sub>, which has a CO ground state. A strong SHG signal at 700 nm appears just below the CO phase transition temperature (136 K). We consider that SHG is related to the ferroelectric property, and that the CO system will become new non-linear optical materials in the near infrared region. (IV-A-5) (5) We examined the  $\kappa$ -(BEDT-TTF)<sub>2</sub>Cu[N(CN)<sub>2</sub>]Br,  $\kappa$ -(BEDT-TTF)<sub>2</sub>Cu[N(CN)<sub>2</sub>]I, and  $\beta$ -(BEDT-TTF)<sub>2</sub>I<sub>3</sub> to find the relation between the Raman shift and linewidth and the structural and electronic anomalies. (IV-A-4) and (IV-A-6) We reasonably determined the site-charge distribution of (EDO-TTF)<sub>2</sub>X (X = ReO<sub>4</sub> and GaCl<sub>4</sub>) and TEA (TCNQ)<sub>2</sub> employing the infrared and Raman spectroscopy. (IV-A-7) and (IV-A-8). (6) We found a phase separation in the temperature region of 160 K–100 K in biferrocenium (F<sub>1</sub>TCNQ)<sub>3</sub>, through the x-ray diffraction experiment, infrared and Raman experiments. In the phase-separation region, nonovalent (D<sup>+</sup>A<sup>3-</sup>) and divalent (D<sup>2+</sup>A<sub>3</sub><sup>2-</sup>) ionic states coexist. A rough mapping of the monovalent and divalent domains was conducted using micro Raman spectroscopy. The domain size was macroscopic and the domain boundary may involve mesoscopic or microscopic domain structure. (IV-A-9) and (IV-A-10).

### Multi-Frequency and Pulsed ESR Investigation for Molecular-Based Materials

**FURUKAWA, Ko; MATSUOKA, Hideto; HARA, Toshifumi; TANATAR, Makariy; MAEDA, Keisuke; NAKAMURA, Toshikazu**

In general, high frequency (high field) ESR measurements are advantageous because they are high sensitive and high resolution spectroscopy. So we can get ESR signals even for very tiny samples. Moreover, as for the solid compounds, *i.e.* conducting and/or magnetic materials, multi-frequency measurements give us information about frequency (magnetic field) dependent ESR parameters. For example, the frequency dependence of the *g*-values tells us the development of the short-range order for the paramagnetic states. In the magnetic long-range order phases, we can estimate the dispersion of their collective mode. From the frequency dependence of the linewidth, we can estimate the characteristic time of the spin diffusive motion, the development of the spin-spin correlation time for the paramagnetic phases. Such kind of information is very important to understand the electronic interaction in functional materials.

Moreover pulsed ESR measurements are advantageous since we can directly obtain the spin-lattice (*T*<sub>1</sub>) and spin-spin (*T*<sub>2</sub>) relaxation times. From these parameters, we can understand detail of electronic phases.

We performed the multi-frequency (X-, Q-, and W-band) and pulsed-ESR measurements for several molecular-based materials in order to clarify low-temperature electronic phase. The following studies are now going on.

- [1] Multi-frequency ESR measurements for charge-ordering phases in (TMTTF)<sub>2</sub>X
- [2] Pulsed ESR investigation of the spin-Peierls phases in (TMTTF)<sub>2</sub>X

- [3] ESR study of Mn-cluster in the S-0 and S-2 states of Cyanobacterial single crystals
- [4] ESR study on low-dimensional antiferromagnet (BEDT-TTF)<sub>2</sub>PF<sub>6</sub>

### Broad-Line Solid State NMR Investigation of Molecular-Based Conductors

**NAKAMURA, Toshikazu; TANATAR, Makariy**

Magnetic resonance measurements may be mature techniques as devices of the so-called chemical analyses. However, from the viewpoint of the solid state material science, magnetic resonance measurement is challenging area still in under the special condition such cases as the extreme low temperature, strong magnetic field, high pressure, electric field, optical response and so on. Moreover they are advantageous for studying the fundamental electronic properties and for understanding the detailed electronic structures of molecular based compounds. Soft materials such as molecule based conductors show huge response to environments from the outside. In fact, competition of the electronic phases in molecular based conductors has attracted much attention. Magnetic resonance measurements under the special condition are absolutely necessary to search of the materials with new functions. The following investigations are now underway.

- [1] NMR Investigation of Charge-Ordering Phenomena in (TMTTF)<sub>2</sub>X

<sup>13</sup>C NMR measurements were performed for one-dimensional organic conductors, (TMTTF)<sub>2</sub>ReO<sub>4</sub>. We firstly clarified the existence of an intermediate charge-ordering (CO) phase for a TMTTF salt with a Td-symmetry counter anion by <sup>13</sup>C NMR absorption line and spin-lattice relaxation rate, <sup>13</sup>C *T*<sub>1</sub><sup>-1</sup>: The NMR spectra, which are characteristic of nuclei in equivalent molecules at room temperature, indicate two inequivalent molecules with unequal electron densities below 225 K. Moreover, the spin-singlet transition associated with the ReO<sub>4</sub> anion ordering was confirmed at around 158 K by <sup>13</sup>C NMR. The drastic change of NMR lines at 158 K also indicates a redistribution of the electronic charge at the anion ordering temperature. The existence of the two independent transitions suggests the possible origin of the charge-ordering phenomena is purely electronic.

- [2] Low temperature electronic state of  $\kappa$ -(BEDT-TTF)<sub>2</sub>Cu[N(CN)<sub>2</sub>]I

Although  $\kappa$ -(BEDT-TTF)<sub>2</sub>Cu[N(CN)<sub>2</sub>]X (X = Cl, Br, I) salts have almost same crystal structures, their low-temperature ground states are quite different.  $\kappa$ -(BEDT-TTF)<sub>2</sub>Cu[N(CN)<sub>2</sub>]Br is the well-known high-*T*<sub>c</sub> superconductors, and  $\kappa$ -(BEDT-TTF)<sub>2</sub>Cu[N(CN)<sub>2</sub>]Br undergoes an antiferromagnetic transition. On the other hand, preparation of  $\kappa$ -(BEDT-TTF)<sub>2</sub>Cu[N(CN)<sub>2</sub>]I single crystal is very difficult, and the electronic structure of it is not clarified so far. The resistivity of  $\kappa$ -(BEDT-TTF)<sub>2</sub>Cu[N(CN)<sub>2</sub>]I shows weak temperature dependence with a minimum around 100 K. However, this resistivity behavior indicates crucial sample dependence which is due to formation of super-lattice probably originated from conformations of the ethylene located at the end of BEDT-TTF molecules. To understand the low tempera-

ture electronic state of  $\kappa$ -(BEDT-TTF)<sub>2</sub>Cu[N(CN)<sub>2</sub>], we are performing <sup>13</sup>C and <sup>1</sup>H NMR measurements for the same crystal. We can understand the detail of electronic state from the <sup>13</sup>C NMR analyses, and the <sup>1</sup>H NMR lineshape gives us the information of the ethylene conformation.

### Synchrotron X-Ray Diffraction Experiments and MEM Analyses for Single Crystals of Organic Conductors

HARA, Toshifumi; FURUKAWA, Ko;  
NAKAMURA, Toshikazu

MEM (The Maximum Entropy Method) analyses for synchrotron X-ray diffraction are powerful method to understand local electric charge distribution on each atom for crystalline samples. We performed these techniques for single crystals of organic conductors to study whether there is a change of symmetry of frontier orbitals (electric charge distribution in molecules), which is believed to be rigid so far, at phase transitions, and to investigate possible relation between the detailed electric charge distribution in molecules and the electronic phases. It is believed that most of physics phenomena can be explained within the framework that the frontier orbital can be treated as if one rigid atomic orbital in an alkaline metal. However, there are several experimental results which suggest a change of electric charge distribution in the molecule in some systems.

Possibility of inter-molecular electric charge redistribution has been ignored so far also for charge-ordering phenomena. Hence, we performed synchrotron X-ray diffraction measurements and MEM analyses to investigate the electric charge distribution of molecules on (TMTTF)<sub>2</sub>PF<sub>6</sub>. Detailed MEM analyses are now going on.

### Development of New Functional Molecular Systems

KOBAYASHI, Hayao; TAKAHASHI, Kazuyuki;  
CUI, HengBo; OKANO, Yoshinori; FUJIWARA,  
Emiko<sup>1</sup>; KOBAYASHI, Akiko<sup>1</sup>  
(<sup>1</sup>Univ. Tokyo)

The molecules are usually assembled by relatively weak intermolecular interactions and tend to retain their intrinsic properties even in the crystalline states. Consequently, it might be easily imagined that the different molecular functions can be accumulated in the same crystal by assembling different building blocks with different characters. In these systems, the multi-functional properties will be realized due to the synergetic actions of different building blocks. The magnetic conductor based on  $\pi$  donors conveying electron conduction and magnetic anions with localized magnetic moments may be a good example. We have recently discovered unprecedented magnetic organic conductors such as the conductors showing superconductor-to-insulator transition, antiferromagnetic organic superconductors and field-induced organic superconductors. We are trying to develop various types of molecular systems with new electronic functions. The main results

of our group in the last year are as follows. (1) We have recently found the possibility of unprecedented "constant resistivity state" below  $T_c$ , in  $\lambda$ -(BETS)<sub>2</sub>Fe<sub>x</sub>Ga<sub>1-x</sub>Cl<sub>4</sub> ( $x \approx 0.35$ ) exhibiting superconductor-to-insulator transition where the resistivity was independent of temperature and magnetic field applied parallel to the  $\pi$  conduction plane. (2) We are trying to develop photo-controllable magnetic molecular conductors by using Ni(dmit)<sub>2</sub> molecules and spin-crossover complex cations. (3) By the improvement of the crystal quality, the antiferromagnetic transition temperature of single-component molecular metal Au(tmtd)<sub>2</sub> was enhanced up to 110 K. This is the first molecular metal where  $\pi$  metal electrons and magnetic order coexist above 100 K. (4) We are developing new molecular systems with unprecedentedly high dielectric constant by combining porous molecular crystals and polar guest molecules. Very recently, we have succeeded to obtain molecular systems with dielectric constants one or two orders of magnitude larger than those of usual organic and inorganic compounds.

### Synthesis and Properties of Novel Chiral Organic-Inorganic Molecule-Based Magnets

AKITA, Motoko; INOUE, Katsuya

The design and synthesis of molecular materials with interesting electrical and/or optical and magnetic properties has been one of the major challenges of the last few years. The aim of this project is synthesis and characterization of new chiral magnetic materials. Novel properties are expected for The MChD (magneto-chiral dichroism) effect depends on the magnitude of the optical activity and the magnetic moment. The chiral ferro/ferrimagnets are expected to exhibit a strong MChD effect.

Organic radicals like aminoxyl radicals have been used to construct molecule-based magnets. A strategy of using  $\pi$ -conjugated high-spin oligonitroxide radicals as bridging ligands for transition metal ions in order to assemble and align the electron spins on a macroscopic scale has been established. The crystal structures and magnetic structures of these complexes are well investigated and can be tuned by using appropriately designed ligands. We have been synthesized new chiral organic radicals as ligands in order to introduce chirality to molecule-based magnets constructed with aminoxyl radicals and magnetic metals.

Chiral organic radical 2-{4'-(*S*)-2"-methylbutoxy phenyl}-4,4,5,5-tetramethylimidazole-1-oxyl-3-oxide (**1**) and its metal complex **1**·M(II)(hfac)<sub>2</sub> (M = Mn, Co, Cu) were synthesized and characterized. The radical **1** crystallizes in the chiral orthorhombic space group  $P2_12_12_1$  with  $a = 11.494(3)$ ,  $b = 25.328(3)$ ,  $c = 6.1281(5)$  Å. **1**·Mn(II)(hfac)<sub>2</sub> crystallized in the same space group with  $a = 14.081(1)$ ,  $b = 15.940(1)$ ,  $c = 16.075(1)$  Å. X-ray crystal structure analysis of the **1**·Mn(II)(hfac)<sub>2</sub> revealed the formation of a helical chain structure. The temperature dependence of the magnetization and the magnetization curve revealed that **1**·Mn(II)(hfac)<sub>2</sub> behaves as a ferrimagnet below  $T_c = 4.3$  K.

## Design and Functions of Novel Soft Nanomaterials Based on Molecular Programming

JIANG, Donglin

In this special project, we focus on creation of novel soft nanomaterials based on molecular programming. By developing new self-assembling protocols, we target at synthesis of soft nanomaterials with highly controlled structures and well-defined morphologies that lead to the discovery of novel functions. In detail, molecular components bearing photoactive, conductive, and/or spin-active moieties are integrated as building blocks for programmed hierarchical fabrication of nanomaterials. Especially, creation of novel nanomaterials for highly efficient photoinduced energy and electron transfers, construction of functional nanomaterials for future-generation spin-based devices, and realization of high efficiency room-temperature light-induced spin transition are important missions.

## Giant Vesicle Fusion on Microelectrodes Fabricated by Femtosecond Laser Ablation Followed by Synchrotron Radiation Etching

RAHMAN, Md. Mashiur; NONOGAKI, Youichi; TERO, Ryugo; KIM, Yong-Hoon; UNO, Hidetaka; ZHANG, Zhen-Long; YANO, Takayuki; AOYAMA, Masaki; URISU, Tsuneo

[*Jpn. J. Appl. Phys.* **44**, L1207–1210 (2005)]

Figure 1 shows the fabrication process for the well structures with microelectrodes. A Co thin film (10 nm thick) was sputter deposited on a mirror-polished Si (100) surface after conventional wet cleaning and Co (10 nm thick) and Ag (100 nm thick) films on the rough back surface [Figure 1(b)]. After that, a SiO<sub>2</sub> thin film consisting of SOG (400 nm thickness) and sputtered SiO<sub>2</sub> (200 nm thickness) were deposited [Figure 1(c)], then the sample was annealed at 540 °C for 10 min. The Co layer was changed to CoSi<sub>2</sub> and the Co/Si interface became ohmic [Figure 1(d)]. The sample was then annealed by SR irradiation to remove gas from SOG [Figure 1(e)]. A Co layer as an etching contact-mask was deposited on the SOG surface by sputtering [Figure 1(f)], and electrode hole mask patterns were made using a femtosecond laser ( $\lambda = 560$  nm, average power = 250 mW, frequency = 258 kHz, pulse width = 900 fs, and irradiation time = 4 ms) [Figure 1(g)]. The diameter of an electrode hole was about 1  $\mu$ m. SR etching of the SiO<sub>2</sub> layer for making the well on the electrode was carried out at beam line 4A2 of the SR facility (UV-SOR) at the Institute for Molecular Science, using a mixture of SF<sub>6</sub> (0.05 Torr) and O<sub>2</sub> (0.002 Torr) as the etching gas [Figure 1(h)]. The SR etching gives a vertical side wall and completely stops at the CoSi<sub>2</sub> surface. The Co contact-mask was successfully removed without damaging the substrate by immersion into 0.1M HNO<sub>3</sub> aq. [Figure 1(i)]. Ag (50 nm thickness) was deposited on CoSi<sub>2</sub> electrode surfaces by electroplating [Figure 1(j)]. Then, AgCl/Ag was formed also by electroplating [Figure 1(k)]. Unilamellar giant vesicles of DPPC :

POPS : Rb (89:5 : 10 : 0:5) were prepared as follows; a chloroform solution of a lipid mixture (10 mg/ml) was dried under N<sub>2</sub> flow using a rotary evaporator for about 30 min and subsequently vacuum-dried for 10 h to clearly remove the solvent; then a buffer solution (10 mM KCl) was added to the obtained lipid thin film and gently agitated. The lipid concentration of the obtained suspension was 0.1 mg/ml. All the processes were carried out at room temperature (RT). Then, after incubation at 48 °C for 10 h, dialysis was carried out for the suspension of giant vesicles by using a 5  $\mu$ m filter for 1 h in the buffer solution (10 mM KCl, pH = 6.6) at RT. For the deposition of lipid bilayer membranes, the substrate was incubated for 1 h at 50 °C under a buffer solution formed by mixing 200 ml of the vesicle suspension and 50 ml of CaCl<sub>2</sub> 50 mM solution. Then the sample was washed five times at room temperature (RT) with the buffer solution [Figure 1(l)]. Atomic force microscope (AFM) observations were performed using a SPI3800 scanning probe microscopy system (Seiko Instruments) in the dynamic-force mode (tapping mode) using a Si cantilever. The spring constant of the cantilever for measuring the surface roughness of the substrate in air was 43 N/m, and 1.5 N/m for the in situ characterization of the lipid bilayer.

The surface around the electrode well is very flat ( $R_a < 0.8$  nm). To obtain such a flat surface, it was important to control the irradiation power of the femtosecond laser such that only the Co film is removed while causing negligible damage to the SiO<sub>2</sub> layer beneath. The electric characteristics were determined using a patch clamp amplifier (CEZ-2400, Nihon-Koden, Japan) through the AgCl/Ag electrode in conjunction with the eCell (ver 2.12) software. The diameter of the bilayer was typically about 200–300  $\mu$ m, large enough to cover the electrode area (10–30  $\mu$ m diameter).

The lipid bilayer covering the electrode well was formed by giant vesicle fusion. A fluorescence microscopy image after lipid bilayer formation on the microelectrode area clearly shows the existence of the homogeneous lipid thin film. From the current-voltage characteristics of the system measured after the lipid bilayer formation, the resistance of the lipid bilayer was estimated to be 1.2 G $\Omega$ .

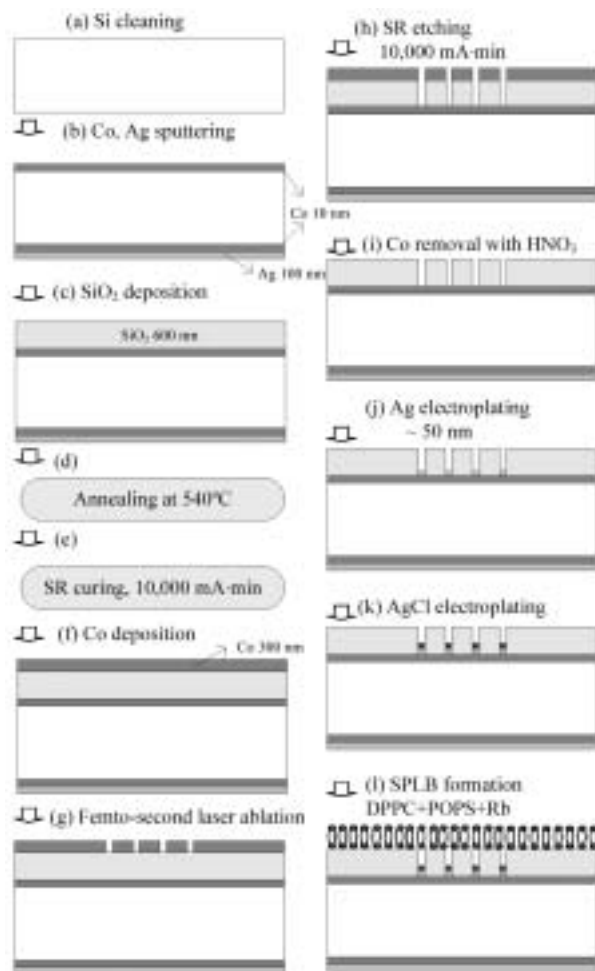


Figure 1.

### Reduction of CO<sub>2</sub> and Oxidation of Organic Molecules Aiming at Reversible Conversion between Chemical and Electrical Energies

TANAKA, Koji

Electro- and photochemical reduction of CO<sub>2</sub> affording methanol has become the crucial issue in line with the progress of fuel energy cells using methanol. Carbon dioxide reacts with coordinatively unsaturated low-valent metal complexes to form  $\eta^1$ -CO<sub>2</sub> adducts, which can be converted to the corresponding metal-CO ones in protic media. Electrochemical reduction of metal-CO complexes usually results in the M-CO bonds cleavages due to accumulation of too much electrons on the central metals. Such reductive cleavage of metal-CO bonds plays the key role in the formation of CO in the electrochemical reduction of CO<sub>2</sub>. On the other hand, the process prevents electrochemical hydrogenation of the CO ligand that would lead to four- and six-electron reduction affording formaldehyde and methanol. To achieve the six-electron reduction of CO<sub>2</sub>, we are designing new types of metal complexes with redox active ligands, which can provide hydrides to carbonyl carbon without increasing electron densities in the metal centers.

Metal complexes that have an ability to oxidize methanol at potentials more negative than the reduction

potential of dioxygen may be applied for electrocatalysts used in methanol fuel cells. Metal-oxo complexes are possible candidates for the oxidation of methanol, since metal-oxo species are believed to work as active centers in various metal enzymes, which oxidize various biological substrates under very mild conditions. Mechanistic understandings of the reactivity of metal-oxo species, however, are limited due to the difficulty of preparation of reactive M-O frameworks in artificial systems. Accordingly, reactivity of high valent Ru=O complexes prepared by sequential electron and proton loss of the corresponding Ru-OH<sub>2</sub> ones have been extensively studied and proven to work as oxidants of organic molecules to some extent. We have succeeded reversible conversion between aqua and oxo ligands on Ru-dioxolene frameworks without using any oxidants by taking advantage of the charge distribution between the metal center and the ligand. Along this line, we have been preparing a variety of metal-aqua and -amine complexes bearing a dioxolene ligand aiming at oxidation of hydrocarbons by the corresponding metal-oxo and -imido complexes.

### Coordination Chemistry of New Multidentate Ligands and Activation of Small Molecules

KAWAGUCHI, Hiroyuki; MATSUO, Tsukasa

The introduction of substituents onto the two *ortho* positions of *para*-substituted phenol can be readily achieved by electrophilic substitution reactions. The availability of these two substituent positions at the phenol allows its ligand systems of podant and linear (or macrocyclic) linkage. This not only leads to a well defined relative orientation of the ligating atoms but opens up manifold possibilities of steric control. In addition, phenoxide functions may be combined with other functionalities which possess differences in formal charge and their interaction with the metal center. In this context, we are studying the coordination chemistry of multidentate ligands derived from phenoxides. Our recent work concentrate on the synthesis, structural characterization, and reactivity of early transition metal complexes supported by multidentate phenoxide ligands. Our main efforts have been directed toward activation of small molecules.

### Studies on Development of Molecules and the Device Fabrications for Molecular Scale Electronics

OGAWA, Takuji; TANAKA, Hirofumi

The aim of this special project is to study the electric and photonic properties of individual single molecules, and to establish the fundamental of molecular nanoscience. The project is composed of two parts; (1) design and synthesis of novel molecules which are important in molecular nano-science and (2) construction of a "molecular tester" which is comprised of double probe conductive AFM. The "molecular tester" is capable of measuring the electric properties of individual molecules by using two conductive cantilevers like probes of conventional electric testers. The machine

can be extended to include SNOM-type cantilever as the third probe, which will be used to measure the photonic properties of the individual molecules. The construction diagram was shown in Figure 1. In many cases multi probe SPMs do not have atomic resolutions because of the complexity of the system. However, our two probe STM has atomic images and  $7 \times 7$  structure of Si(111) surface can be obtained successfully as shown in Figure 2. Figure 3 shows the cooling characteristics of the system. With this setup the sample can be cooled to less than 70 K within three hours.

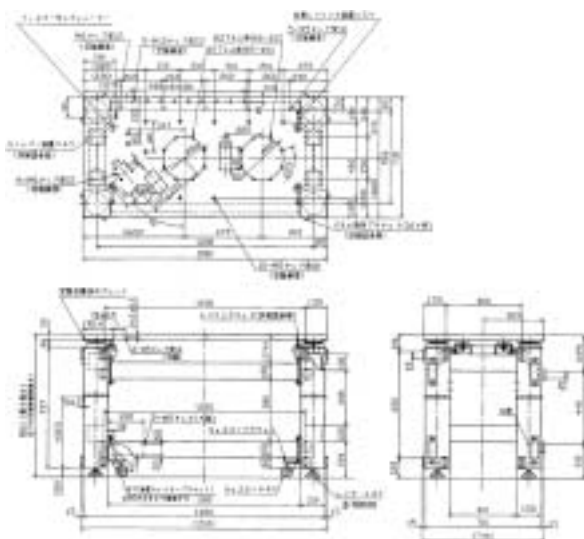


Figure 1.



Figure 2.

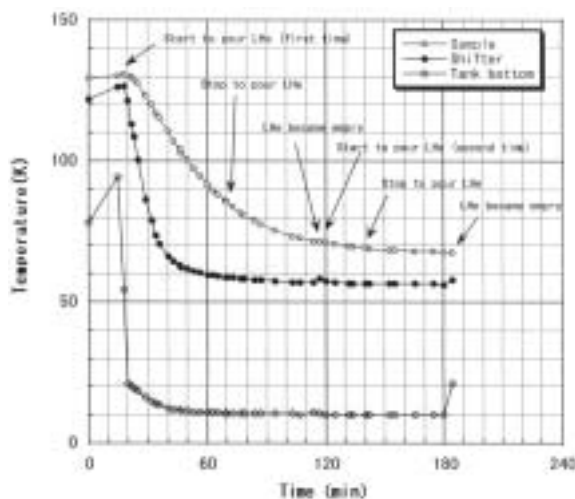


Figure 3.

## Synthesis of Perfluorinated Fluorene Oligomers and Applications for Organic Light-Emitting Diodes

OKUBO, Kimitaka; SUZUKI, Toshiyasu

We have synthesized novel perfluorinated fluorene oligomers up to the tetramer. These oligomers form good amorphous films. Light-emitting diodes using these oligomers as the hole-blocking and electron-transport layers show high quantum efficiencies.

## Novel Pincer Complexes and Their Catalytic Properties

UOZUMI, Yasuhiro

A wide range of NCN pincer palladium complexes, [4-*tert*-2,6-bis(*N*-alkylimino)phenyl]chloropalladium (alkyl = *n*-butyl, benzyl, cyclohexyl, *t*-butyl, adamantyl, phenyl, 4-methoxyphenyl), were readily prepared from *trans*-(4-*tert*-butyl-2,6-diformyl-phenyl)chlorobis(triphenylphosphine)palladium *via* dehydrative introduction of the corresponding alkylimino ligand groups (ligand introduction route) in excellent yields (71–98%). NMR studies on this route for forming pincer complexes revealed the intermediacy of [4-*tert*-2,6-bis(*N*-alkylimino)phenyl]chlorobis(triphenylphosphine)palladium which is in equilibrium with the corresponding NCN pincer complexes *via* coordination/dissociation of the intramolecular imino groups and triphenylphosphine ligands. A series of chiral NCN pincer complexes bearing pyrroloimidazolone units as the *trans*-chelating donor groups, [4-*tert*-butyl-2,6-bis{(3*R*,7*aS*)-2-phenylhexahydro-1*H*-pyrrolo[1,2-*c*]imidazol-1-on-3-yl}phenyl]chloropalladium, were also prepared from the same precursor *via* condensation with proline anilides in high yields. The catalytic properties of the NCN imino and the NCN pyrroloimidazolone pincer palladium complexes were examined in the Heck reaction and the asymmetric Michael reaction to demonstrate their high catalytic activity and high enantioselectivity.

## Asymmetric Aquacatalysis with Polymeric Palladium Complexes

UOZUMI, Yasuhiro

Catalytic asymmetric organic transformations performed in aqueous media with immobilized chiral palladium and rhodium complexes were developed. Amphiphilic polystyrene-poly(ethylene glycol) graft copolymer (PS-PEG) resin-supported MOP, boxax, BINAP, and an imidazoindole phosphine ligands were designed and prepared with a view to use them in asymmetric catalysis under aqueous and heterogeneous conditions. Several carbon–hydrogen, carbon–carbon, carbon–nitrogen, and carbon–oxygen bond forming reactions were achieved in water with high stereoselectivity and recyclability to meet the green chemical requirements.

## Construction of Advanced Redox Materials Based on Organic Molecules and Metal Complexes, as Basis of Chemical Energy Conversion Systems

NAGATA, Toshi; KIKUZAWA, Yoshihiro; NAGASAWA, Takayuki; MAKI, Suguru

The goal of this project is to develop advanced redox catalysis reactions suitable for chemical energy conversion. Our current interest focuses on modeling photosynthesis, that is, driving chemical transformation by using light energy via photoinduced electron transfer. We are trying to mimic the function of photosynthesis by assembling molecular units that perform individual physical/chemical action. The molecular units include porphyrins, redox active organic molecules, transition metal complexes, and metal nanoparticles.

During the last year, we have made progresses on the following three areas: (1) application of molecular dynamic simulations to the composite material of organic molecules and gold nanoparticles in organic solvents, which gives us better understanding of the solution behavior of these composites, (2) electrochemical examination of ferrocene-dendrimer-porphyrin molecules, which gives us some insights about the dynamic feature of these multiple redox-active molecules, and (3) synthesis and characterization of a series of cobalt complexes as candidates of new electrocatalysts.

## Synthesis of Buckybowls and Heterobuckybowls

SAKURAI, Hidehiro; HIGASHIBAYASHI, Shuhei

Bowl-shaped  $\pi$ -conjugated compounds including partial structures of the fullerenes, which are called "buckybowls," are of importance not only as model compounds of fullerenes but also as their own chemical and physical properties. For example, in solution they show the characteristic dynamic behavior such as bowl-to-bowl inversion. On the other hand, they sometimes favor stacking structure in a concave-convex fashion in the solid state, giving excellent electron conductivity. Furthermore, heterobuckybowls, some of whose carbon atoms in the framework are substituted to the appropriate heteroatoms such as N, O, S, Se, Si, B *etc.*, have been expected to exhibit unique physical characters based on the heteroatom induced effects.

However, very few buckybowls/heterobuckybowls has been achieved for preparation mainly due to their strained structure. In addition, most of thus-reported procedures are performed under severe reaction conditions, limiting the sort of the introducible atoms/functional groups. In the present project, we develop the rational route to the various kinds of buckybowls/heterobuckybowls using the organic synthesis approach. Targets of this year are as follows:

- A. Novel and versatile route to  $C_5$  symmetric corannulene and its derivatives.
- B. Synthesis of  $C_2$  symmetric  $C_{60}$  and  $C_{70}$  fragments.
- C. Synthesis of nitrogen-containing heterobuckybowls.
- D. Synthetic route to silicon-containing aromatic compounds.

## Tuning Catalytic Activities of Gold Clusters via Hybridization of Functional Molecules

NEGISHI, Yuichi; TSUNOYAMA, Hironori; YANAGIMOTO, Yasushi; TSUKUDA, Tatsuya

We have recently demonstrated that the polymer-stabilized gold clusters dispersed in water exhibit inherent catalytic activities against aerobic oxidation. This finding shows that the small gold clusters are inherently catalytic active and are promising candidates for environmentally benign catalysts. In the present project, the gold clusters were hybridized with various types of functional organic molecules in order to add new and higher-ordered catalysis, such as catalytic activity, substrate selectivity and enantioselectivity. The molecules we used so far include thiolated cyclodextrine, dendrimers, and chiral phosphines. The catalyses of these gold clusters have been compared with those of the gold clusters stabilized by linear polymers.

## Structural Analyses of Multi-Domain Proteins by Use of Ultra-High Field NMR Spectroscopy Measured at 920 MHz $^1\text{H}$ Resonance Frequency

KATO, Koichi

Recent advances in NMR structural biology have made possible the high throughput structural determination of small simple proteins and protein domains. However, structural analyses of multi-domain proteins, natively unfolded proteins, and glycoproteins remain as tasks with more challenge. Although NMR structural biology of these troublesome proteins is still at a preliminary stage, the ultra-high field NMR spectrometer will be a powerful tool to cope with the difficulty in dealing with them. In the present study, we apply ultra-high field NMR spectroscopy to determination of the relative orientation of individual domains in multi-domain proteins using protein disulfide isomerase (PDI) as a model molecule.

PDI is a folding assistant operating in the endoplasmic reticulum, and catalyzes the formation, breakage and rearrangement of disulfide bonds of its substrate proteins. PDI has a modular structure with four globular domains, *a*, *b*, *b'* and *a'* plus a C-terminal acidic extension. The homologous *a* and *a'* domains contain a cysteine pair in a WCGHCK active site sequence motif directly involved in thiol-disulfide exchange reactions. So far the solution structures of the *a* and *b* domains have been reported to be thioredoxin folds. We have shown that substrate binding site of PDI is primarily composed of the *b'* and *a'* domains.

We performed structural analyses of three-dimensional structures, substrate recognition, and domain-domain interactions of the *b'* and *a'* domains of thermophilic fungal PDI. Isotopically labeled *b'* and *a'* domains as well as the fragments composed of these two domains were expressed in *E. coli*. Inspection of NOE, chemical shift, and residual dipolar coupling (RDC) data revealed that 1) the *b'* and *a'* domain assume typical thioredoxin folds, 2) substrate analogs, *e.g.* somatostatin and mastoparan, bind a hydrophobic area spanning the *b'* and *a'* domains in their oxidized form,

and 3) reduction of the active site of the  $a'$  domain results in its increased contact with the  $b'$  domain, rendering the hydrophobic area less accessible. On the basis of these data, we conclude that this conformational rearrangement causes redox-dependent interaction of PDI with its substrates. In the NMR analyses, the 920 MHz NMR spectrometer plays a crucial role in observation of RDC because the alignment of macromolecules in the presence of liquid crystal media is more enhanced at higher magnetic fields. This study demonstrates that 920 MHz NMR spectroscopy provides us with invaluable information for structural determination of multi-domain proteins in the absence of crystal packing forces.

### Observation of Intense Bursts of Terahertz Synchrotron Radiation at UVSOR-II

**KATO**, Masahiro; **HOSAKA**, Masahito; **MOCHIHASHI**, Akira; **KIMURA**, Shin-ichi; **TAKAHASHI**, Toshiharu<sup>1</sup>; **TAKASHIMA**, Yoshifumi<sup>2</sup>  
(<sup>1</sup>Kyoto Univ.; <sup>2</sup>Nagoya Univ.)

We have detected very intense bursts of terahertz synchrotron radiation at the UVSOR-II electron storage ring operated in single bunch mode. The bursts were observed in the wavelength range from 0.2 to 3.0 mm by using a liquid-helium-cooled InSb hot-electron bolometer. The typical duration and interval of the bursts were about 200  $\mu$ s and 10–15 ms, respectively. Each burst shows the quasi-periodic structure of about 30  $\mu$ s. The peak intensity of the bursts was about 10000 times larger than that of ordinary synchrotron radiation in the same wavelength region. The extremely high intensity strongly suggests that the bursts are coherent synchrotron radiation, although the radiation wavelength was much shorter than the electron bunch length.

We have prepared a TiSa laser which is synchronized with the RF acceleration of the UVSOR-II electron storage ring. By using this laser, we can produce local density modulation in the electron pulses. Such electron pulses are expected to emit intense terahertz radiation. The laser has been successfully commissioned. A preliminary result indicated the successful production of coherent terahertz radiation.

### Optical and Photoelectrical Studies on Fermiology of Strongly Correlated Electron Systems

**KIMURA**, Shin-ichi; **ITO**, Takahiro; **SAKURAI**, Yoko; **NISHI**, Tatsuhiko; **IM**, Hojun; **MIZUNO**, Takafumi; **MIYAZAKI**, Hidetoshi

Strongly correlated electron systems attract much attention because of their various physical properties. To reveal the origin of the physical properties from microscopical viewpoints, we investigate the electronic structure near the Fermi level (Fermiology) by infrared and photoemission spectroscopies using synchrotron radiation. In this year, we investigated the electronic structure near the quantum critical point of rare-earth compounds  $\text{CeNi}_{1-x}\text{Co}_x\text{Ge}_2$  ( $0 \leq x \leq 1$ ). The phase

separation between the metallic and insulating states of partially-deuterated  $\kappa$ -(ET)<sub>2</sub>Cu[N(CN)<sub>2</sub>]Br was directly observed by using infrared magneto-optical imaging spectroscopy and was concluded to originate from the inhomogeneity of the sample itself. Infrared spectroscopy of CeSb under multi-extreme conditions of low-temperature, high-field and high-pressure was successfully performed and the pseudogap formation and its collapse due to magnetic fields were observed.

### Developments and Researches of New Laser Materials

**SARUKURA**, Nobuhiko; **ONO**, Shingo; **MURAKAMI**, Hidetoshi; **QUEMA**, Alex; **ESTACIO**, Elmer; **DIWA**, Girbert; **PONSECA**, Carlito Jr.; **DE LOS REYES**, Glenda

Although development of lasers is remarkable, there are no lasers which lase in ultraviolet and far infrared regions. However, it is expected that these kinds of lasers break out a great revolution in not only the molecular science but also in the industrial world.

In this project we research characters of new materials for ultraviolet and far infrared lasers, and develop new lasers by using these laser materials.

### Development and Research of Advanced Tunable Solid State Lasers

**TAIRA**, Takunori; **ISHIZUKI**, Hideki; **TSUNEKANE**, Masaki; **DASCALU**, Traian; **SATO**, Yoichi; **SAIKAWA**, Jiro; **PAVEL**, Nicolaie

The use of diode lasers to pump solid-state lasers opens new horizon in laser science. Diode-pumped solid-state lasers are compact, reliable, and efficient sources of coherent radiation. They can provide excellent spatial mode quality and narrow linewidths. The high spectral power brightness of these lasers has allowed high efficiency frequency extension by nonlinear frequency conversion. Moreover, the availability of new and improved nonlinear optical crystals makes these techniques more practical. Recently attention has been directed to the trivalent neodymium and ytterbium ion doped materials. The advantages of Yb:YAG lasers for a high power, high stability and wide tunability laser operation are well recognized due to its small quantum defect, long upper-state life time and wide gain width. Recently developed transparent ceramic material enhances the flexibility of the solid-state laser, for example, the doping ions and host structures for the advanced laser systems.

On the other hand, quasi phase matching (QPM) is a new technique instead of conventional birefringent phase matching for compensating phase velocity dispersion in frequency conversion. Inasmuch as the pool of mature nonlinear optical materials is limited and development of new materials takes time and cost, QPM is a useful method for extending the range of available nonlinear optical materials. The ability to pattern a QPM structure allows the nonlinear materials to be engineered for desired interactions, meaning molecular-science-specified lasers are obtainable through these

artificial materials.

In this projects we research and develop new diode-pumped-solid-state lasers and new frequency conversion devices. Especially, we will focus on the combination of microchip lasers and QPM devices. These kinds of advanced tunable solid-state light, so to speak "Chroma-Chip Lasers," will assist the research of molecular science.

### Regulation of Biological Function by the Heme-Based Gas-Molecule Sensor Proteins

**YOSHIOKA, Shiro; KOBAYASHI, Katsuaki;  
OZAWA, Kazumichi; INAGAKI, Sayaka;  
YOSHIMURA, Hideaki; NISHIMURA, Muneto;  
AONO, Shigetoshi**

The heme-based sensor proteins reveal a novel function of hemeproteins, in which the heme acts as the active site for sensing the external environmental signals such as diatomic gas molecules and redox change. As the heme-based sensor protein, O<sub>2</sub>, NO, and CO sensor proteins are reported so far. In this project, we are working on CO sensor protein (CooA), O<sub>2</sub> sensor protein (HemA), and a novel redox sensor protein (DcrA) to elucidate their structure-function relationships.

Elucidating the heme environmental structure is important to understand the structure-function relationships of the heme-based sensor proteins, because the heme is the active site for sensing the physiological effector molecules. Therefore, we have characterized the heme-based sensor proteins by UV/VIS, EPR, NMR, and resonance Raman spectroscopies along with mutagenesis studies. Electrochemical redox titration is also used to determine the redox properties of the heme-based sensor proteins. To determine the molecular structures of the heme-based sensor proteins by X-ray crystallography, screening the condition has been tried for crystallization of sensor proteins.

We are also trying to find novel heme-based sensor proteins by searching DNA data bases, and find a possible candidate so far. It is a Htr8 protein from *Halobacterium salinarum*, which would be a membrane-bound chemotaxis signal transducer protein. Based on the amino acid sequence deduced from the DNA sequence, Htr8 will consist of at least two domains, the N-terminal sensor domain and C-terminal signaling domain. The amino acid sequence of the sensor domain shows a homology to that of cytochrome *c* oxidase  $\alpha$  subunit that contains hemes and copper ions as the active site for respiration. We are now constructing expression systems of Htr8 to obtain and characterize the recombinant Htr8.

### Molecular Mechanism of Metalloenzymes Related to Oxygen Activation and Denitrification Processes

**FUJII, Hiroshi; KURAHASHI, Takuya; KUJIME, Masato**

Metalloenzymes are a class of biologically important macromolecules that have various functions such as

oxygen transport, electron transfer, oxidation, and oxygenation. These diverse functions of metalloenzymes have been thought to depend on the coordination structure of the active site in the protein matrices. In this project, we are studying the molecular mechanism of metalloenzymes related to oxygen activation and denitrification.

(1) Oxidizing intermediates are generated from nonheme iron(III) complexes to investigate the electronic structure and the reactivity, in comparison with the oxoiron(IV) porphyrin  $\pi$ -cation radical (compound I) as a heme enzyme model. The present study explains unique properties of mononuclear nonheme enzymes with Tyr residues, and also a poor epoxidation activity of Fe salen compared to Mn and Cr salens.

(2) In non-heme metalloenzymes, imidazole rings of histidine residues often form part of the metal-binding site. For examples, in the active sites of hemocyanin (Cu), nitrite reductase (Cu), and carbonic anhydrase (Zn), three imidazoles coordinate to one metal ion. We report the synthesis of tris(4-imidazolyl)carbinol ligands having chemically stable methyl group as the NH protective group and bulky substituent (isopropyl or phenyl) for stabilizing reactive species bound to metal center.

(3) Heme oxygenase (HO) catalyzes catabolism of heme to biliverdin, CO and a free iron through three successive oxygenation steps. The third oxygenation, oxidative degradation of verdoheme to biliverdin, has been the least understood step in spite of its importance to regulate the HO activity. We have thoroughly examined degradation of a synthetic verdoheme IXa complexed with rat HO-1. We propose that the HO enzyme activates O<sub>2</sub> and H<sub>2</sub>O<sub>2</sub> on the verdoheme iron with the aid of a nearby water molecule linked with Asp140.

(4) Reduction of nitrite (NO<sub>2</sub><sup>-</sup>) to gaseous nitric oxide (NO) is one of key processes in the global nitrogen cycle and carried out by bacterial copper-containing nitrite reductases (NiR). We report detection and characterization of new reaction intermediates in the nitrite reduction. This study shows that two protons required for the reaction are not provided to the copper bound nitrite simultaneously but stepwise and that the intramolecular electron transfer from the copper(I) ion to the copper bound nitrite occurs in the second protonation step.

### Molecular Science of Proteins Based on Vibrational Spectroscopy

**KITAGAWA, Teizo**

Proteins have an average structure as determined by x-ray crystallographic analysis. The higher order structure, details of which are not always clarified by x-ray crystallography and are easily altered by small energy, is directly related to a function of the molecule. Vibrational spectroscopy can provide some essential information on the higher order structure of proteins and its dynamics. It is the purpose of this group to apply resonance Raman and IR spectroscopy to observe vibrational spectra of proteins in aqueous solutions and to elucidate the structure-function relation in a level of molecular science.

In resonance Raman spectroscopy, various sensory proteins have been treated with visible and UV excitations. The visible excitation explored the structure of the heme site and UV excitation revealed what part of the protein is involved in the signal transduction *via* vibrational spectra of Trp and Tyr residues. For gas sensor proteins, sGC for NO, CooA and NPAS2 for CO and HemAT and Dos for O<sub>2</sub> are examined extensively. In addition, heme Raman spectra of new proteins including SOUL in mouse eyes, a maturation protein of cytochrome *c* (CcmE), and aldoxime dehydratase are also examined. Some basic features of Mb and Hb are also investigated in combination of UV and visible resonance Raman. We have been invited to contribute a mini-review paper on the gas sensory proteins by several international journals (*Acc. Chem. Res.*, *Inorg. Chem.* and *J. Inorg. Biochem.*).

As a very unique study, anti-stokes Raman spectra of dendrimer porphyrins are investigated in the presence and absence of IR irradiation, by which capturing of IR photons through antennae is confirmed. The Raman studies are extended to DNA-photolyse, various oxygen activating enzymes and their model compounds. On the other hand, our IR study is focused on an amyloid fibril. IR microscope technique is applied to several amyloid fibrils derived from fragment peptides of  $\beta_2$  microglobulin. IR spectroscopy will also be used to reveal the coupling mechanism of proton and electron transfers by terminal oxidases.

# JOINT STUDIES PROGRAMS

As one of the important functions of an inter-university research institute, IMS undertakes joint studies programs for which funds are available to cover research expenses as well as travel and living expenses of individuals. The proposals from domestic scientists are reviewed and controlled by an inter-university committee.

The programs are carried out under one of the following categories:

- (1) Joint Studies on Special Projects (a special project of significant relevance to the advancement of molecular science can be carried out by a team of several groups of scientists).
- (2) Research Symposia (a symposium on timely topics organized by collaboration between outside and IMS scientists).
- (3) Cooperative Research (a research program carried out by outside scientists with collaboration from an IMS scientist).
- (4) Use of Facility (a research program carried out by outside scientists at the research facilities of IMS except the UVSOR facility).
- (5) Invited Research Project
- (6) Joint Studies Programs using beam lines of UVSOR Facility.
- (7) Use of Facility Program of the Computer Center (research programs carried out by outside scientists at research facilities in Computer Center).

In 2004 Oct.–2005 Sep., the numbers of joint studies programs accepted for the categories (1)–(7) were 5, 11, 94, 47, 0, 125, and 133, respectively.

## (1) Special Projects

### A. Exchange and Spin-Orbit Interactions in Molecular Inner-Shell Excitation

**KOSUGI, Nobuhiro; GEJO, Tatsuo<sup>1</sup>; ISHIDA, Toshimasa<sup>2</sup>; HIYAMA, Miyabi; RÜHL, Eckart<sup>3</sup>; HATSUI, Takaki**

(<sup>1</sup>Univ. Hyogo; <sup>2</sup>Kyoto Univ.; <sup>3</sup>IMS and Würzburg Univ.)

In the orbital interaction theory,<sup>1)</sup> the electron-hole interaction between occupied and unoccupied orbitals is related to short-range interaction, delocalization or charge transfer, and long-range interaction, polarization (PL) or local excitation. On the other hand, the electron-electron interaction in two occupied orbitals is related to short-range exchange repulsion (EX) and long-range electrostatic interaction. The spin-orbit (SO) interaction is inherently of atomic character. EX and SO interactions involving core electrons of the first-row and second-row elements such as carbon 1s and sulfur 2p are relatively small in comparison with intra-valence EX and deep-core SO, but have been recently essential to understand fine structures newly found in high-resolution and sophisticated measurements of inner-shell phenomena using third-generation synchrotron radiation facilities.

There are some types of EX. EX in closed-shell electrons results in an *exclusion* effect on the electrons in the interacting region. This is completely different from electrons *sharing* in the interacting region and forming covalent bonds. The interatomic core-core and core-valence EX interactions<sup>2)</sup> are important in discussing core hole localization in the core ionization and resonant phenomena such as multi-atom resonant photoemission. The core excitation in the closed-shell system creates an open-shell valence and/or Rydberg electron.

In this case, the intra-atomic core-valence and core-Rydberg EX result in large and small singlet-triplet (ST) exchange splittings, respectively, where the core electron is localized on an atom and the intra-atomic EX component is predominant. On the other hand, the Rydberg electron may have relatively large intermolecular EX interaction with surrounding molecules in cluster, liquid, solid, and adsorbate phases, because of its diffuse character. In the core excitation and ionization of the open-shell system, EX causes more complicated multiplet splittings (MS). The core-valence EX sometimes competes with the intra-valence EX in core excitations of open-shell molecules composed of first-row elements.<sup>2–5)</sup>

The SO splitting on the core electron is directly observed in X-ray photoelectron spectroscopy. Even in 2p photoabsorption spectroscopy, the 2p SO splitting of third-row and heavier elements is large and is easily distinguishable. The singlet and triplet (ST) 2p excited states are strongly and indistinguishably mixed with each other through SO or *jj* coupling. However, in second-row elements such as phosphorus and sulfur, 2p SO is not satisfactorily analyzed due to a small and comparable splitting to the intra-atomic core-valence EX splitting. SO is still a major factor in the core-to-Rydberg excited state with a small ST (EX) splitting, but is only one of some important factors in the core-to-valence excited state with a large ST (EX) splitting.<sup>6)</sup> Recent high-resolution photoelectron spectroscopy is possible to reveal another small splitting in the 2p<sub>3/2</sub> manifold due to the molecular field (MF) effect.<sup>7)</sup>

Now we have to consider SO, MF, and EX splittings in interpreting 2p excitation spectra of molecules involving second-row elements. Furthermore, de-excitation or resonant inner-shell spectroscopy may indicate additional features *via* triplet components in intermediate core-excited states; that is, triplet valence excitation in resonant inelastic X-ray scattering and quartet valence ionization in resonant photoelectron or Auger electron emission. In the present special project, we have discussed various types of EX and intermediate

couplings between SO and EX to analyze experimental evidence in inner-shell spectra of some simple molecules.<sup>8)</sup>

#### References

- 1) for example, K. Hirai and N. Kosugi, *Can. J. Chem.* **70**, 301 (1992).
- 2) N. Kosugi, *Chem. Phys.* **289**, 117 (2003).
- 3) N. Kosugi, E. Shigemasa and A. Yagishita, *Chem. Phys. Lett.* **190**, 481 (1992).
- 4) N. Kosugi, J. Adachi, E. Shigemasa and A. Yagishita, *J. Chem. Phys.* **97**, 8842 (1992).
- 5) A. Yagishita, E. Shigemasa and N. Kosugi, *Phys. Rev. Lett.* **72**, 3961 (1994).
- 6) N. Kosugi, R. G. Cavell and A. P. Hitchcock, *Chem. Phys. Lett.* **265**, 490 (1997).
- 7) N. Kosugi and T. Ishida, *Chem. Phys. Lett.* **329**, 138 (2000).
- 8) N. Kosugi, *J. Electron Spectrosc. Relat. Phenom.* **137**, 335 (2004).

### B. Integration of Bio-Molecular Recognition Reaction System on Solid Surfaces and the Structure Analysis

**URISU, Tsuneo; TERO, Ryugo; MORIGAKI, Kenichi<sup>1</sup>; AOYAGI, Mutsumi<sup>2</sup>; WATANABE, Hidekazu<sup>2</sup>; TANAKA, Keiichi<sup>2</sup>; HARADA, Kensuke<sup>2</sup>; UTSUMI, Yuichi<sup>3</sup>**  
 (<sup>1</sup>AIST; <sup>2</sup>Kyushu Univ.; <sup>3</sup>Univ. Hyogo)

Membrane protein biosensors and biochips are the most important research targets in the post-genome. However, their developments are surprisingly delayed. One of the reasons is due to the difficulty in integrating the membrane protein on solid surfaces without losing their physiological activities. They express their physiological activity only when they are reconstructed in the lipid bilayers under the water. In this research project, we are going to develop elementary technologies of constructing membrane protein/lipid bilayer systems on Si surfaces and conduct the analysis of their structures by atomic force microscopy (AFM) and infrared reflection absorption spectroscopy using buried metal layer substrates (BML-IRRAS).

#### B-1 Development of New Infrared Reflection Absorption Spectroscopy and Application to Bio Materials

We have been developing BML-IRRAS, which shows characteristics of the surface top layer chemically, and shows characteristics of buried metal for the incident electromagnetic wave. We have investigated the surface chemical reactions for relatively simple molecules on the BML substrate to understand basic performance of this technique. An application to biomaterials is another important target of this sub-project. We have designed and constructed a special sample holder and IR beam optics for BML-IRRAS measurements of the biomaterials under water (D<sub>2</sub>O).

#### B-2 Chemical Modification of Si Surfaces and Formation of Supported Lipid Bilayers

Chemical modification of Si surfaces is one of the important elementary processes of the membrane protein biosensor fabrications. In this sub-project, we are developing Si surface chemical modification techniques. Avidin molecules were immobilized on COOH-modified SiO<sub>2</sub>/Si(100) surfaces with subnano-level flatness ( $R_a < 0.1$  nm) forming covalent bonds between COOH groups on the substrate surface and NH<sub>2</sub> groups of the avidin molecules. The avidin-immobilized surfaces were characterized by AFM, BML-IRRAS, transmission infrared absorption spectroscopy (TIRAS), and ellipsometry. It is concluded from these data that the avidin molecules are immobilized with the symmetry axis of the tetramer almost perpendicular to the substrate surface.

The effect of the electrostatic attractive force between vesicles and the substrate surface on Ca<sup>2+</sup> free supported lipid bilayer formation has been investigated by using atomic force microscopy and fluorescence microscopy. When negative-charged giant vesicles were incubated without Ca<sup>2+</sup>, the surface coverage of lipid bilayer was extremely low on the SiO<sub>2</sub> surface. On the other hand, in case of the positive-charged surface modified by aminopropyltrimethoxysilane, the high coverage of the lipid bilayer was obtained without Ca<sup>2+</sup>. The attractive force between the negative-charged giant vesicles and the positive-charged surface is essentially useful to induce the vesicle fusion without addition of Ca<sup>2+</sup>.

Fluorescence recovery after photobleaching (FRAP) method has become an important tool for investigating the lateral mobility and dynamics of biomembranes in living cells and mimicking membranes. Some groups have reported the fabrication of FRAP apparatus. While for those, fluorescence intensities were estimated by some complicated calibrations. In the present study, we successfully fabricated a new FRAP machine. There are two excitations for new FRAP apparatus. One is UV lamp, which is for fluorescence microscope observations. Another is the second harmonic of the 1120 nm semiconductor laser for photobleaching and quantitative high speed monitoring. On the optical pathway, two neutral density filters with different transmission coefficients can be inserted to the filter holder to attenuate the powers of the UV lamp and the laser. Two recording devices are equipped which can continuously record fluorescence recovery resulting in acquisition of images at CCD and the photomultiplier tube (PMT) joined with an oscillograph and computer by which the curve representing the time dependence of fluorescence intensity can be obtained.

#### B-3 Membrane Protein Biosensor Fabrications

High resistance lipid bilayer formation is the most important first step of the supported membrane single ion channel biosensors. In this sub-project, we have recently succeeded in the fabrication of gigaohm seals on the Si substrate with microelectrodes and the guard ring consisted of self assembled monolayer of alkyl silane compounds to reduce the edge leak currents.

Furthermore, we have also started the new subject of integrating the membrane protein biosensor to the micro-fluidic circuit

We have developed a technique to fabricate the hole (well) with about 1  $\mu\text{m}$  diameter for the microelectrode on the surface of  $\text{SiO}_2/\text{Si}$  substrate. The circle pattern was made on the Co thin film by using the femto-second laser ablation, and the hole was made by the succeeding synchrotron radiation etching using this Co pattern as the mask. This process enabled the fabrication of the electrode hole with keeping the original nano-level flatness ( $R_a \sim 0.8 \text{ nm}$ ) of the substrate. A single planar lipid bilayer, deposited on these microelectrodes by the rapture of giant unilamellar vesicles, showed a high resistance (1.2  $\text{G}\Omega$ ) necessary for the single channel recordings.

### C. Development and Application of Short Wave Length Free Electron Laser

**KATOH, Masahiro; HOSAKA, Masahito; MOCHIHASHI, Akira; TAKASHIMA, Yoshifumi<sup>1</sup>; HAMA, Hiroyuki<sup>2</sup>; GEJO, Tatsuo<sup>3</sup>; NISHINO, Hideo<sup>4</sup>; HARA, Toru<sup>5</sup>; COUPRIE, Marie-Emmanuelle<sup>6</sup>; BIELAWSKI, Serge<sup>7</sup>**  
(<sup>1</sup>Nagoya Univ.; <sup>2</sup>Tohoku Univ.; <sup>3</sup>Univ. Hyogo; <sup>4</sup>JST; <sup>5</sup>RIKEN; <sup>6</sup>CEA; <sup>7</sup>Univ. Sci. Tech. Lille)

As the result of the upgrade of the UVSOR-II electron storage ring in 2003, the ring can be operated with a small beam emittance of 17 nm-rad. This small emittance enables high power oscillation of the UVSOR free electron laser (FEL) in deep UV region. We tried the FEL oscillation at the wavelength of 250 nm and achieved a high power oscillation with several hundred mW. This circular polarized laser at 250 nm was used for the experiment on absolute asymmetric photo-reactions of amino acids. We have confirmed the progress of the photoreactions.

We have constructed a feed back system to stabilize the FEL output power. The system observes the change of the out-coupled laser power and control the synchronization between the laser pulse and the electron pulses. The test operation was successful. Even under the operating condition in which the laser was very unstable, the out-coupled power was stabilized sufficiently.

## (2) Research Symposia

(From 2004 Oct. to 2005 Sep.)

1. Studies of Life Science from a Viepoint of Physical Chemistry—From Molecular Organizations to Living Cells—  
(Dec. 20–21, 2004)  
Chair: **TERAZIMA, Masahide**
2. Perspective of Biometal Molecular Science  
(Oct. 1–3, 2004)  
Chair: **SHIRO, Yoshitsugu**

3. Recent Developments of the Studies on Surface Magnetism  
(Nov. 5–6, 2004)  
Chair: **OHTA, Toshiaki**
4. Surface and Interface in Nano-Bioelectronics (Biotronics 2005)  
(March 3–7, 2005)  
Chair: **URISU, Tsuneo**
5. Symposium on Conductive and Photoconductive Organic Solids and Related Phenomena  
(Nov. 12–14, 2004)  
Chair: **YAKUSHI, Kyuya**
6. Frontiers in Biospectroscopy and Molecular Imaging  
(Jan. 17–18, 2005)  
Chair: **TAMURA, Mamoru**
7. Molecular Science of Heterogeneous Systems Observed in Atmospheric Sciences  
(Jan. 20–22, 2005)  
Chair: **TAKAMI, Akinori**
8. Progresses of Molecular Science and Related Fields  
(June 4–5, 2005)  
Chair: **NAKAJIMA, Atsushi**
9. Structure and Function of Retinal Proteins and GPCRs  
(June 15–17, 2005)  
Chair: **TSUDA, Motoyuki**
10. Various Hydrogen-Bonded Systems and Quantum Effects  
(July 8–9, 2005)  
Chair: **SEKIYA, Hiroshi**
11. Physical Chemistry Symposium for Young Researchers  
(June 8, 2005)  
Chair: **MASUHARA, Hiroshi**

## (3) Cooperative Research

This is one of the most important categories that IMS undertakes for conducting its own research of the common interest to both outside and IMS scientists by using the facilities at IMS. In 2004 Oct.–2005 Mar., 118 outside scientists from 48 research groups joined the Cooperative Research programs, and 103 outside scientists from 46 research groups in 2005 Apr.–2005 Sep. The names and affiliations of those collaborations are found in the Research Activities sections in this Review.

## **(4) Use of Facility**

The number of projects accepted for the Use of Facility in 2004 Oct.–2005 Mar. amounted 1, 23, and 0 for the Laser Research Center for Molecular Science (LRCMS), for the Research Center for Molecular-scale Nanoscience (RCMN) and for the Equipment Development Center (EDC), respectively. In 2005 Apr.–2005 Sep., the number of projects accepted amounted 2, 20, and 1 for LRCMS, for RCMN, and for EDC, respectively.

## **(5) Invited Research**

Under this joint-study program, several scientists were invited from other institutions of help for construction and improvement of instruments in IMS. The total number of the projects in this category was 0.

## **(6) Use of UVSOR Projects**

In the UVSOR Facility with the 750 MeV electron storage ring, there are sixteen beam lines available for synchrotron radiation research (see UVSOR ACTIVITY REPORT 2004). Under the Use of UVSOR Projects, many synchrotron radiation experiments have been carried out by outside scientists on eight beam lines in close cooperation with the UVSOR staff. The total number of the projects in this category was 125 (64 in 2004 Oct.–2005 Mar., and 61 in 2005 Apr.–2005 Sep.).

## **(7) Use of Facility Program of the Computer Center**

Computer Center provides three types of research programs for outside scientists: (a) Use-of-Facility Program; (b) Cooperative Research Program; (c) Advanced Research Program. The numbers of projects accepted for each programs during the fiscal year of 2004 were (a) 126 with 501 users, (b) 6 with 12 users and (c) 1 with 3 users. Computer time distributed for these projects amounted to 85% of the total annual CPU time available.

## FOREIGN SCHOLARS

Visitors from abroad are always welcome at IMS and they have always played an important role in the research activities of the Institute. The foreign scientists who visited IMS during the past year (September 2004–August 2005) are listed below.

The mark <sup>\*1</sup> indicates attendance at an Okazaki IMS Conference; <sup>\*2</sup> a MONKASHO (Ministry of Education, Culture, Sports, Science and Technology, Japan) or JSPS (Japan Society for the Promotion of Science) Invited Fellow; <sup>\*3</sup> an IMS councillor; <sup>\*4</sup> an IMS visiting professor or associate professor from abroad (period of stay from 3 to 12 months); <sup>\*5</sup> a JSPS Post-Doctoral or Ronpaku Fellow; <sup>\*6</sup> an IMS visiting scientist and <sup>\*7</sup> a visitor to IMS.

Scientists who would like to visit IMS under programs <sup>\*2</sup> and <sup>\*4</sup> are invited to make contact with IMS staff in their relevant field.

Dr. Digambara Patra <sup>*2</sup>	Humboldt Res.	(Germany)	Sep. '04–Aug. '06
Prof. Rossky Peter J. <sup>*1</sup>	Univ. of Texas	(U.S.A.)	Sep. '04
Prof. OsheroV Vladimir <sup>*2</sup>	Russian Acad. of Sci.	(Russia)	Sep. '04–Jan. '05
Dr. Slanina Zdenek <sup>*1</sup>	Tsukuba Univ.	(Japan)	Sep. '04–Mar. '05
Prof. Ishkhanyan Artur <sup>*6</sup>	Armenian Natl. Acad. of Sci.	(Armenia)	Sep. '04–Dec. '04
Dr. Michael W. Schmidt <sup>*6</sup>	Iowa Univ. Ames Inst.	(U.S.A.)	Sep. '04–Oct. '04
Dr. Simonyan Mkhitar <sup>*6</sup>	Armenian Natl. Acad. of Sci.	(Armenia)	Sep. '04–Dec. '04
Prof. Varotsis Constantinos <sup>*2</sup>	Univ. of Crete	(Greece)	Sep. '04–Jan. '05
Prof. Giedroc David <sup>*1</sup>	Texas A&M Univ.	(U.S.A.)	Oct. '04
Dr. Roy L. Johnston <sup>*1</sup>	Univ. of Birmingham	(U.K.)	Oct. '04
Dr. Anant D. Kulkarni <sup>*6</sup>	Univ. of Pune	(India)	Oct. '04–Mar. '05
Dr. Kokalj Anton <sup>*6</sup>	Jozef Stefan Inst.	(Slovenia)	Oct. '04
Prof. Meneghetti Moreno <sup>*6</sup>	Univ. of Padova	(Italy)	Oct. '04
Prof. Michael Deleuze <sup>*6</sup>	Limburgs Univ.	(Belgium)	Oct. '04
Prof. Sun Wen-Yin <sup>*4</sup>	Nanjing Univ.	(China)	Nov. '04–Oct. '05
Prof. Ernst Richard <sup>*1</sup>	ETH	(Swiss)	Nov. '04
Prof. Zhao Yi <sup>*2</sup>	Univ. of Sci. and Tech. of China	(China)	Nov. '04–Nov. '05
Prof. Gerber Gustav <sup>*6</sup>	Univ. Wurzburg	(Germany)	Nov. '04
Prof. Meyer Michael <sup>*6</sup>	LURE	(France)	Nov. '04–Dec. '04
Dr. Szwaj Christophe <sup>*6</sup>	Univ. of Sci. and Tech. of Lille	(France)	Dec. '04
Dr. Couprie Marie-Emmanuelle <sup>*6</sup>	Commissariat al Energie Atomique	(France)	Dec. '04
Dr. Bielawski Serge <sup>*2</sup>	Univ. of Sci. and Tech. of Lille	(France)	Dec. '04
Prof. Park Tae Jun <sup>*2</sup>	Dongguk Univ.	(Korea)	Dec. '04–Feb. '05
Mr. Choi Young-Cheol <sup>*1</sup>	Pohang Univ. of Sci. and Tech.	(Korea)	Dec. '04
Mr. Choi Hyeonho <sup>*1</sup>	Seoul Natl. Univ.	(Korea)	Dec. '04
Mr. Heo Wonjoon <sup>*1</sup>	KAIST	(Korea)	Dec. '04
Mr. Jung JaeWoon <sup>*1</sup>	KAIST	(Korea)	Dec. '04
Mr. Kim Hyungjun <sup>*1</sup>	KAIST	(Korea)	Dec. '04
Mr. Lee In-Ho <sup>*1</sup>	Korea Res. Inst. of Standards and Sci.	(Korea)	Dec. '04
Mr. Nongmaithem Jiten Singh <sup>*1</sup>	Pohang Univ. of Sci. and Tech.	(Korea)	Dec. '04
Ms. Park Jeongeon <sup>*1</sup>	KAIST	(Korea)	Dec. '04
Ms. Park Mina <sup>*1</sup>	Pohang Univ. of Sci. and Tech.	(Korea)	Dec. '04
Mr. Son Won-joon <sup>*1</sup>	Seoul Natl. Univ.	(Korea)	Dec. '04
Mr. Yoon Ho-jin <sup>*1</sup>	KIAS	(Korea)	Dec. '04
Mr. Yoon Jeseong <sup>*1</sup>	Seoul Natl. Univ.	(Korea)	Dec. '04
Mr. Yoon Yeohoon <sup>*1</sup>	Seoul Natl. Univ.	(Korea)	Dec. '04
Ms. Chak Li Ling <sup>*1</sup>	Natl. Univ. of Singapore	(Singapore)	Dec. '04
Mr. Chiang Samuel <sup>*1</sup>	Natl. Univ. of Singapore	(Singapore)	Dec. '04
Mr. Han Liany <sup>*1</sup>	Natl. Univ. of Singapore	(Singapore)	Dec. '04
Mr. Li Hu <sup>*1</sup>	Natl. Univ. of Singapore	(Singapore)	Dec. '04
Ms. Li Shuiying <sup>*1</sup>	Natl. Univ. of Singapore	(Singapore)	Dec. '04
Mr. Lin Honghuang <sup>*1</sup>	Natl. Univ. of Singapore	(Singapore)	Dec. '04
Mr. Lu Yunpeng <sup>*1</sup>	Natl. Univ. of Singapore	(Singapore)	Dec. '04
Mr. Radjiman Sugiarto <sup>*1</sup>	Natl. Univ. of Singapore	(Singapore)	Dec. '04
Mr. Ung Choong Yong <sup>*1</sup>	Natl. Univ. of Singapore	(Singapore)	Dec. '04
Mr. Wang Jian <sup>*1</sup>	Natl. Univ. of Singapore	(Singapore)	Dec. '04
Mr. Zeng Nan <sup>*1</sup>	Natl. Univ. of Singapore	(Singapore)	Dec. '04
Ms. Zhang Liling <sup>*1</sup>	Natl. Univ. of Singapore	(Singapore)	Dec. '04
Ms. Zheng Chanjuan <sup>*1</sup>	Natl. Univ. of Singapore	(Singapore)	Dec. '04
Ms. Zhu Shizhen <sup>*1</sup>	Natl. Univ. of Singapore	(Singapore)	Dec. '04
Ms. Chumchua Vasunun <sup>*1</sup>	Chulalongkorn Univ.	(Thailand)	Dec. '04
Mr. Pornputtapong Natapol <sup>*1</sup>	Natl. Cent. for Genetic Engineering and BIOTEC	(Thailand)	Dec. '04

Ms. Prommeenate Peerada <sup>*1</sup>	King Mongkut's Univ. of Tech. Thonburi	(Thailand)	Dec. '04
Ms. Roddechcha Supacharee <sup>*1</sup>	Mahidol Univ.	(Thailand)	Dec. '04
Mr. Somsook Ekasith <sup>*1</sup>	Mahidol Univ.	(Thailand)	Dec. '04
Mr. Tantirungrotechai Yuthana <sup>*1</sup>	Mahidol Univ.	(Thailand)	Dec. '04
Mr. Chen Chien-Fu <sup>*1</sup>	Natl.Chung Cheng Univ.	(Taiwan)	Dec. '04
Mr. Hu Chin-Kun <sup>*1</sup>	Acad. Sinica	(Taiwan)	Dec. '04
Mr. Wu Ming-Chya <sup>*1</sup>	Acad. Sinica	(Taiwan)	Dec. '04
Mr. Shaikh Md. Aftab Ali <sup>*1</sup>	Univ. of Dhaka	(Bangladesh)	Dec. '04
Prof. Girard Bertrand <sup>*6</sup>	Univ. Paul Sabatier	(France)	Dec. '04
Prof. Petek Hirvoje <sup>*1</sup>	Univ. of Pittsburgh	(U.S.A.)	Dec. '04
Prof. Boo Bong Hyun <sup>*2</sup>	Chungnam Natl. Univ.	(Korea)	Dec. '04
Prof. Lu Jing <sup>*6</sup>	Beijing Univ.	(China)	Dec. '04
Prof. Marc Simon <sup>*6</sup>	LCPMR	(France)	Jan. '05
Prof. Offenhaeusser Andreas <sup>*1</sup>	Inst. of Thin Films & Interfaces	(Germany)	Jan. '05
Prof. Tanatar Makariy <sup>*4</sup>	Natl. Acad. of Sci. of Ukraine	(Ukraine)	Feb. '05–Jan. '06
Prof. Mo Yu-Jun <sup>*6</sup>	Henan Univ.	(China)	Feb. '05–Mar. '05
Prof. Ishkhanyan Artur <sup>*6</sup>	Armenian Natl. Acad. of Sci.	(Armenia)	Mar. '05
Dr. Manukyan Ashot <sup>*6</sup>	Armenian Natl. Acad. of Sci.	(Armenia)	Mar. '05
Prof. Aka Gerard Philippe <sup>*6</sup>	ENSCP	(France)	Mar. '05
Prof. Lupei Voicu <sup>*6</sup>	Natl. Inst. for Laser, Plasma and Radiation Phys.	(Rumania)	Mar. '05
Prof. Pobre Romeric <sup>*6</sup>	De La Salle Univ.	(Philippines)	Feb. '05–Mar. '05
Dr. Estacio Elmer <sup>*6</sup>	Univ. of Philippines	(Philippines)	Feb. '05–Mar. '06
Prof. Takats Josef <sup>*1</sup>	Univ. of Alberta	(Canada)	Mar. '05
Prof. Varotsis Constantinos <sup>*2</sup>	Univ. of Crete	(Greece)	Feb. '05–Apr. '05
Mr. Daskalakis Evangelos <sup>*6</sup>	Univ. of Crete	(Greece)	Mar. '05–Jun. '05
Dr. Schmidt Michael <sup>*6</sup>	Univ. of Iowa	(U.S.A.)	Mar. '05–Apr. '05
Prof. Heyes David <sup>*6</sup>	Univ. of Surrey	(U.K.)	Apr. '05
Ms. Nickut Patricia <sup>*6</sup>	Univ. of Oldenburg	(Germany)	Apr. '05–Jul. '05
Prof. Long La-Sheng <sup>*4</sup>	Xiamen Univ.	(China)	May '05–Apr. '06
Prof. Bronold Franz Xaver <sup>*6</sup>	Ernst-Moritz-Arndt-Univ. Greifswald	(Germany)	Apr. '05–May '05
Mr. Delagnes Jean-Christophe <sup>*6</sup>	Univ. Paul Sabatier	(France)	Apr. '05–Jun. '05
Prof. Pulay Peter <sup>*4</sup>	Univ. of Arkansas	(U.S.A.)	May '05–Aug. '05
Dr. Chen Zhongfang <sup>*6</sup>	Univ. of Georgia	(China)	May '05–Jun. '05
Prof. Girard Bertrand <sup>*2</sup>	Univ. of Paul Sabatier	(France)	May '05–Jun. '05
Mr. Lee Hun-cheol <sup>*6</sup>	Yeungnam Univ.	(Korea)	Dec. '04–Jan. '05
Prof. Yi Jonghoon <sup>*6</sup>	Yeungnam Univ.	(Korea)	Dec. '04–Jan. '05
Dr. Kim Jeong Ho <sup>*6</sup>	Res. Inst. of Industrial Tech, Korea Maritime Univ.	(Korea)	Mar. '05
Mr. Wisdom Jeffrey <sup>*6</sup>	Stanford Univ.	(U.S.A.)	Mar. '05
Dr. Gaume Romain <sup>*6</sup>	Stanford Univ.	(U.S.A.)	Mar. '05
Prof. Byer Robert L <sup>*6</sup>	Stanford Univ.	(U.S.A.)	Mar. '05
Dr. Sichelschmidt Joerg <sup>*6</sup>	Max-Planck-Inst. for Chem. Phys. of Solids	(Germany)	Feb. '05
Dr. Noh Tae W. <sup>*6</sup>	Seoul Natl.Univ.	(Korea)	Feb. '05–Mar. '05
Dr. Moon Soon Jae <sup>*6</sup>	Seoul Natl.Univ.	(Korea)	Feb. '05–Mar. '05
Prof. Kwon Yong Seoung <sup>*6</sup>	Sungkyunkwan Univ.	(Korea)	Mar. '05
Dr. Feng Guangyao <sup>*7</sup>	Univ. of Sci. and Tech. of China	(China)	Mar. '05
Dr. Zhang Shancai <sup>*7</sup>	Univ. of Sci. and Tech. of China	(China)	Mar. '05
Dr. Couprie Marie Emmanuelle <sup>*1</sup>	Commissariat for Atomic Energy	(France)	Jan. '05–Feb. '05
Prof. Meier Christophe <sup>*6</sup>	Univ. Paul Sabatier	(France)	May '05–Jun. '05
Prof. Y.Ron Shen <sup>*1</sup>	Univ. of California at Berkeley	(U.S.A.)	Jun. '05
Prof. Shi Gaoquan <sup>*1</sup>	Tsinghua Univ.	(China)	Nov. '04
Prof. Tian He <sup>*1</sup>	East China Univ. of Sci. and Tech.	(China)	Nov. '04
Prof. Mu Sholin <sup>*1</sup>	Yangzhou Univ.	(China)	Nov. '04
Prof. Ma Yuguang <sup>*1</sup>	Jilin Univ.	(China)	Nov. '04
Prof. Wang Fosong <sup>*1</sup>	Changchun Inst.	(China)	Nov. '04
Prof. Wang Lixiang <sup>*1</sup>	Changchun Inst. of Applied Chem.	(China)	Nov. '04
Prof. Yan Donghang <sup>*1</sup>	Changchun Inst. of Applied Chem.	(China)	Nov. '04
Prof. Geng Yanhou <sup>*1</sup>	Changchun Inst. of Applied Chem.	(China)	Nov. '04
Prof. Chen Hongzheng <sup>*1</sup>	Zhejiang Univ.	(China)	Nov. '04
Prof. Pei Jian <sup>*1</sup>	Peking Univ.	(China)	Nov. '04
Prof. Qin Jingui <sup>*1</sup>	Wuhan Univ.	(China)	Nov. '04
Prof. Lu Yun <sup>*1</sup>	Nannjing Univ.	(China)	Nov. '04
Prof. Peng Junbiao <sup>*1</sup>	Inst. of Polymer Optoelectronic Materials and Devices	(China)	Nov. '04
Prof. Shi Huahong <sup>*1</sup>	South China Univ. of Tech.	(China)	Nov. '04
Mr. Jiang Jiaying <sup>*1</sup>	South China Univ.	(China)	Nov. '04

Prof. Yang Junlin <sup>*1</sup>	Natl. Natural Sci. Foundation of China	(China)	Nov. '04
Prof. Zhu Daoben <sup>*1</sup>	Inst. of Chem. Chinese Acad. of Sci.	(China)	Nov. '04
Prof. bai Fenglian <sup>*1</sup>	Inst. of Chem. Chinese Acad. of Sci.	(China)	Nov. '04
Prof. Li Yongfang <sup>*1</sup>	Inst. of Chem. Chinese Acad. of Sci.	(China)	Nov. '04
Prof. Shuai Zhigang <sup>*1</sup>	Inst. of Chem. Chinese Acad. of Sci.	(China)	Nov. '04
Prof. Song Yanlin <sup>*1</sup>	Inst. of Chem. Chinese Acad. of Sci.	(China)	Nov. '04
Prof. Hu Wenning <sup>*1</sup>	Inst. of Chem. Chinese Acad. of Sci.	(China)	Nov. '04
Prof. Ye Cheng <sup>*1</sup>	Inst. of Chem. Chinese Acad. of Sci.	(China)	Nov. '04
Prof. Li Yuliang <sup>*1</sup>	Inst. of Chem. Chinese Acad. of Sci.	(China)	Nov. '04
Prof. Liu Yunqi <sup>*1</sup>	Inst. of Chem. Chinese Acad. of Sci.	(China)	Nov. '04
Prof. Wan Meixiang <sup>*1</sup>	Inst. of Chem. Chinese Acad. of Sci.	(China)	Nov. '04
Prof. Zhang Deqing <sup>*1</sup>	Inst. of Chem. Chinese Acad. of Sci.	(China)	Nov. '04
Prof. Guo Zhixing <sup>*1</sup>	Inst. of Chem. Chinese Acad. of Sci.	(China)	Nov. '04
Prof. Liu Minhua <sup>*1</sup>	Inst. of Chem. Chinese Acad. of Sci.	(China)	Nov. '04
Prof. Jiang Lei <sup>*1</sup>	Inst. of Chem. Chinese Acad. of Sci.	(China)	Nov. '04
Prof. Yang Chunhe <sup>*1</sup>	Inst. of Chem. Chinese Acad. of Sci.	(China)	Nov. '04
Prof. Liu Huibiao <sup>*1</sup>	Inst. of Chem. Chinese Acad. of Sci.	(China)	Nov. '04
Prof. Zhang Bin <sup>*1</sup>	Inst. of Chem. Chinese Acad. of Sci.	(China)	Nov. '04
Prof. Liu Caiming <sup>*1</sup>	Inst. of Chem. Chinese Acad. of Sci.	(China)	Nov. '04
Prof. Xu Wei <sup>*1</sup>	Inst. of Chem. Chinese Acad. of Sci.	(China)	Nov. '04
Prof. Jin Zhai <sup>*1</sup>	Inst. of Chem. Chinese Acad. of Sci.	(China)	Nov. '04
Prof. Yu Gui <sup>*1</sup>	Inst. of Chem. Chinese Acad. of Sci.	(China)	Nov. '04
Prof. Li Hongxiang <sup>*1</sup>	Inst. of Chem. Chinese Acad. of Sci.	(China)	Nov. '04
Dr. Mondal Chandan Kumar <sup>*6</sup>	Chonnam Natl. Univ.	(Korea)	Jun. '05–Aug. '05
Prof. Lee Jin Yong <sup>*2</sup>	Chonnam Natl. Univ.	(Korea)	Jun. '05–Aug. '05
Dr. Boyko Sergiy <sup>*1</sup>	Univ. of Ontario Inst. of Tech.	(Canada)	Jul. '05–Aug. '05
Prof. Chakravarty Akhil <sup>*1</sup>	Indian Inst. of Sci.	(India)	Jul. '05
Prof. Petek Hrvoje <sup>*1</sup>	Univ. of Pittsburgh	(U.S.A.)	Jul. '05
Prof. Zhao Xiang <sup>*6</sup>	Xian Jiaotong Univ.	(China)	Jul. '05–Aug. '05
Prof. Fejer Martin <sup>*1</sup>	Edward L. Ginzton Lab. Stanford Univ.	(U.S.A.)	Jul. '05
Prof. Kim Younkyoo <sup>*6</sup>	Hankuk Univ. of Foreign Studies	(Korea)	Jul. '05–Aug. '05
Dr. Couprie Marie Emmanuelle <sup>*6</sup>	Committee of Atomic Energy	(France)	Jul. '05–Aug. '05
Ms. Labat Marie <sup>*6</sup>	Committee of Atomic Energy	(France)	Jul. '05–Aug. '05
Mr. Lambert Guillaume <sup>*6</sup>	Committee of Atomic Energy	(France)	Jul. '05
Prof. Xu Hongliang <sup>*7</sup>	Univ. of Sci. and Tech. of China	(China)	Jul. '05–Aug. '05
Dr. Zhang Shancai <sup>*7</sup>	Univ. of Sci. and Tech. of China	(China)	Jul. '05–Aug. '05
Dr. Huang Guirong <sup>*7</sup>	Univ. of Sci. and Tech. of China	(China)	Jul. '05–Aug. '05
Prof. Wang Lin <sup>*7</sup>	Univ. of Sci. and Tech. of China	(China)	Jul. '05–Aug. '05
Prof. Kwon Yong Seung <sup>*7</sup>	Sungkyuunkwan Univ.	(Korea)	Aug. '05
Mr. Hong Jong Beom <sup>*6</sup>	Sungkyuunkwan Univ.	(Korea)	Aug. '05
Mr. Kim Jeong Woon <sup>*6</sup>	Sungkyuunkwan Univ.	(Korea)	Aug. '05
Prof. Gu Yuzong <sup>*2</sup>	Henan Univ.	(China)	Jul. '05
Dr. El-Mashtoly Samir Fathy Abd El-Monem <sup>*6</sup>	Ain Shams Univ.	(Egypt)	Jul. '04–Sep. '04
Dr. Kim Hyeong-Do <sup>*6</sup>	Pohang Accelerator Lab.	(Korea)	Aug. '05



## AWARDS

### Associate Professor Dr. Ozawa's Scientific Achievement

Prof. Takeaki Ozawa of Department of Molecular Structure received the Young Scientists Award from Minister of MEXT. The award title is "Development of the Methods for Analyzing Molecular Dynamics in Live Cells in the Fields of Chemistry and Biology." A current focus on biological research is to quantify and to image cellular processes in living cells and animals. To detect such cellular processes, many reporter proteins are now extensively being used. The most common reporters include fluorescent and bioluminescent proteins such as firefly luciferase, green fluorescent protein (GFP), and their variants with various spectral properties. Prof. Ozawa developed a novel design of the reporter proteins with general applicability for detecting the biological processes in living cells and animals. The principle is based on reconstitution of split reporter protein fragments by the use of 'protein splicing' technique. He showed the following attractive applications with the split reporter fragments. First, split reporter fragments, connected respectively with a pair of interacting proteins, worked as indicators for protein-protein interactions in live bacteria and mammalian cells. Second, the split GFP reporter provided a genetic method for identifying mitochondrial proteins from large-scale cDNA libraries. Finally, the split luciferase reporter enabled high-throughput sensing and noninvasive imaging of nuclear transport of proteins of interest in living animals. The basic concept of split reporter reconstitution by protein splicing will promise a wide variety of applications to study protein-protein interactions, protein localizations, intracellular protein dynamics, and protein activity in living cells and animals. Thus, the impact of Prof. Ozawa's work on methodological development for analyzing molecular dynamics in living cells is clearly significant.

### Professor Emeritus Hirota's Scientific Achievements

Professor Emeritus Eizi Hirota received E. Bright Wilson Award in Spectroscopy by the American Chemical Society for his outstanding contributions to "high-resolution spectroscopy, in particular to the detection and the characterization of free radicals and ions that have led to deeper understanding of chemical reaction mechanisms." This award was founded 1997 to commemorate the significant establishments of E. B. Wilson, Jr. in physical chemistry, in particular, experimental and theoretical achievements in molecular spectroscopy, and it has been granted to an individual who makes outstanding accomplishments in fundamental or applied spectroscopy in chemistry.

Dr. Hirota had settled high-resolution spectroscopy of radicals and ions as the main subject to be explored since he joined IMS as a professor of Department of Molecular Structure at the occasion of the foundation of the Institute (1975). Free radicals and molecular ions are reactive intermediates that play significant roles in chemical reactions, so importance of decisive characterization *via* spectroscopic investigations had been well recognized even at the moment. Nevertheless, high-resolution spectroscopic studies of them were believed to be too demanding because of inherently low concentration of the species to be detected. Dr. Hirota and his co-workers overcame this difficulty by the development of highly sensitive detection methods, such as millimeter- and submillimeter-wave spectroscopy and infrared diode laser spectroscopy. During his carrier in IMS, Dr. Hirota achieved successful detection and precise structural determination of dozens of free radicals and ions, including prototypical organic free radicals (methyl, vinyl, allyl, methoxy, vinyloxy, *etc.*) and those of fundamental importance in plasma and in space ( $\text{SiH}_3$ ,  $\text{H}_2\text{D}^+$ ,  $\text{FHF}^-$ , *etc.*). In addition, high-resolution spectroscopic detection was applied to monitor elementary chemical reactions with quantum-state resolved manner, and entirely new information was provided on photodissociation dynamics and oxidation mechanisms of several fundamental molecules. In these respects, Dr. Hirota's achievements have an enormous impact not only on molecular spectroscopy but also on varieties of related scientific fields, such as quantum chemistry, chemical reaction studies, plasma chemistry, atmospheric chemistry, and interstellar chemistry.

### Professor Hama's Scientific Achievements

Prof. Hiroyuki Hama at Tohoku University, a former associate professor of the UVSOR facility (1990–2000), received the 2004 FEL (Free Electron Laser) Prize for his contribution to "Storage Ring Free Electron Lasers." He has performed fundamental and pioneering contributions in Storage Ring Free Electron Lasers (SRFELs). Thanks to his deep understanding of the FEL and to his achievements, he has promoted the use of SRFELs in a broad scientific community, from synchrotron radiation to nuclear physics. He Installed the first optical klystron with adjustable planar-to-helical field in 1996 on the UVSOR storage ring. This improvements produced short wavelength records for FELs in 1996. He also demonstrated the production of monochromatic gamma-rays by Compton Back-Scattering with a storage ring free electron laser.

## Mr. Horigome's Technological Achievements

Mr. Toshio Horigome, the chief of the technical section of the UVSOR facility, received "The CSJ Award for Technical Achievement" in the spring of 2005. His contribution is "Experimental Apparatus Design and Fabrication for Molecular Photoscience."

The Chemical Society of Japan (CSJ) awards every year a person who has contributed to the development or improvement of experimental techniques in chemistry and chemical engineering. Mr. Toshio Horigome is recognized for his distinguished and long-standing achievements in high-precision and compact instrumentation for various types of experiments under ultra-high vacuum condition.

## Associate Professor Taira Group's Scientific Achievements

Drs. J. Saikawa, Y. Sato, and T. Taira of Laser Research Center for Molecular Science received the Award from the Laser Society of Japan for the paper on "Short pulse generation in Yb:Y<sub>3</sub>ScAl<sub>4</sub>O<sub>12</sub> disordered ceramic laser" presented in the 324th Conference on "High-performance solid-state lasers and their applications." Recently, they have developed Nd<sup>3+</sup> or Yb<sup>3+</sup> doped mixed garnet materials Y<sub>3</sub>ScAl<sub>4</sub>O<sub>12</sub> ceramics, which are a solid solution of YAG and Y<sub>3</sub>Sc<sub>2</sub>Al<sub>3</sub>O<sub>12</sub> (YSAG), by using sintering methods. They demonstrated that a passively mode-locked Yb<sup>3+</sup>-doped YSAG ceramic laser provides the maximum average output power of 150 mW with a pulse duration of 500 fs and an average output power of 62 mW with a pulse duration of 280 fs at 1035.8 nm. These developments opened a new field of lasers and variety of applications.

## Technical Associate Ishimura's Scientific Achievement

Mr. Kazuya Ishimura, Technical Associate of Department of Theoretical Molecular Science, received the Diamond Award for the presentation of an excellent poster titled "A New Parallel second-order Møller-Plesset algorithm" in the 7<sup>th</sup> Congress of WATOC (World Association of Theoretically Oriented Chemists), the most representative international congress in theoretical and computational chemistry, which was held in Cape town, South Africa, on January 16–21, 2005. He developed a new parallel algorithm of the canonical MP2 method with two-step parallelization and dynamic load-balancing, which is applicable to large molecular systems. The developed MP2 algorithm made it possible to perform reliable calculations of weak non-covalent interactions that play an important role in host-guest chemistry, molecular recognition, and self-assembly.

## Research Associate Dr. Imura's Scientific Achievement

Dr. Kohei Imura, Research Associate of Department of Molecular Structure, received two awards this year. One is the Nano Optics Award in the 14th Annual Symposium of The Nano Optics Research Group (July 2005) and his title of paper was "Plasmon-Mode Imaging of Noble Metal Nanorods and Dispersion Relations." The other one is Young Scientist Award in the 2005 Annual Conference on Molecular Structure and Related Topics (September 2005, the largest conference in the field of physical chemistry in Japan) and his title of paper was "Plasmon-Mode Imaging and Two-Photon Induced Photoluminescence of Gold Nanorods and Nanoplates."

He succeeded in direct observation of the plasmon-mode wavefunctions of noble-metal metal nanorods and nanoplates based on near-field transmission imaging or near-field two-photon induced emission imaging, with a spatial resolution as high as ~50 nm. At the same time, the resonant frequencies of the plasmon modes of nanorods were determined from the near-field transmission spectra. From these measurements, the dispersion relations for the nanorod plasmons were obtained, and the results were discussed based upon electromagnetism. He also investigated spectra and polarization characteristics of the two-photon induced photoluminescence from nanorods and nanoplates and analyzed them in relation to the crystal structures and band structures. These results are important for fundamental understanding and application of optical properties of metal nanoparticles, and those of plasmon resonances in nanometric systems.

## Dr. Tero's Scientific Achievement

Dr. Ryugo Tero, received the Young Scientist Award for the presentation of an Excellent Paper in the Annual Meeting of The Surface Science Society of Japan (November, 2004). The title of the paper was "Fabrication of avidin single molecular layer on silicon oxide surfaces and formation of tethered lipid bilayer membranes." He

fabricated single molecular layer of avidin on an atomically flat SiO<sub>2</sub> surface and characterized using atomic force microscopy (AFM) and infrared reflection absorption spectroscopy. He showed that each of avidin molecules adsorbs as a single molecule and retains the biotin-binding activity from the AFM topographs and function-recognizing images obtained by biotin-modified cantilever. He also succeeded in the depositing and observing tethered lipid bilayer membranes of a biotinylated phospholipid on the single molecular avidin layer. These observation and characterization was achieved due to the atomically flat surface and well-controlled surface modification with biological materials. These results are very important for the modification and characterization of biological materials on silicon surface, which is an attractive research field for the development of new devices, biosensors and screening methods.

## Graduate Student Hino's Scientific Achievement

Miss Takami Hino, Graduate student of Department of Structural Molecular Science, School of Physical Sciences, the Graduate University for Advanced Studies received the Young Scientist Award for the Presentation of an Excellent Paper in the Annual Meeting of The Japan Society of Coordination Chemistry (2004 Autumn). Her title of paper was "Catalytic Oxidation of Alcohols Utilized by Acid-Base Equilibrium of Ruthenium-dioxolene-Amine Complexes." She constructed a new catalytic system composed of Ru-dioxolene-amino complexes and bases that catalyzes alcohols under very mild conditions such as electrolysis at 0 V. She also obtained the direct evidence that the oxidation of alcohols catalyzed by an Ru-dioxolene-aniline complex proceeds *via* a radical mechanism. The outcome that she obtained will give fundamental information about designing of molecular catalysts aimed at electrochemical oxidation of alcohol in fuel cells.

## Dr. Hiyama's Scientific Achievement

Research Associate Dr. Miyabi Hiyama of Department of Vacuum UV Photoscience has received the Society of Atomic Collision Research Award for Young Scientists 2005 for her contribution to "Molecular Inner-shell Excitation Mechanism revealed by the R-matrix/MQDT method," in the summer of 2005.

## Dr. Hiramatsu's Scientific Achievements

Dr. Hirotsugu Hiramatsu, a JSPS fellow in Okazaki Institute for Integrative Bioscience who moved to Tohoku University on September, 2005, received the 2005 William F. Meggers award for his publication entitled "Development of Infrared Electroabsorption Spectroscopy and Its Application to Molecular Structural Studies." [*Applied Spectroscopy* volume 58 number 4] This award is given to the authors of an outstanding paper appearing in *Applied Spectroscopy*. He developed a spectrometer that consists of dispersive IR spectrometer, low-noise MCT detector, AC coupled pre-amplifier, lock-in amplifier, and sample cell for electric field modulation, and realized an electroabsorption (Stark) spectroscopy in mid-IR region on liquid sample at room temperature. This equipment enabled him to detect of an absorbance change as small as  $6 \times 10^{-8}$  generated by electric field modulation. Accordingly, he succeeded in observing an electric field-dependent change of equilibrium between rotational isomers of 1,2-dichloroethane, and also in determining the permanent dipole moment of *N*-methylacetamide for each oligomer, besides finding electric field responses of some molecules. These studies provided a new method of investigating structural chemistry of liquid molecules, and demonstrated a potential of this fundamental spectroscopic approach.

## Research Associate Dr. Yamada's Achievement

Research Associate Dr. Yoichi M. A. Yamada of Research Center for Molecular-scale Nanoscience received the Pharmaceutical Society of Japan Award for Young Scientists 2005 for his contribution to "Development of New Solid-Phase Catalysts and Their Applications to Synthetic Organic Reactions."

This award is given to encourage young researchers in all the field of pharmaceutical sciences (Age up to 38). Dr. Yamada developed highly active and reusable polymeric catalysts produced by self-assembly process of non-cross-linked amphiphilic polymeric ligands with inorganic species. Thus, PWAA prepared from H<sub>3</sub>PW<sub>12</sub>O<sub>40</sub> and poly[(*N*-isopropylacrylamide)-*co*-(acrylamide with ammonium salt)] is suitable for oxidation of alcohols, amines, and sulfides in aqueous hydrogen peroxide. PdAS produced by self-organization of (NH<sub>4</sub>)<sub>2</sub>PdCl<sub>4</sub> and poly[(*N*-isopropylacrylamide)<sub>10</sub>-*co*-diphenylphosphinostyrene] is an excellent recyclable catalyst for Suzuki-Miyaura

reaction in water, water-organic solvents, and organic solvents. PdAS has been commercially supplied from Tokyo Kasei Kogyo (TCI) since 2003. PdAS-V assembled from  $(\text{NH}_4)_2\text{PdCl}_4$  and poly[(*N*-isopropylacrylamide)<sub>5</sub>-*co*-diphenylphosphinostyrene] provides recycling system of itself for Mizorogi-Heck reaction. TiSS made from  $\text{Ti}(\text{O}-i\text{-Pr})_4$  and poly(styryl-linked binaphtholate-*co*-styrene) promotes an enantioselective carbonyl-ene reaction as a recyclable catalyst.

## Professor Suzuki's Scientific Achievement

Professor Toshinori Suzuki, Chief Scientist of Chemical Dynamics Laboratory, RIKEN (Institute of Physical and Chemical Research), a former associate professor of Department of Electronic Structure, IMS, received the JSPS (Japan Society for the Promotion of Science) Prize in 2004 for his contribution to "Imaging of Chemical Reactions using Molecular Beam Scattering Method." This prize was founded in order to raise the level of scientific research in Japan to the world's highest standard and is given to young researchers who have rich creativity and superlative research ability.

He accomplished the visualization of motions of reacting molecules. Integrating the techniques of molecular beams, ultrafast laser spectroscopy and imaging, he realized for the first time the real-time tracking of rotational, vibrational and electronic states of reacting molecules and the imaging of three-dimensional product scattering distributions. He contributed to the elucidation of the quantum dynamics of chemical reactions. His method is expected to develop into versatile techniques applicable to investigations on the nano-scale reaction fields around solvated molecules and also on the vital phenomena.

## Dr. Tahara's Scientific Achievements

It is a great delight to report that the former associate professor of Department of Vacuum UV Photoscience, Dr. Tahei Tahara (1995–2001; currently, Chief Scientist of RIKEN) earned the IBM Japan Science Prize in 2004 for his contribution to "Development of Novel Time-Resolved Spectroscopy and its Application to Dynamics of Condensed-Phase Molecules."

He has been working as a frontier scientist in the research field of molecular photochemistry in condensed phase, by introducing various kinds of time-resolved spectroscopic techniques, based on his original ideas. He has made enormous efforts for research and development on novel experimental methods. Picosecond two-dimensional coherent anti-Stokes Raman scattering spectroscopy, femtosecond impulsive Raman spectroscopy, femtosecond UV-pump/visible-probe photoabsorption spectroscopy can be listed as his known examples. His continuous effort towards utilizing ultrafast molecular spectroscopy has led to successful observation of the excited state vibrational coherence. All his recent results shed light upon dynamics and structures of short-lived species that play an important role in the elementary process of chemical reactions.

# LIST OF PUBLICATIONS

## Department of Theoretical Studies

- J. LU, S. NAGASE, S. ZHANG and L. PENG**, "Counterion-Driven Spontaneous Polymerization of the Linear  $C_{60}^{n-}$  Chains in the *fcc* Fullerides and its Magic Number Behavior," *Chem. Phys. Lett.* **395**, 199–204 (2004).
- J. LU, S. NAGASE, D. YU, H. YE, R. HAN, Z. GAO, S. ZHANG and L. PENG**, "Amphoteric and Controllable Doping of Carbon Nanotubes by Encapsulation of Organic and Organometallic Molecules," *Phys. Rev. Lett.* **93**, 116804 (4 pages) (2004).
- Z. SLANINA, F. UHLIK, L. ADAMOWICZ, K. KOBAYASHI and S. NAGASE**, "Electronic Excited States and Stabilities of Fullerenes: Isomers of  $C_{78}$  and  $Mg@C_{72}$ ," *Int. J. Quantum Chem.* **100**, 610–616 (2004).
- Z. SLANINA, O. V. BOLTALINA, K. KOBAYASHI and S. NAGASE**, "B3LYP/6-31G\* Computations of  $C_{60}F_{36}$  (g) Isomers," *Fullerenes, Nanotubes, Carbon Nanostruct.* **12**, 691–695 (2004).
- Y. ISHIDA, A. SEKIGUCHI, K. KOBAYASHI and S. NAGASE**, "1,6,7-Trigermabicyclo[4.1.0]hept-3-en-7-yl: The Isolable Bicyclic Germyl Radical," *Organometallics* **23**, 4891–4896 (2004).
- K. SHIMADA, K. GOTO, T. KAWASHIMA, N. TAKAGI, Y. -K. CHOE and S. NAGASE**, "Isolation of a *Se*-Nitrososelenol: A New Class of Reactive Nitrogen Species Relevant to Protein *Se*-Nitrosation," *J. Am. Chem. Soc.* **126**, 13238–13239 (2004).
- J. LU, S. NAGASE, S. ZHANG and L. PENG**, "A New Approach to Simulate the Depolymerization Process of a Two-Dimensional Hexagonal  $C_{60}$  Polymer," *Chem. Phys. Lett.* **398**, 486–488 (2004).
- T. WAKAHARA, A. SAKURABA, Y. IIDUKA, M. OKAMURA, T. TSUCHIYA, Y. MAEDA, T. AKASAKA, S. OKUBO, T. KATO, K. KOBAYASHI, S. NAGASE and K. M. KADISH**, "Chemical Reactivity and Redox Property of  $Sc_3@C_{82}$ ," *Chem. Phys. Lett.* **398**, 553–556 (2004).
- T. TSUCHIYA, T. WAKAHARA, S. SHIRAKURA, Y. MAEDA, T. AKASAKA, K. KOBAYASHI, S. NAGASE, T. KATO and K. M. KADISH**, "Reduction of Endohedral Metallofullerenes: A Convenient Method for Isolation," *Chem. Mater.* **16**, 4343–4346 (2004).
- Y. MAEDA, S. KIMURA, Y. HIRASHIMA, M. KANDA, Y. LIAN, T. WAKAHARA, T. AKASAKA, T. HASEGAWA, H. TOKUMOTO, T. SHIMIZU, H. KATAURA, Y. MIYAUCHI, S. MARUYAMA, K. KOBAYASHI and S. NAGASE**, "Dispersion of Single-Walled Carbon Nanotube Bundles in Nonaqueous Solution," *J. Phys. Chem. B* **108**, 18395–18397 (2004).
- S. IWAMATSU, T. KUWAYAMA, K. KOBAYASHI, S. NAGASE and S. MURATA**, "Regioselective Carbon–Carbon Bond Cleavage of an Open-Cage Diketone Derivative of [60]Fullerene by Reaction with Aromatic Hydrazones," *Synthesis* 2962–2964 (2004).
- Z. SLANINA, L. ADAMOWICZ, K. KOBAYASHI and S. NAGASE**, "Gibbs Energy-Based Treatment of Metallofullerenes:  $Ca@C_{72}$ ,  $Ca@C_{74}$ ,  $Ca@C_{82}$ , and  $La@C_{82}$ ," *Mol. Sim.* **31**, 71–77 (2005).
- Y. MAEDA, J. MIYASHITA, T. HASEGAWA, T. WAKAHARA, T. TSUCHIYA, L. FENG, Y. LIAN, T. AKASAKA, K. KOBAYASHI, S. NAGASE, M. KAKO, K. YAMAMOTO and K. M. KADISH**, "Chemical Reactivities of the Cation and Anion of  $M@C_{82}$  ( $M = Y, La, \text{ and } Ce$ )," *J. Am. Chem. Soc.* **127**, 2143–2146 (2005).
- T. SASAMORI, E. MIEDA, N. NAGAHORA, N. TAKEDA, N. TAKAGI, S. NAGASE and N. TOKITOH**, "Systematic Studies on Redox Behavior of Homonuclear Double-Bond Compounds of Heavier Group 15 Elements," *Chem. Lett.* 166–167 (2005).
- M. YAMASHITA, Y. YAMAMOTO, K. -Y. AKIBA, D. HASHIZUME, F. IWASAKI, N. TAKAGI and S. NAGASE**, "Syntheses and Structures of Hypervalent Pentacoordinate Carbon and Boron Compounds Bearing an Anthracene Skeleton—Elucidation of Hypervalent Interaction Based on X-Ray Analysis and DFT Calculation," *J. Am. Chem. Soc.* **127**, 4354–4371 (2005).
- J. LU, S. NAGASE, Y. MAEDA, T. WAKAHARA, T. NAKAHODO, T. AKASAKA, D. YU, Z. GAO, R. HAN, and H. YE**, "Adsorption Configuration of  $NH_3$  on Single-Wall Carbon Nanotubes," *Chem. Phys. Lett.* **405**, 90–92 (2005).
- L. FENG, T. WAKAHARA, T. TSUCHIYA, Y. MAEDA, Y. LIAN, T. AKASAKA, N. MIZOROGI, K. KOBAYASHI, S. NAGASE and K. M. KADISH**, "Structural Characterization of  $Y@C_{82}$ ," *Chem. Phys. Lett.* **405**, 274–277 (2005).
- M. YAMADA, L. FENG, T. WAKAHARA, T. TSUCHIYA, Y. MAEDA, Y. LIAN, M. KAKO, T. AKASAKA, T. KATO, K. KOBAYASHI and S. NAGASE**, "Synthesis and Characterization of Exohedrally Silylated  $M@C_{82}$  ( $M = Y \text{ and } La$ )," *J. Phys. Chem. B* **109**, 6049–6051 (2005).
- K. -Y. AKIBA, Y. MORIYAMA, M. MIZOZOE, H. INOHARA, T. NISHII, Y. YAMAMOTO, M. MINOURA, D. HASHIZUME, F. IWASAKI, N. TAKAGI, K. ISHIMURA and S. NAGASE**, "Synthesis and Characterization of Stable Hypervalent Carbon Compounds (10-C-5) Bearing a 2,6-Bis(*p*-substituted phenyloxy-methyl)benzene Ligand," *J. Am. Chem. Soc.* **127**, 5893–5901 (2005).
- M. KATOUDA, M. KOBAYASHI, H. NAKAI and S. NAGASE**, "Practical Performance Assessment of Accompanying Coordinate Expansion Recurrence Relation Algorithm for Computation of Electron Repulsion Integrals," *J. Theor. Comput. Chem.* **4**, 139–149 (2005).
- T. TSUCHIYA, T. WAKAHARA, Y. MAEDA, T. AKASAKA, M. WAELCHLI, T. KATO, N. MIZOROGI, K. KOBAYASHI and S. NAGASE**, "2D NMR Characterization of the  $La@C_{82}$  Anion," *Angew. Chem., Int. Ed.* **44**, 3282–3285 (2005).

**S. IWAMATSU, S. MURATA, Y. ANDOH, M. MINOURA, K. KOBAYASHI, N. MIZOROGI and S. NAGASE**, "Open-Cage Fullerene Derivatives Suitable for the Encapsulation of a Hydrogen Molecule," *J. Org. Chem.* **70**, 4820–4825 (2005).

**Z. SLANINA, S. -H. LEE, L. ADAMOWICZ, F. UHLIK and S. NAGASE**, "Computed Structure and Energetics of  $\text{La@C}_{60}$ ," *Int. J. Quantum Chem.* **104**, 272–277 (2005).

**Y. RIKIISHI, Y. KASHINO, H. KUSAI, Y. TAKABAYASHI, E. KUWAHARA, Y. KUBOZONO, T. KAMBE, T. TAKENOBU, Y. IWASA, N. MIZOROGI, S. NAGASE and S. OKADA**, "Metallic Phase in the Metal-Intercalated Higher Fullerene  $\text{Rb}_{8,8(7)}\text{C}_{84}$ ," *Phys. Rev. B* **71**, 224118 (6 pages) (2005).

**J. LU, S. NAGASE, S. RE, X. ZHANG, D. YU, J. ZHANG, R. HAN, Z. GAO, H. YE, S. ZHANG and L. PENG**, "Interplay of Single-Wall Carbon Nanotubes and Encapsulated  $\text{La@C}_{82}$ ,  $\text{La}_2\text{@C}_{80}$ , and  $\text{Sc}_3\text{N@C}_{80}$ ," *Phys. Rev. B* **71**, 235417 (5 pages) (2005).

**J. LU, S. NAGASE, X. ZHANG, Y. MAEDA, T. WAKAHARA, T. NAKAHODO, T. TSUCHIYA, T. AKASAKA, D. YU, Z. GAO, R. HAN and H. YE**, "Structural Evolution of [2+1] Cycloaddition Derivatives of Single-Wall Carbon Nanotubes: From Open Structure to Closed Three-Membered Ring Structure with Increasing Tube Diameter," *THEOCHEM* **725**, 255–257 (2005).

**H. NIKAWA, T. KIKUCHI, T. WAKAHARA, T. NAKAHODO, T. TSUCHIYA, G. M. RAHMAN, T. AKASAKA, Y. MAEDA, K. YOZA, E. HORN, K. YAMAMOTO, N. MIZOROGI and S. NAGASE**, "Missing Metallofullerene  $\text{La@C}_{74}$ ," *J. Am. Chem. Soc.* **127**, 9684–9685 (2005).

**Y. IIDUKA, O. IKENAGA, A. SAKURABA, T. WAKAHARA, T. TSUCHIYA, Y. MAEDA, T. NAKAHODO, T. AKASAKA, M. KAKO, N. MIZOROGI and S. NAGASE**, "Chemical Reactivity of  $\text{Sc}_3\text{N@C}_{80}$  and  $\text{La}_2\text{@C}_{80}$ ," *J. Am. Chem. Soc.* **127**, 9956–9957 (2005).

**Y. MAEDA, S. KIMURA, M. KANDA, Y. HIRASHIMA, T. HASEGAWA, T. WAKAHARA, Y. LIAN, T. NAKAHODO, T. TSUCHIYA, T. AKASAKA, J. LU, X. ZHANG, Z. GAO, Y. YU, S. NAGASE, S. KAZAOUI, N. MINAMI, T. SHIMIZU, H. TOKUMOTO and R. SAITO**, "Large-Scale Separation of Metallic and Semiconducting Single-Walled Carbon Nanotubes," *J. Am. Chem. Soc.* **127**, 10287–10290 (2005).

**W. SONG, M. NI, J. LU, Z. GAO, S. NAGASE, D. YU, H. YE and X. ZHANG**, "Encapsulation of  $\text{La@C}_{82}$  and  $\text{La}_2\text{@C}_{80}$  inside Single-Walled Boron Nitride Nanotubes," *THEOCHEM* **730**, 119–122 (2005).

**H. KOKUBO and Y. OKAMOTO**, "Classification and Prediction of Low-Energy Membrane Protein Helix Configurations by Replica-Exchange Monte Carlo Method," *J. Phys. Soc. Jpn.* **73**, 2571–2585 (2004).

**A. MITSUTAKE, M. KINOSHITA, Y. OKAMOTO and F. HIRATA**, "Combination of the Replica-Exchange Monte Carlo Method and the Reference Interaction Site Model Theory for Simulating a Peptide Molecule in Aqueous Solution," *J. Phys. Chem. B* **108**, 19002–19012 (2004).

**H. OKUMURA and Y. OKAMOTO**, "Liquid-Gas Phase Transitions Studied by Multibaric-Multithermal Monte Carlo Simulations," *J. Phys. Soc. Jpn.* **73**, 3304–3311 (2004).

**S. G. ITOH and Y. OKAMOTO**, "Multi-Overlap Molecular Dynamics Methods for Biomolecular Systems," *Chem. Phys. Lett.* **400**, 308–313 (2004).

**H. OKUMURA and D. M. HEYES**, "Comparisons between a Molecular Dynamics and Hydrodynamics Treatment of Non-Stationary Thermal Processes in a Liquid," *Phys. Rev. E* **70**, 061206 (11 pages) (2004).

**T. YODA, Y. SUGITA and Y. OKAMOTO**, "Secondary-Structure Preferences of Force Fields for Proteins Evaluated by Generalized-Ensemble Simulations," *Chem. Phys.* **307**, 269–283 (2004).

**H. OKUMURA and Y. OKAMOTO**, "Monte Carlo Simulations in New Generalized Isobaric-Isothermal Ensemble," *Trans. Mater. Res. Soc.-J.* **29**, 3783–3786 (2004).

**A. MITSUTAKE, Y. SUGITA and Y. OKAMOTO**, "Generalized-Ensemble Monte Carlo Algorithms for Simulations of Proteins," *AIP Conference Proceedings Volume 708: SLOW DYNAMICS IN COMPLEX SYSTEMS*, M. Tokuyama and I. Oppenheim, Eds., American Institute of Physics; Melville, pp. 350–351 (2004).

**Y. TANIMURA, K. AOI, T. HIROYASU, M. MIKI, Y. OKAMOTO and J. DONGARRA**, "Implementation of Protein Tertiary Structure Prediction System with NetSolve," *Proceedings of the 7th International Conference on High Performance Computing and Grid in Asia Pacific Region*, 320–327 (2004).

**H. OKUMURA and Y. OKAMOTO**, "Multibaric-Multithermal Ensemble Simulation for Simple Liquids," *Mol. Sim.* **30**, 847–852 (2004).

**H. KAMISAKA, O.I.TOLSTIKHIN and H. NAKAMURA**, "Full Quantum Dynamics of Atom-Diatom Chemical Reactions in Hyperspherical Elliptic Coordinates," *J. Phys. Chem. A* **108**, 8827–8839 (2004).

**K. YAGI, G. V. MIL'NIKOV, T. TAKETSUGU, K. HIRAO and H. NAKAMURA**, "Effect of Out-Of-Plane Vibration on the Hydrogen Atom Transfer Reaction in Malonaldehyde," *Chem. Phys. Lett.* **397**, 435–440 (2004).

**Y. ZHAO, G. V. MIL'NIKOV and H. NAKAMURA**, "Evaluation of Canonical and Microcanonical Non-adiabatic Reaction Rate Constants by Using the Zhu-Nakamura Formulas," *J. Chem. Phys.* **121**, 8854–8860 (2004).

**A. ISHKHANYAN, G. P. CHERNIKOV and H. NAKAMURA**, "Rabi Dynamics of Coupled Atomic and Molecular Bose-Einstein Condensates," *Phys. Rev. A* **70**, 053611 (9 pages) (2004).

**A. KONDORSKIY and H. NAKAMURA**, "Semiclassical Frozen Gaussian Propagation Method for Electronically Nonadiabatic Chemical Dynamics: Møller Operator Formulation and Incorporation of the Zhu-Nakamura Theory," *J. Theor. Comput. Chem.* **4**, 89–102 (2005).

- A. KONDORSKIY and H. NAKAMURA**, "Semiclassical Formulation of Optimal Control Theory," *J. Theor. Comput. Chem.* **4**, 75–87 (2005).
- H. TAMURA, S. NANBU, H. NAKAMURA and T. ISHIDA**, "A Theoretical Study of Cyclohexadiene/Hexatriene Photochemical Interconversion: Multireference Configuration Interaction Potential Energy Surfaces and Transition Probabilities for the Radiationless Decays," *Chem. Phys. Lett.* **401**, 487 (2005).
- S. ZOU, A. KONDORSKIY, G. V. MIL'NIKOV and H. NAKAMURA**, "Laser Control of Electronic Transitions of Wave Packet by Using Quadratically Chirped Pulses," *J. Chem. Phys.* **122**, 084112 (2005).
- H. NAKAMURA**, "Nonadiabatic Transition and Chemical Dynamics: Multi-Dimensional Tunneling Theory and Applications of the Zhu-Nakamura Theory," *J. Theor. Comput. Chem.* **4**, 127–137 (2005).
- A. ISHKHANYAN, J. JAVANAINEN and H. NAKAMURA**, "A Basic Two-State Model for Bosonic Field Theories with a Cubic Nonlinearity," *J. Phys. A* **38**, 3505–3516 (2005).
- G. V. MIL'NIKOV and H. NAKAMURA**, "Instanton Theory for the Tunneling Splitting of Low Vibrationally Excited States," *J. Chem. Phys.* **122**, 124311 (11 pages) (2005).
- G. V. MIL'NIKOV, O. KÜHN and H. NAKAMURA**, "Ground State and Vibrationally Assisted Tunneling in the Formic Acid Dimer," *J. Chem. Phys.* **123**, 074308 (9 pages) (2005).
- K. NOBUSADA and K. YABANA**, "High-Order Harmonic Generation from Silver Clusters: Laser-Frequency Dependence and the Screening Effect of *d* Electrons," *Phys. Rev. A* **70**, 043411 (7 pages) (2004).
- K. NOBUSADA**, "Electronic Structure and Photochemical Properties of a Monolayer-Protected Gold Cluster," *J. Phys. Chem. B* **108**, 11904–11908 (2004).
- K. SHIRATORI, K. NOBUSADA and K. YABANA**, "Multiple Ionization of a Silver Diatomic Molecule in an Intense Laser Field," *Chem. Phys. Lett.* **404**, 365–369 (2005).
- Y. NEGISHI, K. NOBUSADA and T. TSUKUDA**, "Glutathione-Protected Gold Clusters Revisited: Bridging the Gap between Gold(I)-Thiolate Complexes and Thiolate-Protected Gold Nanocrystals," *J. Am. Chem. Soc.* **127**, 5261–5270 (2005).
- A. MITSUTAKE, M. KINOSHITA, Y. OKAMOTO and F. HIRATA**, "Combination of the Replica-Exchange Monte Carlo Method and the Reference Interaction Site Model Theory for Simulating a Peptide Molecule in Aqueous Solution," *J. Phys. Chem. B* **108**, 19002–19012 (2004).
- I. OMEL'YAN, A. KOVALENKO and F. HIRATA**, "Microscopic Description of a Liquid-Vapor Interface by an Inhomogeneous Integral Equation Theory," *Chem. Phys. Lett.* **397**, 368–373 (2004).
- T. IMAI and F. HIRATA**, "Hydrophobic Effects on Partial Molar Volume," *J. Chem. Phys.* **122**, 94509 (2005).
- A. KOBRYN, T. YAMAGUCHI and F. HIRATA**, "Pressure Dependence of Diffusion and Orientational Relaxation Time for Acetonitrile and Methanol in Water: RISM/Mode-Coupling Study," *J. Mol. Liq.* **119**, 7–13 (2005).
- K. NISHIYAMA, T. YAMAGUCHI, F. HIRATA and T. OKADA**, "Solvation Dynamics in Water Investigated by RISM/Mode-Coupling Theory," *J. Mol. Liq.* **119**, 63–66 (2005).
- T. IMAI, A. KOVALENKO and F. HIRATA**, "Partial Molar Volume of Proteins Studied by the Three-Dimensional Reference Interaction Site Model Theory," *J. Phys. Chem. B* **109**, 6658–6665 (2005).
- A. KOBRYN, T. YAMAGUCHI and F. HIRATA**, "Site-Site Memory Equation Approach in Study of Density/Pressure Dependence of Translational Diffusion Coefficient and Rotational Relaxation Time of Polar Molecular Solutions: Acetonitrile in Water, Methanol in Water, and Methanol in Acetonitrile," *J. Chem. Phys.* **122**, 184511–184524 (2005).
- A. KOVALENKO and F. HIRATA**, "A Molecular Theory of Liquid Interface," *Phys. Chem. Chem. Phys.* **7**, 1785–1793 (2005).
- T. IMAI, T. TAKEKIYO, A. KOVALENKO, F. HIRATA, M. KATO and Y. TANIGUCHI**, "Theoretical Study of Conformational Changes Associated with the Helix-Coil Transition of an Alanine-Rich Peptide in Aqueous Solutions," *Biopolymers* **79**, 97–105 (2005).
- K. YONEMITSU**, "Phase Transition in a One-Dimensional Extended Peierls-Hubbard Model with a Pulse of Oscillating Electric Field: I. Threshold Behavior in Ionic-to-Neutral Transition," *J. Phys. Soc. Jpn.* **73**, 2868–2878 (2004).
- K. YONEMITSU**, "Phase Transition in a One-Dimensional Extended Peierls-Hubbard Model with a Pulse of Oscillating Electric Field: II. Linear Behavior in Neutral-to-Ionic Transition," *J. Phys. Soc. Jpn.* **73**, 2879–2886 (2004).
- K. YONEMITSU**, "Phase Transition in a One-Dimensional Extended Peierls-Hubbard Model with a Pulse of Oscillating Electric Field: III. Interference Caused by a Double Pulse," *J. Phys. Soc. Jpn.* **73**, 2887–2893 (2004).
- K. YONEMITSU**, "Theory of Photoinduced Phase Dynamics in Organic Charge-Transfer Complexes," *J. Lumin.* **112**, 279–282 (2005).
- N. MAESHIMA, K. OKUNISHI, K. OKAMOTO and T. SAKAI**, "Frustration-Induced  $\eta$  Inversion in the  $S = 1/2$  Bond-Alternating Spin Chain," *Phys. Rev. Lett.* **93**, 127203 (4 pages) (2004).
- N. MAESHIMA, K. OKUNISHI, K. OKAMOTO, T. SAKAI and K. YONEMITSU**, "Field-Induced Phase Transitions and Long-Range Orders in the  $S = 1/2$  Spin Bond-Alternating Chain with Frustrating Interaction," *J. Phys. Soc. Jpn.* **74**, Suppl. 63–66 (2005).

**M. INDERGAND, Y. YAMASHITA, H. KUSUNOSE and M. SIGRIST**, “Effective Interaction between the Interpenetrating Kagome Lattices in  $\text{Na}_x\text{CoO}_2$ ,” *Phys. Rev. B* **71**, 214414 (19 pages) (2005).

**K. UEDA and Y. YAMASHITA**, “Magnetism in Strongly Correlated and Frustrated Systems,” *Physica B* **359**, 626–632 (2005).

**T. NAKAJIMA and G. BUICA**, “Modification of the Photoelectron Angular Distribution through Laser-Induced Continuum Structure,” *Phys. Rev. A* **71**, 013413 (2005).

**T. NAKAJIMA**, “Control of the Spin-Polarization of Photoelectrons/Photoions Using Short Laser Pulses,” in *Ultrafast Phenomena in Semiconductors and Nanosctrucure Materials IX*, Kong-Thon Tsen, Jin-Joo Song and HongXing Jiang, Eds., Proc. SPIE Int. Soc. Opt. Eng. **5725**, 169–179 (2005).

### Department of Molecular Structure

**K. IMURA, T. NAGAHARA and H. OKAMOTO**, “Plasmon Mode Imaging of Single Gold Nanorods,” *J. Am. Chem. Soc.* **126**, 12730–12731 (2004).

**K. IMURA, T. NAGAHARA and H. OKAMOTO**, “Imaging of Surface Plasmon and Ultrafast Dynamics in Gold Nanorods by Near-Field Microscopy,” *J. Phys. Chem. B* **108**, 16344–16347 (2004).

**T. NAGAHARA, K. IMURA and H. OKAMOTO**, “Near-Field Spectroscopy of Water-Soluble and Water-Insoluble Porphyrin J-Aggregates,” *Scanning* **26** (Suppl. I), 10–15 (2004).

**T. NAGAHARA, K. IMURA and H. OKAMOTO**, “Time-Resolved Scanning Near-Field Optical Microscopy with Supercontinuum Light Pulses Generated in Microstructure Fiber,” *Rev. Sci. Instrum.* **75**, 4528–4533 (2004).

**K. IMURA, T. NAGAHARA and H. OKAMOTO**, “Characteristic Near-Field Spectra of Single Gold Nanoparticles,” *Chem. Phys. Lett.* **400**, 500–505 (2004).

**K. IMURA, T. NAGAHARA and H. OKAMOTO**, “Near-Field Optical Imaging of Plasmon Modes in Gold Nanorods,” *J. Chem. Phys.* **122**, 154701 (2005).

**K. IMURA, T. NAGAHARA and H. OKAMOTO**, “Near-Field Two-Photon Induced Photoluminescence from Single Gold Nanorods and Imaging of Plasmon Modes,” *J. Phys. Chem. B* **109**, 13214–13220 (2005).

**J. K. LIM, K. IMURA, T. NAGAHARA, S. K. KIM and H. OKAMOTO**, “Imaging and Dispersion Relations of Surface Plasmon Modes in Silver Nanorods by Near-Field Spectroscopy,” *Chem. Phys. Lett.* **412**, 41–45 (2005).

**T. NOMOTO, T. ISHIBASHI, H. OKAMOTO and H. HAMAGUCHI**, “Structure of the  $S_1$  State of Diphenylacetylene as Studied by Time-Resolved CARS and Infrared Spectroscopy,” *J. Mol. Struct.* **735-736**, 197–202 (2005).

**T. NAGAHARA, K. IMURA and H. OKAMOTO**, “Pump-Probe Near-Field Optical Microscopy of Molecular Aggregates Using Supercontinuum,” in *Ultrafast phenomena XIV*, T. Kobayashi, T. Okada, T. Kobayashi, K. A. Nelson and S. De Silvestri, Eds., Springer-Verlag; Berlin, pp. 434–436 (2005).

**K. IMURA, T. NAGAHARA and H. OKAMOTO**, “Ultrafast Near-Field Microscope Imaging of Electron and Phonon Relaxation in Single Gold Nanoparticle,” in *Ultrafast phenomena XIV*, T. Kobayashi, T. Okada, T. Kobayashi, K. A. Nelson, and S. De Silvestri, Eds., Springer-Verlag; Berlin, pp. 655–657 (2005).

**Y. MORIWAKI and N. MORITA**, “Laser Spectroscopic Investigation of Ca Atoms in Liquid Helium—Comparison between Spectral Properties for Liquid Helium-3 and Helium-4,” *Eur. Phys. J. D* **33**, 323–327 (2005).

**Y. HOU, H. KONDOH, T. KOGURE and T. OHTA**, “Preparation and Characterization of Highly Monodisperse FePd Nanoparticles,” *Chem. Mater.* **16**, 5149 (2004).

**K. TONO, T. TERASAKI, T. OHTA and T. KONDOW**, “Electronic Structure of  $\text{Mn}_2\text{O}^-$ : Ferromagnetic Spin Coupling Stabilized by Oxidation,” *Chem. Phys. Lett.* **388**, 374–378 (2004).

**I. NAKAI, H. KONDOH, K. AMEMIYA, M. NAGASAKA, A. NAMBU, T. SHIMADA and T. OHTA**, “Reaction-Path Switching Induced by Spatial-Distribution Change of Reactants: CO Oxidation on Pt(111),” *J. Chem. Phys.* (Comm.) **121**, 5035–5038 (2004).

**H. KONDOH, A. NAMBU, Y. EHARA, F. MATSUI, T. YOKOYAMA and T. OHTA**, “Substrate Dependence of Self-Assembly of Alkanethiol: X-Ray Absorption Fine Structure,” *J. Phys. Chem. B* **108**, 12946–12954 (2004).

**K. AMEMIYA, D. MATSUMURA, H. ABE, S. KITAGAWA, T. OHTA and T. YOKOYAMA**, “Direct Observation of an Oscillatory Behavior in the Surface Magnetization of Fe Thin Films Grown on a Ni/Cu(100) Film,” *Phys. Rev. B* **70**, 195405 (6 pages) (2004).

**Y. HOU, H. KONDOH, T. OHTA and S. GAO**, “Size-Controlled Synthesis of Nickel Nanoparticles,” *Appl. Surf. Sci.* **241**, 218–222 (2005).

**Y. NAKAYAMA, H. KONDOH and T. OHTA**, “Nanometer-Scale Mapping of Local Work Function with a Photon-Assisted STM Technique,” *Appl. Surf. Sci.* **241**, 18–22 (2005).

**Y. HOU, H. KONDOH and T. OHTA**, “Self-Assembly of Co Nanoplatelets into Spheres: Synthesis and Characterization,” *Chem. Mater.* **17**, 3994–3996 (2005).

**T. SHIMADA, H. KONDOH, I. NAKAI, M. NAGASAKA, R. YOKOTA and T. OHTA**, “Structure of Hexanethiol,  $n\text{-C}_6\text{H}_{13}\text{SH}$ , “Striped” Phase on Au(111),” *Chem. Phys. Lett.* **406**, 232–236 (2005).

- M. NAGASAKA, H. KONDOH, I. NAKAI and T. OHTA**, "Oxygen Island Formation on Pt(111) Studied by Dynamic Monte Carlo Simulation," *J. Chem. Phys.* **122**, 044715 (2005).
- M. NAGASAKA, H. KONDOH and T. OHTA**, "Water Formation Reaction on Pt(111); Role of the Proton Transfer," *J. Chem. Phys.* **122**, 204704 (2005).
- I. NAKAI, H. KONDOH, K. AMEMIYA, M. NAGASAKA, T. SHIMADA, R. YOKOTA, A. NAMBU and T. OHTA**, "Mechanism of the CO Oxidation Reaction on O-Pre-Covered Pt(111) Surfaces Studied with Near Edge X-Ray Absorption Fine Structure Spectroscopy," *J. Chem. Phys.* **122**, 134709 (2005).
- K. AMEMIYA, D. MATSUMURA, H. ABE, S. KITAGAWA, T. YOKOYAMA and T. OHTA**, "Direct Observation of Surface and Interface Magnetism with the Probing-Depth Dependent X-Ray Magnetic Circular Dichroism," *J. Electron Spectrosc. Relat. Phenom.* **144-147**, 689–693 (2005).
- Y. HOU, H. KONDOH, M. SHIMOJO, E. O. SAKO, N. OZAKI, T. KOGURE and T. OHTA**, "Inorganic Nanocrystals Self-Assembly via the Inclusion Interaction of  $\beta$ -Cyclodextrins; Toward 3D Spherical Magnetite," *J. Phys. Chem. B* **109**, 4845–4852 (2005).
- T. NAKAMURA, T. MIYAMAE, I. NAKAI, H. KONDOH, T. KAWAMOTO, N. KOBAYASHI, S. YASUDA, D. YOSHUMURA, T. OHTA, H. NOZOYE and M. MATSUMOTO**, "Adsorption States of Dialkyl Ditelluride Autooxidized Monolayers on Au(111)," *Langmuir* **21**, 3344–3353 (2005).
- H. KONDOH, K. AMEMIYA, I. NAKAI, M. NAGASAKA, A. NAMBU, T. SHIMADA, T. YOKOYAMA and T. OHTA**, "Energy-Dispersive Near-Edge X-Ray Absorption Fine Structure: A New Technique to Study Dynamic Surface Process," *Phys. Scr.* **T115**, 88–92 (2005).
- D. MATSUMURA, K. AMEMIYA, S. KITAGAWA, T. OHTA and T. YOKOYAMA**, "CO Induced Spin Reorientation Transition of Co/Pd(111) Studied by XMCD and XPS," *Phys. Scr.* **T115**, 583–585 (2005).
- K. OKAMOTO, K. KOHDATE, K. NAGAI, J. MIYAWAKI, H. KONDOH, T. YOKOYAMA, A. NOJIMA and T. OHTA**, "Light-Modulated XAFS Spectroscopy for Photo-Induced Structural Changes," *Phys. Scr.* **T115**, 1050–1052 (2005).
- K. AMEMIYA, S. KITAGAWA, T. YOKOYAMA, D. MATSUMURA, H. ABE, H. WATANABE and T. OHTA**, "Direct Observation of Magnetic Depth Profile with a Depth-Resolved X-Ray Magnetic Dichroism Technique," *Phys. Scr.* **T115**, 1035–1037 (2005).
- K. AMEMIYA, E. SAKAI, D. MATSUMURA, H. ABE, T. OHTA and T. YOKOYAMA**, "Spin Reorientation Transition of Ni/Cu(100) and CO/Ni/Cu(100): Separation of the Surface and Bulk Components of the X-Ray Magnetic Circular Dichroism Spectrum," *Phys. Rev. B* **71**, 214420 (2005).
- H. KONDOH, A. NAMBU, Y. EHARA, F. MATSUI, T. YOKOYAMA and T. OHTA**, "Substrate Dependence of Self-Assembly of Alkanethiol: X-Ray Absorption Fine Structure Study," *J. Phys. Chem. B* **108**, 12946–12954 (2004).
- H. HACHISUKA, K. AWAGA and T. YOKOYAMA**, "Structure and Magnetic Properties of the Single-Molecule Magnet  $[\text{Mn}_{11}\text{CrO}_{12}(\text{O}_2\text{CCH}_3)_{16}(\text{H}_2\text{O})_4]\cdot 2\text{CH}_3\text{COOH}\cdot 4\text{H}_2\text{O}$ : Magnetization Manipulation and Dipolar-Biased Tunneling in a  $\text{Mn}_{11}\text{Cr}/\text{Mn}_{12}$  Mixed Crystal," *Phys. Rev. B* **70**, 104427 (2004).
- S. SHIMIZU, V. G. ANAND, R. TANIGUCHI, K. FURUKAWA, T. KATO, T. YOKOYAMA and A. OSUKA**, "Biscopper Complexes of Meso-Aryl-Substituted Hexaphyrin: Gable Structures and Varying Antiferromagnetic Coupling," *J. Am. Chem. Soc.* **126**, 12280–12281 (2004).
- K. AMEMIYA, D. MATSUMURA, H. ABE, S. KITAGAWA, T. OHTA and T. YOKOYAMA**, "Direct Observation of Oscillatory Behavior in the Surface Magnetization of Fe Thin Films Grown on a Ni/Cu(100) Film," *Phys. Rev. B* **70**, 195405 (2004).
- D. MATSUMURA, T. YOKOYAMA, K. AMEMIYA, S. KITAGAWA and T. OHTA**, "CO Induced Spin Reorientation Transition of Co/Pd(111) Studied by XMCD and XPS," *Phys. Scr.* **T115**, 583–585 (2005).
- K. AMEMIYA, S. KITAGAWA, T. YOKOYAMA, D. MATSUMURA, H. ABE, H. WATANABE and T. OHTA**, "Direct Observation of Magnetic Depth Profile with a Depth-Resolved X-Ray Magnetic Dichroism Technique," *Phys. Scr.* **T115**, 1035–1037 (2005).
- T. NAKAGAWA, H. WATANABE and T. YOKOYAMA**, "Opposite Spin Reorientation Transitions Driven by a Magnetic Orbital Moment: Ultrathin Ni Films on Cu Surfaces," *Phys. Rev. B* **71**, 235403 (2005).
- M. MITSUMI, H. GOTO, S. UMEBAYASHI, Y. OZAWA, M. KOBAYASHI, T. YOKOYAMA, H. TANAKA, S. KURODA and K. TORIUMI**, "A Neutral Mixed-Valent Conducting Polymer Formed by Electron Transfer between Metal  $d$  and Ligand  $\pi$  Orbitals," *Angew. Chem., Int. Ed.* **117**, 4164–4168 (2005).

#### Department of Electronic Structure

- C. OKABE, T. NAKABAYASHI, Y. INOKUCHI, N. NISHI and H. SEKIYA**, "Ultrafast Excited-State Dynamics in Photochromic *N*-Salicylideneaniline Studied by Femtosecond Time-Resolved REMPI Spectroscopy," *J. Chem. Phys.* **121**, 9436–9422 (2004).
- H. MACHINAGA, K. OHASHI, Y. INOKUCHI, N. NISHI and H. SEKIYA**, "Infrared Photodissociation Spectra and Solvation Structure of  $\text{Mg}^+(\text{CH}_3\text{OH})_n$  ( $n = 1-4$ )," *Chem. Phys. Lett.* **391**, 85–90 (2004).
- K. OHASHI, K. TERANOBU, Y. INOKUCHI, Y. MUNE, H. MACHINAGA, N. NISHI and H. SEKIYA**, "Infrared Photodissociation Spectroscopy of  $\text{Mg}^+(\text{NH}_3)_n$  ( $n = 3-6$ ): Direct Coordination or Solvation through Hydrogen Bonding," *Chem. Phys. Lett.* **393**, 264–270 (2004).

**A. HARA, Y. KOMOTO, K. SAKOTA, R. MIYOSHI, Y. INOKUCHI, K. OHASHI, K. KUBO, E. YAMAMOTO, A. MORI, N. NISHI and H. SEKIYA**, “Electronic Spectra of Jet-Cooled 3-Methyl-7-Azaindole Dimer. Symmetry of the Lowest Excited Electronic State and Double-Proton Transfer,” *J. Phys. Chem. A* **108**, 10789–10793 (2004).

**A. MURAOKA, Y. INOKUCHI, N. NISHI and T. NAGATA**, “Structure of  $[(\text{CO}_2)_n(\text{H}_2\text{O})_m]^-$  ( $n = 1-4, m = 1,2$ ) Cluster Anions. 1. Infrared Photodissociation Spectroscopy,” *J. Chem. Phys.* **122**, 094303 (2005).

**K. WATANABE, A. KOKAJI, Y. INOKUCHI, I. RZEZNICKA, K. OHSHIMO, N. NISHI and T. MATSUSHIMA**, “Orientation of Nitrous Oxide on Palladium (110) by STM,” *Chem. Phys. Lett.* **406**, 474–478 (2005).

**K. SAKOTA, C. OKABE, N. NISHI and H. SEKIYA**, “Excited State Double Proton Transfer in the 7-Azaindole Dimer in the Gas Phase. 3. Reaction Mechanism Studied by Picosecond Time-Resolved REMPI Spectroscopy,” *J. Phys. Chem. A* **109**, 5245–5247 (2005).

**J. NISHIJO, C. OKABE, J. BUSHIRI, K. KOSUGI, N. NISHI and H. SAWA**, “Formation of Carbon-Encapsulated Metallic Nano-Particles from Metal Acetylides by Electron Beam Irradiation,” *Eur. Phys. J. D* **34**, 219–222 (2005).

**S. -Y. LEE, B. -H. BOO, H. -K. KANG, D. KANG, K. JUDAI, J. NISHIJO and N. NISHI**, “Reexamination of the Structures and Energies of  $\text{Li}_2\text{C}_2$  and  $\text{Li}_4\text{C}_4$ ,” *Chem. Phys. Lett.* **411**, 484–491 (2005).

**R. KANYA and Y. OHSHIMA**, “Pendular-Limits Representation of Energy Levels and Spectra of Symmetric- and Asymmetric-Top Molecules,” *Phys. Rev. A* **70**, 013403 (19 pages) (2004).

**R. KANYA and Y. OHSHIMA**, “Pendular-State Spectroscopy of the  $S_1-S_0$  Transition of 9-Cyanoanthracene,” *J. Chem. Phys.* **121**, 9489–9497 (2004).

**Y. OHSHIMA, K. SATO, Y. SUMIYOSHI and Y. ENDO**, “Rotational Spectrum and Hydrogen Bonding of the  $\text{H}_2\text{O}-\text{HO}$  Radical Complex,” *J. Am. Chem. Soc.* **127**, 1108–1109 (2005).

**Y. MATSUSHITA, T. SUZUKI, T. ICHIMURA and T. HIKITA**, “Cavity Size Effect on the Excited State Dynamics of Methyl 4-(Dimethylamino)benzoate-Cyclodextrin Complexes,” *J. Phys. Chem. A* **108**, 7490–7496 (2004).

**Y. HARADA, S. WATANABE, T. SUZUKI and T. ICHIMURA**, “Photochemical Reaction Dynamics of 9,10-Phenanthrenequinone and 1,2-Naphthoquinone with Hydrogen Donors in Solution,” *J. Photochem. Photobiol., A* **170**, 161–167 (2004).

**R. MATSUMOTO, K. SAKEDA, Y. MATSUSHITA, T. SUZUKI and T. ICHIMURA**, “Spectroscopy and Relaxation Dynamics of Photoexcited Anisole and Anisole- $d_3$  Molecules in a Supersonic Jet,” *J. Mol. Struct.* **735–736**, 153–167 (2005).

**R. MATSUMOTO, T. SUZUKI and T. ICHIMURA**, “Internal Rotational Motion of the Chloromethyl Group of Jet-Cooled Benzyl Chloride Molecule,” *J. Phys. Chem. A* **109**, 3331–3336 (2005).

**M. ANDO, S. YOSHIKE, T. SUZUKI, T. ICHIMURA, T. OKUTSU, M. UEDA, H. HORIUCHI, H. HIRATSUKA, A. KAWAI and K. SHIBUYA**, “Evidence of Phenoxyethyl Radical Formation in Laser Photolysis of Anisole in Solution,” *J. Photochem. Photobiol., A* **174**, 194–198 (2005).

**T. ISOZAKI, K. SAKEDA, T. SUZUKI, T. ICHIMURA, K. TSUJI and K. SHIBUYA**, “Evidence for Non-Planar Conformer and Conformational Isomerization of *o*-Fluoroanisole in Low-Temperature Ar Matrix,” *Chem. Phys. Lett.* **409**, 93–97 (2005).

**T. ICHIMURA**, “Production and Excited State Dynamics of Photo-Rearranged Isomer of Benzyl Chloride and Its Methyl Derivatives Studied by Stepwise Two-Color Laser Excitation Transient Absorption and Time-Resolved Thermal Lensing Techniques,” *J. Phys. Chem.* **109**, 5825–5831 (2005).

**O. NAKAGOE, K. WATANABE, N. TAKAGI and Y. MATSUMOTO**, “In-Situ Observation of CO Oxidation on  $\text{Ag}(110)(2\times 1)-\text{O}$  by Scanning Tunneling Microscopy: Structural Fluctuation and Catalytic Activity,” *J. Phys. Chem. B* **109**, 14536–14543 (2005).

**D. INO, K. WATANABE, N. TAKAGI and Y. MATSUMOTO**, “The Electronic Structure and Femtosecond Electron Transfer Dynamics at Noble Metal/Tris-(8-Hydroxyquinoline) Aluminum Interfaces,” *Phys. Rev. B* **71**, 115427 (2005).

**K. WATANABE, N. TAKAGI and Y. MATSUMOTO**, “Mode-Selective Excitation of Coherent Surface Phonons on Alkali-Covered Metal Surfaces,” *Phys. Chem. Chem. Phys.* **7**, 2697–2700 (2005).

**M. NISHIJIMA, H. OKUYAMA, N. TAKAGI, T. ARUGA and W. BREINIG**, “Quantum Delocalization of Hydrogen on Metal Surfaces,” *Surf. Sci. Rep.* **57**, 113–156 (2005).

#### Department of Molecular Assemblies

**T. YAMAMOTO, M. URUICHI, K. YAKUSHI, J. YAMAURA and H. TAJIMA**, “Infrared and Raman Evidence for the Charge-Ordering in  $\beta''$ -(BEDT-TTF) $_3(\text{ReO}_4)_2$ ,” *Phys. Rev. B* **70**, 125102 (11 pages) (2004).

**K. YAMAMOTO, K. YAKUSHI, M. MENEGHETTI and C. PECILE**, “Bond and Charge Density Waves in the Charge Localized Phase of  $(\text{DI-DCNQI})_2\text{Ag}$  Studied by Single-Crystal Infrared and Raman Spectra,” *Phys. Rev. B* **71**, 045118 (10 pages) (2005).

- M. MAKSIMUK, K. YAKUSHI, H. TANIGUCHI, K. KANODA and A. KAWAMOTO**, "Influence of the Cooling Rate on Low-Temperature Raman and Infrared-Reflection Spectra of Partially Deuterated  $\kappa$ -(BEDT-TTF)<sub>2</sub>Cu[N(CN)<sub>2</sub>]Br," *Synth. Met.* **149**, 13–18 (2005).
- R. SWIETLIK, K. YAKUSHI, K. YAMAMOTO, T. KAWAMOTO and T. MORI**, "Infrared and Raman Studies of the Phase Transition in the Organic Conductor (TTM-TTP)I<sub>3</sub>," *Synth. Met.* **150**, 83–92 (2005).
- T. YAMAMOTO, M. URUICHI, K. YAMAMOTO, K. YAKUSHI, A. KAWAMOTO and H. TANIGUCHI**, "Examination of the Charge Sensitive Vibrational Modes in ET Molecule," *J. Phys. Chem. B* **109**, 15226–15235 (2005).
- A. F. BANGURA, A. I. COLDEA, J. SINGLETON, A. ARDAVAN, A. AKUTSU-SATO, H. AKUTSU, S. S. TURNER, P. DAY, T. YAMAMOTO and K. YAKUSHI**, "The Robust Superconducting State in the Low-Quasiparticle-Density Organic Metals  $\beta$ "-(BEDT-TTF)<sub>4</sub>[(H<sub>3</sub>O)M(C<sub>2</sub>O<sub>4</sub>)<sub>3</sub>]Y; Superconductivity due to Proximity to a Charge-Ordered State," *Phys. Rev. B* **72**, 014543 (13 pages) (2005).
- S. FUJIYAMA and T. NAKAMURA**, "Charge Disproportionation in (TMTTF)<sub>2</sub>SCN Observed by <sup>13</sup>C NMR," *Phys. Rev. B* **70**, 045102 (6 pages) (2004).
- T. SEKINE, N. SATOH, M. NAKAZAWA and T. NAKAMURA**, "Sliding Spin-Density Wave of (TMTSF)<sub>2</sub>PF<sub>6</sub> Studied with Narrow-Band Noise," *Phys. Rev. B* **70**, 214201 (13 pages) (2004).
- R. CHIBA, K. HIRAKI, T. TAKAHASHI, H. M. YAMAMOTO and T. NAKAMURA**, "Extremely Slow Charge Fluctuations in the Metallic State of the Two-Dimensional Molecular Conductor  $\theta$ -(BEDT-TTF)<sub>2</sub>RbZn(SCN)<sub>4</sub>," *Phys. Rev. Lett.* **93**, 216405 (4 pages) (2004).
- S. SHIMIZU, V. G. ANAND, R. TANIGUCHI, K. FURUKAWA, T. KATO, T. YOKOKAWA and A. OSUKA**, "Biscopper(II) Complexes of Hexaphyrin-(1.1.1.1.1.1) : Gable Structures and Varying Antiferromagnetic Coupling," *J. Am. Chem. Soc.* **126**, 12280–12281 (2004).
- T. TAKAHASHI, N. TAKAHASHI, T. NAKAMURA, T. KATO, K. FURUKAWA, G. M. SMITH and P. C. RIEDI**, "Magnetic Characteristics of Fe<sub>4</sub>N Epitaxial Films Grown by Halide Vapor Phase Deposition under Atmospheric Pressure," *Solid State Sci.* **6**, 97–99 (2004).
- A. KAWAMORI, J. R. SHEN, K. FURUKAWA, H. MATSUOKA and T. KATO**, "W-Band EPR Studies of Mn-Cluster in the S-0 and S-2 States of Cyanobacterial Single Crystals," *Plant Cell Physiol.* **45**, S81–S81 (2004).
- M. HIRAOKA, H. SAKAMOTO, K. MIZOGUCHI, T. KATO, K. FURUKAWA, R. KATO, K. HIRAKI and T. TAKAHASHI**, "Spin Soliton Dynamics and Pressure Effects in the Spin-Peierls System (DMe-DCNQI)<sub>2</sub>M (M = Li, Ag)," *J. Magn. Magn. Mater.* **272**, 1077–1078 (2004).
- L. O. HUSEBO, B. SITHARAMAN, K. FURUKAWA, T. KATO and L. J. WILSON**, "Fullerenols Revisited as Stable Radical Anions," *J. Am. Chem. Soc.* **126**, 12055–12064 (2004).
- H. MATSUOKA, N. OZAWA, T. KODAMA, H. NISHIKAWA, I. IKEMOTO, K. KIKUCHI, K. FURUKAWA, K. SATO, D. SHIOMI, T. TAKUI and T. KATO**, "Multifrequency EPR Study of Metallofullerenes: Eu@C<sub>82</sub> and Eu@C<sub>74</sub>," *J. Phys. Chem. B* **108**, 13972–13976 (2004).
- H. TANAKA, M. MOKUMOTO, S. ISHIBASHI, D. GRAF, E. S. CHOI, J. S. BROOKS, S. YASUZUKA, Y. OKANO, H. KOBAYASHI and A. KOBAYASHI**, "Observation of Three-Dimensional Fermi Surfaces in a Single-Component Molecular Metal, [Ni(tmdt)<sub>2</sub>]," *J. Am. Chem. Soc.* **126**, 10518–10519 (2004).
- H. FUJIWARA, H. -J. LEE, H. -B. CUI, H. KOBAYASHI, E. KOBAYASHI and A. KOBAYASHI**, "Synthesis, Structure and Physical Properties of a New Organic Conductor Based on a  $\pi$ -Extended Donor Containing a Stable PROXYL Radical," *Adv. Mater.* **16**, 1765–1769 (2004).
- T. KONOIKE, S. UJI, T. TERASHIMA, M. NISHIMURA, S. TASUZUKA, K. ENOMOTO, H. FUJIWARA, B. ZHANG and H. KOBAYASHI**, "Magnetic-Field-Induced Superconductivity in the Antiferromagnetic Organic Superconductor  $\kappa$ -(BETS)<sub>2</sub>FeBr<sub>4</sub>," *Phys. Rev. B* **70**, 094514 (5 pages) (2004).
- T. OTSUKA, H. -B. CUI, H. FUJIWARA, H. KOBAYASHI, E. FUJIWARA and A. KOBAYASHI**, "The Pressure Effect on the Antiferromagnetic and Superconducting Transitions of  $\kappa$ -(BETS)<sub>2</sub>FeBr<sub>4</sub>," *J. Mater. Chem.* **14**, 1682–1685 (2004).
- E. FUJIWARA, A. KOBAYASHI, H. FUJIWARA, T. SUGIMOTO and H. KOBAYASHI**, "Novel  $\pi$ -Extended Donors Containing a 2,2,5,5-Tetramethylpyrrolin-1-yloxy Radical Designed for Magnetic Molecular Conductors," *Chem. Lett.* 964–965 (2004).
- Z. WANG, B. ZHANG, T. OTSUKA, K. INOUE, H. KOBAYASHI and M. KURMOO**, "Anionic NaCl-Type Frameworks of [Mn(HCOO)<sub>3</sub>]<sup>-</sup>, Templated by Alkylammonium, Exhibit Weak Ferromagnetism," *Dalton Trans.* **15**, 2209–2216 (2004).
- R. M. VLASOVA, N. V. DRICHIKO, B. V. PETROV, V. N. SEMKIN, E. I. ZHILYAEVA, R. N. LYBOVSKAYA, I. OLEJNICZAK, A. KOBAYASHI and H. KOBAYASHI**, "Optical Properties of New Organic Conductors Based on the BEDT-TSeF Molecule, the  $\kappa$ -(BETS)<sub>4</sub>Hg<sub>2.84</sub>Br<sub>8</sub> Superconductor and  $\kappa$ -(BETS)<sub>4</sub>Hg<sub>3</sub>Cl<sub>8</sub> Metal in the Range 300–15 K," *Phys. Solid State* **46**, 1985–1993 (2004).
- N. V. DRICHIKO, B. V. PETROV, V. N. SEMKIN, R. M. VLASOVA, O. A. BOGDANOVA, E. I. ZHILYAEVA, R. N. LYBOVSKAYA, I. OLEJNICZAK, H. KOBAYASHI and A. KOBAYASHI**, "A Comparative Mid-Infrared Study of Superconductor BETS<sub>4</sub>Hg<sub>2.84</sub>Br<sub>8</sub> and Metal BETS<sub>4</sub>Hg<sub>3</sub>Cl<sub>8</sub>," *J. Phys. IV France* **114**, 305–307 (2004).

S. TAKAHASHI, A. E. KOVALEV, S. HILL, S. TAKASAKI, J. YAMADA, H. ANZAI, J. S. QUALLS, K. KAWANO, M. TAMURTA, T. NAITO and H. KOBAYASHI, "Fermi Surface Studies of Quasi-1D and Quasi-2D Organic Superconductors Using Periodic Orbit Resonance in High Magnetic Fields," *Int. J. Mod. Phys. B* **18**, 3499–3504 (2004).

M. SASA, E. FUJIWARA, A. KOBAYASHI, S. ISHIBASHI, K. TERAKURA, Y. OKANO, H. FUJIWARA and H. KOBAYASHI, "Crystal Structure and Physical Properties of Single-Component Molecular Conductors Consisting of Nickel and Gold Complexes with Bis(trifluoromethyl)tetrathiafulvalenedithiolate Ligands," *J. Mater. Chem.* **15**, 155–163 (2005).

H. -B. CUI, S. OTSUBO, Y. OKANO and H. KOBAYASHI, "Structural and Physical Properties of  $\lambda$ -(BEST)<sub>2</sub>MCl<sub>4</sub> (BEST = Bis(ethylenediseleno) Tetrathia-fulvalene; M = Fe, Ga) and Analogous Magnetic Organic Conductor," *Chem. Lett.* 254–255 (2005).

S. ISHIBASHI, H. TANAKA, M. KOHYAMA, M. TOKUMOTO, A. KOBAYASHI, H. KOBAYASHI and K. TERAKURA, "Ab Initio Electronic Structure Calculation for Single-Component Molecular Conductor Au(tmdt)<sub>2</sub> (tmdt = Trimethylenetetrathiafulvalenedithiolate)," *J. Phys. Soc. Jpn.* **74**, 843–846 (2005).

Z. WANG, B. ZHANG, M. KURMOO, H. FUJIWARA, T. OTSUKA and H. KOBAYASHI, "Synthesis and Characterization of a Porous Magnetic Diamond Framework, Co<sub>3</sub>(HCOO)<sub>6</sub>, and Its N<sub>2</sub> Sorption Characteristic," *Inorg. Chem.* **44**, 1230–1237 (2005).

S. UJI, T. TERASHIMA, Y. TERAJ, S. YASUZUKA, M. TOKUMOTO, H. TANAKA, A. KOBAYASHI and H. KOBAYASHI, "Superconductivity and Vortex Phases in the Two-Dimensional Organic Conductor  $\lambda$ -(BETS)<sub>2</sub>Fe<sub>x</sub>Ga<sub>1-x</sub>Cl<sub>4</sub> (x = 0.45)," *Phys. Rev. B* **71**, 104525 (7 pages) (2005).

T. KONOIKE, S. UJI, M. NISHIMURA, K. ENOMOTO, H. FUJIWARA, B. ZHANG and H. KOBAYASHI, "Magnetic Properties of Field-induced Superconductor,  $\kappa$ -(BETS)<sub>2</sub>FeBr<sub>4</sub>," *Physica B* **359**, 457–459 (2005).

A. ZHANG, Z. WANG, H. FUJIWARA, H. KOBAYASHI, M. KURMOO, K. INOUE, T. MORI, S. GAO Y. ZHANG and D. ZHU, "Tetrathiafulvalene [Fe<sup>III</sup>(C<sub>2</sub>O<sub>4</sub>)Cl<sub>2</sub>]: An Organic-Inorganic Hybrid Exhibiting Canted Antiferromagnetism," *Adv. Mater.* **17**, 1988–1991 (2005).

K. TAKAHASHI, H. -B. CUI, H. KOBAYASHI, Y. EINAGA and O. SATO, "The Light-Induced Excited Spin State Trapping Effect on Ni(dmit)<sub>2</sub> Salt with an Fe(III) Spin-Crossover Cation: [Fe(qsal)<sub>2</sub>][Ni(dmit)<sub>2</sub>]CH<sub>3</sub>CN," *Chem. Lett.* 1240–1241 (2005).

E. P. SAJITHA, V. PRASAD, S. V. SUBRAMANYAM, S. ETO, K. TAKAI and T. ENOKI, "Synthesis and Characteristics of Iron Nanoparticles in Carbon Matrix along with Catalytic Graphitization of Amorphous Carbon," *Carbon* **42**, 2815–2820 (2004).

L. KUMARI, S. V. SUBRAMANYAM, S. ETO, K. TAKAI and T. ENOKI, "Metal-Insulator Transition in Iodinated Amorphous Conducting Carbon Films," *Carbon* **42**, 2133–2137 (2004).

T. ENOKI, "Diamond-to-Graphite Conversion in Nanodiamond and Electronic Properties of Nanodiamond-Derived Carbon System," *Phys. Solid State* **46**, 635–640 (2004).

A. I. SHAMES, A. M. PANICH, W. KEMPINSKI, M. V. BAIDAKOVA, V. YU. OSIPOV, T. ENOKI and A. YA. VUL', "Magnetic Resonance Study of Nanodiamonds. In: Synthesis, Properties and Applications of Ultrananocrystalline Diamond," *NATO Science Series*, E. D. M. Gruen, O. A. Shenderova and A. Ya. Vul', Eds., Kluwer Academic Publishers; Dordrecht/Boston/London, pp. 271–282 (2005).

J. NISHIJO, A. MIYAZAKI, T. ENOKI, R. WATANABE, Y. KUWATANI and M. IYODA, "d-Electron-Induced Negative Magnetoresistance of  $\pi$ -d Interaction System Including Brominated-TTF Donor," *Inorg. Chem.* **44**, 2493–2506 (2005).

K. OKABE, J. -I. YAMAURA, A. MIYAZAKI and T. ENOKI, "Electronic and Magnetic Properties of  $\pi$ -d Interaction System (EDTDM)<sub>2</sub>FeBr<sub>4</sub>," *J. Phys. Soc. Jpn.* **74**, 1508–1520 (2005).

Y. KOBAYASHI, K. KUSAKABE, K. FUKUI, T. ENOKI and Y. KABURAGI, "STM/STS Observation of Zigzag- and Armchair-Edges of Graphite," *Phys. Rev. B* **71**, 193406 (4 pages) (2005).

M. ITOI, A. TAIRA, M. ENOMOTO, N. MATSUSHITA, N. KOJIMA, Y. KOBAYASHI, K. ASAI, K. KOYAMA, T. NAKANO, Y. UWATOKO and J. YAMAURA, "Crystal Structure and Structural Transition Caused by Charge-Transfer Phase Transition for Iron Mixed-Valence Complex, (n-C<sub>3</sub>H<sub>7</sub>)<sub>4</sub>N[Fe<sup>II</sup>Fe<sup>III</sup>(dto)<sub>3</sub>](dto = C<sub>2</sub>O<sub>2</sub>S<sub>2</sub>)," *Solid State Commun.* **130**, 415–420 (2004).

M. ITOI, M. ENOMOTO and N. KOJIMA, "Ferromagnetism of Iron Mixed-Valence Complex, (n-C<sub>3</sub>H<sub>7</sub>)<sub>4</sub>N[Fe<sup>II</sup>Fe<sup>III</sup>(dto)<sub>3</sub>] (dithiooxalato: dto = C<sub>2</sub>O<sub>2</sub>S<sub>2</sub>)," *J. Magn. Magn. Mater.* **272-276**, 1093–1094 (2004).

Y. KOBAYASHI, M. ITOI, N. KOJIMA and K. ASAI, "Pressure-Induced Charge-Transfer Phase Transition in a Mixed-Valence Iron Complex," *J. Magn. Magn. Mater.* **272-276**, 1091–1092 (2004).

N. KOJIMA, Y. ONO, Y. KOBAYASHI and M. SETO, "Control of Charge Transfer Phase Transition in Iron Mixed-Valence System, (n-C<sub>n</sub>H<sub>2n+1</sub>)<sub>4</sub>N[Fe<sup>II</sup>Fe<sup>III</sup>(dto)<sub>3</sub>](n = 3–6; dto = C<sub>2</sub>O<sub>2</sub>S<sub>2</sub>)," *Hyperfine Interact.* **156-157**, 175–179 (2004).

K. IKEDA, N. KOJIMA, Y. ONO, Y. KOBAYASHI, M. SETO, X. J. LIU and Y. MORITOMO, "Study on Chemical Bond and Electronic State of New Gold Mixed-Valence Complexes, Cs<sub>2</sub>[Au<sup>I</sup>X<sub>2</sub>][Au<sup>III</sup>Y<sub>4</sub>](X, Y = Cl, Br, I, etc.)," *Hyperfine Interact.* **156-157**, 311–314 (2004).

M. SAKATA, T. ITSUBO, E. NISHIBORI, Y. MORITOMO, N. KOJIMA, Y. OHISHI and M. TAKATA, "Charge Density Study under High Pressure," *J. Phys. Chem. Solids* **65**, 1973–1976 (2004).

**K. IKEDA, Y. ONO, M. ENOMOTO, N. KOJIMA, Y. KOBAYASHI, M. SETO, K. KOYAMA and Y. UWATOKO**, “*P-T* Phase Diagram and Gold Valence State of New Gold Mixed-Valence Complexes,  $\text{Cs}_2[\text{Au}^{\text{I}}\text{X}_2][\text{Au}^{\text{III}}\text{Y}_4]$  ( $\text{X}, \text{Y} = \text{Cl}, \text{Br}, \text{I}; \text{X} \neq \text{Y}$ ),” *Ceram. Silik.* **48**, 159–164 (2004).

**I. KASHIMA, M. OKUBO, Y. ONO, M. ITOI, N. KODA, M. HIKITA, M. ENOMOTO and N. KOJIMA**, “Ferromagnetism and Its Photo-Induced Effect in 2D Iron Mixed-Valence Complex Coupled with Photochromic Spiropyran,” *Synth. Met.* **153**, 473–476 (2005).

**M. ENOMOTO and N. KOJIMA**, “Charge Transfer Phase Transition and Ferromagnetism in a Novel Iron Mixed-Valence Complex  $(n\text{-C}_3\text{H}_7)_4\text{N}[\text{Fe}^{\text{II}}\text{Fe}^{\text{III}}(\text{tto})_3](\text{tto} = \text{C}_2\text{OS}_3)$ ,” *Synth. Met.* **152**, 457–460 (2005).

**M. OKUBO, M. ENOMOTO and N. KOJIMA**, “Study on Photomagnetism of 2D Magnetic Compounds Coupled with Photochromic Diarylethene Cations,” *Synth. Met.* **152**, 461–464 (2005).

**M. OKUBO, M. ENOMOTO and N. KOJIMA**, “Reversible Photomagnetism in a Cobalt Layered Compound Coupled with Photochromic Diarylethene,” *Solid State Commun.* **134**, 777–782 (2005).

**M. OKUBO, M. ENOMOTO, K. KOYAMA, Y. UWATOKO and N. KOJIMA**, “Hybrid Organic-Inorganic Conductor Coupled with BEDT-TTF and Photochromic Nitrosyl Ruthenium Complex,” *Bull. Chem. Soc. Jpn.* **78**, 1054–1060 (2005).

**M. TADA, N. KOJIMA, Y. IZUMI, T. TANIKE and Y. IWASAWA**, “Chiral Self-Dimerization of Vanadium Complexes on a  $\text{SiO}_2$  Surface for Asymmetric Catalytic Coupling of 2-Naphthol: Structure, Performance, and Mechanism,” *J. Phys. Chem. B* **109**, 9905–9916 (2005).

**N. MATSUSHITA, F. FUKUHARA and N. KOJIMA**, “A Three-Dimensional Bromo-Bridged Mixed-Valence Gold(I,III) Compound,  $\text{Cs}_2\text{Au}^{\text{I}}\text{Au}^{\text{III}}\text{Br}_6$ ,” *Acta Crystallogr., Sect. E* **61**, 1123–1125 (2005).

**T. NAITO, T. INABE, H. NIIMI and K. ASAKURA**, “Light-Induced Transformation of Molecular Materials into Devices,” *Adv. Mater.* **16**, 1786–1790 (2004).

**T. NAITO and T. INABE**, “Molecular Conductors Containing Photoreactive Species,” *J. Phys. IV France* **114**, 553–555 (2004).

**M. MATSUDA, N. HANASAKI, S. IKEDA, H. TAJIMA, T. NAITO and T. INABE**, “Molecular Unit Based on Metal Phthalocyanine; Designed for Molecular Electronics,” *J. Phys. IV France* **114**, 541–543 (2004).

**M. MATSUDA, N. HANASAKI, H. TAJIMA, T. NAITO and T. INABE**, “Anisotropic Giant Magnetoresistance Originating from the  $\pi$ -d Interaction in a Molecule,” *J. Phys. Chem. Solids* **65**, 749–752 (2004).

**Y. OHTSUKA, T. NAITO and T. INABE**, “Phthalocyanine-Phthalocyanine Salt Crystal: A Unique Assembly Design,” *J. Porphyrins Phthalocyanines* **9**, 68–71 (2005).

**T. NAITO, N. MATSUMURA, T. INABE, M. MATSUDA and H. TAJIMA**, “Physical Properties of Electrically Conducting and Stable Molecular Neutral Radical Solid  $[\text{Co}(2,3\text{-Nc})(\text{CN})_2]\text{CH}_3\text{CN}$  (2,3-Nc = 2,3-naphthalocyanine),” *J. Porphyrins Phthalocyanines* **8**, 1258–1268 (2004).

**T. NAITO and T. INABE**, “Structural, Electrical and Magnetic Properties of  $\alpha\text{-(ET)}_7[\text{MnCl}_4]_2 \cdot (1,1,2\text{-C}_2\text{H}_3\text{Cl}_3)_2$  (ET = bis(ethylenedithio)tetrathiafulvalene),” *Bull. Chem. Soc. Jpn.* **77**, 1987–1995 (2004).

**T. NAITO, K. NISHIBE and T. INABE**, “New Binuclear Copper Complexes  $[(9\text{S}3)\text{Cu}(\text{CN})\text{Cu}(9\text{S}3)]\text{X}_n$  ( $\text{X} = \text{BF}_4$ ,  $n = 1$ ;  $\text{X} = \text{TCNQ}$ ,  $n = 2$ ) (9S3 = 1,4,7-trithiacyclononane): Syntheses, Crystal Structures and Magnetic Properties,” *Z. Anorg. Allg. Chem.* **630**, 2725–2730 (2004).

**T. INABE, N. KOBAYASHI and T. NAITO**, “Crystal Design of Cation-Radical Salts Based on the Supramolecular Self-Organizing Arrangement of Mellitate Anions,” *J. Phys. IV France* **114**, 449–453 (2004).

**N. KOBAYASHI, T. NAITO and T. INABE**, “A Helical  $\pi$ -Radical Cation Column in the Double Helix of Mellitate Anions,” *Adv. Mater.* **16**, 1803–1806 (2004).

**N. KOBAYASHI, T. NAITO and T. INABE**, “Network Formation of Mellitate Anions ( $[\text{C}_6(\text{COO})_6\text{H}_{6-n}]^{n-}$ ) in the Salts with Piperidinium Derivatives and *o*-Phenylenediammonium,” *CrystEngComm* **6**, 189–196 (2004).

**A. KAWAMOTO, M. YAMASHITA and K. KUMAGAI**, “Field-Induced Metal-Insulator Transition in Partially Deuterated  $\kappa\text{-(BEDT-TTF)}_2\text{Cu}[\text{N}(\text{CN})_2]\text{Br}$ ,” *Phys. Rev. B* **70**, 212506 (2004).

**A. KAWAMOTO, Y. HONMA and K. KUMAGAI**, “Electron Localization in the Strongly Correlated Organic System  $\kappa\text{-(BEDT-TTF)}_2\text{X}$  Probed with Nuclear Magnetic Resonance  $^{13}\text{C}$  NMR,” *Phys. Rev. B* **70**, 060510 (2004).

**T. NISHI, S. KIMURA, T. TAKAHASHI, T. ITO, H. J. IM, Y. S. KWON, K. MIYAGAWA, H. TANIGUCHI, A. KAWAMOTO and K. KANODA**, “The Origin of the Phase Separation in Partially Deuterated  $\kappa\text{-(ET)}_2\text{Cu}[\text{N}(\text{CN})_2]\text{Br}$  Studied by Infrared Magneto-Optical Imaging Spectroscopy,” *Solid State Commun.* **134**, 189–193 (2005).

**A. MAKSIMUK, K. YAKUSHI, H. TANIGUCHI, K. KANODA and A. KAWAMOTO**, “Influence of the Cooling Rate on Low-Temperature Raman and Infrared-Reflection Spectra of Partially Deuterated  $\kappa\text{-(BEDT-TTF)}_2\text{Cu}[\text{N}(\text{CN})_2]\text{Br}$ ,” *Synth. Met.* **149**, 13–18 (2005).

#### Department of Applied Molecular Science

**R. DAVYDOV, S. CHEMERISOV, D. E. WERST, T. RAJH, T. MATSUI, M. IKEDA-SAITO and B. M. HOFFMAN**, “Proton Transfer at Helium Temperatures during Dioxygen Activation by Heme Monooxygenases,” *J. Am. Chem. Soc.* **126**, 15960–15961 (2004).

**T. MATSUI, M. FURUKAWA, M. UNNO, T. TOMITA and M. IKEDA-SAITO**, “Roles of Distal Asp in Heme Oxygenase from *Corynebacterium diphtheriae*, HmuO: A Water-Driven Oxygen Activation Mechanism,” *J. Biol. Chem.* **280**, 2981–2989 (2005).

**A. -L. BULTEAU, K. C. LUNDBERG, M. IKEDA-SAITO, G. ISAYA and L. I. SZWEDA**, “Reversible Redox-Dependent Modulation of Mitochondrial Aconitase and Proteolytic Activity during *in vivo* Cardiac Ischemia/Reperfusion,” *Proc. Natl. Acad. Sci. U.S.A.* **102**, 5987–5991 (2005).

#### Department of Vacuum UV Photochemistry

**N. KOSUGI**, “Valence in the Rydberg/Continuum Region in Molecular Inner-Shell Spectroscopy,” *J. Electron Spectrosc. Relat. Phenom.* **144**, 1203–1207 (2005).

**K. WIESNER, A. N. DE BRITO, S. L. SORENSEN, N. KOSUGI and O. BJORNEHOLM**, “Core Excitation in O<sub>3</sub> Localized to One of Two Symmetry-Equivalent Chemical Bonds: Molecular Alignment through Vibronic Coupling,” *J. Chem. Phys.* **122**, 154303 (2005).

**S. MASUDA, T. GEJO, M. HIYAMA and N. KOSUGI**, “Vibronic Couplings in the C 1s-Rydberg and Valence Excitations of C<sub>2</sub>H<sub>2</sub>, Revealed by Angle-Resolved Photoion Yield Spectroscopy,” *J. Electron Spectrosc. Relat. Phenom.* **144**, 215–218 (2005).

**H. SETOYAMA, T. HATSUI and N. KOSUGI**, “S 2p Excited States of OCS in Rare Gas Matrices,” *J. Electron Spectrosc. Relat. Phenom.* **144**, 87–89 (2005).

**T. HATSUI, H. SETOYAMA, E. SHIGEMASA and N. KOSUGI**, “Design of a Novel Transmission-Grating Spectrometer for Soft X-Ray Emission Studies,” *J. Electron Spectrosc. Relat. Phenom.* **144**, 1059–1062 (2005).

**M. HIYAMA and N. KOSUGI**, “Ab Initio R-Matrix/Multi-Channel Quantum Defect Theory Applied to Molecular Core Excitation and Ionization,” *J. Electron Spectrosc. Relat. Phenom.* **144**, 1223–1226 (2005).

**M. HIYAMA and N. KOSUGI**, “Ab Initio R-Matrix/Multi-Channel Quantum Defect Theory Approach to Study Molecular Core Excitation and Ionization: GSCF4R,” *J. Theor. Comput. Chem.* **4**, 35–47 (2005).

**M. HIYAMA and N. KOSUGI**, “Ab Initio R-Matrix/MQDT Method for Near-Edge X-Ray Absorption Fine Structure,” *Phys. Scr.* **T115**, 135–138 (2005).

**R. FLESCH, N. KOSUGI, I. L. BRADEANU, J. J. NEVILLE and E. RUHL**, “Cluster Size Effects in Core Excitons of 1s-Excited Nitrogen,” *J. Chem. Phys.* **121**, 8343–8350 (2004).

**A. HISHIKAWA, H. HASEGAWA and K. YAMANOUCHI**, “Hydrogen Migration in Acetonitrile in Intense Laser Fields in Competition with Two-Body Coulomb Explosion,” *J. Electron Spectrosc. Relat. Phenom.* **141**, 195–200 (2004).

**A. HISHIKAWA, M. UEYAMA and K. YAMANOUCHI**, “Probing the Ultrafast Nuclear Motion in CS<sub>2</sub><sup>2+</sup> in Intense Laser Fields,” *J. Chem. Phys.* **122**, 151104 (4 pages) (2005).

**S. FUJIKI, Y. KUBOZONO, Y. RIKIISHI and T. URISU**, “Scanning Tunneling Microscopy/Spectroscopy Studies of Two Isomers of Ce@C-82 on Si(111)-(7×7) Surfaces,” *Phys. Rev. B* **70**, 235421 (7 pages) (2004).

**Y. -J. LI, R. TERO, T. NAGASAWA, T. NAGATA and T. URISU**, “Deposition of 10-Undecenoic Acid Self-Assembled Layers on H-Si(111) Surfaces Studied with AFM and FT-IR,” *Appl. Surf. Sci.* **238**, 238–241 (2004).

**Y. NONOGAKI, M. KATOH, K. MATSUSHITA, M. SUZUI and T. URISU**, “Construction of the Undulator Beamline Equipped with a UHV-STM for Observations of Synchrotron-Radiation-Stimulated Surface Reaction,” *J. Electron Spectrosc.* **144**, 1113–1116 (2005).

**G. R. RAO, Z. H. WANG, H. WATANABE, M. AOYAGI and T. URISU**, “A Comparative Infrared Study of H<sub>2</sub>O Reactivity on Si(100)-(2×1), (2×1)-H, (1×1)-H and (3×1)-H Surfaces,” *Surf. Sci.* **570**, 178–188 (2004).

**R. TERO, M. TAKIZAWA, Y. -J. LI, M. YAMAZAKI and T. URISU**, “Deposition of Phospholipid Layers on SiO<sub>2</sub> Surface Modified Alkyl-SAM Islands,” *Appl. Surf. Sci.* **238**, 218–222 (2004).

**R. TERO, T. URISU, H. OKAWARA and K. NAGAYAMA**, “Deposition of Lipid Bilayers on OH-Density-Controlled Silicon Dioxide Surfaces,” *J. Vac. Sci. Technol., A* **23**, 751–754 (2005).

**R. TERO, N. MISAWA, S. YAMAMURA, Y. NONOGAKI and T. URISU**, “Fabrication of Avidin Single Molecular Layer on Silicon Oxide Surfaces and Formation of Tethered Lipid Bilayer Membranes,” *Hyomenkagaku* (in Japanese) **26**, 454–459 (2005).

**R. TERO, N. MISAWA, H. WATANABE, S. YAMAMURA, S. NAMBU, Y. NONOGAKI and T. URISU**, “Fabrication of Avidin Single Molecular Layer on Silicon Oxide Surfaces and Formation of Tethered Lipid Bilayer Membranes,” *e-J. Surf. Sci. Nanotech.* **3**, 236–242 (2005).

**C. S. WANG and T. URISU**, “Synchrotron Radiation Stimulated Etching SiO<sub>2</sub> Thin Films with a Contact Cobalt Mask,” *Appl. Surf. Sci.* **242**, 276–280 (2005).

**Z. H. WANG, T. URISU, H. WATANABE, K. OOI, G. R. RAO, S. NAMBU, J. MAKI and M. AOYAGI**, “Assignment of Surface IR Absorption Spectra Observed in the Oxidation Reactions: 2H+H<sub>2</sub>O/Si(100) and H<sub>2</sub>O+H/Si(100),” *Surf. Sci.* **575**, 330–342 (2005).

**J. KOU, T. MORI, Y. KUBOZONO and K. MITSUKE**, “Photofragmentation of C<sub>60</sub> in the Extreme Ultraviolet: Statistical Analysis on the Appearance Energies of C<sub>60-2n</sub><sup>z+</sup> (n ≥ 1, z = 1–3),” *Phys. Chem. Chem. Phys.* **7**, 119–123 (2005).

- K. MITSUKE**, "Photofragmentation Mechanisms of H<sub>2</sub>O Studied by Ultraviolet Dispersed Spectroscopy," *J. Electron Spectrosc. Relat. Phenom.* **144-147**, 131–133 (2005).
- T. MORI, J. KOU, Y. HARUYAMA, Y. KUBOZONO and K. MITSUKE**, "Absolute Photoabsorption Cross Section of C<sub>60</sub> in the Extreme Ultraviolet," *J. Electron Spectrosc. Relat. Phenom.* **144-147**, 243–246 (2005).
- J. KOU, T. MORI, Y. KUBOZONO and K. MITSUKE**, "Photofragmentation of C<sub>60</sub> in Valence Ionization," *J. Electron Spectrosc. Relat. Phenom.* **144-147**, 247–250 (2005).
- K. MITSUKE, T. MORI, J. KOU, Y. HARUYAMA and Y. KUBOZONO**, "4d → 4f Dipole Resonance of the Metal Atom Encapsulated in a Fullerene Cage: Ce@C<sub>82</sub>," *J. Chem. Phys.* **122**, 064304 (5 pages) (2005).
- K. MITSUKE, T. MORI, J. KOU, Y. HARUYAMA, Y. TAKABAYASHI and Y. KUBOZONO**, "Photoion Yield Curves of Dy@C<sub>82</sub> in the Vacuum UV Region," *Int. J. Mass Spectrom.* **243**, 121–125 (2005).

### Department of Computational Molecular Science

- M. SATO and S. OKAZAKI**, "Mixed Quantum-Classical Molecular Dynamics Study of Vibrational Relaxation of CN<sup>-</sup> Ion in Water: An Analysis of Coupling as a Function of Time," *J. Mol. Liq.* **119**, 15–22 (2005).
- M. SATO and S. OKAZAKI**, "Vibrational Relaxation Time of CN<sup>-</sup> Ion in Water Studied by Mixed Quantum-Classical Molecular Dynamics: Comparison with Fermi's Golden Rule and Influence Functional Theory," *Mol. Sim.* **30**, 835–839 (2004).
- T. KOMATSU, N. YOSHII, S. MIURA and S. OKAZAKI**, "A Large-Scale Molecular Dynamics Study of Dynamic Structure Factor and Dispersion Relation of Acoustic Mode in Liquid and Supercritical Water," *Fluid Phase Equilib.* **226**, 345–350 (2004).
- S. MIURA**, "On the Solvation Structure of a Rare-Gas Solute in Superfluid Helium-4," *J. Mol. Liq.* **119**, 41–46 (2005).
- A. MORITA, M. SUGIYAMA and S. KODA**, "Reply to 'Comment on 'Gas-Phase Flow and Diffusion Analysis of the Droplet Train/Flow Reactor Technique for the Mass Accommodation Processes,''" *J. Phys. Chem. A* **108**, 8544–8545 (2004).
- S. IUCHI, A. MORITA and S. KATO**, "Potential Energy Surfaces and Dynamics of Ni<sup>2+</sup> Ion Aqueous Solution: Molecular Dynamics Simulation of the Electronic Absorption Spectrum," *J. Chem. Phys.* **121**, 8446–8457 (2004).
- A. MORITA**, "Toward Computation of Bulk Quadrupolar Signals in Vibrational Sum Frequency Generation Spectroscopy," *Chem. Phys. Lett.* **398**, 361–366 (2004).
- S. IUCHI, A. MORITA and S. KATO**, "Electronic Relaxation Dynamics of Ni<sup>2+</sup> Ion Aqueous Solution: Molecular Dynamics Simulation," *J. Chem. Phys.* **123**, 024505 (2005).
- A. MORITA, M. SUGIYAMA, S. KODA and D. R. HANSON**, "Reply to 'Comment on 'Mass Accommodation Coefficient of Water: Molecular Dynamics Simulation and Revised Analysis of Droplet Train/Flow Reactor Experiment,''" *J. Phys. Chem. B* **109**, 14747–14749 (2005).
- S. NANBU and M. S. JOHNSON**, "Analysis of the Ultraviolet Absorption Cross Sections of Six Nitrous Oxide Isotopomers Using 3D Wavepacket Propagation," *J. Phys. Chem. A (Memorial Festschrift for Professor Gert Billing)* **108**, 8905–8913 (2004).
- Z. -H. WANG, T. URISU, H. WATANABE, K. OOI, G. R. RAO, S. NANBU, J. MAKI and M. AOYAGI**, "Assignment of Surface IR Absorption Spectra Observed in the Oxidation Reactions: 2H + H<sub>2</sub>O/Si(100) and H<sub>2</sub>O + H/Si(100)," *Surf. Sci.* **575**, 330–342 (2005).
- H. TAMURA, S. NANBU, T. ISHIDA and H. NAKAMURA**, "Ab Initio Potential Energy Surfaces for the Cyclohexadiene/Hexatriene Photochemical Interconversion," *Chem. Phys. Lett.* **401**, 487–491 (2005).
- I. TOKUE, K. YAMASAKI, S. MINAMINO and S. NANBU**, "Theoretical Transition Probabilities for the A<sup>2</sup>A<sub>1</sub>-X<sup>2</sup>B<sub>1</sub> System of H<sub>2</sub>O<sup>+</sup> and D<sub>2</sub>O<sup>+</sup> and Related Franck-Condon Factors Based on Global Potential Energy Surfaces," *J. Theor. Comput. Chem.* **4**, 225–245 (2005).
- I. TOKUE, K. YAMASAKI and S. NANBU**, "Vibrational Energies for the X<sup>1</sup>A<sub>1</sub>, A<sup>1</sup>B<sub>1</sub>, and B<sup>1</sup>A<sub>1</sub> States of SiH<sub>2</sub>/SiD<sub>2</sub> and Related Transition Probabilities Based on Global Potential Energy Surfaces," *J. Chem. Phys.* **122**, 144307–144316 (2005).
- J. -I. CHOE, S. -K. CHANG, S. LEE and S. NANBU**, "Ab Initio Calculated Structures of Conformers for 1,3-Dimethoxy-p-tert-Butylcalix[4] Crown-5-Ether Complexed with Potassium Cation," *THEOCHEM* **722**, 117–123 (2005).
- H. WATANABE, S. NANBU, Z. -H. WANG, J. MAKI, T. URISU, M. AOYAGI and K. OOI**, "Theoretical Study of the Oxidation Reaction for the H Atom-Induced Water-Terminated Si Surface 2H+H<sub>2</sub>O/Si(100)-(2×1)," *Chem. Phys. Lett.* **412**, 347–352 (2005).

### Coordination Chemistry Laboratories

- T. HINO, T. WADA, T. FUJIHARA and K. TANAKA**, "Redox Behavior of New Ru-Dioxolene-Ammine Complexes and Catalytic Activity toward Electrochemical Oxidation of Alcohol under Mild Conditions," *Chem. Lett.* **33**, 1596–1597 (2004).

- H. OHTUS and K. TANAKA**, "Chemical Control of Valence Tautomerism of Nickel(II) Semiquinone and Nickel(III) Catecholate States," *Angew. Chem., Int. Ed.* **43**, 6301–6303 (2004).
- H. OHTSU and K. TANAKA**, "Equilibrium of Low- and High-Spin States of Ni(II) Complexes Controlled by the Donor Ability of the Bidentate Ligands," *Inorg. Chem.* **43**, 3024–3030 (2004).
- R. OKAMURA, T. WADA, K. AIKAWA, T. NAGATA and K. TANAKA**, "A Platinum-Ruthenium Dinuclear Complex Bridged by Bis(terpyridyl)xanthene," *Inorg. Chem.* **43**, 7210–7217 (2004).
- H. SUGIMOTO, H. TSUKUBE and K. TANAKA**, "Immobilization of a High-Valent Rhenium Complex on an Indium-Doped Tin-Oxide Electrode: Enhanced Catalytic Activity of a Trans-Dioxorhenium(V) Complex in Electrochemical Oxidation of Alcohols," *Eur. J. Inorg. Chem.* 4550–4553 (2004).
- T. KOIZUMI and K. TANAKA**, "Synthesis, Chemical- and Electrochemical Properties of Ruthenium(II) Complexes Bearing 2,6-Bis(2-naphthyridyl)pyridine," *Inorg. Chim. Acta* **358**, 1999–2004 (2005).
- T. KOIZUMI, T. TOMON and K. TANAKA**, "Synthesis, Structures and Electrochemical Properties of Ruthenium (II) Complexes Bearing Bidentate 1,8-Naphthyridine and Terpyridine Analogous (N,N,C)-Tridentate Ligands," *J. Organomet. Chem.* **690**, 4272–4279 (2005).
- T. KOIZUMI, T. TOMON and K. TANAKA**, "Synthesis and Electrochemical Properties of Bis(bipyridine) ruthenium(II) Complexes Bearing Pyridinyl- and Pyridinylidene Ligands Induced by Cyclometalation of N'-Methylated Bipyridinium Analogs," *J. Organomet. Chem.* **690**, 1258–1264 (2005).
- H. OHTSU and K. TANAKA**, "Electronic Structural Changes between Nickel(II)-Semiquinonato and Nickel(III)-Catecholato States Driven by Chemical and Physical Perturbation," *Chem. Eur. J.* **11**, 3420–3426 (2005).
- H. SUGIMOTO, Y. FURUKAWA, M. TARUMIZU, H. MIYAKE, K. TANAKA and H. TSUKUBE**, "Synthesis and Crystal Structures of  $[W(3,6\text{-dichloro-1,2-benzenedithiolate})_3]^{n-}$  ( $n = 1, 2$ ) and  $[Mo(3,6\text{-dichloro-1,2-benzenedithiolate})_3]^{2-}$ : Dependence of the Coordination Geometry on the Oxidation Number and Counter-Cation in Trigonal-Prismatic and Octahedral Structures," *Eur. J. Inorg. Chem.* 3088–3092 (2005).
- H. SUGIMOTO, M. HARIHARA, M. SHIRO, K. SUGIMOTO, K. TANAKA, H. MIYAKE and H. TSUKUBE**, "Dioxo-Molybdenum(VI) and Mono-oxo-Molybdenum(IV) Complexes Supported by New Aliphatic Dithiolene Ligands: New Models with Weakened Mo=O Bond Characters for the Arsenite Oxidase Active Site," *Inorg. Chem.* **44**, 6386–6392 (2005).
- T. TOMON, T. KOIZUMI and K. TANAKA**, "Electrochemical Hydrogenation of  $[Ru(bpy)_2(napy-kN)(CO)]^{2+}$ : Inhibition of Reductive Ru–CO Bond Cleavage by a Ruthenacycle," *Angew. Chem., Int. Ed.* **44**, 2229–2232 (2005).
- T. TOMON, T. KOIZUMI and K. TANAKA**, "Stabilization and Destabilization of the Ru–CO Bond during the 2,2'-Bipyridin-6-Onato (bpyO)-Localized Redox Reaction of  $[Ru(terpy)(bpyO)(CO)](PF_6)$ ," *Eur. J. Inorg. Chem.* 285–293 (2005).
- M. KONDO, Y. HAYAKAWA, M. MIYAZAWA, A. OYAMA, K. UNOURA, H. KAWAGUCHI, T. NAITO, K. MAEDA and F. UCHIDA**, "New Redox-Active Coordination Polymer with Cobalticinium Dicarboxylate," *Inorg. Chem.* **43**, 5801–5803 (2004).
- M. KONDO, Y. IRIE, Y. SHIMUZU, M. MIYAZAWA, H. KAWAGUCHI, A. NAKAMURA, T. NAITO, K. MAEDA and F. UCHIDA**, "Dynamic Coordination Polymers with 4,4'-Oxybis(benzoate): Reversible Transformations of Nano- and Nonporous Coordination Frameworks Responding to Present Solvents," *Inorg. Chem.* **43**, 6139–6141 (2003).
- H. OKU, T. OHYAMA, A. HIROKI, K. YAMADA, K. FUKUYAMA, H. KAWAGUCHI and R. KATAKAI**, "Addition of a Peptide Fragment on an  $\alpha$ -Helical Depsipeptide Induces  $\alpha/3_{10}$ -Conjugated Helix: Synthesis, Crystal Structure, and CD Spectra of Boc-Leu-Leu-Ala-(Leu-Leu-LaC)<sub>3</sub>-Leu-Leu-OEt," *Biopolymer* **75**, 242–254 (2004).
- T. KOMURO, T. MATSUO, H. KAWAGUCHI and K. TATSUMI**, "Synthesis of a Vanadium(III) Tris(arylthiolato) Complex and Its Reactions with Azide and Azo Compounds; Formation of a Sulfenamide Complex via Cleavage of an Azo N=N Bond," *Inorg. Chem.* **44**, 175–177 (2005).
- W. ZHAO, J. FAN, Y. SONG, H. KAWAGUCHI, T. OKAMURA, W. -Y. SUN and N. UEYAMA**, "Synthesis, Crystal Structures and Properties of Novel Copper(II) Complexes Obtained by Reactions of Copper(II) Sulfate Pentahydrate with Tripodal Ligands," *Dalton Trans.* 1509–1517 (2005).
- L. -Y. KONG, Z. -H. ZHANG, H. -F. ZHU, H. KAWAGUCHI, T. OKAMURA, M. DOI, Q. CHU, W. -Y. SUN and N. UEYAMA**, "Copper(II) and Zinc(II) Complexes Can Fix Atmospheric Carbon Dioxide," *Angew. Chem., Int. Ed.* **44**, 4352–4355 (2005).
- F. AKAGI, T. MATSUO and H. KAWAGUCHI**, "Titanium and Zirconium Complexes of Preorganized Tripodal Triaryloxy Ligands," *J. Am. Chem. Soc.* **127**, 11936–11937 (2005).
- S. TAKEMOTO, S. OSHIO, T. SHIROMOTO and H. MATSUZAKA**, "A Dinuclear Ru(II)  $\kappa^2$ -Diamido/ $\eta^6$ -Naphthalene Complex Featuring a Coordinatively Unsaturated Yet Highly  $\pi$ -Basic ( $\eta^5$ -C<sub>5</sub>Me<sub>5</sub>)Ru Diamide Fragment," *Organometallics* **24**, 801–804 (2005).
- M. HIROTSU, N. OHNO, T. NAKAJIMA and K. UENO**, "Synthesis of a Cofacial Schiff-Base Dimanganese(III) Complex for Asymmetric Catalytic Oxidation of Sulfides," *Chem. Lett.* **34**, 848–849 (2005).
- S. KAMIMURA, T. MATSUNAGA, S. KUWATA, M. IWASAKI and Y. ISHII**, "Synthesis, Structures, and Solution Behavior of Di- and Trinuclear Titanium(IV)-Cyclophosphato Complexes," *Inorg. Chem.* **43**, 6127–6129 (2004).

**H. KAJITANI, Y. TANABE, S. KUWATA and Y. ISHII**, "A Cyanamido-Bridged Iridium Complex: A Reactive Building Block for Polynuclear Cyanamido Complexes," *Organometallics* **24**, 2251–2254 (2005).

**T. YUTAKA, S. OBARA, S. OGAWA, K. NOZAKI, N. IKEDA, T. OHNO, Y. ISHII, K. SAKAI and M. HAGA**, "Syntheses and Properties of Emissive Iridium(III) Complexes with Tridentate Benzimidazole Derivatives," *Inorg. Chem.* **44**, 4737–4746 (2005).

**H. FUKUMOTO and K. MASHIMA**, "Unique Preferential Conformation and Movement of Ru(acac)<sub>2</sub> Fragment(s) Coordinated in an  $\eta^4$ -*s-trans* Fashion to All Diene Unit(s) of  $\alpha,\omega$ -Diphenylpolyenes," *Organometallics* **24**, 3932–3938 (2005).

**T. YASUMOTO, T. YAMAGATA and K. MASHIMA**, "Living Polymerization of 1-Hexene Catalyzed by Half-metallocene Dimethyl Complexes of Hafnium with Bidentate *N*-Substituted Iminomethylpyrrolyl Ligands," *Organometallics* **24**, 3375–3377 (2005).

**S. TAKABAYASHI, M. OHASHI, K. MASHIMA, Y. LIU, S. YAMAZAKI and Y. NAKATO**, "Surface Structures, Photovoltages, and Stability of n-Si(111) Electrodes Surface-Modified with Metal Nano-Dots and Various Organic Groups," *Langmuir* **21**, 8832–8838 (2005).

**T. RÜFFER, M. OHASHI, A. SHIMA, H. MIZOMOTO, Y. KANEDA and K. MASHIMA**, "Unique Oxidative Metal–Metal Bond Formation of Linearly Aligned Tetranuclear Rh–Mo–Mo–Rh Clusters," *J. Am. Chem. Soc.* **126**, 12244–12245 (2004).

**Y. KATAOKA, Y. NAKAGAWA, A. SHIBAHARA, T. YAMAGATA, K. MASHIMA and K. TANI**, "Construction of Metal-Centered Chirality: Diastereoselective Addition of the Meerwein Reagent (Me<sub>3</sub>OBF<sub>4</sub>) to Rhodium Carbonyl Complexes Having the Cp<sup>+</sup>-P Ligand," *Organometallics* **23**, 2095–2099 (2004).

**H. TSURUGI, Y. MATSUO, T. YAMAGATA and K. MASHIMA**, "Intramolecular Benzoylation of an Imino Group of Tridentate 2,5-Bis(*N*-aryliminomethyl)pyrrolyl Ligands Bound to Zirconium and Hafnium Gives Amido-pyrrolyl Complexes That Catalyze Ethylene Polymerization," *Organometallics* **23**, 2797–2805 (2004).

**J. -J. YI, T. MIYABAYASHI, M. OHASHI, T. YAMAGATA and K. MASHIMA**, "Unique Interaction of Mo<sub>2</sub>(O<sub>2</sub>CCF<sub>3</sub>)<sub>4</sub> with 1,2-Dichlorodipalladium compound," *Inorg. Chem.* **43**, 6596–6599 (2004).

**K. OHNO, Y. KATAOKA and K. MASHIMA**, "Asymmetric Transfer Hydrogenation of Aryl Ketones Catalyzed by Salt-free Two Samarium Centers Supported by a Chiral Multidentate Alkoxy Ligand," *Org. Lett.* **6**, 4695–4697 (2004).

**K. KAMADA, K. OHTA, Y. SHIMOYAMA, T. MIYABAYASHI and K. MASHIMA**, "Off-Resonant Third-Order Nonlinear Optical Properties of Multiply-Bonded Multinuclear Organometallic Complexes Measured with Femtosecond Pulses," *Opt. Mater.* **27**, 573–578 (2004).

## Research Center for Molecular-scale Nanoscience List of Publications

**H. UNO, Y. YAMASHITA, M. KIKUCHI, H. WATANABE, T. OGAWA, H. N. YAMADA and N. ONO**, "Photo Precursor for Pentacene," *Tetrahedron. Lett.* **46**, 1981–1983 (2005).

**H. YAMADA, Y. YAMASHITA, M. KIKUCHI, H. WATANABE, T. OKUJIMA, H. UNO, T. OGAWA, K. OHARA, K. MUKAI and N. ONO**, "Novel Photochemical Synthesis of Pentacene and Its Derivatives," *Chem. Eur. J.* **11**, 6212–6220 (2005).

**Y. INOUE, Y. SAKAMOTO, T. SUZUKI, M. KOBAYASHI, Y. GAO and S. TOKITO**, "Organic Thin-Film Transistors with High Electron Mobility Based on Perfluoropentacene," *Jpn. J. Appl. Phys., Part 1* **44**, 3663–3668 (2005).

**T. TSUZUKI, N. SHIRASAWA, T. SUZUKI and S. TOKITO**, "Organic Light-Emitting Diodes Using Multifunctional Phosphorescent with Iridium-Complex Core and Charge-Transporting Dendrons," *Jpn. J. Appl. Phys., Part 1* **44**, 4151–4154 (2005).

**M. MURATSUBAKI, Y. FURUKAWA, T. NOGUCHI, T. OHNISHI, E. FUJIWARA and H. TADA**, "Field-Effect Transistors Based on Poly(*p*-phenylvinylene) Derivatives," *Chem. Lett.* **33**, 1480–1481 (2004).

**Y. MORIOKA, J. NISHIDA, E. FUJIWARA, H. TADA and Y. YAMASHITA**, "Novel Field-Effect Transistors Based on Bis(1,3-dithiol-2-ylidene) Compounds with a Conjugated Spacer Group," *Chem. Lett.* **33**, 1632–1633 (2004).

**E. FUJIWARA, M. TAKADA, Y. YAMASHITA and H. TADA**, "Field-Effect Transistors Based on Single-Crystalline Wires of Bis-(1, 2, 5-Thiadiazolo)-*p*-Quinobis(1, 3-Dithiole)," *Jpn. J. Appl. Phys.* **33**, L82–L84 (2005).

**T. SKANAOUÉ, E. FUJIWARA, R. YAMADA and H. TADA**, "Preparation of Organic Light-Emitting Field-Effect Transistors with Asymmetric Electrodes," *Chem. Lett.* **34**, 494–495 (2005).

**R. YAMADA and H. TADA**, "Manipulation of Droplets by Dynamically Controlled Wetting Gradients," *Langmuir* **21**, 4254–4256 (2005).

**S. ANDO, J. NISHIDA, E. FUJIWARA, H. TADA, Y. INOUE, S. TOKITO and Y. YAMASHITA**, "Novel *p*- and *n*-Type Organic Semiconductors with an Anthracene Unit," *Chem. Mater.* **17**, 1261–1264 (2005).

**S. ANDO, J. NISHIDA, H. TADA, Y. INOUE, S. TOKITO and Y. YAMASHITA**, "High Performance *n*-Type Organic Field-Effect Transistors Based on  $\pi$ -Electronic Systems with Trifluoromethylphenyl Groups," *J. Am. Chem. Soc.* **127**, 5336–5337 (2005).

**M. TAKADA and H. TADA**, "Scanning Tunneling Microscopy and Spectroscopy of Phthalocyanine Molecules on Metal Surfaces," *Jpn. J. Appl. Phys.* **44**, 5332–5335 (2005).

**NARASO, J. NISHIDA, S. ANDO, J. YAMAGUCHI, K. ITAKA, H. KOINUMA, H. TADA, S. TOKITO and Y. YAMASHITA**, "High Performance Organic Field-Effect Transistors Based on  $\pi$ -Extended Tetrathiafulvalene Derivatives," *J. Am. Chem. Soc.* **127**, 10142–10143 (2005).

**MD. AKHTARUZZAMAN, N. KAMATA, J. NISHIDA, S. ANDO, H. TADA, M. TOMURA and Y. YAMASHITA**, "Synthesis, Characterization and FET Properties of Novel Dithiazolybenzothiadiazole Derivatives," *Chem. Commun.* 3183–3185 (2005).

**K. TAKENAKA and Y. UOZUMI**, "An N-C-N Pincer Palladium Complex as an Efficient Catalyst Precursor for the Heck Reaction," *Adv. Synth. Catal.* **346**, 1693–1696 (2004).

**H. HOCHE and Y. UOZUMI**, "PS-PEG Resin-Supported Palladium-MOP Complexes: Application in Asymmetric  $\pi$ -Allylic Reduction," *Tetrahedron* **60**, 9297–9306 (2004).

**Y. NAKAI and Y. UOZUMI**, "Cycloisomerization of 1,6-Enynes: Asymmetric Multistep Preparation of a Hydrindane Framework in Water with Polymeric Catalysts," *Org. Lett.* **7**, 291–293 (2005).

**R. NAKAO, H. RHEE and Y. UOZUMI**, "Hydrogenation and Dehalogenation under Aqueous Conditions with an Amphiphilic Polymer-Supported Nanopalladium Catalyst," *Org. Lett.* **7**, 163–165 (2005).

**Y. UOZUMI and M. KIKUCHI**, "Controlled Monoarylation of Dibromoarenes in Water with a Polymeric Palladium Catalyst," *Synlett* 1775–1778 (2005).

**K. WATANABE, N. TAKAGI and Y. MATSUMOTO**, "Femtosecond Wavepacket Dynamics of Cs Adsorbates on Pt(111): Coverage and Temperature Dependences," *Phys. Rev. B* **71**, 085414 (9 pages) (2005).

**D. INO, K. WATANABE, N. TAKAGI and Y. MATSUMOTO**, "The Electronic Structure and Femtosecond Electron Transfer Dynamics at Noble Metal/tris-(8-hydroxyquinoline) Aluminum Interfaces," *Phys. Rev. B* **71**, 115427 (10 pages) (2005).

**K. WATANABE, N. TAKAGI and Y. MATSUMOTO**, "Mode Selective Excitation of Coherent Surface Phonons on Alkali-Covered Metal Surfaces," *Phys. Chem. Chem. Phys.* **7**, 2697–2700 (2005).

**O. NAKAGOE, K. WATANABE, N. TAKAGI and Y. MATSUMOTO**, "In-Situ Observation of CO Oxidation on Ag(110)(2 $\times$ 1)-O by Scanning Tunneling Microscopy: Structural Fluctuation and Catalytic Activity," *J. Phys. Chem. B* **109**, 14536–14543 (2005).

**H. TSUNOYAMA, H. SAKURAI, N. ICHIKUNI, Y. NEGISHI and T. TSUKUDA**, "Colloidal Gold Nanoparticles as Catalyst for Carbon–Carbon Bond Formation: Application to Aerobic Homocoupling of Phenylboronic Acid in Water," *Langmuir* **20**, 11293–11296 (2004).

**Y. NEGISHI, K. NOBUSADA and T. TSUKUDA**, "Glutathione-Protected Gold Clusters Revisited: Bridging the Gap between Gold(I)-Thiolate Complexes and Thiolate-Protected Gold Nanocrystals," *J. Am. Chem. Soc.* **127**, 5261–5270 (2005).

**H. TSUNOYAMA, H. SAKURAI, Y. NEGISHI and T. TSUKUDA**, "Size-Specific Catalytic Activity of Polymer-Stabilized Gold Nanoclusters for Aerobic Alcohol Oxidation in Water," *J. Am. Chem. Soc.* **127**, 9374–9375 (2005).

**M. TAKAHASHI and Y. UDAGAWA**, "Development and Use of a Multichannel ( $e,2e$ ) Spectrometer for Electron Momentum Densities of Molecules," *J. Phys. Chem. Solids* **65**, 2055–2059 (2004).

**M. TAKAHASHI, N. WATANABE, Y. KHAJURIA, K. NAKAYAMA, Y. UDAGAWA and J. H. D. ELAND**, "Observation of Molecular Frame ( $e,2e$ ) Cross Section Using an Electron-Electron-Fragment Ion Triple Coincidence Apparatus," *J. Electron Spectrosc. Relat. Phenom.* **141**, 83–93 (2004).

**N. WATANABE, J. W. COOPER, R. W. VAN BOEYEN, J. P. DOERING, J. H. MOORE and M. A. COPLAN**, " $(e,3e)$  Collisions on Mg in the Impulsive Regime Studied by Second Born Approximation," *J. Phys. B: At., Mol. Opt. Phys.* **37**, 4551–4560 (2004).

**N. WATANABE, Y. KHAJURIA, M. TAKAHASHI and Y. UDAGAWA**, "Electron Momentum Spectroscopy of Valence Satellites of Neon," *J. Electron Spectrosc. Relat. Phenom.* **142**, 325–334 (2005).

**A. V. GOLOVIN, J. ADACHI, S. MOTOKI, M. TAKAHASHI and A. YAGISHITA**, "Inner-Shell Photoelectron Angular Distributions from Fixed-in-Space OCS Molecules," *J. Phys. B: At., Mol. Opt. Phys.* **38**, L63–L68 (2005).

**M. EHARA, Y. OHTSUKA, H. NAKATSUJI, M. TAKAHASHI and Y. UDAGAWA**, "Theoretical Fine Spectroscopy with Symmetry-Adapted-Cluster Configuration-Interaction Method: Outer- and Inner-Valence Ionization Spectra of Furan, Pyrrole, and Thiophene," *J. Chem. Phys.* **122**, 234319 (10 pages) (2005).

**M. TAKAHASHI, N. WATANABE, Y. KHAJURIA, Y. UDAGAWA and J. H. D. ELAND**, "Observation of a Molecular Frame ( $e,2e$ ) Cross Section: An ( $e,2e+M$ ) Triple Coincidence Study on H<sub>2</sub>," *Phys. Rev. Lett.* **94**, 213202 (4 pages) (2005).

**H. YAMANE, H. FUKAGAWA, S. NAGAMATSU, M. ONO, S. KERA, K. K. OKUDAIRA and N. UENO**, "Direct Observation of the HOMO-Hole/Vibration Coupling in Pentacene Thin Films by means of High-Resolution Ultraviolet Photoelectron Spectroscopy," *IPAP Conf. Ser.* **6**, 19–22 (2005).

- M. ONO, H. YAMANE, H. FUKAGAWA, S. KERA, D. YOSHIMURA, E. MORIKAWA, K. SEKI and N. UENO**, "Possibility of the Fermi Level Control by VUV-Induced Doping of an Organic Thin Film: Polytetrafluoroethylene," *IPAP Conf. Ser.* **6**, 27–30 (2005).
- S. KERA and N. UENO**, "Deep Insight into a Valence Hole in Organic Semiconductors: High-Resolution Ultraviolet Photoemission Spectroscopy," *IPAP Conf. Ser.* **6**, 51–56 (2005).
- H. FUKAGAWA, H. YAMANE, S. KERA, K. K. OKUDAIRA and N. UENO**, "Effects of the Dipole Density on the Electronic Structures of Oriented Thin Films of the Polarized Organic Molecule," *IPAP Conf. Ser.* **6**, 73–75 (2005).
- K. K. OKUDAIRA, E. KOBAYASHI, H. YAGI, S. KERA, K. MASE and N. UENO**, "Site-Specific Ion Desorption of Poly(tetrafluoroethylene) Studied Using Electron-Ion Coincidence Spectroscopy," *IPAP Conf. Ser.* **6**, 80–83 (2005).
- S. NAGAMATSU, M. ONO, S. KERA, K. K. OKUDAIRA, T. FUJIKAWA and N. UENO**, "Multiple Scattering Approach to Polarization-Dependent F K-Edge XANES Spectra of Polytetrafluoroethylene," *IPAP Conf. Ser.* **6**, 84–87 (2005).
- A. PATNAIK, K. K. OKUDAIRA, S. KERA, H. SETOYAMA, K. MASE and N. UENO**, "Polarized Near-Edge X-Ray-Absorption Fine Structure Spectroscopy of C<sub>60</sub>-Functionalized 11-Amino-1-Undecane Thiol Self-Assembled Monolayer: Molecular Orientation and Evidence for C<sub>60</sub> Aggregation," *J. Chem. Phys.* **122**, 154703 (9 pages) (2005).
- H. FUKAGAWA, H. YAMANE, S. KERA, K. K. OKUDAIRA and N. UENO**, "UPS Fine Structures of Highest Occupied Band in Vanadyl-Phthalocyanine Ultrathin Film," *J. Electron Spectrosc. Relat. Phenom.* **144-147**, 475–478 (2005).
- K. K. OKUDAIRA, T. WATANABE, S. KERA, E. KOBAYASHI, K. MASE and N. UENO**, "Site-Specific Ion Desorption of Fluorinated Phthalocyanine Studied with Electron-Ion Coincidence Spectroscopy," *J. Electron Spectrosc. Relat. Phenom.* **144-147**, 464–464 (2005).
- M. ONO, H. YAMANE, H. FUKAGAWA, S. KERA, D. YOSHIMURA, K. K. OKUDAIRA, E. MORIKAWA, K. SEKI and N. UENO**, "UPS Study of VUV-Photodegradation of Polytetrafluoroethylene (PTFE) Ultrathin Film by using Synchrotron Radiation," *Nucl. Instrum. Methods Phys. Res., Sect. B* **236**, 377–382 (2005).

## UVSOR Facility

- A. MOCHIHASHI, M. KATOH, M. HOSAKA, K. HAYASHI, J. YAMAZAKI, Y. TAKASHIMA and Y. HORI**, "Ion Trapping Phenomenon in UVSOR Electron Storage Ring," *Jpn. J. Appl. Phys.* **44**, 430–437 (2005).
- Y. TAKASHIMA, M. KATOH, M. HOSAKA, A. MOCHIHASHI, S. KIMURA and T. TAKAHASHI**, "Observation of Intense Bursts of Terahertz Synchrotron Radiation at UVSOR-II," *Jpn. J. Appl. Phys.* **44**, L1131–L1133 (2005).
- Y. HIKOSAKA and E. SHIGEMASA**, "Velocity Imaging Spectrometer for Negative Fragment Ions: Application to Dynamics of O<sub>2</sub> and N<sub>2</sub>O Ion-Pair Dissociation," *J. Electron Spectrosc. Relat. Phenom.* **148**, 5–10 (2005).
- P. LABLANQUIE, S. SEINERMAN, F. PENENT, T. AOTO, Y. HIKOSAKA and K. ITO**, "Dynamics of Double Photoionization near the Ar 2p Threshold Investigated by Threshold Electron-Auger Electron Coincidence Spectroscopy," *J. Phys. B* **38**, L9–L18 (2005).
- T. AOTO, Y. HIKOSAKA, R. HALL, F. PENENT, P. LABLANQUIE and K. ITO**, "Origin of Threshold Electrons Produced in Decay of the Xe 4d<sup>-1</sup>np Resonance," *J. Electron Spectrosc. Relat. Phenom.* **142**, 319–323 (2005).
- F. PENENT, P. LABLANQUIE, R. I. HALL, J. PALAUDOUX, K. ITO, Y. HIKOSAKA, T. AOTO and J. H. D. ELAND**, "Coincidence Auger Spectroscopy," *J. Electron Spectrosc. Relat. Phenom.* **144-147**, 7–11 (2005).
- T. KANEYASU, T. AZUMA and K. OKUNO**, "Collision Dynamics of the Kr<sup>8+</sup> + N<sub>2</sub> System Studied by a Multi-Coincidence Technique," *J. Phys. B* **38**, 1341 (2005).
- T. KANEYASU, T. AZUMA and K. OKUNO**, "Collision Dynamics of MCI-Molecule Systems Studied by Multi-Coincidence Technique," *Nucl. Instrum. Methods Phys. Res., Sect. B* **235**, 352 (2005).
- J. SICHELSDMIDT, V. VOEVODIN, V. PACHECO, YU. GRIN, F. STEGLICH, T. NISHI and S. KIMURA**, "Optical Investigations of the Clathrate  $\alpha$ -Eu<sub>8</sub>Ga<sub>16</sub>Ge<sub>30</sub>," *Eur. Phys. J. B* **46**, 363–366 (2005).
- I. ZEREC, W. CARRILLO-CABRERA, V. VOEVODIN, J. SICHELSDMIDT, F. STEGLICH, Y. GRIN, A. YARESKO and S. KIMURA**, "Influence of Cage Distortions on the Electronic Structure and Optical Properties of Ba<sub>6</sub>Ge<sub>25</sub>," *Phys. Rev. B* **72**, 045122 (7 pages) (2005).
- H. OKAMURA, T. MICHIZAWA, T. NANBA, S. KIMURA, F. IGA and T. TAKABATAKE**, "Indirect and Direct Energy Gaps in Kondo Semiconductor YbB<sub>12</sub>," *J. Phys. Soc. Jpn.* **74**, 1954–1957 (2005).
- B. K. LEE, J. B. HONG, J. W. KIM, K. -H. JANG, E. D. MUN, D. Y. KIM, M. H. JUNG, S. KIMURA, T. PARK, J. -G. PARK and Y. S. KWON**, "Kondo Ground States and Non-Fermi-Liquid Behavior in CeNi<sub>1-x</sub>Co<sub>x</sub>Ge<sub>2</sub>," *Phys. Rev. B* **71**, 214433 (9 pages) (2005).
- T. NISHI, S. KIMURA, T. TAKAHASHI, Y. MORI, Y. S. KWON, H. J. IM and H. KITAZAWA**, "Infrared Spectroscopy under Multi-Extreme Conditions: Direct Observation of Pseudo Gap Formation and Collapse in CeSb," *Phys. Rev. B* **71**, 220401(R) (4 pages) (2005).

- S. KIMURA, T. NISHI, Y. MORI, Y. SUMIDA, T. TAKAHASHI, Y. S. KWON, H. J. IM and H. KITAZAWA, "Infrared Study on CeSb under High Pressures," *Physica B* **359-361**, 190–192 (2005).
- K. SODA, K. SHIMBA, S. YAGI, M. KATO, T. TAKEUCHI, U. MIZUTANI, T. ZHANG, M. HASEGAWA, A. INOUE, T. ITO and S. KIMURA, "Electronic Structure of Bulk Metallic Glass  $Zr_{55}Al_{10}Cu_{30}Ni_5$ ," *J. Electron Spectrosc. Relat. Phenom.* **144-147**, 585–587 (2005).
- T. NISHI, S. KIMURA, T. TAKAHASHI, T. ITO, H. J. IM, Y. S. KWON, K. MIYAGAWA, H. TANIGUCHI, A. KAWAMOTO and K. KANODA, "The Origin of the Phase Separation in Partially Deuterated  $\kappa$ -(ET) $_2$ Cu[N(CN) $_2$ ]Br Studied by Infrared Magneto-Microspectroscopy," *Solid State Commun.* **134**, 189–193 (2005).
- H. OKAMURA, T. KORETSUNE, S. KIMURA, T. NANBA, H. IMAI, Y. SHIMAKAWA and Y. KUBO, "Carrier-Induced Infrared Magnetic Circular Dichroism in the Magnetoresistive Pyrochlore  $Tl_2Mn_2O_7$ ," *J. Phys. Soc. Jpn.* **74**, 970–974 (2005).
- B. K. LEE, D. H. RYU, D. Y. KIM, J. B. HONG, M. H. JUNG, H. KITAZAWA, O. SUZUKI, S. KIMURA and Y. S. KWON, "Magnetic Ordering in Frustrated  $Ce_5Ni_2Si_3$ ," *Phys. Rev. B* **70**, 224409 (5 pages) (2004).
- I. OUCHI, I. NAKAI, M. ONO and S. KIMURA, "Features of Fluorescence Spectra of Polyethylene Terephthalate Films," *Jpn. J. Appl. Phys.* **43**, 8107–8114 (2004).
- D. Y. KIM, D. H. RYU, J. B. HONG, J. -G. PARK, Y. S. KWON, M. A. JUNG, M. H. JUNG, N. TAKEDA, M. ISHIKAWA and S. KIMURA, "Anomalous Magnetic Properties and Non-Fermi-Liquid Behavior in Single Crystals of the Kondo Lattice  $CeNiGe_{2-x}Si_x$ ," *J. Phys.: Condens. Matter* **16**, 8323–8334 (2004).

### Laser Research Center for Molecular Science

- A. YOSHIKAWA, H. OGINO, J. B. SHIM, V. V. KOCHURIKIN, M. NIKL, N. SOLOVIEVA, S. ONO, N. SARUKURA, M. KIKUCHI and T. FUKUDA, "Growth and Scintillation Properties of Yb Doped Aluminate, Vanadate and Silicate Single Crystals," *Opt. Mater.* **26**, 529–534 (2004).
- A. QUEMA, M. GOTO, M. SAKAI, G. JANAIRO, R. E. OUEZERFI, H. TAKAHASHI, S. ONO and N. SARUKURA, "Onset Detection of Solid-State Phase Transition in Estrogen-Like Chemical *via* Terahertz Transmission Spectroscopy," *Appl. Phys. Lett.* **85**, 3914–3916 (2004).
- R. E. OUEZERFI, S. ONO, A. QUEMA, M. GOTO, M. SAKAI, N. SARUKURA, T. NISHIMATSU, N. TERAKUBO, H. MIZUSEKI, Y. KAWAZOE, H. SATO, A. YOSHIKAWA and T. FUKUDA, "Design Principle of Wide-Gap Fluoride Hetero-Structures for Deep Ultraviolet Optical Devices," *J. Appl. Phys.* **96**, 7655–7659 (2004).
- K. YAMAMOTO, K. TOMINAGA, H. SASAKAWA, A. TAMURA, H. MURAKAMI, H. OHTAKE and N. SARUKURA, "Terahertz Time-Domain Spectroscopy of Amino Acids and Polypeptides," *Biophys. J.* **L22-L24** (2005).
- K. MIZUUCHI, A. MORIKAWA T. SUGITA, K. YAMAMOTO, N. PAVEL and T. TAIRA, "Continuous-Wave Deep Blue Generation in a Periodically Poled MgO:LiNbO $_3$  Crystal by Single-Pass Frequency Doubling of a 912-nm Nd:GdVO $_4$  Laser," *Jpn. J. Appl. Phys.* **43**, 1293–1295 (2004).
- M. HARADA, K. MURAMATSU, Y. IWASAKI, S. KURIMURA and T. TAIRA, "Periodic Twinning in Crystal Quartz for Optical Quasi-Phase Matched Secondary Harmonic Conversion," *J. Mater. Res.* **19**, 969–972 (2004).
- J. SAIKAWA, Y. SATO, T. TAIRA and A. IKESUE, "Absorption, Emission Spectrum Properties, and Efficient Laser Performances of Yb:Y $_3$ ScAl $_4$ O $_{12}$  Ceramics," *Appl. Phys. Lett.* **85**, 1898–1900 (2004).
- H. ISHIZUKI, I. SHOJI and T. TAIRA, "High-Energy Quasi-Phase-Matched Optical Parametric Oscillation in a 3-mm-Thick Periodically Poled MgO:LiNbO $_3$  Device," *Opt. Lett.* **29**, 2527–2529 (2004).
- K. MIZUUCHI, A. MORIKAWA, T. SUGITA, K. YAMAMOTO, N. PAVEL and T. TAIRA, "Continuous-Wave Ultraviolet Generation at 354 nm in a Periodically Poled MgO:LiNbO $_3$  by Frequency Tripling of a Diode End-Pumped Nd:GdVO $_4$  Microlaser," *Appl. Phys. Lett.* **85**, 3959–3961 (2004).
- J. SAIKAWA, Y. SATO, T. TAIRA and A. IKESUE, "Passive Mode Locking of a Mixed Garnet Yb:Y $_3$ ScAl $_4$ O $_{12}$  Ceramic Laser," *Appl. Phys. Lett.* **85**, 5845–5847 (2004).
- Y. SATO, T. TAIRA, O. NAKAMURA and Y. FURUKAWA, "Stark Levels, Selection Rules, and Polarized Cross Sections of Yb:GdVO $_4$  Single Crystal," *OSA TOPS on Advanced Solid-State Photonics* **98**, 13–17 (2005).
- H. ISHIZUKI and T. TAIRA, "Periodically Poled 5mm-Thick MgO-Doped Congruent LiNbO $_3$  for High Power/Energy Wavelength Conversion," *OSA TOPS on Advanced Solid-State Photonics* **98**, 97–101 (2005).
- J. SAIKAWA, Y. SATO, T. TAIRA, O. NAKAMURA and Y. FURUKAWA, "879-nm Direct-Pumped Nd:GdVO $_4$  Lasers: 1.3- $\mu$ m Laser Emission and Heat Generation Characteristics," *OSA TOPS on Advanced Solid-State Photonics* **98**, 183–187 (2005).
- N. PAVEL, Y. SATO, T. TAIRA, Y. TAMAOKI and H. KAN, "Generation of 5 W Continuous-Wave Green Power at 531 nm Based on a Frequency-Doubled Nd:GdVO $_4$  Micro-Laser Pumped into the Emitting Level at 879 nm," *OSA TOPS on Advanced Solid-State Photonics* **98**, 462–467 (2005).
- N. PAVEL, T. TAIRA, K. MIZUUCHI, A. MORIKAWA, T. SUGITA and K. YAMAMOTO, "Continuous-Wave 456-nm Blue Light Generation in a Bulk Periodically Poled MgO:LiNbO $_3$  Crystal," *OSA TOPS on Advanced Solid-State Photonics* **98**, 468–472 (2005).

- M. TSUNEKANE, T. DASCALU and T. TAIRA**, "High-Power Operation of Diode Edge-Pumped, Microchip Yb:YAG Laser Composed with YAG Ceramic Pump Wave-Guide," *OSA TOPS on Advanced Solid-State Photonics* **98**, 603–607 (2005).
- N. PAVEL, V. LUPEI and T. TAIRA**, "1.34- $\mu\text{m}$  Efficient Laser Emission in Highly-Doped Nd:YAG under 885-nm Diode Pumping," *Optics Express* **13**, 7948–7953 (2005).
- M. TSUNEKANE and T. TAIRA**, "High-Power Operation of Diode Edge-Pumped, Glue-Bonded, Composite Yb:YAG Microchip Laser with Ceramic YAG Pump Light-Guide," *Jpn. J. Appl. Phys.* **44**, 1164–1167 (2005).
- N. PAVEL and T. TAIRA**, "High-Power Continuous-Wave Intracavity Frequency-Doubled Nd:GdVO<sub>4</sub>-LBO Laser under Diode Pumping into the Emitting Level," *IEEE J. Sel. Top. Quantum Electron.* **11**, 631–637 (2005).
- Y. SATO and T. TAIRA**, "Comparative Study on the Spectroscopic Properties of Nd:GdVO<sub>4</sub> and Nd:YVO<sub>4</sub> with Hybrid Process," *IEEE J. Sel. Top. Quantum Electron.* **11**, 613–620 (2005).

### Safty Office

- J. NISHIDA, NARASO, S. MURAI, E. FUJIWARA, H. TADA, M. TOMURA and Y. YAMASHITA**, "Preparation, Characterization and FET Properties of Novel Dicyanopyrazinoquinoxaline Derivatives," *Org. Lett.* **6**, 2007–2010 (2004).
- K. ONO, T. IWAO, H. UCHIUMI, T. SUZUKI, M. TOMURA, M. OHKITA and K. SAITO**, "Molecular Arrangement in the Cocrystals of 1,1',3,3'-Tetramethyl-2,2'-bi-1*H*-imidazolium Bis(tetraphenylborate) with Ketone, Aldehyde, and Nitrile as Guest Molecules," *Bull. Chem. Soc. Jpn.* **78**, 867–872 (2005).
- K. ONO, S. EZAKA, A. HIGASHIBATA, R. HOSOKAWA, M. OHKITA, K. SAITO, M. SUTO, M. TOMURA, Y. MATSUSHITA, S. NAKA, H. OKADA and H. ONNAGAWA**, "Macrocyclic and Acyclic Bis(2,5-diphenyl-1,3,4-oxadiazole)s with Electron-Transporting and Hole-Blocking Ability in Organic Electroluminescent Devices," *Macromol. Chem. Phys.* **206**, 1576–1582 (2005).
- M. AKHTARUZZAMAN, N. KAMATA, J. NISHIDA, S. ANDO, H. TADA, M. TOMURA and Y. YAMASHITA**, "Synthesis, Characterization and FET Properties of Novel Dithazolylbenzothiadiazole Derivatives," *Chem. Commun.* 3183–3185 (2005).

### Okazaki Institute for Integrative Bioscience

- N. SAKAKI, R. SHIMO-KON, K. ADACHI, H. ITOH, S. FURUIKE, E. MUNHEYUKI, M. YOSHIDA and K. KINOSITA, Jr.**, "One Rotary Mechanism for F<sub>1</sub>-ATPase over ATP Concentrations from Millimolar down to Nanomolar," *Biophys. J.* **88**, 2047–2056 (2005).
- H. UENO, T. SUZUKI, K. KINOSITA, Jr. and M. YOSHIDA**, "ATP-Driven Stepwise Rotation of F<sub>0</sub>F<sub>1</sub>-ATP Synthase," *Proc. Natl. Acad. Sci. U.S.A.* **102**, 1333–1338 (2005).
- Y. HIRONO-HARA, K. ISHIZUKA, K. KINOSITA, Jr., M. YOSHIDA and H. NOJI**, "Activation of Pausing F<sub>1</sub> Motor by External Force," *Proc. Natl. Acad. Sci. U.S.A.* **102**, 4288–4293 (2005).
- T. OHTA, H. YOSHIMURA, S. YOSHIOKA, S. AONO and T. KITAGAWA**, "Oxygen Sensing Mechanism of HemAT from *B. subtilis*: A Resonance Raman Spectroscopic Study," *J. Am. Chem. Soc.* **126**, 15000–15001 (2004).
- S. INAGAKI, C. MASUDA, T. AKAISHI, H. NAKAJIMA, S. YOSHIOKA, T. OHTA, T. KITAGAWA and S. AONO**, "Spectroscopic and Redox Properties of a CooA Homologue from *Carboxydotherrmus hydrogenoformans*," *J. Biol. Chem.* **280**, 3269–3274 (2005).
- K. KOBAYASHI, S. YOSHIOKA, Y. KATO, Y. ASANO and S. AONO**, "Regulation of Aldoxime Dehydratase Activity by Redox-Dependent Change in the Coordination Structure of the Aldoxime-Heme Complex," *J. Biol. Chem.* **280**, 5486–5490 (2005).
- M. KUJIME and H. FUJII**, "Synthesis of Sterically Hindered Tris(4-imidazolyl)carbinol Ligands and Their Copper(I) Complexes Related to Metalloenzymes," *Tetrahedron Lett.* **46**, 2809–2812 (2005).
- A. WADA, Y. HONDA, S. YAMAGUCHI, S. NAGATOMO, T. KITAGAWA, K. JITSUKAWA and H. MASUDA**, "Steric and Hydrogen-Bonding Effects on the Stability of Copper Complexes with Small Molecules," *Inorg. Chem.* **43**, 5725–5735 (2004).
- E. SATO, I. SAGAMI, T. UCHIDA, A. SATO, T. KITAGAWA, J. IGARASHI and T. SHIMIZU**, "SOUL in Mouse Eyes Is a New Hexameric Heme-Binding Protein with Characteristic Optical Absorption, Resonance Raman Spectral, and Heme-Binding Properties," *Biochemistry* **43**, 14189–14198 (2004).
- K. KONISHI, K. ISHIDA, K. OINUMA, T. OHTA, Y. HASHIMOTO, H. HIGASHIBATA, T. KITAGAWA and M. KOBAYASHI**, "Identification of Crucial Histidines Involved in Carbon-Nitrogen Triple Bond Synthesis by Aldoxime Dehydratase," *J. Biol. Chem.* **279**, 47619–47625 (2004).
- T. UCHIDA, J. M. STEVENS, O. DALTROP, E. M. HARVAT, L. HONG, S. J. FERGUSON and T. KITAGAWA**, "The Interaction of Covalently Bound Heme with the Cytochrome *c* Maturation Protein CcmE," *J. Biol. Chem.* **279**, 51981–51988 (2004).

- T. UCHIDA, T. MOGI, H. NAKAMURA and T. KITAGAWA**, "Role of Tyr-288 at the Dioxygen Reduction Site of Cytochrome *bo* Studied by Stable Isotope Labeling and Resonance Raman Spectroscopy," *J. Biol. Chem.* **279**, 53613–53620 (2004).
- S. YAMAGUCHI, A. WADA, S. NAGATOMO, T. KITAGAWA, K. JITSUKAWA and H. MASUDA**, "Thermal Stability of Mononuclear Hydroperoxocopper(II) Species. Effects of Hydrogen Bonding and Hydrophobic Field," *Chem. Lett.* **33**, 1556–1557 (2004).
- X. ZHANG, H. FURUTACHI, S. FUJINAMI, S. NAGATOMO, Y. MAEDA, Y. WATANABE, T. KITAGAWA and M. SUZUKI**, "Structural and Spectroscopic Characterization of ( $\mu$ -Hydroxo or  $\mu$ -Oxo)( $\mu$ -Peroxo)Diiron(III) Complexes: Models for Peroxo Intermediates of Non-Heme Diiron Proteins," *J. Am. Chem. Soc.* **127**, 826–827 (2005).
- H. FURUTACHI, K. HASHIMOTO, S. NAGATOMO, T. ENDO, S. FUJINAMI, Y. WATANABE, T. KITAGAWA and M. SUZUKI**, "Reversible O–O Bond Cleavage and Formation of a Peroxo Moiety of a Peroxo-carbonate Ligand Mediated by an Iron(III) Complex," *J. Am. Chem. Soc.* **127**, 4550–4551 (2005).
- K. ITOH, H. HAYASHI, H. FURUTACHI, T. MATSUMOTO, S. NAGATOMO, T. TOSHA, S. TERADA, S. FUJINAMI, M. SUZUKI and T. KITAGAWA**, "Synthesis and Reactivity of a ( $\mu$ -1,1-Hydroperoxo)( $\mu$ -Hydroxo) Dicopper(II) Complex: Ligand Hydroxylation by a Bridging Hydroperoxo Ligand," *J. Am. Chem. Soc.* **127**, 5212–5223 (2005).
- H. HIRAMATSU, Y. GOTO, H. NAIKI and T. KITAGAWA**, "Structural Model of the Amyloid Fibril Formed by  $\beta_2$ -Microglobulin #21–31 Fragment Based on Vibrational Spectroscopy," *J. Am. Chem. Soc.* **127**, 7988–7989 (2005).
- Y. J. MO, D. L. JIANG, M. UYEMURA, T. AIDA and T. KITAGAWA**, "Energy Funneling of IR Photons Captured by Dendritic Antennae and Acceptor Mode Specificity: Anti-Stokes Resonance Raman Studies on Iron(III) Porphyrin Complexes with a Poly(Aryl Ether) Dendrimer Framework," *J. Am. Chem. Soc.* **127**, 10020–10027 (2005).
- S. INAGAKI, C. MASUDA, T. AKAISHI, H. NAKAJIMA, S. YOSHIOKA, T. OHTA, B. PAL, T. KITAGAWA and S. AONO**, "Spectroscopic and Redox Properties of a CooA Homologue from *Carboxydothermus hydrogenoformans*," *J. Biol. Chem.* **280**, 3269–3274 (2005).
- K. MATSUURA, S. YOSHIOKA, T. TOSHA, H. HORI, K. ISHIMORI, T. KITAGAWA, I. MORISHIMA, N. KAGAWA and M. R. WATERMAN**, "Structural Diversities of Active Site in Clinical Azole-Bound Forms between Sterol 14 $\alpha$ -Demethylases (Cyp51s) from Human and *Mycobacterium tuberculosis*," *J. Biol. Chem.* **280**, 9088–9096 (2005).
- T. UCHIDA, E. SATO, A. SATO, I. SAGAMI, T. SHIMIZU and T. KITAGAWA**, "CO-Dependent Activity-Controlling Mechanism of Heme-Containing CO-Sensor Protein, Neuronal PAS Domain Protein," *J. Biol. Chem.* **280**, 21358–21368 (2005).
- Z. Q. LI, B. PAL, S. TAKENAKA, S. TSUYAMA and T. KITAGAWA**, "Resonance Raman Evidence for the Presence of Two Heme Pocket Conformations with Varied Activities in CO-Bound Bovine Soluble Guanylate Cyclase and Their Conversion," *Biochemistry* **44**, 939–946 (2005).
- Y. NAGANO, J. G. LIU, Y. NARUTA and T. KITAGAWA**, "UV Resonance Raman Study of Model Complexes of the Cu<sub>B</sub> Site of Cytochrome *c* Oxidase," *J. Mol. Struct.* **735-736**, 279–291 (2005).
- K. OINUMA, H. KUMITA, T. OHTA, K. KONISHI, Y. HASHIMOTO, H. HIGASHIBATA, T. KITAGAWA, Y. SHIRO and M. KOBAYASHI**, "Stopped-Flow Spectrophotometric and Resonance Raman Analyses of Aldoxime Dehydratase Involved in Carbon-Nitrogen Triple Bond Synthesis," *FEBS Lett.* **579**, 1394–1398 (2005).
- S. YAMAGUCHI, A. KUMAGAI, S. NAGATOMO, T. KITAGAWA, Y. FUNAHASHI, T. OZAWA, K. JITSUKAWA and H. MASUDA**, "Synthesis, Characterization, and Thermal Stability of New Mononuclear Hydrogenperoxocopper(II) Complexes with N<sub>3</sub>O-Type Tripodal Ligands Bearing Hydrogen-Bonding Interaction Sites," *Bull. Chem. Soc. Jpn.* **78**, 116–124 (2005).
- R. KOUDO, H. KUROKAWA, E. SATO, J. IGARASHI, T. UCHIDA, I. SAGAMI, T. KITAGAWA and T. SHIMIZU**, "Spectroscopic Characterization of the Isolated Heme-Bound PAS-B Domain of Neuronal PAS Domain Protein 2 (NPAS2) Associated with Circadian Rhythms," *FEBS J.* **272**, 4153–4162 (2005).
- S. NAGATOMO, M. NAGAI, Y. MIZUTANI, T. YONETANI and T. KITAGAWA**, "Quaternary Structures of Intermediately Ligated Hemoglobin and Influences from Strong Allosteric Effectors; Resonance Raman Investigation," *Biophys. J.* **89**, 1203–1213 (2005).
- J. M. STEVENS, T. UCHIDA, O. DALTROP and S. J. FERGUSON**, "Covalent Cofactor Attachment to Proteins: Cytochrome *c* Biogenesis," *Biochem. Soc. Trans.* **33**, 792–795 (2005).

P. CARNINCI, T. KASUKAWA, S. KATAYAMA, J. GOUGH, M. C. FRITH, N. MAEDA, R. OYAMA, T. RAVASI, B. LENHARD, C. WELLS, R. KODZIUS, K. SHIMOKAWA, V. B. BAJIC, S. E. BRENNER, S. BATALOV, A. R. R. FORREST, M. ZAVOLAN, M. J. DAVIS, L. G. WILMING, V. AIDINIS, J. E. ALLEN, A. AMBESI-IMPIOMBATO, R. APWEILER, R. N. ATURALIYA, T. L. BAILEY, M. BANSAL, L. BAXTERI, K. W. BEISEL, T. BERSANO-BEGEY, H. BONO, A. M. CHALK, K. P. CHIU, V. CHOUDHARY, A. CHRISTOFFELS, D. R. CLUTTERBUCK, M. L. CROWE, E. DALLA, B. P. DALRYMPLE, B. DE BONO, G. DELLA GATTA, D. DI BERNARDO, T. DOWN, P. ENGSTROM, M. FAGIOLINI, G. FAULKNER, C. F. FLETCHER, T. FUKUSHIMA, M. FURUNO, S. FUTAKI, M. GARIBOLDI, P. GEORGII-HEMMING, T. R. GINGERAS, T. GOJOBORI, R. E. GREEN, S. GUSTINCICH, M. HARBERS, Y. HAYASHI, T. K. HENSCH, N. HIROKAWA, D. HILL, L. HUMINIECKI, M. IACONO, K. IKEO, A. IWAMA, T. ISHIKAWA, M. JAKT, A. KANAPIN, M. KATOH, Y. KAWASAWA, J. KELSO, H. KITAMURA, H. KITANO, G. KOLLIAS, S. P. T. KRISHNAN, A.F. KRUGER, S. K. KUMMERFELD, I. V. KUROCHKIN, L. F. LAREAU, D. LAZAREVIC, L. LIPOVICH, J. LIU, S. LIUNI, S. MCWILLIAM, M. MADAN BABU, M. MADERA, L. MARCHIONNI H. MATSUDA, S. MATSUZAWA, H. MIKI, F. MIGNONE, S. MIYAKE, K. MORRIS, S. MOTTAGUI-TABAR, N. MULDER, N. NAKANO, H. NAKAUCHI, P. NG, R. NILSSON, S. NISHIGUCHI, S. NISHIKAWA, F. NORI, O. OHARA, Y. OKAZAKI, V. ORLANDO, K. C. PANG, W. J. PAVAN, G. PAVESI, G. PESOLE, N. PETROVSKY, S. PIAZZA, J. REED, J. F. REID, B. Z. RING, M. RINGWALD, B. ROST, Y. RUAN, S. L. SALZBERG A. SANDELIN, C. SCHNEIDER, C. SCHÖNBACH, K. SEKIGUCHI, C. A. M. SEMPLE, S. SENO, L. SESSA, Y. SHENG, Y. SHIBATA, H. SHIMADA, K. SHIMADA, D. SILVA, B. SINCLAIR, S. SPERLING, E. STUPKA, K. SUGIURA, R. SULTANA, Y. TAKENAKA, K. TAKI, K. TAMMOJA, S. L. TAN, S. TANG, M. S. TAYLOR, J. TEGNER, S. A. TEICHMANN, H. R. UEDA, E. VAN NIMWEGENE, R. VERARDO, C. L. WEI, K. YAGI, H. YAMANISHI, E. ZABAROVSKY, S. ZHU, A. ZIMMER, W. HIDE, C. BULT, S. M. GRIMMOND, R. D. TEASDALE, E. T. LIU, V. BRUSIC, J. QUACKENBUSH, C. WAHLESTEDT, J. S. MATTICK, D. A. HUME, C. KAI, D. SASAKI, Y. TOMARU, S. FUKUDA, M. KANAMORI-KATAYAMA, M. SUZUKI, J. AOKI, T. ARAKAWA, J. IIDA, K. IMAMURA, M. ITOH, T. KATO, H. KAWAJI, N. KAWAGASHIRA, T. KAWASHIMA, M. KOJIMA, S. KONDO, H. KONNO, K. NAKANO, N. NINOMIYA, T. NISHIO, M. OKADA, C. PLESSY, K. SHIBATA, T. SHIRAKI, S. SUZUKI, M. TAGAMI, K. WAKI, A. WATAHIKI, Y. OKAMURA-OHO, H. SUZUKI, J. KAWAI and Y. HAYASHIZAKI, "The Transcriptional Landscape of the Mammalian Genome," *Science* **309**, 1559–1563 (2005).



## REVIEW ARTICLES AND TEXTBOOKS

### Department of Theoretical Studies

**Z. SIANINA, K. KOBAYASHI and S. NAGASE**, “Gibbs Energy Treatment of Ca@C<sub>74</sub>, Ca@C<sub>82</sub>, and La@C<sub>82</sub>,” in *Fullerenes and Nanotubes: Materials for the New Chemical Frontier*, P. V. Kamat, D. M. Guldi, F. D’Souza and S. Fukuzumi, Eds., The Electrochemical Society; Pennington, **14**, pp. 71–83 (2004).

**Z. SLANINA, F. UHLIK, O. V. BOLTALINA, K. KOBAYASHI and S. NAGASE**, “Computations of New Observations for C<sub>60</sub>F<sub>36</sub> and C<sub>60</sub>H<sub>36</sub>,” in *Fullerenes and Nanotubes: Materials for the New Chemical Frontier*, P. V. Kamat, D. M. Guldi, F. D’Souza and S. Fukuzumi, Eds., The Electrochemical Society; Pennington, **14**, pp. 94–102 (2004).

**Z. SLANINA, F. UHLIK, L. ADAMOWICZ, K. KOBAYASHI and S. NAGASE**, “Excited Electronic States and Relative Stabilities of C<sub>80</sub> Isomers,” in *Fullerenes and Nanotubes: Materials for the New Chemical Frontier*, P. V. Kamat, D. M. Guldi, F. D’Souza and S. Fukuzumi, Eds., The Electrochemical Society; Pennington, **14**, pp. 168–177 (2004).

**Z. SLANINA and S. NAGASE**, “Computing Encapsulation of Non-Metallic Molecules,” in *NANOTECH 2005—Technical Proceedings of the 2005 NSTI Nanotechnology Conference and Trade Show*, NanoScience and Technology Institute; Cambridge, 2005, pp. 222–225 (2005).

**Z. SLANINA and S. NAGASE**, “Computational Chemistry of Isomeric Fullerenes and Endofullerenes,” in *Theory and Application of Computational Chemistry: The First Forty Years*, C. E. Dykstra, G. Frenking, K. S. Kim and G. E. Scuseria, Eds., Elsevier; Amsterdam, Chapter 32, pp. 891–917 (2005).

**Y. TANIMURA, H. SATO, T. YODA, R. AKIYAMA, S. FUJIWARA and H. OKUMURA**, (translation), P.R. BERGETHON, *The Physical Basis of Biochemistry: The Foundations of Molecular Biophysics*, (translation into Japanese), Springer-Verlag; Tokyo (2004).

**Y. OKAMOTO and S. TAKADA**, “Approaching Protein Tertiary Structure Prediction Problem from Protein Folding Simulations,” in *Special Series: Water and Biomolecules* (in Japanese), *Modern Chemistry* (GENDAI KAGAKU), No. **408**, 47–53 (2005).

**C. ZHU, G. V. MIL’NIKOV and H. NAKAMURA**, “Semiclassical Theory of Nonadiabatic Transition and Tunneling,” in *Modern Trends in Chemical Reaction Dynamics*, X. Yang and K. Liu, Eds., World Scientific; Singapore, Chap 10 (2004).

**H. NAKAMURA**, “Nonadiabatic Transition—An Origin of Mutability of This World,” in *Nonadiabatic Transition in Quantum Systems*, V. I. Osherov and L. I. Ponomarev, Eds., Institute of Problems of Chemical Physics, Russian Academy of Sciences; Chernogolovka, pp. 12–36 (2004).

**V. I. OSHEROV, V. G. USHAKOV and H. NAKAMURA**, “Nonadiabatic Transition—between Asymptotically Degenerate States,” in *Theory of Chemical Reaction Dynamics*, A. Lagana and G. Lendvay, Eds., Kluwer Academic Publisher, pp. 105–127 (2004).

**H. NAKAMURA**, *Chemical Reaction Dynamics* (in Japanese), Asakura Publ. Co.; Tokyo (2004).

### Department of Molecular Structure

**K. IMURA, T. NAGAHARA and H. OKAMOTO**, “Plasmon-Mode Imaging and Dynamics of Gold Nanorods,” *OYO BUTURI* (in Japanese) **74**, 492–496 (2005).

### Department of Electronic Structure

**K. OHMORI**, “Coherent Control with Attosecond Precision Applied to Vibrational Wave-Packets in Molecules,” *BUTSURI* (the monthly membership journal of the Physical Society of Japan) (in Japanese) **59**, 615 (4 pages) (2004).

### Department of Molecular Assemblies

**A. KOBAYASHI, E. FUJIWARA and H. KOBAYASHI**, “Single-Component Molecular Metals with Extended-TTF Dithiolate Ligands,” *Chem. Rev.* **104**, 5243–5264 (2004).

**H. KOBAYASHI, H. CUI and A. KOBAYASHI**, “Organic Metals and Superconductors Based on BETS (BETS = bis(ethylenedithio)tetraseleno-fulvalene),” *Chem. Rev.* **104**, 5265–5288 (2004).

**T. ENOKI, M. AIMATSU, H. YAMAZAKI, K. OKABE, J. NISHIJO, K. ENOMOTO, A. MIYAZAKI, K. UGAWA, E. OGURA, Y. KUWATANI, M. IYODA, O. NAUMENKO and Y. V. SUSHKO**, "Unconventional Properties of TTF-Based Organic Magnetic Conductors, Organic Conductors, Superconductors and Magnets: From Synthesis to Molecular Electronics," in *NATO Science Series II*, Lahcène Ouahab and Edward Yagubskii, Eds., Kluwer Academic Publishers; Dordrecht/Boston/London, **139**, 113–126 (2004).

**T. ENOKI**, "Intercalation and Guest-Host Interaction in Nano-Graphite," *J. Phys. Chem. Solids* **65**, 103–108 (2004).

**L. OUAHAB and T. ENOKI**, "Multiproperty Molecular Materials: TTF-Based Conducting and Magnetic Molecular Materials," *Eur. J. Inorg. Chem.* 933–941 (2004).

**T. ENOKI and A. MIYAZAKI**, "Magnetic TTF-Based Charge Transfer Complexes," *Chem. Rev.* **104**, 5449–5477 (2004).

**T. NAITO**, "Can Light Convert Molecular Material into Molecular Devices?" *Chemistry and Chemical Industry* (in Japanese), The Chemical Society of Japan, **58**, 227–228 (2005).

**K. MIYAGAWA, K. KANODA and A. KAWAMOTO**, "NMR Studies on Two-Dimensional Molecular Conductors and Superconductors: Mott Transition in  $\kappa$ -(BEDT-TTF)<sub>2</sub>X," *Chem. Rev.* **104**, 5635–5653 (2004).

### Department of Applied Molecular Science

**D. -L. JIANG**, "Molecular Design of Light-Harvesting Antennae," in *Dendritic Polymers* (in Japanese), NTS; Tokyo (2005).

### Department of Vacuum UV Photoscience

**J. ADACHI, N. KOSUGI and A. YAGISHITA**, "Symmetry-Resolved Soft X-Ray Absorption Spectroscopy: Its Application to Simple Molecules," *J. Phys. B: At., Mol. Opt. Phys.* **38**, R127–R152 (2005).

### Coordination Chemistry Laboratories

**H. KAWAGUCHI and T. MATSUO**, "Aryloxide-Based Multidentate Ligands for Early Transition Metals and f-Element Metals," *J. Organomet. Chem.* **689**, 4228–4243 (2004). (special issue "40<sup>th</sup> Anniversary of *J. Organomet. Chem.*")

**K. MASHIMA**, "Ligand Architecture on Stereocontrol of Half-Metallocene Benzylidene Complexes of Niobium and Tantalum," *Advanced Synthesis & Catalysis (special issue dedicated to Professor R. Schrock)* **47**, 323–328 (2005).

**A. NAKAMURA and K. MASHIMA**, "Diene Complexes of Early Transition Metals: Ideas and Progresses at Osaka University," *J. Organomet. Chem.* **689**, 4552–4563 (2004). (special issue "40<sup>th</sup> Anniversary of *J. Organomet. Chem.*")

**K. MASHIMA**, "Catalytic and Stoichiometric Reactions by Half-Metallocene Diene Complexes of Niobium and Tantalum," *J. Synth. Org. Chem. Jpn.* **62**, 1166–1171 (2004).

### Research Center for Molecular-scale Nanoscience

**T. OGAWA**, "Electrical Conductance of Single Molecules," *Surface Science* (in Japanese) **25**, 732–737 (2004).

**T. OGAWA**, "Recent Trend in the Studies of Single Molecular Conductance," *Chemistry* (in Japanese) **60**, 72–73 (2005).

**T. OGAWA**, "Single Molecular Device," in *The Fifth Series of Experimental Chemistry* (in Japanese), Maruzen; Tokyo, **28**, pp. 179–197 (2005).

**Y. UOZUMI**, "Recent Progress in Polymeric Palladium Catalysts for Organic Synthesis," *Top. Curr. Chem.* **242**, 77–112 (2004).

**H. ADACHI, H. UNO, A. KAMIMURA, S. KAWABATA, M. KURAMOTO, S. SHINODA, H. TSUKUBE, T. NAGATA, Y. NISHIGAICHI, K. MITSUKURA, Y. MORIMOTO and H. YAMADA**, *First Step in Organic Spectroscopic Analysis*, H. Uno and H. Tsukube, Eds, Maruzen; Japan (in Japanese) (2004).

**T. HIRAO and H. SAKURAI**, "Synthesis of Sumanene, a Bowl-Shaped Conjugated Compound," *Chemistry and Chemical Industry* (in Japanese) **57**, 954–956 (2004).

**Y. MATSUMOTO**, "Surface Dynamics Studied by Time-Resolved Nonlinear Spectroscopy," *Rev. Laser Engineering* (in Japanese) **32**, 694–700 (2004).

**Y. MATSUMOTO**, "Dynamic Formation of Surface Reaction Sites by Structural Fluctuations," *Shokubai* (in Japanese) **46**, 558–563 (2004).

**Y. KAMIYA, Y. YAMAGUCHI and K. KATO**, "NMR for Structural Glycobiology," in *Tousa Kagaku No Shintenkai* (in Japanese), N. Taniguchi and Y. Ito, Eds., NTS; Tokyo, pp. 76–83 (2005).

**M. C. COPLAN, R. W. VAN BOEYEN, J. H. MOORE, J. P. DOERING, J. W. COOPER and N. WATANABE**, "Identification of Double Ionization Mechanisms, Results Bearing on Electron Correlation Measurements," in *Electron and Photon Impact Ionization and Related Topics 2004*, B. Piraux, Ed., Inst. Phys. Conf. Ser. No. 183, Institute of Physics; Bristol and Philadelphia (2004).

**M. TAKAHASHI, T. SAITO and Y. UDAGAWA**, "An Investigation of the Two Outermost Orbitals of Glyoxal and Biacetyl by Electron Momentum Spectroscopy," in *Electron Scattering from Atoms, Molecules, Nuclei and Bulk Matter*, C. T. Whelan and N. J. Mason, Eds., Kluwer Academic/Plenum Publishers; New York (2005).

**M. TAKAHASHI**, "Some Recent Highlights of Electron-Molecule Collision Studies," *Parity* (in Japanese) **20**, 6–8 (2005).

**M. TAKAHASHI**, "Detection of Charged Particles," *The Fifth Series of Experimental Chemistry* (in Japanese), Maruzen: Tokyo, **10**, pp. 315–320 (2005).

### **Okazaki Institute for Integrative Bioscience**

**S. AONO**, "Regulation of Biological Function by Carbon Monoxide," *Chemistry & Education* (in Japanese) **381**, 132–135 (2005).

**B. PAL and T. KITAGAWA**, "Interactions of Soluble Guanylate Cyclase with Diatomics as Probed by Resonance Raman Spectroscopy," *J. Inorg. Biochem.* **99**, 267–279 (2005).

**T. UCHIDA and T. KITAGAWA**, "Mechanism for Transduction of the Ligand-Binding Signal in Heme-Based Gas Sensory Proteins Revealed by Resonance Raman Spectroscopy," *Acc. Chem. Res.* **38**, 662–670 (2005).

**T. OHTA and T. KITAGAWA**, "Resonance Raman Investigation on the Specific Sensing Mechanism of a Target Molecule by Gas Sensory Proteins," *Inorg. Chem.* **44**, 758–769 (2005).



## AUTHOR INDEX

## to “Research Activities” and “Special Research Projects”

**A**

ABE, Hitoshi 54–55  
 ADACHI, Junichi 175  
 ADACHI, Kengo 195  
 ADAMOWICZ, Ludwik 17, 19, 21  
 AIDA, Takuzo 204  
 AIKAWA, Katsuji 136  
 AKAGI, Fumio 139  
 AKAISHI, Tetsuhiro 197, 207  
 AKASAKA, Takeshi 18–22  
 AKHTARUZZAMAN, Md. 193  
 AKIBA, Kin-ya 19–20  
 AKITA, Motoko 225  
 AKUTSU, H. 82  
 AKUTSU-SATO, A. 82  
 AMEMIYA, Kenta 54–55  
 ANDO, Mayaka 76  
 ANDO, Shinji 193  
 ANDOH, Yukihiro 21  
 AONO, Shigetoshi 197–198, 207, 231  
 AOTO, Tomohiro 179–180  
 AOYAGI, Mutsumi 118, 133  
 AOYAMA, Masaki 117, 121, 191, 226  
 ARA, Masato 157  
 ARAKI, Koiti 153  
 ARDAVAN, A. 82  
 ASAKURA, Kiyotaka 101–102  
 ASANO, Yasuhisa 198  
 AWAGA, Kunio 62  
 AZUMA, Toshiyuki 180

**B**

BABA, Akinori 46–47  
 BAIDAKOVA, M. V. 98  
 BANGURA, A. F. 82  
 BJORNEHOLM, Olle 114  
 BOO, Bong-Hyun 67  
 BOYKO, Sergiy 83

BRADEANU, Ioana 114  
 BRONOLD, Franz X. 39  
 BUICA, Gabriela 44  
 BULTEAU, Anne-Laure 111  
 BUSHIRI, Junaid M. 67

**C**

CARRILLO-CABRERA, Wilder 181  
 CHANG, Suk-Kyu 132  
 CHEREMISOV, Sergey 110  
 CHEREPKOV, Nikolai A. 175  
 CHERNIKOV, G. P. 27  
 CHIBA, Hisashi 71  
 CHIBA, Ryo 88  
 CHIKAZUMI, Shinpei 26  
 CHO, Tegyon 173  
 CHOE, Jong-In 132  
 CHOE, Yoong-Kee 18  
 CHONG, Song-Ho 35  
 CHULUUNBAATAR, Ochbadrakh 173  
 COLDEA, A. I. 82  
 COOPER, John W. 172  
 COPLAN, Michael A. 172  
 CUI, HengBo 91, 93, 95–96, 225

**D**

DALTROP, Oliver 209–210  
 DASCALU, Traian 189, 230  
 DAVYDOV, Roman 110  
 DAY, P. 82  
 DE LOS REYES, Glenda 230  
 DEJIMA, Hirohisa 143  
 DIWA, Gilbert 230  
 DOERING, John P. 172  
 DROZDOVA, Olga 83–84, 223  
 DÖRNER, Reinhard 174, 218

**E**

EHARA, Masahiro 42, 173  
 EINAGA, Yasuaki 95–96  
 EITOKU, Takeshi 58  
 EL-MASHTOLY, Samir F. 206  
 ELAND, John H. D. 172–173, 180, 218  
 ENDO, Taichi 207  
 ENOKI, Toshiaki 98–99  
 ENOMOTO, Masaya 100  
 ESTACIO, Elmer 230  
 ETO, Soichiro 98  
 EZAKA, Seiichi 193

**F**

FEHSKE, Holger 39  
 FENG, Lai 19–20  
 FERGUSON, Stuart J. 209–210  
 FRIEDLEIN, Rainer 177  
 FUCHIZAKI, Kazuhiro 43  
 FUJII, Hiroshi 110, 199–200, 231  
 FUJINAMI, Shuhei 206–207, 209  
 FUJIWARA, Eiichi 156  
 FUJIWARA, Emiko 94, 225  
 FUJIWARA, Hideki 93–94  
 FUJIWARA, Katsutoshi 71  
 FUJIWARA, Tetsunori 135  
 FUJIYAMA, Shigeaki 86  
 FUKAGAWA, Hirohiko 176–177  
 FUKUDA, Tsuguo 184  
 FUKUI, Ken-ichi 99  
 FUKUMOTO, Hiroki 148  
 FUKUYAMA, Naoshi 191  
 FUNAHASHI, Yasuhiro 208  
 FURUIKE, Shou 195  
 FURUKAWA, Ko 87–90, 224–225  
 FURUKAWA, Momoko 110  
 FURUKAWA, Yasunori 186  
 FURUKAWA, Yuuki 137

- FURUTACHI, Hideki 206–207, 209  
 FUYUKI, Masanori 166
- G**
- GAO, Song 93  
 GAO, Ying 206  
 GAO, Yuan 155  
 GAO, Zhengxiang 17, 20–22  
 GIRARD, Bertrand 71  
 GOLOVIN, Alexander V. 175  
 GOTO, Kei 18  
 GOTO, Masahiro 184  
 GOTO, Yuji 202, 204  
 GREEN, Mark, A. 92  
 GRIN, Yuri 180–181
- H**
- HACHISUKA, Hidekazu 62  
 HADA, Masahiko 41–42  
 HAGIHARA, Yusuke 71  
 HAKAHODO, Tsukasa 22  
 HALL, Richard 180  
 HAN, Rushan 17, 20–22  
 HANASAKI, Noriaki 102–104  
 HANSON, David R. 131  
 HARA, Akihiko 69  
 HARA, Toshifumi 87–89, 224–225  
 HARADA, Katsuyoshi 206  
 HARADA, Yosuke 75  
 HARIHARA, Makoto 137  
 HARUNA, Atsuyuki 72  
 HARUYAMA, Yusuke 123–125  
 HASEGARA, M. 182  
 HASEGAWA, Hirokazu 72–73, 115, 220  
 HASEGAWA, Hiroyuki 104  
 HASEGAWA, Tadashi 18–19, 22  
 HASHIMOTO, Kazuhito 63  
 HASHIMOTO, Koji 207  
 HASHIMOTO, Yoshiteru 203, 208  
 HASHIZUME, Daisuke 19–20  
 HATSUI, Takaki 113–114, 190, 217  
 HAYASHI, Hideo 207  
 HAYASHI, Kenji 179  
 HAYASHI, Takashi 143–144, 206  
 HAYASHIZAKI, Yoshihide 211  
 HEYES, David M. 25  
 HIGASHIBATA, Akinori 193  
 HIGASHIBATA, Hiroki 203, 208  
 HIGASHIBAYASHI, Shuhei 229  
 HIKONAKA, Yoichiro 112  
 HIKOSAKA, Yasumasa 179–180, 183, 221  
 HINO, Takami 135  
 HIRAKI, Ko-ichi 88  
 HIRAMATSU, Fukiko 83  
 HIRAMATSU, Hirotugu 202, 204, 206
- HIRAO, Kimihiko 27  
 HIRAOKA, Ryusuke 34  
 HIRASHIMA, Yuya 18, 22  
 HIRATA, Fumio 24, 32–36  
 HIRATSUKA, Hiroshi 76  
 HIRONAKA, Yoichiro 112  
 HIROTA, Shun 143  
 HIROTSU, Masakazu 145  
 HISAEDA, Yoshio 143–144  
 HISHIKAWA, Akiyoshi 115, 220  
 HIYAMA, Miyabi 113, 217  
 HOCKE, Heiko 161  
 HOFFMAN, Brian M. 110  
 HONDA, Hiroyuki 176  
 HONDA, Masahiro 71  
 HONDA, Yasushi 41–42  
 HONDA, Yasutaka 203  
 HONG, J. B. 181–183  
 HONMA, Yosuke 107  
 HORI, Hiroshi 56–57, 143, 208  
 HORI, Yoichiro 179  
 HORIGOME, Toshio 113, 190  
 HORIMOTO, Noriko 219  
 HORIUCHI, Hiroaki 76  
 HORN, Ernst 22  
 HOSAKA, Kouichi 71, 175  
 HOSAKA, Masahito 179, 230  
 HOSOKAWA, Ryohei 193  
 HOSOKAWA, Youichi 162  
 HOSSAIN, M. Kamal 52  
 HOZUMI, Toshiya 63  
 HUANG, Wei 152  
 HÜLSEN, Björn 39
- I**
- ICHIMURA, Teijiro 75–78  
 IGA, Fumitoshi 181  
 IGA, Hiroshi 78  
 IGARASHI, Jotaro 203, 209  
 IIDUKA, Yuko 18, 22  
 IKEDA, Shingo 102  
 IKEDA-SAITO, Masao 110–111, 200  
 IKEGAMI, Takahiro 143  
 IKENAGA, Ozora 22  
 IKESUE, Akio 186–187  
 IKUTA, Yasuhiro 32  
 IM, Hojun 181–182, 230  
 IMAEDA, Minoru 188  
 IMAHORI, Hiroshi 49  
 IMAI, Hideto 182  
 IMAI, Takashi 33–34  
 IMURA, Kohei 49–52, 219  
 INABE, Tamotsu 101–106  
 INAGAKI, Sayaka 197, 207, 231  
 INDERGAND, Martin 39  
 INO, Daisuke 166  
 INOHARA, Hideki 20  
 INOKUCHI, Yoshiya 68–70  
 INOUE, Akihisa 182  
 INOUE, Katsuya 93, 225  
 INOUE, Youji 155  
 ISAYA, Grazia 111
- ISHIBASHI, Shoji 94–95  
 ISHIDA, Kyoko 203  
 ISHIDA, Tateki 221  
 ISHIDA, Toshimasa 29, 132  
 ISHIDA, Yutaka 17  
 ISHII, Youichi 147  
 ISHIKAWA, Haruto 57  
 ISHIKAWA, Masakazu 183  
 ISHIMORI, Koichiro 56–57, 208  
 ISHIMURA, Kazuya 20, 222  
 ISHIOKA, Kunie 52  
 ISHIYAMA, Tatsuya 221  
 ISHIZUKA, Koji 195  
 ISHIZUKI, Hideki 189, 230  
 ISHKHANYAN, Artur 27  
 ISOZAKI, Tasuku 77–78  
 ITO, Kenji 179–180, 183  
 ITO, Shinobu 209  
 ITO, Takahiro 230  
 ITOH, Hiroyasu 195  
 ITOH, Kyosuke 207  
 ITOH, Satoru G. 24, 217  
 IWAI, Kozuhiro 57  
 IWAI, Makato 188  
 IWAI, Shinichiro 83  
 IWAMATSU, Sho-ichi 19, 21  
 IWAO, Takeshi 193  
 IWASA, Yoshihiro 21  
 IWASAKI, Fujiko 19–20  
 IWASAKI, Masakazu 147  
 IYODA, Masahiko 98
- J**
- JACKSON, Timothy A. 206  
 JAGUTZKI, Ottmar 174, 218  
 JANAIRO, Gerardo 184  
 JANG, K. -H. 181  
 JAVANAINEN, Juha 27  
 JIANG, Donglin 109, 204, 226  
 JITSUKAWA, Koichiro 203–204, 208  
 JOHNSON, Matthew S. 132  
 JUDAI, Ken 65–67, 223  
 JUNG, M. A. 183  
 JUNG, M. H. 181–183
- K**
- KABURAGI, Yutaka 99  
 KADISH, Karl M. 18–20  
 KAFLE, Bhim Prasad 125–126  
 KAGAWA, Norio 56, 208  
 KAJITANI, Hidenobu 147  
 KAKIUCHI, Toru 89  
 KAKO, Masahiro 19–20, 22  
 KAMATA, Naoto 193  
 KAMBE, Takashi 21  
 KAMIKAWA, Ken 141  
 KAMIMURA, Sou 147  
 KAMIYA, Yukiko 170  
 KANDA, Makoto 18, 22  
 KANEYASU, Tatsuo 180, 183, 221

- KANG, Dongeun 67  
 KANG, Heun-Kag 67  
 KANODA, Kazushi 82  
 KASHINO, Yoko 21  
 KASHIWAZAKI, Akimitsu 83  
 KATAURA, Hiromichi 18  
 KATAYANAGI, Hideki 124–126, 220  
 KATO, Koichi 170, 229  
 KATO, Masahiko 182  
 KATO, Michihiko 57  
 KATO, Tatsuhisa 18, 20–21, 90  
 KATO, Yasuo 198  
 KATOH, Masahiro 179, 230  
 KATOUDA, Michio 20  
 KATSUKI, Hiroyuki 71  
 KAWADA, Norifumi 210  
 KAWAGUCHI, Hiroyuki 139, 227  
 KAWAI, Akio 76  
 KAWAMORI, Asako 90  
 KAWAMOTO, Atsushi 81–82, 107  
 KAWANO, Hidetaka 112  
 KAWAO, Masahiro 151, 153  
 KAWASHIMA, Takayuki 18  
 KAWASHIMA, Yukio 217  
 KAWAUCHI, Susumu 76  
 KAWAZOE, Yoshiyuki 184  
 KAZAOUI, Said 22  
 KEMPIŃSKI, W. 98  
 KERA, Satoshi 176–177  
 KHAJURIA, Yugal 172–174, 218  
 KIKUCHI, M. 184  
 KIKUCHI, Makoto 151–152, 161  
 KIKUCHI, Takashi 22  
 KIKUZAWA, Yoshihiro 163, 229  
 KIM, D. Y. 182–183  
 KIM, J. W. 181  
 KIM, Jinheung 207  
 KIM, Seong Keun 51  
 KIM, Sung Bae 64  
 KIM, Yong-Hoon 117, 120, 226  
 KIMURA, Shin-ichi 18, 22, 180–183, 230  
 KINOSHITA, Masahiro 24, 34  
 KINOSITA, Kazuhiko, Jr. 195  
 KIRISAKO, Takayoshi 57  
 KISHIMURA, Hiroaki 112  
 KITAGAWA, Soichiro 54  
 KITAGAWA, Teizo 56, 197, 199, 202–210, 231  
 KITAJIMA, Masahiro 52  
 KITAJIMA, Yoshinori 102  
 KITAZAWA, Hideaki 181–182  
 KOBAYASHI, Akiko 91–95, 225  
 KOBAYASHI, Eiichi 177  
 KOBAYASHI, Hayao 91–96, 191, 225  
 KOBAYASHI, J. Akiko 91  
 KOBAYASHI, Kaoru 17–21  
 KOBAYASHI, Katsuaki 198, 231  
 KOBAYASHI, Masafumi 155  
 KOBAYASHI, Masato 20  
 KOBAYASHI, Michihiko 203, 208  
 KOBAYASHI, Norihito 105–106  
 KOBAYASHI, Yoshio 199  
 KOBAYASHI, Yousuke 99  
 KOBRYN, Alexander 35  
 KOCHURIKIN, V. V. 184  
 KODA, Seiichiro 131  
 KODA, Shinobu 35  
 KODAMA, Katsuaki 104  
 KOIZUMI, Take-aki 136–138  
 KOJIMA, Norimichi 100  
 KOKALJ, Anton 68  
 KOKUBO, Hironori 24, 217  
 KOMATSU, Takahiro 130  
 KOMATSUZAKI, Tamiki 46–47  
 KOMOTO, Yusuke 69  
 KOMURO, Takashi 139  
 KONDO, Ken-ichi 112  
 KONDO, Takuhiko 190  
 KONDORSKIY, Alexey 28  
 KONISHI, Kazunobu 203, 208  
 KORETSUNE, Toshihisa 182  
 KOSHIKAWA, Hidenori 145  
 KOSUGI, Kentaroh 67  
 KOSUGI, Nobuhiro 113–114, 217  
 KOU, Junkei 123–125, 220  
 KOUDO, Ryoji 209  
 KOVALENKO, Andriy 33–34, 36  
 KOZAKOV, Konstantin A. 173–174  
 KUBO, Kanji 69  
 KUBO, Yoshimi 182  
 KUBOZONO, Yoshihiro 21, 123–125  
 KUJIME, Masato 199–200, 231  
 KUMADA, Shinji 78  
 KUMAGAI, Akinori 208  
 KUMAGAI, Ken-ichi 107  
 KUMARU, Latha 98  
 KUMITA, Hideyuki 208  
 KURAHASHI, Takuya 199, 231  
 KURIHARA, Masato 150  
 KURMOO, Mohamedally 92–93  
 KUROKAWA, Hirofumi 209  
 KUSAI, Haruka 21  
 KUSAKABE, Koichi 99  
 KUSHCH, N. D. 83  
 KUSUNOSE, Hiroaki 39  
 KUWAHARA, Eiji 21, 125  
 KUWATA, Shigeaki 147  
 KUWATANI, Yoshiyuki 98  
 KUWAYAMA, Toshiki 19  
 KUZUOKA, Chie 42  
 KWON, Yong-seung 181–183  
 KÜHN, O. 28  
 L  
 LABLANQUIE, Pascal 179–180  
 LEE, B. K. 181–182  
 LEE, Jimin 207  
 LEE, Sang-Yeon 67  
 LEE, Shyi-Long 21  
 LEE, Sik 132  
 LI, Chun Biu 46  
 LIAN, Yongfu 18–20, 22  
 LIANG, Wanzhen 26  
 LIM, Jong Kuk 51, 219  
 LIU, Jin-Gang 205  
 LONG, La-Sheng 91  
 LU, Jing 17–18, 20–22  
 LUNDBERG, Kathleen C. 111  
 M  
 MA, Xiao-Dong 63  
 MACHINAGA, Hironobu 69  
 MAEDA, Keisuke 224  
 MAEDA, Seisuke 152  
 MAEDA, Yonezo 206  
 MAEDA, Yutaka 18–22  
 MAEHARA, Keiko 144  
 MAESHIMA, Nobuya 37, 39, 222  
 MAKI, Jun 118, 133  
 MAKI, Suguru 162, 229  
 MAKINO, Masatomo 210  
 MAKSIMUK, M. 82  
 MANSFIELD MATERA, Kathryn 110  
 MARUYAMA, Koichi 222  
 MARUYAMA, Shigeo 18  
 MASE, Kazuhiko 177  
 MASHIMA, Kazushi 148  
 MASUDA, Chiaki 197, 207  
 MASUDA, Gou 152  
 MASUDA, Hideki 203–204, 208  
 MASUDA, Kouki 104  
 MASUDA, Tadashi 190  
 MATSUDA, Masaki 102–104  
 MATSUI, Toshitaka 110, 200  
 MATSUMOTO, Ryu 77  
 MATSUMOTO, Shun-ichi 145  
 MATSUMOTO, Takahiro 207  
 MATSUMOTO, Taketoshi 165–166, 218  
 MATSUMOTO, Takuya 153  
 MATSUMOTO, Yoshiyasu 80, 165–167, 218  
 MATSUMURA, Daiju 54–55  
 MATSUMURA, Naoko 103  
 MATSUNAGA, Noriaki 107  
 MATSUNAGA, Tsukasa 147  
 MATSUNAGA, Yasuhiro 46  
 MATSUO, Takashi 143–144  
 MATSUO, Tsukasa 139, 227  
 MATSUOKA, Daisuke 58  
 MATSUOKA, Hideto 90, 224  
 MATSUOKA, Tatsuro 35  
 MATSUSHIMA, Tatsuo 68  
 MATSUSHITA, Yoshihisa 77–78  
 MATSUSHITA, Yosuke 193  
 MATSUURA, Koji 56, 208  
 MATSUZAKA, Hiroyuki 141  
 MEIER, Christophe 71  
 MICHIZAWA, Takahiro 181  
 MICHL, J. 42  
 MIEDA, Eiko 19

- MIGITA, Catharina T. 110  
MIKAMI, Taiji 217  
MIL'NIKOV, Gennady V. 26–28  
MINAMI, Nobutsugu 22  
MINEGISHI, Kouji 174  
MINO, Hiroyuki 90  
MINOURA, Mao 20  
MINOURA, Masayuki 21  
MISAWA, Nobuo 118–119  
MITSUKE, Koichiro 122–126, 220  
MITSUTAKE, Ayori 24, 34  
MIURA, Kazuhiro 174  
MIURA, Shinichi 130, 217  
MIYAKE, Hiroyuki 137  
MIYAKE, Shin-ichiro 74  
MIYAKE, Yusuke 174  
MIYAMOTO, Takeshi 102  
MIYASHITA, Jun 19  
MIYASHITA, Satoshi 222  
MIYAUCHI, Yuhei 18  
MIYAZAKI, Akira 98–99  
MIYAZAKI, Hidetoshi 230  
MIYAZAKI, Mitsuhiro 72, 74, 220  
MIYOSHI, Riko 69  
MIZOROGI, Naomi 20–22  
MIZOZOE, Mitsuhiro 20  
MIZUGUCHI, Eisuke 153  
MIZUNO, Takafumi 230  
MIZUSEKI, Hiroshi 184  
MIZUTANI, Nobuo 174  
MIZUTANI, Uichiro 182  
MIZUTANI, Yasuhisa 210  
MIZUUCHI, Kiminori 188  
MO, Yu-Jun 121, 204  
MOCHIDA, Tomoyuki 84–85  
MOCHIHASHI, Akira 179, 230  
MOORE, John H. 172  
MORI, Akira 69  
MORI, Takanori 123–125, 220  
MORI, Takehiko 93  
MORI, Yoshihisa 181–182  
MORIKAWA, Akihiro 188  
MORIKAWA, Eiji 177  
MORISHIMA, Isao 56, 208  
MORISHITA, Hiroto 112  
MORITA, Akihiro 131, 221  
MORITA, Norio 53, 219  
MORIWAKI, Yoshiki 53, 219  
MORIYAMA, Yuji 20  
MOTOKI, Souhei 175  
MUKAI, Kazuo 152  
MUKOYAMA, Takeshi 174  
MUN, E. D. 181  
MUNCK, Eckard 207  
MUNE, Yutaka 69  
MUNEYUKI, Eiro 195  
MURAKAMI, Hidetoshi 184, 230  
MURAOKA, Azusa 70  
MURATA, Dai 143  
MURATA, Shizuaki 19, 21
- N**  
NADA, Tomokazu 58  
NAGAHARA, Tetsuhiko 49–51, 219  
NAGAHORA, Noriyoshi 19  
NAGAI, Hiroyuki 117, 191  
NAGAMATSU, Shin-ichi 177  
NAGANO, Mayumi 170  
NAGANO, Mika 76  
NAGANO, Yasutomo 205  
NAGASAWA, Takayuki 164, 229  
NAGASE, Shigeru 17–22, 222  
NAGATA, Takashi 70  
NAGATA, Toshi 136, 162–164, 229  
NAGATOMO, Shigenori 199, 203–204, 206–209  
NAGAYAMA, Kuniaki 119  
NAIKI, Hironobu 202, 204  
NAITO, Toshio 101–106  
NAKA, Shigeki 193  
NAKABAYASHI, Takakazu 68  
NAKAGAWA, Takeshi 59–61, 222  
NAKAGAWA, Tomoyuki 206  
NAKAGOE, Osamu 80, 167  
NAKAHODO, Tsukasa 20, 22  
NAKAI, Hiromi 20  
NAKAI, Ikuo 182  
NAKAI, Naohito 120  
NAKAI, Yasushi 161  
NAKAJIMA, Aya 110, 200  
NAKAJIMA, Hiroshi 197, 207  
NAKAJIMA, Takashi 44, 145  
NAKAMURA, Akira 148  
NAKAMURA, Hiroki 26–29, 132  
NAKAMURA, Kazutaka 112  
NAKAMURA, Osamu 186  
NAKAMURA, Toshikazu 86–89, 224–225  
NAKAO, Ryu 161  
NAKASONE, Yusuke 58  
NAKATSUJI, Hiroshi 41–42, 173  
NAKAYAMA, Kazuya 172  
NAKAZAWA, Mitsuhiro 88  
NAM, Wonwoo 207  
NANBA, Takao 181–182  
NANBU, Shinkoh 29, 118–119, 132–133  
NARUTA, Yoshinori 205  
NASU, Keiichiro 38  
NAVES DE BRITO, Arnaldo 114  
NEGISHI, Yuichi 31, 168–169, 229  
NEMOTO, Koshichi 112  
NI, Ming 22  
NIIMI, Hironobu 101–102  
NIKAWA, Hidefumi 22  
NIKL, M. 184  
NISHI, Nobuyuki 65–70, 83, 223  
NISHI, Tatsuhiko 180–182, 230  
NISHIBE, Kunimasa 105  
NISHIDA, Jun-ichi 193
- NISHIDA, Shinpei 58  
NISHII, Takako 20  
NISHIJO, Junichi 65–67, 98, 223  
NISHIMATSU, Takeshi 184  
NISHIMURA, Muneto 231  
NISHIYAMA, Katsura 35  
NOBUSADA, Katsuyuki 30–31, 168, 219  
NODA, Satoshi 47  
NOJI, Hiroyuki 196  
NOMURA, Kazushige 107  
NONOGAKI, Youichi 117–120, 226
- O**  
OGAWA, Takuji 49, 151–153, 227  
OGINO, Hiraku 184  
OGINO, Hiroshi 145  
OGURA, Shin-ichiro 141  
OGURA, Takashi 107, 202  
OGURO, Akane 49  
OHARA, Keishi 152  
OHASHI, Kazuhiko 69  
OHIZUMI, Tomohiro 150  
OHKITA, Masakazu 193  
OHKOSHI, Shin-ichi 63  
OHMACHI, Eiji 104  
OHMORI, Kenji 71, 220  
OHNO, Naoki 145  
OHSHIMA, Takashi 148  
OHSHIMA, Yasuhiro 72–74, 220  
OHSHIMO, Keijiro 68  
OHTA, Takehiro 197, 203, 205–208, 210  
OHTA, Toshiaki 54–55  
OHTAKE, Hideyuki 184  
OHTSU, Hideki 135, 137  
OHTSUKA, Yoshikazu 103  
OHTSUKA, Yuhki 173  
OHTSUKI, Yukiyoshi 71  
OINUMA, Ken-Ichi 203, 208  
OISHI, Osamu 66  
OISHI, Yuji 112  
OKABE, Chie 65–68, 83  
OKABE, K. 99  
OKADA, Hiroyuki 193  
OKADA, Susumu 21  
OKADA, Tadashi 35  
OKAMOTO, Hiromi 49–52, 219  
OKAMOTO, Kiyomi 39  
OKAMOTO, Yuko 24–25, 34, 217  
OKAMURA, Hidekazu 181–182  
OKAMURA, Mutsuo 18  
OKAMURA, Rei 136  
OKANO, Yasuaki 112  
OKANO, Yasuhisa 112  
OKANO, Yoshinori 91, 94, 96, 225  
OKAWARA, Hiroshi 119  
OKAZAKI, Masaaki 145

- OKAZAKI, Susumu 129–130, 217  
 OKUBO, Hiroshi 21  
 OKUBO, Kimitaka 228  
 OKUBO, Masashi 100  
 OKUBO, Shingo 18  
 OKUDAIRA, K. Koji 176–177  
 OKUJIMA, Tetsuo 151–152  
 OKUMURA, Hisashi 25, 217  
 OKUNISHI, Kouichi 39  
 OKUNO, Kazuhiko 180  
 OKUTSU, Tetsuo 76  
 OLOYEDE, Oluwaponmile 26  
 ONNAGAWA, Hiroyoshi 193  
 ONO, Katsuhiko 193  
 ONO, Masaki 177  
 ONO, Mitsumasa 182  
 ONO, Noboru 151–152  
 ONO, Shingo 184, 230  
 ONO, Yuriko 217  
 ONO-HARA, Yoko 195  
 OOI, Kenta 118, 133  
 OSADA, Toshihito 104  
 OSAKO, Takao 209  
 OSHIO, Shinya 141  
 OSIPOV, V. Yu. 98  
 OTA, Akira 84  
 OTO, Takahiro 182  
 OTSUKA, Takeo 92  
 OTSUKA, Yoichi 153  
 OUCHI, Isuke 182  
 OUENZERFI, Riadh 184  
 OZAWA, Hiroaki 49, 151  
 OZAWA, Kazumichi 231  
 OZAWA, Takeaki 64, 219  
 OZAWA, Tomohiro 208  
 O'BRIAN, Mark R. 57
- P**
- PACHECO, J. 180  
 PAL, Biswajit 205–207  
 PALAUDOUX, Jerome 180  
 PANICH, A. M. 98  
 PARK, J. -G. 181, 183  
 PARK, Mi Joo 206  
 PARK, T. 181  
 PATNAIK, Archita 177  
 PAVEL, Nicolaie 188–189, 230  
 PENENT, Francis 179–180  
 PENG, Lianmao 17–18, 21  
 PONSECA, Carlito Jr. 230  
 POPOV, Yuri V. 173–174
- Q**
- QUE, Lawrence Jr. 207  
 QUEMA, Alex 184, 230
- R**
- RAHMAN, G. M. Aminur 22  
 RAHMAN, Md. Mashiur 117, 120, 191, 226
- RAJH, Tijana 110  
 RE, Suyong 21  
 RHEE, Hakjune 161  
 RIKIISHI, Yoshie 21  
 RYU, D. H. 182–183  
 RZEZNICKA, Izabela 68  
 RÜHL, Eckart 114
- S**
- SAGAMI, Ikuko 203, 209  
 SAIKAWA, Jiro 187, 230  
 SAITO, Gunzi 84  
 SAITO, Katsuhiko 193  
 SAITO, Riichiro 22  
 SAKAI, Enju 55  
 SAKAI, Masahiro 184  
 SAKAI, Tôru 39  
 SAKAI, Yasuhiro 174  
 SAKAKI, Naoyoshi 195  
 SAKAMOTO, Masatomi 150  
 SAKAMOTO, Youichi 155  
 SAKANOUÉ, Tomo 156  
 SAKEDA, Kosaku 77–78  
 SAKOTA, Kenji 68–69  
 SAKURABA, Akihiro 18, 22  
 SAKURAI, Hidehiro 169, 229  
 SAKURAI, Yoko 230  
 SARUKURA, Nobuhiko 184, 230  
 SASA, Masaaki 94  
 SASAKAWA, Hiroaki 170, 184  
 SASAKI, Ryuichiro 117, 191  
 SASAMORI, Takahiro 19  
 SASTRI, Chivukula V. 206  
 SATO, Akira 203  
 SATO, Emiko 209  
 SATO, Hideaki 143–144  
 SATO, Hirokazu 152  
 SATO, Hiroki 184  
 SATO, Masahiro 129, 217  
 SATO, Osamu 95–96  
 SATO, Yoichi 186–187, 230  
 SATO, Yukinori 71  
 SATOH, Norikazu 88  
 SAWA, Hiroshi 67, 89  
 SAWAI, Hitomi 210  
 SEINERMAN, Sergei 179  
 SEINO, Junji 41  
 SEKI, Kazuhiko 177  
 SEKIGUCHI, Akira 17  
 SEKINE, Tomoyuki 88  
 SEKIYA, Hiroshi 68–69  
 SEMENOV, Sergei K. 175  
 SEO, Mi Sook 207  
 SETOYAMA, Hiroyuki 114, 177  
 SHAMES, Alexander I. 98  
 SHEN, Jian-Ren 90  
 SHIBUYA, Kazuhiko 76–77  
 SHIBUYA, Masahiro 174  
 SHICHIBU, Yukatsu 168  
 SHIGEMASA, Eiji 179, 183, 221  
 SHIM, Jan Bo 184  
 SHIMADA, Keiichi 18  
 SHIMAKAWA, Yuichi 182
- SHIMBA, Kurando 182  
 SHIMIZU, Tetsuo 18, 22  
 SHIMIZU, Toru 203, 209  
 SHIMO-KON, Rieko 195  
 SHIRAKURA, Shingo 18  
 SHIRASAWA, Nobuhiko 155  
 SHIRATORI, Kazuya 30, 219  
 SHIRO, Motoo 137  
 SHIRO, Yoshitsugu 208, 210  
 SHIROMOTO, Takayuki 141  
 SHOJI, Ichiro 189  
 SICHELSCHEMIDT, Joerg 180–181  
 SIGRIST, Manfred 39  
 SINGLETON, J. 82  
 SLANINA, Zdenek 17, 19, 21  
 SODA, Kazuo 182  
 SOLOVIEVA, N. 184  
 SONG, Wei 22  
 SORENSEN, Stacey 114  
 STEGLICH, Frank 180–181  
 STEVENS, Julie M. 209–210  
 STUBNA, Audria 206  
 SUBRAMANYAM, S. V. 98  
 SUGAWARA, Hideyuki 102  
 SUGIMOTO, Hideki 136–137  
 SUGIMOTO, Hiroshi 210  
 SUGIMOTO, Kunihisa 137  
 SUGITA, Tomoya 188  
 SUGITA, Yuji 24  
 SUGIYAMA, Masakazu 131  
 SUMIDA, Yukitsune 182  
 SUTO, Michitaka 193  
 SUZUI, Mitsukazu 174, 190–191  
 SUZUKI, Kenji 81  
 SUZUKI, Masatatsu 206–207, 209  
 SUZUKI, Osamu 182  
 SUZUKI, Tadashi 75–78  
 SUZUKI, Takahisa 193  
 SUZUKI, Toshiharu 195  
 SUZUKI, Toshiyasu 155, 228  
 SZWEDA, Luke I. 111
- T**
- TADA, Hirokazu 156–159, 193  
 TAIRA, Takunori 186–189, 230  
 TAJIMA, Hiroyuki 102–104  
 TAKABATAKE, Toshiro 181  
 TAKABAYASHI, Yasuhiro 21, 125  
 TAKADA, Masaki 156–157  
 TAKAGI, Noriaki 80, 165–167  
 TAKAGI, Nozomi 18–20  
 TAKAHASHI, Eiji J. 115, 220  
 TAKAHASHI, Hiroshi 184  
 TAKAHASHI, Kazuyuki 91, 93, 95–96, 191, 225  
 TAKAHASHI, Masahiko 172–175, 218  
 TAKAHASHI, Toshiharu 181–182, 230  
 TAKAHASHI, Toshihiro 88

- TAKAI, Kazuyuki 98  
 TAKAO, Ryohei 64  
 TAKASHIMA, Yoshifumi 179, 230  
 TAKEDA, Kazuyoshi 152  
 TAKEDA, Naoya 183  
 TAKEDA, Nobuhiro 19  
 TAKEKIYO, Takahiro 33  
 TAKEMOTO, Shin 141  
 TAKENOBU, Taishi 21  
 TAKETSUGU, Tetsuya 27  
 TAKEUCHI, Tsunehiro 182  
 TAKIGAWA, Masashi 104  
 TAMURA, Atsuo 184  
 TAMURA, Hiroyuki 29  
 TANABE, Yoshiaki 147  
 TANAKA, Hirofumi 151–153, 227  
 TANAKA, Hisashi 92, 95  
 TANAKA, Koji 135–138, 150, 227  
 TANAKA, Shinji 177  
 TANAKA, Shoji 160  
 TANATAR, Makariy 83, 224  
 TANIGUCHI, H. 82  
 TANIGUCHI, Hiromi 81, 107  
 TANIGUCHI, Yoshihiro 33  
 TARUMIZU, Makoto 137  
 TARUNO, Shinsuke 145  
 TERABARU, Kazutaka 69  
 TERADA, Shohei 209  
 TERADA, Shoichi 207  
 TERAUBO, Noriaki 184  
 TERAURA, Kiyoyuki 94–95  
 TERAMOTO, Takahiro 175  
 TERANISHI, Toshiharu 168  
 TERANISHI, Yoshiaki 71  
 TERASHIMA, Taichi 92  
 TERAZIMA, Masahide 58  
 TERO, Ryugo 117–121, 226  
 TOBITA, Hiromi 145  
 TODA, Mikito 46  
 TOKITO, Shizuo 155  
 TOKITOH, Norihiro 19  
 TOKUE, Ikuo 132  
 TOKUMOTO, Hiroshi 18, 22  
 TOKUMOTO, Madoka 92, 95  
 TOKUNAGA, Fuminori 57  
 TOKUTOMI, Satoru 58  
 TOMINAGA, Keisuke 184  
 TOMITA, Takeshi 110  
 TOMON, Takashi 136–138  
 TOMURA, Masaaki 193  
 TORII, Tatsuharu 190  
 TOSHA, Takehiko 56, 199, 207–209  
 TSUCHIYA, Takahiro 18–20, 22  
 TSUJI, Kazuhide 77  
 TSUKUBE, Hiroshi 136–137  
 TSUKUDA, Tatsuya 31, 168–169, 229  
 TSUNEKANE, Masaki 187, 230  
 TSUNOYAMA, Hironori 169, 229  
 TSURUTA, Takashi 144  
 TSUTSUMI, Osamu 152  
 TSUZUKI, Toshimitsu 155  
 TURNER, S. S. 82  
**U**  
 UCHIDA, Takeshi 205, 209–210  
 UCHIUMI, Hideki 193  
 UDAGAWA, Yasuo 172–174, 218  
 UEDA, Kazuo 40  
 UEDA, Kiyoshi 71  
 UEDA, Minoru 76  
 UENO, Hiroshi 195  
 UENO, Keiji 145  
 UENO, Nobuo 176–177  
 UEYAMA, Mazakuni 115  
 UHLÍK, Filip 17, 21  
 UJI, Shinya 92  
 UMEZAWA, Yoshio 64  
 UNNO, Masaki 110  
 UNO, Hidemitsu 151–152  
 UNO, Hidetaka 117, 120, 226  
 UNO, Tadayuki 210  
 UOZUMI, Yasuhiro 161, 191, 228  
 URISU, Tsuneo 117–121, 133, 191–192, 226  
 URUICHI, Mikio 81, 84–85, 223  
 UYEMURA, Makoto 204  
**V**  
 VAN BOEYEN, Roger W. 172  
 VINITSKY, Pavel S. 173–174  
 VOEVODIN, Vladimir 180–181  
 VUL', A. Ya. 98  
**W**  
 WADA, Akira 203–204  
 WADA, Tohru 135–136, 150  
 WAELCHLI, Markus 21  
 WAKABAYASHI, Kazuhito 78  
 WAKAHARA, Takatsugu 18–20, 22  
 WANG, Zheming 91–93  
 WANG, Zhi-Hong 118, 133  
 WASSERMANN, Bernhard 114  
 WATANABE, Hidekazu 118–119, 133  
 WATANABE, Hikaru 151–152  
 WATANABE, Hirokazu 59–60, 222  
 WATANABE, Kazuo 68  
 WATANABE, Kazuya 80, 165–167, 218  
 WATANABE, Masahito 143  
 WATANABE, Noboru 172–175, 218  
 WATANABE, Ryoji 98  
 WATANABE, Sadayuki 75  
 WATANABE, Shuntaro 44  
 WATANABE, Takahiro 177  
 WATANABE, Yoshihito 206–207  
 WATERMAN, Michael R. 56, 208  
 WERST, David E. 110  
 WIESNER, Karoline 114  
**Y**  
 YABANA, Kazuhiro 30, 219  
 YAGI, Kiyoshi 27  
 YAGI, Shinya 182  
 YAGISHITA, Akira 175  
 YAJIMA, Takashi 153  
 YAKUSHI, Kyuya 81–85, 107, 223  
 YAMADA, Hiroko 151–152  
 YAMADA, Michio 20  
 YAMADA, Ryo 156–159  
 YAMADA, Yoichi M. A. 191  
 YAMAGATA, Tsuneaki 148  
 YAMAGUCHI, Dai 165  
 YAMAGUCHI, Syuhei 203–204, 208  
 YAMAGUCHI, Tsuyoshi 35  
 YAMAGUCHI, Yoshiki 170  
 YAMAMOTO, Emi 69  
 YAMAMOTO, Kaoru 81, 83, 107, 223  
 YAMAMOTO, Kazuhisa 188  
 YAMAMOTO, Kazunori 19, 22  
 YAMAMOTO, Koji 184  
 YAMAMOTO, M. Hiroshi 88  
 YAMAMOTO, Takashi 81–82, 223  
 YAMAMOTO, Yohsuke 19–20  
 YAMAMURA, Shusaku 118–119  
 YAMANE, Hiroyuki 176–177  
 YAMANOCHI, Kaoru 115  
 YAMASAKI, Katsuyoshi 132  
 YAMASHITA, Makoto 19  
 YAMASHITA, Yasufumi 37, 39–40, 222  
 YAMASHITA, Yoshiro 156, 193  
 YAMASHITA, Yuko 151–152  
 YAMAUCHI, Seigo 203  
 YAMAURA, J. -I. 99  
 YAMAZAKI, Jun-ichiro 179  
 YAMAZAKI, Takeshi 32  
 YAMOCHI, Hideki 84  
 YANAGIDA, Satomi 174  
 YANAGIMOTO, Yasushi 169, 229  
 YANG, Jianhua 57  
 YANO, Takayuki 117, 191, 226  
 YARESKO, Alexander 181  
 YASUMOTO, Takahiro 148  
 YASUZUKA, Shuma 92  
 YE, Hengqiang 17, 20–22  
 YODA, Takao 24  
 YOKOYAMA, Toshihiko 54–55, 59–63, 222  
 YONEMITSU, Kenji 37–39, 222  
 YOSHIDA, Hisashi 121, 192

YOSHIDA, Makoto	117, 191
YOSHIDA, Masasuke	195
YOSHIDA, Norio	32
YOSHIDA, Tadashi	110, 200
YOSHII, Noriyuki	130
YOSHIIKE, Shigeru	76
YOSHIKAWA, Akira	184
YOSHIMURA, Daisuke	177
YOSHIMURA, Hideaki	197, 231
YOSHIMURA, Takashi	145
YOSHIMURA, Tetsuhiko	203
YOSHINO, Tae	174
YOSHINO, Takeshi	188
YOSHIOKA, Shiro	
56, 197–198, 207–208, 231	
YOSHIKAWA, Katsutoshi	210
YOZA, Kenji	22
YU, Dapeng	17, 20–22
YU, Yapeng	22

## Z

ZEREC, Ivica	181
ZHANG, Bin	92–93
ZHANG, Jin	21
ZHANG, Shuang	17–18, 21
ZHANG, T.	182
ZHANG, Xi	206
ZHANG, Xinwei	21–22
ZHANG, Yan	93
ZHANG, Zhen-Long	
117, 120–121, 226	
ZHAO, Yi	26
ZHOU, Biao	94
ZHU, Daoben	93
ZOU, Shiyang	27–28

